DIFFERENTIATION AND REGULATION OF BONE MARROW MESENCHYMAL STROMAL CELLS

EDITED BY: Xiao Chen, Chao Xie, Ce Dou and Zhenhong Ni
PUBLISHED IN: Frontiers in Cell and Developmental Biology and
Frontiers in Molecular Biosciences

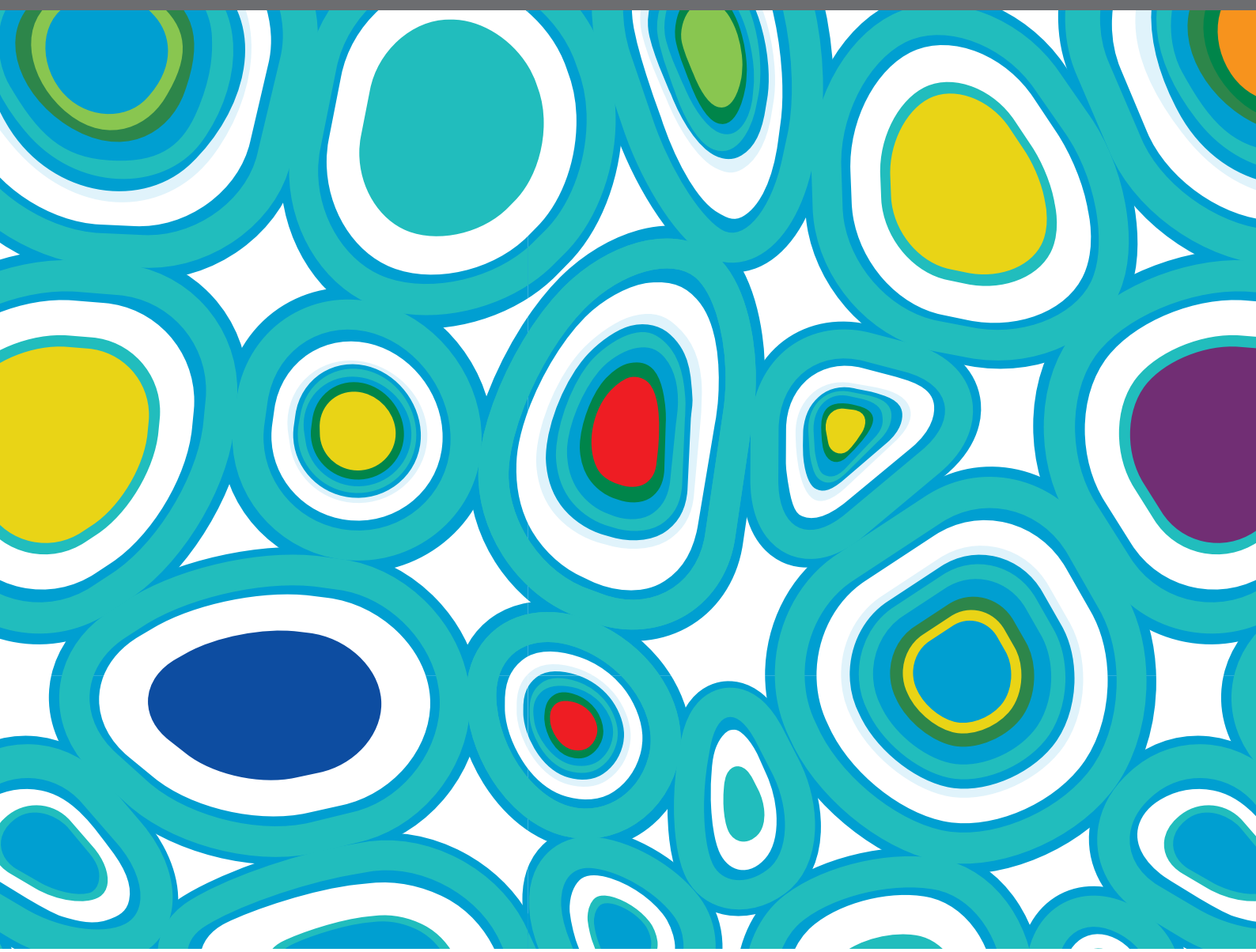

frontiers Research Topics

frontiers

ISSN 1664-8714
ISBN 978-2-88976-756-4
DOI 10.3389/978-2-88976-756-4

About Frontiers

Frontiers is more than just an open-access publisher of scholarly articles: it is a pioneering approach to the world of academia, radically improving the way scholarly research is managed. The grand vision of Frontiers is a world where all people have an equal opportunity to seek, share and generate knowledge. Frontiers provides immediate and permanent online open access to all its publications, but this alone is not enough to realize our grand goals.

Frontiers Journal Series

The Frontiers Journal Series is a multi-tier and interdisciplinary set of open-access, online journals, promising a paradigm shift from the current review, selection and dissemination processes in academic publishing. All Frontiers journals are driven by researchers for researchers; therefore, they constitute a service to the scholarly community. At the same time, the Frontiers Journal Series operates on a revolutionary invention, the tiered publishing system, initially addressing specific communities of scholars, and gradually climbing up to broader public understanding, thus serving the interests of the lay society, too.

Dedication to Quality

Each Frontiers article is a landmark of the highest quality, thanks to genuinely collaborative interactions between authors and review editors, who include some of the world's best academicians. Research must be certified by peers before entering a stream of knowledge that may eventually reach the public - and shape society; therefore, Frontiers only applies the most rigorous and unbiased reviews.
Frontiers revolutionizes research publishing by freely delivering the most outstanding research, evaluated with no bias from both the academic and social point of view. By applying the most advanced information technologies, Frontiers is catapulting scholarly publishing into a new generation.

What are Frontiers Research Topics?

Frontiers Research Topics are very popular trademarks of the Frontiers Journals Series: they are collections of at least ten articles, all centered on a particular subject. With their unique mix of varied contributions from Original Research to Review Articles, Frontiers Research Topics unify the most influential researchers, the latest key findings and historical advances in a hot research area! Find out more on how to host your own Frontiers Research Topic or contribute to one as an author by contacting the Frontiers Editorial Office: frontiersin.org/about/contact

DIFFERENTIATION AND REGULATION OF BONE MARROW MESENCHYMAL STROMAL CELLS

Topic Editors:
Xiao Chen, Second Military Medical University, China
Chao Xie, University of Rochester, United States
Ce Dou, Army Medical University, China
Zhenhong Ni, Army Medical University, China

Citation: Chen, X., Xie, C., Dou, C., Ni, Z., eds. (2022). Differentiation and Regulation of Bone Marrow Mesenchymal Stromal Cells.
Lausanne: Frontiers Media SA. doi: 10.3389/978-2-88976-756-4

Table of Contents

frontiers | Frontiers in Molecular Biosciences

EDITORIAL
published: 13 July 2022
doi: 10.3389/fmolb.2022.950930

Editorial: Differentiation and Regulation of Bone Marrow Mesenchymal Stromal Cells

Hao Zhang[1,2,3], *Lipeng Wang*[2,3] *and Xiao Chen*[1]*

[1]*Department of Orthopedics, Shanghai Changhai Hospital, Naval Medical University, Shanghai, China,* [2]*Institute of Translational Medicine, Shanghai University, Shanghai, China,* [3]*Musculoskeletal Organoid Research Center, Shanghai University, Shanghai, China*

Keywords: bone marrow mesenchymal stromal cells, differentiation, regulation, bone disease, osteoporosis

Editorial on the Research Topic

Differentiation and Regulation of Bone Marrow Mesenchymal Stromal Cells

Bone marrow mesenchymal stromal cells (BMSCs, also known as bone marrow mesenchymal stem cells) are a group of heterogeneous stromal cells with various differentiation potentials contributing to the postnatal genesis of osteoblasts, chondrocytes, and adipocytes as well as the maintenance of hemopoietic niches. Under pathological conditions like osteoporosis, osteoarthritis, etc., the differentiation shift of BMSCs has gained attention and been ever in the spotlight in recent decades. This Research Topic focuses on the mechanisms and regulations of BMSCs differentiation as well as therapeutic strategies for altering BMSC differentiation shifts for bone diseases. This Research Topic contains 16 reports, 5 literature reviews, and 11 pieces of original researche.

Identification and isolation of BMSCs is the first step to study the differentiation of BMSCs. Gao et al. comprehensively reviewed the current knowledge about several new subgroups of BMSCs. They could be divided into multipotent stem cells and skeletal stem cells, and the former cells are expected to mainly differentiate into adipocytes while the latter are the stem cells of osteoblast and chondrocyte. The differential lineages of skeletal stem cells were also compared between humans and mice in this review. Wei et al. identified and isolated a new subtype of MSCs derived from lateral mesoderm (LM-MSCs) using a novel protocol. LM-MSCs are similar to BMSCs but showed a homeodomain transcription factor (HOX) gene expression pattern. This new type of MSCs showed increased osteogenic and chondrogenic differentiation capacity and hematopoietic support potential compared to BMSCs. LM-MSCs might be an ideal cell source for bone and blood diseases after further confirmation.

Insight into mechanisms controlling BMSCs differentiation is also interesting. Differentiation of BMSCs in normal organisms may be related to epigenetic and gene expression. The contribution by Liu et al. provided updated insights into the role of epigenetic modifier proteins, chromodomain helicase DNA-binding (CHD) proteins, in BMSCs. CHD proteins promote disruption of histone-DNA contacts and exhibit regulatory effects in stem cell proliferation, differentiation, and functioning. It is involved in neurodevelopmental disorders, including CHARGE syndrome and Kallmann syndrome, cancers, and bone diseases. Thus, epigenetic regulation in stem cells could be a clinical target.

The development of high-throughput sequencing technologies and transcriptomics has provided new methods to create a deeper understanding of key genes in BMSC differentiation. Data from rat BMSC differentiation high-throughput transcription factors sequencing presented by Zhang et al. demonstrated that Hopx and other early responder TFs may control the osteogenic cell fate of BMSCs and participate in the development of osteoporosis. Gbx2 and other early responder TFs

OPEN ACCESS

Edited and reviewed by:
Cecilia Giulivi,
University of California, Davis, United States

***Correspondence:**
Xiao Chen
sirchenxiao@126.com

Specialty section:
This article was submitted to Cellular Biochemistry, a section of the journal Frontiers in Molecular Biosciences

Received: *23 May 2022*
Accepted: *02 June 2022*
Published: *13 July 2022*

Citation:
Zhang H, Wang L and Chen X (2022) Editorial: Differentiation and Regulation of Bone Marrow Mesenchymal Stromal Cells. Front. Mol. Biosci. 9:950930. doi: 10.3389/fmolb.2022.950930

should be considered in mechanistic models that clarify the anabolic changes in cartilage during the clinical progression of osteoarthritis. As was shown by Liu et al., Ccna2, Cdc20, and Il6 may act as common hub genes in initiating osteogenesis, adipogenesis, and chondrogenesis. Expression of Mex3b, Sertad1, and Hopx was only increased throughout three early phases during the osteogenic differentiation. Dtx4 and Ibsp expression occurred in adipogenesis and chondrogenesis, respectively. Bioinformatics makes it easier to screen key genes in BMSC differentiation. In human, Sun et al. found a key gene in BMSC osteogenic differentiation *via* bioinformatics-guided analysis. Aldehyde oxidase (AOX) was screened out in his study which showed a strong association with osteoblast-related pathways. AOX increased during BMSCs differentiation and AOX overexpression significantly increased the expression of osteo-specific genes. More transcriptome sequences of BMSCs in different species should be down to piece together a panorama of gene regulation in BMSC differentiation.

BMSCs reside in a complex microenvironment with multiple cells including adipocytes, immunocytes and osteoclasts. Cross-talks between BMSCs and different neighbors regulate BMSCs differentiation and exert important physiological action. In the review contributed by Gao et al., cross-talks occurred between bone and fat to control the bone mass through several pathways. RANKL and adipokines secreted by adipo-lineage cells negatively regulate BMSC osteogenic differentiation. The role of fat in the bone marrow and its regulatory effect on BMSCs was highlighted in the review article by Wang et al. Bone marrow adipocytes (BMAs) are critical regulators in hematopoiesis, osteogenesis, and osteoclastogenesis. As a cell type derived from BMSCs, BMAs inhibit osteoclast formation *via* bone morphogenetic protein receptor (BMPR) and epidermal growth factor receptor pathways and adipokines. An inflammatory response is essential for bone formation and BMSC osteogenic differentiation during fracture healing. Deng et al. uncovered that macrophages could express four kinds of osteoinductive cytokines, including BMP2, FGF2, TGFβ3, and OSM, under co-culture with hucMSC-derived extracellular matrix (hucMSC-ECM). They believed that macrophage-mediated osteogenesis depended on MIF/CD74 signal transduction. Crosstalk between osteoclast and osteoblast has been well investigated, and the OPG-RANK-RANKL axis is essential in coupling bone remodeling. Though a prior study (Xie et al., 2014) revealed that pre-osteoclast could increase angiogenesis *via* PDGF-BB to regulate BMSCs osteogenic differentiation, direct crosstalks between pro-osteoclast and BMSCs remain mysterious. Data presented by Bai et al. demonstrated tartrate acid phosphatase (TRAP)-positive monocytes secreted CTGF to activate BMSCs in periosteum during bone regeneration. Usually, pre-osteoclasts are TRAP-positive monocytes. CTGF derived from pre-osteoclast promoted bone healing by activating BMSCs and directing lineage commitment directly. Cross-talks between BMSCs and related cells could provide novel clinical targets in curing fracture and osteoporosis.

Differentiation of BMSCs is precisely regulated by a variety of factors including genes, microenvironment, and metabolism. In pathological conditions, differentiation of BMSCs is disturbed, leading to a decrease in tissue repair capacity and worsening disease. Diabetes mellitus (DM) is widely known for its susceptibility to multiple complications in the elderly. Xu and Zuo reviewed the research of stem cell fate alteration under DM in depth. Hyperglycemia of DM patients induced both dysfunctions and quantity alteration of stem cells *via* diabetic microenvironment. Stem cells showed abnormal mobilopathy, differentiation, migration, and secretion because of a rising level of oxidative stress and pro-inflammatory factors. Lipid metabolism also influences BMSCs differentiation. As was discovered by Lin et al., lipid availability could modulate the osteogenesis of skeletal progenitors. They found that lipoprotein receptor-related protein 5 (LRP5) participated in lipid uptake during BMSC osteogenesis. Lipid scarcity or Lrp5 ablation could decrease bone quality and suppresses BMSC osteogenic differentiation. Normal glucose and lipid metabolism are essential for maintaining stem cell proliferation and differentiation, but the changes in stem cell differentiation in different systemic diseases still need to be further explored.

Osteogenic differentiation ability of BMSCs plays a vital role in the development of orthopedic diseases. Exploring the mechanisms of osteogenic differentiation of BMSCs and developing therapeutic strategies are the current hot topics of research on BMSCs. In this Research Topic, Ni et al. investigated that IL-18 promoted the osteogenic differentiation of hBMSCs *via* the SLC7A5/c-MYC pathway. This research provided a possible pathway of IL-18 in promoting bone formation, but they only provided *in vitro* data. The contribution by Xu et al. provided both *in vitro* and *in vivo* evidence that Zinc finger E-box-binding homeobox 1 (ZEB1) could regulate osteogenesis. Silencing of ZEB1 in BMSCs promoted osteogenic activity and mineralization partly through the Wnt/β-catenin pathway, which is a major pathway regulating BMSC osteogenic differentiation. In-depth mechanistic studies provide therapeutic targets for regulating the differentiation of BMSCs, but target-specific drug development remains challenging. Small molecules derived from traditional Chinese medicine could regulate the differentiation of BMSCs. Wang et al. investigated that curculigoside (CCG), a bioactive component of Curculigo orchioides, could regulate the bone-fat balance in the marrow of aging mice *via* transcriptional co-activator with PDZ-binding motif (TAZ) expression.

Overall, the studies included in this Research Topic expand our knowledge of BMSCs subtype. The differentiation process and several key regulatory genes of BMSCs in physiological status have been revealed in three studies. The shift of BMSC differentiation in some pathological conditions were explored and reviewed by articles in this Research Topic. Osteogenic differentiation of BMSCs as a main clinical translation point was well researched in this topic, and several key regulatory proteins and novel drugs were developed to cure related bone diseases.

AUTHOR CONTRIBUTIONS

HZ and LW wrote the manuscript. XC edited the manuscript. LW and XC did the final checks of the manuscript and submitted it. All authors contributed to the article and approved the submitted version.

FUNDING

This work was supported by the National Natural Science Foundation of China (82172098), National Natural Science Foundation of China (81972254), National Natural Science Foundation of China (81871099), Shanghai Rising Star Program (21QA1412000).

REFERENCES

Xie, H., Cui, Z., Wang, L., Xia, Z., Hu, Y., Xian, L., et al. (2014). PDGF-BB Secreted by Preosteoclasts Induces Angiogenesis during Coupling with Osteogenesis. *Nat. Med.* 20 (11), 1270–1278. doi:10.1038/nm.3668

Conflict of Interest: The authors declare that the research was conducted in the absence of any commercial or financial relationships that could be construed as a potential conflict of interest.

frontiers in Molecular Biosciences

ORIGINAL RESEARCH
published: 24 May 2021
doi: 10.3389/fmolb.2021.682728

ZEB1 Mediates Bone Marrow Mesenchymal Stem Cell Osteogenic Differentiation Partly via Wnt/β-Catenin Signaling

Cuidi Xu[1], Hongli Shi[1], Xin Jiang[1], Yongqian Fan[2], Donghui Huang[2], Xinming Qi[3] and Qun Cheng[1]**

[1] Department of Osteoporosis and Bone Disease, Huadong Hospital Affiliated to Fudan University, Research Section of Geriatric Metabolic Bone Disease, Shanghai Geriatric Institute, Shanghai, China, [2] Department of Orthopedics, Huadong Hospital Affiliated to Fudan University, Shanghai, China, [3] Center for Drug Safety Evaluation and Research, State Key Laboratory of Drug Research, Shanghai Institute of Materia Medica, Chinese Academy of Sciences, Shanghai, China

OPEN ACCESS

Edited by:
Xiao Chen,
Second Military Medical University, China

Reviewed by:
Hongyuan Zhang,
Duke University, United States
Xiao Zhai,
Changhai Hospital, China
Ce Dou,
Army Medical University, China
Yingying Jing,
Shanghai University, China
Jin Cui,
Second Military Medical University, China

***Correspondence:**
Xinming Qi
xmqi@cdser.simm.ac.cn
Qun Cheng
chengqun@fudan.edu.cn

Specialty section:
This article was submitted to Cellular Biochemistry, a section of the journal Frontiers in Molecular Biosciences

Received: 19 March 2021
Accepted: 14 April 2021
Published: 24 May 2021

Citation:
Xu C, Shi H, Jiang X, Fan Y, Huang D, Qi X and Cheng Q (2021) ZEB1 Mediates Bone Marrow Mesenchymal Stem Cell Osteogenic Differentiation Partly via Wnt/β-Catenin Signaling. Front. Mol. Biosci. 8:682728. doi: 10.3389/fmolb.2021.682728

Zinc finger E-box-binding homebox 1 (ZEB1) is a zinc-finger transcription factor best known for its role in promoting the epithelial-mesenchymal transition, which is also related to osteogenesis. Here, ZEB1 was investigated for its role in the commitment of bone marrow mesenchymal stem cells (BMSCs) to osteoblasts. *In vitro*, ZEB1 expression decreased following osteogenic differentiation. Furthermore, silencing of ZEB1 in BMSCs promoted osteogenic activity and mineralization. The increase in osteogenic differentiation induced by si-ZEB1 could be partly rescued by the inhibition of Wnt/β-catenin (si-β-catenin). *In vivo*, knockdown of ZEB1 in BMSCs inhibited the rapid bone loss of ovariectomized (OVX) mice. ZEB1 expression has also been negatively associated with bone mass and bone formation in postmenopausal women. In conclusion, ZEB1 is an essential transcription factor in BMSC differentiation and may serve as a potential anabolic strategy for treating and preventing postmenopausal osteoporosis (PMOP).

Keywords: ZEB1, osteogenesis, Wnt/β-catenin, postmenopausal osteoporosis, BMSCs

INTRODUCTION

Bone marrow mesenchymal stem cells (BMSCs) are multipotent cells that represent a promising source for regenerative medicine. BMSCs are capable of osteogenic, chondrogenic, and adipogenic differentiation (Bartscherer et al., 2006); regeneration of cells in injured tissues requires the ability to maintain differentiation toward the desired cell fate, and therefore, cellular and molecular signaling pathways and micro-environmental changes have been studied to understand the role of cytokines, chemokines, and transcription factors on the differentiation of BMSCs. The differentiation of BMSCs can be genetically manipulated and inhibited by specific transcription factors associated with a particular cell lineage.

Abbreviations: BMSCs, bone marrow mesenchymal stem cells; ZEB1, zinc finger E-box-binding homebox 1; Col1a1, collagen 1A1; RUNX2, runt-related transcription factor 2; TGFβ, transforming growth factor beta; BMP, bone morphogenetic protein; PMOP, postmenopausal osteoporosis; BMD, bone mineral density; MAR, bone mineral apposition rate; ALP, alkaline phosphatase; EC, endothelial cell; MMP-1, matrix metalloproteinase-1.

In this study, we critically investigated the role of the transcription factor, zinc finger E-box-binding homebox 1 (ZEB1), and related signaling pathways that affect the differentiation of BMSCs toward osteoblasts. ZEB1, a member of the zinc finger E-box-binding protein family, is a transcription factor that triggers the epithelial-to-mesenchymal transition (EMT) (Bracken et al., 2008; Sanchez-Tillo et al., 2010). A previous investigation reported that ZEB1 is involved in early skeletal development. Yang et al. reported that ZEB1, which was downregulated as BMSCs were differentiated to osteoblasts, repressed the differentiation of C2C12 myoblasts into the osteoblast lineage induced by BMP_2 (Yang et al., 2007). However, mice with a homozygous mutation in ZEB1 display skeletal defects in craniofacial bones, ribs, intervertebral disc, sternum, and limb skeletons (Takagi et al., 1998). Recently, Rong et al. (Fu et al., 2020) reported that specific deletion of ZEB1 in the endothelial cells (ECs) could reduce bone angiogenesis and osteogenesis, and injecting a pcDNA3.1 + C-eGFP-ZEB1 vector that expressed enhanced ZEB1 protein in bone ECs restored the impaired bone formation in ovariectomized (OVX) mice, suggesting that ZEB1 plays a significant role in crosstalk between angiogenesis and osteogenesis. ZEB1 was shown to be closely related to the EMT in osteosarcoma, and miR-126 and miR-708-5p played an inhibitory role in the proliferation and invasion of osteosarcoma cells by directly targeting ZEB1 and subsequently suppressed the EMT (Jiang et al., 2017; Feng et al., 2020). Therefore, the function of ZEB1 is extremely complex and may even have contradictory effects on bone metabolism, and its role in osteogenesis in osteoblast lineage deserves further investigation.

MATERIALS AND METHODS

Cell Culture

Human bone marrow-derived mesenchymal stem cell lines were purchased from Cyagen (Shanghai, China). BMSCs were maintained in hBMSC basal medium (Cyagen). BMSCs were re-plated at a density of 8,000 cells/100 μl and were subcultured when they were 80–90% confluent.

Osteogenic Differentiation and Alizarin Red Staining

The differentiation medium used in this study was human BMSC osteogenic differentiation basal medium purchased from Cyagen. Briefly, BMSCs were seeded at 5,000cells/100 μl in 96-well plates. For evaluating mineralization, cells were induced for 21 days, washed 1–2 times with PBS, and fixed with 4% paraformaldehyde for 30 min. This was supplemented with 50μl of freshly prepared alizarin red S solution (Cyagen), and cells were incubated for 3–5 min.

Clinical Bone Sample Preparation

A total of 20 bone specimens were collected from patients (aged 70–85 years) who had a fragile fracture that necessitated hip arthroplasty surgery at the department of orthopedics in the Huadong Hospital. All patients were women who had incurred a low-energy hip fracture and had undergone arthroplasty within 48 h following the fracture. Individuals were excluded if they had malignant, metabolic, or endocrine diseases; chronic renal failure; or other severe systemic diseases. We collected the trabecular bone core from the intertrochanteric region of the proximal femur because it is not exactly the fracture site and is available during arthroplasty. All clinical procedures were approved by the Ethics Committee of Huadong Hospital affiliated with Fudan University (2019K055).

Alkaline Phosphatase Activity and ALP Staining

For measuring alkaline phosphatase (ALP) activity, cells were cultured for 7 days and incubated with p-nitrophenyl phosphate (pNPP) in 1 M diethanolamine buffer containing 0.5 mM $MgCl_2$ (pH 9.8) at 37°C for 15 min. The absorbance was measured at 405 nm. For ALP staining, the BCIP/NBT Alkaline Phosphatase Color Development Kit (Beyotime, Shanghai, China) was carried out according to the instructions of the manufacturer.

RNA Interference

Negative control siRNA (si-NC) and ZEB1-specific siRNAs (si-ZEB1) were purchased from RiboBio (Guangzhou, China). BMSCs were cultured to 75–80% confluence in six-well plates and were transfected with 40 nM of ZEB1 siRNAs using RNAiMAX (Invitrogen, United States). After transfection for 24 h, the medium was replaced with an osteogenic medium to determine their cell fate-specific differentiation potential.

Lentiviral Vector Preparation and Infection

For ZEB1 overexpression, lentiviruses expressing ZEB1 and empty vectors were purchased from OBIO (Shanghai, China). BMSCs were infected with these viruses in the presence of polybrene for 24–48 h. The packaged lentiviruses were named lenti-NC and lenti-ZEB1.

Reverse Transcription and Real-Time PCR

Total RNA was isolated from BMSCs using TRIzol reagent (Takara, Japan). cDNA was obtained using a PrimeScript RT Master Mix (Takara, Japan) according to the instructions of the manufacturer. Relative sequences are listed in the **Supplementary Materials**.

Western Blotting

Bone marrow mesenchymal stem cells were lysed in RIPA lysis buffer, and 30 ng of protein was loaded and separated by 10% SDS—polyacrylamide gel electrophoresis, followed by transfer onto membranes, which were then blocked in non-fat milk (5%) for 1–2 h at room temperature. Membranes were then incubated overnight at 4°C with primary antibodies against GAPDH (1:3,000, Proteintech, Chicago, TL, United States), β-catenin (1:1,000, Proteintech), ZEB1 (1:1,000, Proteintech), and smad3 (1:1,000, Cell Signaling Technology, Beverly, MA, United States).

Membranes were washed three times with Tris-buffered saline with 0.1% Tween® 20 Detergent (TBST), followed by incubation with secondary antibodies for 45–60 min.

In vivo Studies

Sham and OVX-operated mice (4 weeks old, 13–15 g) were used to determine the effect of ZEB1 *in vivo*. All female C57BL/6J mice were purchased from Shanghai Model Organisms (Shanghai, China). A recombinant adeno-associated virus (AAV9) for the knockdown of ZEB1 in osteoblast lineage cells in the bone was purchased from HANBIO (Shanghai, China). Recombinant adeno-associated virus9 (rAVV9) is highly effective for transducing osteoblast lineage cells in the bone, as reported in Yang et al. (2019). A total of 24 mice were divided into four groups: (1) sham group: mice were subjected to sham operation; (2) OVX group: mice were subjected to bilateral oophorectomy to establish the osteoporosis model; (3) OVX + AAV9-amiR-Ctrl group: OVX mice were injected with empty adenovirus; and (4) OVX + AAV9-amiR-ZEB1 group: OVX mice were injected with ZEB1 knockdown adenovirus. A volume of 200 μl of rAVV9 carrying Ctrl or ZEB1 was intravenously injected through the tail at 4 weeks after model establishment. At 12 weeks after model establishment, mice in all groups were euthanized after anesthesia, and femurs were collected for μCT or bone histomorphometry. Each procedure was performed under aseptic conditions, and general anesthesia was carried out in accordance with the Animal Ethics and Experimental Safety of Fudan University (JS-004).

Micro-Computed Tomography and Bone Histomorphometry

Femurs were fixed in 4% paraformaldehyde for 12 h and transferred to 75% ethanol at 4°C. Samples were then used for micro-computed tomography (μCT), and relative images were analyzed by SCANCO evaluation software to perform the three-dimensional structural parameter analysis including bone mineral density (BMD), bone volume/tissue volume (BV/TV), trabecular thickness (Tb.Th), and trabecular separation (Tb.Sp). For assessing new bone formation, we injected tetracycline (25 mg/kg) at 14 days before the mice were euthanized, and calcein (5 mg/kg) was injected at 7 days prior to sacrifice. The bone mineral apposition rate (MAR, μm/d) was measured by image analysis software (ImageJ; NIH, Bethesda, MD, United States). Undecalcified sections were subjected to Goldner's trichrome staining and examined and photographed using a high-quality microscope.

Statistical Analysis

Differences between two groups were tested by independent sample *t*-test and one-way analysis of variance (ANOVA); the Tukey' *post hoc* test was applied to compare three or more groups. Correlation analysis was used to test the association of ZEB1 expression in bone tissue with BMD and with osteogenesis genes in bone tissue. Each experiment *in vitro* was repeated three times with similar results. All data were analyzed by GraphPad Prism 7 software and presented as means plus standard deviation. $^{*}p < 0.05$, $^{**}p < 0.01$, and $^{***}p < 0.001$ were considered indicative of statistical significance.

RESULTS

ZEB1 Expression Was Negatively Related With BMD and Osteogenesis Genes in Bone Tissue in Postmenopausal Women

We detected the mRNA expression of ZEB1 in bone tissue from postmenopausal osteoporosis (PMOP) patients, and results showed that in PMOP patients, the expression of osteogenesis genes such as osterix, RUNX2, and Col1a1 in bone tissue was positively related with BMD, while ZEB1 expression was negatively related with osteogenesis genes and BMD (**Figure 1**).

Downregulation of Endogenous ZEB1 Promotes Osteogenesis of hBMSCs *in vitro*

By assaying the endogenous expression of ZEB1 during hBMSCs osteogenesis, we demonstrated that ZEB1 expression in hBMSCs was significantly decreased at days 4, 7, and 14 following osteogenic differentiation at both the mRNA (**Figure 2A**) and protein levels (**Figures 2B,C**).

To explore the effect of ZEB1 on osteogenesis, siRNA-mediated knockdown was performed to downregulate ZEB1 expression, and the efficiency of knockdown was tested at 48 h post-infection by real-time PCR (**Figure 2D**) and western blot analysis (**Figure 2E,F**). ZEB1 mRNA and protein levels were reduced by over 70 and 90%, respectively, after siRNA transfection. hBMSCs transfected with si-ZEB1 showed higher ALP activity (**Figure 2I**) and enhanced ALP staining (**Figure 2G**) and alizarin red staining (**Figure 2H**) compared with siNC. Consistent with these changes, qRT-PCR showed that mRNA levels of ALP, osterix, RUNX2, and Col1a1 were significantly increased in the si-ZEB1 group on day 7, compared with the siNC group (**Figure 2J**).

Upregulation of Endogenous ZEB1 Inhibits Osteogenic Differentiation of hBMSCs *in vitro*

To further investigate the role of ZEB1 in the osteogenesis of hBMSCs, lentivirus-infected hBMSCs were induced to differentiate into the osteogenic lineage. The overexpression efficiency of ZEB1 was tested after 48 h of infection by real-time PCR (**Figure 3A**) and western blot analysis (**Figures 3B,C**). Levels of mRNA and protein were increased by nearly fivefold compared to the control group.

As elucidated by ALP activity (**Figure 3F**) and ALP staining (**Figure 3D**), compared with the lenti-NC group, the expression and activity of ALP clearly decreased in lenti-ZEB1-infected cells. Alizarin red staining demonstrated that calcium mineralization was also reduced (**Figure 3E**). qRT-PCR showed that mRNA levels of ALP, osterix, RUNX2, and Col1a1 were significantly decreased in the overexpression lenti-ZEB1 group compared with the lenti-NC group (**Figure 3G**).

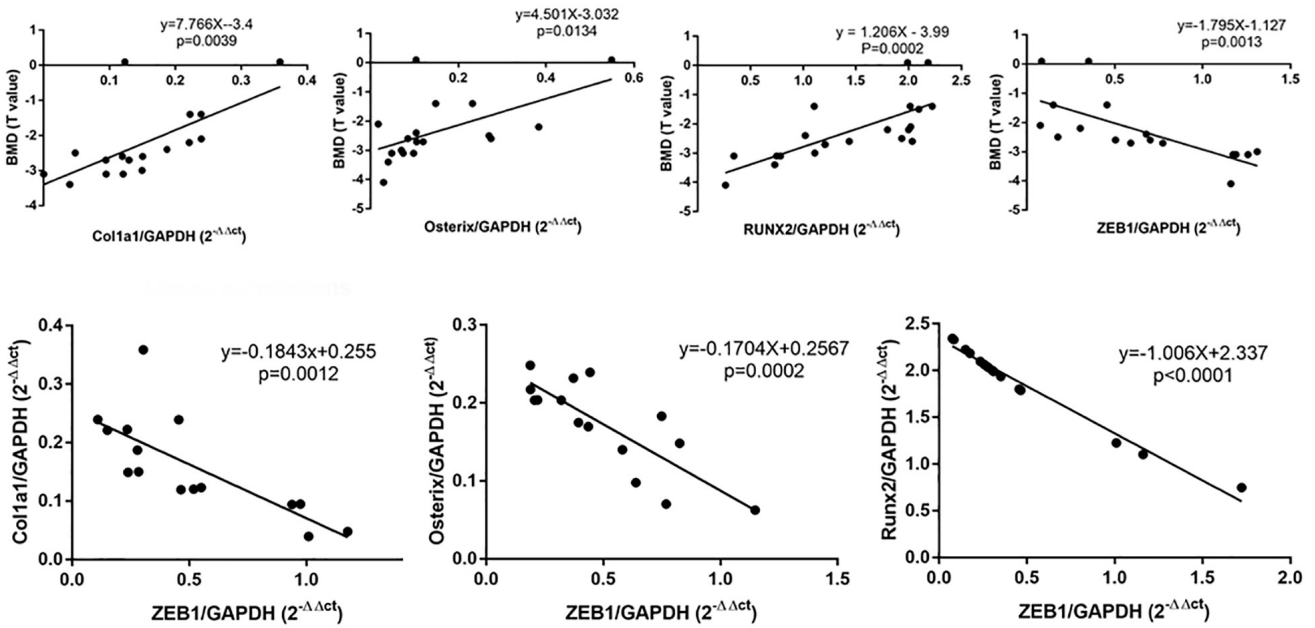

FIGURE 1 | qRT-PCR analysis showed that Col1a1, osterix, and RUNX2 were significantly decreased in PMOP patients-derived bone tissue. Correlation analysis demonstrated that ZEB1 was negatively correlated with BMD and Col1a1, osterix, and RUNX2 in bone tissue derived from PMOP patients.

si-β-Catenin Counteracted ZEB1 Downregulation-Induced Osteogenesis

Previous studies have demonstrated that the differentiation of BMSC into osteoblasts is regulated by various signaling pathways, including the important Wnt/β-catenin pathway (Fan et al., 2018). To further determine if si-ZEB1 promotes osteogenesis through Wnt/β-catenin signaling, we measured mRNA (**Figure 4C**) and protein (**Figures 4A,B**) levels of β-catenin expression after si-ZEB1 treatment. The si-ZEB1 group showed significantly increased expression of β-catenin, especially in the nucleus (**Figures 4D,E**), along with Oct4, Cyclin D1, C-myc, and CD44 compared to the control (**Supplementary Materials**). However, western blotting showed that there was no significant difference in the smad3 expression between the si-ZEB1 group and the control (**Supplementary Materials**).

To further confirm that enhanced osteogenesis of si-ZEB1 was correlated with activated canonical Wnt signaling, the specific inhibitor, si-β-catenin, was added to the cell culture in the osteogenic induction medium. The efficacy of inhibition of Wnt/β-catenin signaling was tested by western blotting (**Figure 4F**), which showed that β-catenin was remarkably downregulated by this inhibitor. Importantly, with si-β-catenin treatment, the enhanced ALP activity (**Figure 4H**) and ALP staining (**Figure 4G**) in the si-ZEB1 group was abolished. Alizarin red demonstrated that fewer bone nodules were present in the si-β-catenin group compared with the si-ZEB1 group (**Figure 4G**), and there were decreased mRNA levels of the osteogenic genes ALP, osterix, RUNX2, and Col1a1 in the si-β-catenin group (**Figures 4I–K**).

Downregulation of ZEB1 Attenuated the Bone Loss Induced by Ovariectomy

To investigate the anabolic effect of ZEB1 *in vivo*, we injected AAV9-amiR-Ctrl and AAV9-amiR-ZEB1 into OVX mice. ZEB1 mRNA levels were reduced by over 60% (**Figure 5A**), and β-catenin increased after injection with AAV9-amiR-ZEB1 (**Figure 5B**). μCT and relative images were analyzed to perform the three-dimensional structural parameter analysis including BMD, BV/TV, Tb.Th, and Tb.Sp (**Figures 5C–G**). Compared to sham mice, OVX mice exhibited reduced bone mass, indicated by a 19.73% decrease of BMD, 58.40% decrease of BV/TV, 55.74% decrease of Tb.N, and 31.68% increase of Tb.Sp. Moreover, AAV9-amiR-ZEB1 treatment significantly increased the bone mass, demonstrated by micro-CT analysis, with an increase of BMD, BV/TV, and Tb.N and a decrease of Tb.Sp compared with both the OVX group and the AAV9-amiR-Ctrl group. Interestingly, compared with the sham group, OVX + AAV9-amiR-ZEB1 showed a 17.93% increase of BMD, 32.09% increase of BV/TV, 27.67% increase of Tb.N, and 9.28% decrease of Tb.Sp (**Figures 5C–G**). Similarly, the bone formation ability *in vivo* was clearly increased in the ZEB1 knockdown group, as confirmed by the Goldner's trichrome staining and double fluorescence labeling of calcein and tetracycline, which measured the bone formation-related parameter MAR (**Figures 5H–I**).

DISCUSSION

The balance between the activities of bone-forming osteoblasts and bone-resorbing osteoclasts is fundamental to the strength and integrity of bone (Yi et al., 2017). With aging, the balance

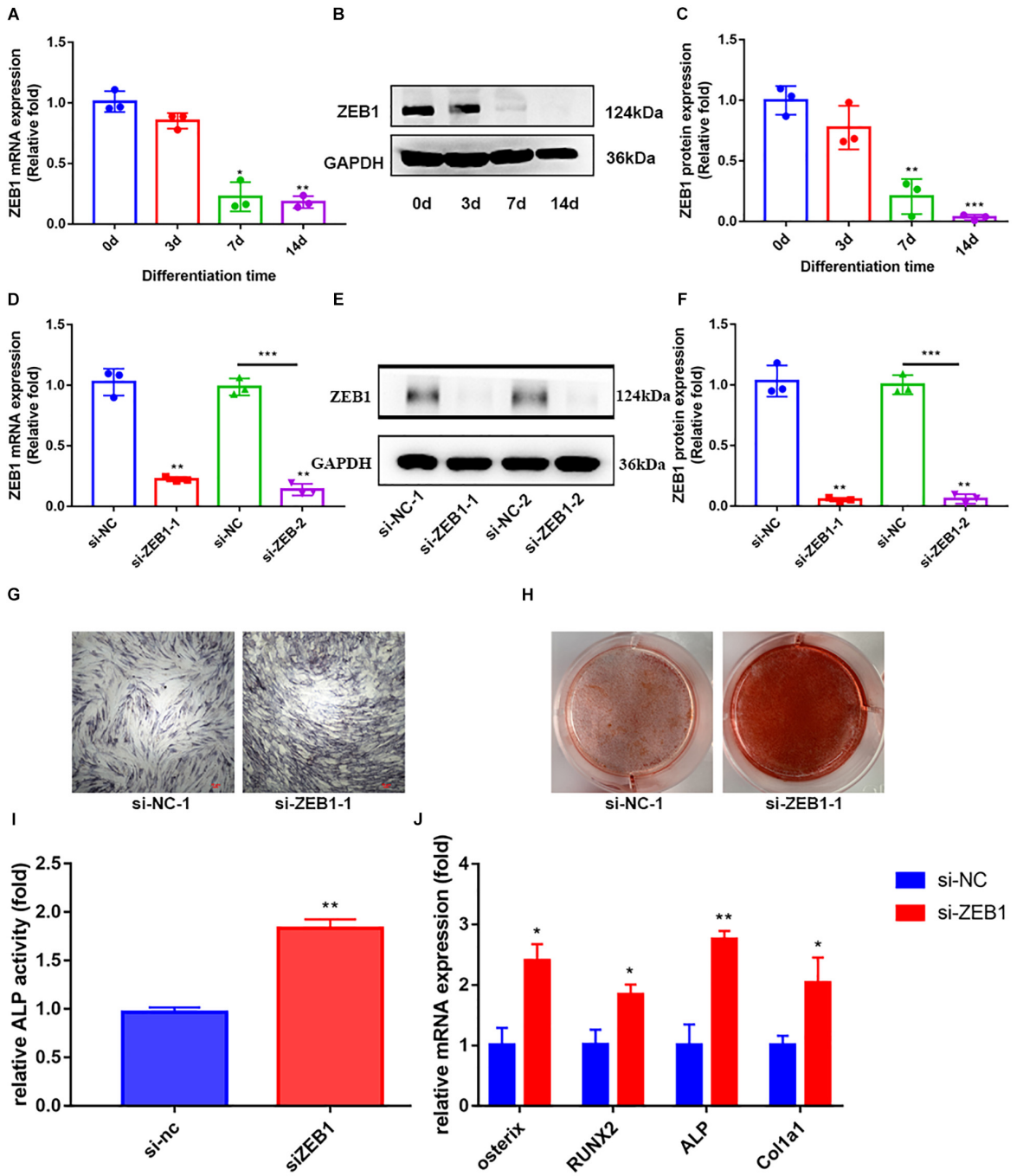

FIGURE 2 | Zinc finger E-box-binding homebox 1 (ZEB1) knockdown enhanced the osteogenesis of hBMSCs. **(A)** qRT-PCR analysis demonstrated that the mRNA expression of ZEB1 decreased after osteogenic differentiation. **(B,C)** Western blotting analysis showed that the protein expression of ZEB1 decreased after osteogenic differentiation. **(D)** ZEB1 expression decreased after siZEB1 treatment – evaluated by qRT-PCR. **(E,F)** ZEB1 expression decreased after siZEB1 treatment – evaluated by western blotting. **(G,H)** ALP staining and alizarin red staining of hBMSCs after transfecting with siZEB1. **(I)** ALP activity of hBMSCs after transfection with siZEB1. **(J)** qRT-PCR analysis demonstrated that siZEB1 transfection increased the mRNA level of ALP, osterix, RUNX2, and Col1a1. *p-value < 0.05, **p-value < 0.01 and ***p-value < 0.001.

is swayed in favor of bone resorption so that the osteoclast activity exceeds the osteoblast activity, causing the bones to become brittle and prone to fracture (Ishtiaq et al., 2015). Age-related osteoporosis is related to a deficit of bone formation caused by reduced capacity in proliferation and differentiation of BMSCs (Kiernan et al., 2016). Therefore, unveiling the mechanism that regulates the differentiation of osteoblasts is of great therapeutic potential. Here, we showed that ZEB1 is

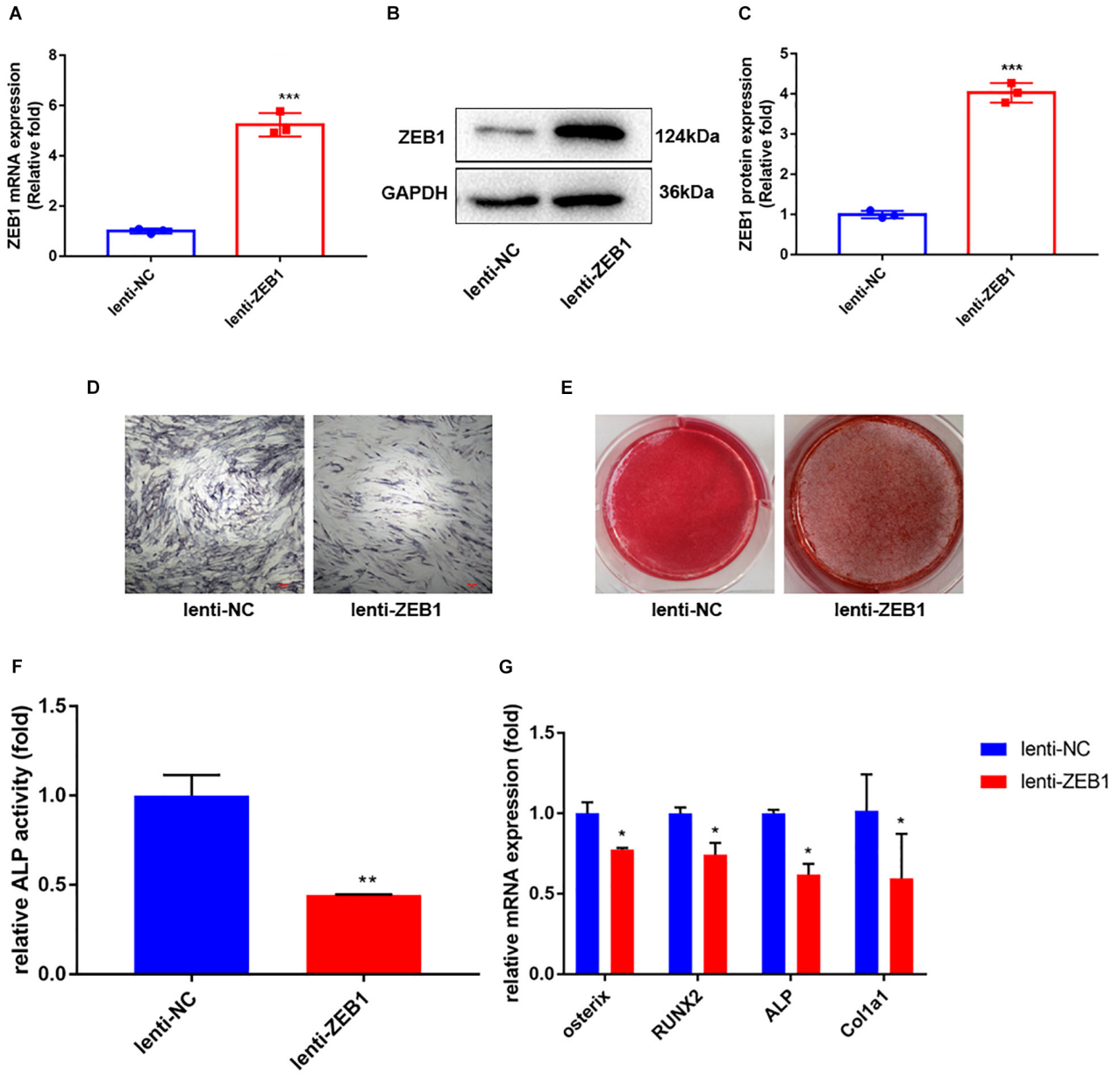

FIGURE 3 | Zinc finger E-box-binding homebox 1 (ZEB1) upregulation inhibited the osteogenesis of hBMSCs. **(A)** ZEB1 expression increased after lenti-ZEB1 treatment – evaluated by qRT-PCR. **(B,C)** ZEB1 expression increased after lenti-ZEB1 treatment – evaluated by western blotting. **(D,E)** ALP staining and alizarin red staining of hBMSCs after lenti-ZEB1 treatment. **(F)** ALP activity of hBMSCs after lenti-ZEB1 treatment. **(G)** qRT-PCR analysis demonstrated that lenti-ZEB1 treatment decreased the mRNA level of ALP, osterix, RUNX2, and Col1a1. *p-value < 0.05, **p-value < 0.01 and ***p-value < 0.001.

endogenously expressed in BMSCs, and the expression pattern of ZEB1 during the osteogenic differentiation period also showed that ZEB1 gradually decreased over time.

The osteogenic activity of BMSCs decreases progressively as a function of increasing lifespan, and a decrease in the number of BMSCs and a reduction in their osteogenic capacity are the main causes of osteoporosis in the elderly (Qadir et al., 2020). Darryl et al. reported that ZEB1 was highly expressed in early limb mesenchyme, and ZEB1 expression was lost in these cells after condensation; by binding to a CACCT sequence contained within an E2 box, ZEB1 was shown to inhibit the activity of the rat Col2a1 promoter, suggesting that ZEB1 was involved in skeletal patterning during limb development and can serve as a negative regulator of chondrocyte-specific genes (Murray et al., 2000; Terraz et al., 2001). However, ZEB1 has not been reported to be functionally related to the osteogenesis of BMSCs. We found that silencing ZEB1 positively increased the osteogenic potential of BMSCs *in vitro*. ZEB1 silencing promoted ALP activity and mineralization and increased the expression of osteogenesis markers such as ALP, osterix, RUNX2, and

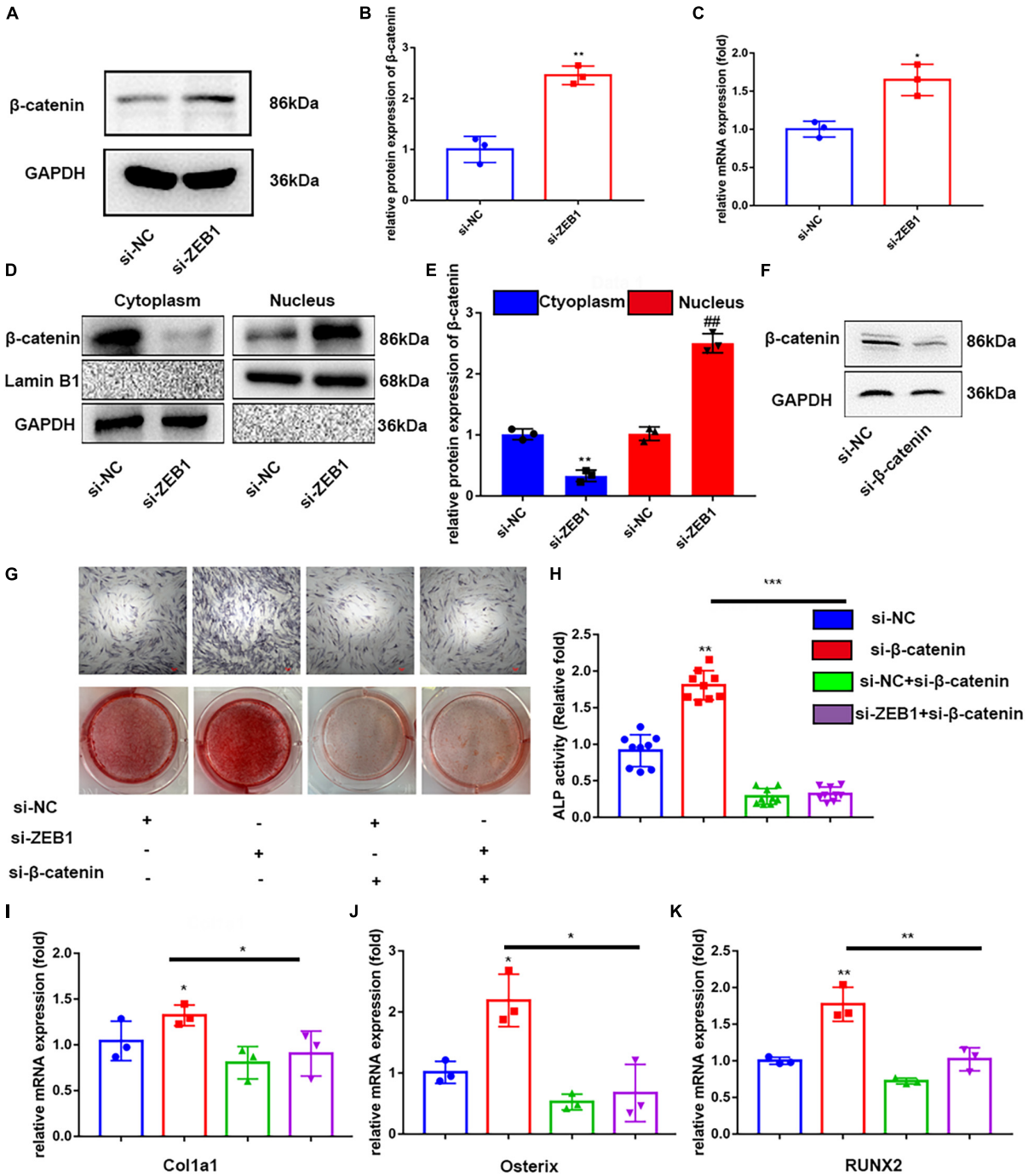

FIGURE 4 | Downregulation of endogenous ZEB1 activated wnt/β-catenin signaling pathway. **(A,B)** Western blotting analysis showed that ZEB1 knockdown promoted the protein level of β-catenin. **(C)** qRT-PCR analysis revealed that ZEB1 knockdown promoted the mRNA level of β-catenin. **(D,E)** β-catenin protein level was increased in the nucleus evaluated by qRT-PCR. **(F)** β-catenin expression was decreased after siβ-catenin treatment – evaluated by western blotting. **(G)** ALP staining and alizarin red staining of hBMSCs after siβ-catenin and siZEB1 treatment. **(H)** ALP activity of hBMSCs after siβ-catenin and siZEB1 treatment. **(I–K)** qRT-PCR exhibited that siβ-catenin transfection rescued the increased ALP, osterix, RUNX2, and Col1a1 induced by siZEB1. **p*-value < 0.05, ***p*-value < 0.01 and ****p*-value < 0.001.

Col1a1, indicating that ZEB1 is likely to inhibit the osteogenesis of BMSCs. In order to verify the possible role of endogenous ZEB1 in BMSCs, the lentivirus-based approach was applied to upregulate ZEB1 expression. Overexpression of ZEB1 limited the osteogenic differentiation ability compared to the NC group. Moreover, ZEB1 is inappropriately highly expressed in various

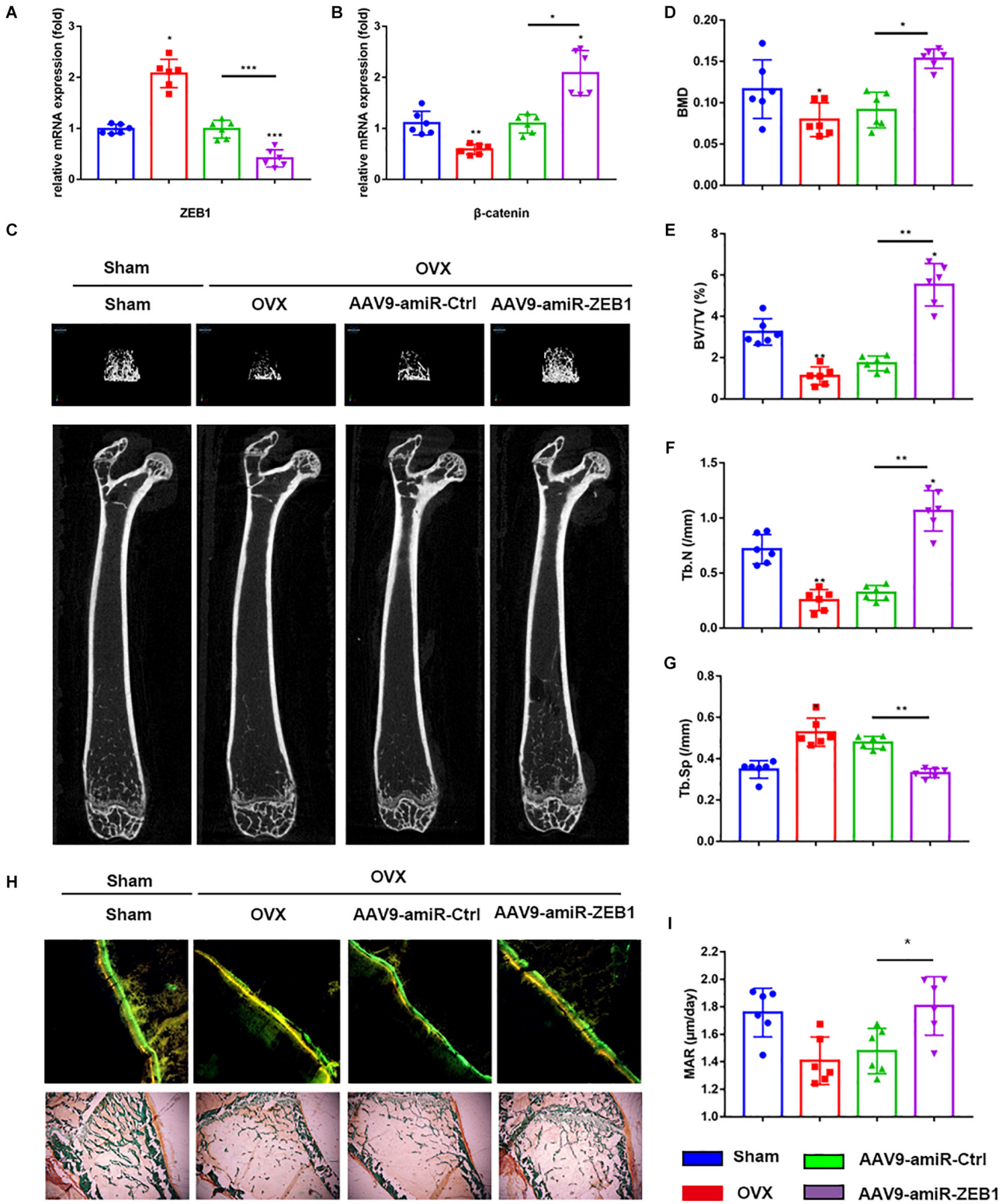

FIGURE 5 | Downregulation of ZEB1 attenuates the bone loss induced by ovariectomy. **(A)** qRT-PCR analysis revealed that ZEB1 was decreased after injection with AAV9-amiR-ZEB1. **(B)** qRT-PCR analysis revealed that ZEB1 knockdown promoted the mRNA level of β-catenin *in vivo*. **(C–G)** Representative images of microCT. $n = 6$ biologically independent samples. 3D structural parameters-BMD, BV/TV, Tb.N, and Tb.Sp of femurs measured by microCT in all groups. **(H,I)** Representative images showing new bone formation were assessed by double fluorescence labeling of calcein and tetracycline and Goldner's trichrome staining of femurs. 100×. Histomorphometric analysis of the bone formation-related parameter MAR in all groups. *p-value < 0.05, **p-value < 0.01 and ***p-value < 0.001.

malignant tumors and functions as a stimulating factor of tumor invasion and bone metastasis. The conditioned medium derived from ZEB1-overexpressing MDA-MB-231 cells can stimulate osteoclast maturation by upregulating MMP-1 and subsequently promote breast cancer metastasis to bone (Hu et al., 2011). ZEB1 promotes tumor invasion and metastasis by inducing the EMT in osteosarcoma, causing carcinoma cells to acquire cancer stem cell properties such as self-renewal. Our findings are consistent with the results investigated by Manuel et al., who found that MSCs from complete knockout of ZEB1 mice ($ZEB1^{flox/flox}$) exhibited increased ALP staining and alizarin red staining. Manuel also translated his findings to the cancer context and demonstrated that high ZEB1 expression can prevent osteogenesis in osteosarcoma cells and eventually lock the tumor cells in an aggressive, undifferentiated state (Hu et al., 2011), indicating that ZEB1 may maintain the stemness of stem cells in both physiological and pathophysiological conditions. Therefore, in patients with decreased bone mass caused by tumor bone metastasis, targeting ZEB1 for therapeutic purposes may serve to "kill two birds with a stone."

Activation of the Wnt/β-catenin signaling is crucial during the osteogenic differentiation of BMSCs (Gozo et al., 2013; Shen et al., 2020). The Wnt family comprises 19 closely secreted glycoproteins that mediate multiple cellular and biological processes (Cadigan and Nusse, 1997), including the formation of the body axis, development of the central nervous system, axial specification in limb development, and mouse mammary gland development. It has been reported that Wnt signaling stabilizes and causes the accumulation of β-catenin (Kikuchi, 2000; Bartscherer et al., 2006), which is an important trigger of osteoblastic differentiation. ZEB1 also has a Smad-binding domain (SBD), which binds to Smad family proteins and regulates TGF-β/BMP signaling (Postigo et al., 2003). In addition, the odontoblastic differentiation of murine dental papilla cells (mDPCs) was repressed in ZEB1-silenced cells. In the case of tooth germ at the cap stage, ZEB1 expression was lost in the epithelium-separated dental mesenchyme, but was recovered by BMP4 signaling (Xiao et al., 2021). Therefore, the function of ZEB1 in the differentiation of mDPCs was achieved via the BMP pathway. It is possible that the promoting function of ZEB1 depends on BMP/smad signaling, and its inhibitory regulation relies on Wnt signaling. In this study, we did not find any differences in Smad3 protein levels after siZEB1 treatment; however, the expression of β-catenin was significantly enhanced, suggesting that the effect of ZEB1 in osteogenesis is regulated via the Wnt/β-catenin pathway rather than the TGF-β/BMP pathway. Some studies have also reported that ZEB1 correlated with β-catenin levels. Xinghai et al. found that conditional β-catenin knockdown led to the decrease of ZEB1 expression, which, in turn, inhibited bone metastasis in lung cancer (Yang et al., 2015). Tan et al. (2019) demonstrated that the upregulation of ZEB1 induced by β-catenin could enhance the differentiation of BMSCs into hepatocytes. Moreover, hypoxia improved vasculogenesis in distraction osteogenesis through Wnt/β-catenin signaling, with a concomitant decrease in ZEB1 (He et al., 2020). The different outcomes of these studies imply that there may be synergistic or opposite effects of the identical transcription factors in different tissues or different cell lineages. However, our results proved that ZEB1 silencing led to an increase in Wnt signaling demonstrated by the increased mRNA and protein levels of β-catenin. Furthermore, si-β-catenin, used as an antagonist of Wnt/β-catenin, rescued the increase in ALP activity, mineralization, and osteogenesis gene expression induced by ZEB1 knockdown. In conclusion, ZEB1 regulates the osteogenic differentiation of hBMSCs partly via Wnt/β-catenin signaling.

Oral bisphosphonates and intravenous receptor activator of nuclear factor kappa-B ligand antibodies are the main clinical therapeutic drugs for osteoporosis (Tella and Gallagher, 2014), which both repress osteoclast activity. However, there are currently limited drugs for promoting osteogenesis. Teriparatide has been used as an anabolic drug in most countries, but it poses a risk of developing osteosarcoma. As our *in vivo* study showed, ZEB1 could be a strong potential candidate for osteoporosis therapy. AAV9-amiR-ZEB1 markedly alleviated trabecular bone loss and promoted bone formation after being injected into OVX mice. Moreover, the changes in bone-formation markers, Goldner's trichrome staining, and double fluorescence labeling of calcein and tetracycline indicated that the anabolic effect of AAV9-amiR-ZEB1 mainly contributes to promoting bone formation. In addition, we reported that the expression levels of ZEB1 were negatively associated with bone mass and osteogenesis markers in bone tissue from PMOP patients. These results revealed that treatment aimed at the downregulation of ZEB1 in BMSCs may provide a new strategy by enhancing the osteogenic differentiation of BMSCs.

In summary, we are the first to provide experimental and clinical evidence that ZEB1 negatively regulates osteogenesis of BMSCs. ZEB1 is involved in regulating osteoblast differentiation and maintenance of bone mass. Silencing ZEB1 expression promoted osteoblast differentiation *in vitro* and slowed bone loss *in vivo*. Clinically, ZEB1 expression was negatively correlated with bone mass and osteogenesis markers in bone tissue in PMOP patients. Our data suggested that ZEB1 could be a pathogenic factor of PMOP and a potential therapeutic target for osteoporosis.

CONCLUSION

In this study, ZEB1 was investigated for its correlation with bone formation genes and BMD in the bone tissue of postmenopausal women. Furthermore, it was found that ZEB1 could regulate osteogenesis through Wnt/β-catenin signaling *in vitro*, and silencing ZEB1 enhanced bone formation *in vivo*. Thus, ZEB1 could be a valuable therapeutic target for osteoporosis and other bone disorders induced by damaged osteogenesis.

DATA AVAILABILITY STATEMENT

The original contributions presented in the study are included in the article/**Supplementary Material**, further inquiries can be directed to the corresponding author/s.

ETHICS STATEMENT

The studies involving human participants were reviewed and approved by Ethics Committee of the Huadong hospital. The patients/participants provided their written informed consent to participate in this study. The animal study was reviewed and approved by Animal Ethics and Experimental Safety of the Fudan University.

AUTHOR CONTRIBUTIONS

CX, QC, and XQ conceptualized and designed the study. QC was responsible for the administrative support. QC, DH, and YF were responsible for the provision of study materials or patients. CX and QC were responsible for the collection and assembly of data. CX was responsible for the data analysis and interpretation. All authors contributed to the manuscript writing and made the final approval of manuscript.

FUNDING

This study was supported by grants from the National Natural Science Foundation of China (NSFC; No. 81471089) and National Key R&D Program of China (2018YFC2000201).

SUPPLEMENTARY MATERIAL

The Supplementary Material for this article can be found online at: https://www.frontiersin.org/articles/10.3389/fmolb.2021.682728/full#supplementary-material

REFERENCES

Bartscherer, K., Pelte, N., Ingelfinger, D., and Boutros, M. (2006). Secretion of wnt ligands requires evi, a conserved transmembrane protein. *Cell* 125, 523–533. doi: 10.1016/j.cell.2006.04.009

Bracken, C. P., Gregory, P. A., Kolesnikoff, N., Bert, A. G., Wang, J., Shannon, M. F., et al. (2008). A double-negative feedback loop between ZEB1-SIP1 and the microRNA-200 family regulates epithelial-mesenchymal transition. *Cancer Res.* 68, 7846–7854. doi: 10.1158/0008-5472.CAN-08-1942

Cadigan, K. M., and Nusse, R. (1997). Wnt signaling: a common theme in animal development. *Genes Dev.* 11, 3286–3330. doi: 10.1101/gad.11.24.3286

Fan, J., An, X., Yang, Y., Xu, H., Fan, L., Deng, L., et al. (2018). MiR-1292 targets FZD4 to regulate senescence and osteogenic differentiation of stem cells in TE/SJ/Mesenchymal tissue system via the wnt/β-catenin pathway. *Aging Dis.* 9, 1103–1121. doi: 10.14336/AD.2018.1110

Feng, T., Zhu, Z., Jin, Y., Wang, H., Mao, X., Liu, D., et al. (2020). The microRNA-708-5p/ZEB1/EMT axis mediates the metastatic potential of osteosarcoma. *Oncol. Rep.* 43, 491–502. doi: 10.3892/or.2019.7452

Fu, R., Lv, W., Xu, Y., Gong, M., Chen, X., Jiang, N., et al. (2020). Endothelial ZEB1 promotes angiogenesis-dependent bone formation and reverses osteoporosis. *Nat. Commun.* 11:460. doi: 10.1038/s41467-019-14076-3

Gozo, M. C., Aspuria, P. J., Cheon, D. J., Walts, A. E., Berel, D., Miura, N., et al. (2013). Foxc2 induces Wnt4 and Bmp4 expression during muscle regeneration and osteogenesis. *Cell Death. Differ.* 20, 1031–1042. doi: 10.1038/cdd.2013.34

He, X., Han, Z., Jiang, W., Huang, F., Ren, C., Wei, Q., et al. (2020). Hypoxia improved vasculogenesis in distraction osteogenesis through mesenchymal-epithelial transition (MET), Wnt/β-catenin signaling pathway, and autophagy. *Acta Histochem.* 122:151593. doi: 10.1016/j.acthis.2020.151593

Hu, F., Wang, C., Guo, S., Sun, W., Mi, D., Gao, Y., et al. (2011). DeltaEF1 promotes osteolytic metastasis of MDA-MB-231 breast cancer cells by regulating MMP-1 expression. *Biochim. Biophys. Acta* 1809, 200–210. doi: 10.1016/j.bbagrm.2011.01.003

Ishtiaq, S., Fogelman, I., and Hampson, G. (2015). Treatment of post-menopausal osteoporosis: beyond bisphosphonates. *J. Endocrinol. Invest.* 38, 13–29. doi: 10.1007/s40618-014-0152-z

Jiang, R., Zhang, C., Liu, G., Gu, R., and Wu, H. (2017). MicroRNA-126 inhibits proliferation, migration, invasion, and EMT in osteosarcoma by targeting ZEB1. *J. Cell. Biochem.* 118, 3765–3774. doi: 10.1002/jcb.26024

Kiernan, J., Hu, S., Grynpas, M. D., Davies, J. E., and Stanford, W. L. (2016). Systemic mesenchymal stromal cell transplantation prevents functional bone loss in a mouse model of age-related osteoporosis. *Stem Cells Transl. Med.* 5, 683–693. doi: 10.5966/sctm.2015-0231

Kikuchi, A. (2000). Regulation of β-Catenin signaling in the wnt pathway. *Biochem. Biophys. Res. Commun.* 268, 243–248. doi: 10.1006/bbrc.1999.1860

Murray, D., Precht, P., Balakir, R., Walter, E., and Horton, J. (2000). The transcription factor î'EF1 is inversely expressed with type II collagen mRNA and can repress col2a1 promoter activity in transfected chondrocytes. *J. Biol. Chem.* 275:3610. doi: 10.1074/jbc.275.5.3610

Postigo, A. A., Kroll, K. L., Depp, J. L., and Taylor, J. J. (2003). Regulation of Smad signaling through a differential recruitment of coactivators and corepressors by ZEB proteins. *EMBO J.* 22, 2453–2462. doi: 10.1093/emboj/cdg226

Qadir, A., Liang, S., Wu, Z., Chen, Z., Hu, L., and Qian, A. (2020). Senile osteoporosis: the involvement of differentiation and senescence of bone marrow stromal cells. *Int. J. Mol. Sci.* 21:349. doi: 10.3390/ijms21010349

Sanchez-Tillo, E., Lazaro, A., Torrent, R., Cuatrecasas, M., Vaquero, E. C., Castells, A., et al. (2010). ZEB1 represses E-cadherin and induces an EMT by recruiting the SWI/SNF chromatin-remodeling protein BRG1. *Oncogene* 29, 3490–3500. doi: 10.1038/onc.2010.102

Shen, G., Ren, H., Shang, Q., Zhao, W., Zhang, Z., Yu, X., et al. (2020). Foxf1 knockdown promotes BMSC osteogenesis in part by activating the Wnt/β-catenin signalling pathway and prevents ovariectomy-induced bone loss. *EBioMedicine* 52:102626. doi: 10.1016/j.ebiom.2020.102626

Takagi, T., Moribe, H., Kondoh, H., and Higashi, Y. (1998). DeltaEF1, a zinc finger and homeodomain transcription factor, is required for skeleton patterning in multiple lineages. *Development* 125, 21–31.

Tan, Y. F., Tang, L., OuYang, W. X., Jiang, T., Zhang, H., and Li, S. J. (2019). Beta-catenin-coordinated lncRNA MALAT1 up-regulation of ZEB-1 could enhance the telomerase activity in HGF-mediated differentiation of bone marrow mesenchymal stem cells into hepatocytes. *Pathol. Res. Pract.* 215, 546–554. doi: 10.1016/j.prp.2019.01.002

Tella, S. H., and Gallagher, J. C. (2014). Prevention and treatment of postmenopausal osteoporosis. *J. Steroid Biochem. Mol. Biol.* 142, 155–170. doi: 10.1016/j.jsbmb.2013.09.008

Terraz, C., Toman, D., Delauche, M., Ronco, P., and Rossert, J. (2001). ΔEF1 binds to a far upstream sequence of the mouse Pro-α1(I) collagen gene and represses its expression in osteoblasts. *J. Biol. Chem.* 276, 37011–37019. doi: 10.1074/jbc.M104185200

Xiao, Y., Lin, Y. X., Cui, Y., Zhang, Q., Pei, F., Zuo, H. Y., et al. (2021). Zeb1 promotes odontoblast differentiation in a stage-dependent manner. *J. Dent. Res.* doi: 10.1177/0022034520982249 [Online ahead of print].

Yang, S., Zhao, L., Yang, J., Chai, D., Zhang, M., Zhang, J., et al. (2007). ΔEF1 represses BMP-2-induced differentiation of C2C12 myoblasts into the osteoblast lineage. *J. Biomed. Sci.* 14, 663–679. doi: 10.1007/s11373-007-9155-5

Yang, X., Li, L., Huang, Q., Xu, W., Cai, X., Zhang, J., et al. (2015). Wnt signaling through Snail1 and Zeb1 regulates bone metastasis in lung cancer. *Am. J. Cancer Res.* 5, 748–755.

Yang, Y., Xie, J., Wang, D., Kim, J., Tai, P. W. L., Gravallese, E., et al. (2019). Bone-targeting AAV-mediated silencing of Schnurri-3 prevents bone loss in osteoporosis. *Nat. Commun.* 10:2958. doi: 10.1038/s41467-019-10809-6

Yi, S., Yu, M., Yang, S., Miron, R. J., and Zhang, Y. (2017). Tcf12, a member of basic Helix-Loop-Helix transcription factors, mediates bone marrow mesenchymal stem cell osteogenic differentiation in vitro and in vivo. *Stem Cells* 35, 386–397. doi: 10.1002/stem.2491

Conflict of Interest: The authors declare that the research was conducted in the absence of any commercial or financial relationships that could be construed as a potential conflict of interest.

frontiers in Cell and Developmental Biology

ORIGINAL RESEARCH
published: 17 August 2021
doi: 10.3389/fcell.2021.726549

TMT-Based Proteomic Explores the Influence of DHEA on the Osteogenic Differentiation of hBMSCs

*Xiaonan Liang[1†], Mingwei He[2†], Bo Zhu[3†], Yongjia Zhu[4], Xixi He[1], Dachang Liu[1] and Qingjun Wei[1]**

[1] Department of Orthopedics Trauma and Hand Surgery, The First Affiliated Hospital of Guangxi Medical University, Nanning, China, [2] Guangxi Collaborative Innovation Center for Biomedicine, Guangxi Medical University, Nanning, China, [3] Guangxi Engineering Center in Biomedical Materials for Tissue and Organ Regeneration, The First Affiliated Hospital of Guangxi Medical University, Nanning, China, [4] Nanning Second People's Hospital, The Third Affiliated Hospital of Guangxi Medical University, Nanning, China

OPEN ACCESS

Edited by:
Ce Dou,
Army Medical University, China

Reviewed by:
Miriam Zacchia,
University of Campania Luigi Vanvitelli, Italy
Paula Rozenfeld,
CONICET Instituto de Estudios Inmunológicos y Fisiopatalógicos (IIFP), Argentina

***Correspondence:**
Qingjun Wei
weiqingjungxnn@163.com

† These authors have contributed equally to this work

Specialty section:
This article was submitted to Cellular Biochemistry, a section of the journal Frontiers in Cell and Developmental Biology

Received: *18 June 2021*
Accepted: *26 July 2021*
Published: *17 August 2021*

Citation:
Liang X, He M, Zhu B, Zhu Y, He X, Liu D and Wei Q (2021) TMT-Based Proteomic Explores the Influence of DHEA on the Osteogenic Differentiation of hBMSCs. Front. Cell Dev. Biol. 9:726549. doi: 10.3389/fcell.2021.726549

Dehydroepiandrosterone (DHEA) has been revealed to implicate in facilitating osteoblast differentiation of human bone marrow mesenchymal stem cells (hBMSCs) and inhibiting osteoporosis (OP). However, the underlying molecular mechanism remains largely unknown. Here, we induced osteogenic differentiation of hBMSCs derived from elders using an osteogenic induction medium with or without DHEA. The results showed that osteogenic induction medium (OIM) with DHEA could significantly promote the proliferation and osteogenic differentiation of hBMSCs than OIM alone. By using a Tandem Mass Tag (TMT) labeling and liquid chromatography-tandem mass spectrometry (LC-MS/MS) technology, we screened out 604 differentially expressed proteins (DEPs) with at least one unique peptide were identified [524: OIM vs. complete medium (CM), and 547: OIM+DHEA vs. CM], among these proteins, 467 DEPs were shared in these two different comparative groups. Bioinformatic analysis revealed these DEPs are mainly enriched in metabolic pathways. Interestingly, the expression levels of the DEPs in the metabolic pathways showed a more noticeable change in the OIM+DHEA vs. CM group than OIM vs. CM group. Moreover, the protein-protein interaction (PPI) network analysis revealed that three potential proteins, ATP5B, MT-CYB, and MT-ATP6, involved in energy metabolism, might play a key role in osteogenic differentiation induced by OIM+DHEA. These findings offer a valuable clue for us to better understand the underlying mechanisms involved in osteoblast differentiation of hBMSCs caused by DHEA and assist in applying DHEA in hBMSCs-based therapy for osteogenic regeneration.

Keywords: hBMSCs, DHEA, osteogenic differentiation, TMT, bioinformatic analysis

INTRODUCTION

Osteoporosis (OP) is a systemic disorder that is characterized by bone fragility, accompanied by a sharp decrease in bone strength (Ginaldi et al., 2005; Franco-Trepat et al., 2019). With increasing age, these bone losses are raised, in turn resulted in a higher risk of fragility fractures (Lynn et al., 2005; Chen et al., 2019). Thus, the morbidity of OP increases with the aging of the

population, severely affecting the quality of life and physical health of the elderly (Chen et al., 2019). According to statistics, osteoporosis-induced disabling injuries have become the third most serious disease affecting the life and health of the elderly following hypertension, cardiovascular, and cerebrovascular diseases (An et al., 2016; Tan and Dai, 2019). However, although the approved anti-osteoporosis drugs currently have some therapeutic effect on the treatment of osteoporosis, the risk of osteonecrosis of the jaw and atypical femoral fractures was increased after long-term intake, thereby leading to their limited utility in clinical (Voss et al., 2018). Hence, it is urgent to develop new therapeutic strategies for OP.

Mesenchymal stem cells derived from human bone marrow (hBMSCs) are multipotent stromal cells that can differentiate into osteoblasts, chondrocytes, adipocytes, and many other cell types (Pittenger et al., 1999). It is currently believed that proliferation and differentiation of hBMSCs, especially the osteogenic differentiation, have close correlations with the onset and recovery of OP, providing new ideas for the treatment and study of the disease (Wang et al., 2007, 2009). Furthermore, in recent years, the regenerative medical potential of human mesenchymal stem cells (hMSCs), specifically bone marrow-derived MSCs, have attracted increasing attention, and these cells were used frequently for augmenting bone tissue repair and regeneration in bone tissue engineering, and were considered as a promising tool for bone regeneration in OP (Ciapetti et al., 2006; Annamalai et al., 2019; Liu et al., 2019). Hence, enhancing the proliferation and osteogenesis differentiation of BMSCs and understanding the underlying mechanisms may significantly improve the therapeutic efficacy of OP.

Dehydroepiandrosterone (DHEA) and its sulfate ester, the prominent adrenal steroids in human circulation, are used as a nutritional supplement in the United States and can be obtained without a prescription. DHEA is touted for its putative anti-aging peculiarities and potential advantage in metabolic and cardiovascular health (Allolio and Arlt, 2002; Formoso et al., 2006). Recent studies reported that DHEA could accelerate the growth of osteoblast and morphometry of bone tissue, and oppose osteoporosis by inhibiting certain activities of endogenous glucocorticoids (GC) in rodents (Malik et al., 2010). DHEA has been reported to promote the proliferation of osteoblast and inhibit apoptosis of osteoblast and maturation of osteoclast. In addition, DHEA significantly boosts the production of osteoblast by modulating the expression of genes associated with osteoblast in MSC (Qiu et al., 2015). Our previous study evaluated the effect of DHEA on hBMSCs and showed that the higher ALP activity was recorded at 10 nM of DHEA in the medium (Liang et al., 2016). As the literature grew, DHEA will become widely used as a promising agent to treat osteoporosis by affecting the osteogenic differentiation of hBMSCs. However, systemic approaches for specifying the influence of DHEA on osteogenic differentiation of hBMSCs have not yet to be investigated, and the molecular mechanism of osteogenic differentiation remains unclear. Proteins, as the actual functional molecules involved in various biological effects in the human body, should be translated from messenger RNA and then undergo a variety of modifications before they can be used as the available proteins. Therefore, the expression of biological molecules at the genomic level alone cannot wholly reflect the truth.

Recently, proteomics methodology has been employed for the investigations of a series of mesenchymal stem cells (MSCs), including the differential expression profile analysis of membrane proteins in MSCs during differentiation of osteoblast (Foster et al., 2005), the analysis of the secretome of MSCs differentiated from embryonic stem cells (Sze et al., 2007), the proteomic analysis of rat MSCs subcultures (Celebi and Elçin, 2009), and proteomic profiling of transforming growth factor-β acting on MSCs (Wang et al., 2004; Kurpinski et al., 2009). Nevertheless, data on the proteome profile of bone tissue-derived MSCs was still limited, and further studies are needed to provide information for better application of these populations of MSCs. Therefore, to gain further understanding of the underlying molecular mechanism of the osteogenic differentiation of hBMSCs, we applied a Tandem Mass Tag (TMT) peptide labeling combined with liquid chromatography-tandem mass spectrometry (LC-MS/MS) approach to quantitatively evaluate the protein expression profile of the osteogenesis model *in vitro*. The TMT labeling coupled with LC-MS/MS is a gel-free quantitative proteomics technology that enables isobaric labeling of proteins and was used for the quantification and identification of biological macromolecules, such as peptides and proteins, which is one of the most sensitive techniques currently used for quantitative analysis of proteomes (Zhang and Elias, 2017).

Herein, we explored the promote effects of DHEA on the osteogenic differentiation of hBMSCs, and analyzed differentially expressed proteins (DEPs) of hBMSCs cultured in three different mediums under the two-dimensional system using TMT peptide labeling combined with LC-MS/MS technology. We particularly focused on the differential expression of proteins during osteoblast differentiation of hBMSCs induced by osteogenic induction medium (OIM) and OIM with DHEA and conducted bioinformatics analysis. The DEPs identified in this study may serve essential roles in the progression of osteogenic differentiation. Our findings provide an important insight into the crucial proteins and the underlying intracellular mechanisms of osteogenic differentiation, further promoting their application of DHEA in OP therapy.

MATERIALS AND METHODS

Extracting and Culturing of hBMSCs

All studies involving human stem cells were approved by the Ethics Committee of The First Affiliated Hospital of Guangxi Medical University. HBMSCs were isolated from the iliac crest of donors who received a total hip replacement for osteoporosis in the Department of Orthopedics Trauma and Hand Surgery, The First Affiliated Hospital of Guangxi Medical University. Patients gave informed written consent before they participated in this study. The criteria for exclusion have been explained in our previous reports (Liang et al., 2016; Zhou and Glowacki, 2017). Briefly, the mononuclear cells were extracted from bone marrow that had been treated with heparin by using Ficoll-Hypaque

density gradient centrifugation with a density of 1.077 g/L. Subsequently, the cells were seeded in a six-well plate and cultured with α-minimal essential medium (α-MEM, Gibco-BRL, United States) containing 10% fetal bovine serum (FBS, Gibco-BRL, United States) and 100 units/mL penicillin and 100 μg/mL streptomycin (Solarbio, China), which is called as complete medium (CM), and then incubated in an incubator (Thermo Fisher Scientific, United States) at 37°C with 5% CO_2 humidified atmosphere. After 7 days of culture, the hBMSCs were harvested and re-cultured in 10 cm of plastic dishes at the density of 4×10^3 cells/cm^2, and the cultured medium was replaced with a fresh medium every 3 days. The trypsin-EDTA solution containing 0.02% EDTA and 0.25% trypsin (Solarbio, China) was applied to detach the cells, and a subculture was conducted at 1:3 split when the cells reached 100% confluence. The cells from passage three were used for further experimentation.

Cytotoxicity Assay

To determine the toxic effect of DHEA on hBMSCs, the cytotoxicity was detected by an MTT (Gibco-BRL, United States) assay following the manufacturer's instruction. In brief, the hBMSCs with a density of 1,000 cells/well were cultured in a 96-well plate. After 3 days of treatment with DHEA with a variety of concentrations (0–100 μM of DHEA where 0 μM was employed as a control), and the plates were incubated at 37°C in the dark for 4 h after the addition of 20 μL of MTT reagents (5 mg/ml) into each well. After removing MTT reagents, 200 μL of dimethyl sulfoxide (DMSO, Sigma-Aldrich, United States) was added to the cells for crystal solubilization. After that, the spectrometric absorbance at the wavelength of 570 nm was obtained by Multiskan^{TM} GO microplate spectrophotometer (Thermo Fisher Scientific Inc., United States). Every experiment was performed in triplicate. An optimal concentration of 10 nM was chosen for further investigation according to the results of MTT analysis.

Treatment and Grouping of hBMSCs

The hBMSCs were divided into three groups as follows: CM group: hBMSCs were cultured with complete medium; osteogenic induction medium (OIM) group: hBMSCs were induced with OIM (Shen et al., 2019), which composed of α-MEM, 10% FBS, β-glycerophosphate (10 mM) (Sigma-Aldrich, United States), dexamethasone (10 mM), and ascorbic acid-2 phosphate (50 μg/mL); OIM+DHEA group: hBMSCs were cultured in OIM containing 10 nM of DHEA.

Alkaline Phosphatase Activity Test

The cultured cells were lysed with RIPA lysis buffer (Beyotime, China) after wash twice with Phosphate Buffer Saline (PBS). Subsequently, the Alkaline Phosphatase Assay Kit (Beyotime, China) was used to assess the cellular alkaline phosphatase (ALP) activity quantitatively in the light of the manufacturer's protocol. After that, the cellular ALP activity was measured under the wavelength of 405 nm by using a microplate reader (Thermo Fisher Scientific, United States).

Alizarin Red Staining for Calcium Deposit

After 7 and 14 days of culture, the process of fixation with 4% paraformaldehyde was carried out after the cultured cells were washed twice with PBS. Subsequently, the cells underwent evaluation of calcium levels using alizarin red staining according to the standard protocols. Light microscopic images were observed and captured using an Olympus BX53 microscope (Olympus, Japan).

Real-Time Quantitative Polymerase Chain Reaction Analysis

Total RNA was purified using an RNA isolation kit (Tiangen Biotech, China) according to the manufacturer's specifications. The cDNA was synthesized from the RNA by using a reverse transcription kit (Takara, Japan). The real-time quantitative polymerase chain reaction (qRT-PCR) was performed with Fast Start Universal SYBR Green Master Mix (Roche, Germany) in the procedure with 40 cycles of 95°C for 15 s, 60°C for 30 s, following by 72°C for 30 s by using ABI Step One Real-Time PCR System machine. Every reaction was repeated three times. The relative expression levels of target genes were measured by employing $2^{-\Delta\Delta CT}$ method. The sequences of gene primer employed for the amplification of the target gene were presented in **Table 1**.

Proteomic Analysis by TMT

Human bone marrow mesenchymal stem cells were cultured in a 55 cm^2 plastic culture dish at a density of 10,000 cells/cm^2 with a culture medium as formerly indicated. The cells were lysed with 2 mL of cell lysis buffer after detachment with trypsin when 14 days of growth. Subsequently, the protein concentrations were determined using a Bradford Quant Kit (Amresco) according to the manufacturer's protocol. And then, 100 g of each protein sample was treated with 3.3 L of trypsin (1 g/L) at 37°C for 24 h, and following by labeled with the TMT. After desalting of the TMT-labeled peptides by C18 reversed-phase column, the lyophilized products were further separated by using the Dionex capillary/nano-HPLC system, and then transported to the Q-Exactive Plus spectrometer for further analysis. The mass spectrum was obtained by the software Proteome Discoverer 2.1 in a data-dependent manner. The analytical cycle consisted of a single full-scan mass spectrum (350–2000 Da), followed by 15 data-dependent MS/MS scans. Under this scan, to generate reporter ions and fragment ions, TMT-labeled peptides were

TABLE 1 | Primer used in the qRT-PCR.

Gene name	Forward primer	Reverse primer
ALPL	GCAAGAAAGGGGACCCAAGA	CAGAATGTTCCACGGAGGCT
COL1A1	GCTTCACCTACAGCGTCACT	AAGCCGAATTCCTGGTCTGG
RUNX2	TGTCATGGCGGGTAACGATG	CCCTAAATCACTGAGGCGGT
BMP2	TCCATGTGGACGCTCTTTCA	AGCAGCAACGCTAGAAGACA
GAPDH	CTATAAATTGAGCCCGCAGC	GACCAAATCCGTTGACTCCG

ALPL, Alkaline phosphatase; COL1A1, Collagen type I alpha 1 chain; RUNX2, RUNX family transcription factor 2; BMP2, Bone morphogenetic protein 2; GAPDH, Glyceraldehyde-3-phosphate dehydrogenase.

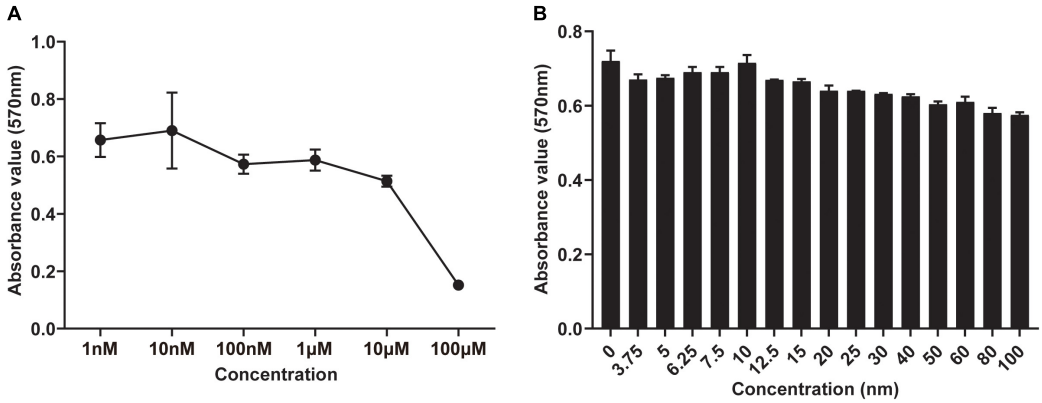

FIGURE 1 | Screening of the optimal concentration of DHEA in the viability of hBMSCs by MTT assay. **(A)** The viability of hBMSCs was measured after 3 days of co-culture with DHEA at various concentrations (0–100 μM). **(B)** The viability of hBMSCs was measured after 3 days of co-culture with DHEA at multiple concentrations (0–100 nM).

fragmented. The ratio of reporter ions reflected the relative abundance of the peptides or proteins in the sample. Fragment ions were applied to identify the labeled peptide sequences and their corresponding proteins. The data acquired in the TMT experiments were analyzed with Mascot 2.5 using the UniProt-Homo Sapiens database[1].

Bioinformatics Analysis

Compared with the Control group, the proteins with a threshold of fold change (FC) more or less than 1.2 and *p*-value less than 0.05 were defined as differentially expressed proteins (DEPs). The functional classifications, pathway enrichment, and Gene Ontology (GO) term analysis on the DEPs were conducted after the identification of proteins using the bioinformatics method. By using the Gene Ontology analysis database[2], GO enrichment analyses classified proteins based on biological process, cell component, and molecular function. The pathway analysis of the DEPs was carried out applying the Kyoto Encyclopedia of Genes and Genomes (KEGG) online database[3]. KEGG pathways and GO terms with corrected $p < 0.05$ were considered significant enrichment.

Western Blot Analysis

The western blot analysis was performed as previously described (Ma et al., 2020). Briefly, hBMSCs were seeded at a density of 10,000 cells/cm^2 in six-well plates and allowed to grow for 14 days in different mediums as the former indicated. After that, cells in the diverse group were harvested to detect the expression of ATP5B, MT-CYB, and MT-ATP6. For extraction of proteins, RIPA buffer (Beyotime, Shanghai, China) was used to lyse the cells. The concentrations of proteins were determined using A BCA protein assay kit (Beyotime, China). Furthermore, 60 micrograms of each protein lysate were resolved using 10% SDS polyacrylamide gel and transferred to polyvinylidene difluoride membranes (Millipore, Bedford, MA, United States). The membranes were then incubated at 4°C overnight with an appropriate concentration of primary antibodies as follows: ATP5B (1:500, Proteintech, Catalog No. 17247-1-AP), MT-CYB (1:500, Proteintech, Catalog No. 55090-1-AP), MT-ATP6 (1:500, Proteintech, Catalog No. 55313-1-AP), and β-actin (1:1000, Proteintech, Catalog No. 66009-1-Ig). After washing the membrane three times for 10 min with 1× TBST, the membranes were incubated with a secondary antibody on a rocking platform for 30 min at room temperature. Finally, the membranes were exposed to Odyssey infrared imaging system (LI-COR Biosciences, Lincoln, NE, United States) for the appropriate period to acquire the images. Quantitative analysis of the band intensity was analyzed by Image J.

Statistical Analysis

The statistical analysis of data was carried out using GraphPad Software (GraphPad Prism 5.0). All values are presented as the mean ± standard deviation (SD). The data were evaluated using one-way ANOVA and the Tukey's *t*-test using SPSS 16.0 (IBM, United States). *P*-value < 0.05 was considered statistically significant.

RESULTS

The Optimal Concentration of DHEA Without Cytotoxicity and Contributes to the Proliferation of hBMSCs

To evaluate the cytotoxicity of DHEA toward hBMSCs and its effect on the proliferation of BMSCs, we conducted an MTT assay. In the traditional complete medium, no apparent cytotoxicity was observed in the hBMSCs treated with DHEA at a range of 1–10 nM for 3 days, but a gradually reduce cell viability was observed at higher concentrations (100 nM–100 μM) (**Figure 1A**). It is worth noting that cell viability was significantly

[1]http://www.uniprot.org

[2]http:// www.geneontology.org/

[3]http://www.genome.jp/kegg/pathway.html

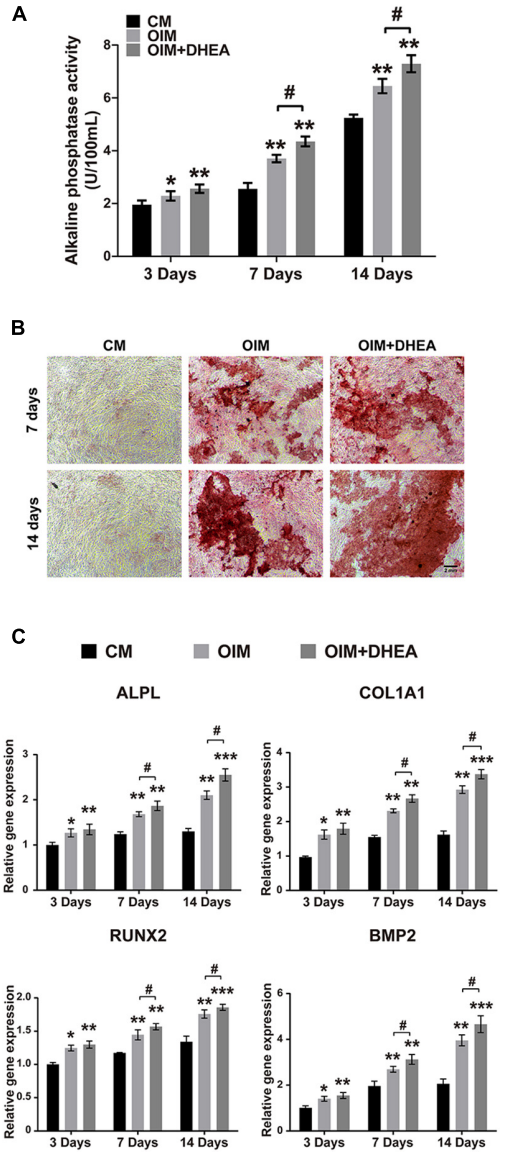

FIGURE 2 | DHEA promotes the osteogenic differentiation of BMSCs *in vitro*. **(A)** ALP activity was analyzed after 3, 7, and 14 days of hBMSCs culturing with CM, OIM, and OIM supplemented with 10 nM of DHEA. Error bars: mean ± SD. $N = 3$, *, # indicates $p < 0.05$, **indicates $p < 0.01$. **(B)** Alizarin red staining of osteogenic hBMSCs treated with or without 10 nM of DHEA for 7 and 14 days (Scale bar = 2 mm). **(C)** The mRNA expression of Alpl, Col1a1, Runx2, and Bmp2 was detected in the CM, OIM, and OIM+DHEA groups at the indicated time by qRT-PCR analysis. Error bars: mean ± SD. $N = 3$, *, # indicates $p < 0.05$, **indicates $p < 0.01$, ***indicates $p < 0.001$.

increased in the hBMSCs treated with DHEA at a range of 6.25–10 nM, a concentration of 10 mM arrived a peak increase in viability, where thereafter, there was a gradual decline in vitality at higher concentrations (**Figure 1B**). These results indicated that 10 nM is the lowest and most proper functional concentration of DHEA on hBMSCs. Therefore, the concentration of 10 nM for DHEA was selected for subsequent investigations.

DHEA Promotes Osteoblastic Differentiation of hBMSCs *in vitro*

To explore the functions of DHEA on osteoblastic differentiation, we performed a quantitative alkaline phosphatase (ALP) assay and Alizarin red staining when hBMSCs were cultured in the osteogenic induction medium (OIM) with or without DHEA for 3, 7, and 14 days, respectively. As shown in **Figure 2A**, our results showed no significant difference in ALP activity observed in the OIM group and OIM+DHEA group at 3 days. However, the ALP activity in the OIM+DHEA group was significantly higher than that in the OIM group at 7 days and 14 days. Meanwhile, alizarin red staining yielded comparable results, where the formation of calcification deposits was markedly increased in the OIM+DHEA group compared with the CM and OIM group at 7 days and 14 days (**Figure 2B**). In addition, the expression levels of osteoblast-specific genes, Bone morphogenetic protein-2 (Bmp2), Runt-related transcription factor 2 (Runx2), Collagen type I alpha 1 (Col1a1), and Alkaline phosphatase (Alp) were detected in hBMSCs treated with 10 μM of DHEA for 3, 7, and 14 days by RT-PCR analysis. As shown in **Figure 2C**, compared to the hBMSCs cultured in CM, the mRNAs expression level of Col1a1, Runx2, Bmp2, and Alp was markedly increased in the OIM group and OIM+DHEA group. What's more, the expression of osteogenic-specific genes was dramatically elevated after 7 and 14 days of DHEA treatment compared with the hBMSCs cultured in OIM without DHEA. The above results suggested that the addition of DHEA is more effective than conventional inducer in inducing osteogenic differentiation of hBMSCs.

Identify the DEPs in OIM and OIM+DHEA Groups Through TMT Proteomic Analysis

To explore the patterns of proteome during the osteogenic differentiation of hBMSCs induced by DHEA, comparative proteome analysis was performed in hBMSCs cultured with CM, OIM, and OIM+DHEA by using TMT. Under the condition of FC > 1.2 or FC < −1.2 and *P* value < 0.05, a total of 45614 spectra were obtained in the comparison between OIM and CM (OIM vs. CM), and 50590 spectra were obtained in the comparison between OIM+DHEA and CM (OIM+DHEA vs. CM). By searching UniProt-Homo Sapiens database, we identified 604 proteins containing at least one unique peptide from these spectra (**Table 2**). Among these proteins, the number of differentially expressed proteins (DEPs) between OIM and CM groups was 524, containing 222 down- and 302 up-regulated proteins. However, there were 547 DEPs, including 230 down- and 317 up-regulated proteins in OIM+DHEA vs. CM. And 467 DEPs were shared in these two different comparative groups, including 269 up- and 198 down-regulated proteins (**Figure 3**).

Gene Ontology Enrichment Analysis

Base on the Gene Ontology (GO) database, we investigated the enrichment of DEPs during osteogenic differentiation induced by two different induction mediums. In the OIM vs. CM, DEPs are mainly enriched in 25 GO terms, 15 GO terms, and 18 GO terms of the biological process (BP), molecular

TABLE 2 | Quantitative results of protein.

Comparisons	Spectra	Peptides	Proteins		
			Up-	Down-	All
OIM vs. CM	45,614	3,348	302	222	524
OIM+DHEA vs. CM	50,590	3,633	317	230	547

FC > 1.2 or FC < −1.2 and P value < 0.05.

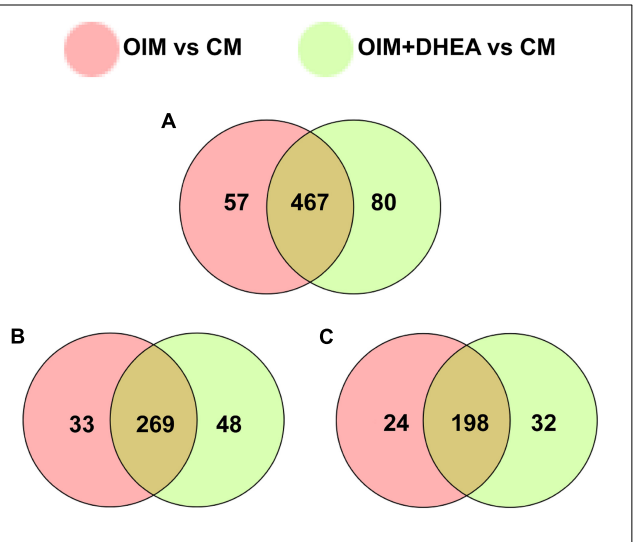

FIGURE 3 | Analysis of differentially expressed proteins (DEPs) between two different comparative groups. **(A)** Venn diagram of DEPs comparing between OIM vs. CM and OIM+DHEA vs. CM. **(B)** Venn diagram of up-regulated proteins comparing between OIM vs. CM and OIM+DHEA vs. CM. **(C)** Venn diagram of down-regulated proteins comparing between OIM vs. CM and OIM+DHEA vs. CM.

function (MF), and cellular component (CC), respectively. In the BP category, cellular process, single-organism process, and biological regulation were the top three terms. The first three terms of the MF category were catalytic activity, binding, and molecular function regulator. Cell, cell part, and organelle dominated the CC category (**Figure 4A**). These results indicated that OIM promotes the differentiation of hBMSCs into the osteoblasts might through promoting the activities of cell and organelle, and regulating the cellular process and binding-related molecular functions.

Interestingly, in the OIM+DHEA vs. CM, DEPs were enriched in similar GO terms in the BP, MF, and CC categories, separately. The most enriched three terms in the BP category were cellular process, regulation of biological process, and single-organism process. Transporter activity, catalytic activity, and binding were highly clustered terms in the MF category. The most significant three terms in the CC category were also the same as OIM+DHEA vs. CM, which was cell, cell part, and organelle (**Figure 4B**). These results suggested that DEPs in OIM vs. CM and OIM+DHEA vs. CM had a similar biological function in BP, MF, and CC categories.

Kyoto Encyclopedia of Genes and Genomes Pathway Enrichment Analysis for the DEPs

To map the DEPs to the reference pathways and uncover their unique biological significance, the pathway enrichment analysis was carried out by employing the Kyoto Encyclopedia of Genes and Genomes (KEGG) database. As shown in **Figure 5**, among the top 30 enriched pathways (ranked by count), 24 pathways were identical, including Metabolic pathways, PPAR signaling pathway, Alzheimer's disease, Oxidative phosphorylation, Huntington's disease, and Focal adhesion in OIM vs. CM group and OIM+DHEA vs. CM group. Notably, among the 24 shared pathways, more proteins were enriched in the Metabolic pathways. A total of 30 proteins in the OIM vs. CM group and 37 proteins in the OIM+DHEA vs. CM group were involved in the metabolic pathways (**Table 3**). Of note, the top 20 DEPs in both OIM vs. CM group and OIM+DHEA vs. CM group all were enriched in the metabolic pathways, indicating that the metabolic pathways were more specific for osteogenic differentiation than other pathways. These results suggested that DHEA and OIM had similar molecular mechanisms, especially metabolic pathways, during osteogenic differentiation.

Analysis of Differentially Expressed Proteins in Metabolic Pathways

To further investigate the critical proteins that participated in metabolic pathways, the intersection of these proteins enriched in the metabolic pathways in each group was analyzed, and 29 shared proteins were harvested. As shown in **Table 4**, the changing trend of metabolic pathways protein was consistent between the two groups, and the change of most differentially expressed proteins in OIM + DHEA vs. CM group was more significant. Moreover, it's worth noting that alkaline phosphatase (ALPL, a specific protein of biomineralization) was implicated in the metabolic pathways and was located on both the OIM+DHEA vs. CM and OIM vs. CM. Notably, compared with group OIM vs. CM, the expression of the ALPL was higher in group OIM+DHEA vs. CM, which is consistent with the result of qRT-PCR analysis (**Figure 2C**). Collectively, we concluded that DHEA could activate the metabolic pathways more effectively than OIM, thereby accelerating osteogenic differentiation.

Analysis of Protein-Protein Interaction Network for These Proteins Involved in Metabolic Pathways

To further research the differences and similarities of the interaction of proteins involved in metabolic pathways in OIM vs. CM and OIM+DHEA vs. CM groups, the protein-protein interaction (PPI) network was constructed. As shown in **Figure 6**, we found that three proteins, ATP5B, MT-CYB, and MT-ATP6, are highly connected protein nodes, interacting with many more partners than average. Therefore, three proteins, ATP synthase subunit beta (ATP5B), Cytochrome b (MT-CYB), and ATP synthase subunit an (MT-ATP6), were considered to be key proteins in the whole network. Besides, combined protein

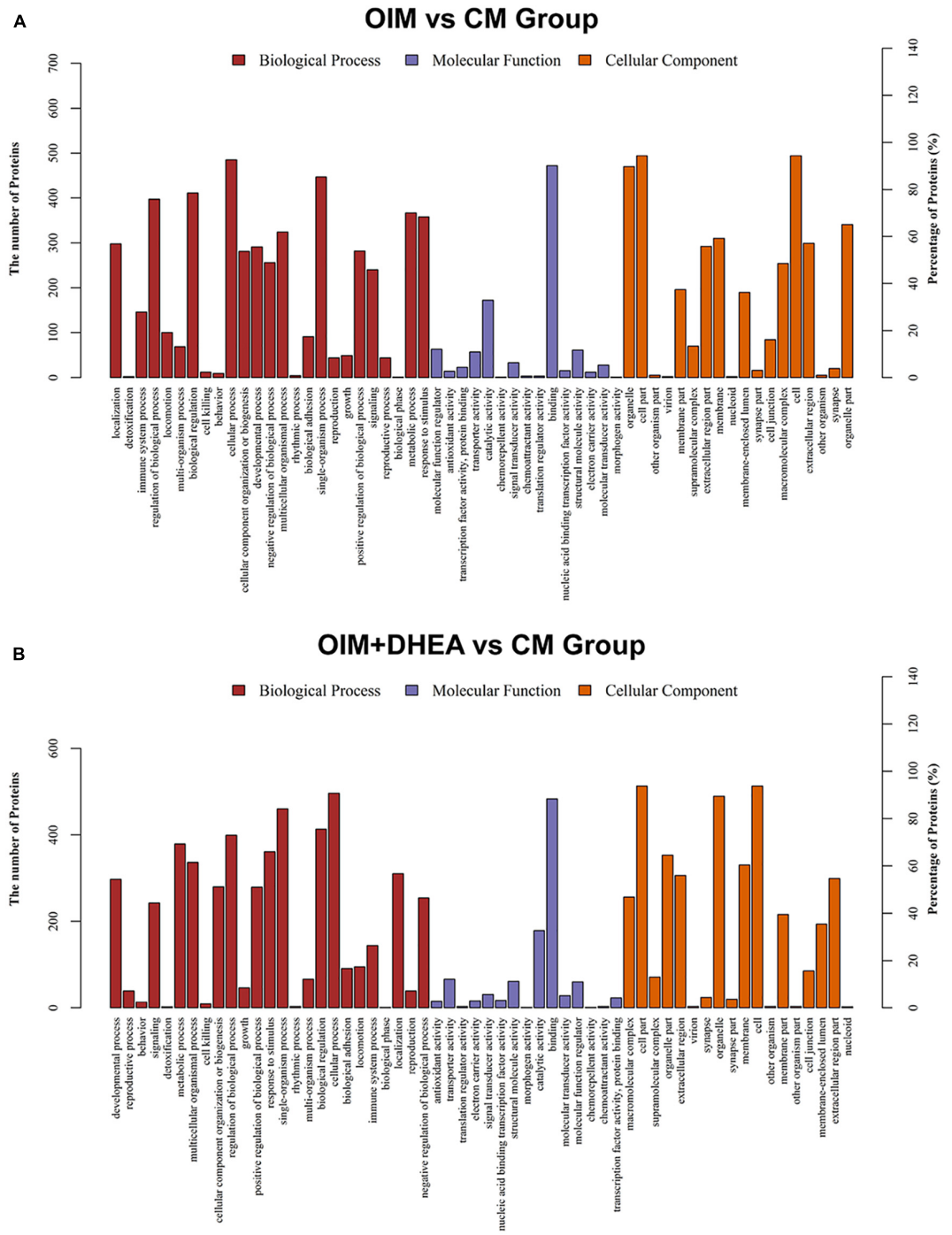

FIGURE 4 | Gene ontology (GO) classification of differentially expressed proteins (DEGs). GO analysis of DEGs in OIM+DHEA vs. CM group **(A)** and OIM+DHEA vs. CM group **(B)**. Cut-off value: p-value < 0.05, and count > 2.

expression profile, expression of ATP5B, MT-CYB, and MT-ATP6 was increased in group OIM+DHEA vs. CM compared with OIM vs. CM. In addition, to confirm the expression of ATP5B, MT-CYB, and MT-ATP6, we performed a western blot analysis. Indeed, the expression of ATP5B, MT-CYB, and MT-ATP6 proteins was markedly increased in the OIM group and OIM+DHEA group compared with that in the CM group. In particular, their expression in the OIM+DHEA group was significantly higher than that in the OIM group (**Figure 7**). These results indicated that three proteins, ATP5B, MT-CYB, and MT-ATP6, may play a key role in osteogenic differentiation induced by OIM+DHEA.

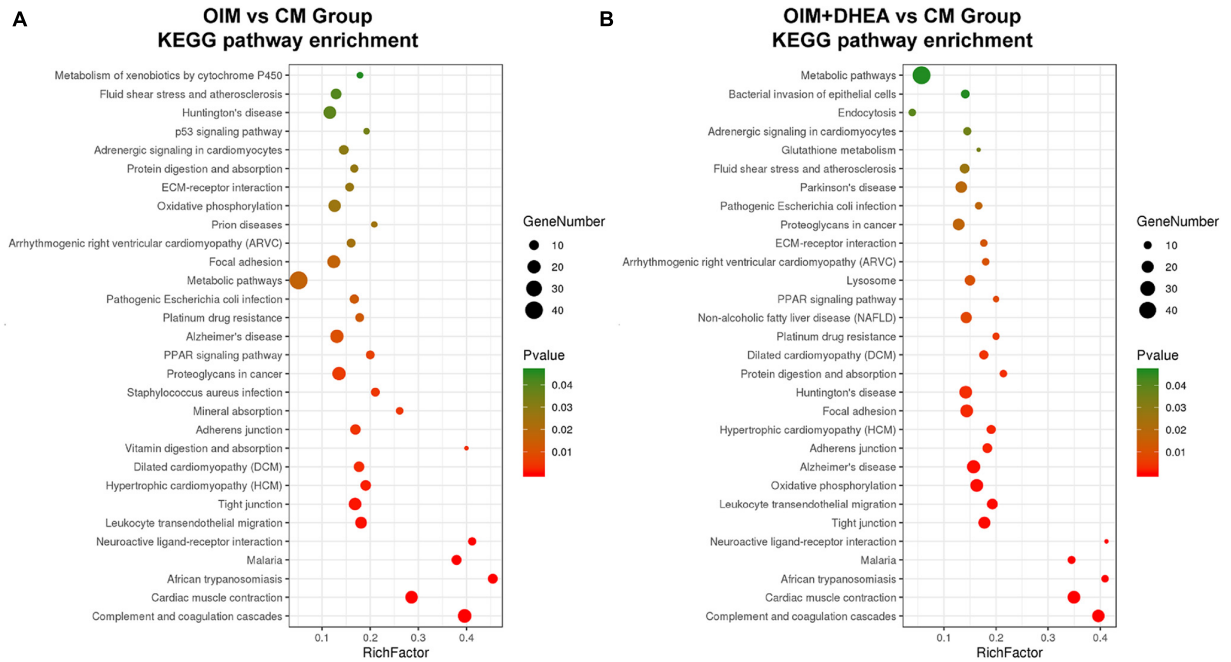

FIGURE 5 | The enriched KEGG pathways of differentially expressed proteins (DEGs). The top 30 enriched KEGG pathways of the DEPs in OIM vs. CM **(A)** and OIM+DHEA vs. CM **(B)**. Cut-off value: p-value < 0.05.

TABLE 3 | Proteins enriched in metabolic pathways.

Group	Enriched genes
OIM vs. CM	CHIA, RFK, ATP6, COX1, COX2, ATP8, CYTB, UGP2, PFAS, AMY1A, ATP6V0C, UQCR11, ATP5L, LDHA, ALDOA, ARG1, ALPL, COX4I1, MAOA, ATP6V0C, ATP5D, NNMT, PRPS1, EXT1, Q59E93, Q6ZMU0, HGD, CYP2S1, HEL-S-271, HEL-S-41, HSD11B1
OIM+DHEA vs. CM	CHIA, RFK, GUK1, ATP6, COX1, COX2, ATP8, CYTB, UGP2, PFAS, AMY1A, ATP6V0C, PLPP1, UQCR11, ATP5L, LDHA, ALDOA, ARG1, ALPL, COX6C, COX4I1, MAOA, ATP6V0C, ATP5D, NNMT, UQCRFS1, XDH, PRPS1, ATP6AP1, EXT1, Q59E93, P4HA3, HGD, CYP2S1, HEL-S-271 (ATP5B), HEL-S-41, HSD11B1

DISCUSSION

As a metabolic bone disease, the main feature of OP is loss of bone mineral density and high risk of fractures, in which osteogenesis of osteoblasts and bone resorption of osteoclasts is vital for the occurrence and development of OP (Wu et al., 2018). Therefore, it is critical to explore osteoblast differentiation of hBMSCs to provide novel and highly effective treatment options for OP. We found that DHEA could significantly improve osteoblast differentiation of hBMSCs *in vitro*. Although the research on osteogenic differentiation of hBMSCs induced by DHEA has provided significant insights into the occurrence, development, and therapy of OP, there are still outstanding insufficient in the mechanism research of osteogenesis. Thus, the identification and characterization of proteins that are expressed differently during the osteogenic differentiation of hBMSCs induced by DHEA might contribute to an in-depth understanding of the complexity of the osteogenic commitment and their therapeutic effect for OP.

In this study, we confirmed that DHEA addition could more significantly promote the proliferation and osteogenic differentiation of hBMSCs from elders than OIM alone, which agrees with the former research that DHEA stimulation promotes osteoblast differentiation (Malik et al., 2010; Qiu et al., 2015; Liang et al., 2016). DHEA has been reported to potentiate cell proliferation, differentiation, and osteocalcin production (Scheven and Milne, 1998). In addition, we also used a powerful proteomics tool, TMT, to investigate the underlying molecular mechanism of osteogenesis induced by DHEA. The TMT-labeled quantitative proteomics is an efficient and systematic method that improves the reliability of the data analysis to accurately quantifying relative protein levels. As untargeted research, TMT-labeled quantitative proteomics is increasingly being used to study the pathogenesis of a disease or cellular biological processes because of its ability to conduct systematic and unbiased analysis of various proteins in samples, as well as its advantages of high sensitivity and good reproducibility (Thompson et al., 2003; Moulder et al., 2018). Untargeted studies can provide a broader perspective on the molecular phenotypes of pathophysiological processes and have the prospect of studying a more comprehensive range of signal pathways (Ismail et al., 2019). Especially proteomics, untargeted studies of the proteome can provide some clues into the understanding of biological processes. For instance, Zhou et al. (2019) found multiple protein factors involved in the pathogenesis of osteoporosis

TABLE 4 | Common DEPs associated with metabolic pathways in OIM vs. CM and OIM+DHEA vs. CM groups.

Accession	Gene name	Description	Coverage% (unique peptide)	OIM vs CM	OIM+DHEA vs CM
Up-regulated					
P05186	ALPL	Alkaline phosphatase, tissue-nonspecific isozyme OS=Homo sapiens GN=ALPL PE=1 SV=4	59.16	2.69	3.00
B7ZMD7	AMY1A	Alpha-amylase OS=Homo sapiens GN=AMY1A PE=2 SV=1	5.87	6.24	5.23
P05089	ARG1	Arginase-1 OS=Homo sapiens GN=ARG1 PE=1 SV=2	5.59	5.17	5.20
P30049	ATP5D	ATP synthase subunit delta, mitochondrial OS=Homo sapiens GN=ATP5D PE=1 SV=2	13.69	2.50	2.67
O75964	ATP5L	ATP synthase subunit g, mitochondrial OS=Homo sapiens GN=ATP5L PE=1 SV=3	47.57	2.52	2.69
A0A059QB80	ATP6 (MT-ATP6)	ATP synthase subunit a OS=Homo sapiens GN=ATP6 PE=4 SV=1	4.42	2.63	3.00
P27449	ATP6V0C	V-type proton ATPase 16 kDa proteolipid subunit OS=Homo sapiens GN=ATP6V0C PE=1 SV=1	11.61	2.32	2.36
A0A059QPX7	ATP8	ATP synthase protein 8 OS=Homo sapiens GN=ATP8 PE=3 SV=1	29.41	3.01	2.94
A0A024R0D9	CHIA	Chitinase, acidic, isoform CRA_a OS=Homo sapiens GN=CHIA PE=3 SV=1	3.99	4.24	3.36
A0A059QJB6	COX1	Cytochrome c oxidase subunit 1 OS=Homo sapiens GN=COX1 PE=3 SV=1	6.04	2.85	2.96
A0A059RTG7	COX2	Cytochrome c oxidase subunit 2 (Fragment) OS=Homo sapiens GN=COX2 PE=3 SV=1	31.53	2.91	2.45
P13073	COX4I1	Cytochrome c oxidase subunit 4 isoform 1, mitochondrial OS=Homo sapiens GN=COX4I1 PE=1 SV=1	51.48	2.34	2.58
Q96SQ9	CYP2S1	Cytochrome P450 2S1 OS=Homo sapiens GN=CYP2S1 PE=1 SV=2	1.79	2.44	2.82
A0A059RS35	CYTB (MT-CYB)	Cytochrome b OS=Homo sapiens GN=CYTB PE=3 SV=1	4.21	2.60	2.66
Q16394	EXT1	Exostosin-1 OS=Homo sapiens GN=EXT1 PE=1 SV=2	4.69	3.77	2.50
V9HW31	HEL-S-271 (MT-ATP5B)	ATP synthase subunit beta OS=Homo sapiens GN=HEL-S-271 PE=1 SV=1	74.10	3.46	3.79
V9HWF8	HEL-S-41	Epididymis secretory protein Li 41 OS=Homo sapiens GN=HEL-S-41 PE=2 SV=1	14.72	11.32	11.75
Q93099	HGD	Homogentisate 1,2-dioxygenase OS=Homo sapiens GN=HGD PE=1 SV=2	9.44	4.28	4.02
X5D2L1	HSD11B1	Hydroxysteroid 11-beta dehydrogenase 1 isoform A (Fragment) OS=Homo sapiens GN=HSD11B1 PE=2 SV=1	19.18	2.29	2.61
P21397	MAOA	Amine oxidase [flavin-containing] A OS=Homo sapiens GN=MAOA PE=1 SV=1	48.39	3.41	3.17
P40261	NNMT	Nicotinamide N-methyltransferase OS=Homo sapiens GN=NNMT PE=1 SV=1	45.83	2.37	2.68
A8K8N7	PFAS	Phosphoribosylformylglycinamidine synthase (FGAR amidotransferase), isoform CRA_b OS=Homo sapiens GN=PFAS PE=2 SV=1	4.71	2.59	2.44
Q59E93	Q59E93	Aminopeptidase (Fragment) OS=Homo sapiens PE=2 SV=1	49.85	2.57	2.67
A0A024R275	RFK	Riboflavin kinase, isoform CRA_a OS=Homo sapiens GN=RFK PE=4 SV=1	6.79	2.27	2.39
A0A087WYS1	UGP2	UTP–glucose-1-phosphate uridylyltransferase OS=Homo sapiens GN=UGP2 PE=1 SV=1	50.79	2.60	2.80
O14957	UQCR11	Cytochrome b-c1 complex subunit 10 OS=Homo sapiens GN=UQCR11 PE=3 SV=1	21.43	3.19	3.92
Down-regulated					
P04075	ALDOA	Fructose-bisphosphate aldolase A OS=Homo sapiens GN=ALDOA PE=1 SV=2	71.98	0.38	0.38
P00338	LDHA	L-lactate dehydrogenase A chain OS=Homo sapiens GN=LDHA PE=1 SV=2	57.83	0.52	0.50
P60891	PRPS1	Ribose-phosphate pyrophosphokinase 1 OS=Homo sapiens GN=PRPS1 PE=1 SV=2	43.08	0.52	0.51

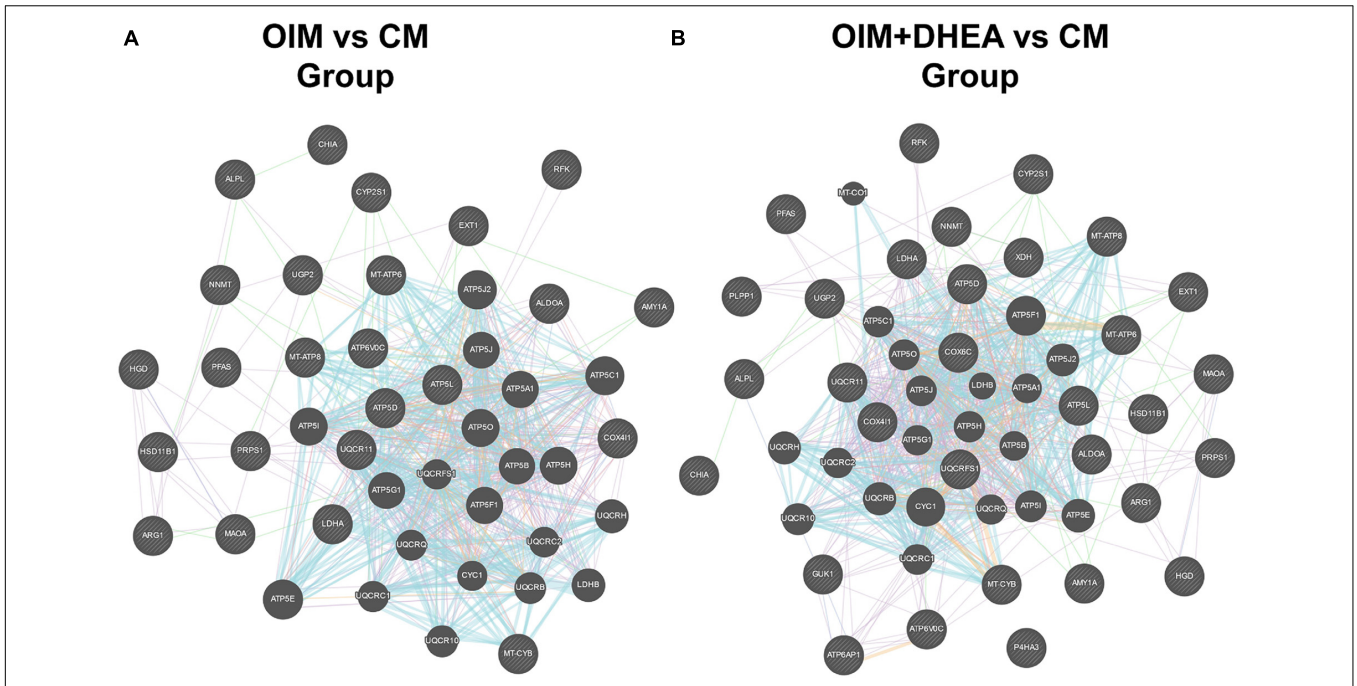

FIGURE 6 | Protein-protein interaction network for the proteins in the metabolic pathways of OIM vs. CM group **(A)** and OIM+DHEA vs. CM group **(B)**.

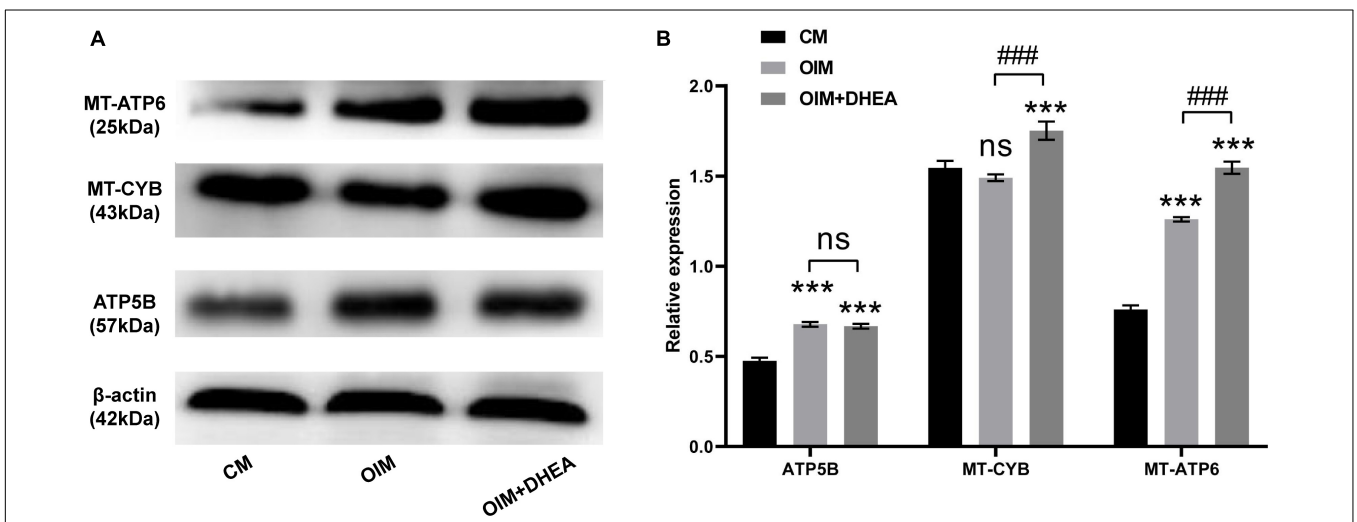

FIGURE 7 | Protein expressions of ATP5B, MT-CYB, and MT-ATP6 were increased in the OIM group and OIM+DHEA group. **(A)** The expression of ATP5B, MT-CYB, and MT-ATP6 protein were assessed by western blot analysis, β-actin as a loading control. **(B)** The quantification of expression levels of ATP5B, MT-CYB, and MT-ATP6 proteins, the data were presented as the mean ± SD for each group (***$p < 0.001$; ###$p < 0.001$).

through investigating protein alterations in the bone marrow microenvironment of osteoporotic patients undergoing spine fusion using TMT-based proteomics. Zhang et al. (2021) also applied TMT-based quantitative proteomic analysis to unveil the impact of BMSCs on hair follicle regeneration and confirm key hair regeneration-related protein targets in this therapeutic context.

To the best of our knowledge, this is the first time to apply this method to assess the underlying molecular mechanism in the osteogenic differentiation of BMSCs induced by DHEA *in vitro*. In our research, the more differentially expressed proteins of hBMSCs in the CM, OIM, and OIM+DHEA groups were obtained through TMT peptide labeling, combined with LC-MS/MS, as a set of 604 DEPs were identified from OIM vs. CM group (524 DEPs) and OIM+DHEA vs. CM group (547 DEPs). These proteins could play an important role in the osteoblast differentiation of hBMSCs induced by DHEA and may be closely related to osteogenesis.

Further bioinformatics analysis demonstrated that these differential proteins from OIM vs. CM group and OIM+DHEA vs. CM group were mainly enriched into metabolic pathways. Metabolic pathways have been reported to regulate the expression of genes via epigenetic modifications, and most of the cofactors, substrates, or allosteric regulators involved in epigenetic changes are produced by way of bioenergetic pathways (Motyl et al., 2017). Thus, control of metabolic pathways has a profound impact in controlling adenosine triphosphate (ATP) generation involved in energy metabolism and controlling the expression of genes, and these effects will affect the lineage determination of stem cells. Energy metabolism as one of the metabolic pathways has been confirmed to participate in osteoblast differentiation and osteogenesis (Smith and Eliseev, 2021). Increasing evidence revealed that substantial amounts of energy were necessary for the synthetic phase of osteoblast differentiation as osteoblasts required huge energy-producing capability (Dirckx et al., 2019). Together with our findings, these results support the fact that metabolic pathways, especially energy metabolism, play a vital role in the DHEA osteoinduction of hBMSCs.

Interestingly, we observed increased expression of proteins (ATP5B, MT-CYB, and MT-ATP6) related to oxidative phosphorylation (OXPHOS) in the OIM+DHEA vs. CM group compared with the OIM vs. CM group. Cumulating evidence has revealed that OXPHOS is a crucial supplementary pathway for ATP synthesis in energy metabolism (Wilson, 2017), and increasing evidence has recently announced that human MSCs (hMSCs) primarily generate ATP through OXPHOS-dependent metabolism during osteogenic differentiation (Guntur et al., 2014; Meleshina et al., 2016). Thus, we speculated that DHEA promotes osteogenic differentiation of hBMSCs may through regulating energy metabolism of metabolic pathways by up-regulating three OXPHOS-related proteins (ATP5B, MT-CYB, and MT-ATP6). ATP is mainly synthesized by mitochondrial ATP synthetase. As one of the principal subunits of ATP synthase, ATP5B could promote cellular ATP levels and play a key role in the differentiation and proliferation of stem cells (Xiaoyun et al., 2017). MT-ATP6 protein that is a component of a large enzyme was known as ATP synthase, is encoded by the mitochondrial genome and responsible for catalyzing the final step of oxidative phosphorylation (Andrews et al., 1999; Demir et al., 2014). MT-CYB protein, as the only mitochondrial genome-encoded subunit of respiratory complex III, is encoded by the MT-CYB gene and exerts important functions in the electron transport system (Demir et al., 2014). Although the precise role of each of these three proteins alone in osteogenic differentiation induced by DHEA currently not know, these observations point to the increased expression of ATP5B, MT-CYB, and MT-ATP6 observed in osteocytes differentiation of hBMSCs caused by DHEA may represent a regulated mechanism of mitochondrial function to up-regulate ATP synthesis by OXPHOS. Further investigations are needed to address the precise tasks of DEPs these possibilities in osteogenic differentiation of hBMSCs and determine whether ATP5B, MT-CYB, and MT-ATP6 cause changes in energy metabolism, which impact the differentiation of hBMSCs into osteocytes induced by DHEA.

In short, our findings suggested that DHEA possesses osteoinduction properties and could foster the proliferation and osteoblast differentiation of hBMSCs in OIM. The proteomics and bioinformatics analysis revealed that DHEA-induced osteogenic differentiation of hBMSCs mechanically is mainly through energy metabolism as one of the metabolic pathways. Three key proteins, ATP5B, MT-CYB, and MT-ATP6, may act as the essential regulators for promoting the osteogenic differentiation of hBMSCs, and their specific functions need to be further studied. Our results offered novel information about the underlying molecular mechanisms involved in osteogenic differentiation of hBMSCs induced by DHEA, and DHEA is likely to be an ideal reagent for the prevention and treatment of OP.

DATA AVAILABILITY STATEMENT

The datasets presented in this study can be found in online repositories. The names of the repository/repositories and accession number(s) can be found below: MassIVE database, accession no: MSV000087888.

ETHICS STATEMENT

The studies involving human participants were reviewed and approved by the Ethics Committee of The First Affiliated Hospital of Guangxi Medical University. The patients/participants provided their written informed consent to participate in this study.

AUTHOR CONTRIBUTIONS

XL, MH, and BZ contributed to the design and conception of the research, analysis of the data, interpretation of the results, and the writing of the manuscript. YZ, XH, and DL performed some experiments, provided reagents, and critical comments on the manuscript. QW reviewed and edited the manuscript. All authors read and approved the final manuscript.

FUNDING

This study was financially supported by the National Natural Science Foundation of China (Grant No. 81560371), the Guangxi Key R&D Program (Grant No. GuiKeAB17292073), and the Guangxi Natural Science Foundation of China (Grant No. 2019GXNSFAA245072).

ACKNOWLEDGMENTS

We thank the Shanghai Genechem Co., Ltd., for TMT quantitative proteomics detection.

REFERENCES

Allolio, B., and Arlt, W. (2002). DHEA treatment: myth or reality? *Trends Endocrinol. Metab.* 13, 288–294. doi: 10.1016/S1043-2760(02)00617-3

An, J., Yang, H., Zhang, Q., Liu, C., Zhao, J., Zhang, L., et al. (2016). Natural products for treatment of osteoporosis: the effects and mechanisms on promoting osteoblast-mediated bone formation. *Life Sci.* 147, 46–58. doi: 10.1016/j.lfs.2016.01.024

Andrews, R. M., Kubacka, I., Chinnery, P. F., Lightowlers, R. N., Turnbull, D. M., and Howell, N. (1999). Reanalysis and revision of the Cambridge reference sequence for human mitochondrial DNA. *Nat. Genet.* 23, 147. doi: 10.1038/13779

Annamalai, R. T., Hong, X., Schott, N. G., Tiruchinapally, G., Levi, B., and Stegemann, J. P. (2019). Injectable osteogenic microtissues containing mesenchymal stromal cells conformally fill and repair critical-size defects. *Biomaterials* 208, 32–44. doi: 10.1016/j.biomaterials.2019.04.001

Celebi, B., and Elçin, Y. M. (2009). Proteome analysis of rat bone marrow mesenchymal stem cell subcultures. *J. Proteome Res.* 8, 2164–2172. doi: 10.1021/pr800590g

Chen, X. H., Shi, Z. G., Lin, H. B., Wu, F., Zheng, F., Wu, C. F., et al. (2019). Resveratrol alleviates osteoporosis through improving the osteogenic differentiation of bone marrow mesenchymal stem cells. *Eur. Rev. Med. Pharmacol. Sci.* 23, 6352–6359.

Ciapetti, G., Ambrosio, L., Marletta, G., Baldini, N., and Giunti, A. (2006). Human bone marrow stromal cells: *in vitro* expansion and differentiation for bone engineering. *Biomaterials* 27, 6150–6160. doi: 10.1016/j.biomaterials.2006.08.025

Demir, D., Türkkahraman, D., Samur, A. A., Lüleci, G., Akçurin, S., and Alper, M. (2014). Mitochondrial ATPase subunit 6 and cytochrome B gene variations in obese Turkish children. *J. Clin. Res. Pediatr. Endocrinol.* 6, 209–215. doi: 10.4274/Jcrpe.1601

Dirckx, N., Moorer, M. C., Clemens, T. L., and Riddle, R. C. (2019). The role of osteoblasts in energy homeostasis. *Nat. Rev. Endocrinol.* 15, 651–665. doi: 10.1038/s41574-019-0246-y

Formoso, G., Chen, H., Kim, J. A., Montagnani, M., Consoli, A., and Quon, M. J. (2006). Dehydroepiandrosterone mimics acute actions of insulin to stimulate production of both nitric oxide and endothelin 1 via distinct phosphatidylinositol 3-kinase- and mitogen-activated protein kinase-dependent pathways in vascular endothelium. *Mol. Endocrinol.* 20, 1153–1163. doi: 10.1210/me.2005-0266

Foster, L. J., Zeemann, P. A., Li, C., Mann, M., Jensen, O. N., and Kassem, M. (2005). Differential expression profiling of membrane proteins by quantitative proteomics in a human mesenchymal stem cell line undergoing osteoblast differentiation. *Stem Cells* 23, 1367–1377. doi: 10.1634/stemcells.2004-0372

Franco-Trepat, E., Guillán-Fresco, M., Alonso-Pérez, A., Jorge-Mora, A., Francisco, V., Gualillo, O., et al. (2019). Visfatin connection: present and future in osteoarthritis and osteoporosis. *J. Clin. Med.* 8:1178. doi: 10.3390/jcm8081178

Ginaldi, L., Di Benedetto, M. C., and De Martinis, M. (2005). Osteoporosis, inflammation and ageing. *Immun. Ageing I A* 2:14.

Guntur, A. R., Le, P. T., Farber, C. R., and Rosen, C. J. (2014). Bioenergetics during calvarial osteoblast differentiation reflect strain differences in bone mass. *Endocrinology* 155, 1589–1595. doi: 10.1210/en.2013-1974

Ismail, I. T., Showalter, M. R., and Fiehn, O. (2019). Inborn errors of metabolism in the Era of untargeted metabolomics and lipidomics. *Metabolites* 9:242. doi: 10.3390/metabo9100242

Kurpinski, K., Chu, J., Wang, D., and Li, S. (2009). Proteomic profiling of mesenchymal stem cell responses to mechanical strain and TGF-beta1. *Cell. Mol. Bioeng.* 2, 606–614. doi: 10.1007/s12195-009-0090-6

Liang, X., Glowacki, J., Hahne, J., Xie, L., LeBoff, M. S., and Zhou, S. (2016). Dehydroepiandrosterone stimulation of osteoblastogenesis in human MSCs requires IGF-I signaling. *J. Cell. Biochem.* 117, 1769–1774. doi: 10.1002/jcb.25475

Liu, Y., Kuang, B., Rothrauff, B. B., Tuan, R. S., and Lin, H. (2019). Robust bone regeneration through endochondral ossification of human mesenchymal stem cells within their own extracellular matrix. *Biomaterials* 218:119336. doi: 10.1016/j.biomaterials.2019.119336

Lynn, H. S., Lau, E. M., Au, B., and Leung, P. C. (2005). Bone mineral density reference norms for Hong Kong Chinese. *Osteoporo. Int.* 16, 1663–1668. doi: 10.1007/s00198-005-1899-z

Ma, K., Zhu, B., Wang, Z., Cai, P., He, M., Ye, D., et al. (2020). Articular chondrocyte-derived extracellular vesicles promote cartilage differentiation of human umbilical cord mesenchymal stem cells by activation of autophagy. *J. Nanobiotechnol.* 18:163. doi: 10.1186/s12951-020-00708-0

Malik, A. K., Khaldoyanidi, S., Auci, D. L., Miller, S. C., Ahlem, C. N., Reading, C. L., et al. (2010). 5-Androstene-3beta,7beta,17beta-triol (beta-AET) slows thermal injury induced osteopenia in mice: relation to aging and osteoporosis. *PLoS One* 5:e13566. doi: 10.1371/journal.pone.0013566

Meleshina, A. V., Dudenkova, V. V., Shirmanova, M. V., Shcheslavskiy, V. I., Becker, W., Bystrova, A. S., et al. (2016). Probing metabolic states of differentiating stem cells using two-photon FLIM. *Sci. Rep.* 6:21853. doi: 10.1038/srep21853

Motyl, K. J., Guntur, A. R., Carvalho, A. L., and Rosen, C. J. (2017). Energy metabolism of bone. *Toxicol. Pathol.* 45, 887–893. doi: 10.1177/0192623317737065

Moulder, R., Bhosale, S. D., Goodlett, D. R., and Lahesmaa, R. (2018). Analysis of the plasma proteome using iTRAQ and TMT-based Isobaric labeling. *Mass Spectrom. Rev.* 37, 583–606. doi: 10.1002/mas.21550

Pittenger, M. F., Mackay, A. M., Beck, S. C., Jaiswal, R. K., Douglas, R., Mosca, J. D., et al. (1999). Multilineage potential of adult human mesenchymal stem cells. *Science* 284, 143–147. doi: 10.1126/science.284.5411.143

Qiu, X., Gui, Y., Xu, Y., Li, D., and Wang, L. (2015). DHEA promotes osteoblast differentiation by regulating the expression of osteoblast-related genes and Foxp3(+) regulatory T cells. *Biosci. Trends* 9, 307–314. doi: 10.5582/bst.2015.01073

Scheven, B. A., and Milne, J. S. (1998). Dehydroepiandrosterone (DHEA) and DHEA-S interact with 1,25-dihydroxyvitamin D3 (1,25(OH)2D3) to stimulate human osteoblastic cell differentiation. *Life Sci.* 62, 59–68. doi: 10.1016/s0024-3205(97)01038-2

Shen, W.-C., Lai, Y.-C., Li, L.-H., Liao, K., Lai, H.-C., Kao, S.-Y., et al. (2019). Methylation and PTEN activation in dental pulp mesenchymal stem cells promotes osteogenesis and reduces oncogenesis. *Nat. Commun.* 10:2226. doi: 10.1038/s41467-019-10197-x

Smith, C. O., and Eliseev, R. A. (2021). Energy metabolism during osteogenic differentiation: the role of Akt. *Stem Cells Dev.* 30, 149–162. doi: 10.1089/scd.2020.0141

Sze, S. K., de Kleijn, D. P., Lai, R. C., Khia Way Tan, E., Zhao, H., Yeo, K. S., et al. (2007). Elucidating the secretion proteome of human embryonic stem cell-derived mesenchymal stem cells. *Mol. Cell. Proteomics* 6, 1680–1689. doi: 10.1074/mcp.M600393-MCP200

Tan, F. Z., and Dai, H. L. (2019). TAZ accelerates osteogenesis differentiation of mesenchymal stem cells via targeting PI3K/Akt. *Eur. Rev. Med. Pharmacol. Sci.* 23, 81–88.

Thompson, A., Schäfer, J., Kuhn, K., Kienle, S., Schwarz, J., Schmidt, G., et al. (2003). Tandem mass tags: a novel quantification strategy for comparative analysis of complex protein mixtures by MS/MS. *Anal. Chem.* 75, 1895–1904. doi: 10.1021/ac0262560

Voss, P. J., Steybe, D., Poxleitner, P., Schmelzeisen, R., Munzenmayer, C., Fuellgraf, H., et al. (2018). Osteonecrosis of the jaw in patients transitioning from bisphosphonates to denosumab treatment for osteoporosis. *Odontology* 106, 469–480. doi: 10.1007/s10266-018-0362-5

Wang, D., Park, J. S., Chu, J. S., Krakowski, A., Luo, K., Chen, D. J., et al. (2004). Proteomic profiling of bone marrow mesenchymal stem cells upon transforming growth factor beta1 stimulation. *J. Biol. Chem.* 279, 43725–43734. doi: 10.1074/jbc.M407368200

Wang, L., Wang, Y. D., Wang, W. J., and Li, D. J. (2009). Differential regulation of dehydroepiandrosterone and estrogen on bone and uterus in ovariectomized mice. *Osteoporos. Int.* 20, 79–92. doi: 10.1007/s00198-008-0631-1

Wang, L., Wang, Y. D., Wang, W. J., Zhu, Y., and Li, D. J. (2007). Dehydroepiandrosterone improves murine osteoblast growth and bone tissue morphometry via mitogen-activated protein kinase signaling pathway independent of either androgen receptor or estrogen receptor. *J. Mol. Endocrinol.* 38:467. doi: 10.1677/jme.1.02173

Wilson, D. F. (2017). Oxidative phosphorylation: regulation and role in cellular and tissue metabolism. *J. Physiol.* 595, 7023–7038. doi: 10.1113/JP273839

Wu, Q. Y., Li, X., Miao, Z. N., Ye, J. X., Wang, B., Zhang, F., et al. (2018). Long non-coding RNAs: a new regulatory code for osteoporosis. *Front. Endocrinol.* 9:587. doi: 10.3389/fendo.2018.00587

Xiaoyun, X., Chaofei, H., Weiqi, Z., Chen, C., Lixia, L., Queping, L., et al. (2017). Possible involvement of F1F0-ATP synthase and intracellular ATP in keratinocyte differentiation in normal skin and skin lesions. *Sci. Rep.* 7:42672. doi: 10.1038/srep42672

Zhang, C., Li, Y., Qin, J., Yu, C., Ma, G., Chen, H., et al. (2021). TMT-based quantitative proteomic analysis reveals the effect of bone marrow derived mesenchymal stem cell on hair follicle regeneration. *Front. Pharmacol.* 12:658040. doi: 10.3389/fphar.2021.658040

Zhang, L., and Elias, J. E. (2017). Relative protein quantification using tandem mass tag mass spectrometry. *Methods Mol. Biol. (Clifton N. J.)* 1550, 185–198. doi: 10.1007/978-1-4939-6747-6_14

Zhou, Q., Xie, F., Zhou, B., Wang, J., Wu, B., Li, L., et al. (2019). Differentially expressed proteins identified by TMT proteomics analysis in bone marrow microenvironment of osteoporotic patients. *Osteoporos. Int.* 30, 1089–1098. doi: 10.1007/s00198-019-04884-0

Zhou, S. H., and Glowacki, J. (2017). Chronic kidney disease and vitamin D metabolism in human bone marrow-derived MSCs. *Ann. N. Y. Acad. Sci.* 1402, 43–55. doi: 10.1111/nyas.13464

Conflict of Interest: The authors declare that the research was conducted in the absence of any commercial or financial relationships that could be construed as a potential conflict of interest.

Publisher's Note: All claims expressed in this article are solely those of the authors and do not necessarily represent those of their affiliated organizations, or those of the publisher, the editors and the reviewers. Any product that may be evaluated in this article, or claim that may be made by its manufacturer, is not guaranteed or endorsed by the publisher.

frontiers in Cell and Developmental Biology

ORIGINAL RESEARCH
published: 14 September 2021
doi: 10.3389/fcell.2021.730095

Connective Tissue Growth Factor From Periosteal Tartrate Acid Phosphatase-Positive Monocytes Direct Skeletal Stem Cell Renewal and Fate During Bone Healing

Yun Bai[1†], Tao Yu[1†], Jiezhong Deng[1], Yusheng Yang[1], Jiulin Tan[1], Qijie Dai[1], Zehua Zhang[1], Shiwu Dong[1,2] and Jianzhong Xu[1*]*

[1] Department of Orthopedics, Southwest Hospital, Third Military Medical University, Chongqing, China, [2] Department of Biomedical Materials Science, School of Biomedical Engineering, Third Military Medical University, Chongqing, China

OPEN ACCESS

Edited by:
Chao Xie,
University of Rochester, United States

Reviewed by:
Rupesh K. Srivastava,
All India Institute of Medical Sciences, India
Luca Persano,
University of Padua, Italy

***Correspondence:**
Shiwu Dong
dongshiwu@tmmu.edu.cn
Jianzhong Xu
brianbai@tmmu.edu.cn

[†] These authors have contributed equally to this work

Specialty section:
This article was submitted to Cellular Biochemistry, a section of the journal Frontiers in Cell and Developmental Biology

Received: *24 June 2021*
Accepted: *20 August 2021*
Published: *14 September 2021*

Citation:
Bai Y, Yu T, Deng J, Yang Y, Tan J, Dai Q, Zhang Z, Dong S and Xu J (2021) Connective Tissue Growth Factor From Periosteal Tartrate Acid Phosphatase-Positive Monocytes Direct Skeletal Stem Cell Renewal and Fate During Bone Healing. Front. Cell Dev. Biol. 9:730095. doi: 10.3389/fcell.2021.730095

The periosteum is critical for bone healing. Studies have shown that the periosteum contains periosteal stem cells (PSCs) with multidirectional differentiation potential and self-renewal ability. PSCs are activated in early fracture healing and are committed to the chondrocyte lineage, which is the basis of callus formation. However, the mechanism by which PSCs are activated and committed to chondrocytes in bone regeneration remains unclear. Here, we show that tartrate acid phosphatase (TRAP)-positive monocytes secrete CTGF to activate PSCs during bone regeneration. The loss function of TRAP-positive monocytes identifies their specific role during bone healing. Then, the secreted CTGF promotes endochondral ossification and activates PSCs in mouse bone fracture models. The secreted CTGF enhances PSC renewal by upregulating the expression of multiple pluripotent genes. CTGF upregulates c-Jun expression through αVβ5 integrin. Then, c-Jun transcription activates the transcription of the pluripotent genes *Sox2*, *Oct4*, and *Nanog*. Simultaneously, CTGF also activates the transcription and phosphorylation of Smad3 through αVβ5 integrin, which is the central gene in chondrogenesis. Our study indicates that TRAP-positive monocyte-derived CTGF promotes bone healing by activating PSCs and directing lineage commitment and that targeting PSCs may be an effective strategy for preventing bone non-union.

Keywords: skeletal stem cell, ctgf, TRAP-positive monocytes, fracture healing, bone regeneration

INTRODUCTION

Bones are repeatedly and routinely healed wounds or acute injuries for regeneration, which is different from many other tissues that repair scars (Vi et al., 2018). However, the healing process is not completely flawless and sometimes fails, resulting in a delayed healing rate of 5–10% (Hu et al., 2017). In clinical practice, approximately one-sixth patients exhibit fracture non-union, which results in a huge physical and economic burden on the affected individuals and the society. Fracture non-union or delayed union may occur due to many reasons, including infection at the fracture site, insufficient blood supply to the bone, and insufficient bone stability. These factors hinder effective

bone callus formation owing to the limited ability of cartilage generation. Therefore, studying the mechanism of fracture healing is crucial for solving the problem of failure of fracture healing.

Endochondral ossification is the primary means of bone regeneration in bone defects (Raggatt et al., 2014). Bone marrow mesenchymal stem cells (BMSCs) were believed to be the cellular source of endochondral ossification. Although BMSCs are widely used in bone tissue engineering, evidence suggests that BMSCs are not the main cellular origin of bone callus during fracture healing. On the other hand, the periosteum directly participates in the maintenance of bone integrity. Furthermore, the periosteum is crucial for typical fracture healing (Ho-Shui-Ling et al., 2018; Li et al., 2019). Studies have shown that the periosteum contains periosteal stem cells (PSCs) that possess higher ability to repair bones. The PSC is a population of high-purity skeletal stem cells (SSCs) with multipotent capacity, which can differentiate into bone, cartilage, and bone marrow cells (Chan et al., 2015, 2018). Compared with BMSCs, PSCs, which are activated in the early stage of bone regeneration, have enhanced cell growth and clonal formation capabilities and excellent regeneration capabilities, which are fundamental to bone regeneration. For lineage tracing, MSCs were labeled with GFP and transferred into mice with bone injury (Duchamp De Lageneste et al., 2018). The transplanted PSCs merged into the callus at its center, but a majority of the BMSCs remained at the periphery of the callus. These results indicate that PSCs contribute more to callus formation than BMSCs. Another study revealed that no PSC-derived chondrocytes were observed at the baseline. However, when a fracture occurs, PSCs contribute to approximately half of the cartilage tissue in the fractured callus. In a renal capsule transplantation model, PSCs isolated from the bone callus differentiated into cartilage tissue (Debnath et al., 2018), indicating that the fate of PSCs in bone repair shifts from osteoblast to chondrocyte differentiation and that PSCs explain this functional transformation of the periosteum by converting the ability of intramembranous bone formation at baseline into the ability to obtain endochondral bone formation after a fracture. However, how PSCs are activated and committed to the chondrocyte lineage during bone regeneration remains unclear.

Fracture healing occurs in a microenvironment where various cells cooperate and interact with each other in different ways. In the process of bone remodeling, osteoclast precursors migrate and differentiate because of endocrine and paracrine factors. This process is accompanied by both bone resorption by osteoclasts and bone formation by osteoblasts (Tang et al., 2009). After responding to the stimulation of M-CSF and RANKL, monocytes and macrophages first commit to the osteoclast lineage (mononuclear preosteoclast), which is characterized by resistance to tartrate acid phosphatase (tartrate-resistant acid phosphatase; $TRAP^+$). Subsequently, fusion of the preosteoclasts leads to the formation of TRAP-positive mature osteoclasts. These osteoclasts are multinucleated and possess bone resorption capacity. Studies have shown that TRAP-positive monocytes reside in the periosteum and secrete PDGF-BB during bone modeling. This PDGF-BB induces angiogenesis coupled with osteogenesis by S1P signaling (Xie et al., 2014). TRAP-positive monocyte-conditioned medium induces the migration of MSCs and endothelial progenitor cells (EPCs) and enhances EPC tube formation. Results of the aforementioned studies and the existing regulation of bone remodeling by TRAP-positive monocytes suggest that TRAP-positive monocytes may participate in PSC activation.

CTGF, a member of the CCN protein family, can promote proliferation, adhesion, migration of multiple types of cells, as well as angiogenesis (Carlstrom et al., 2015). CTGF participates in endochondral ossification by acting on many types of cells (Takigawa, 2013). CTGF expression is also important for chondrocyte hypertrophy to form a calcified matrix. CTGF overexpression promoted growth plate growth and increased the length of long bones in transgenic mice (Arnott et al., 2011). Research has also proven that CTGF is the main regulator of cartilage formation. The multidomain feature allows CTGF to interact with other growth factors such as TGF-β, BMP, IGF, and VEGF (Shen et al., 2021). Simultaneously, CTGF interacts with the extracellular matrix and cell surface receptors, such as integrins (Perbal, 2004).

This study reported that TRAP-positive monocytes secrete CTGF to activate PSCs and direct chondrocyte lineage commitment during fracture healing. First, the number and distribution of TRAP-positive monocytes were identified in the periosteum after injury. We then found that TRAP-positive monocytes secrete CTGF to promote endochondral ossification and PSC renewal in bone callus. The mechanism by which CTGF derived from TRAP-positive monocytes acts on PSCs was also elucidated.

MATERIALS AND METHODS

Mice

Rosa26-iDTR ($DTR^{fl/fl}$) mice (#007900) and tdTomato reporter mice (#007909) were purchased from Jackson laboratory (United States). Acp5-Cre mice were purchased from GemPharmatech Co., Ltd (Chengdu, China). $Ccn2^{fl/fl}$ mice–bearing loxP sites flanking exon 4 of the cellular communication network factor 2 gene were also purchased from Jackson laboratory (# 035182). All mice were bred under SPF conditions in the Laboratory Animals Center of Army Medical University (Third Military Medical University, Chongqing, China). Age- and sex-matched littermates were used as control mice. All experiments were conducted according to the Third Military Medical University Sciences Guide for Laboratory Animals.

Primary Cultures of Periosteal Stem Cells

The mice were sacrificed and their femurs and tibias were dissected. After removing the epiphysis, the bone was flushed for removing total bone marrow cells. To obtain primary PSCs, the remaining bone-washed explants without muscles and tendons were cultured using Mouse MesenCult™ Expansion Kit (# 05513, STEMCELL Technologies, United States) supplemented with L-Glutamine (# 07100, STEMCELL Technologies); the PSCs migrated from the explants within 3 days. After 2 weeks, the bones were removed, and the PSCs were digested with trypsin

and directly used for *in vitro* and *in vivo* experiments without further amplification.

Colony-Forming Efficiency Assay and Differentiation of Periosteal Stem Cells *in vitro*

PSCs obtained were directly plated at a density of 1,000 cells/cm^2 in stem cell growth media (# 05513, STEMCELL Technologies) for 2 weeks, with the medium being changed every 3 days. Clones were fixed in 4% paraformaldehyde for 0.5 h, stained with Giemsa stain (# G5637, Sigma-Aldrich, United States), and counted.

For chondrogenic differentiation, cells were grown in micromass culture. About 5×10^5 PSCs were plated in the center of a culture plate and incubated at 37°C with 5% CO_2 for 3 h. Without disturbing the pellet, the chondrogenic medium (# MUBMX-9004, Cyagen, China) was carefully added to the cells. The cell micromass was fixed in 4% paraformaldehyde for 0.5 h on day 14. Alcian blue staining (Cyagen) was performed to demonstrate the presence of matrix proteoglycans. The stain was then extracted for quantification through measurement of absorbance at 620 nm.

For osteogenic differentiation, the PSCs were treated with an osteogenic differentiation medium kit (# MUBMD-90021, Cyagen) in accordance with the manufacturer's instructions. Mineralized nodules were stained with alizarin red solution in osteogenic differentiation medium kit. This staining procedure was quantitatively analyzed by measuring absorbance at 405 nm.

In some experiments, the Src inhibitor PP2 (10 μM, # P0042, Sigma–Aldrich), anti-integrin αvβ5 (1 μg/mL, # MAB1961, Sigma–Aldrich), and recombinant CTGF (rCTGF, 100 ng/mL, # sc-515116, Santa Cruz) were added to the medium.

Preparation of Osteoclast Conditioned Medium

The bone marrow of the femur and tibia of 4-week-old wild-type male mice were washed to collect monocytes and macrophages (BMMs). The washed bone marrow cells were cultured in α-MEM culture media containing 10% FBS, 100 U/mL penicillin, 100 μg/mL streptomycin sulfate, and 30 ng/mL M-CSF (# 416-ML-010/CF, R&D, United States) for 6 h. After the adherent cells were discarded, the floating cells were incubated with α-MEM culture media containing M-CSF (30 ng/mL) to obtain pure BMMs. When the BMMs were incubated in a 12-well plate (2×10^5 cells/well) containing 30 ng/mL M-CSF and 50 ng/mL RANKL (# 462-TEC-010, R&D), all cells became precursor osteoclasts after 3 days of culture. The incubation was continued with 30 ng/mL M-CSF and 100 ng/mL RANKL for 7 days to form mature multinucleated osteoclasts. Then, the conditioned media was harvested from preosteoclasts and mature osteoclasts. After centrifugation (2,500 r.p.m., 10 min at 4°C), the conditioned medium was aliquoted and stored at −80°C. In subsequent experiments, neutralizing antibodies for certain factors, including IGFBP5 (# sc-515116, Santa Cruz, 1 μg/mL), CXCL12 (# sc-74271, Santa Cruz, 1 μg/mL), and CTGF (# sc-365970, Santa Cruz, 1 μg/mL), were added to the conditioned media for 3d (CFE) or for 7d (chondrogenesis).

Flow Cytometry

We harvested the fractured callus of wild-type or Ccn2Acp5 mice on the 14th day after the fracture. Using a mortar and pestle, each sample was crushed separately and placed in separate 50-ml centrifuge tubes with 10 mL collagenase at 37°C for 30 min Each sample was subjected to continuous enzymatic digestion with collagenase and DNase at 37°C with gentle shaking for 30 min. The digestion step was repeated thrice. The digested cells were filtered through a 70-μm nylon mesh, centrifuged at 200 × g at 4°C, and resuspended in PBS containing 2% FBS. After the cells were washed with PBS, they were resuspended in 50 μL PBS containing 2% FBS. The pellet was stained using fluorescent dye-conjugated antibodies against CD45 (1:100, # 147718, Biolegend, United States), Tie2 (1:100, # 124009, Biolegend), CD51 (alpha V, 1:100, # 104105, Biolegend), Ly-51 (6C3, 1:100, # 108314, Biolegend), Ter119 (1:100, # 116228, Biolegend), CD105 (1:100, # 120406, Biolegend), CD200 (1:50, # 565547, BD Biosciences, United States), and Thy (CD90.2, 1:100, # 105335, Biolegend) for flow cytometry analysis.

Plasmids and siRNA

To construct the dual-luciferase reporter vector, the 1-kb upstream promoter regions of Jun and Smad3 were cloned into the pLG3 vector (Promega, Madison, WI, United States). Luciferase activity was detected using the double Luciferase Assay System (Promega) and normalized with the co-expressed Renilla luciferase. siRNAs of c-Jun (# sc-29224, Santa Cruz, United States) and Smad3 (# sc-37239, Santa Cruz) were purchased from Santa Cruz Biotechnology.

Mice Bone Fracture Model and Periosteum Grafting

Eight-week-old male or female mice were used for the model. The mice were anaesthetized with 0.5% sodium pentobarbital (# P3761, Sigma-Aldrich). A closed, transverse fracture was made in the tibia by three-point bending, which was confirmed by radiography. Periosteum grafts isolated from the tibia tdTomato donor mice were transplanted. Briefly, we anaesthetized wild-type or $Ccn2^{Acp5}$ mice to make open and unstable fractures. Then, we carefully scraped off the two tibial periosteums of a tdTomato donor using microdissection surgical instruments and collected and transplanted them at the site of non-stabilized tibial fractures in 8-week-old $Ccn2^{fl/fl}$ or $Ccn2^{Acp5}$ host mice. The muscle was then sutured to fix the grafted periosteum and then the skin was closed.

Micro-Computed Tomography Analysis

Tibia specimens from different mice groups were fixed overnight in 4% paraformaldehyde. The specimens were scanned using micro-computed tomography (μCT; Skyscan1272, Bruker microCT, Kontich, Belgium). The scanner was set to a voltage of 60 kV and a resolution of 8 μm per pixel. NRecon v1.6 software (Bioz, Inc., United States) was used to reconstruct the scanned image. The reconstruction was analyzed using CTAn v1.9 software (Bruker micro-CT), and CTVol v2.0 software (Bruker micro-CT) was used to visualize the 3D model. The area

of interest was defined according to the "fracture callus analysis" section of Bruker micro-CT method annotation.

Histochemistry

The sample was analyzed by CT and then decalcified using 0.5 M EDTA decalcification solution for a week at 25°C. The samples are embedded in paraffin. Using a paraffin microtome, 4-μm-thick bone sections were prepared for TRAP staining (# 387A-1KT, Sigma-Aldrich) and safranin O (# S2255, Sigma-Aldrich)/fast green (# F7252, Sigma-Aldrich) staining. For safranin O/fast green staining, the sections were dewaxed and washed thrice with phosphate-buffered saline (PBS). The sections were stained with fast green for 5 min, followed by differentiation with 1% acetic acid for 10 s. Subsequently, the sections were counterstained with safranin O for 5 min. For TRAP staining, the TRAP staining solution was first prepared according to the manufacturer's instructions. The sections were dewaxed, washed thrice with PBS, stained with TRAP staining solution for 5 min at 70°C, and counterstained with methyl green (#M884, Sigma-Aldrich) for 10 s.

Real-Time Quantitative PCR

For total RNA extraction, RNAiso Plus reagent (# 91089, Takara, Japan) was used. cDNA was prepared from 1 μg of total RNA using PrimeScript™ RT reagent Kit with gDNA Eraser (# RR047B, Takara), according to the manufacturer's instructions. PCR amplifications were performed using specific primers for each gene as follows: *Sox2* (F) 5′-GCGGAGTGGAAACTTTTGTCC- 3′, (R) 5′-CGGGAAGCGTGTACTTATCCTT-3′; *Oct4* (F) 5′-GGCTTCAGACTTCGCCTCC-3′, (R) 5′-AACCTGAGGTCCACAGTATGC-3′; *Nanog* (F) 5′-TCTTCCTGGTCCCCACAGTTT-3′, (R) 5′-GCAAGAATAGTTCTCGGGATGAA-3′; *Sox9* (F) 5′-GAGCCGGATCTGAAGAGGGA-3′, (R) 5′-GCTTGACGTGTGGCTTGTTC-3′; *Col2a1* (F) 5′-GGGAATGTCCTCTGCGATGAC-3′, (R) 5′-CAGGCGCACCATCTCTGAT-3′.

Western Blots and Antibodies

Cells were lysed in cell lysis buffer (#P0013, Beyotime Biotechnology, China). In total, 20 μg of protein samples was subjected to SDS-PAGE. Next, the proteins were transferred onto PVDF membranes (#ISEQ00010, Merck Millipore, Germany). Then, the membranes were blocked in 5% skim milk for 2 h and incubated with primary antibodies overnight at 4°C. The primary antibodies for GAPDH (1:1,000, # 5,174), Smad3 (1:1,000, # 9,523T), phospho-Smad3 (Ser423/425) (1:1,000, # 9,520), c-Jun (1:1,000, # 9,165), and phospho-c-Jun (Ser63) (1:1,000, # 2,361) were purchased from Cell Signaling Technology (Danvers, MA, United States). Then, the membranes were incubated for 2 h with secondary antibodies (1:2,000, # 7074, Cell Signaling Technology) at 25°C. After the membranes were washed in TBST, chemiluminescent signals were detected using the Bio-Rad Molecular Imager ChemiDoc™ XRS + system (Bio-Rad, United States). GAPDH was used as the loading control.

Protein 3D Structure Construction and Docking

An online server was used to model the protein sequence, and the template was searched using Homology detection and structure prediction by HMM-HMM comparison[1] provided by the Max-Planck Institute of Developmental Biology, Germany. The protein sequence was submitted to the HHpred database, the latest PDB database was selected in the database search column, and a template with homology to the target was searched. The single-template modeling script model_singal.py in Modeler 9.23 was used to perform single-template modeling for 3D structure simulation. The energy of the constructed structure was minimized. ZDOCK was used for protein–protein docking, and PyMOL was used to analyse the results before plotting.

Statistical Analysis

The unpaired, two-tailed Student's *t*-test was used for comparison between two groups, and one-way analysis of variance (ANOVA) with the Bonferroni *post hoc* test was used for multiple comparisons. For all experiments, $P < 0.05$ was considered significant and indicated by "*"; $P < 0.01$ was indicated by "**."

RESULTS

Tartrate Acid Phosphatase-Positive Cell Deficiency Impairs Callus Formation During Bone Healing

Studies have identified that TRAP-positive cells on the periosteum are mononuclear osteoclast precursors (Xie et al., 2014). However, the precise location of fracture-associated TRAP-positive mononuclear osteoclast precursor remains unknown. To determine the distribution of TRAP-positive cells during fracture healing, we established a closed tibia fracture model in wild-type mice. TRAP staining revealed that TRAP-positive cells increased significantly on the surface of the callus at 2 and 4 weeks after the fracture compared with that at week 0 (**Figure 1A**).

To further explore the functions of TRAP-positive lineage cells in bone healing, we genetically ablated TRAP-positive cells by crossing Acp5-Cre mice with DTR mice to generate Acp5-Cre; DTR mice (DTR^{Acp5}), which have TRAP-positive cell deficiency after administering diphtheria toxin (DT) injection. The DTR^{Acp5} mice were injected with DT 2 weeks before surgery and analyzed at 2 weeks after the fracture. We induced tibial fractures on 8-week-old DTR^{Acp5} mice and their littermate controls ($DTR^{fl/fl}$) and found that the mice failed to achieve maximum callus volume at 2 weeks, characterized by delayed cartilage formation leading to fibrosis (**Figure 1B**). To further investigate mineralized bone callus, we performed μCT analysis. μCT found that the DTR^{Acp5} mice exhibited an impaired bone healing process marked by a decrease in the total fracture callus size and hard bone callus volume at 2 weeks after the fracture compared with the $DTR^{fl/fl}$ mice (**Figure 1C**). The

[1] http://toolkit.tuebingen.mpg.de/hhpred

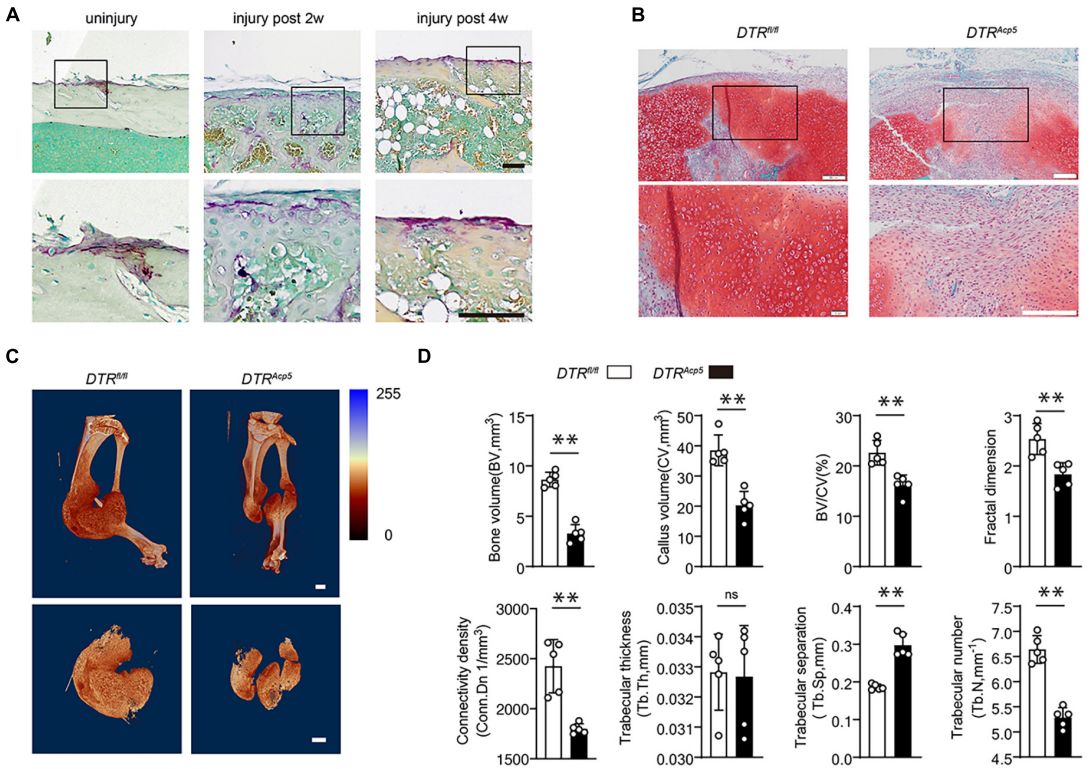

FIGURE 1 | Tartrate-resistant acid phosphatase (TRAP)-positive cell deficiency impairs callus formation during bone healing. **(A)** Localization of TRAP-positive cells in the periosteum and fracture callus during fracture healing in WT mice. Scale bars, 200 μm. **(B)** Representative images of tibia callus Safranin O/Fast green staining on14 days post fractures in WT and DTR^{Acp5} mice. Scale bars, 200 μm. **(C)** Representative 3D micro-computer tomography (μCT) images of tibia bone callus 14 days post fractures. Scale bars, 2 mm. **(D)** Quantitative μCT analysis of tibia fractures in DTR^{Acp5} mice on 14 days post fractures. The μCT parameters includes CV (callus volume), BV (bone volume), BV/CV, FD (Fractal dimension), Tb.Th (trabecular thickness), Tb.Sp (trabecular separation), Tb.N (trabecular number), and Conn.Dn (Connectivity density). Data are expressed as mean ± SD. $^{**}P < 0.01$.

VOI volume indicates the total volume of the callus. As shown in **Figures 1C,D**, the callus volume significantly decreased in the DTR^{Acp5} mice compared with the $DTR^{fl/fl}$ mice. Other 3D morphometric parameters of μCT including bone volume (BV), callus volume (CV), BV/CV, fractal dimension (FD), connective density (Conn. Dn), trabecular thickness (Tb.Th), trabecular separation (Tb.Sp), and trabecular number (Tb.N), which are sensitive to the connectivity and microstructure of the complex porous callus, were used to evaluate the mineralized callus. As indicated by these morphological parameters, the DTR^{Acp5} mice had significantly reduced bone callus connectivity and microstructure compared with littermate controls (**Figure 1D**). These results suggest lower quality of the callus in TRAP-positive cell-deficient mice with decreased callus volume and a complex porous callus.

Connective Tissue Growth Factor From Preosteoclasts Induces Periosteal Stem Cell Renewal and Promotes the Chondrogenic Potential of SSCs *in vitro*

PSC activation at an early stage of fracture healing is the basis of callus formation. PSCs exhibit the stem cell properties of clonal multipotency. To explore the possible mechanism of TRAP-positive monocytes (preosteoclasts) in regulating callus formation and PSC activation, we induced differentiation of BMMs into preosteoclasts and mature osteoclasts and collected the different groups of conditioned media. The colony-forming efficiency assay (CFE) was used to detect the cell renewal activity. Compared with the medium derived from mature osteoclasts, the conditioned medium derived from preosteoclasts induced significantly higher PSC clonogenicity (**Figure 2A** upper panel, **Figure 2B**), indicating that the factor that promotes PSCs renewal is derived from preosteoclasts. In addition, the conditioned medium derived from preosteoclasts induced significantly more chondrogenesis than that derived from mature osteoclasts (**Figure 2A** middle panel, **Figure 2C**). However, the conditioned medium from preosteoclasts rarely affected the osteogenic differentiation activity of PSCs compared with that from mature osteoclasts (**Figure 2A** lower panel, **Figure 2D**).

To identify the functional factors, we analyzed protein profile data from a previous study (Dong et al., 2020). In this study, preosteoclasts were introduced to bone tissue engineering as seed cells. iTRAQ-labeled mass spectrometry was performed to analyze the difference between proteins secreted by MSCs alone

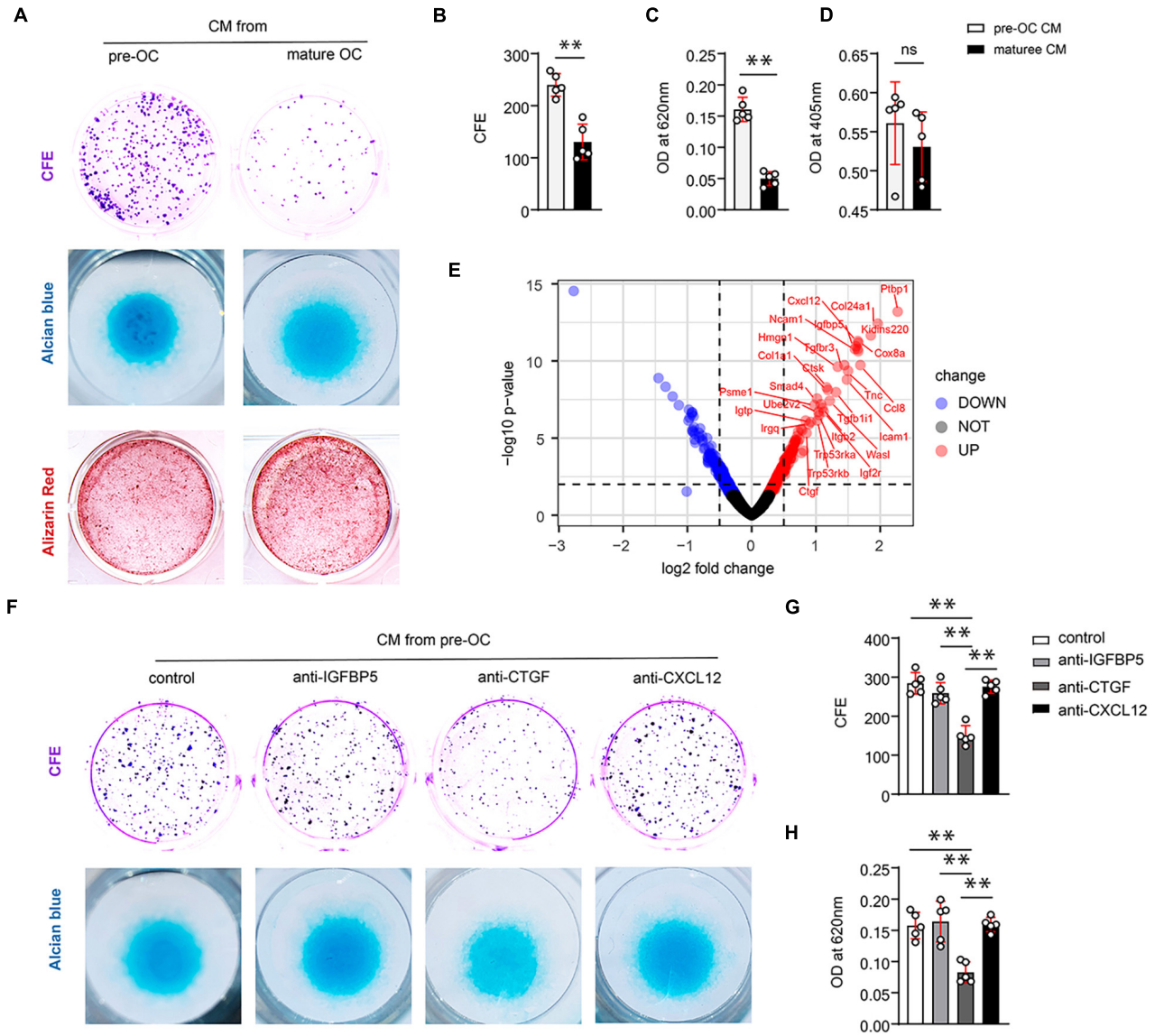

FIGURE 2 | CTGF from preosteoclasts induces periosteal stem cells (PSCs) renewal and promotes the chondrogenic potential of PSCs *in vitro*. **(A)** Representative images of clone formation efficiency (CFE), alcian blue, and alizarin red staining of PSCs. **(B)** Quantitative analysis of the CFE of PSCs. **(C)** Quantitative analysis of alcian blue staining 620 nm absorbance. **(D)** Quantitative analysis of alizarin red staining at 405 nm absorbance. **(E)** Volcano map of differentially expressed proteins in the extracellular matrix after adding TRAP$^+$ monocytes. Neutralizing antibodies of IGFBP5, CTGF, and CXCL12 were added to the conditioned medium of preosteoclasts and mature osteoclasts to investigate their effects on PSCs self-renewal and chondrogenesis. **(F)** Representative images of clone formation efficiency (CFE) and Alcian blue. **(G)** Quantitative analysis of the CFE of PSCs. **(H)** Quantitative analysis of Alcian blue staining 620 nm absorbance. Data are shown as mean ± SD. $^{**}P < 0.01$.

and MSCs + preosteoclast. Volcano maps were used to show differentially expressed proteins, indicating the secreted protein from preosteoclast (TRAP-positive monocyte) (**Figure 2E**). Among the differentially expressed proteins, we observed that IGFBP5, CXCL12, and CTGF might be the potential regulators of differentiation and fate of stem cells. To clarify the role of the aforementioned proteins in PSC self-renewal, we tested neutralizing antibodies against IGFBP5, CXCL12, and CTGF in the conditioned media. Only the antibodies against CTGF abolished preosteoclast-induced PSC renewal (**Figure 2F** upper panel, **Figure 2G**). Alcian blue staining revealed that only the CTGF neutralizing antibody reduced the chondrogenic ability of the conditioned medium on PSCs (**Figure 2F**, lower panel, **Figure 2H**). ELISA revealed that preosteoclasts secreted more CTGF than mature osteoclasts (**Supplementary Figures 1A,B**). Taken together, our results suggest that preosteoclasts, a TRAP-positive monocyte, secrete CTGF to induce PSC activation after bone fracture and facilitate the bone healing process.

Connective Tissue Growth Factor From Preosteoclasts Induces Callus Formation During Bone Healing

We next examined the function of CTGF secreted by preosteoclasts in callus formation during bone healing. CTGF floxed mice ($Ccn2^{fl/fl}$ mice) were crossed with Acp5-Cre mice to generate TRAP lineage-specific Ccn2 deletion mice (*Acp5-Cre; Ccn2* $^{fl/fl}$, short as $Ccn2^{Acp5}$). We performed immunofluorescence double staining to verify CTGF suppression in TRAP-positive cells in the $Ccn2^{Acp5}$ mice (**Supplementary Figure 1C**). Tibial fractures were induced in 8-week-old $Ccn2^{Acp5}$ and $Ccn2^{fl/fl}$ mice. The callus size and bone volume were all lower in the $Ccn2^{Acp5}$ mice relative to the $Ccn^{fl/fl}$ mice (**Figure 3**). The $Ccn2^{Acp5}$ mice failed to achieve maximum cartilage volume by day 14, leading to non-union at day 28 (**Figures 3E,F**). To further investigate mineralized callus formation, the μCT analysis was performed. The $Ccn2^{Acp5}$ mice exhibited an impaired bone healing process marked by a decrease in the total fracture callus size and hard callus volume both at week 2 after the fracture compared with the $Ccn2^{fl/fl}$ mice (**Figure 3A**). Furthermore, the $Ccn2^{Acp5}$ mice had significantly reduced bone callus connectivity and microstructure compared with the $Ccn2^{fl/fl}$ mice, marked by the morphological parameters as previously described in **Figures 1D**, **3B**. The callus usually begins to remodel at 2 weeks after the fracture; however, μCT results showed that bone non-union appeared in the $Ccn2^{Acp5}$ mice 4 weeks after the fracture, which was characterized by a significant decrease in BV and BV/TV (**Figures 3C,D**). The aforementioned results indicated that CTGF from preosteoclasts induces callus formation by promoting cartilage formation during bone healing, and CTGF depletion in preosteoclasts leads to bone non-union.

Connective Tissue Growth Factor From Preosteoclasts Is Required to Maintain the Pool of Periosteal Stem Cells and Commit Periosteal Stem Cells to Chondrogenic Lineage

Studies have reported that [$CD45^-$ Ter-119^- $Tie2^-$ $AlphaV^+$ Thy^- $6C3^-$ $CD105^-CD200^+$] PSCs exhibit clonal multipotency and self-renewal and sit at the apex of a stem cell differentiation hierarchy in the periosteum (Chan et al., 2015). To investigate the role of CTGF from preosteoclasts in PSC activation after a bone fracture, flow cytometry was used to detect the PSC population (**Figure 4A**). After establishing a fracture model using 8-week-old $Ccn2^{Acp5}$ mice and their littermate controls, the callus tissue was dissected and digested. The flow cytometry gating strategy of PSCs was based on previously reported literature (Chan et al., 2015). According to the results of flow cytometry, the frequency of $CD105^-$ $CD200^+$ PSCs in the $Ccn2^{Acp5}$ mice was significantly decreased compared with that in the littermates (**Figures 4B,C**). As [$CD45^-$ Ter-119^- $Tie2^-$ $AlphaV^+$ Thy^- $6C3^-$ $CD105^+$ $CD200^+$] pro-chondrogenic progenitors (PCPs) predominantly gave rise to cartilage with minimal bone and no marrow, considering the importance of chondrogenesis to the callus formation after a bone fracture, we focused on not only the PCPs (subpopulation **e**) but also the PCPs (subpopulation **g**).

To investigate the role of CTGF from preosteoclasts in regulating PSCs and their periosteum niche, we used periosteum transplantation and examined PSC contribution to bone repair after two rounds of fractures (**Figure 4D**). After the first round of fracture, the $Ccn2^{Acp5}$ mice showed a non-union at day 28, whereas the littermate mice achieved bone healing. After the second round of injury, the littermates formed ossified calluses and new periosteum at day 28, but the $Ccn2^{Acp5}$ mice formed fibrosis callus (**Figure 4E**). After transplantation of the tdTomato periosteal grafts at the fracture site of wild-type hosts, periosteum-derived tdTomato-positive cells largely contributed to cartilage in the callus, and rare tdTomato-positive cells were localized in the newly formed periosteum by day 28. This indicated that PSCs in the periosteum of the tdTomato donor could be activated after transplantation to continue to participate in the formation of a new periosteum. After the second injury, these rare tdTomato-positive PSCs continued to be reactivated for fracture healing and were detected in the callus cartilage by day 7. When we transplanted the tdTomato periosteal grafts into the $Ccn2^{Acp5}$ hosts, the regenerative ability of PSCs was abolished and could not be detected in the cartilage in the callus, which resulted in failed callus formation and fibrosis. Thus, these data indicate that the non-union phenotype in the $Ccn2^{Acp5}$ mice was due to the impaired PSC renewal activity, and absence of CTGF from preosteoclasts affected the ability of the periosteum to maintain the PSC niche, resulting in obstructed callus formation.

Connective Tissue Growth Factor From Preosteoclasts Induces Periosteal Stem Cell Renewal and Directs Periosteal Stem Cell Fate via αVβ5

Although CTGF functions through AlphaV (αV) integrins, αV needs to bind to β subunits, which exist in many forms in the stem cells. αβ integrin interacts with CTGF in the stem cells. To identify which integrin that may have more affinity for CTGF, we used a method that mimics protein molecule docking. First, we performed 3D modeling of protein molecules based on homologous templates according to the protein sequence. The structure of αV integrin (Uniport ID: P43406) was determined by homologous template 3IJE (A chain, similarity: 95%). The structure of CTGF is modeled using templates 5NB8 (similarity: 56%) and 4JPH (similarity: 22%). Then, after modeling the protein structure of CTGF, αVβ3, αVβ5, and αVβ6, protein–protein docking was performed using Zdock. The results revealed that the ternary complex structure of αVβ5 (P43406_O70309) and CTGF had the largest binding surface, followed by those of αVβ6 (Q9Z0T9) and αVβ3 (O54890) (**Figure 5A**).

To further investigate whether CTGF affects PSC self-renewal and chondrogenesis through αVβ5 integrin, we used αVβ5 integrin neutralizing antibody to block αVβ5 activity. CFE assays demonstrated that the neutralizing antibody partially blocked the effect of CTGF on PSC self-renewal (**Figure 5B** upper panel, **Figure 5C**). The results of the alcian blue staining were consistent

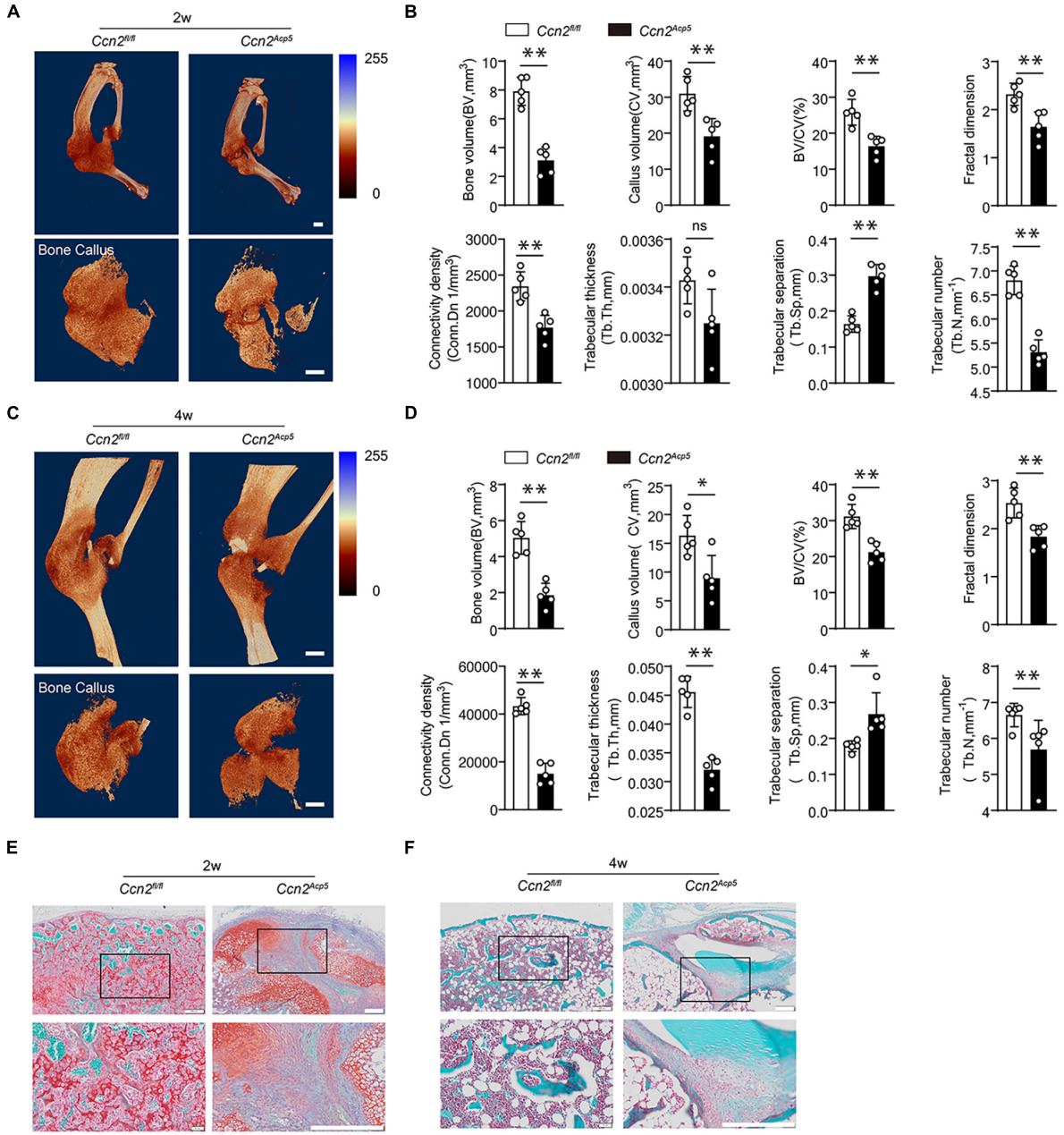

FIGURE 3 | CTGF from preosteoclasts induces callus formation during bone healing. CTGF floxed mice (*Ccn2*$^{fl/fl}$ mice) were crossed with Acp5-Cre mice to generate TRAP lineage-specific Ccn2 deletion mice (*Acp5-Cre; Ccn2* $^{fl/fl}$, short as *Ccn2*^{Acp5}). The tibial fractures were induced on 8-week-old *Ccn2*^{Acp5} mice and *Ccn2*$^{fl/fl}$ mice. **(A)** Representative 3D micro-computer tomography (μCT) images of tibia bone callus 14 days post fractures in *Ccn2*$^{fl/fl}$ and *Ccn2*^{Acp5} mice. Scale bars, 2 mm. **(B)** Quantitative μCT analysis of **(A)**. **(C)** Representative 3D micro-computer tomography (μCT) images of tibia bone callus 28 days post fractures in *Ccn2*$^{fl/fl}$ and *Ccn2*^{Acp5} mice. Scale bars, 2 mm. **(D)** Quantitative μCT analysis of **(C)**. The μCT parameters includes CV (callus volume), BV (bone volume), BV/CV, FD (Fractal dimension), Tb.Th (trabecular thickness), Tb.Sp (trabecular separation), Tb.N (trabecular number), and Conn.Dn (Connectivity density). **(E)** Representative images of tibia callus Safranin O/Fast green staining on 14 days post fractures in *Ccn2*$^{fl/fl}$ and *Ccn2*^{Acp5} mice. Scale bars, 200 μm. **(F)** Representative images of tibia callus Safranin O/Fast green staining on 28 days post fractures in *Ccn2*$^{fl/fl}$ and *Ccn2*^{Acp5} mice. Scale bars, 200 μm. Data are expressed as mean ± SD. $^{*}P < 0.05$, $^{**}P < 0.01$.

with those of the CFE assay. Blocking αVβ5 activity significantly reduced the effect of CTGF on PSC chondrogenesis (**Figure 5B** middle panel, **Figure 5D**). Next, RT-qPCR was used to detect the expression of pluripotent genes and cartilage marker genes. After CTGF stimulation, αVβ5 blockade significantly decreased the expression of the pluripotent genes *Sox2*, *Oct4*, and *Nanog*. αVβ5 blockade also decreased the expression of the chondrogenic marker genes *Sox9* and *Col2a1* (**Figure 5E**).

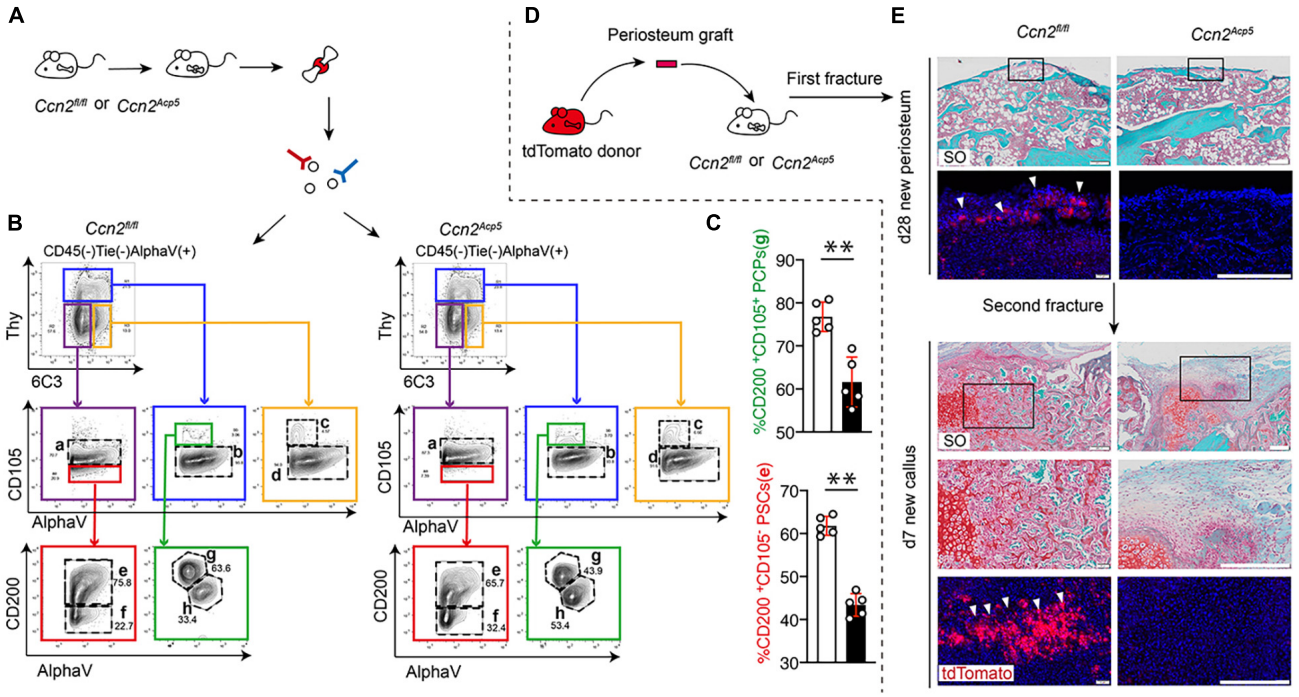

FIGURE 4 | CTGF from preosteoclasts is required to maintain the pool of PSCs and commit PSCs to chondrogenic lineage. After performing fractures on *Ccn2*^{Acp5} mice and *Ccn2*$^{fl/fl}$ controls, the callus tissue was dissected and digested for Flow cytometry analysis **(A)**. Representative plots **(B)** and quantification **(C)** of [CD45$^-$ Ter-119$^-$ Tie2$^-$ AlphaV$^+$ Thy$^-$ 6C3$^-$ CD105$^-$CD200$^+$] PSCs and [CD45$^-$ Ter-119$^-$ Tie2$^-$ AlphaV$^+$ Thy$^-$ 6C3$^-$ CD105$^+$CD200$^+$] PCPs in the bone callus. **(D)** Schematic diagram of separating the periosteal graft from Tomato donor mice and transplanting it to the fracture site of *Ccn2*^{Acp5} mice and *Ccn2*$^{fl/fl}$ controls. **(E)** Representative images of SO staining and DAPI/tdTomato immunofluorescence of fracture tibia after transplantation with tdTomato periosteal graft. In the new periosteum formed 28 days after the fracture, high magnification shows that the scarce periosteum-derived tdTomato$^+$ cells are integrated into the new periosteum (white arrow). After the second fracture, a large number of tdTomato$^+$ cells derived from periosteum were found in day 7 callus and formed cartilage tissue (white arrow). Scale bars, 200 μm. Data are shown as mean ± SD. $^{**}P < 0.01$.

αVβ3 directly upregulates the expression of pluripotent genes through c-Jun; therefore, we hypothesized that CTGF affects c-Jun expression through αVβ5. To verify this hypothesis, we first used western blotting to determine whether CTGF directly increases the c-Jun protein level and phosphorylated c-Jun also significantly increases after the introduction of CTGF (**Figure 6A**). Smad3 is the core controller of chondrocyte differentiation. Western blotting found that CTGF significantly upregulates the protein and phosphorylation levels of Smad3 (**Figure 6A**). To further investigate whether CTGF functions through c-Jun and Smad3, three different siRNAs targeting c-Jun and Smad3 were introduced into the PSCs. RT-qPCR results showed that the siRNAs targeting *Jun* and *Smad3* effectively reduced the expression of c-Jun and Smad3 (**Supplementary Figure 2A**). The Western blotting revealed that c-Jun and Smad3 knockdown downregulates pluripotent gene expression and cartilage marker gene expression, respectively (**Figures 6B,C**). The αβ integrins usually function through the FAK-Src axis. We found that the Src inhibitor PP2 significantly reduced Src phosphorylation caused by rCTGF (**Supplementary Figure 2B**). To investigate the mechanism of action of CTGF on c-Jun and Smad3 promoter activities, the promoter sequences of c-Jun and Smad3 were cloned into the dual fluorescein reporter gene vector. The αVβ5 blockade and administration of the Src inhibitor PP2 inhibited c-Jun and Smad3 promoter activities, respectively (**Figures 6D,E**). The mechanism of CTGF on PSCs is shown in **Figure 6F**.

DISCUSSION

A new era of bone regeneration-related research has begun with the identification of a series of skeletal stem cells (SSCs) (Chan et al., 2018; Duchamp De Lageneste et al., 2018; Gulati et al., 2018). SSCs in the periosteum that are capable of full-time intramembranous osteogenesis are called PSCs (Debnath et al., 2018). Lineage tracking and renal capsule transplantation experiments have shown that the most important cell source in endochondral ossification in the fracture area is PSCs from the periosteum rather than the BMSCs (Duchamp De Lageneste et al., 2018). PSCs isolated from the periosteum at baseline rarely differentiate into chondrocytes, whereas those isolated from the bone injury site mediate endochondral ossification when transplanted into the kidney capsule model (Chan et al., 2018; Duchamp De Lageneste et al., 2018). This proves that

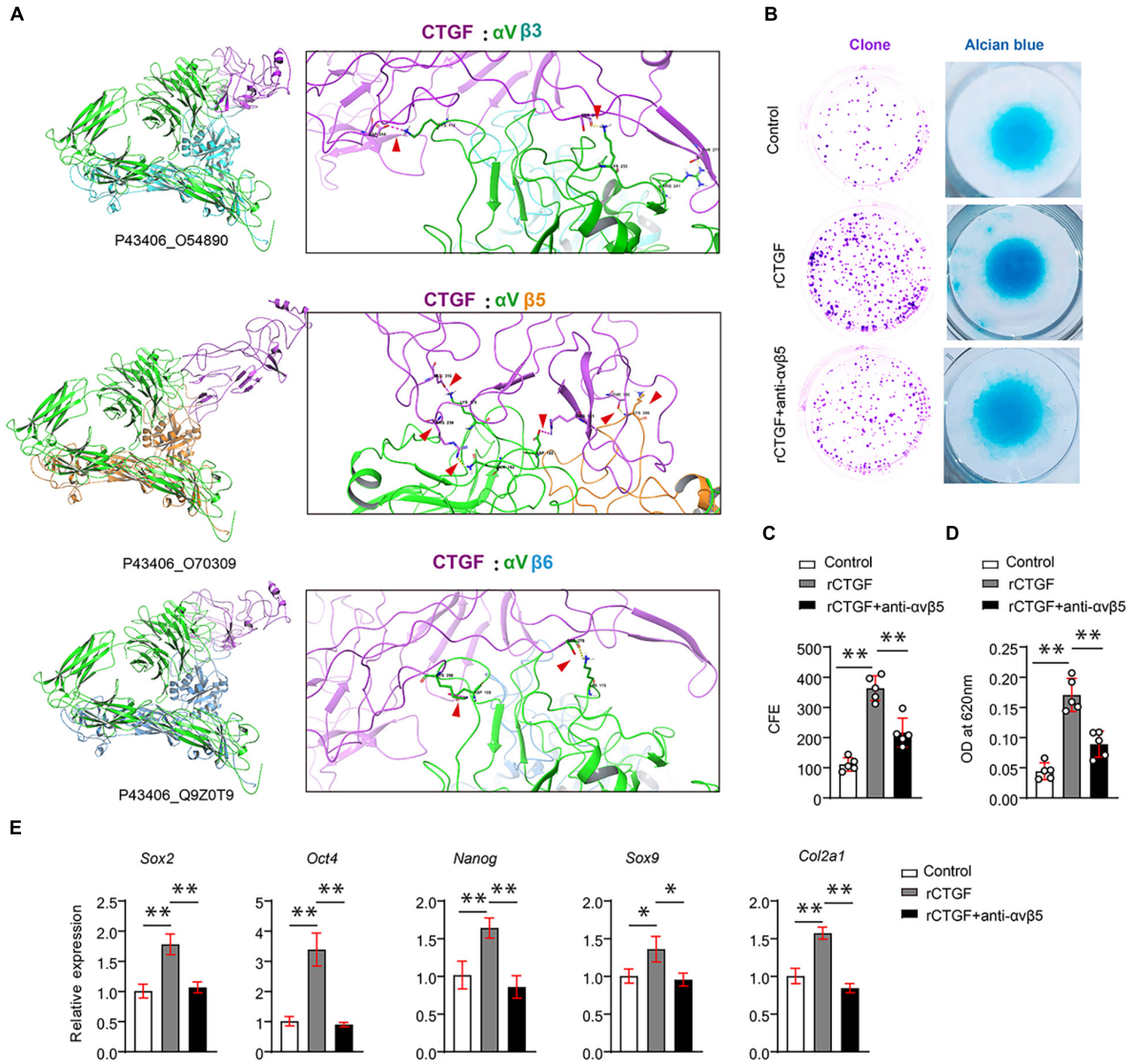

FIGURE 5 | CTGF induces PSCs renewal and chondrogenesis via αVβ5. **(A)** Results of protein docking showed that the ternary complex structure of αVβ5 (P43406_O70309) and CTGF had the largest binding surface, followed by Q9Z0T9, and O54890 was the worst. **(B)** Representative images of clone formation efficiency (CFE) and Alcian blue staining. **(C)** Quantitative analysis of the CFE. **(D)** Quantitative analysis of Alcian blue staining 620 nm absorbance. **(E)** Quantitative PCR analysis of *Sox2*, *Oct4*, *Nanog*, *Sox9*, and *Col2a1* after recombinant CTGF (rCTGF) treatment with or without anti-αVβ5 antibody. Data are shown as mean ± SD. $^{*}P < 0.05$, $^{**}P < 0.01$.

PSCs are activated to mediate endochondral ossification during bone defects (Debnath et al., 2018). This study investigated the mechanism by which PSCs are activated during bone defects. Our results demonstrated that CTGF from TRAP-positive monocytes induces bone callus formation during fracture healing. TRAP-positive monocytes locate at the periosteal and endosteal bone surface through fracture healing. The secreted CTGF directs PSC renewal and commitment to chondrogenic lineage after injury.

The periosteum is a local source of SSCs for bone repair (Debnath et al., 2018; Wang et al., 2019). It is a microvascular connective tissue that covers the outer surface of the cortical bone. The periosteum provides a special microenvironment that promotes bone growth and remodeling (Raggatt et al., 2014). Osteoclasts are abundant on the bone surface. Most osteoclasts in the periosteum are TRAP-positive monocytes and are important for bone remodeling and regeneration. PDGF-BB derived from TRAP-positive precursor osteoclasts on the bone surface can couple angiogenesis in time and space in bone growth and remodeling. TRAP-positive monocyte-conditioned medium induces MSC and EPC migration and enhances angiogenesis. PDGF-BB from periosteal precursor osteoclasts stimulates S1P secretion to promote bone formation, which further couples angiogenesis with bone formation in the periosteal environment (Xie et al., 2014). We achieved similar results and proved that

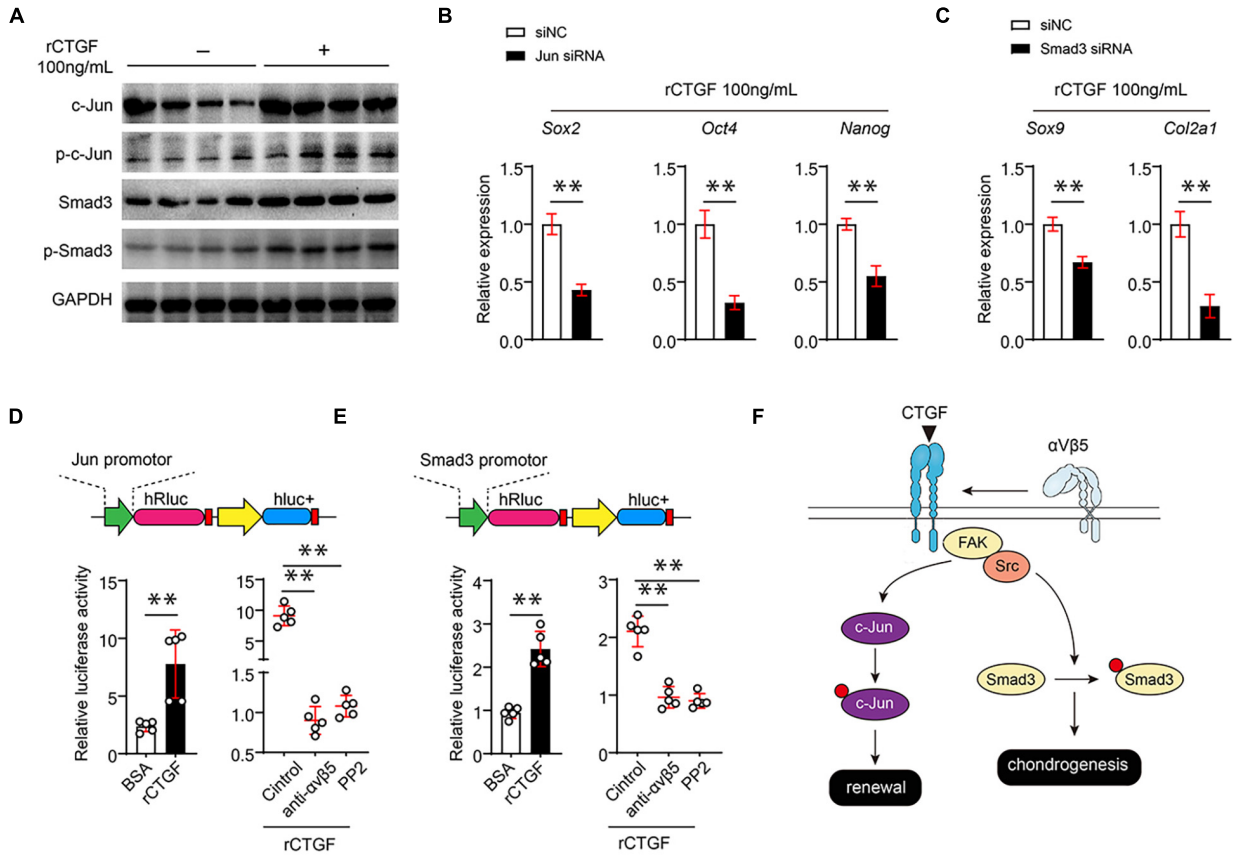

FIGURE 6 | CTGF directly induces the transcriptional activity of c-Jun and Smad3 αVβ5-FAK/Src axis. **(A)** Representative images of western blot of c-Jun, p-c-Jun, Smad3, and p-Smad3 of PSCs treated with or without rCTGF. **(B)** Quantitative PCR analysis of *Sox2*, *Oct4*, and *Nanog* of PSCs treated with rCTGF with or without c-Jun siRNA. **(C)** Quantitative PCR analysis of *Sox9* and *Col2a1* after rCTGF treatment with or without Smad3 siRNA. **(D,E)** The 1,000 bp upstream of the Jun transcription start site (TSE) was cloned in front of the firefly luciferin expression gene (hRluc). rCTGF was added to study its effect on the transcription of Jun and Smad3. At the same time, αVβ5 neutralizing antibody and Src inhibitor PP1 were used to study the effect of αVβ5-FAK/Src axis on the transcription of Jun and Smad3 by rCTGF. The ratio of hRluc to hluc were detected for quantitative statistics. **(F)** Data are shown as mean ± SD. $^{**}P < 0.01$.

TRAP cells not only play a role in physiological bone remodeling but also promote PSC self-renewal during fracture healing. Our study proves that TRAP cells constitute the niche in the periosteum of PSCs, which are vital for maintaining PSCs in injury and baseline.

CTGF, a CCN family member, performs chemotaxis, induces adhesion, and regulates cell proliferation and migration (Ramazani et al., 2018; Shen et al., 2021). CTGF also regulates bone formation in the cartilage (Takigawa et al., 2003). Moreover, it plays a role in endochondral osteogenesis by regulating almost all types of cells (Takigawa, 2013). CTGF stimulates the proliferation and differentiation of chondrocytes on the growth plate and promotes their hypertrophy to form a calcified matrix. Recombinant CTGF promotes osteoblast proliferation, differentiation, and calcification (Nishida et al., 2000). CTGF promotes the proliferation, adhesion, migration, and lumen formation of vascular endothelial cells (Markiewicz et al., 2011). The main role of CTGF is to promote chondrocyte differentiation. CTGF overexpression in transgenic mice can accelerate endochondral ossification by promoting the proliferation and differentiation of growth plate chondrocytes and promote the increase in the length of their long bones (Tomita et al., 2013). CTGF promotes the differentiation of various chondrocytes, including articular chondrocytes. Another study showed that cartilage-specific CTGF overexpression in transgenic mice can prevent osteoarthritis (Macdonald et al., 2021). Our study proves that CTGF functions by acting on αVβ5 on PSCs. The activated αVβ5 enhances the transcriptional activity of c-Jun and Smad3 through the FAK-Src axis, thereby promoting the expression of pluripotent genes and cartilage marker genes.

The present research has several limitations. The detailed mechanism by which CTGF stimulates PSC activation, such as the cell cycle regulation mechanism, has not been studied. Moreover, high-throughput methods such as gene sequencing and single-cell sequencing should be used to further study the complete molecular mechanism underlying the effect of CTGF on PSCs.

In this study, we demonstrated that TRAP-positive monocytes secrete CTGF to active PSCs during bone regeneration.

CTGF from TRAP-positive monocytes promotes endochondral ossification and activates PSCs in mouse bone fracture models. CTGF induces c-Jun expression through αVβ5 integrin, and c-Jun directly activates the transcription of the pluripotent genes *Nanog*, *Sox2*, and *Oct4*. Our research shows that TRAP-positive monocyte-derived CTGF promotes bone healing by activating PSC and directing lineage orientation. Developing technologies targeting PSCs and TRAP-positive monocytes may be an effective strategy to prevent non-union.

DATA AVAILABILITY STATEMENT

The original contributions presented in the study are included in the article/**Supplementary Material**, further inquiries can be directed to the corresponding author/s.

ETHICS STATEMENT

The animal study was reviewed and approved by the Laboratory Animal Welfare and Ethics Committee of Third Military Medical University.

AUTHOR CONTRIBUTIONS

YB conceived the idea, conducted most of the experiments, and prepared the manuscript. TY collected some specimens and did some of the experiments. TY, SD, and JT helped with processing some of the statistical results. JD and YY provided suggestions for experiments. QD helped in planning the projects and provided suggestions for experiments. SD and JX supervised the project, reviewed, and edited the manuscript. All authors have read and approved the manuscript.

FUNDING

This work was funded by grants from the Nature Science Foundation of China (81902218, 81972082, and 81772365).

SUPPLEMENTARY MATERIAL

The Supplementary Material for this article can be found online at: https://www.frontiersin.org/articles/10.3389/fcell.2021.730095/full#supplementary-material

REFERENCES

Arnott, J. A., Lambi, A. G., Mundy, C., Hendesi, H., Pixley, R. A., Owen, T. A., et al. (2011). The role of connective tissue growth factor (CTGF/CCN2) in skeletogenesis. *Crit. Rev. Eukaryot. Gene Expr.* 21, 43–69. doi: 10.1615/critreveukargeneexpr.v21.i1.40

Carlstrom, M., Wilcox, C. S., and Arendshorst, W. J. (2015). Renal autoregulation in health and disease. *Physiol. Rev.* 95, 405–511. doi: 10.1152/physrev.00042.2012

Chan, C. K. F., Gulati, G. S., Sinha, R., Tompkins, J. V., Lopez, M., Carter, A. C., et al. (2018). Identification of the human skeletal stem cell. *Cell* 175, 43–56.e21.

Chan, C. K., Seo, E. Y., Chen, J. Y., Lo, D., Mcardle, A., Sinha, R., et al. (2015). Identification and specification of the mouse skeletal stem cell. *Cell* 160, 285–298. doi: 10.1016/j.cell.2014.12.002

Debnath, S., Yallowitz, A. R., Mccormick, J., Lalani, S., Zhang, T., Xu, R., et al. (2018). Discovery of a periosteal stem cell mediating intramembranous bone formation. *Nature* 562, 133–139. doi: 10.1038/s41586-018-0554-8

Dong, R., Bai, Y., Dai, J., Deng, M., Zhao, C., Tian, Z., et al. (2020). Engineered scaffolds based on mesenchymal stem cells/preosteoclasts extracellular matrix promote bone regeneration. *J. Tissue Eng.* 11:204173142092 6918.

Duchamp De Lageneste, O., Julien, A., Abou-Khalil, R., Frangi, G., Carvalho, C., Cagnard, N., et al. (2018). Periosteum contains skeletal stem cells with high bone regenerative potential controlled by Periostin. *Nat. Commun.* 9:773.

Gulati, G. S., Murphy, M. P., Marecic, O., Lopez, M., Brewer, R. E., Koepke, L. S., et al. (2018). Isolation and functional assessment of mouse skeletal stem cell lineage. *Nat. Protoc.* 13, 1294–1309. doi: 10.1038/nprot.2018.041

Ho-Shui-Ling, A., Bolander, J., Rustom, L. E., Johnson, A. W., Luyten, F. P., and Picart, C. (2018). Bone regeneration strategies: engineered scaffolds, bioactive molecules and stem cells current stage and future perspectives. *Biomaterials* 180, 143–162. doi: 10.1016/j.biomaterials.2018.07.017

Hu, D. P., Ferro, F., Yang, F., Taylor, A. J., Chang, W., Miclau, T., et al. (2017). Cartilage to bone transformation during fracture healing is coordinated by the invading vasculature and induction of the core pluripotency genes. *Development* 144, 221–234. doi: 10.1242/dev.130807

Li, Z., Meyers, C. A., Chang, L., Lee, S., Li, Z., Tomlinson, R., et al. (2019). Fracture repair requires TrkA signaling by skeletal sensory nerves. *J. Clin. Invest.* 129, 5137–5150.

Macdonald, I. J., Huang, C. C., Liu, S. C., Lin, Y. Y., and Tang, C. H. (2021). Targeting CCN proteins in rheumatoid arthritis and osteoarthritis. *Int. J. Mol. Sci.* 22:4340, doi: 10.3390/ijms22094340

Markiewicz, M., Nakerakanti, S. S., Kapanadze, B., Ghatnekar, A., and Trojanowska, M. (2011). Connective tissue growth factor (CTGF/CCN2) mediates angiogenic effect of S1P in human dermal microvascular endothelial cells. *Microcirculation* 18, 1–11. doi: 10.1111/j.1549-8719.2010.00058.x

Nishida, T., Nakanishi, T., Asano, M., Shimo, T., and Takigawa, M. (2000). Effects of CTGF/Hcs24, a hypertrophic chondrocyte-specific gene product, on the proliferation and differentiation of osteoblastic cells in vitro. *J. Cell. Physiol.* 184, 197–206. doi: 10.1002/1097-4652(200008)184:2<197::aid-jcp7>3.0.co;2-r

Perbal, B. (2004). CCN proteins: multifunctional signalling regulators. *Lancet* 363, 62–64. doi: 10.1016/s0140-6736(03)15172-0

Raggatt, L. J., Wullschleger, M. E., Alexander, K. A., Wu, A. C., Millard, S. M., Kaur, S., et al. (2014). Fracture healing via periosteal callus formation requires macrophages for both initiation and progression of early endochondral ossification. *Am. J. Pathol.* 184, 3192–3204. doi: 10.1016/j.ajpath.2014.08.017

Ramazani, Y., Knops, N., Elmonem, M. A., Nguyen, T. Q., Arcolino, F. O., Van Den Heuvel, L., et al. (2018). Connective tissue growth factor (CTGF) from basics to clinics. *Matrix Biol.* 68–69, 44–66. doi: 10.1016/j.matbio.2018.03.007

Shen, Y. W., Zhou, Y. D., Chen, H. Z., Luan, X., and Zhang, W. D. (2021). Targeting CTGF in cancer: an emerging therapeutic opportunity. *Trends Cancer* 7, 511–524. doi: 10.1016/j.trecan.2020.12.001

Takigawa, M. (2013). CCN2: a master regulator of the genesis of bone and cartilage. *J. Cell Commun. Signal.* 7, 191–201. doi: 10.1007/s12079-013-0204-8

Takigawa, M., Nakanishi, T., Kubota, S., and Nishida, T. (2003). Role of CTGF/HCS24/ecogenin in skeletal growth control. *J. Cell. Physiol.* 194, 256–266. doi: 10.1002/jcp.10206

Tang, Y., Wu, X., Lei, W., Pang, L., Wan, C., Shi, Z., et al. (2009). TGF-beta1-induced migration of bone mesenchymal stem cells couples bone resorption with formation. *Nat. Med.* 15, 757–765. doi: 10.1038/nm.1979

Tomita, N., Hattori, T., Itoh, S., Aoyama, E., Yao, M., Yamashiro, T., et al. (2013). Cartilage-specific over-expression of CCN family member 2/connective tissue growth factor (CCN2/CTGF) stimulates insulin-like growth factor expression and bone growth. *PLoS One* 8:e59226. doi: 10.1371/journal.pone.0059226

Vi, L., Baht, G. S., Soderblom, E. J., Whetstone, H., Wei, Q., Furman, B., et al. (2018). Macrophage cells secrete factors including LRP1 that orchestrate the rejuvenation of bone repair in mice. *Nat. Commun.* 9: 5191.

Wang, L., Tower, R. J., Chandra, A., Yao, L., Tong, W., Xiong, Z., et al. (2019). Periosteal mesenchymal progenitor dysfunction and extraskeletally-derived fibrosis contribute to atrophic fracture nonunion. *J. Bone Miner. Res.* 34, 520–532. doi: 10.1002/jbmr.3626

Xie, H., Cui, Z., Wang, L., Xia, Z., Hu, Y., Xian, L., et al. (2014). PDGF-BB secreted by preosteoclasts induces angiogenesis during coupling with osteogenesis. *Nat. Med.* 20, 1270–1278. doi: 10.1038/nm.3668

Conflict of Interest: The authors declare that the research was conducted in the absence of any commercial or financial relationships that could be construed as a potential conflict of interest.

frontiers in Cell and Developmental Biology

MINI REVIEW
published: 20 September 2021
doi: 10.3389/fcell.2021.710203

Advances in Chromodomain Helicase DNA-Binding (CHD) Proteins Regulating Stem Cell Differentiation and Human Diseases

Caojie Liu, Ning Kang, Yuchen Guo and Ping Gong**

State Key Laboratory of Oral Diseases, West China School of Stomatology, Sichuan University, Chengdu, China

Background: Regulation of gene expression is critical for stem cell differentiation, tissue development, and human health maintenance. Recently, epigenetic modifications of histone and chromatin remodeling have been verified as key controllers of gene expression and human diseases.

Objective: In this study, we review the role of chromodomain helicase DNA-binding (CHD) proteins in stem cell differentiation, cell fate decision, and several known human developmental disorders and cancers.

Conclusion: CHD proteins play a crucial role in stem cell differentiation and human diseases.

Keywords: epigenetic, chromodomain helicase DNA-binding protein, chromatin remodeling, histone modification, CHARGE syndrome

OPEN ACCESS

Edited by:
Ce Dou,
Army Medical University, China

Reviewed by:
Fernando Moreira Simabuco,
State University of Campinas, Brazil
Shaohua Ge,
Shandong University, China

****Correspondence:***
Yuchen Guo
dent.guo@qq.com
Ping Gong
dentistgong@hotmail.com

Specialty section:
This article was submitted to Cellular Biochemistry, a section of the journal Frontiers in Cell and Developmental Biology

Received: *15 May 2021*
Accepted: *29 July 2021*
Published: *20 September 2021*

Citation:
Liu C, Kang N, Guo Y and Gong P (2021) Advances in Chromodomain Helicase DNA-Binding (CHD) Proteins Regulating Stem Cell Differentiation and Human Diseases. Front. Cell Dev. Biol. 9:710203. doi: 10.3389/fcell.2021.710203

INTRODUCTION OF CHD SUPERFAMILY

There are three classes of epigenetic modifier proteins, including chromatin writers, erasers, and readers. We center around a chromatin reader superfamily and review their functions and structures as well as known roles in human diseases. In eukaryotic organisms, ATP-dependent chromatin remodeling enzymes are commonly divided into three major superfamilies, including SWItch/sucrose non-fermentable (SWI/SNF), Imitation SWI (ISWI), and chromodomain helicase DNA-binding (CHD) proteins (Dann et al., 2017; Barisic et al., 2019).

CHD comprises nine proteins, which are classified as three subfamilies on account of domain homology. These nine CHDs all involve tandem chromatin organization modifier domains (chromodomain) as well as sucrose non-fermentable2 (SNF2)-like ATP-dependent helicase domains (Flanagan et al., 2005; Bajpai et al., 2010; He et al., 2016; Farnung et al., 2017). Recently, a study reviewed the structure of these four domains and the differences between CHDs (Mills, 2017; Goodman and Bonni, 2019). CHDs read and/or interpret histone modifications by specialized domains. When reading the chromatin state, CHDs disrupt the DNA–histone interaction via translocating the nucleosomes along the same or the other DNA strand (Clapier et al., 2017; Mashtalir et al., 2018).

CHDs share highly similar helicase-ATPase domains with the SWItch2/SNF2 superfamily (Noh et al., 2015; Mashtalir et al., 2018). These helicase-ATPase domains provide energy. At the same time, they promote disruption of histone-DNA contacts as mentioned above (Clapier et al., 2017; Mashtalir et al., 2018). Moreover, the three subfamilies described above are defined by specific

domains (**Figure 1**). Briefly, subfamily I, including CHD1 and 2, share DNA-binding domains that demonstrate similar function with SWI3, ADA2. Subfamily II, including CHD3-5, contain the PHD zinc finger domain in addition to the three domains mentioned above, which promotes its binding to methylated histone residues and protein cofactors. Subfamily III, including CHD6-9, its specific SANT domain could promote non-specific DNA binding (Mills, 2017; Platt et al., 2017).

Chromodomains were first recognized in *Drosophila* heterochromatin protein 1. Heterochromatin protein 1 owns a chromodomain that binds to nucleosomes to facilitate a closed chromatin state as well as regulate homeotic genes (Flanagan et al., 2005; Farnung et al., 2017; Zhao et al., 2020). It is known nowadays that binding to methylated histone residues is the primary function of chromodomains. CHDs contain a special variant of the chromodomains with methy1-binding cages, which promote interactions with H3K4me (Flanagan et al., 2005; Dann et al., 2017; Barisic et al., 2019). For instance, CHD1 chromodomains interact with H3K4me, and CHD5 chromodomains bind to H3K27me3 (Dorighi and Tamkun, 2013; Link et al., 2018; Goodman and Bonni, 2019). Therefore, CHDs demonstrate special functions and preferences for active or repressive histone marks. CHD chromodomains are essential for proper gene expression and maintaining dynamic chromatin structures.

CHD AND STEM CELLS

CHD superfamily proteins are essential to regulate gene expression. Thus, CHDs are crucial for the survival, maintenance, and proliferation of stem cells as well as regulating the cell fate of their daughter cells (**Figure 2**).

Embryonic Stem Cells (ESCs)

ESCs demonstrate an open chromatin environment. Via activation or repression of different genetic pathways, ESCs differentiate toward mesenchymal, hematopoietic, neural, and other lineage cells. By maintaining open chromatin, CHD1 participates in the mediator complex, a regulator of ESCs (Gaspar-Maia et al., 2009; Bulut-Karslioglu et al., 2018). This complex is a multiprotein complex that pre-initiates gene transcription through binding to CHD1 and recruiting it to express genes (de Dieuleveult et al., 2016; Percharde et al., 2017). If lacking CHD1, chromatin would condense to form heterochromatin. In that case, due to increased ectodermal lineage gene expression and decreased endodermal lineage gene expression, pluripotent differentiation would be impaired (Lin et al., 2011; Koh et al., 2015; Suzuki et al., 2015). Furthermore, induction of *CHD1* is necessary for efficient programming of induced pluripotent stem cells (de Dieuleveult et al., 2016; Percharde et al., 2017; Bulut-Karslioglu et al., 2018). Therefore, CHD1 is essential to maintain pluripotency in stem cells.

By regulating epigenetic and signaling pathways, CHD7 is also crucial for cell fate decisions. In mouse ESCs, the *Chd7* gene is highly expressed and associated with gene expression active signals. In stem and progenitor cells, the euchromatic chromatin environment is poised between activation and repression (Yang et al., 2017). Different from active or inactive states, those promoters as well as enhancers typically express both active and inactive marks (Schnetz et al., 2009; Yang et al., 2017). Via binding to active as well as poised enhancers of ectodermal lineage genes, CHD7 plays an important role in histone modifying, transcription factor recruiting, and other chromatin remodeling (Platt et al., 2017; Goodman and Bonni, 2019). Meanwhile, it promotes open chromatin at enhancers of critical genes such as *Sox2, Nanog,* and *Oct4* (Engelen et al., 2011; Puc and Rosenfeld, 2011; Fujita et al., 2016).

In brief, the CHD family is essential to regulating the function of ESCs.

Neural Stem Cells (NSCs)

NSCs produce both neuron and supporting cells and, thus, play a pivotal role in the nervous system as well as sensory organs. In the dentate gyrus of the hippocampus and subventricular zone of the forebrain, CHD4, CHD5, and CHD7 cooperate with signaling pathways and transcription factors, which are critical for the differentiation and function of NSC niches (Feng et al., 2017; Weiss et al., 2020; Parenti et al., 2021).

Binding to the polycomb repressive complex 2 (PRC2) during cortical neurogenesis, CHD4 was found to express in the murine subventricular zone neural progenitor (Mohd-Sarip et al., 2017; Pierson et al., 2019; Shieh et al., 2020). This complex represses the expression of glial fibrillary acidic protein gene (*Gfap)* as well as blocks glial differentiation (Dorighi and Tamkun, 2013; Sparmann et al., 2013). During neurogenesis, this complex promotes neuronal differentiation by inhibiting the *Gfap* locus (Sparmann et al., 2013). Moreover, CHD4, together with other nucleosome remodeling and deacetylase (NuRD) complex, can repress several genes that downregulate neuronal differentiation (Mohd-Sarip et al., 2017; Link et al., 2018; Pierson et al., 2019; Shieh et al., 2020).

CHD5 also binds to PRC2 and H3K27me3 in NSCs (Egan et al., 2013; Xie et al., 2015; Hayashi et al., 2016). In the subventricular and subgranular zones in the hippocampus, high expression of CHD5 is found in neuroblast cells as well as neural progenitors (Egan et al., 2013). CHD5 is pivotal for learning and memory. It is also found that depletion of *Chd5* in the developing cortex leads to reduction of migratory neuroblasts (Egan et al., 2013).

CHD7 is also vital for fine function of NSCs. CHD7 is highly expressed in both the subgranular and subventricular zones in adult mice. In these areas, CHD7 colocalizes with markers of NSCs, neural progenitor cells, and neuroblasts (Feng et al., 2017; Goodman and Bonni, 2019). Studies in which *Chd7* was conditionally deleted in the adult subventricular zone demonstrate that CHD7 deletion resulted in a reduction of mature dopaminergic NSCs (Feng et al., 2013). Such *Chd7* deficiency also downregulates the expression of proneural genes, such as *Sox4* and *Sox11* (Feng et al., 2013; Brajadenta et al., 2019). Conditional knockout of *Chd7* in the subgranular zone also reduces neurogenesis (Feng et al., 2013). Furthermore, in the otic placodes and olfactory, CHD7 promotes NSC progenitor proliferation (Jones et al., 2015; Ohta et al., 2016;

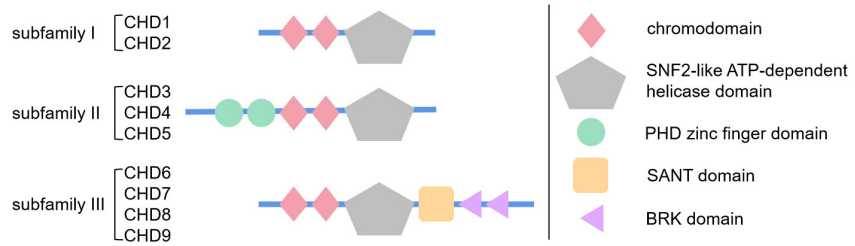

FIGURE 1 | Schematic diagram showing the structure and specific domains of three subfamilies of chromodomain helicase DNA-binding (CHD) proteins. This figure briefly demonstrates the basic structure and domains of CHD protein family. As is reviewed in section "Introduction of CHD Superfamily" of this article, CHD proteins are mainly divided in three subfamilies by their specific domains, subfamily I with basic chromodomian and sucrose non-fermentable2 (SNF2)-like ATP-dependent helicase domain, subfamily II with additional PHD zinc finger domain, and subfamily III with additional SANT domain and BRK domain. The simple geometric patterns represent the protein domains, whose size or location are not strictly to scale, just for brief demonstration.

Whittaker et al., 2017). CHD7 is critical for NSC function although the mechanisms by which CHD7 regulates NSC function remain to be determined.

Mesenchymal Stem Cells (MSCs)

As a kind of multipotent mesoderm-derived cell differentiating into myoblasts, adipocytes, osteoblasts, and chondrocytes, MSCs are shown to be regulated by CHD proteins (Mohd-Sarip et al., 2017). Several different CHD proteins regulate the differentiation of MSCs into four distinct lineages. CHD2 is critical for induction of myogenic cell fates (Harada et al., 2012; de Dieuleveult et al., 2016; Semba et al., 2017; Nieto-Estevez and Hsieh, 2018). CHD9 could bind to osteocalcin, which is one of the master transcriptional factors for bone development, and promote its expression (Shur et al., 2006a,b; de Dieuleveult et al., 2016). Recently, we found that CHD7 is essential for osteogenic differentiation of human MSCs. Depletion of *CHD7* via siRNA impairs the osteogenesis potential of MSCs, and overexpression of *CHD7* via lentivirus vector could promote the osteogenesis potential of MSCs. Mechanically, we found that CHD7 might bind to the enhancer of *Sp7*, and it also interacts with SMAD1, indicating that CHD7 is crucial to the osteogenesis potential of MSCs (Chen et al., 2016).

Besides the above-described biological processes, the CHD family also affect the development and functional maintenance of many organ systems, such as the hematopoietic and circulatory systems (Koh et al., 2015; Sperlazza et al., 2015; Zhen et al., 2017; Arends et al., 2019; Hsu et al., 2020; Tu et al., 2021). For example, CHD7 promotes the osteogenesis potential of dental follicle cells to form cementum by upregulating the PTH/PTH1R signaling pathway (Liu et al., 2020).

CHD AND HUMAN DISEASES

CHD in Neurodevelopmental Disorders (NDDs)

Due to the important regulatory role of the CHD family in the differentiation and function of NSCs, the deletion or mutation of CHD genes often leads to NDDs, featuring as intellectual disability (ID), autism spectrum disorders (ASDs), and epilepsy.

Several *CHD*, such as *CHD2*, *CHD6*, *CHD7*, and *CHD8*, were found non-sense, heterozygous, or other kinds of mutations in patients with ASD, ID, and epilepsy (Allen et al., 2013; Suls et al., 2013; Sugathan et al., 2014; Ellingford et al., 2021; Parenti et al., 2021). In patients with ASD and/or ID that associate with gastrointestinal disturbance and macrocephaly, 13 recurrent alleles of *CHD8* were figured out (Bernier et al., 2014; Sugathan et al., 2014; Ellingford et al., 2021). Using RNA- and ChIP-sequencing, a recent study indicates that knockdown of *CHD8* could not alter the neural ectodermal or morphology markers of neural progenitors, but could impair their gene expression (Sugathan et al., 2014; Goodman and Bonni, 2019). CHD8 was found to bind CHD7 as well as p53, regulate p53, and inhibit cell proapoptotic effects during development (Nishiyama et al., 2009; Hurley et al., 2021; Tu et al., 2021). Interestingly, CHD7 could also bind to and repress p53 (Van Nostrand et al., 2014; Corsten-Janssen and Scambler, 2017). Thus, some CHD proteins might share common target genes, interacting factors, and downstream mechanisms. CHD2 mutations were also observed in patients with epilepsy (Allen et al., 2013; Suls et al., 2013; Nieto-Estevez and Hsieh, 2018). All these data raise the possibility that the region of *CHD* mutation may be wider than the previous hypothesis. Due to the intricacy of CHD targets as well as associating partners, a main goal of future studies is making clear the mechanisms by which *CHD* mutation disturbs NSCs and neuronal development.

CHD in CHARGE Syndrome and Kallmann Syndrome

CHARGE is the acronym of an autosomal dominant genetic syndrome, which is characterized by six main symptoms, including ocular coloboma, congenital heart defects, choanal atresia, developmental retardation, genital anomalies, and ear anomalies (Pagon et al., 1981; Brajadenta et al., 2019). According to a Canadian study, this syndrome occurs in approximately 1 in 10,000 live births (Issekutz et al., 2005; Van Nostrand et al., 2014). *CHD7* has been closely linked to this disorder because heterozygous mutations in this gene were found in more than 90% of these patients (Vissers et al., 2004; Ghaoui et al., 2015; Brajadenta et al., 2019). Therefore, CHD7 is also one of the most researched members among the CHD

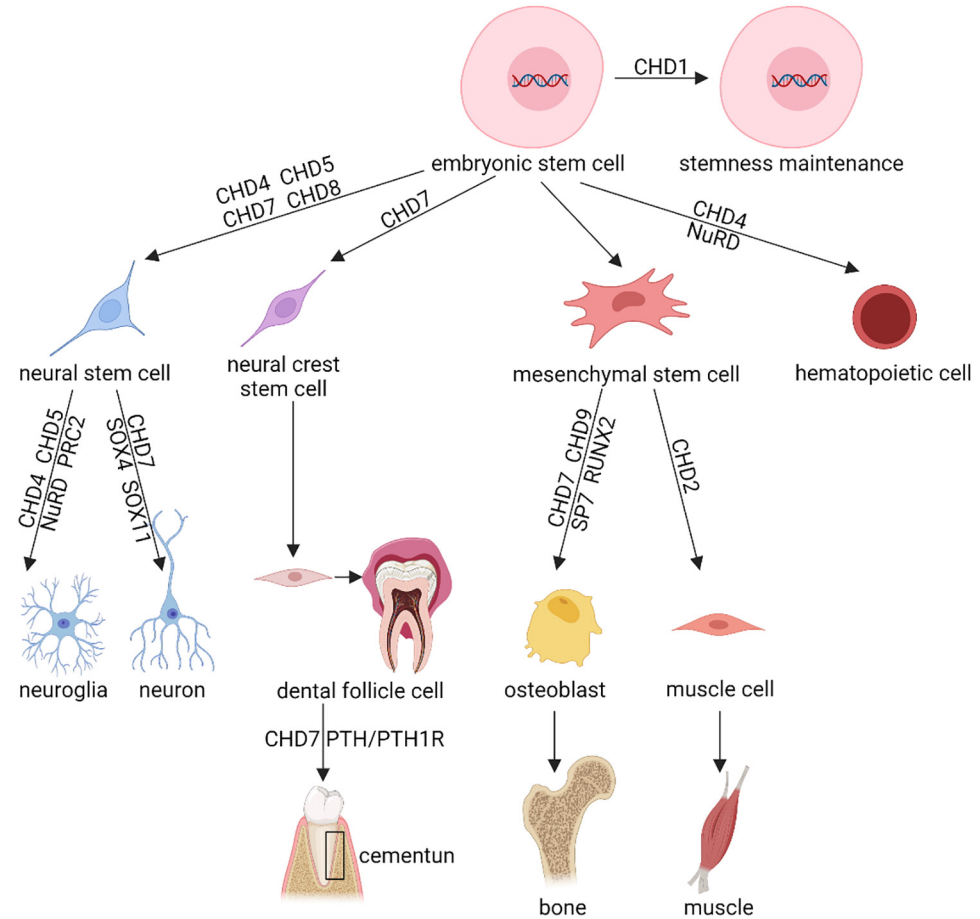

FIGURE 2 | Schematic diagram showing the regulatory effects of CHD proteins in stem cell proliferation, differentiation, and functioning. This figure briefly demonstrates the known function of the CHD protein family in various stem cells, including the stemness maintenance, cellular differentiation, lineage commitment, cell fate decision, etc. Shown are representative stem cells, e.g., Embryonic Stem Cells (ESCs), Neural Stem Cells (NSCs), neural crest stem cells, Mesenchymal Stem Cells (MSCs), reviewed in section "CHD and Stem Cells" of this article. This diagram only exhibits the certified function of CHD protein family, the uncertain or controversial effects of CHDs have been omitted. NuRD, nucleosome remodeling and deacetylase; PRC2, Polycomb Repressive Complex 2.

superfamily. The embryologic expression of CHD7 involves several sites, including eyes, olfactory bulb cells, inner ears, etc. (Vissers et al., 2004; Jamadagni et al., 2021). Additionally, high expression of *CHD7* is also observed in undifferentiated neuroepithelium and neural crest mesenchyme as mentioned above. Thus, CHARGE is a monogenic disorder with variable expressivity (Jones et al., 2015; Yan et al., 2020). However, due to the multiplicity of *CHD7* mutations as well as the variable expressivity of this syndrome, no critical genotype/phenotype correlations can be found (Bajpai et al., 2010; Butcher et al., 2017). In an *in vitro* study, intact recombinant CHD7 protein was purified and proved to be an ATP-dependent nucleosome remodeling factor (Bouazoune and Kingston, 2012; Yan et al., 2020). Interestingly, when CHARGE patients were administrated with recombinant CHD7 protein, their enzymatic activity, which is related to chromatin remodeling, reduced in a mutation-specific mode (Rother et al., 2020; Yan et al., 2020). This study supports the hypothesis that CHD7 haploinsufficiency is the main cause of CHARGE syndrome (Whittaker et al., 2017; Brajadenta et al., 2019). Although other functions of CHD7 should be discovered, these functions might help explain the clinical features in CHARGE patients.

CHD7 haploinsufficiency leads to dysfunction in sensory processes as well as impaired vision, hearing, balance, and olfaction. A mouse model has been established and analyzed to learn more about the role of CHD7 in CHARGE. *Chd7* knockout mice embryos cannot survive over embryonic day 10.5, but heterozygous mice show several similar defects observed in CHARGE syndrome (Kim et al., 2008; Gage et al., 2015; Jones et al., 2015). Moreover, there is no CHARGE syndrome patient who is figured out to have *CHD7* homozygous mutations (Vissers et al., 2004; Basson and van Ravenswaaij-Arts, 2015). These facts suggest that homozygous mutations in *CHD7* might cause embryonic lethality, possibly due to the wide expression of the *CHD7* gene in tissues affected in CHARGE syndrome (Yan et al., 2020). Using conditional $Chd7^{flox}$ allele mating with tissue-specific *Cre* transgenes, a recent study found that CHD7 is necessary for eye development in multiple embryonic tissues and

also essential for lens development in the surface ectoderm (Gage et al., 2015; Goodman and Bonni, 2019). *Chd7*$^{+/-}$ mice showed hypoplasia and aplasia of posterior and lateral semicircular canals as well as innervation defects of the vestibular sensory epithelium (Yan et al., 2020; Jamadagni et al., 2021). In all, this evidence suggests that CHD7 might play a similar role in sensory tissues as in NSCs.

As two major phenotypes observed in CHARGE syndrome patients, hyposmia and anosmia mean decrease and loss of the smell sense, respectively (Brajadenta et al., 2019; Yan et al., 2020). Olfactory deficiency is usually accompanied by aplasia or hypoplasia of the olfactory bulbs (Ghaoui et al., 2015). Through behavioral assays and electrophysiological study, *Chd7* heterozygous mice were found lacking in odor discrimination, olfactory bulb hypoplasia, and complete anosmia (Layman et al., 2009). As an essential gene in stem cell differentiation, high expression of CHD7 could be found in olfactory NSCs as well as progenitor cells (Whittaker et al., 2017; Jamadagni et al., 2021). Depletion of *Chd7* results in a significant reduction of NSC proliferation in olfactory epithelials, thus leading to a decrease in olfactory receptor neurons and delayed recovery post damage (Feng et al., 2017; Whittaker et al., 2017). Moreover, efferent neurons in the olfactory epithelium as well as olfactory bulb neurogenesis from the subventricular NSC niches of such mutant mice are impaired, resulting in the reduction of tyrosine hydroxylase-positive interneurons in the olfactory bulb (Ohta et al., 2016; Feng et al., 2017). Taken together, olfactory processing counts on CHD7 function.

Through co-IP and chromatin immunoprecipitation studies, CHD7 was proved to interact with *SOX2*, which associated with several diseases, such as Feingold syndrome, Alagille syndrome, and Pallister–Hall syndrome (Engelen et al., 2011; Puc and Rosenfeld, 2011; Fujita et al., 2016). These syndromes share several similar phenotypes with CHARGE syndrome, including tracheoesophageal defects, genital abnormalities, semicircular canal hypoplasia, and pituitary and endocrine dysfunction (Puc and Rosenfeld, 2011; Stamou et al., 2020). It is reported that CHD7 binds to SOX2 because of the massive overlap in expression as well as function of these two proteins. Besides this, CHD7 and SOX2 share similar functions in the development of ectodermal lineages that are influenced in CHARGE syndrome (Schnetz et al., 2010; Doi et al., 2017). As one of the characters of CHARGE syndrome, craniofacial malformations are also commonly observed (Van Nostrand et al., 2014; He et al., 2016). It was found that *Chd7* is necessary for proper craniofacial development via immunofluorescence and *Cre* lineage tracing (Sperry et al., 2014). Importantly, CHD7 also interacts with SMAD1 and could bind to the enhancer region of *Sp7*, which is a master transcription factor of osteogenic differentiation (Chen et al., 2016).

Besides this, CHD7 is also closely associated with Kallmann syndrome, which is a genetic heterogeneous congenital disease mainly characterized by idiopathic hypogonadotrophic hypogonadism (IHH) (Kim et al., 2008; Stamou et al., 2020). Such manifestation is largely caused by impaired gonadotropin-releasing hormone (GnRH) (Balasubramanian and Crowley, 2017; Stamou et al., 2020). The pathogenic mechanism of Kallmann syndrome is complicated and could be partially explained by several mutated genes, including the missence mutation of *CHD7*, leading to the alteration of the domain or function of CHD7 protein (Kim et al., 2008; Boehm et al., 2015). Some of the clinical symptoms of Kallmann syndrome, e.g., anosmia, IHH, heart defect, cleft lip, cleft palate, etc., also often appear in CHARGE syndrome, so these two syndromes are often compared in clinical work and need differential diagnosis (Ufartes et al., 2018; Stamou et al., 2020).

CHD in Cancers

CHD proteins are also involved in cancers. Genomic and epigenomic changes are correlated and could predict the tumor phenotypes and progression.

CHD1 was proved to be frequently deleted in prostate cancer (Attard et al., 2016; Zhang et al., 2020). Researchers conducted and analyzed whole-genome, whole-transcriptome, and DNA methylation data from patients with primary prostate cancer and healthy controls. Deletions in CHD1 occurred in 18% of the tumors (Li et al., 2020). Further studies confirm that CHD1 plays a key role in myeloid-derived suppressor cell recruitment and find that CHD1/IL6 is a major regulator of the immunosuppressive tumor microenvironment in prostate cancer (Zhao et al., 2020).

CHD4 is closely associated with breast, endometrial, and colorectal cancer (Novillo et al., 2021). As a crucial ingredient in NuRD complex, the upstream regulating effects of CHD4 involves the recruitment of DNA methyl transferase and key transcriptional repressors (Hata et al., 2019; Wang et al., 2020). CHD4 could recruit inhibitory chromatin remodelers to the DNA damage repair sites and initiate and support the silencing of tumor suppressor gene. Such functions confirm the oncogenic effect of CHD4 (Chang et al., 2019; Novillo et al., 2021). In addition, CHD4, as a co-activator of hypoxia-inducible factor (HIF), is upregulated in human breast tumors and is related to the expression of HIF target genes (Shieh et al., 2020; Wang et al., 2020). Besides this, CHD4 was associated with poorer overall survival in breast cancer patients (Novillo et al., 2021).

According to the position, expression pattern, and function of CHD5 in neuroblastoma cells and xenograft cells, CHD5 was identified as a tumor suppressor gene (Kolla et al., 2014; Liu et al., 2018). CHD5 also functions as one of the tumor suppressor genes in other types of tumors, e.g., gliomas, breast, colon, lung, ovarian, and prostate cancers (Bagchi et al., 2007; Xie et al., 2015). Especially, low expression of CHD5 is strongly associated with poorer clinical and biological characteristics and prognosis (Kolla et al., 2014; Higashi et al., 2015).

To sum up, all of the associations among these diseases emphasize the variety of cell processes that require proper chromatin remodeling.

CONCLUSION

Here, we review the CHD superfamily as well as known functions in several kinds of stem cells. The CHD family is widely involved in and regulates many physiological and biochemical pathways in

the organism, which is of great significance for normal growth, development, and functional maintenance of the body as well as the occurrence and development of several diseases. Future studies aiming at revealing the proper mechanisms by which CHDs mediate these effects will uncover more important cues about this important chromatin remodeler.

AUTHOR CONTRIBUTIONS

CL: drafting manuscript. PG: approval of article and funding secured. YG: literature summary, article revision, and funding secured. NK: concept, design, and funding secured. All authors contributed to the article and approved the submitted version.

FUNDING

This research was supported by the National Natural Science Foundation of China (NSFC Grant Nos. 81701009 and 82001017), the West China Hospital of Stomatology (Grant No. RCDWJS2020-23), and the China Postdoctoral Science Foundation Grant (Grant Nos. 2019TQ0218 and 2020M683328).

ACKNOWLEDGMENTS

We appreciate the website BioRender for the technical support in schematic diagram drawing (https://app.biorender.com/).

REFERENCES

Allen, A., Berkovic, S., Cossette, P., Delanty, N., Dlugos, D., Eichler, E., et al. (2013). De novo mutations in epileptic encephalopathies. *Nature* 501, 217–221. doi: 10.1038/nature12439

Arends, T., Dege, C., Bortnick, A., Danhorn, T., Knapp, J., Jia, H., et al. (2019). CHD4 is essential for transcriptional repression and lineage progression in B lymphopoiesis. *Proc. Natl. Acad. Sci. U. S. A.* 116, 10927–10936. doi: 10.1073/pnas.1821301116

Attard, G., Parker, C., Eeles, R., Schröder, F., Tomlins, S., Tannock, I., et al. (2016). Prostate cancer. *Lancet* 387, 70–82. doi: 10.1016/s0140-6736(14)61947-4

Bagchi, A., Papazoglu, C., Wu, Y., Capurso, D., Brodt, M., Francis, D., et al. (2007). . CHD5 is a tumor suppressor at human 1p36. *Cell* 128, 459–475. doi: 10.1016/j.cell.2006.11.052

Bajpai, R., Chen, D., Rada-Iglesias, A., Zhang, J., Xiong, Y., Helms, J., et al. (2010). CHD7 cooperates with PBAF to control multipotent neural crest formation. *Nature* 463, 958–962. doi: 10.1038/nature08733

Balasubramanian, R., and Crowley, W. (2017). Reproductive endocrine phenotypes relating to CHD7 mutations in humans. *Am. J. Med. Genet. C Semin. Med. Genet.* 175, 507–515. doi: 10.1002/ajmg.c.31585

Barisic, D., Stadler, M., Iurlaro, M., and Schübeler, D. (2019). Mammalian ISWI and SWI/SNF selectively mediate binding of distinct transcription factors. *Nature* 569, 136–140. doi: 10.1038/s41586-019-1115-5

Basson, M., and van Ravenswaaij-Arts, C. (2015). Functional Insights into Chromatin Remodelling from Studies on CHARGE Syndrome. *Trends Genet.* 31, 600–611. doi: 10.1016/j.tig.2015.05.009

Bernier, R., Golzio, C., Xiong, B., Stessman, H., Coe, B., Penn, O., et al. (2014). Disruptive CHD8 mutations define a subtype of autism early in development. *Cell* 158, 263–276. doi: 10.1016/j.cell.2014.06.017

Boehm, U., Bouloux, P., Dattani, M., de Roux, N., Dodé, C., Dunkel, L., et al. (2015). Expert consensus document: European Consensus Statement on congenital hypogonadotropic hypogonadism–pathogenesis, diagnosis and treatment. *Nat. Rev. Endocrinol.* 11, 547–564. doi: 10.1038/nrendo.2015.112

Bouazoune, K., and Kingston, R. (2012). Chromatin remodeling by the CHD7 protein is impaired by mutations that cause human developmental disorders. *Proc. Natl. Acad. Sci. U. S. A.* 109, 19238–19243. doi: 10.1073/pnas.1213825109

Brajadenta, G., Bilan, F., Gilbert-Dussardier, B., Kitzis, A., and Thoreau, V. (2019). A functional assay to study the pathogenicity of CHD7 protein variants encountered in CHARGE syndrome patients. *Eur. J. Hum. Genet.* 27, 1683–1691. doi: 10.1038/s41431-019-0465-7

Bulut-Karslioglu, A., Macrae, T., Oses-Prieto, J., Covarrubias, S., Percharde, M., Ku, G., et al. (2018). The Transcriptionally Permissive Chromatin State of Embryonic Stem Cells Is Acutely Tuned to Translational Output. *Cell Stem Cell* 22, 369–383.e8. doi: 10.1016/j.stem.2018.02.004

Butcher, D., Cytrynbaum, C., Turinsky, A., Siu, M., Inbar-Feigenberg, M., Mendoza-Londono, R., et al. (2017). CHARGE and Kabuki Syndromes: gene-Specific DNA Methylation Signatures Identify Epigenetic Mechanisms Linking These Clinically Overlapping Conditions. *Am. J. Hum. Genet.* 100, 773–788. doi: 10.1016/j.ajhg.2017.04.004

Chang, S., Yim, S., and Park, H. (2019). The cancer driver genes IDH1/2, JARID1C/KDM5C, and UTX/ KDM6A: crosstalk between histone demethylation and hypoxic reprogramming in cancer metabolism. *Exp. Mol. Med.* 51, 1–17. doi: 10.1038/s12276-019-0230-6

Chen, Y., Wang, M., Chen, D., Wang, J., and Kang, N. (2016). Chromatin remodeling enzyme CHD7 is necessary for osteogenesis of human mesenchymal stem cells. *Biochem. Biophy. Res. Commun.* 478, 1588–1593. doi: 10.1016/j.bbrc.2016.08.161

Clapier, C., Iwasa, J., Cairns, B., and Peterson, C. (2017). Mechanisms of action and regulation of ATP-dependent chromatin-remodelling complexes. *Nat. Rev. Mol. Cell Biol.* 18, 407–422. doi: 10.1038/nrm.2017.26

Corsten-Janssen, N., and Scambler, P. (2017). Clinical and molecular effects of CHD7 in the heart. *Am. J. Med. Genet. C Semin. Med. Genet.* 175, 487–495. doi: 10.1002/ajmg.c.31590

Dann, G., Liszczak, G., Bagert, J., Müller, M., Nguyen, U., Wojcik, F., et al. (2017). ISWI chromatin remodellers sense nucleosome modifications to determine substrate preference. *Nature* 548, 607–611. doi: 10.1038/nature23671

de Dieuleveult, M., Yen, K., Hmitou, I., Depaux, A., Boussouar, F., Dargham, D. Bou, et al. (2016). Genome-wide nucleosome specificity and function of chromatin remodellers in ES cells. *Nature* 530, 113–116. doi: 10.1038/nature16505

Doi, T., Ogata, T., Yamauchi, J., Sawada, Y., Tanaka, S., and Nagao, M. (2017). Chd7 Collaborates with Sox2 to Regulate Activation of Oligodendrocyte Precursor Cells after Spinal Cord Injury. *J. Neurosci.* 37, 10290–10309. doi: 10.1523/jneurosci.1109-17.2017

Dorighi, K., and Tamkun, J. (2013). The trithorax group proteins Kismet and ASH1 promote H3K36 dimethylation to counteract Polycomb group repression in Drosophila. *Development* 140, 4182–4192. doi: 10.1242/dev.095786

Egan, C., Nyman, U., Skotte, J., Streubel, G., Turner, S., O'Connell, D., et al. (2013). CHD5 is required for neurogenesis and has a dual role in facilitating gene expression and polycomb gene repression. *Dev. Cell* 26, 223–236. doi: 10.1016/j.devcel.2013.07.008

Ellingford, R., Panasiuk, M., de Meritens, E., Shaunak, R., Naybour, L., Browne, L., et al. (2021). Cell-type-specific synaptic imbalance and disrupted homeostatic plasticity in cortical circuits of ASD-associated Chd8 haploinsufficient mice. *Mol. Psychiatry*. doi: 10.1038/s41380-021-01070-9 [Online ahead of print].

Engelen, E., Akinci, U., Bryne, J., Hou, J., Gontan, C., Moen, M., et al. (2011). Sox2 cooperates with Chd7 to regulate genes that are mutated in human syndromes. *Nat. Genet.* 43, 607–611. doi: 10.1038/ng.825

Farnung, L., Vos, S., Wigge, C., and Cramer, P. (2017). Nucleosome-Chd1 structure and implications for chromatin remodelling. *Nature* 550, 539–542. doi: 10.1038/nature24046

Feng, W., Kawauchi, D., Körkel-Qu, H., Deng, H., Serger, E., Sieber, L., et al. (2017). Chd7 is indispensable for mammalian brain development through activation of a neuronal differentiation programme. *Nat. Commun.* 8:14758. doi: 10.1038/ncomms14758

Feng, W., Khan, M., Bellvis, P., Zhu, Z., Bernhardt, O., Herold-Mende, C., et al. (2013). The chromatin remodeler CHD7 regulates adult neurogenesis via activation of SoxC transcription factors. *Cell Stem Cell* 13, 62–72. doi: 10.1016/j.stem.2013.05.002

Flanagan, J., Mi, L., Chruszcz, M., Cymborowski, M., Clines, K., Kim, Y., et al. (2005). Double chromodomains cooperate to recognize the methylated histone H3 tail. *Nature* 438, 1181–1185. doi: 10.1038/nature04290

Fujita, K., Ogawa, R., and Ito, K. (2016). CHD7, Oct3/4, Sox2, and Nanog control FoxD3 expression during mouse neural crest-derived stem cell formation. *FEBS J.* 283, 3791–3806. doi: 10.1111/febs.13843

Gage, P., Hurd, E., and Martin, D. (2015). Mouse Models for the Dissection of CHD7 Functions in Eye Development and the Molecular Basis for Ocular Defects in CHARGE Syndrome. *Invest. Ophthalmol. Vis. Sci.* 56, 7923–7930. doi: 10.1167/iovs.15-18069

Gaspar-Maia, A., Alajem, A., Polesso, F., Sridharan, R., Mason, M., Heidersbach, A., et al. (2009). Chd1 regulates open chromatin and pluripotency of embryonic stem cells. *Nature* 460, 863–868. doi: 10.1038/nature08212

Ghaoui, R., Cooper, S., Lek, M., Jones, K., Corbett, A., Reddel, S., et al. (2015). Use of Whole-Exome Sequencing for Diagnosis of Limb-Girdle Muscular Dystrophy: outcomes and Lessons Learned. *JAMA Neurol.* 72, 1424–1432. doi: 10.1001/jamaneurol.2015.2274

Goodman, J., and Bonni, A. (2019). Regulation of neuronal connectivity in the mammalian brain by chromatin remodeling. *Curr. Opin. Neurobiol.* 59, 59–68. doi: 10.1016/j.conb.2019.04.010

Harada, A., Okada, S., Konno, D., Odawara, J., Yoshimi, T., Yoshimura, S., et al. (2012). Chd2 interacts with H3.3 to determine myogenic cell fate. *EMBO J.* 31, 2994–3007. doi: 10.1038/emboj.2012.136

Hata, T., Rajabi, H., Takahashi, H., Yasumizu, Y., Li, W., Jin, C., et al. (2019). MUC1-C Activates the NuRD Complex to Drive Dedifferentiation of Triple-Negative Breast Cancer Cells. *Cancer Res.* 79, 5711–5722. doi: 10.1158/0008-5472.can-19-1034

Hayashi, M., Maehara, K., Harada, A., Semba, Y., Kudo, K., Takahashi, H., et al. (2016). Chd5 Regulates MuERV-L/MERVL Expression in Mouse Embryonic Stem Cells Via H3K27me3 Modification and Histone H3.1/H3.2. *J. Cell. Biochem.* 117, 780–792. doi: 10.1002/jcb.25368

He, D., Marie, C., Zhao, C., Kim, B., Wang, J., Deng, Y., et al. (2016). Chd7 cooperates with Sox10 and regulates the onset of CNS myelination and remyelination. *Nat. Neurosci.* 19, 678–689. doi: 10.1038/nn.4258

Higashi, M., Kolla, V., Iyer, R., Naraparaju, K., Zhuang, T., Kolla, S., et al. (2015). Retinoic acid-induced CHD5 upregulation and neuronal differentiation of neuroblastoma. *Mol. Cancer* 14:150. doi: 10.1186/s12943-015-0425-y

Hsu, J., Huang, H., Lee, C., Choudhuri, A., Wilson, N., Abraham, B., et al. (2020). CHD7 and Runx1 interaction provides a braking mechanism for hematopoietic differentiation. *Proc. Natl. Acad. Sci. U. S. A.* 117, 23626–23635. doi: 10.1073/pnas.2003228117

Hurley, S., Mohan, C., Suetterlin, P., Ellingford, R., Riegman, K., Ellegood, J., et al. (2021). Distinct, dosage-sensitive requirements for the autism-associated factor CHD8 during cortical development. *Mol. Autism* 12:16. doi: 10.1186/s13229-020-00409-3

Issekutz, K., Graham, J., Prasad, C., Smith, I., and Blake, K. (2005). An epidemiological analysis of CHARGE syndrome: preliminary results from a Canadian study. *Am. J. Med. Genet. A* 133A, 309–317. doi: 10.1002/ajmg.a.30560

Jamadagni, P., Breuer, M., Schmeisser, K., Cardinal, T., Kassa, B., Parker, J., et al. (2021). Chromatin remodeller CHD7 is required for GABAergic neuron development by promoting PAQR3 expression. *EMBO Rep.* 22:e50958. doi: 10.15252/embr.202050958

Jones, K., Sarić, N., Russell, J., Andoniadou, C., Scambler, P., and Basson, M. (2015). CHD7 maintains neural stem cell quiescence and prevents premature stem cell depletion in the adult hippocampus. *Stem Cells* 33, 196–210. doi: 10.1002/stem.1822

Kim, H., Kurth, I., Lan, F., Meliciani, I., Wenzel, W., Eom, S., et al. (2008). Mutations in CHD7, encoding a chromatin-remodeling protein, cause idiopathic hypogonadotropic hypogonadism and Kallmann syndrome. *Am. J. Hum. Genet.* 83, 511–519. doi: 10.1016/j.ajhg.2008.09.005

Koh, F., Lizama, C., Wong, P., Hawkins, J., Zovein, A., and Ramalho-Santos, M. (2015). Emergence of hematopoietic stem and progenitor cells involves a Chd1-dependent increase in total nascent transcription. *Proc. Natl. Acad. Sci. U. S. A.* 112, E1734–E1743. doi: 10.1073/pnas.1424850112

Kolla, V., Zhuang, T., Higashi, M., Naraparaju, K., and Brodeur, G. (2014). Role of CHD5 in human cancers: 10 years later. *Cancer Res.* 74, 652–658. doi: 10.1158/0008-5472.can-13-3056

Layman, W., McEwen, D., Beyer, L., Lalani, S., Fernbach, S., Oh, E., et al. (2009). Defects in neural stem cell proliferation and olfaction in Chd7 deficient mice indicate a mechanism for hyposmia in human CHARGE syndrome. *Hum. Mol. Genet.* 18, 1909–1923. doi: 10.1093/hmg/ddp112

Li, J., Xu, C., Lee, H., Ren, S., Zi, X., Zhang, Z., et al. (2020). A genomic and epigenomic atlas of prostate cancer in Asian populations. *Nature* 580, 93–99. doi: 10.1038/s41586-020-2135-x

Lin, J., Lehmann, L., Bonora, G., Sridharan, R., Vashisht, A., Tran, N., et al. (2011). Mediator coordinates PIC assembly with recruitment of CHD1. *Genes Dev.* 25, 2198–2209. doi: 10.1101/gad.17554711

Link, S., Spitzer, R., Sana, M., Torrado, M., Völker-Albert, M., Keilhauer, E., et al. (2018). PWWP2A binds distinct chromatin moieties and interacts with an MTA1-specific core NuRD complex. *Nat. Commun.* 9:4300. doi: 10.1038/s41467-018-06665-5

Liu, C., Li, Q., Xiao, Q., Gong, P., and Kang, N. (2020). CHD7 Regulates Osteogenic Differentiation of Human Dental Follicle Cells via PTH1R Signaling. *Stem Cells Int.* 2020:8882857. doi: 10.1155/2020/8882857

Liu, Z., Su, D., Qi, X., and Ma, J. (2018). MiR-500a-5p promotes glioblastoma cell proliferation, migration and invasion by targeting chromodomain helicase DNA binding protein 5. *Mol. Med. Rep.* 18, 2689–2696. doi: 10.3892/mmr.2018.9259

Mashtalir, N., D'Avino, A., Michel, B., Luo, J., Pan, J., Otto, J., et al. (2018). Modular Organization and Assembly of SWI/SNF Family Chromatin Remodeling Complexes. *Cell* 175, 1272–1288.e20. doi: 10.1016/j.cell.2018.09.032

Mills, A. (2017). The Chromodomain Helicase DNA-Binding Chromatin Remodelers: family Traits that Protect from and Promote Cancer. *Cold Spring Harb. Perspect. Med.* 7:a026450. doi: 10.1101/cshperspect.a026450

Mohd-Sarip, A., Teeuwssen, M., Bot, A., De Herdt, M., Willems, S., Baatenburg de Jong, R., et al. (2017). DOC1-Dependent Recruitment of NURD Reveals Antagonism with SWI/SNF during Epithelial-Mesenchymal Transition in Oral Cancer Cells. *Cell Rep.* 20, 61–75. doi: 10.1016/j.celrep.2017.06.020

Nieto-Estevez, V., and Hsieh, J. (2018). CHD2: one Gene, Many Roles. *Neuron* 100, 1014–1016. doi: 10.1016/j.neuron.2018.11.036

Nishiyama, M., Oshikawa, K., Tsukada, Y., Nakagawa, T., Iemura, S., Natsume, T., et al. (2009). CHD8 suppresses p53-mediated apoptosis through histone H1 recruitment during early embryogenesis. *Nat. Cell Biol.* 11, 172–182. doi: 10.1038/ncb1831

Noh, K., Maze, I., Zhao, D., Xiang, B., Wenderski, W., Lewis, P., et al. (2015). ATRX tolerates activity-dependent histone H3 methyl/phos switching to maintain repetitive element silencing in neurons. *Proc. Natl. Acad. Sci. U. S. A.* 112, 6820–6827. doi: 10.1073/pnas.1411258112

Novillo, A., Fernández-Santander, A., Gaibar, M., Galán, M., Romero-Lorca, A., El Abdellaoui-Soussi, F., et al. (2021). Role of Chromodomain-Helicase-DNA-Binding Protein 4 (CHD4) in Breast Cancer. *Front. Oncol.* 11:633233. doi: 10.3389/fonc.2021.633233

Ohta, S., Yaguchi, T., Okuno, H., Chneiweiss, H., Kawakami, Y., and Okano, H. (2016). CHD7 promotes proliferation of neural stem cells mediated by MIF. *Mol. Brain* 9:96. doi: 10.1186/s13041-016-0275-6

Pagon, R., Graham, J., Zonana, J., and Yong, S. (1981). Coloboma, congenital heart disease, and choanal atresia with multiple anomalies: CHARGE association. *J. Pediatr.* 99, 223–227. doi: 10.1016/s0022-3476(81)80454-4

Parenti, I., Lehalle, D., Nava, C., Torti, E., Leitão, E., Person, R., et al. (2021). Missense and truncating variants in CHD5 in a dominant neurodevelopmental disorder with intellectual disability, behavioral disturbances, and epilepsy. *Hum. Genet.* 140, 1109–1120. doi: 10.1007/s00439-021-02283-2

Percharde, M., Bulut-Karslioglu, A., and Ramalho-Santos, M. (2017). Hypertranscription in Development, Stem Cells, and Regeneration. *Dev. Cell* 40, 9–21. doi: 10.1016/j.devcel.2016.11.010

Pierson, T., Otero, M., Grand, K., Choi, A., Graham, J., Young, J., et al. (2019). The NuRD complex and macrocephaly associated neurodevelopmental disorders.

Am. J. Med. Genet. C Semin. Med. Genet. 181, 548–556. doi: 10.1002/ajmg.c.31752

Platt, J., Kent, N., Kimmel, A., and Harwood, A. (2017). . DictyosteliumRegulation of nucleosome positioning by a CHD Type III chromatin remodeler and its relationship to developmental gene expression in. *Genome Res.* 27, 591–600. doi: 10.1101/gr.216309.116

Puc, J., and Rosenfeld, M. (2011). SOX2 and CHD7 cooperatively regulate human disease genes. *Nat. Genet.* 43, 505–506. doi: 10.1038/ng.843

Rother, M., Pellegrino, S., Smith, R., Gatti, M., Meisenberg, C., Wiegant, W., et al. (2020). CHD7 and 53BP1 regulate distinct pathways for the re-ligation of DNA double-strand breaks. *Nat. Commun.* 11:5775. doi: 10.1038/s41467-020-19502-5

Schnetz, M., Bartels, C., Shastri, K., Balasubramanian, D., Zentner, G., Balaji, R., et al. (2009). Genomic distribution of CHD7 on chromatin tracks H3K4 methylation patterns. *Genome Res.* 19, 590–601. doi: 10.1101/gr.086983.108

Schnetz, M., Handoko, L., Akhtar-Zaidi, B., Bartels, C., Pereira, C., Fisher, A., et al. (2010). CHD7 targets active gene enhancer elements to modulate ES cell-specific gene expression. *PLoS Genet.* 6:e1001023. doi: 10.1371/journal.pgen.1001023

Semba, Y., Harada, A., Maehara, K., Oki, S., Meno, C., Ueda, J., et al. (2017). Chd2 regulates chromatin for proper gene expression toward differentiation in mouse embryonic stem cells. *Nucleic Acids Res.* 45, 8758–8772. doi: 10.1093/nar/gkx475

Shieh, C., Jones, N., Vanle, B., Au, M., Huang, A., Silva, A., et al. (2020). GATAD2B-associated neurodevelopmental disorder (GAND): clinical and molecular insights into a NuRD-related disorder. *Genet. Med.* 22, 878–888. doi: 10.1038/s41436-019-0747-z

Shur, I., Socher, R., and Benayahu, D. (2006a). In vivo association of CReMM/CHD9 with promoters in osteogenic cells. *J. Cell. Physiol.* 207, 374–378. doi: 10.1002/jcp.20586

Shur, I., Solomon, R., and Benayahu, D. (2006b). Dynamic interactions of chromatin-related mesenchymal modulator, a chromodomain helicase-DNA-binding protein, with promoters in osteoprogenitors. *Stem Cells* 24, 1288–1293. doi: 10.1634/stemcells.2005-0300

Sparmann, A., Xie, Y., Verhoeven, E., Vermeulen, M., Lancini, C., Gargiulo, G., et al. (2013). The chromodomain helicase Chd4 is required for Polycomb-mediated inhibition of astroglial differentiation. *EMBO J.* 32, 1598–1612. doi: 10.1038/emboj.2013.93

Sperlazza, J., Rahmani, M., Beckta, J., Aust, M., Hawkins, E., Wang, S., et al. (2015). Depletion of the chromatin remodeler CHD4 sensitizes AML blasts to genotoxic agents and reduces tumor formation. *Blood* 126, 1462–1472. doi: 10.1182/blood-2015-03-631606

Sperry, E., Hurd, E., Durham, M., Reamer, E., Stein, A., and Martin, D. (2014). The chromatin remodeling protein CHD7, mutated in CHARGE syndrome, is necessary for proper craniofacial and tracheal development. *Dev. Dyn.* 243, 1055–1066. doi: 10.1002/dvdy.24156

Stamou, M., Ng, S., Brand, H., Wang, H., Plummer, L., Best, L., et al. (2020). A Balanced Translocation in Kallmann Syndrome Implicates a Long Noncoding RNA, RMST, as a GnRH Neuronal Regulator. *J. Clin. Endocrinol. Metab.* 105, e231–e244. doi: 10.1210/clinem/dgz011

Sugathan, A., Biagioli, M., Golzio, C., Erdin, S., Blumenthal, I., Manavalan, P., et al. (2014). CHD8 regulates neurodevelopmental pathways associated with autism spectrum disorder in neural progenitors. *Proc. Natl. Acad. Sci. U. S. A.* 111, E4468–E4477. doi: 10.1073/pnas.1405266111

Suls, A., Jaehn, J., Kecskés, A., Weber, Y., Weckhuysen, S., Craiu, D., et al. (2013). De novo loss-of-function mutations in CHD2 cause a fever-sensitive myoclonic epileptic encephalopathy sharing features with Dravet syndrome. *Am. J. Hum. Genet.* 93, 967–975. doi: 10.1016/j.ajhg.2013.09.017

Suzuki, S., Nozawa, Y., Tsukamoto, S., Kaneko, T., Manabe, I., Imai, H., et al. (2015). CHD1 acts via the Hmgpi pathway to regulate mouse early embryogenesis. *Development* 142, 2375–2384. doi: 10.1242/dev.120493

Tu, Z., Wang, C., Davis, A., Hu, M., Zhao, C., Xin, M., et al. (2021). Chromatin remodeler CHD8 governs hematopoietic stem/progenitor survival by regulating ATM-mediated P53 protein stability. *Blood.* doi: 10.1182/blood.2020009997 [Online ahead of print].

Ufartes, R., Schwenty-Lara, J., Freese, L., Neuhofer, C., Möller, J., Wehner, P., et al. (2018). Sema3a plays a role in the pathogenesis of CHARGE syndrome. *Hum. Mol. Genet.* 27, 1343–1352. doi: 10.1093/hmg/ddy045

Van Nostrand, J., Brady, C., Jung, H., Fuentes, D., Kozak, M., Johnson, T., et al. (2014). Inappropriate p53 activation during development induces features of CHARGE syndrome. *Nature* 514, 228–232. doi: 10.1038/nature13585

Vissers, L., van Ravenswaaij, C., Admiraal, R., Hurst, J., de Vries, B., Janssen, I., et al. (2004). Mutations in a new member of the chromodomain gene family cause CHARGE syndrome. *Nat. Genet.* 36, 955–957. doi: 10.1038/ng1407

Wang, Y., Chen, Y., Bao, L., Zhang, B., Wang, J., Kumar, A., et al. (2020). CHD4 Promotes Breast Cancer Progression as a Coactivator of Hypoxia-Inducible Factors. *Cancer Res.* 80, 3880–3891. doi: 10.1158/0008-5472.can-20-1049

Weiss, K., Lazar, H., Kurolap, A., Martinez, A., Paperna, T., Cohen, L., et al. (2020). The CHD4-related syndrome: a comprehensive investigation of the clinical spectrum, genotype-phenotype correlations, and molecular basis. *Genet. Med.* 22, 389–397. doi: 10.1038/s41436-019-0612-0

Whittaker, D., Riegman, K., Kasah, S., Mohan, C., Yu, T., Pijuan-Sala, B., et al. (2017). The chromatin remodeling factor CHD7 controls cerebellar development by regulating reelin expression. *J. Clin. Investig.* 127, 874–887. doi: 10.1172/jci83408

Xie, C., Li, Z., Sun, H., Wang, F., Sun, Y., Zhao, W., et al. (2015). Mutual regulation between CHD5 and EZH2 in hepatocellular carcinoma. *Oncotarget* 6, 40940–40952. doi: 10.18632/oncotarget.5724

Yan, S., Thienthanasit, R., Chen, D., Engelen, E., Brühl, J., Crossman, D., et al. (2020). CHD7 regulates cardiovascular development through ATP-dependent and -independent activities. *Proc. Natl. Acad. Sci. U. S. A.* 117, 28847–28858. doi: 10.1073/pnas.2005222117

Yang, P., Oldfield, A., Kim, T., Yang, A., Yang, J., and Ho, J. (2017). Integrative analysis identifies co-dependent gene expression regulation of BRG1 and CHD7 at distal regulatory sites in embryonic stem cells. *Bioinformatics* 33, 1916–1920. doi: 10.1093/bioinformatics/btx092

Zhang, Z., Zhou, C., Li, X., Barnes, S., Deng, S., Hoover, E., et al. (2020). Loss of CHD1 Promotes Heterogeneous Mechanisms of Resistance to AR-Targeted Therapy via Chromatin Dysregulation. *Cancer Cell* 37, 584–598.e11. doi: 10.1016/j.ccell.2020.03.001

Zhao, D., Cai, L., Lu, X., Liang, X., Li, J., Chen, P., et al. (2020). Chromatin Regulator CHD1 Remodels the Immunosuppressive Tumor Microenvironment in PTEN-Deficient Prostate Cancer. *Cancer Discov.* 10, 1374–1387. doi: 10.1158/2159-8290.cd-19-1352

Zhen, T., Kwon, E., Zhao, L., Hsu, J., Hyde, R., Lu, Y., et al. (2017). Chd7 deficiency delays leukemogenesis in mice induced by Cbfb-MYH11. *Blood* 130, 2431–2442. doi: 10.1182/blood-2017-04-780106

Conflict of Interest: The authors declare that the research was conducted in the absence of any commercial or financial relationships that could be construed as a potential conflict of interest.

Publisher's Note: All claims expressed in this article are solely those of the authors and do not necessarily represent those of their affiliated organizations, or those of the publisher, the editors and the reviewers. Any product that may be evaluated in this article, or claim that may be made by its manufacturer, is not guaranteed or endorsed by the publisher.

frontiers in Cell and Developmental Biology

ORIGINAL RESEARCH
published: 21 September 2021
doi: 10.3389/fcell.2021.714011

Macrophage-Mediated Bone Formation in Scaffolds Modified With MSC-Derived Extracellular Matrix Is Dependent on the Migration Inhibitory Factor Signaling Pathway

Moyuan Deng†, Jiulin Tan†, Qijie Dai, Fei Luo and Jianzhong Xu**

Department of Orthopaedics, Southwest Hospital, Army Medical University, Chongqing, China

OPEN ACCESS

Edited by:
Chao Xie,
University of Rochester, United States

Reviewed by:
Rupesh K. Srivastava,
All India Institute of Medical Sciences, India
Ritu Chakravarti,
The University of Toledo, United States

***Correspondence:**
Moyuan Deng
betty.deng@126.com
Jianzhong Xu
jianz_xu@126.com

†*These authors have contributed equally to this work and share first authorship*

Specialty section:
This article was submitted to Cellular Biochemistry, a section of the journal Frontiers in Cell and Developmental Biology

Received: *24 May 2021*
Accepted: *09 August 2021*
Published: *21 September 2021*

Citation:
Deng M, Tan J, Dai Q, Luo F and Xu J (2021) Macrophage-Mediated Bone Formation in Scaffolds Modified With MSC-Derived Extracellular Matrix Is Dependent on the Migration Inhibitory Factor Signaling Pathway. Front. Cell Dev. Biol. 9:714011. doi: 10.3389/fcell.2021.714011

The positive role of macrophages in the osteogenesis of mesenchymal stem cells (MSCs) has been a recent research focus. On the other hand, MSCs could carefully regulate the paracrine molecules derived from macrophages. Human umbilical cord mesenchymal stem cells (hucMSCs) can reduce the secretion of inflammatory factors from macrophages to improve injury healing. hucMSC-derived extracellular matrix (hucMSC-ECM) has the similar effect to hucMSCs, which could combat the inflammatory response of macrophages. Additionally, MSC-derived extracellular matrix also enhanced bone regeneration by inhibiting osteoclastic differentiation of monocyte/macrophage lineage. However, whether hucMSC-ECM could improve bone formation by guiding macrophage-induced osteogenic differentiation of MSCs is unknown. Here, we present decalcified bone scaffolds modified by hucMSC-derived extracellular matrix (*DBM-ECM*), which maintained multiple soluble cytokines from hucMSCs, including macrophage migration inhibitory factor (MIF). Compared with DBM, the *DBM-ECM* scaffolds induced bone formation in an improved heterotopic ossification model of severe combined immunodeficiency (SCID) mice in a macrophage-dependent manner. Macrophages cocultured with *DBM-ECM* expressed four osteoinductive cytokines (BMP2, FGF2, TGFβ3 and OSM), which were screened out by RNA sequencing and measured by qPCR and western blot. The conditioned medium from macrophages cocultured with *DBM-ECM* improved the osteogenic differentiation of hBMSCs. Furthermore, *DBM-ECM* activated CD74/CD44 (the typical MIF receptors) signal transduction in macrophages, including phosphorylation of P38 and dephosphorylation of c-jun. On the other side, the inhibitory effects of the *DBM-ECM* scaffolds with a deficient of MIF on osteogenesis *in vitro* and *in vivo* revealed that macrophage-mediated osteogenesis depended on MIF/CD74 signal transduction. The results of this study indicate that the coordinated crosstalk of macrophages and MSCs plays a key role on bone regeneration, with an emphasis on hucMSC-ECM constructing a macrophage-derived osteoinductive microenvironment.

Keywords: mesenchymal stem cells, macrophages, extracellular matrix, osteogenic differentiation, migration inhibitory factor, osteoimmunological microenviroment

INTRODUCTION

Large bone defects healing requires implants to achieve the classic stages of endochondral ossification and bone tissue regeneration, which caused by trauma, spinal injury, osteitis and tumor resection. In this mode of bone regeneration, the repair is initiated by the infiltration of immune cells, particularly macrophages. In addition to phagocytosing necrotic cells and tissue debris, macrophages initiate the recruitment of mesenchymal stem cells (MSCs) and other progenitor cells (Pajarinen et al., 2019). MSCs and other progenitor cells differentiate to form granulation tissue and ultimately form cartilage calli for bone regeneration (Pajarinen et al., 2019). The differentiation of MSCs and the subsequent formation of bone are regulated by the microenvironment. Recently, in addition to recruiting MSCs, it has been determined that macrophages play a key role in the osteogenic differentiation of MSCs and the maintenance bone tissue homeostasis (Niu et al., 2017). However, how macrophages improve bone formation remains unclear. And how to construct a macrophage-induced osteogenic microenvironment for MSCs remains unknown.

Mesenchymal stem cells (MSCs) have a good immunomodulatory ability, especially for macrophages (Swartzlander et al., 2015). MSCs derived from umbilical cord Wharton's jelly (hucMSCs) are regarded to be significantly superior to those derived from bone marrow and adipose tissue due to their non-invasive tissue sources and, most importantly, increased immunomodulatory properties (Zhao et al., 2010; Wang et al., 2015). As MSC-derived extracellular matrix has the similar nature to native cells, the extracellular matrix of hucMSCs (hucMSC-ECM) also achieves immunomodulatory potency in combating macrophage-derived inflammation (Deng et al., 2020). Additionally, extracellular matrix or vesicles derived from MSCs inhibited the osteoclastic differentiation of monocyte/macrophage and this demonstrated that MSC-derived ECM or vesicles could improve bone formation by inhibiting osteoclastogenesis (Li et al., 2018; Hu et al., 2020). On the other hand, whether hucMSC-ECM could improve bone formation by conducting macrophage-induced osteogenic differentiation of MSCs needs to be investigated. Recent studies showed that macrophages or monocytes in a co-culture with MSCs could increase bone formation, which was mediated by Oncostain M(OSM) secreted by monocytes (Pajarinen et al., 2019). Based on hucMSC-ECM has a similar effect to hucMSCs, it is logical to hypothesize that hucMSC-ECM might induce some osteoinductive cytokines expressed by macrophages, and these cytokines improved osteogenesis of MSCs and bone formation.

The aim of this study was to investigate whether bone regeneration of hucMSC-ECM is mediated by macrophages. Firstly, the characterization of scaffolds modified by hucMSC-derived ECM was examined. Next, the role and mechanism of hucMSC-ECM on expression of macrophage-derived paracrine osteogenic molecules were estimated. Lastly, the efficacy of hucMSC-ECM on macrophage-mediated osteogenic differentiation of bone marrow MSCs (BMSCs) and bone regeneration in improved heterotopic ossification model of severe combined immunodeficiency (SCID) mice were investigated (**Figure 1**).

MATERIALS AND METHODS

Cell Culture

hucMSCs and hBMSCs were purchased from Cyagen (Cyagen Biosciences Inc., Guangzhou, China). MSCs were cultured in DMEM/F12 (HyClone, GE Healthcare Life Sciences, United States) with 10% fetal bovine serum (FBS; HyClone, United States) and 1% penicillin-streptomycin (HyClone). Passage 3-5 hucMSCs were used for the preparation of scaffolds. Passage 3-6 hBMSCs were used for osteogenic differentiation. The human monocytic cell line THP-1 (Shanghai Cell Bank, Chinese Academy of Sciences, China) was maintained in RPMI 1640 medium (HyClone, United States) supplemented with 10% FBS as previously described (Shiratori et al., 2017). THP-1 cells (5×10^5/mL) were differentiated into macrophages with 50 ng/mL PMA (Sigma, United States) for 48 h and cultured in RPMI 1640 medium supplemented with 10% FBS without PMA. Cells were cultured at 37°C with 5% CO_2.

Preparation of Scaffolds

Demineralized bone matrix (DBM) (3 mm × 3 mm × 3 mm) was prepared with OX cancellous bone (Chongqing Datsing Bio-Tech Co., Ltd, Chongqing, China). DBM scaffolds were seeded with hucMSCs and cultured in complete medium for 12 days, rinsed with PBS, flash frozen in liquid nitrogen for 10 min, thawed in a 37°C water bath with shaking at 60 rpm for 20 min, rinsed with PBS, frozen at −80°C overnight, and freeze-dried to prepare the *DBM-ECM*. To assess the effect of MIF (macrophage migration inhibitory factor) in the *DBM-ECM* scaffolds on macrophage-mediated bone formation, *DBM-ECM*, *shCtr*l and *shmif* were prepared. The *DBM-ECM* with a deficient of MIF expression was used. Lentiviruses carrying short hairpin RNA (shRNA) were transfected into hucMSCs. hucMSCs were cultured in DMEM/F12 medium supplemented with mif shRNA or non-silencing shRNA (OBIO Technology Co., Ltd., Shanghai, China) for 24 h, and then the culture medium was changed to complete culture medium supplemented with 2.5 pM puromycin amino nucleoside (Sigma, Saint Louis, MO, United States) to eliminate untransfected cells. The cells transfected with mif (*shmif*) or the control (*shCtrl*) shRNA were used to prepare the *DBM-ECM*.

Scanning Electron Microscopy (SEM) Analysis

Scaffolds were fixed with glutaraldehyde, dehydrated in a gradient ethanol, and sealed with tert-butyl alcohol. The scaffolds were then sprayed with gold and examined using a scanning electron microscope (Crossbeam 340; ZEISS, German) with an accelerating voltage of 1 kV and a working distance of 4–6 mm.

Elemental Distribution

Scaffolds were determined using energy-dispersive X-ray spectroscopy at an electron acceleration voltage of 5 kV (Deng et al., 2020).

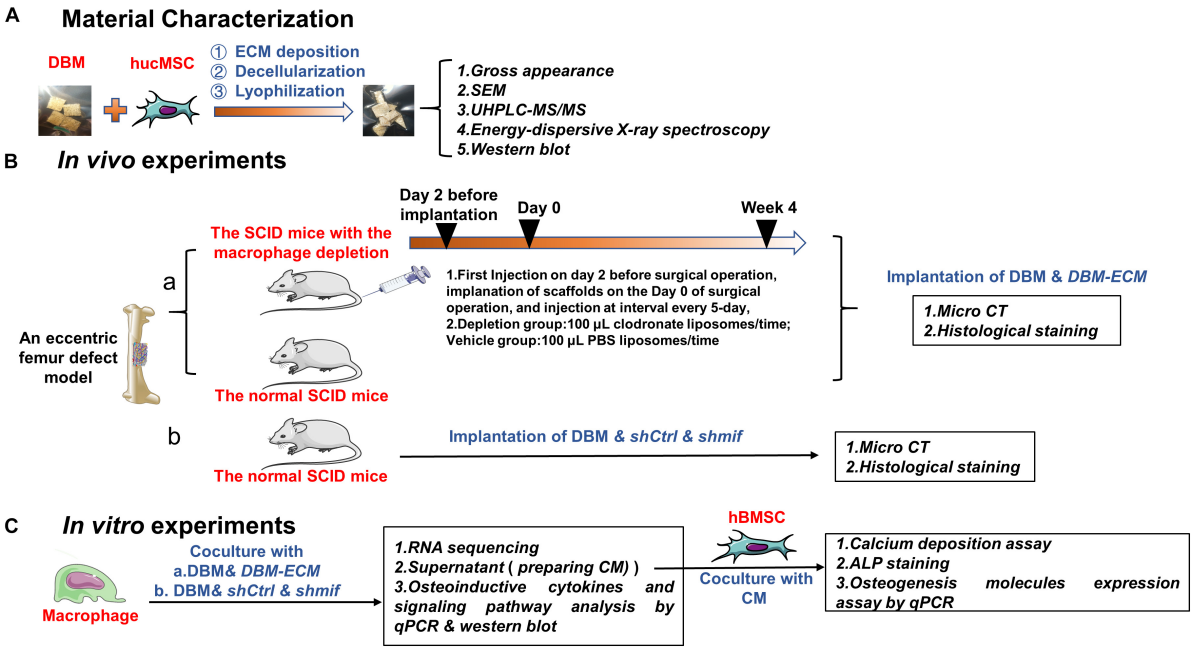

FIGURE 1 | Schematic diagram of the experiments assessing macrophage-mediated bone formation of *DBM-ECM in vivo* and *in vitro*. **(A)** Material preparation and characterization. **(B)** *In vivo* experiments assessing the role of macrophages in ECM-induced bone formation **(a)** and the effect of the MIF signaling pathway on macrophage-mediated bone formation **(b)**. **(C)** *In vitro* experiments investigating the role of conditioned media of macrophages on osteogenesis of hBMSCs and the mechanism of macrophage-mediated osteogenesis of MSCs induced by ECM.

UHPLC-MS/MS

The total protein of scaffolds (DBM and *DBM-ECM*) was extracted with 250 μL RIPA lysis buffer (Beyotime, Jiangsu, China). Protein samples were digested and assessed by LC-MS/MS (LTQ Orbitrap Velos Pro, Thermo Fisher), and data analysis was performed as previously described (Yin et al., 2014).

Animal Model and Macrophage Depletion

All animal care and experimental protocols complied with the Animal Management Rule of the Ministry of Public Health of China (documentation 55, 2001). Ten-week-old SCID mice weighing approximately 20 ± 2 g from the Animal Experiment Center of Southwest Hospital of China were used to prepare the unilateral femoral eccentric femoral defect model. To analyze the role of macrophages in scaffold-induced bone formation, SCID mice were divided into the following two sets: those that received selective macrophage depletion and those that did not receive macrophage depletion. The method of using clodronate liposomes to deplete macrophages is well established (Cho et al., 2014; Wu et al., 2014). Forty-eight hours before surgery, depletion of the macrophages was induced by intravenous injection of 100 μL clodronate liposomes (5 mg/mL) into the tail vein (Schlundt et al., 2018). Clodronate liposome injection was repeated every 5 days to target the different phases of the bone healing process. The surgical procedure was performed as previously described (Luo et al., 2016). Mice were randomly assigned to the following two groups: the DBM group (n = 6 for normal mice and n = 6 for macrophage-depleted mice) and the *DBM-ECM* group (n = 6 for normal mice and n = 6 for macrophage-depleted mice). To estimate the role of MIF in the macrophage-mediated bone formation ability of hucMSC-ECM, mice were also randomly assigned to the following three groups: the DBM group (n = 6), the *shCtrl* group (n = 6) and the *shmif* group (n = 6). Bone formation was assessed by micro-CT detection and Masson's staining at harvesting at postoperative week 4.

Micro CT

New bone formation at week 4 was evaluated with micro-CT (Skyscan 1272, Antwerp, Belgium). The retrieved femora with muscles removed were fixed in 4% paraformaldehyde and scanned as previously described (Deng et al., 2020). The data were subsequently analyzed and imaged using CT Analyser software (version 1.16.1.0, Skyscan1272, Bruker Microct, Kontich, Belgium). 3-D pictures were created with CTvox software (version 3.2.0r1294, Skyscan1272, Bruker Microct). Relative bone volume per tissue volume (BV/TV), trabecular number (Tb. N), and bone mineral density (BMD) (0.25 g/cm^3 CaHA of BMD phantom) were calculated for each scaffold using CTvox software (version 3.2.0r1294, Skyscan, Antwerp, Kontich, Belgium).

Histochemistry Assessment

The scaffolds were retrieved 4 weeks postoperatively. The muscle and soft tissue were removed. Next, the scaffolds and regenerated tissue were fixed in 4% buffered paraformaldehyde, decalcified

in 4% EDTA solution, embedded in paraffin and sectioned at 4–6 mm thickness. The slides were used for Masson's trichrome staining.

Osteogenesis-Related Assays *in vitro*

***Preparation of conditioned media (CM)*:** THP-1 cells (5×10^5/mL) were seeded in 6-well plates and differentiated into macrophages; next, scaffolds cut into small pieces were added. After 2 days of induction, the medium derived from the DBM and *DBM-ECM* groups was harvested and centrifuged at 2,000 × *g* for 10 min to collect the supernatant. The conditioned medium was the DMEM/F12 mixed with the collected supernatant at a ratio of 1:1 containing 10% FBS,100 nM dexamethasone, 50 nM ascorbic acid, and 10 nM β-sodium glycerophosphate (Solarbio, Beijing, China), which was stored at −80°C for subsequent experiments (Chen et al., 2014).

Calcium deposition assay: To assess calcium nodule formation and calcium deposition, hBMSCs were cultured with CM for 14 days. The cells were fixed and stained with 1% Alizarin red solution (Cyagen, Guangzhou, China). For the quantitation of calcium deposition, Alizarin red binding with calcium nodules was desorbed by 10% cetylpyridinium chloride (Aladdin, Shanghai, China), and OD measurements were obtained at a wavelength of 570 nm (Li et al., 2019).

ALP staining: After 10 days of incubation, hBMSCs were fixed and stained with an alkaline phosphatase assay kit (Beyotime, Jiangsu, China). ALP expression was observed by microscopy (Ma et al., 2019).

RNA Sequencing

THP-1 cells (5×10^5/mL) were seeded in 6-well plates, differentiated into macrophages, and incubated with DBM and *DBM-ECM* scaffolds for 3 to 7-day. Cells were collected for RNA sequencing. Total RNA extraction, cDNA library construction, RNA sequencing and data analyses (Dif-gene-finder, Pathway analysis and GO analysis) were carried out as previously described (Novel Bio, Shanghai, China) (Deng et al., 2020). Dif-genes of interest were selected from the results of the GO term and pathway term analysis with the key gene descriptions of "osteoblast/chondrocyte differentiation, mineralization, cartilage development, bone remodeling, chondrocyte/osteoblast/cell proliferation and endochondral ossification". Dif-genes of interest were normalized using the log 10 value and used to generate a heatmap with Heatmap illustrator (HemI.1.0, CUCKOO Work group, Hubei, China).

Quantitative Real-Time Polymerase Chain Reaction

To estimate the profile of osteoinductive cytokines expressed by macrophages induced by scaffolds, 5×10^5/mL THP-1 cells were seeded in 6-well culture plates, differentiated into macrophages, and incubated with scaffolds. After 2 days of incubation, the expression levels of macrophage genes involved in osteoinduction (TGFβ3, BMP1, BMP6, BMP2, FGF2, Wnt5a, PTHLH, OSM, WNT7β and IL-6) were examined by quantitative PCR. For the osteogenic differentiation assay, after 14 days of incubation with CM, the gene expression of hBMSCs (OPN, OCN and OSX) was examined by quantitative PCR. Briefly, total RNA was extracted from the cells with TRIzol reagent (Takara, Beijing, China) and reverse transcribed with the PrimeScript™ RT reagent kit (Takara, Beijing, China) according to the manufacturer's instructions. Real-time PCR was performed using 2 × SYBR Green PCR Master Mix. All primer sequences were obtained from Sangon Biotech Co., Ltd. (Shanghai, China), and these sequences are summarized in **Supplementary Table S1**.

Western Blotting

To assess MIF deposited on scaffolds, the total protein of the DBM and *DBM-ECM* was extracted by 250 μL RIPA lysis buffer (Beyotime, Jiangsu, China). To investigate the molecular mechanism of osteoinductive cytokines expressed by macrophages induced by scaffolds, 5×10^5/mL THP-1 cells were seeded in 6-well culture plates, differentiated into macrophages, and incubated with scaffolds for 0–240 min or 2 days. To estimate the knockdown level of MIF in hucMSCs, the total protein was extracted from normal cells and the cells that were transfected with lentivirus carrying mif shRNA and non-silencing shRNA. The total protein of the cells was extracted with 120 μL RIPA lysis buffer (Beyotime, Jiangsu, China), subjected to SDS-PAGE, transferred onto nitrocellulose membranes (Millipore, Billerica) and probed overnight at 4°C with specific primary antibodies against OSM, FGF2, TGFβ3, BMP2, BMP6, CD74, CD44, phspho-p38, phspho-c-jun, phspho-AKT, Erk1/2, c-jun and AKT at a dilution of 1:1000 (Abcam, United States); MIF, phspho-Erk1/2, and p38 at a dilution of 1:1000 (Cell Signaling Technology, United States); BMP1 (Bioss, Beijing, China), Wnt7β, Wnt5a, and PTHLH at a dilution of 1:500-1:1000 (Proteintech, Wuhan, China), and control antibodies Tubulin and GAPDH were used at a dilution of 1:1000 (Proteintech, Wuhan, China). Immunoreactive protein bands were visualized using ECL chemiluminescence detection plus a Western blot detection system (Viber, Viber Lourmat, France).

Statistical Analysis

One-way ANOVA followed by a multiple comparisons test was utilized to determine the statistical significance for the micro-CT analysis (DBM, *shCtrl* and *shmif* scaffolds in normal mice), Alizarin red staining and qPCR assay (for the analysis of mRNA associated with osteogenic differentiation). T-tests were used for the analysis of the results of UHPLC-MS/MS and the qPCR assay for the analysis of osteoinductive cytokines expressed in macrophages. Two-way ANOVA followed by a multiple comparisons test was used for the micro-CT analysis of the scaffolds in normal and macrophage-depleted mice. EB-seq was used for Dif-Gene-Finder, and Fisher's exact test was used to select significant pathways or GO terms. The results are displayed as the mean ± standard deviation. Sample numbers and repeats are for $n \geq 3$ per group. For all the statistical tests, differences were considered to be significant if $P < 0.05$.

RESULTS

MIF Abundantly Deposited on the *DBM-ECM* Scaffold Was Derived From hucMSC-Derived ECM

In our previous studies, tissue engineering technology, followed by decellularization and lyophilization, was used to deposit hucMSC-ECM on scaffolds and enhance the osteoinductive potential of the scaffolds (Deng et al., 2016, 2020). After modification of DBM scaffolds, white, tubular hucMSC-ECM proteins appeared on the surface of the scaffolds (**Figures 2A,B**). The elemental distribution data showed that the contents of four elements (C, S, Cl, and Na) were remarkably different between the DBM and *DBM-ECM* scaffolds, in which the content level of C and S decreased, while the others increased (**Figure 2C** and **Supplementary Figure S1**). Furthermore, LC-MS/MS high-throughput analysis showed the presence of soluble proteins originating from the *DBM-ECM* scaffold (**Figure 2D**). The top 10 soluble protein peak area values were as follows: serum albumin (ALB), macrophage migration inhibitory factor (MIF), collagen alpha-1 (XII) (COL12A1), thrombospondin-1 (THBS1), transforming growth factor-beta-induced protein ig-h3 (TGFβI), neuroblast differentiation-associated protein (AHNAK), collagen alpha-1 (VI) (COL6A1), brain acid soluble protein 1 (BASP1), fibronectin (FN1) and prohibitin-2 (PHB2) (**Figure 2D**). Among the top ten soluble proteins, the content of macrophage migration inhibitory factor (MIF) ranked second, and a clear MIF protein band in the total protein extracted from the *DBM-ECM* was detected by Western blot (**Figures 2D,E**).

Macrophage Depletion Inhibited Bone Regeneration Induced by hucMSC-ECM

To estimate the role of macrophages in the bone formation ability of hucMSC-ECM, SCID mice with macrophage depletion were injected with clodronate liposomes and were compared with control mice without macrophage depletion that were injected with PBS liposomes. The DBM and the *DBM-ECM* scaffolds were harvested for micro-CT and histochemistry staining after week 4 postimplantation (**Figure 3A**). In control mice, the implanted DBM scaffolds formed hollow nest-like bone tissue, while the *DBM-ECM* formed dense bone tissue (**Figure 3B**). In the macrophage-depleted mice, all the DBM and *DBM-ECM* scaffolds exhibited similar hollow nest-like bone tissue, indicating that the surfaces of these scaffolds induced bone formation and

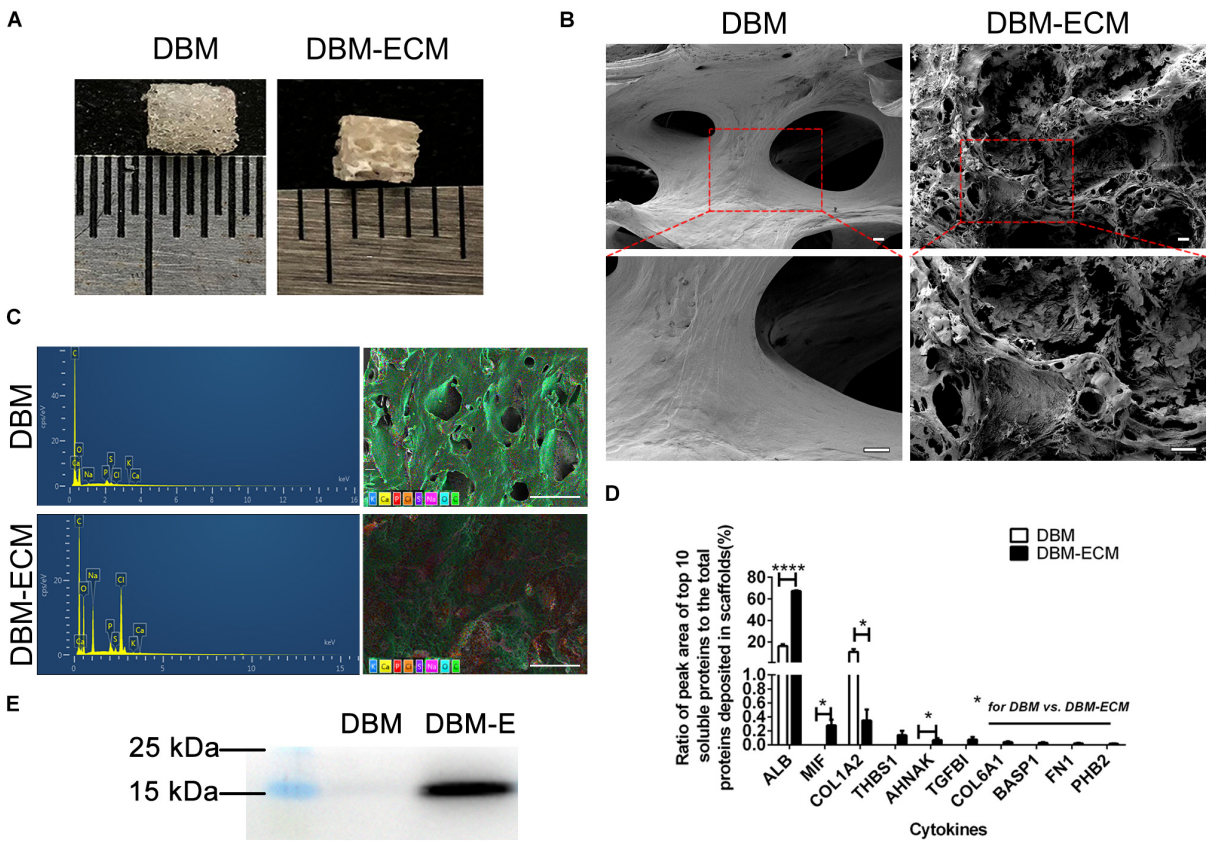

FIGURE 2 | Evaluation of the surface modification of DBM scaffolds with hucMSC-ECM. **(A)** The gross appearance of the DBM scaffold with or without surface modification. **(B)** Scanning electron microscopy (SEM) images of scaffolds. **(C)** Energy dispersive spectroscopy (EDS) of scaffolds. **(D)** HPLC-MS/MS high-throughput analysis for the top 10 principal soluble protein components highly deposited in the *DBM-ECM*. **(E)** Protein expression of MIF tested by Western blot. Scale bar for the top panel of **(B)**: 100 μm, Scale bar for the down panel of **(B)**: 50 μm; Scale bar for **(C)**: 500 μm; *$p < 0.05$, ****$p < 0.001$.

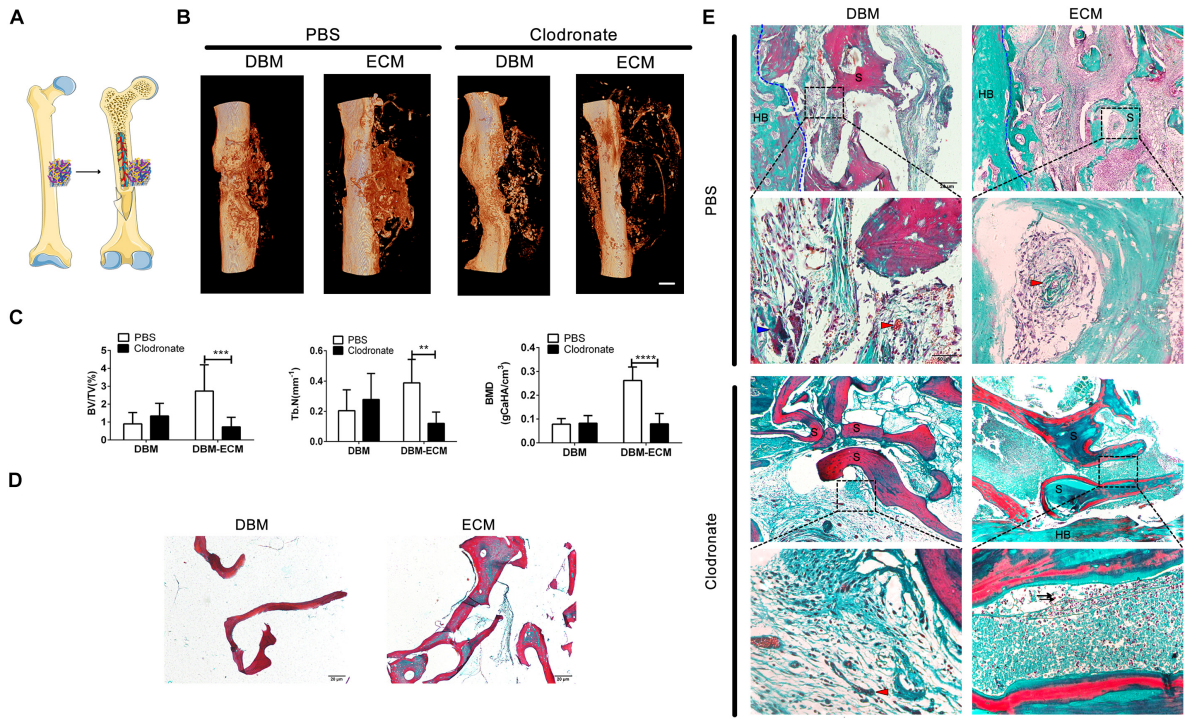

FIGURE 3 | Macrophage depletion inhibited bone regeneration induced by hucMSC-ECM. **(A)** Schematic outline of surgical operation model. **(B)** 3D images of bone regeneration of the DBM and *DBM-ECM* scaffolds adjacent to the femoral shaft at 4 weeks postimplantation in SCID mice with or without macrophage depletion. **(C)** BMD, BV/TV, and Tb. N of the regenerated bone of the DBM and *DBM-ECM* scaffolds at 4 weeks postimplantation. **(D)** Masson's staining of the DBM and *DBM-ECM* scaffolds. **(E)** Masson's staining of the DBM and *DBM-ECM* scaffolds at 4 weeks postimplantation; HB, host bone; S, scaffold fragment; blue arrowhead, necrotic tissue; red arrowhead, new blood vessels; black arrow, granulocytes. Scale bar: 1 mm for **(B)**; Scale bar: 20 μm for **(D)**; Scale bar for upper images of panel **(E)** is 20 μm and lower images of panel **(E)** is 50 μm; $^{**}p < 0.01$, $^{***}p < 0.005$, $^{****}p < 0.001$.

the internal part of the scaffolds were degraded and absorbed (**Figure 3B**). The quantitative analysis of micro-CT data verified this observation (**Figure 3C**). Compared to the control mouse model, macrophage depletion did not significantly change the bone regeneration indexes of DBM scaffolds (**Figure 3C**). In contrast, macrophage depletion dramatically decreased the values of BV/TV, Tb. N and BMD in the *DBM-ECM* group compared with those in the control mouse model (2.73 ± 1.47- vs. 0.74 ± 0.53-fold for BV/TV, 0.38 ± 0.15- vs. 0.12 ± 0.07-fold for Tb. N, 0.26 ± 0.05 vs. 0.08 ± 0.04 folds for BV/TV; **Figure 3C**).

Masson's staining of sections (5 μm) of DBM scaffolds showed red mature collagen fibers, and the collagen fibers of *DBM-ECM* scaffolds were red and green, indicating that the scaffolds had been modified by hucMSC-ECM (**Figure 3D**). In the control mice, Masson's staining of implanted DBM scaffolds showed a few red collagen fibers with some necrotic tissue scattered in the scaffold pores (blue arrowhead), while the *DBM-ECM* scaffolds had been replaced by green collagen fibers indicating new bone tissue formation that was densely granular and had a rich blood vessel network (red arrowhead). On the other hand, in the macrophage-depleted mice, the collagen fiber color in the DBM and the *DBM-ECM* scaffolds was unchanged in comparison with non-transplanted scaffolds, and sparse fibrous tissue was scattered in the scaffold pores, indicating that these scaffolds had not been replaced by new bone formation. In addition, compared to the tissue in normal mice, the new tissue of the *DBM-ECM* group macrophage-depleted mice contained numerous granulocytes, indicating severe inflammation (black arrow, **Figure 3E**).

hucMSC-ECM Improved Macrophage-Mediated Osteogenic Differentiation of hBMSCs

Furthermore, the effect of macrophages on the osteogenic differentiation of MSCs induced by the *DBM-ECM* scaffolds was estimated *in vitro*. Alizarin red staining showed that conditioned medium from macrophages incubated with the *DBM-ECM* scaffolds (Mφ + ECM-CM group) induced deeper red color reaction and a higher OD value per 10^4 cells compared to those in the other groups (ECM-CM and Mφ-CM), which was 82.32 ± 5.19% and 41.45 ± 11.09% higher than those of the ECM-CM and Mφ-CM groups, respectively (**Figure 4A**). Alkaline phosphatase (ALP) staining suggested a similar trend with the results of Alizarin red staining that the staining of the Mφ + ECM-CM group showed a deeper blue color reaction, indicating higher ALP activity (**Figure 4B**). Furthermore, qPCR data demonstrated that the osteocalcin (*ocn*)and osterix (*osx*) levels of the Mφ + ECM-CM group were significantly higher

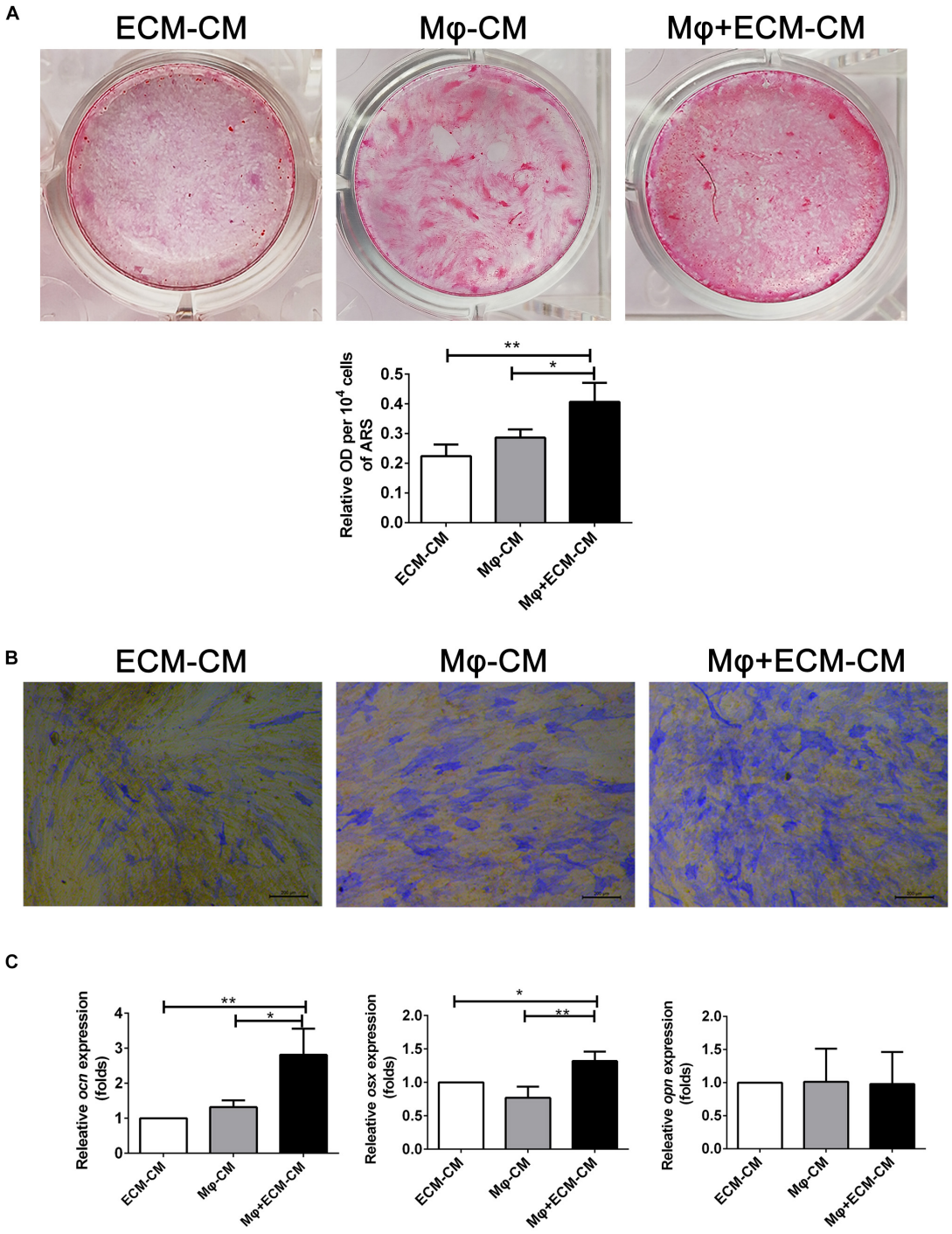

FIGURE 4 | hucMSC-ECM improved macrophage-mediated osteogenesis of hBMSCs. **(A)** Alizarin red staining and OD value per 10^4 cells of Alizarin red deposited in calcic nodules of different groups. **(B)** Alkaline phosphatase (ALP) staining of different groups. **(C)** mRNA levels of osteogenic genes of different groups; ECM-CM: conditioned medium from *DBM-ECM* scaffolds, Mφ-CM: conditioned medium from macrophages, Mφ + ECM-CM: conditioned medium from macrophages with coculture of *DBM-ECM* scaffolds. Scale bar: 200 μm for panel **(B)**. $^{**}p < 0.01$; $^{*}p < 0.05$.

than those of the other two groups (2.81 ± 0.75-fold of the Mφ + ECM-CM group vs. 1.32 ± 0.19-fold of the Mφ-CM group for the *ocn* level, 1.32 ± 0.14-fold of the Mφ + ECM-CM group vs. 0.77 ± 0.17-fold of the Mφ-CM group for the *osx* level), which are key indexes for pro-osteogenic differentiation (**Figure 4C**). However, there were no significant differences in Osteopontin (*opn*) levels among the three groups, which is a key gene indicating bone resorption (**Figure 4C**; Kelly et al., 2020).

hucMSC-ECM Enhanced the Expression of Multiple Osteoinductive Cytokines in Macrophages

To investigate the mechanism of macrophage-mediated osteogenesis induced by *DBM-ECM*, macrophages cocultured with *DBM-ECM* scaffolds were sequenced and compared with macrophages from the DBM group. The gene expression profile of macrophages cocultured with the DBM or *DBM-ECM* scaffolds was then analyzed (GSE174477)[1]. Twenty genes involved in bone formation were screened out, of which there were 8 genes that encoded for osteoinductive secretory cytokines and 3 genes that encoded for receptors (red frame for cytokine and blue frame for receptor, **Figure 5A**). Next, the expression of 8 screened cytokine genes and two of the other relevant genes (bone morphogenetic protein, BMP2 and Oncostatin M, OSM), a total of 10 genes, was verified by qPCR. Except for IL-6, which exhibited downregulated expression, the mRNA expression level of 4 genes in was increased in the *DBM-ECM* group compared with the expression level in the DBM group, and the difference was determined to be significant by a *t*-test (3.59 ± 1.20-fold for FGF2, 2.11 ± 0.21-fold for PTHLH, 11.20 ± 2.74-fold for TGFβ3 and 3.58 ± 1.57-fold for BMP2) (**Figure 5B**). To further confirm the protein expressions of cytokines screened out, except for IL-6, the expression levels of the proteins encoded for by the 9 remaining genes were verified by western blot. The results suggested that the protein expression level of TGFβ3, OSM, FGF2 and BMP2 increased, while the protein expression level of BMP6, WNT5α and PTHLH in the *DBM-ECM* group did not change compared to that in the DBM group (**Figure 5C**). In addition, WNT7β and BMP1 were not observed (data not shown), indicating that these proteins were only present at trace levels.

hucMSC-ECM Upregulated the Expression of Osteoinductive Cytokines From Macrophages by the MIF Signaling Pathway

It has been reported that MIF plays important roles in macrophage behaviors and bone healing (Liu et al., 2021; Zhu et al., 2021). **Figure 2D** showed that MIF deposited in hucMSC-ECM was rich in content. Thus, the role of the MIF deposited in the *DBM-ECM* scaffolds and MIF signaling pathway on the upregulation of osteoinductive cytokine expression by macrophages was estimated. CD74 and its chaperone protein CD44 have been reported to be typical MIF receptors (Jankauskas et al., 2019; Farr et al., 2020). The *DBM-ECM* scaffolds obviously enhanced the expression of CD74 and CD44, indicating that the MIF deposited in the *DBM-ECM* might activate CD74/CD44 of macrophages (**Figure 6A**). The latest study showed that macrophage-derived osteoinductive cytokines might

[1]https://www.ncbi.nlm.nih.gov/geo/query/acc.cgi?acc=GSE174477

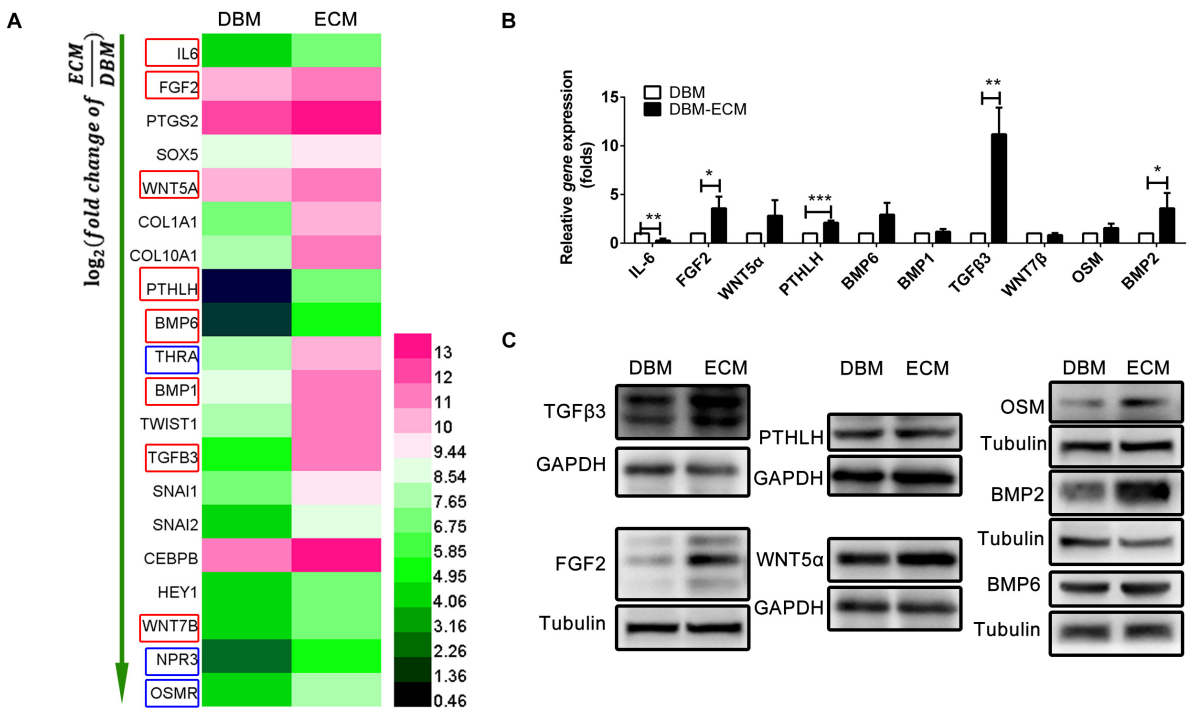

FIGURE 5 | hucMSC-ECM enhanced the expression of multiple osteoinductive cytokines in macrophages. **(A)** Heatmap of upregulated Dif genes of interest in macrophages cocultured with the DBM and *DBM-ECM* scaffolds as identified by mRNA sequencing; red frame: cytokine, blue frame: receptor. **(B)** The mRNA levels of 10 cytokines in macrophages cocultured with the DBM and *DBM-ECM* scaffolds. **(C)** The protein expression of the seven cytokines in macrophages cocultured with the DBM and *DBM-ECM* scaffolds, which were screened out from qPCR results. ***$p < 0.005$; **$p < 0.01$; *$p < 0.05$.

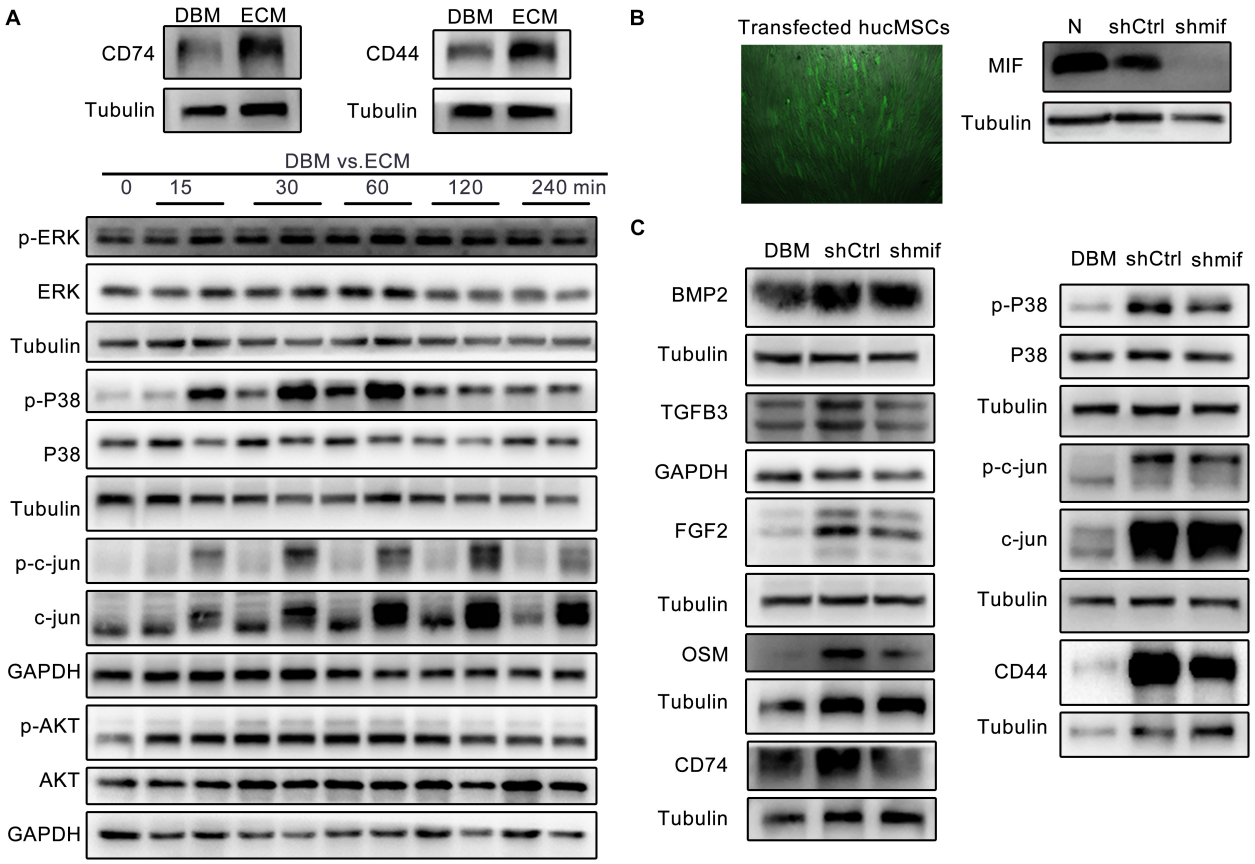

FIGURE 6 | hucMSC-ECM upregulated the expression of osteoinductive cytokines in macrophages via the MIF pathway. **(A)** The protein and phosphorylation levels of key molecules involved in the MIF signaling pathway. **(B)** MIF expression of hucMSCs transfected with the lentiviral vector containing mif shRNA or no shRNA; left panel: fluorescence expression of hucMSCs transfected with the GFP lentiviral vector, right image: protein level of MIF. **(C)** The expression of cytokines and key molecules of the MIF signaling pathway derived from macrophages in the DBM, *shCtrl* and *shmif* groups.

be induced via CD74 downstream signaling (the MAPK and PI3K-AKT signaling pathways) (Subbannayya et al., 2016). The phosphorylation of three key transcription factors, including ERK, P38 and c-Jun of the MAPK pathway and AKT of the PI3K pathway, were tested. Western blot results showed that in the time span of 0–240 min, the *DBM-ECM* improved the phosphorylation of P38 from 15 to 60 min and the dephosphorylation of c-jun from 60 to 240 min. On the other hand, the phosphorylation levels of ERK1/2 and AKT were not affected by hucMSC-ECM (**Figure 6A**). To investigate the relationship between the expression of osteoinductive cytokines and MIF deposited in *DBM-ECM*, hucMSC-ECM with the knockdown of *mif* and hucMSC-ECM transfected with control shRNA were prepared. The transfection efficiency of the lentiviruses was high, as indicated by strong expression of GFP (left panel of **Figure 6B**). Western blot analysis showed that MIF expression in the *shCtrl* group decreased slightly compared to that in the normal hucMSCs without transfection of lentiviral vector, while MIF expression in the *shmif* group was almost completely suppressed (right panel of **Figure 6B**). Furthermore, after macrophages were incubated with scaffolds (DBM, the *shCtrl* and *shmif* scaffolds), the expression of the previously screened cytokines and the aforementioned signaling pathways was tested. Among the 4 cytokines (BMP2, TGFβ3, FGF2 and OSM), only the BMP2 level among the 3 groups (DBM, *shCtrl* and *shmif*) was not significantly changed, suggesting that MIF deposited in hucMSCs-ECM did not improve BMP2 expression (**Figure 6C**). The expression levels of TGFβ3, FGF2 and OSM in the *shmif* group were heavily decreased compared with those in the *shCtrl* group, indicating that MIF deposited in the ECM played a major role in upregulating the expression of these three cytokines (**Figure 6C**). In addition, the expression of CD74/CD44 and phosphorylation of P38 in the *shmif* group were inhibited compared with those in the *shCtrl* group, while dephosphorylation of c-jun was not changed as a result of MIF knockdown (**Figure 6C**).

hucMSC-ECM Improved Macrophage-Mediated Osteogenesis of hBMSCs and Bone Formation by MIF Signaling Pathway

To further investigate the role of the MIF signaling pathway in macrophage-mediated osteogenesis and bone formation induced

by *DBM-ECM*, Alizarin red staining and the expression levels of genes involved in osteogenic differentiation *in vitro* and bone regeneration *in vivo* were compared between the *shCtrl* and *shmif* groups. Compared with the Mφ + DBM-CM group, Alizarin red staining showed increasingly larger calcic nodules in the Mφ + shCtrl-CM group, which had a higher OD value per 10^4 cells (2.62 ± 0.14-fold in the Mφ + shCtrl-CM group vs. 1.96 ± 0.17-fold in the Mφ + DBM-CM group). The BMSCs in the Mφ + shmif-CM group detached during the 14-day culture period, and Alizarin red staining showed no cell or calcic nodules in the middle of the 6-well plate, and the OD value per 10^4 cells also decreased (1.96 ± 0.16-fold) (**Figure 7A**). qPCR results showed that the expression of *ocn* and *osx* (indicating osteogenic differentiation) in the Mφ + shCtrl-CM group remarkably increased compared with that in the Mφ + DBM-CM group (3.39 ± 1.21-fold in the Mφ + shCtrl-CM group for *ocn*, 2.00 ± 0.40-fold in the Mφ + shCtrl-CM group for *osx*), while it was obviously decreased compared with that of the Mφ + shmif-CM group (1.69 ± 0.20-fold in the Mφ + shmif-CM group for *ocn*, 0.93 ± 0.62-fold in the Mφ + shmif-CM group for *osx*). In addition, the *opn* level of the Mφ + shCtrl-CM group showed a striking decrease compared with that of the Mφ + DBM-CM group (0.14 ± 0.04-fold of the Mφ + shCtrl-CM group), and the deficient of mif slightly reversed this trend (0.37 ± 0.11-fold of the Mφ + shmif-CM group) (**Figure 7B**). Furthermore, the bone formation ability of the three groups *in vivo* verified the results of qPCR and Alizarin red staining *in vitro*. 3D micro-CT images showed that more new bone tissue appeared in the *shCtrl* group and less new bone tissue appeared in the *shmif* group and DBM group. Three key evaluation indexes of micro-CT (relative bone volume, trabecular number and bone mineral density) also maintained a similar trend. The BV/TV, Tb. N and BMD of the *shmif* group (0.43 ± 0.14-fold for BV/TV, 0.05 ± 0.01-fold for Tb. N and 0.08 ± 0.02-fold for BMD) was lower than that of the *shCtrl* group (2.46 ± 1.24-fold for BV/TV, 1.10 ± 0.31-fold for Tb. N and 0.13 ± 0.03 folds for BMD) (**Figure 7C**). Based on Masson's staining, the implanted DBM retained many red scaffold fragments that had not been replaced by new bone tissue and some necrotic tissue was scattered between the scaffold fragments. The *shCtrl* scaffold fragment was replaced with new bone tissue, as indicated by endochondral ossification appearing between the scaffold fragments. The *shmif* scaffolds did not show any sign of degradation or replacement by new bone tissue as indicated by the maintenance of the scaffold structure by red collagen fibers with few green fibers (**Figure 7D**).

DISCUSSION

Osteogenic differentiation and bone formation are determined by the microenvironment, which involves many cells and cytokines, including innate immune cells and the extracellular matrix niche (Torossian et al., 2017; Rowley et al., 2019). Recently, with the emergence of osteoimmunology, the increasing studies have focused on regulating macrophage behavior to create an osteoinductive niche (Takayanagi et al., 2000; Chen et al., 2015). In this study, we created a macrophage-mediated osteoinductive niche based on hucMSC-ECM. Compared to some previous ECM-based immunomodulatory biomaterials incorporated with ECM-derived molecules, the modification by the facile tissue engineering technique not only changes the elemental distribution of DBM scaffolds, but also deposits the full natural context of the original ECM protein on DBM scaffolds, containing multiple bioactive soluble cytokines (**Figures 2C,D**; Rowley et al., 2019). The variety of cytokines deposited on scaffolds improves the ability of macrophages to express some osteoinductive cytokines, including FGF2, TGFβ3, OSM and BMP2, which provides an osteogenic microenvironment (**Figures 4–6**). Indeed, approximately eight osteoinductive genes were identified by RNA sequencing and qPCR, but the protein expression of only four cytokines was increased (**Figure 5**). Previous studies revealed that MSCs can induce monocytes/macrophages to secrete OSM, and OSM from activated macrophages could promote osteoblastic differentiation and mineralization of human muscle-derived stromal cells surrounding neurogenic heterotopic ossification (Nicolaidou et al., 2012; Torossian et al., 2017). Our results verified that hucMSC-ECM can also upregulate the expression of OSM from macrophages and improve bone formation of the *DBM-ECM* scaffolds attached to the femur with an improved heterotopic ossification model (**Figures 3**, **5**, **7**). In addition, BMP2 levels had been reported to increase in the medium of cocultured M2 macrophages and MSCs (Ekstrom et al., 2013). This study also achieved similar results that hucMSC-ECM could also upregulate macrophage-derived BMP2 expression. Furthermore, the *DBM-ECM* scaffolds enhanced FGF2 and TGFβ3 expression in addition to BMP2 (**Figure 5**). This result is consistent with observation of Chen et al. in which β-tricalcium phosphate increased the mRNA levels of BMP2, VEGF and TGFβ3 in macrophages (Chen et al., 2014, 2015). The difference is that *DBM-ECM* scaffolds can't upregulate VEGF level of macrophages. It's worth noting that *DBM-ECM* upregulated FGF2 mRNA and protein expression levels, which has rarely been observed in previous studies. Lastly, the conditioned media derived from macrophages induced by the *DBM-ECM* (Mφ + ECM-CM group) improved osteogenic differentiation and mineralization level of hBMSCs compared to ECM-CM group and Mφ-CM group (**Figure 4**). Importantly, Mφ + ECM-CM upregulated the mRNA levels of OCN and OSX in hBMSCs except for OPN (**Figure 4C**). OCN and OSX are the key molecules indicating osteogenic differentiation, while OPN is thought to enhance bone resorption by anchoring osteoclasts to bone matrix (Fukuda et al., 2018; Si et al., 2020; Sun et al., 2020). These results suggested that *DBM-ECM in vitro* could promote osteogenesis of BMSCs in a macrophage-mediated manner.

In this study, an improved heterotopic ossification model of SCID mice with clodronate liposomes or not was used to estimate the role of macrophages on bone formation of the *DBM-ECM* scaffolds. SCID mouse has no functional T and B cells, but has functional macrophages, which is usually used to build the model with engraftment human organ or cell to avoid rejection caused by human derived proteins in normal mice (Barry et al., 1991; Ronchese and Hausmann, 1993; Andoh et al., 2003). In this study, SCID mice were suitable for DBM scaffolds modified by human umbilical cord mesenchymal stem

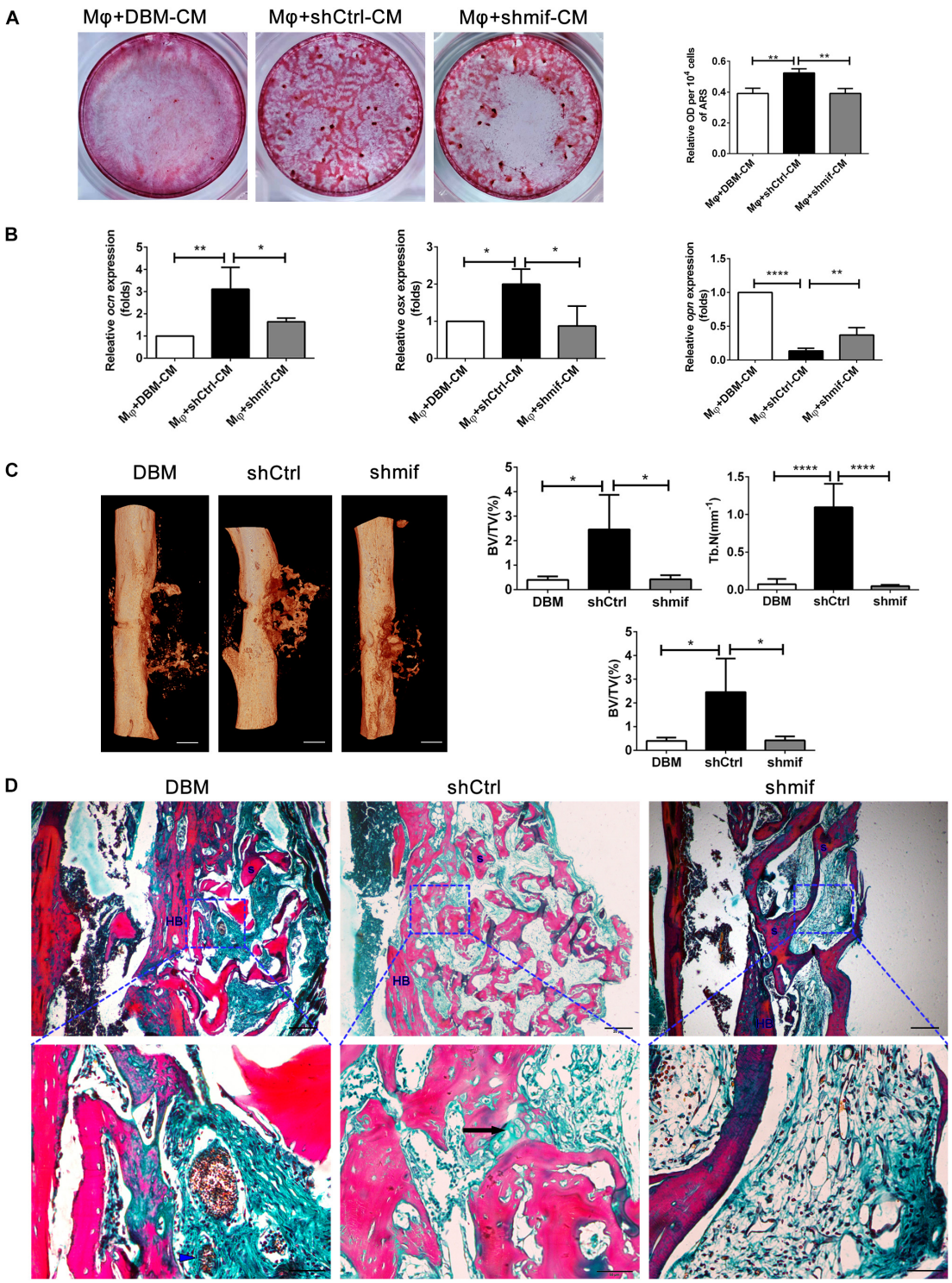

FIGURE 7 | hucMSCs-ECM improved macrophage-mediated osteogenesis of hBMSCs and bone formation via the MIF signaling pathway. **(A)** Alizarin red staining and OD value per 10^4 cells of Alizarin red deposited in calcic nodules of different groups. **(B)** mRNA levels of osteogenic genes of different groups. **(C)** Micro-CT analysis of regenerated bone induced by different scaffolds at 4 weeks postimplantation. **(D)** Masson's staining for regenerated bone induced by different scaffolds at 4 weeks postimplantation; HB, host bone; S, scaffold fragment; blue arrowhead, necrotic tissue; black arrow, endochondral ossification. Mφ + DBM-CM: the conditioned medium from macrophages cocultured with DBM scaffolds; Mφ + shCtrl-CM: the conditioned medium from macrophages cocultured with the *shCtrl* scaffolds; Mφ + shmif-CM: the conditioned medium from macrophages cocultured with the *shmif* scaffolds. Scale bar: 1 mm for **(C)**, scale bar for upper images of panel **(D)** is 20 μm and lower images of panel **(D)** is 50 μm; $^{****}p < 0.001$; $^{**}p < 0.01$; $^{*}p < 0.05$.

cells derived ECM (the *DBM-ECM*). Clodronate liposomes are usually used to deplete macrophages *in vivo*, and SCID mice with clodronate liposomes were used for estimating the role of macrophages on bone formation of the *DBM-ECM* (Beatty et al., 2015; Han et al., 2019; Michalski et al., 2019). In addition, heterotopic ossification (HO) model is suitable for estimating osteoinductive effect of scaffolds *in vivo*, which consists of ectopic bone formation within soft tissues following surgery or trauma (Shimono et al., 2011). Muscle pouch model is usually as a HO model and used to estimate ectopic bone-formation of scaffolds with or without medicine (Dong et al., 2021). In this study, an improved heterotopic ossification model was a unilateral femoral eccentric femoral defect model with the destruction of cortical bone and overflow of bone marrow, which brought much more macrophages from bone marrow compared to the muscle pouch model (**Figure 3A**). This improved heterotopic ossification model can much better reflect the role of macrophages on bone formation.

This improved heterotopic ossification model introduced a new understanding of the mechanism of MSC-induced bone formation. The earlier hypothesis was that exogenous MSCs differentiated into osteoblasts and then formed bone tissue *in vivo* (Kuznetsov et al., 1997). With the increasing evidences that massive exogenous MSCs would be dead in the early postimplantation period, the role of exogenous MSCs is recruiting endogenous stem cells to participate in bone regeneration (Caplan and Correa, 2011; Vanden, 2014). In this study, the comparison of normal and macrophage-depleted mice revealed by micro CT images that the indexes for new bone in DBM scaffolds were not significantly different, while the indexes of the *DBM-ECM* scaffolds implanted in macrophage-depleted mice were heavily decreased, suggesting that macrophages are required for bone formation induced by hucMSC-ECM (**Figure 3**). As hucMSC-ECM was similar to intact cells, and it is logical to assume that bone formation enhanced by exogenous hucMSCs might depend on the regulation of macrophages, similar to hucMSC-ECM. This new understanding of this mechanism is different from previous hypotheses and emphasizes that exogenous MSCs promote bone regeneration in a macrophage-mediated manner.

The results of this study furtherly confirmed the positive role of the MIF/CD74 signaling pathway in bone formation. Previously, MIF was regarded as a pleiotropic inflammatory cytokine involved in exaggerated inflammation and immunopathology (Farr et al., 2020). Recently, it has become appreciated that the MIF signaling pathway protects

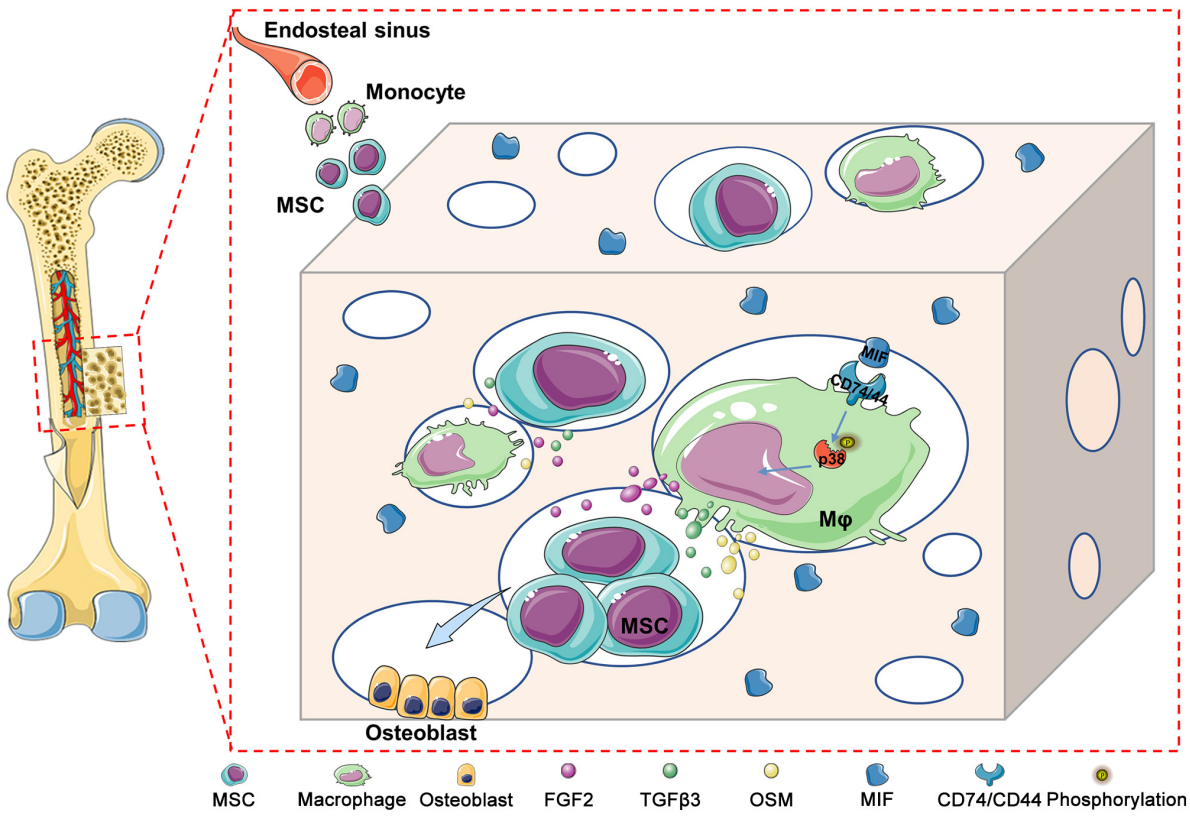

FIGURE 8 | Schematic diagram illustrating the underlying mechanism of macrophage-mediated bone formation in DBM modified by hucMSC-ECM. Briefly, *DBM-ECM*-induced bone regeneration depends on the osteogenic niche constructed by macrophage-derived paracrine molecules. MIF highly deposited in the *DBM-ECM* scaffolds activates CD74/CD44 expression in macrophages, subsequently enhances the phosphorylation of P38 and finally upregulates the expression of multiple osteoinductive cytokines, including FGF2, TGFβ3 and OSM, in macrophages, which directs the osteogenesis of BMSCs and promotes bone regeneration.

against injury and promotes repair in many tissues, including the intestine, lung, neurologic system, heart, kidney, liver, skin and hair (Farr et al., 2020; Oh et al., 2020). However, the role of MIF in bone disease healing is controversial. Shin Onodera et al. demonstrated that transgenic mice overexpressing MIF exhibit osteoporosis, and some studies have also revealed that MIF induced osteoclastogenesis in arthritic mice (Onodera et al., 2006; Gu et al., 2015). Additionally, the MIF inhibitor 4-IPP reverses osteoclast formation (Zheng et al., 2019). On the other hand, MIF-deficient mice exhibited impaired fracture healing (Kobayashi et al., 2011). In addition, mice with deletion of CD74 (the receptor of MIF) exhibited enhanced osteoclastogenesis and decreased bone mass (Mun et al., 2013). The latest studies revealed that MIF plays a protective role in osteoarthritis (Liu et al., 2021). It has even been documented that MIF induces TNF production in monocytes, activates β-catenin in osteoblasts and promotes the mineralization of osteoblasts, indicating that the MIF/CD74 axis is linked to inflammation and new bone formation seen in ankylosing spondylitis (Ranganathan et al., 2017). In this study, hucMSC-ECM enhanced the expression of osteoinductive cytokines (FGF2, TGFβ3, OSM and BMP2) in macrophages and improved osteogenic differentiation of BMSCs (**Figures 4**, **5**). MIF abundantly deposited on the *DBM-ECM* was derived from hucMSC-ECM, and this finding was consistent with that in Hyun Ah Oh et al.'s study, which showed that the content of MIF was the highest out of 57 growth factors in the conditioned medium of human umbilical cord blood-derived MSCs (**Figures 2D,E**; Oh et al., 2020). Furthermore, the Western blot results demonstrated that hucMSC-ECM with mif knockdown decreased the expression of osteoinductive cytokines (FGF2, TGFβ3 and OSM, not BMP2) in macrophages (**Figure 6C**). The downregulation of cytokine levels resulted in the decreases in calcium deposition and the mRNA expression of osteogenic genes in BMSCs (**Figures 7A,B**). Furthermore, the implanted *shmif* scaffolds *in vivo* achieved a small bone mass, which was significantly smaller than that of *shCtrl* scaffolds (**Figure 7C**). Many fragments of the *shmif* scaffolds were not replaced by new bone tissue, whereas new tissue and endochondral ossification was observed with *shCtrl* scaffolds (**Figure 7D**). These results revealed that MIF deposited in the *DBM-ECM* plays an important role in upregulating the osteoinductive cytokine expression level in macrophages, thus improving bone formation.

In addition, CD74 is a known MIF receptor, and CD44 is a coreceptor (Farr et al., 2020). The MIF/CD74 signaling pathway induces tissue repair by triggering the activation of AMP-activated protein kinase (AMPK) and the PI3K-Akt signal transduction cascade (Subbannayya et al., 2016; Farr et al., 2020). In this study, western blot results showed that *DBM-ECM* upregulated the levels of CD74 and CD44, the phosphorylation of P38 and the dephosphorylation of c-jun, while the knockdown of *mif* downregulated the expression of CD74/CD44 and p-P38 and did not affect the MAPK-c-jun or MAPK-ERK pathway. These results suggested that MIF in the *DBM-ECM* activated the CD74/CD44-P38 signal cascade (**Figures 6A,C**, **8**).

In conclusion, we constructed a macrophage-mediated niche that could guide the osteogenic differentiation of BMSCs and promote bone regeneration. We revealed the underlying mechanism of the MIF signaling cascade in the osteogenesis of BMSCs by an indirect immunomodulatory manner. Overall, the results of this study highlight that the osteoimmunomodulatory niche created by MSC-ECM might hold potential for bone healing.

DATA AVAILABILITY STATEMENT

The datasets presented in this study can be found in online repositories. The names of the repository/repositories and accession number(s) can be found below: https://www.ncbi.nlm.nih.gov/geo/query/acc.cgi?acc=GSE174477.

ETHICS STATEMENT

The animal study was reviewed and approved by the Animal Management Rule of the Ministry of Public Health, China (documentation 55, 2001).

AUTHOR CONTRIBUTIONS

MD, FL, and JX conceived and designed the study. MD completed the experiments, including animal modeling, western blotting, SEM, collected and analyzed the data, and drafted and edited the manuscript. JT completed the experiments, including cell culture, surface modification of DBM, qPCR, and osteogenesis-related assays. QD performed micro CT analysis and results statistics. All authors contributed to the article and approved the submitted version.

FUNDING

This work was supported by grants from the General Program of the National Natural Science Foundation of China (No. 81771995).

ACKNOWLEDGMENTS

We wish to acknowledge the assistance of the following individuals in the elemental distribution assay: Changshun Ruan and Juan Liu (Research Center for Human Tissue and Organs Degeneration, Shenzhen Institutes of Advanced Technology Chinese Academy of Sciences); and the preparation of the DBM scaffold: Zen Gai (Chongqing Datsing Bio-Tech Co., Ltd, Chongqing, China).

SUPPLEMENTARY MATERIAL

The Supplementary Material for this article can be found online at: https://www.frontiersin.org/articles/10.3389/fcell.2021.714011/full#supplementary-material

REFERENCES

Andoh, M., Naganawa, T., Hotta, A., Yamaguchi, T., Fukushi, H., Masegi, T., et al. (2003). SCID mouse model for lethal Q fever. *Infect. Immun.* 71, 4717–4723. doi: 10.1128/IAI.71.8.4717-4723.2003

Barry, T. S., Jones, D. M., Richter, C. B., and Haynes, B. F. (1991). Successful engraftment of human postnatal thymus in severe combined immune deficient (SCID) mice: differential engraftment of thymic components with irradiation versus anti-asialo GM-1 immunosuppressive regimens. *J. Exp. Med.* 173, 167–180. doi: 10.1084/jem.173.1.167

Beatty, G. L., Winograd, R., Evans, R. A., Long, K. B., Luque, S. L., Lee, J. W., et al. (2015). Exclusion of t cells from pancreatic carcinomas in mice is regulated by Ly6C(low) f4/80(+) extratumoral macrophages. *Gastroenterology* 149, 201–210. doi: 10.1053/j.gastro.2015.04.010

Caplan, A. I., and Correa, D. (2011). The MSC: an injury drugstore. *Cell Stem Cell* 9, 11–15. doi: 10.1016/j.stem.2011.06.008

Chen, Z., Wu, C., Gu, W., Klein, T., Crawford, R., and Xiao, Y. (2014). Osteogenic differentiation of bone marrow MSCs by beta-tricalcium phosphate stimulating macrophages via BMP2 signalling pathway. *Biomaterials* 35, 1507–1518. doi: 10.1016/j.biomaterials.2013.11.014

Chen, Z., Yuen, J., Crawford, R., Chang, J., Wu, C., and Xiao, Y. (2015). The effect of osteoimmunomodulation on the osteogenic effects of cobalt incorporated beta-tricalcium phosphate. *Biomaterials* 61, 126–138. doi: 10.1016/j.biomaterials.2015.04.044

Cho, S. W., Soki, F. N., Koh, A. J., Eber, M. R., Entezami, P., Park, S. I., et al. (2014). Osteal macrophages support physiologic skeletal remodeling and anabolic actions of parathyroid hormone in bone. *Proc. Natl. Acad. Sci. U.S.A.* 111, 1545–1550. doi: 10.1073/pnas.1315153111

Deng, M., Chang, Z., Hou, T., Dong, S., Pang, H., Li, Z., et al. (2016). Sustained release of bioactive protein from a lyophilized tissue-engineered construct promotes the osteogenic potential of mesenchymal stem cells. *J. Orthop. Res.* 34, 386–394. doi: 10.1002/jor.23027

Deng, M., Tan, J., Hu, C., Hou, T., Peng, W., Liu, J., et al. (2020). Modification of PLGA scaffold by MSC-derived extracellular matrix combats macrophage inflammation to initiate bone regeneration via TGF-β-induced protein. *Adv. Healthc. Mater.* 9:2000353. doi: 10.1002/adhm.202000353

Dong, J., Xu, X., Zhang, Q., Yuan, Z., and Tan, B. (2021). Critical implication of the PTEN/PI3K/AKT pathway during BMP2-induced heterotopic ossification. *Mol. Med. Rep.* 23:254. doi: 10.3892/mmr.2021.11893

Ekstrom, K., Omar, O., Graneli, C., Wang, X., Vazirisani, F., and Thomsen, P. (2013). Monocyte exosomes stimulate the osteogenic gene expression of mesenchymal stem cells. *PLoS One* 8:e75227. doi: 10.1371/journal.pone.0075227

Farr, L., Ghosh, S., and Moonah, S. (2020). Role of MIF Cytokine/CD74 receptor pathway in protecting against injury and promoting repair. *Front. Immunol.* 11:1273. doi: 10.3389/fimmu.2020.01273

Fukuda, M., Yoshizawa, T., Karim, M. F., Sobuz, S. U., Korogi, W., Kobayasi, D., et al. (2018). SIRT7 has a critical role in bone formation by regulating lysine acylation of SP7/Osterix. *Nat. Commun.* 9:2833. doi: 10.1038/s41467-018-05187-4

Gu, R., Santos, L. L., Ngo, D., Fan, H., Singh, P. P., Fingerle-Rowson, G., et al. (2015). Macrophage migration inhibitory factor is essential for osteoclastogenic mechanisms in vitro and in vivo mouse model of arthritis. *Cytokine* 72, 135–145. doi: 10.1016/j.cyto.2014.11.015

Han, X., Li, Q., Lan, X., El-Mufti, L., Ren, H., and Wang, J. (2019). Microglial depletion with clodronate liposomes increases proinflammatory cytokine levels, induces astrocyte activation, and damages blood vessel integrity. *Mol. Neurobiol.* 56, 6184–6196. doi: 10.1007/s12035-019-1502-9

Hu, Y., Zhang, Y., Ni, C. Y., Chen, C. Y., Rao, S. S., Yin, H., et al. (2020). Human umbilical cord mesenchymal stromal cells-derived extracellular vesicles exert potent bone protective effects by CLEC11A-mediated regulation of bone metabolism. *Theranostics* 10, 2293–2308. doi: 10.7150/thno.39238

Jankauskas, S. S., Wong, D. W. L., Bucala, R., Djudjaj, S., and Boor, P. (2019). Evolving complexity of MIF signaling. *Cell. Signal.* 57, 76–88. doi: 10.1016/j.cellsig.2019.01.006

Kelly, R. R., Sidles, S. J., and LaRue, A. C. (2020). Effects of Neurological Disorders on Bone Health. *Front. Psychol.* 11:612366. doi: 10.3389/fpsyg.2020.612366

Kobayashi, T., Onodera, S., Kondo, E., Tohyama, H., Fujiki, H., Yokoyama, A., et al. (2011). Impaired fracture healing in macrophage migration inhibitory factor-deficient mice. *Osteoporos Int.* 22, 1955–1965. doi: 10.1007/s00198-010-1385-0

Kuznetsov, S. A., Krebsbach, P. H., Satomura, K., Kerr, J., Riminucci, M., Benayahu, D., et al. (1997). Single-colony derived strains of human marrow stromal fibroblasts form bone after transplantation in vivo. *J. Bone Miner. Res.* 12, 1335–1347. doi: 10.1359/jbmr.1997.12.9.1335

Li, M., Chen, X., Yan, J., Zhou, L., Wang, Y., He, F., et al. (2018). Inhibition of osteoclastogenesis by stem cell-derived extracellular matrix through modulation of intracellular reactive oxygen species. *Acta Biomater.* 71, 118–131. doi: 10.1016/j.actbio.2018.03.003

Li, S., Song, C., Yang, S., Yu, W., Zhang, W., Zhang, G., et al. (2019). Supercritical CO2 foamed composite scaffolds incorporating bioactive lipids promote vascularized bone regeneration via Hif-1α upregulation and enhanced type H vessel formation. *Acta Biomater.* 94, 253–267. doi: 10.1016/j.actbio.2019.05.066

Liu, M., Xie, Z., Sun, G., Chen, L., Qi, D., Zhang, H., et al. (2021). Macrophage migration inhibitory factor may play a protective role in osteoarthritis. *Arthritis Res. Ther.* 23:59. doi: 10.1186/s13075-021-02442-w

Luo, K., Mei, T., Li, Z., Deng, M., Zhang, Z., Hou, T., et al. (2016). A High-Adhesive Lysine-Cyclic RGD peptide designed for selective cell retention technology. *Tissue Eng. Part C Methods* 22, 585–595. doi: 10.1089/ten.TEC.2015.0517

Ma, Y., Hu, N., Liu, J., Zhai, X., Wu, M., Hu, C., et al. (2019). Three-Dimensional printing of biodegradable Piperazine-Based Polyurethane-Urea scaffolds with enhanced osteogenesis for bone regeneration. *ACS Appl. Mater. Interfaces* 11, 9415–9424. doi: 10.1021/acsami.8b20323

Michalski, M. N., Zweifler, L. E., Sinder, B. P., Koh, A. J., Yamashita, J., Roca, H., et al. (2019). Clodronate-Loaded liposome treatment has Site-Specific skeletal effects. *J. Dent. Res.* 98, 459–467. doi: 10.1177/0022034518821685

Mun, S. H., Won, H. Y., Hernandez, P., Aguila, H. L., and Lee, S. K. (2013). Deletion of CD74, a putative MIF receptor, in mice enhances osteoclastogenesis and decreases bone mass. *J. Bone Miner. Res.* 28, 948–959. doi: 10.1002/jbmr.1787

Nicolaidou, V., Wong, M. M., Redpath, A. N., Ersek, A., Baban, D. F., Williams, L. M., et al. (2012). Monocytes induce STAT3 activation in human mesenchymal stem cells to promote osteoblast formation. *PLoS One* 7:e39871. doi: 10.1371/journal.pone.0039871

Niu, Y., Li, Q., Xie, R., Liu, S., Wang, R., Xing, P., et al. (2017). Modulating the phenotype of host macrophages to enhance osteogenesis in MSC-laden hydrogels: design of a glucomannan coating material. *Biomaterials* 139, 39–55. doi: 10.1016/j.biomaterials.2017.05.042

Oh, H. A., Kwak, J., Kim, B. J., Jin, H. J., Park, W. S., Choi, S. J., et al. (2020). Migration inhibitory factor in conditioned medium from human umbilical cord Blood-Derived mesenchymal stromal cells stimulates hair growth. *Cells* 9:1344. doi: 10.3390/cells9061344

Onodera, S., Sasaki, S., Ohshima, S., Amizuka, N., Li, M., Udagawa, N., et al. (2006). Transgenic mice overexpressing macrophage migration inhibitory factor (MIF) exhibit high-turnover osteoporosis. *J. Bone Miner. Res.* 21, 876–885. doi: 10.1359/jbmr.060310

Pajarinen, J., Lin, T., Gibon, E., Kohno, Y., Maruyama, M., Nathan, K., et al. (2019). Mesenchymal stem cell-macrophage crosstalk and bone healing. *Biomaterials* 196, 80–89. doi: 10.1016/j.biomaterials.2017.12.025

Ranganathan, V., Ciccia, F., Zeng, F., Sari, I., Guggino, G., Muralitharan, J., et al. (2017). Macrophage migration inhibitory factor induces inflammation and predicts spinal progression in ankylosing spondylitis. *Arthritis Rheumatol.* 69, 1796–1806. doi: 10.1002/art.40175

Ronchese, F., and Hausmann, B. (1993). B lymphocytes in vivo fail to prime naive T cells but can stimulate antigen-experienced T lymphocytes. *J. Exp. Med.* 177, 679–690. doi: 10.1084/jem.177.3.679

Rowley, A. T., Nagalla, R. R., Wang, S. W., and Liu, W. F. (2019). Extracellular matrix-based strategies for immunomodulatory biomaterials engineering. *Adv. Healthc. Mater.* 8:1801578. doi: 10.1002/adhm.201801578

Schlundt, C., El Khassawna, T., Serra, A., Dienelt, A., Wendler, S., Schell, H., et al. (2018). Macrophages in bone fracture healing: their essential role in endochondral ossification. *Bone* 106, 78–89. doi: 10.1016/j.bone.2015.10.019

Shimono, K., Tung, W. E., Macolino, C., Chi, A. H., Didizian, J. H., Mundy, C., et al. (2011). Potent inhibition of heterotopic ossification by nuclear retinoic acid receptor-gamma agonists. *Nat. Med.* 17, 454–460. doi: 10.1038/nm.2334

Shiratori, H., Feinweber, C., Luckhardt, S., Linke, B., Resch, E., Geisslinger, G., et al. (2017). THP-1 and human peripheral blood mononuclear cell-derived macrophages differ in their capacity to polarize in vitro. *Mol. Immunol.* 88, 58–68. doi: 10.1016/j.molimm.2017.05.027

Si, J., Wang, C., Zhang, D., Wang, B., and Zhou, Y. (2020). Osteopontin in bone metabolism and bone diseases. *Med. Sci. Monit.* 26:e919159. doi: 10.12659/MSM.919159

Subbannayya, T., Variar, P., Advani, J., Nair, B., Shankar, S., Gowda, H., et al. (2016). An integrated signal transduction network of macrophage migration inhibitory factor. *J. Cell Commun. Signal.* 10, 165–170. doi: 10.1007/s12079-016-0326-x

Sun, P., He, L., Jia, K., Yue, Z., Li, S., Jin, Y., et al. (2020). Regulation of body length and bone mass by Gpr126/Adgrg6. *Sci. Adv.* 6:z368. doi: 10.1126/sciadv.aaz0368

Swartzlander, M. D., Blakney, A. K., Amer, L. D., Hankenson, K. D., Kyriakides, T. R., and Bryant, S. J. (2015). Immunomodulation by mesenchymal stem cells combats the foreign body response to cell-laden synthetic hydrogels. *Biomaterials* 41, 79–88. doi: 10.1016/j.biomaterials.2014.11.020

Takayanagi, H., Ogasawara, K., Hida, S., Chiba, T., Murata, S., Sato, K., et al. (2000). T-cell-mediated regulation of osteoclastogenesis by signalling cross-talk between RANKL and IFN-gamma. *Nature* 408, 600–605. doi: 10.1038/35046102

Torossian, F., Guerton, B., Anginot, A., Alexander, K. A., Desterke, C., Soave, S., et al. (2017). Macrophage-derived oncostatin M contributes to human and mouse neurogenic heterotopic ossifications. *JCI Insight* 2:e96034. doi: 10.1172/jci.insight.96034

Vanden, B. W. (2014). In situ tissue regeneration: chemoattractants for endogenous stem cell recruitment. *Tissue Eng. Part B Rev.* 20, 28–39. doi: 10.1089/ten.TEB.2013.0100

Wang, P., Liu, X., Zhao, L., Weir, M. D., Sun, J., Chen, W., et al. (2015). Bone tissue engineering via human induced pluripotent, umbilical cord and bone marrow mesenchymal stem cells in rat cranium. *Acta Biomater.* 18, 236–248. doi: 10.1016/j.actbio.2015.02.011

Wu, X., Schulte, B. C., Zhou, Y., Haribhai, D., Mackinnon, A. C., Plaza, J. A., et al. (2014). Depletion of M2-like tumor-associated macrophages delays cutaneous T-cell lymphoma development in vivo. *J. Invest. Dermatol.* 134, 2814–2822. doi: 10.1038/jid.2014.206

Yin, X., Liu, X., Zhang, Y., Yan, G., Wang, F., Lu, H., et al. (2014). Rapid and sensitive profiling and quantification of the human cell line proteome by LC-MS/MS without prefractionation. *Proteomics* 14, 2008–2016. doi: 10.1002/pmic.201300510

Zhao, L., Weir, M. D., and Xu, H. H. (2010). An injectable calcium phosphate-alginate hydrogel-umbilical cord mesenchymal stem cell paste for bone tissue engineering. *Biomaterials* 31, 6502–6510. doi: 10.1016/j.biomaterials.2010.05.017

Zheng, L., Gao, J., Jin, K., Chen, Z., Yu, W., Zhu, K., et al. (2019). Macrophage migration inhibitory factor (MIF) inhibitor 4-IPP suppresses osteoclast formation and promotes osteoblast differentiation through the inhibition of the NF-kappaB signaling pathway. *FASEB J.* 33, 7667–7683. doi: 10.1096/fj.201802364RR

Zhu, W., Sun, L., Zhao, P., Liu, Y., Zhang, J., Zhang, Y., et al. (2021). Macrophage migration inhibitory factor facilitates the therapeutic efficacy of mesenchymal stem cells derived exosomes in acute myocardial infarction through upregulating miR-133a-3p. *J. Nanobiotechnol.* 19:61. doi: 10.1186/s12951-021-00808-5

Conflict of Interest: The authors declare that the research was conducted in the absence of any commercial or financial relationships that could be construed as a potential conflict of interest.

Publisher's Note: All claims expressed in this article are solely those of the authors and do not necessarily represent those of their affiliated organizations, or those of the publisher, the editors and the reviewers. Any product that may be evaluated in this article, or claim that may be made by its manufacturer, is not guaranteed or endorsed by the publisher.

frontiers in Cell and Developmental Biology

ORIGINAL RESEARCH
published: 26 October 2021
doi: 10.3389/fcell.2021.768316

Dynamics of Transcription Factors in Three Early Phases of Osteogenic, Adipogenic, and Chondrogenic Differentiation Determining the Fate of Bone Marrow Mesenchymal Stem Cells in Rats

*Qingyu Zhang, Jun Dong, Peng Zhang, Dongsheng Zhou and Fanxiao Liu**

Department of Orthopaedics, Shandong Provincial Hospital Affiliated to Shandong First Medical University, Jinan, China

OPEN ACCESS

Edited by:
Xiao Chen,
Second Military Medical University, China

Reviewed by:
Changliang Peng,
Second Hospital of Shandong University, China
Yan Wang,
Peking Union Medical College Graduate School, China

***Correspondence:**
Fanxiao Liu
woshi631@126.com;
liufanxiao@sdfmu.edu.cn
orcid.org/0000-0002-1412-849X

Specialty section:
This article was submitted to Cellular Biochemistry, a section of the journal Frontiers in Cell and Developmental Biology

Received: *31 August 2021*
Accepted: *05 October 2021*
Published: *26 October 2021*

Citation:
Zhang Q, Dong J, Zhang P, Zhou D and Liu F (2021) Dynamics of Transcription Factors in Three Early Phases of Osteogenic, Adipogenic, and Chondrogenic Differentiation Determining the Fate of Bone Marrow Mesenchymal Stem Cells in Rats. Front. Cell Dev. Biol. 9:768316. doi: 10.3389/fcell.2021.768316

The imbalance of osteogenic, adipogenic, and chondrogenic differentiation in bone marrow mesenchymal stem cells (BMSCs) occurred in multiple age-related degenerative diseases such as osteoporosis and osteoarthritis. In order to improve our understanding and control of multi-directional differentiation of BMSCs in rats, using high-throughput sequencing, we identified key gene regulatory events in the early stages of lineage commitment. Data analysis revealed two transcription factors (TFs, Tsc22d3, and Epas1) with elevated expression throughout the initiation of differentiation (3 h), lineage acquisition (12 h), and early lineage progression (72 h) of three-directional differentiation. For osteogenic differentiation, 792, 1,042, and 638 differentially expressed genes including 48, 59, and 34 TFs were identified at three time points, respectively. Moreover, the functional analysis demonstrated that 4, 12, and 5 TFs were only differentially expressed during osteogenic differentiation at 3, 12, and 72 h, respectively, and not during other two-directional differentiation. Hopx showed enhanced expression throughout three early phases during the osteogenic differentiation but no significant change in other two-directional differentiation. A similar pattern of Gbx2 expression occurred in chondrogenic differentiation. Thus, Hopx and other early responder TFs may control the osteogenic cell fate of BMSCs and participate in the development of osteoporosis. Gbx2 and other early responder TFs should be considered in mechanistic models that clarify cartilage-anabolic changes in the clinical progression of osteoarthritis.

Keywords: bone marrow mesenchymal stem cells (BMSCs), high-throughput sequencing, osteogenic differentiation, chondrogenic differentiation, transcription factors, adipogenic differentiation

INTRODUCTION

Bone mesenchymal stem/stromal cells (BMSCs) have the potentials of differentiating into several mesodermal derivatives, in particular osteogenic (osteogenic progenitors, osteocytes, osteoblasts, and bone lining cells), adipogenic and chondrogenic cells in the existence of physiological demands or pathological changes (Arthur and Gronthos, 2020; Jiang et al., 2021). Systematic cell-based

therapy by administration of *in vivo* expanded BMSCs could serve as an excellent alternative for bone regeneration and tissue engineering (Arthur and Gronthos, 2020; Robert et al., 2020; Jiang et al., 2021), but it is not yet a standard clinical practice due to donor variation among patients and unpredictable direction for cell differentiation (Crapnell et al., 2013; O'Connor, 2019).

The adipogenesis and osteogenesis of BMSCs are competing and reciprocal, keeping homeostasis within the bone. The primary role of BMSCs-derived osteoblasts is to produce and secrete osteoid and mineralizing factors to remodel bone according to the metabolic and structural needs of the body (Yu and Wang, 2016). During aging and the development of bone remodeling disorders such as osteoporosis and osteonecrosis, the normal balance between osteogenic and adipogenic cell populations can shift toward the latter and result in increased formation of marrow fat (Zhang et al., 2018; Pittenger et al., 2019; Robert et al., 2020; Saeedi et al., 2021). Hyaline cartilage is responsible for bone formation in the embryo and can be found in the articular surface of the bones of adults (Carballo et al., 2017). Until now, the *in vitro* differentiation process is unable to produce cartilage similar to articular cartilage formed under normal physiological conditions (Huynh et al., 2019). Further understanding the mechanism for the three-directional differentiation of BMSCs is imperative.

The differentiation of BMSCs is a two-step process, lineage commitment (from MSCs to lineage-specific progenitors) and maturation (from progenitors to specific cell types) (Robert et al., 2020). The lineage commitment of MSCs to adipocytes, osteoblasts and chondrocytes share a common precursor (Chen et al., 2016; Yianni and Sharpe, 2020), and intensive studies in recent decades have demonstrated that a number of signaling pathways and transcription factors (TFs) are critical for this process (van de Peppel et al., 2017). RUNX2, SP7/Osterix, and SOX9 are among the leading TFs involved in the differentiation of MSCs into osteoblasts or chondrocytes, while PPARγ and cyclic AMP response element-binding protein (CREB) are required for adipogenic differentiation (Chen et al., 2016; Pittenger et al., 2019; Robert et al., 2020). Overexpression of RUNX2 in non-osteoblastic cells and adipose-tissue-derived MSCs elevates the level of osteoblastic markers, promotes mineralization and inhibits lineage commitment to adipocytes, indicating that a single TF is important for bone development and osteoblast differentiation (Robert et al., 2020). During adipogenesis, the production of cyclic AMP is augmented, resulting in phosphorylation of CREB and an increased expression of CEBPβ (Merrett et al., 2020). CEBPβ, together with the other two CEBP family members (CEBPα and CEBPδ), was reported to be implicated in adipogenic differentiation (Chen et al., 2016; Hu et al., 2018; Robert et al., 2020).

Although the enriched biological processes and TFs are mostly identical between these lineages within the first 4 days after induction (van de Peppel et al., 2017; Fang et al., 2020), the early stages of lineage commitment of human BMSCs could be further divided into three distinct phases with own mRNA dynamics: initiation of differentiation (0–3 h, phase I), lineage acquisition (6–24 h, phase II), and early lineage progression (48–96 h, phase III) (van de Peppel et al., 2017). Downstream analyses of four TFs (TP53, FOSl1, ESR1, and HOXA9) identified during the first phase of osteogenic differentiation are capable of regulating more than 50% of the differentially expressed genes (DEGs) in the second and third phases. However, the expression of TFs in chondrogenic differentiation during this stage was not systematically investigated. Meanwhile, this study used human BMSCs, while key TFs playing critical roles in lineage commitment of rat BMSCs were not considered.

BMSCs from 4 different species (human, pig, rat, guinea pig) fail to elicit a proliferative response from allogeneic lymphocytes and therefore can function across the species barrier (Li et al., 2012). Given the unique immunologic properties of rat BMSC, BMSC from rats is an attractive option for xenografts. In the current study, *in vivo* differentiation of rat BMSCs from a two-dimensional culture system was applied, and by using high-throughput transcriptome sequencing technique and multiple bioinformatics methods, we systematically investigated genes, especially TFs being regulated upon lineage commitment of rat BMSCs into adipocytes, chondrocytes, and osteocytes. One of our key findings was the characterization of genes and regulatory programs controlling the early stages of lineage commitment of rat BMSCs. Progress in this area will be of great value to understand age- and pathology-related fractures and metabolic syndromes, and to guide a better application of BMSCs in tissue engineering and regenerative medicine.

MATERIALS AND METHODS

Cell Isolation and Induced Differentiation

This study was approved by the Animal Ethics Committee of Shandong Provincial Hospital affiliated to Shandong First Medical University. BMSCs were collected from femurs and tibia of 3 female Sprague Dawley (SD) rats (3 weeks old) by washing the marrow cavity using high glucose Dulbecco's Modified Eagle Medium (DMEM) (Gibco, Rockville, MD, United States) until bones appear white. Obtained cell clumps were dispersed to cell suspension by using 21-gauge needles. The cells were cultured in DMEM supplemented with 10% fetal bovine serum (FBS) in an incubator of 5% CO_2 and 95% humidity at 37°C. BMSCs at passage 2 were seeded in 12-well cell culture plates and after 2 days, cells were induced to differentiate into osteoblasts using mesenchymal stem cell osteogenic differentiation medium (Promocell, Germany, C-28013), or to adipocytes using mesenchymal stem cell adipogenic differentiation medium (Promocell, Germany, C-28016), or to chondrocytes using mesenchymal stem cell chondrogenic differentiation medium (Promocell, C-28012). Differentiation media were replaced every 3–4 day.

Protein Concentration Assay and Bone Marrow Mesenchymal Stem Cells Staining

Protein concentration assay, Elisa assay, alizarin red staining, Oil Red O staining and Alcian blue staining were performed as previously described (Bruedigam et al., 2011; Gari et al., 2016).

RNA Isolation

To obtain enough RNA for the gene expression profiling analyses, we pooled three individual cultures in TRIzol (Life Technologies), resulting in a total of three experimental samples per time point (3 time points, namely, 3, 12, and 72 h) per lineage (osteogenic, adipogenic, or chondrogenic) to be used for gene expression profiling analyses. Plus, the control samples, there were a total of 30 samples. RNA was isolated as previously described (Bruedigam et al., 2011).

High-Throughput Sequencing

The quality of RNA was analyzed using NanoDrop™ One (Thermo Fisher Scientific, United States). An mRNA library was constructed by NEBNext® Ultra™ II mRNA Library Prep Kit for Illumina® (NEB, United States). Qubit™ dsDNA HS Assay Kit (Invitrogen, United States), D1000 Screen Tape (Agilent, United States), and KAPA Library Quant kit (illumine, United States) universal qPCR Mix were used to assess the quality and yield of the constructed library. Finally, the mRNA was sequenced by NovaSeq 6000 (Illumina, United States).

Sequencing Result Analysis

After standardization and quality control of the sequencing data, the differential expression of mRNA was analyzed. | log2fold change (FC)| in mRNA expression $\geq$ 1 with an adjusted p-value < 0.05 was used as the threshold for determining gene upregulation or downregulation. Differentially expressed TFs were identified by using the AnimalTFDB 3.0 database.[1] Gene Ontology (GO) enrichment[2] and Kyoto Encyclopedia of Genes and Genomes (KEGG) enrichment[3] analysis was utilized to determine the biological function of the differentially expressed TFs and investigate its possible involvement in the lineage-commitment of rat BMSCs. The protein-protein interaction (PPI) network of identified genes was predicted using the multiple protein online tool in STRING database (Liu et al., 2021), a search tool for the Retrieval of Interacting Genes database (version 11.0b)[4] and visualized in Cytoscape software (Version 3.6.2). Relationships between critical TFs and their differentially expressed target genes were predicted to construct the TF-target regulatory network based on the previous method (Zhang et al., 2017; Zhou et al., 2021).

Statistical Analysis

Statistical analyses were conducted by using SPSS Software, version 17.0 (IBM SPSS Statistics, United States). One-way analysis of variance (ANOVA) followed by LSD method was used to compare the protein concentration and ALP

[1]http://bioinfo.life.hust.edu.cn/AnimalTFDB/#!/
[2]http://www.geneontology.org/
[3]https://david.ncifcrf.gov/summary.jsp
[4]http://string-db.org

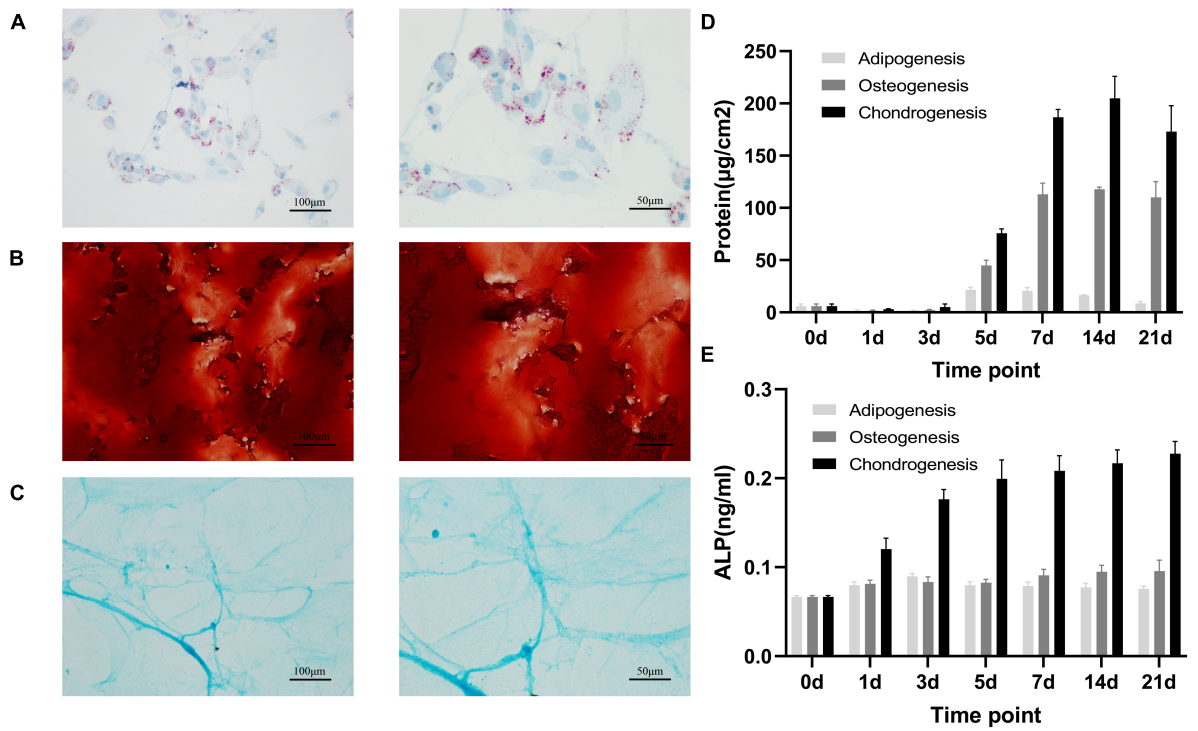

FIGURE 1 | Adipogenic, osteogenic and chondrogenic differentiation of rat BMSCs. Histochemical staining of calcium **(A)** with Alizarin red or adipocyte **(B)** with oil red O or cartilage **(C)** with Alcian blue staining after 21 days of osteogenic or adipogenic or chondrogenic differentiation. Scale bars, 100 and 50 μm; total protein **(D)** and ALP **(E)** concentration in osteogenesis, adipogenesis and chondrogenesis of rat BMSC. Error bars indicate SD. Mean and SD of three independent experiments with three technical replicates.

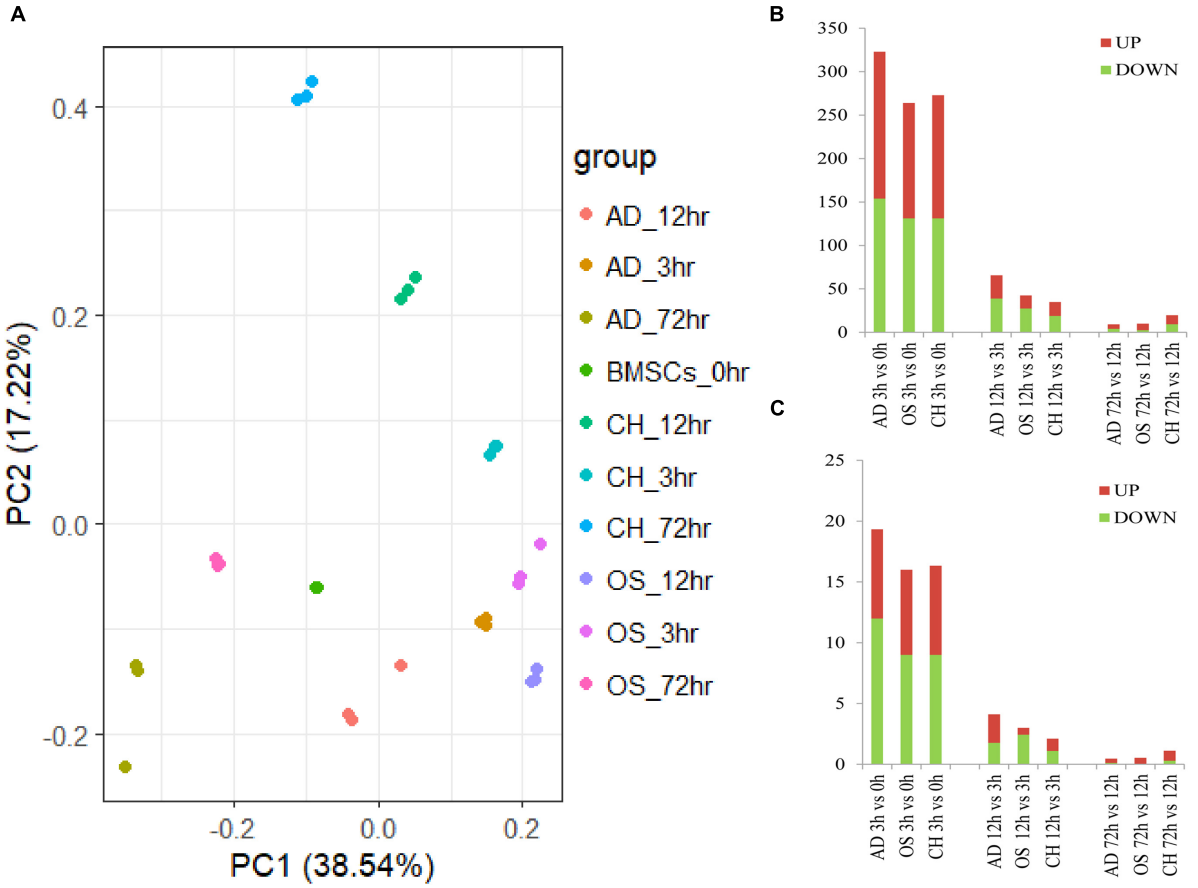

FIGURE 2 | Dynamic transcriptional changes upon osteogenic, adipogenic, and chondrogenic differentiation of rat BMSCs. **(A)** Principal component analyses of the gene expression profile in osteogenic, adipogenic, and chondrogenic groups at three time points; **(B)** number of significant differential TFs relative to the previous time point (based on three independent experiments); and **(C)** the number of differentially expressed TFs per hour compared to the previous time point (based on three independent experiments). AD, adipogenesis; OS, osteogenesis; CH, chondrogenesis.

expression between different groups, which are expressed as the means ± standard deviation. Differences between means were considered statistically significant when p-values were < 0.05.

RESULTS

Differentiation of Rat Bone Marrow Mesenchymal Stem Cells Into Osteoblasts, Adipocytes, and Chondrocytes

On day 21 after induced differentiation, histological staining for calcium in the osteogenic differentiation group showed that extracellular matrix (ECM) was mineralized (**Figure 1A**), Oil Red O staining for lipids in the adipogenic differentiation group showed that cells accumulated intracellular lipid vesicle (**Figure 1B**), and Alcian blue staining in the chondrocyte differentiation group showed cartilage formation (**Figure 1C**). Biochemical analyses of samples during differentiation revealed that total protein and alkaline phosphatase (ALP) concentration transiently increased during adipogenic, osteogenic, and chondrogenic differentiation (**Figures 1D,E**). Together, our observations established that rat BMSCs differentiated into three lineages, consistent with their expected multi-lineage potential.

Identification of Differentially Expressed Transcription Factors in Three Phases

Data cross−comparability was evaluated via principal component analysis (PCA) for confirming biological variability between different samples. All samples were grouped separately (**Figure 2A**), indicating globally distinct expression profiles. Analysis of gene expression dynamics during rat BMSC differentiation revealed that transcript levels changed significantly 3 h upon induction of differentiation (**Figure 2B**). During induction of osteogenic differentiation, 792, 1,042, and 638 DEGs were identified at three time points, respectively. At least 48 TFs (21 upregulated and 27 downregulated ones) were significantly different at 3 h and this increased further to 59 (25 upregulated and 34 downregulated ones) at 12 h. The number of significantly modulated TFs decreased to 34

TABLE 1 | The same differential expressed TFs at three time points after differentiation into osteoblasts, adipocytes, and chondroblasts.

Groups	Total	TFs	Groups	Total	TFs
OS3h, 12h, 72h; AD3h, 12h, 72h, CH3h, 12h, 72h	2	Tsc22d3, Epas1	CH3h, 12h, 72h; OS72h	1	Plscr1
OS3h, 12h, 72h; AD3h, 12h, 72h, CH3h, 72h	2	Rab24, Cenpa	CH3h, 12h; OS3h, 12h	1	Atoh8
OS12h; AD3h, 12h, 72h; CH3h, 12h, 72h	1	Sox9	AD3h, 12h; CH12h	1	Klf5
OS3h, 12h; AD3h, 12h, 72h, CH3h, 12h	2	Id3, Id2	AD3h; CH3h; OS3h	1	Hmg20a
OS72h; AD3h, 12h, 72h; CH12h, 72h	1	Snai2	AD3h; OS3h, 12h	2	Phb, Emx2
OS3h, 12h; AD3h, 12h; CH3h, 72h	1	Ahrr	AD12h; CH72h; OS12h	1	Bhlhe41
OS12h, 72h; AD3h, 72h; CH12h, 72h	1	Klf10	AD72h; CH72h; OS72h	1	Tfcp2l1
OS3h, 12h, 72h; AD3h; CH3h, 12h	1	Meox2	CH3h, 12h, 72h	1	Gbx2
OS72h; AD12h, 72h; CH3h, 12h, 72h	1	Hic1	CH3h, 12h; OS3h	2	Sox11, AABR07001099.1
AD3h, 12h, 72h; CH3h, 72h	1	Irf5	CH3h, 12h; OS12h	1	Tbx4
AD3h, 12h, 72h; CH12h, 72h	1	Bhlhe40	CH3h; OS3h, 12h	1	Hoxd13
OS3h, 12h; AD3h, 12h; CH3h	2	Cenpt, Foxm1	CH12h; OS3h, 12h	1	Nme2
OS3h, 12h, 72h; AD3h, 72h	1	Klf4	CH12h; OS12h, 72h	1	AABR07015743.1
OS3h, 12h; AD3h; CH3h, 12h	1	Hbp1	OS3h, 12h, 72h	1	Hopx
OS3h, 12h; AD3h; CH3h, 72h	1	Zfp467	AD3h; CH3h	2	Zfp668, Mef2a
OS3h, 12h, 72h; AD3h; CH72h	1	Dlx3	AD3h; CH72h	1	Ets2
OS3h, 12h; AD12h, 72h; CH72h	1	Ehf	AD3h; OS3h	1	Foxf1
OS72h; AD72h; CH3h, 12h, 72h	2	Nfia, Scx	AD72h; CH12h	1	Nr1d1
OS12h, 72h; AD72h; CH3h, 72h	1	Pax8	AD72h; OS72h	2	Ascl2, Zfp503
OS3h, 12h, 72h; AD72h; CH3h	1	Mafb	OS12h; CH3h	1	Hey2
OS3h, 12h; CH3h, 12h, 72h	1	Tshz2	AD3h, 12h	2	Zfp667, Nr4a1
OS12h, 72h; CH3h, 12h, 72h	1	Tsc22d1	AD12h, 72h	1	Arid3b
OS12h; AD3h, 12h, 72h	1	Hoxd9	CH3h, 12h	2	Zfp394, Jun
AD3h, 12h, 72h; OS72h	1	Zfp536	CH12h, 72h	2	Gsc, Terf1
AD3h, 12h; CH3h; OS12h	1	Relb	OS3h, 12h	4	Zfp773-ps1, Klf16, Zfp367, Foxn1
AD3h, 72h; CH3h; OS3h	1	Klf3	OS3h, 72h	1	Zfp296
AD3h, 72h; OS3h, 12h	1	Zfp521	OS12h, 72h	2	Rfx2, Hif1a
AD3h; CH3h, 12h; OS3h	1	Hoxc6	OS3h	4	Ybx3, Zbtb25, Hes6, Zfp879
AD3h; CH3h, 72h; OS12h	1	Rfx3	OS12h	12	Gtf3a, Hoxd3, LOC500584, Csdc2, Maf, Zfp113, Zfp174, LOC108349189, E2f2, Rbpjl, Pou5f2, AABR07029613.1
AD3h; CH3h; OS3h, 12h	3	Tbx6, Foxc2, Mxd4	OS72h	5	Tmf1, Msx2, Tcf23, Rfx8, Pparg
AD3h; CH12h; OS3h, 72h	1	Zfp39	AD3h	15	Pou6f1, Sp5, L3mbtl1, Lhx9, Zbtb38, Hoxd10, Pax4, Arid2, Zfp317, Zeb1, Tulp1, Zfp541, Pou2f3, Foxc1, Zbtb12
AD3h; OS3h, 12h, 72h	1	Tead3	AD12h	1	Atf4
AD12h, 72h; CH12h, 72h	1	Creb3l1	AD72h	5	RGD1560108, Hlx, Foxo3, Osr1, LOC100362054
AD12h; CH3h, 72h; OS12h	1	Hmgb2	CH3h	7	Preb, Csrnp3, Mafa, Lef1, Stat6, Prdm16, Zfp395
AD72h; OS3h, 12h, 72h	1	Zfhx2	CH12h	4	Lrrfip2, Zfp62, Tfam, AABR07060287.1
CH3h, 12h, 72h; OS3h	1	Runx3	CH72h	8	Smarca1, Myrfl, Mlxip, Dlx5, Rarb, Heyl, Foxd2, Gli1

OS, osteogenic differentiation; CH, chondrogenic differentiation AD, adipogenic differentiation; TF, transcription factor.

(22 upregulated and 12 downregulated ones) at 72 h. During adipogenic differentiation, the number of differentially expressed TFs was 58 at 3 h, 26 at 12 h, and 36 at 72 h. During chondrogenic differentiation, the number was 49 at 3 h, 38 at 12 h, and 39 at 72 h. Remarkably, at 3 and 12h after differentiation, the number of downregulated TFs was higher than the upregulated ones. Next, we calculated the number of differentially expressed TFs at each time point compared with the preceding time point and in three directions of differentiation, the number of TFs that changed per hour decreased as time extends (**Figure 2C**). Differentially expressed TFs in three time points during three-directional differentiation were summarized in **Table 1**.

The volcano plot and heatmap of differentially expressed TFs at 3, 12, and 72 h of osteogenesis were shown in **Figure 3**, while results of comparison between every two lineage-commitment at 3 h after inductive differentiation were presented in **Figure 4**.

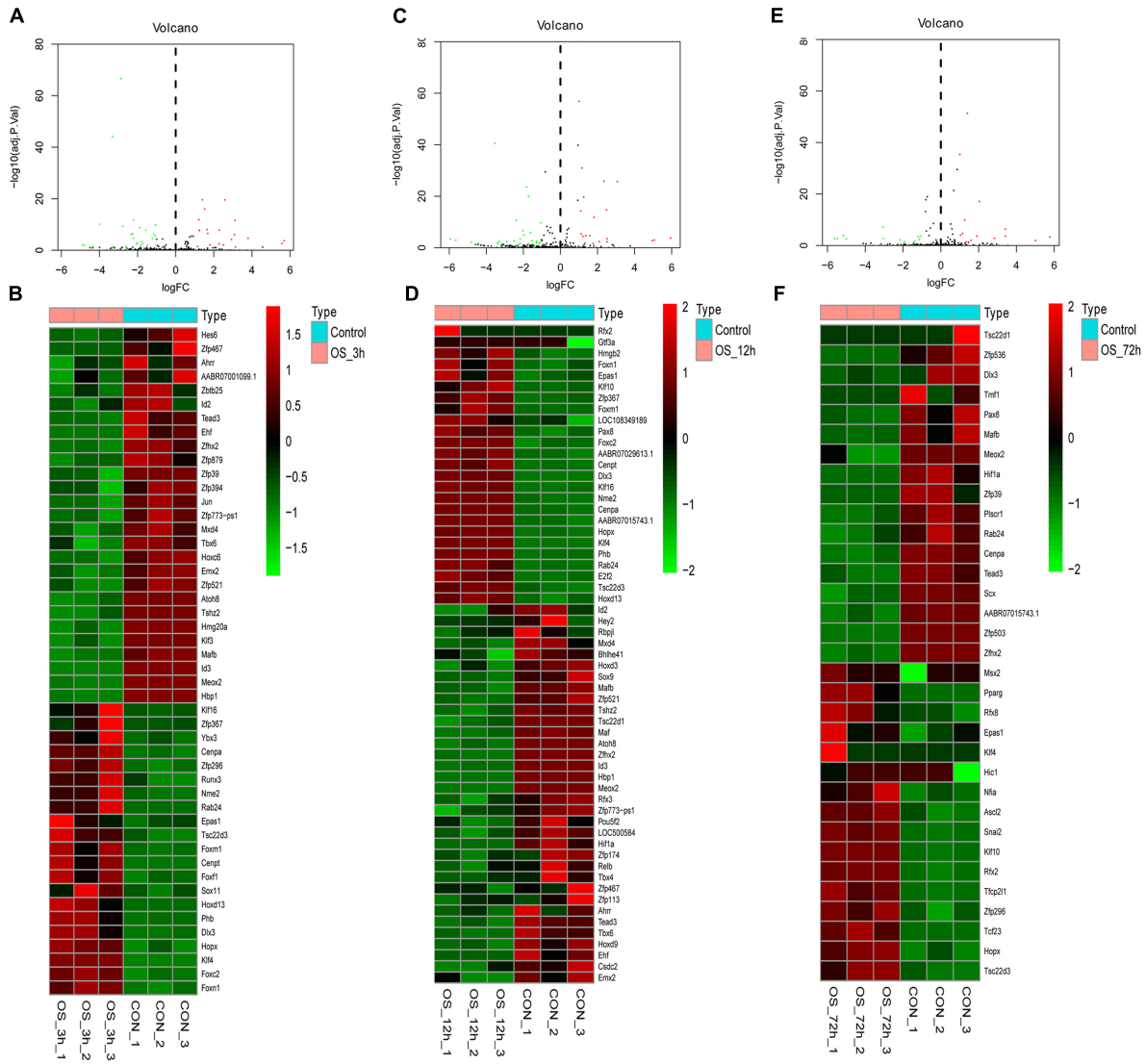

FIGURE 3 | Volcano plot and heatmap of differentially regulated TFs during osteogenesis at 3 h **(A,B)**, 12 h **(C,D)**, and 72 h **(E,F)** compared with undifferentiated cells (t = 0 h).

Supplementary Figures 1, 2 described the visualized results of differentially expressed TFs at three time points of adipogenic and chondrogenic differentiation.

Identification of Specific Differentially Expressed Transcription Factors in Three Phases

In osteogenesis of BMSCs, there were 13, 20, and 14 TFs being identified to be differentially expressed only at 3, 12, and 72 h after inductive differentiation (**Figure 5A**). In adipogenesis, the numbers were 33, 3, and 14 (**Figure 5B**), and for chondrogenesis, the numbers were 20, 11, and 13 (**Figure 5C**). Notably, 11 (e.g., Hopx and Tsc22d3), 12 (e.g., Irf5 and Rab24), and 11 (e.g., Gbx2 and Epas1) TFs showed differentially expressed levels at all three time points in osteogenesis, adipogenesis, and chondrogenesis, respectively.

Comparison of Differentially Expressed Transcription Factors Between Different Lineages

At 3 h after induction of differentiation, it was noticed that there were 15, 24, and 17 TFs only differentially expressed in osteogenesis, adipogenesis, and chondrogenesis, respectively (**Figure 5D**). At 12 h, the numbers were 35, 6, and 18 (**Figure 5E**), and at 72 h, the numbers were 13, 12, and 19 (**Figure 5F**). Notably, 11 (e.g., Hmg20a and Hoxc6), 5 (e.g., Id2 and Id3), and 11(e.g., Tfcp2l1 and Scx) TFs showed differential expression at all three directions of differentiation at 3, 12, and 72 h after inductive differentiation, respectively.

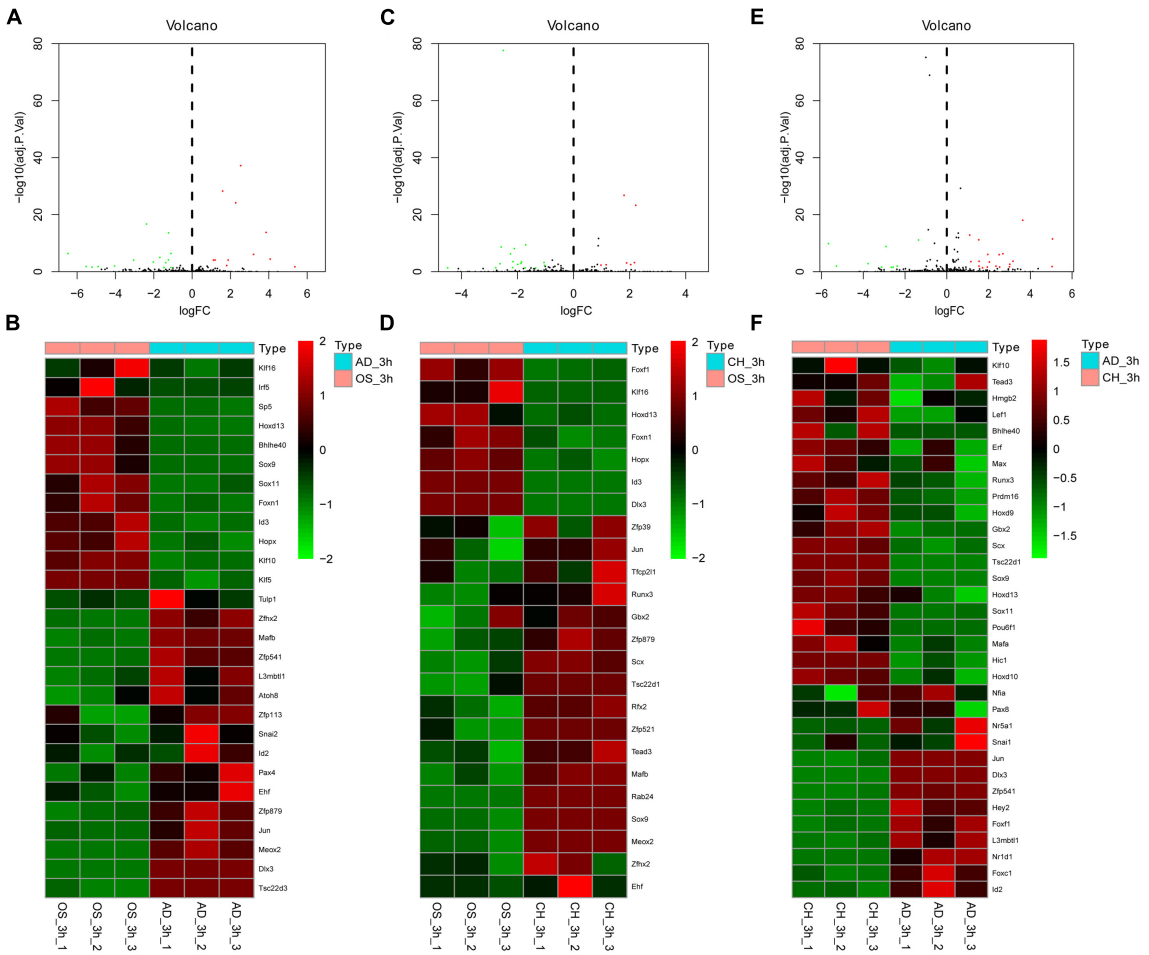

FIGURE 4 | Volcano plot and heatmap of differentially regulated TFs between every two lineages at 3 h after inductive differentiation (t = 0 h). **(A,B)** comparison between osteogenesis and adipogenesis; **(C,D)** comparison between osteogenesis and chondrogenesis, and **(E,F)** comparison between chondrogenesis and adipogenesis. AD, adipogenesis; OS, osteogenesis; CH, chondrogenesis.

Functional Enrichment Analysis of Differentially Expressed Transcription Factors

GO and KEGG pathway enrichment analysis of differentially expressed TFs at different time points of three directions of differentiation was performed to identify the most relevant biological processes (BPs), molecular functions (MFs), cellular components (CCs), and pathways. The top enriched terms in BP, CC, MF, and KEGG at 3 h after osteogenesis were presented in **Figure 6A**. For instance, the enriched BPs terms included "negative regulation of transcription from RNA polymerase II promoter," "regulation of transcription, DNA-templated," and "positive regulation of transcription from RNA polymerase II promoter." The enriched terms at 12 and 72 h after osteogenesis were presented in **Figures 6B,C**, respectively, while results of the other two directions of differentiation were presented in **Supplementary Figures 3, 4**.

The differentially expressed TFs between osteogenesis and adipogenesis at 3 h after inductive differentiation were also significantly enriched in BPs terms such as "negative regulation of transcription from RNA polymerase II promoter," "regulation of transcription, DNA-templated." Results of functional enrichment analysis of the differentially expressed TFs between every two lineage-commitment at 3 h of inductive differentiation were presented in **Figure 7**.

Protein Interaction Network Construction of Differentially Expressed Transcription Factors

The interactions between the proteins expressed from differentially expressed TFs at 3 h of osteogenesis consisted of 17 nodes and 13 edges, with Klf4 gene being identified to have a relatively high connectivity degree (**Figure 8A**). The PPI networks at 12 and 72 h after osteogenesis were presented in **Figures 8B,C**, respectively. Meanwhile, the PPI networks of the other two-direction differentiation at three time points were presented in **Supplementary Figure 5**.

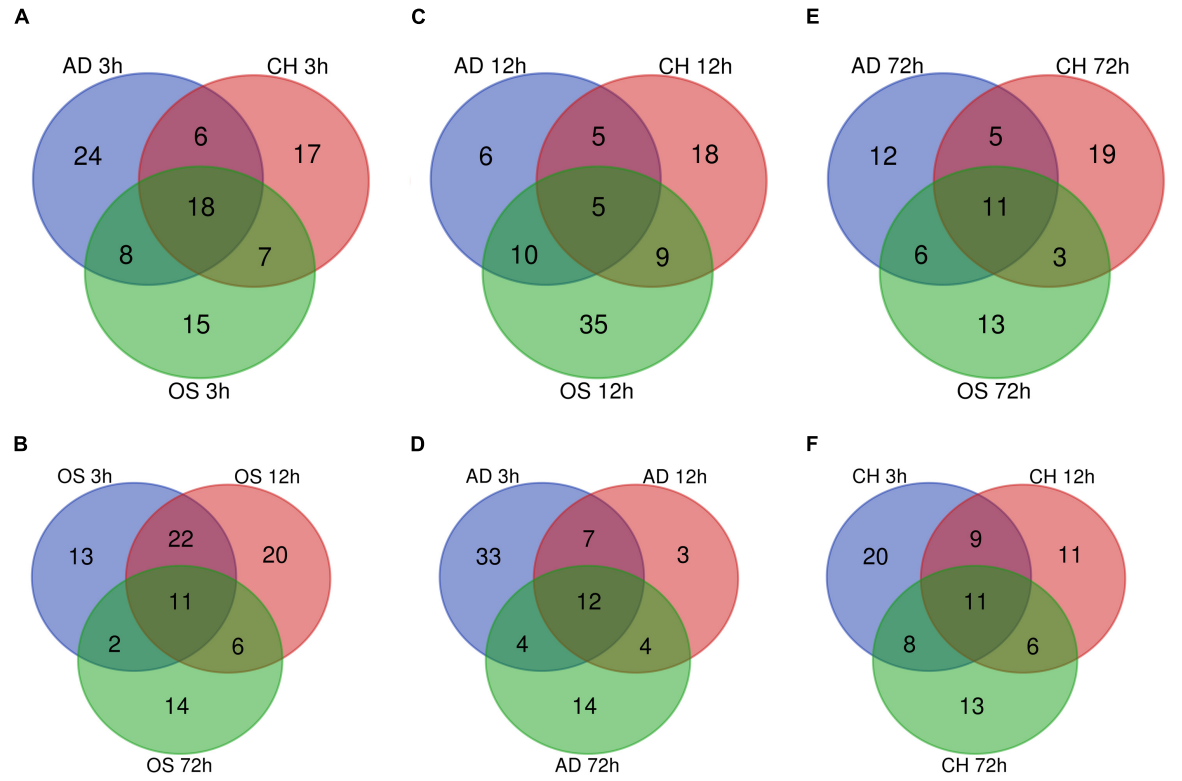

FIGURE 5 | Venn Diagrams of differentially regulated TFs at 3 h **(A)**, 12 h **(C)**, and 72 h **(E)** of three directions of differentiation compared with undifferentiated cells (t = 0 h). Venn Diagrams of differentially regulated TFs during osteogenesis **(B)**, adipogenesis **(D)**, and chondrogenesis **(F)** at three time points compared with undifferentiated cells (t = 0 h). AD, adipogenesis; OS, osteogenesis; CH, chondrogenesis.

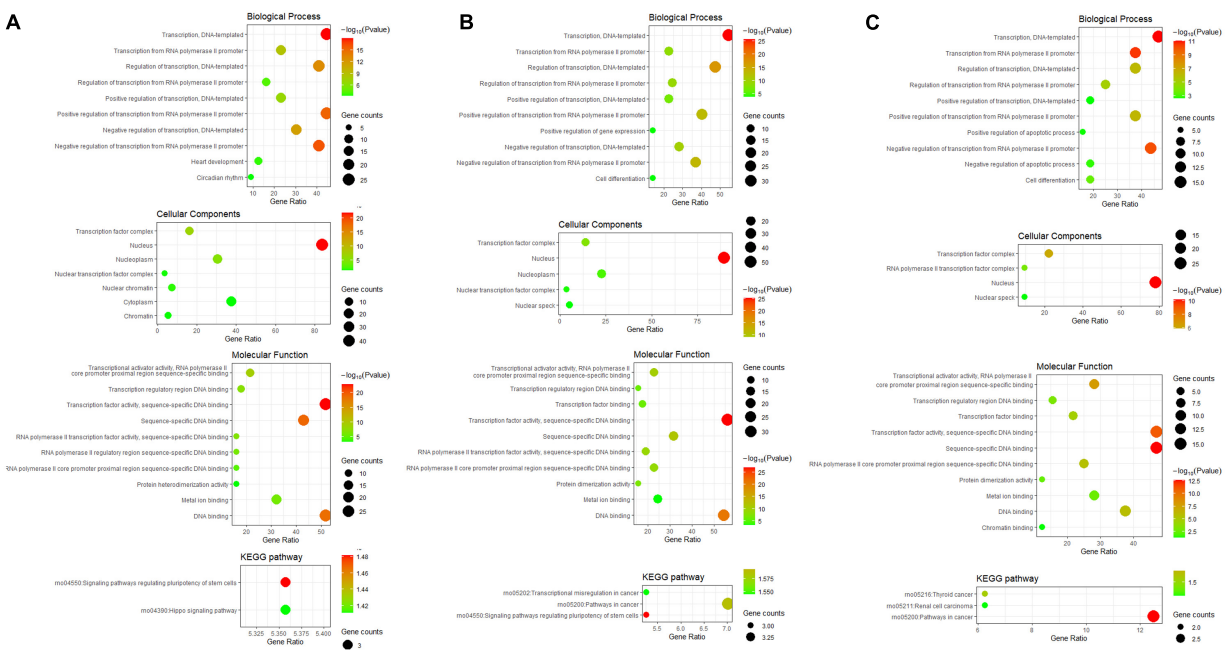

FIGURE 6 | GO including biological process, cellular components and molecular function analysis, and KEGG enrichment analysis of differentially expressed TFs at 3 h **(A)**, 12 h **(B)**, and 72 h **(C)** of osteogenesis compared with undifferentiated cells (t = 0 h).

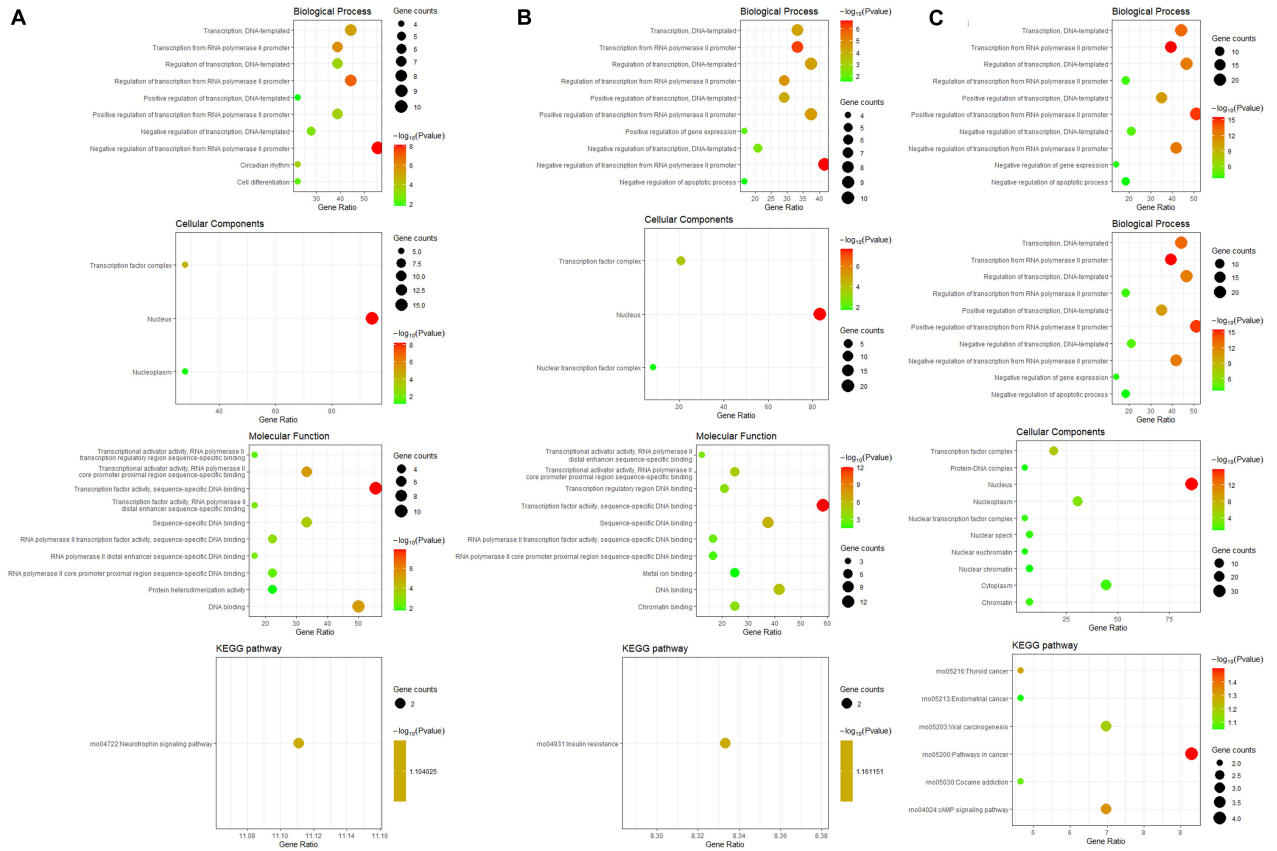

FIGURE 7 | GO including biological process, cellular components and molecular function analysis, and KEGG enrichment analysis of differentially expressed TFs between every two lineages at 3 h after inductive differentiation (t = 0 h). **(A)** comparison between osteogenesis and adipogenesis; **(B)** comparison between osteogenesis and chondrogenesis, and **(C)** comparison between chondrogenesis and adipogenesis.

The interactions between the proteins expressed from differentially expressed TFs between osteogenesis and adipogenesis at 3 h after inductive differentiation consisted of 6 nodes and 6 edges, with the Sox9 gene being identified to have a relatively high connectivity degree (**Figure 8D**). The interactions between the proteins expressed from differentially expressed TFs between osteogenesis and chondrogenesis, and between adipogenesis and chondrogenesis at 3 h after inductive differentiation were presented in **Figures 8E,F**.

Construction of Differentially Expressed Transcription Factors and Differentially Expressed Genes Regulatory Network

Based on the integrated analysis between TFs and DEGs, it could be noticed that during osteogenesis, the differentially expressed TFs at 3 h were able to regulate 111, 92, and 46 DEGs at 3, 12, and 72 h after differentiation (**Figures 9A–C**). Four differentially expressed TFs (Tead3, Cenpa, Epas1, and Klf4) identified at 3 h could function at all three time points. Meanwhile, during adipogenesis, the differentially expressed TFs at 3 h were able to regulate 113, 85, and 61 DEGs at 3, 12, and 72 h after differentiation (**Figures 10A–C**). Six differentially expressed TFs (Sox9, Snai2, Epas1, Id2, Cenpa, and Bhlhe40) occurred in three regulatory networks. For chondrogenesis, the differentially expressed TFs at 3 h were able to regulate 115, 33, and 60 DEGs at 3, 12, and 72 h after differentiation (**Figures 11A–C**). Six differentially expressed TFs (Runx3, Hic1, Scx, Sox9, Epas1, and Nfia) identified at 3 h could function at all three time points.

The regulatory networks between TFs and DEGs at 12 and 72 h after differentiation were presented in **Supplementary Figure 6**. The regulatory networks of the differentially expressed TFs and DEGs between every two lineage-commitment at 3 h after inductive differentiation were presented in **Supplementary Figure 7**.

DISCUSSION

Most previous studies investigating the differentiation process of BMSCs used primary cells isolated from humans. BMSCs isolated from rat functions across barriers and could be used as a source of regenerative therapy for bone metabolic diseases and bone defects. van de Peppel et al. (2017) discriminated the first 4 days of human BMSCs differentiation into three distinct phases

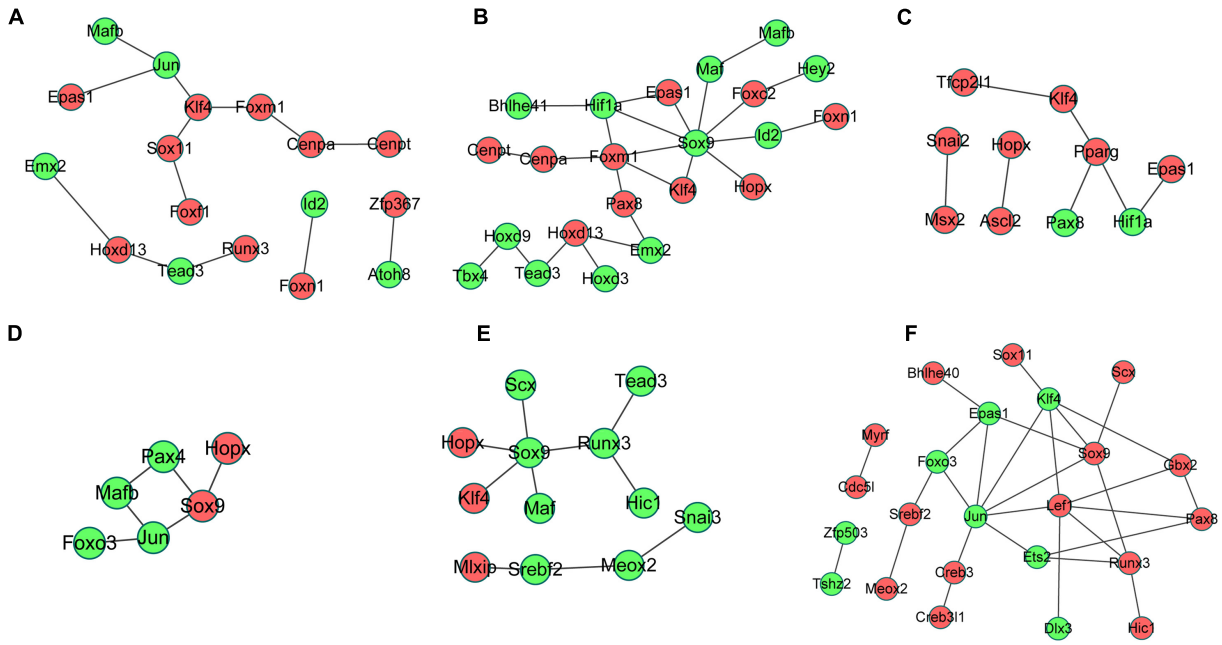

FIGURE 8 | Protein-protein interaction (PPI) network analysis of differentially expressed TFs. PPI network of differentially expressed TFs at 3 h **(A)**, 12 h **(B)**, and 72 h **(C)** of osteogenesis compared with undifferentiated cells (t = 0 h); the PPI network of differentially regulated TFs between osteogenesis and adipogenesis **(D)**, between osteogenesis and chondrogenesis **(E)**, and between chondrogenesis and adipogenesis **(F)** at 3 h after inductive differentiation (t = 0 h). Red indicates upregulated TFs, and green indicates the downregulated TFs.

and presented candidate genes for early regulation of osteogenic and adipogenic lineage-commitment. In the present study, we focused on the mechanism underlying the determination of osteogenesis, adipogenesis, and chondrogenesis of rat BMSCs. Primary rat BMSCs represent a heterogeneous cell population, but by using inductive differentiation mediums, the clock of the cells was synchronized to limit cell-cycle heterogeneity. Three time points (3, 12, and 72 h) in three phases of early lineage-commitment of rat BMSCs differentiation were chosen and the high-throughput sequencing data we generated discovered the key transcription factors guiding the differentiation direction. These processes occurred before time windows examined by most previous studies but were proved to play critical roles in the differentiation (Ng et al., 2008; Piek et al., 2010). Hopx and other early responder TFs may control the osteogenic cell fate of BMSCs and participate in the development of osteoporosis. Gbx2 and other early responder TFs should be considered in mechanistic models that clarify cartilage-anabolic changes in the clinical progression of osteoarthritis.

In the first phase of differentiation, gene expression analyses revealed a high number of differentially expressed TFs in all three directions of differentiation. In the regulatory model derived from our data, the first phase represents the initiation stage of the differentiation program and is characterized by expression changes of many transcription-related genes that regulate lineage commitment and set the stage for further differentiation toward a stable phenotype. Downstream analyses of the differentially expressed TFs identified at 3 h of osteogenic differentiation showed that they were capable of regulating 92 and 46 DEGs in the second and third phases, respectively. As for the second phase, differentiating lineages begin to deviate, as reflected by the fact that many transcriptional changes are direct targets of the differentially expressed TFs in the first phases. In the current study, TFs that changed per hour decreased as time extended, which suggested that the differentiating cells had reached a stable phenotype. This illustrates the transition from proliferation to differentiation and reflects the inverse correlation between these processes as has been described in various other differentiating cells.

Interestingly, we identified two TFs (Tsc22d3 and Epas1) that were upregulated in three lineages at all three time points, which may play an important role in the initiation of osteogenesis, adipogenesis, and chondrogenesis. Tsc22d3, also known as glucocorticoid−induced leucine zipper, is a glucocorticoid−responsive anti−inflammatory molecule that could regulate intracellular signaling pathways via hypoxia-induced factor-1α (HIF−1α) as well as AP−1 (Kanda et al., 2020). Tsc22d3 is also one of the most regulated genes in Cushing's syndrome (CS) and has been demonstrated to regulate osteoblast and bone turnover. Epas1, also known as HIF-2, is an active nucleoprotein and transcription factor induced by hypoxia. It could regulate hundreds of genes including VEGF, Ang-2, and HO-1, acting to enhance the production of corresponding proteins, and launch the process of angiogenesis and osteogenesis (Zhou et al., 2020). Thus, transfection of Epas1 into BMSCs provides an alternative for treating bone defects in the clinic. Other noteworthy TF is Hopx, which is the smallest member of the homeodomain-containing protein family (Hng et al., 2020).

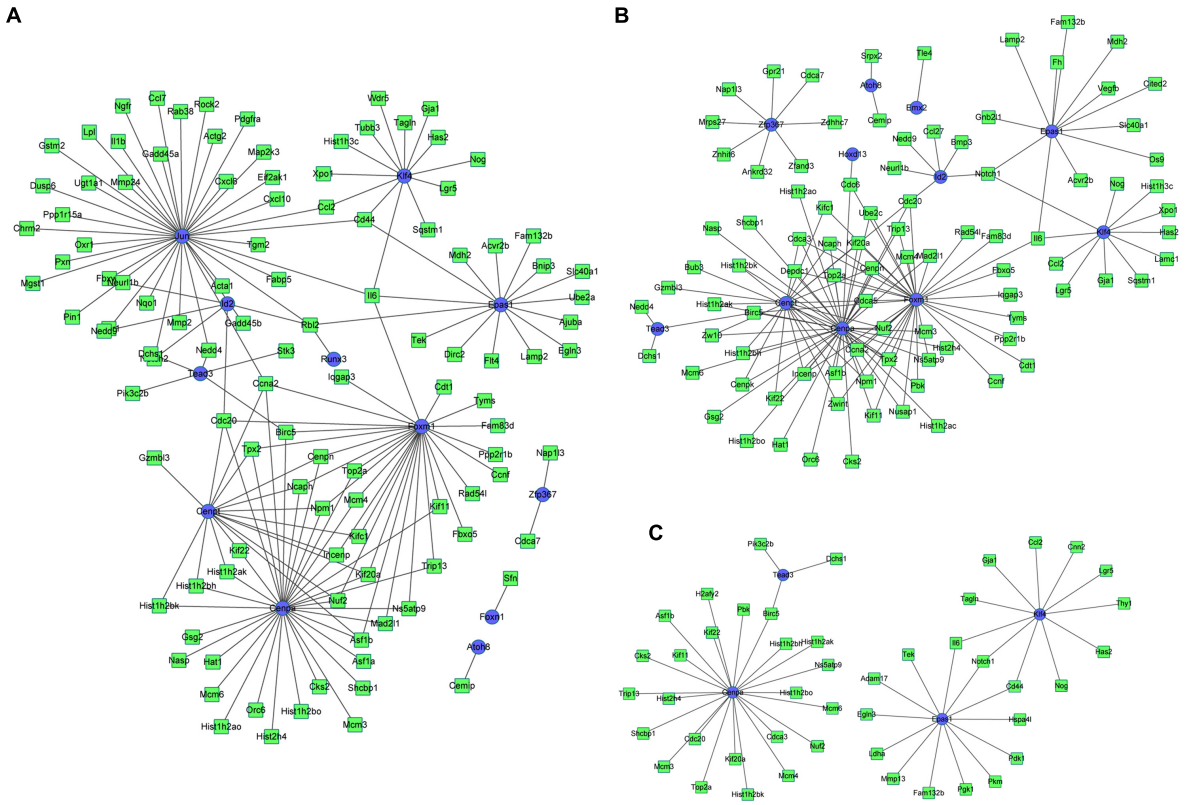

FIGURE 9 | The regulatory network between differentially expressed TFs at 3 h and targeted differentially expressed genes at 3 h **(A)**, 12 h **(B)**, and 72 h **(C)** in osteogenesis compared with undifferentiated cells (t = 0 h). Blue indicates TFs, and green indicates targeted genes.

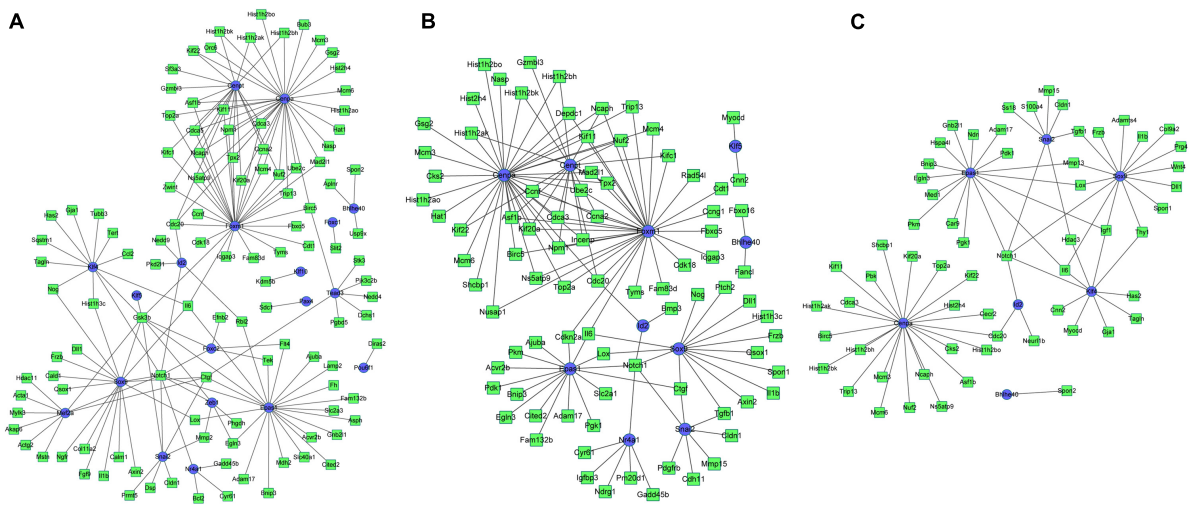

FIGURE 10 | The regulatory network between differentially expressed TFs at 3 h and targeted differentially expressed genes at 3 h **(A)**, 12 h **(B)**, and 72 h **(C)** in adipogenesis compared with undifferentiated cells (t = 0 h). Blue indicates TFs, and green indicates targeted genes.

Hopx manifested an up-regulated transcription level only under the condition of osteogenesis (3, 12, and 72 h). Unlike other typical homeobox proteins, Hopx binds to different protein partners and therefore recruits transcription factors to gene promoter regions (Trivedi et al., 2010; Hng et al., 2020). Hemming et al. (2016) have demonstrated a correlation between the Enhancer of zeste homolog 2 (EZH2) and Hopx, implicating a regulatory effect of Hopx during BMSC osteogenesis. Similarly,

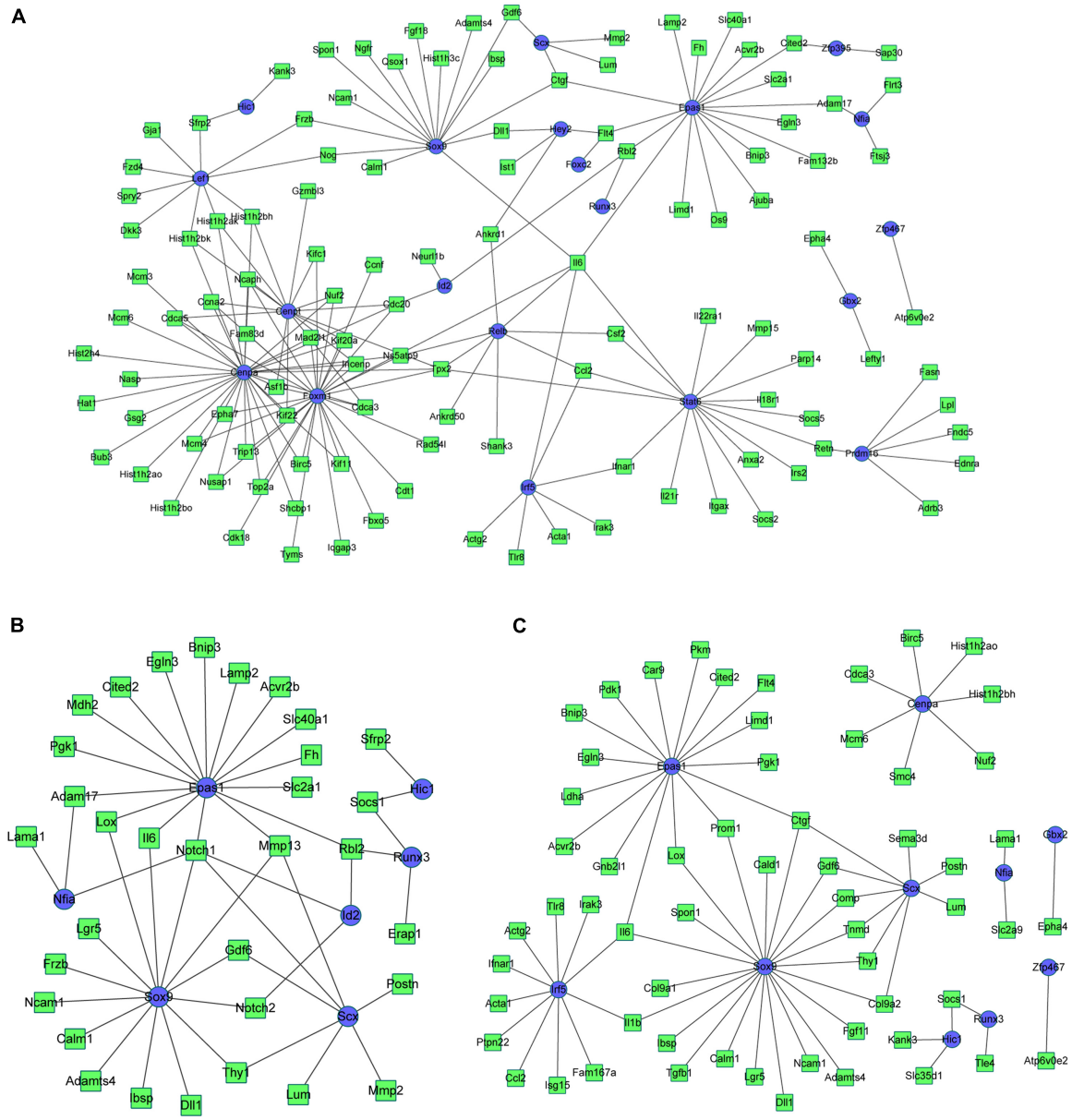

FIGURE 11 | The regulatory network between differentially expressed TFs at 3 h and targeted differentially expressed genes at 3 h **(A)**, 12 h **(B)**, and 72 h **(C)** in chondrogenesis compared with undifferentiated cells (t = 0 h). Blue indicates TFs, and green indicates targeted genes.

Gbx2 may participate in the decision of chondrogenesis of BMSCs. This TF is a LIF/STAT3 signaling downstream target that could allow long-term expansion of the undifferentiated embryonic stem cells (Wang et al., 2017). Sox9 was up-regulated in chondrogenesis but down-regulated in adipogenesis in tree time points, which was consistent with previous studies that this TF was essential for lineage differentiation of BMSCs (Lefebvre et al., 2019). Cooperation between GLI, JUN/FOSL2, and Sox9 is based on multiple binding sites near those of Sox9 and therefore transactivates many cartilage-specific genes (Liu and Lefebvre, 2015). Four TFs including Ybx3, Zbtb25, Hes6, and Zfp879 were inclusively upregulated at 3 h of osteogenesis. Further studies are needed to elucidate their role in the initiation of osteogenesis.

Then we used a variety of bioinformatics analysis methods to analyze these differentially expressed TFs to obtain a comprehensive understanding. As a result, GO terms of the differentially expressed TFs at 3 h of osteogenesis, adipogenesis, and chondrogenesis for biological process categories included "negative regulation of transcription from RNA polymerase II promoter," "transcription, DNA-templated," and "regulation of transcription, DNA-templated." Furthermore, the KEGG pathway enrichment analysis revealed that the differentially expressed TFs at 3 h of osteogenesis and adipogenesis

were predominantly associated with the "signaling pathways regulating pluripotency of stem cells" (Id2, Id3, and Klf4). Id2 and Id3 were downregulated in three lineages while Klf4 was upregulated in the process of adipogenesis and osteogenesis. This suggests that the initiation of BMSCs differentiation is similarly activated in both lineages, and changes of these signaling pathways and TFs are necessary to exit the immature multi-potent cell stage and acquire a specialized mesenchymal phenotype. While in the second phase, the enriched KEGG pathways begin to deviate. For osteogenesis, "signaling pathways regulating pluripotency of stem cells" was still significantly enriched, while for adipogenesis, "PI3K-Akt signaling pathway" and "MAPK signaling pathway" were significantly enriched. For chondrogenesis, "cAMP signaling pathway" was significantly enriched.

The regulatory network provided potential connections between identified DEGs and TFs. There were four, six, and six differentially expressed TFs identified at 3 h during osteogenesis, adipogenesis, and chondrogenesis possessing targets among DEGs identified at all three time points. It could be noticed that Cenpa and Epas1 overlap in osteogenesis and adipogenesis while Sox9 overlaps in adipogenesis and chondrogenesis. Like Epas1, Cenpa was also upregulated in both osteogenesis and adipogenesis at 3 h. Cenpa is a functionally conserved molecule about 17kDa that forms a centromere-specific nucleosome with H2A, H2B, and H4, whose overexpression is crucial for multiple kinds of cancers (Saha et al., 2020; Zhang et al., 2020). The role of Cenpa in lineage-commitment of BMSCs has not to be raised by former studies.

It could be noticed that there are some variations at the transcriptional level between the differentiation of human and rat BMSCs. At present, mechanism investigation regarding the lineage-commitment of rat BMSCs is still lacking. We performed high-throughput transcriptome sequencing and conducted a rigorous informatics analysis based on multiple databases, proposing multiple key transcription factors that may participate in the lineage-commitment of rat BMSCs. These findings provide research directions and potential molecular candidates for further studies investigating the underlying mechanisms of three-directional differentiation of rat BMSCs. However, this study has some shortcomings. First, this is an *in vitro* experiment based on isolated rat BMSCs. The differentiation processes may possess different characteristics *in vivo*. Findings obtained from *in vitro* experiments cannot simply be transposed to predict the reaction of an entire organism *in vivo*. Second, only three time points were selected in this study. These time points were separately locating in three phases and were used as delegates. Third, further in-depth studies are needed to establish whether MSCs from adipose tissue or other anatomical locations undergo a similar cascade of transcriptional events. Adipose-derived MSCs may respond very differently with respect to their clonogenic potential and doubling time in comparison with BMSCs (Russo et al., 2014). Fourth, the detailed functional mechanism of identified TFs was not clearly elucidated, and we could not attribute the lineage-commitment to a particular TF (or set of TFs). Last but not least, because there was a large and diverse amount of data, we could not validate these TFs by western blotting. Proteomics study may be needed in the future.

CONCLUSION

These transcription factors, functional terms and predicted targeted genes identified in the current study can help shed light on the molecular mechanism underlying the lineage-commitment of rat bone mesenchymal stem cells. Changes in TF activity during the early stage may play pivotal roles in the regulation of subsequent later phases of mesenchymal differentiation. Hopx and other early responder TFs may control the osteogenic cell fate of BMSCs, while Gbx2 and other early responder TFs should be considered in mechanistic models that clarify cartilage-anabolic changes. The latter finding exhibits possibilities for efficiently inducing osteoblast and chondrocytes differentiation, as part of a bone anabolic strategy for osteoporosis and osteoarthritis. In-depth experiments are required to further clarify the effect of these transcription factors.

DATA AVAILABILITY STATEMENT

The datasets presented in this study can be found in online repositories. The names of the repository/repositories and accession number(s) can be found below: https://www.ncbi.nlm.nih.gov/geo/query/acc.cgi?acc=GSE185140.

ETHICS STATEMENT

The animal study was reviewed and approved by the Animal Ethics Committee of Shandong Provincial Hospital affiliated to Shandong First Medical University.

AUTHOR CONTRIBUTIONS

FL and QZ conceived and designed the study. FL, QZ, JD, and DZ analyzed RNA sequencing data. FL, QZ, and PZ performed the basic experiment. FL and QZ wrote the manuscript, which was commented on by all authors.

FUNDING

This work was partially supported by the China Scholarship Council (CSC) (Grant No. 201808080126), the incubation fund of Shandong Provincial Hospital (Grant No. 2020FY019), the Young Scholars Program of Shandong Provincial Hospital, the Young Taishan Scholars Program of Shandong Province (Grant No. tsqn201909183), the Academic Promotion Program of Shandong First Medical University (Grant No. 2020RC008), and the Natural Science Foundation of Shandong Province (Grant Nos. ZR201911090016 and ZR202102180575).

SUPPLEMENTARY MATERIAL

The Supplementary Material for this article can be found online at: https://www.frontiersin.org/articles/10.3389/fcell.2021.768316/full#supplementary-material

Supplementary Figure 1 | Volcano plot and heatmap of differentially regulated TFs during adipogenesis at 3 h **(A,B)**, 12 h **(C,D)**, and 72 h **(E,F)** compared with undifferentiated cells (t = 0 h).

Supplementary Figure 2 | Volcano plot and heatmap of differentially regulated TFs during chondrogenesis at 3 h **(A,B)**, 12 h **(C,D)**, and 72 h **(E,F)** compared with undifferentiated cells (t = 0 h).

Supplementary Figure 3 | GO including biological process, cellular components and molecular function analysis, and KEGG enrichment analysis of differentially expressed TFs at 3 h **(A)**, 12 h **(B)**, and 72 h **(C)** of adipogenesis compared with undifferentiated cells (t = 0 h).

Supplementary Figure 4 | GO including biological process, cellular components and molecular function analysis, and KEGG enrichment analysis of differentially expressed TFs at 3 h **(A)**, 12 h **(B)**, and 72 h **(C)** of chondrogenesis compared with undifferentiated cells (t = 0 h).

Supplementary Figure 5 | Protein-protein interaction (PPI) network analysis of differentially expressed TFs at 3 h **(A)**, 12 h **(B)**, and 72 h **(C)** of osteogenesis, and 3 h **(D)**, 12 h **(E)**, and 72 h **(F)** of chondrogenesis compared with undifferentiated cells (t = 0 h). Red indicates upregulated TFs, and green indicates the downregulated TFs.

Supplementary Figure 6 | The regulatory network between differentially expressed TFs and targeted differentially expressed genes at 12 and 72 h in osteogenesis **(A,B)**, adipogenesis **(C,D)**, and chondrogenesis **(E,F)** compared with undifferentiated cells (t = 0 h). Blue indicates TFs, and green indicates targeted genes.

Supplementary Figure 7 | The regulatory network between differentially expressed TFs and targeted differentially expressed genes between every two lineages at 3 h after inductive differentiation (t = 0 h). **(A)** comparison between osteogenesis and adipogenesis; **(B)** comparison between osteogenesis and chondrogenesis, and **(C)** comparison between chondrogenesis and adipogenesis. Blue indicates TFs, and green indicates targeted genes.

REFERENCES

Arthur, A., and Gronthos, S. (2020). Clinical application of bone marrow mesenchymal Stem/Stromal cells to repair skeletal tissue. *Int. J. Mol. Sci.* 21:21249759. doi: 10.3390/ijms21249759

Bruedigam, C., Driel, M., Koedam, M., Peppel, J., van der Eerden, B. C., Eijken, M., et al. (2011). Basic techniques in human mesenchymal stem cell cultures: Differentiation into osteogenic and adipogenic lineages, genetic perturbations, and phenotypic analyses. *Curr. Protoc. Stem Cell Biol.* 1:17. doi: 10.1002/9780470151808.sc01h03s17

Carballo, C. B., Nakagawa, Y., Sekiya, I., and Rodeo, S. A. (2017). Basic science of articular cartilage. *Clin. Sports Med.* 36, 413–425. doi: 10.1016/j.csm.2017.02.001

Chen, Q., Shou, P., Zheng, C., Jiang, M., Cao, G., Yang, Q., et al. (2016). Fate decision of mesenchymal stem cells: Adipocytes or osteoblasts? *Cell Death Differ.* 23, 1128–1139. doi: 10.1038/cdd.2015.168

Crapnell, K., Blaesius, R., Hastings, A., Lennon, D. P., Caplan, A. I., and Bruder, S. P. (2013). Growth, differentiation capacity, and function of mesenchymal stem cells expanded in serum-free medium developed via combinatorial screening. *Exp. Cell Res.* 319, 1409–1418. doi: 10.1016/j.yexcr.2013.04.004

Fang, F., Li, Z., Zhao, Q., Xiong, C., and Ni, K. (2020). Analysis of multi-lineage gene expression dynamics during primordial germ cell induction from human induced pluripotent stem cells. *Stem Cell Res. Ther.* 11:100. doi: 10.1186/s13287-020-01620-y

Gari, M., Alsehli, H., Gari, A., Abbas, M., Alkaff, M., Abuzinadah, M., et al. (2016). Derivation and differentiation of bone marrow mesenchymal stem cells from osteoarthritis patients. *Tissue Eng. Regen. Med.* 13, 732–739. doi: 10.1007/s13770-016-0013-2

Hemming, S., Cakouros, D., Vandyke, K., Davis, M. J., Zannettino, A. C., and Gronthos, S. (2016). Identification of novel EZH2 targets regulating osteogenic differentiation in mesenchymal stem cells. *Stem Cells Dev.* 25, 909–921. doi: 10.1089/scd.2015.0384

Hng, C. H., Camp, E., Anderson, P., Breen, J., Zannettino, A., and Gronthos, S. (2020). HOPX regulates bone marrow-derived mesenchymal stromal cell fate determination via suppression of adipogenic gene pathways. *Sci. Rep.* 10:11345. doi: 10.1038/s41598-020-68261-2

Hu, L., Yin, C., Zhao, F., Ali, A., Ma, J., and Qian, A. (2018). Mesenchymal stem cells: Cell fate decision to osteoblast or adipocyte and application in osteoporosis treatment. *Int. J. Mol. Sci.* 19:360. doi: 10.3390/ijms19020360

Huynh, N., Zhang, B., and Guilak, F. (2019). High-depth transcriptomic profiling reveals the temporal gene signature of human mesenchymal stem cells during chondrogenesis. *FASEB J.* 33, 358–372. doi: 10.1096/fj.201800534R

Jiang, Y., Zhang, P., Zhang, X., Lv, L., and Zhou, Y. (2021). Advances in mesenchymal stem cell transplantation for the treatment of osteoporosis. *Cell Prolif.* 54:e12956. doi: 10.1111/cpr.12956

Kanda, A., Hirose, I., Noda, K., Murata, M., and Ishida, S. (2020). Glucocorticoid-transactivated TSC22D3 attenuates hypoxia- and diabetes-induced Muller glial galectin-1 expression via HIF-1alpha destabilization. *J. Cell. Mol. Med.* 24, 4589–4599. doi: 10.1111/jcmm.15116

Lefebvre, V., Angelozzi, M., and Haseeb, A. (2019). SOX9 in cartilage development and disease. *Curr. Opin. Cell Biol.* 61, 39–47. doi: 10.1016/j.ceb.2019.07.008

Li, J., Ezzelarab, M. B., and Cooper, D. K. (2012). Do mesenchymal stem cells function across species barriers? Relevance for xenotransplantation. *Xenotransplantation.* 19, 273–285. doi: 10.1111/xen.12000

Liu, C. F., and Lefebvre, V. (2015). The transcription factors SOX9 and SOX5/SOX6 cooperate genome-wide through super-enhancers to drive chondrogenesis. *Nucleic Acids Res.* 43, 8183–8203. doi: 10.1093/nar/gkv688

Liu, F., Dong, J., Zhou, D., and Zhang, Q. (2021). Identification of key candidate genes related to inflammatory osteolysis associated with vitamin E-Blended UHMWPE debris of orthopedic implants by integrated bioinformatics analysis and experimental confirmation. *J. Inflamm. Res.* 14, 3537–3554. doi: 10.2147/JIR.S320839

Merrett, J. E., Bo, T., Psaltis, P. J., and Proud, C. G. (2020). Identification of DNA response elements regulating expression of CCAAT/enhancer-binding protein (C/EBP) beta and delta and MAP kinase-interacting kinases during early adipogenesis. *Adipocyte* 9, 427–442. doi: 10.1080/21623945.2020.1796361

Ng, F., Boucher, S., Koh, S., Sastry, K. S., Chase, L., Lakshmipathy, U., et al. (2008). PDGF, TGF-beta, and FGF signaling is important for differentiation and growth of mesenchymal stem cells (MSCs): Transcriptional profiling can identify markers and signaling pathways important in differentiation of MSCs into adipogenic, chondrogenic, and osteogenic lineages. *Blood* 112, 295–307. doi: 10.1182/blood-2007-07-103697

O'Connor, K. C. (2019). Molecular profiles of Cell-to-Cell variation in the regenerative potential of mesenchymal stromal cells. *Stem. Cells Int.* 2019:5924878. doi: 10.1155/2019/5924878

Piek, E., Sleumer, L. S., van Someren, E. P., Heuver, L., de Haan, J. R., de Grijs, I., et al. (2010). Osteo-transcriptomics of human mesenchymal stem cells: Accelerated gene expression and osteoblast differentiation induced by vitamin D reveals c-MYC as an enhancer of BMP2-induced osteogenesis. *Bone* 46, 613–627. doi: 10.1016/j.bone.2009.10.024

Pittenger, M. F., Discher, D. E., Peault, B. M., Phinney, D. G., Hare, J. M., and Caplan, A. I. (2019). Mesenchymal stem cell perspective: Cell biology to clinical progress. *NPJ Regen. Med.* 4:22. doi: 10.1038/s41536-019-0083-6

Robert, A. W., Marcon, B. H., Dallagiovanna, B., and Shigunov, P. (2020). Adipogenesis, osteogenesis, and chondrogenesis of human mesenchymal Stem/Stromal cells: A comparative transcriptome approach. *Front. Cell Dev. Biol.* 8:561. doi: 10.3389/fcell.2020.00561

Russo, V., Yu, C., Belliveau, P., Hamilton, A., and Flynn, L. E. (2014). Comparison of human adipose-derived stem cells isolated from subcutaneous, omental, and

intrathoracic adipose tissue depots for regenerative applications. *Stem Cells Transl. Med*. 3, 206–217. doi: 10.5966/sctm.2013-0125

Saeedi, M., Nezhad, M. S., Mehranfar, F., Golpour, M., Esakandari, M. A., Rashmeie, Z., et al. (2021). Biological aspects and clinical applications of mesenchymal stem cells: Key features you need to be aware of. *Curr. Pharm. Biotechnol*. 22, 200–215. doi: 10.2174/1389201021666200907121530

Saha, A. K., Contreras-Galindo, R., Niknafs, Y. S., Iyer, M., Qin, T., Padmanabhan, K., et al. (2020). The role of the histone H3 variant CENPA in prostate cancer. *J. Biol. Chem.* 295, 8537–8549. doi: 10.1074/jbc.RA119.010080

Trivedi, C. M., Zhu, W., Wang, Q., Jia, C., Kee, H. J., Li, L., et al. (2010). Hopx and Hdac2 interact to modulate Gata4 acetylation and embryonic cardiac myocyte proliferation. *Dev. Cell* 19, 450–459. doi: 10.1016/j.devcel.2010.08.012

van de Peppel, J., Strini, T., Tilburg, J., Westerhoff, H., van Wijnen, A. J., and van Leeuwen, J. P. (2017). Identification of three early phases of Cell-Fate determination during osteogenic and adipogenic differentiation by transcription factor dynamics. *Stem Cell Rep*. 8, 947–960. doi: 10.1016/j.stemcr.2017.02.018

Wang, M., Tang, L., Liu, D., Ying, Q. L., and Ye, S. (2017). The transcription factor Gbx2 induces expression of Kruppel-like factor 4 to maintain and induce naive pluripotency of embryonic stem cells. *J. Biol. Chem.* 292, 17121–17128. doi: 10.1074/jbc.M117.803254

Yianni, V., and Sharpe, P. T. (2020). Epigenetic mechanisms driving lineage commitment in mesenchymal stem cells. *Bone* 134:115309. doi: 10.1016/j.bone.2020.115309

Yu, B., and Wang, C. Y. (2016). Osteoporosis: The result of an 'Aged' bone microenvironment. *Trends Mol. Med.* 22, 641–644. doi: 10.1016/j.molmed.2016.06.002

Zhang, J., Guo, F., Wei, J., Xian, M., Tang, S., Zhao, Y., et al. (2017). An integrated approach to identify critical transcription factors in the protection against hydrogen peroxide-induced oxidative stress by Danhong injection. *Free Radic. Biol. Med*. 112, 480–493. doi: 10.1016/j.freeradbiomed.2017.07.002

Zhang, Q. Y., Li, Z. R., Gao, F. Q., and Sun, W. (2018). Pericollapse stage of osteonecrosis of the femoral head: A last chance for joint preservation. *Chin. Med. J.* 131, 2589–2598. doi: 10.4103/0366-6999.244111

Zhang, Y., Yang, L., Shi, J., Lu, Y., Chen, X., and Yang, Z. (2020). The oncogenic role of CENPA in hepatocellular carcinoma development: Evidence from bioinformatic analysis. *Biomed. Res. Int.* 2020:3040839. doi: 10.1155/2020/3040839

Zhou, L., Qiu, M., Yang, L., Yang, L., Zhang, Y., Mu, S., et al. (2020). MicroRNA-1-3p enhances osteoblast differentiation of MC3T3-E1 cells by interacting with hypoxia-inducible factor 1 alpha inhibitor (HIF1AN). *Mech. Dev*. 162:103613. doi: 10.1016/j.mod.2020.103613

Zhou, R., Guo, F., Xiang, C., Zhang, Y., Yang, H., and Zhang, J. (2021). Systematic Study of Crucial Transcription Factors of Coptidis rhizoma Alkaloids against Cerebral Ischemia-Reperfusion Injury. *ACS Chem. Neurosci.* 12, 2308–2319. doi: 10.1021/acschemneuro.0c00730

Conflict of Interest: The authors declare that the research was conducted in the absence of any commercial or financial relationships that could be construed as a potential conflict of interest.

Publisher's Note: All claims expressed in this article are solely those of the authors and do not necessarily represent those of their affiliated organizations, or those of the publisher, the editors and the reviewers. Any product that may be evaluated in this article, or claim that may be made by its manufacturer, is not guaranteed or endorsed by the publisher.

frontiers in Molecular Biosciences

REVIEW
published: 02 November 2021
doi: 10.3389/fmolb.2021.745035

The Fate Status of Stem Cells in Diabetes and its Role in the Occurrence of Diabetic Complications

Jinyi Xu and Chengguo Zuo**

State Key Laboratory of Ophthalmology, Zhongshan Ophthalmic Center, Sun Yat-sen University, Guangzhou, China

Diabetes mellitus (DM) is becoming a growing risk factor for public health worldwide. It is a very common disease and is widely known for its susceptibility to multiple complications which do great harm to the life and health of patients, some even lead to death. To date, there are many mechanisms for the complications of diabetes, including the generation of reactive oxygen species (ROS) and the abnormal changes of gas transmitters, which ultimately lead to injuries of cells, tissues and organs. Normally, even if injured, the body can quickly repair and maintain its homeostasis. This is closely associated with the repair and regeneration ability of stem cells. However, many studies have demonstrated that stem cells happen to be damaged under DM, which may be a nonnegligible factor in the occurrence and progression of diabetic complications. Therefore, this review summarizes how diabetes causes the corresponding complications by affecting stem cells from two aspects: stem cells dysfunctions and stem cells quantity alteration. In addition, since mesenchymal stem cells (MSCs), especially bone marrow mesenchymal stem cells (BMMSCs), have the advantages of strong differentiation ability, large quantity and wide application, we mainly focus on the impact of diabetes on them. The review also puts forward the basis of using exogenous stem cells to treat diabetic complications. It is hoped that through this review, researchers can have a clearer understanding of the roles of stem cells in diabetic complications, thus promoting the process of using stem cells to treat diabetic complications.

Keywords: diabetic complications, stem cells, mesenchymal stem cells, bone marrow mesenchymal stem cells, stem cells dysfunctions, stem cells quantity changes, stem cells therapy

OPEN ACCESS

Edited by:
Zhenhong Ni,
Army Medical University, China

Reviewed by:
Hongyuan Zhang,
Amgen, United States
Lijun Li,
Zhejiang University, China
Qun Cheng,
Fudan University, China
Jian Jun Li,
China Medical University, China
Peng Xue,
Third Hospital of Hebei Medical University, China

****Correspondence:***
Jinyi Xu
1003543669@qq.com
Chengguo Zuo
chengguozuo@163.com

Specialty section:
This article was submitted to Cellular Biochemistry, a section of the journal Frontiers in Molecular Biosciences

Received: *21 July 2021*
Accepted: *20 October 2021*
Published: *02 November 2021*

Citation:
Xu J and Zuo C (2021) The Fate Status of Stem Cells in Diabetes and its Role in the Occurrence of Diabetic Complications. Front. Mol. Biosci. 8:745035. doi: 10.3389/fmolb.2021.745035

INTRODUCTION

At present, with the improvement of living standard, the morbidity and incidence of diabetes are increasing rapidly all over the world, projected to affect 10.9% (700 million) people worldwide by 2045 (Saeedi et al., 2019). Diabetes mellitus (DM) is a chronic disease with the volatility of hyperglycemic state caused by the deficiency of insulin secretion or the damage of its biological function, or both (Alberti and Zimmet, 1998; Tripathi and Srivastava, 2006). There are two major forms of diabetes, type 1 diabetes mellitus (T1DM) and type 2 diabetes mellitus (T2DM). T1DM is usually attributed to autoimmune β-cell destruction and characterized by insulin dependence, which occurs mostly in children and adolescents. T2DM is prone to occur in adults and is characterized by insulin resistance (Classification and Diagno, 2020).

Polydipsia, polyuria, polyphagia and emaciation are typical symptoms of DM, which reduce patients' quality of life. In addition to the harm that "more than three a little" symptoms bring to

patients, the complications caused by diabetes are the major cause of death in diabetic patients (Nathan et al., 1993; Intensive blood-glucose c, 1998; Brownlee, 2001). Among all the complications, long-term vascular complications are considered to be the most devastating consequence of diabetes. The vascular complications are due at least in part to chronic hyperglycemia leading to sustained blood vessel damage. They can be divided into microvascular (retinopathy, neuropathy, and nephropathy) and macrovascular (cerebrovascular, coronary artery, and peripheral artery diseases) complications, representing the main contributors to diminished quality of life and increased mortality rate in patients with both T1DM and T2DM (van den Born et al., 2016). Compared with individuals without diabetes, they have a two to four folds increased risk of vascular diseases (Fox et al., 2004). Other chronic complications of diabetes include osteoporosis-associated fracture, diabetic ulcer, sexual dysfunction and et al.

The burden of diabetic complications is directly related to cell, tissue and organ damage, and is also associated with defects in endogenous repair mechanisms. The role of their imbalance in the occurrence and development of the diseases cannot be ignored (Fadini et al., 2017). As we all know, stem cells play an important role in the maintenance of homeostasis and the damaged tissue repair. Therefore, their dysfunctions, or a decline in quantity, may inevitably impair the ability of tissue repair and regeneration, then accelerate the progression of diseases and contribute to diabetic complications. Although diabetes is an extremely complicated disease process with many pathological consequences, some of which have been well established, little is known about whether and how the function and quantity of stem cells, especially MSCs and BMMSCs, are damaged in diabetic microenvironment, and affect the occurrence and progression of diabetic complications.

The aim of this review was to address the specific alteration of the quality and quantity of stem cells, especially MSCs and BMMSCs, in diabetes, briefly discuss the mechanisms of stem cells damage in DM and the relationship between diabetic complications and stem cells changes, and propose a potential modality to manage diabetic complications with stem cell-based therapies. In particular, we explored the properties of diabetic stem cells in terms of 1) dysfunctions, including mobilization, differentiation potential, migration ability, cytokine secretion and et al. 2) the alteration of quantity. By understanding the body of literature devoted to these topics, researchers and practitioners may gain valuable insights into prevention, treatment, and management of diabetic complications. Additionally, it is important to illuminate the changes in the diabetic stem cells microenvironment, which may facilitate the development and improvement of future stem cell-based therapies.

Mechanisms of Diabetes Induced Injury

Despite the difference in pathophysiology, chronic hyperglycemia is the master switch of diabetic complications in both T1DM and T2DM. As the initiating factor, hyperglycemia ultimately results in endothelial dysfunctions and a variety of cells, tissues and organs damages through different pathways (Forbes and Cooper, 2013; Sena et al., 2013). The underlying molecular mechanisms have been proposed in many researches, including increased polyol pathway flux through aldose reductase, raised advanced glycation end-product (AGE) formation, protein kinase C (PKC) activation, excess glucose flow to hexosamine pathway and et al. (Brownlee, 2001; Forbes and Cooper, 2013). These biochemical pathways can further lead to 1) increase in oxidative stress mainly caused by overproduction of reactive oxygen species (ROS) (Du et al., 2000; Nishikawa et al., 2000; Giacco and Brownlee, 2010) 2) abnormal level of gas transmitters such as nitric oxide (NO), carbon monoxide (CO), and hydrogen sulfide (H2S) (van den Born et al., 2016) 3) increased expression of pro-inflammatory cytokines and pro-coagulant molecules. These factors can then lead to inflammation, endothelial dysfunction and hypercoagulability, which correlate and interact with one another, playing an important role in the development of diabetic complications, especially vascular damages in diabetic patients (Domingueti et al., 2016).

Under the condition of DM, the homeostasis of body is also damaged through the above mechanisms, leading to changes in cell microenvironment. Long-term exposure to diabetic microenvironment could do great harm to stem cells. The combined effects of oxidative stress, inflammation, abnormal levels of cytokines and et al. initiated by high glucose in diabetic patients may be responsible for the adverse changes in quality and quantity of stem cells (Fadini et al., 2017). In addition to the above mechanisms considering high glucose as the starting factor of the damages, many other mechanisms for the injuries of stem cells induced by diabetes also exist, some of which are mentioned in the review later. **Figure 1** shows the main mechanism of diabetic complications and stem cell injuries caused by DM.

Roles of Stem Cells in Tissue Repair and Homeostasis Maintenance

Stem cells are one of the damaged members which play a significant role in the development of diabetic complications. Stem cells are a population of relatively undifferentiated cells that retain the ability to divide and proliferate throughout postnatal life to provide progenitor cells that can differentiate into specialized cells. Self-renewal and differentiation ability are the most prominent characteristics of stem cells. The ability of self-renewal refers to the process in which stem cells divide symmetrically or asymmetrically to produce at least one daughter cell that retains the characteristics of stem cells (Lodi et al., 2011). The differentiation capacity indicates that stem cells have single or multi-directional differentiation potential and can differentiate into specific or various types of specialized cells. Many studies have reported that these two properties play an important role in tissue regeneration and repair. The ability of self-renewal ensures enough number of stem cells, while the ability of differentiation ensures stem cells to differentiate into damaged cells in time. Under the circumstances of injury and repair, stem cells can proliferate to supplement cells or replace damaged cells (Angelini et al., 2004; Lodi et al., 2011; Chen et al., 2012; Falanga, 2012). Besides directly differentiating into damaged cells in cell replacement manner, stem cells,

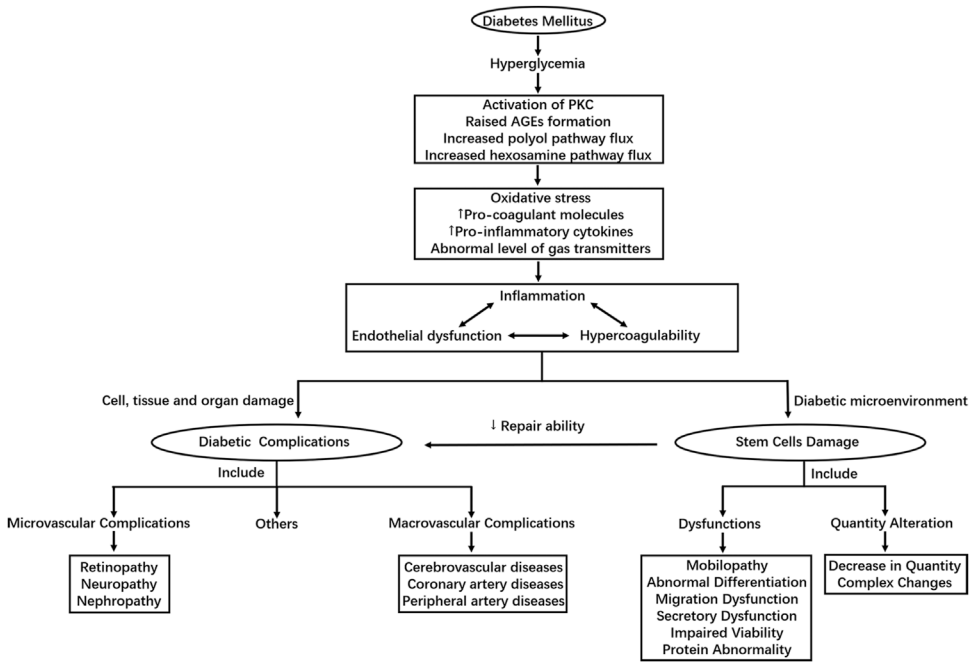

FIGURE 1 | Shows the main mechanism of diabetic complications and stem cell injuries caused by DM.

especially exogenous or nonlocal stem cells, are involved in tissue repair and regeneration mainly through secreting a series of cytokines, as well as a lot of exosomes containing various of miRNAs and lncRNAs. In addition, stem cells have many other characteristics, such as migration and mobilization ability. All of which are of great significance in maintaining tissue homeostasis and repairing damaged tissue. However, when stem cells are damaged under diabetes, whether functionally or qualitatively, their abilities of tissue repair and regeneration are impaired, thus accelerating the progression of diabetic complications.

Among different types of stem cells, mesenchymal stem cells (MSCs), especially bone marrow mesenchymal stem cells (BMMSCs), are most widely applied in treatments for various diseases as a novel potential therapeutic intervention (Charbord, 2010; Berebichez-Fridman and Montero-Olvera, 2018). This can be attributed to their various advantages in biology and medicine. Firstly, they are multipotent and can differentiate into mesodermal lineages, such as adipocytes, osteocytes and chondrocytes. Secondly, MSCs are numerous and can be easily obtained from bone marrow (BM), adipose tissue or umbilical cord tissue. Thirdly, BMMSCs can be derived from autologous, so there is no problem of matching or immune rejection. Fourth, they still have strong immunoregulatory abilities besides their abilities of tissue repair and regeneration. These characteristics make them valuable in a wide range of applications in biological and medical sciences (Naji et al., 2019). Therefore, the review mainly focuses on the impact of diabetes on them. **Table 1** summarizes the mechanisms, objects, complications, and the corresponding references of stem cells dysfunctions in diabetes.

Stem Cells Dysfunctions in Diabetes

Stem Cells Mobilopathy

Mobilization from BM into the circulation is the primary step for stem cells to realize their effects in cell recovery and tissue repair after injury. However, under the condition of DM, stem cells and progenitor cells suffer from "mobilopathy" and are unable to be activated for tissue repair, inducing the progression of diabetic complications.

The BM niches provide the essential microenvironment for maintenance of stem cells function. Hematopoietic stem and progenitor cells (HSPCs) are important kinds of stem cells in BM which can differentiate into mature blood cells with various functions and maintain the homeostasis of blood system. Their abnormalities are related to lowered immunity, difficulty of wound healing and et al. which aggravate the complications. Adhesion molecules, chemokines, cytokines, and proteolytic enzymes form part of the microenvironment and their complex interactions are involved in the regulation of HSPCs mobilization (Lapidot and Petit, 2002). In diabetic mouse, DM compromises the BM niches by down-regulating adhesion molecule VCAM1, chemokine SDF-1, pro-angiogenic cytokine VEGF, peptidase DPP-4 and et al. The disturbed stem cells niche leads to stem cells dysfunctions, thereby, impairing the mobilization of HSPCs (Orlandi et al., 2010). Similarly, in a parallel human group study, HSPCs mobilization in response to subcutaneous injection of human recombinant granulocyte colony–stimulating factor (hrG-CSF) is found to be impaired in patients with DM. This "mobilopathy" is associated with the inability to upregulate protease DPP-4, a regulator of the mobilizing chemokine SDF-1, which is required for the

TABLE 1 | Summarizes the mechanisms, objects, complications and the corresponding references of stem cells dysfunctions in diabetes.

Dysfunction	Mechanism	Object	Complication	References
Mobilopathy	disturbed stem cell niches: VCAM1↓SDF-1↓VEGF↓DPP-4↓in BM	HSPCs	various	Orlandi et al. (2010)
	impaired mobilization in response to G-CSF: inability to upregulate DPP-4→SDF-1↓	HSPCs	various	(Fadini et al., 2013a), (Fadini et al., 2013b)
	SNS terminals↑→response of MSCs to β-adrenergic stimulation or G-CSF↓→inability to downregulate CXCL12	HSPCs	neuropathy	Ferraro et al. (2011)
	p66Shc↑Sirtuin1↑→adhesion molecules↑	BM-derived stem cells	neuropathy	Albiero et al. (2014)
	M1/CD169 BMMΦ↑→OSM↑→release of CXCL12 by MSCs↑	Stem cells	various	Albiero et al. (2015)
	APN↓→MC3T3-E1 osteoblastic cells↓→Smad1/5/8 phosphorylation and nuclear localization↓→SDF-1↓	BMMSCs	bone disease	Yu et al. (2015)
Abnormal Differentiation	aberrant angiogenic potential	MSCs	abnormal repair of ischemia	Kim et al. (2015)
	high glucose→adipogenic potential↑	MPCs	vascular disease	Keats and Khan, (2012)
	Nox4↑→ROS↑→adipogenic potential↑	MSCs	vascular disease	Yan et al. (2012)
	differentiation potential toward active fibroblasts↑osteogenic and adipogenic potential↓	Cardiac MSCs	diabetic cardiomyopathy	de Paula et al. (2017)
	T1DM→ERK↓WNT↓p38↑→osteogenic potential↓adipogenic potential↑	MSCs	osteoporosis	Silva et al. (2015)
	T2DM→circulation changes→osteogenic potential↓adipogenic potential↑	MSCs	osteoporosis	Moseley et al. (2018)
	T2DM→BMP-2↓→disturbed BMP signaling pathway→osteogenic potential↓	BMMSCs	osteoporosis	Wang et al. (2013)
	high glucose→osteogenic potential↓	MSCs	osteoporosis	Deng et al. (2018)
	high glucose→osteogenic and chondrogenic potential↓adipogenic potential↑	ASCs	various	Cramer et al. (2010)
	unable to differentiate into mature and functional adipocytesa→hypertrophy of existing mature adipocytes	ASCs	obesity	Barbagallo et al. (2017)
	BMP4↑glucose↑→endothelial and adipogenic potential↑	ASCs	lipodystrophy	Jumabay et al. (2015)
	T1DM→inflammation→Leydig cells↓→testosterone level↓	SSCs	male reproductive disorder	Skurikhin et al. (2017)
	myogenic differentiation ability↓	BMMSCs	various	Jin et al. (2010)
Migration Dysfunction	high glucose	MPCs	neovascularization dysfunction	Keats and Khan, (2012)
	chemokine receptor CXCR4↓	ASCs	various	Kočí et al. (2014)
	high glucose→ERK1/2 and p38 MAPK activities↓→SCF expression↓	CSCs	myocardial infarction	She et al. (2012)
	unknown	ASCs	diabetic ulcer	Cianfarani et al. (2013)
	high glucose→GSK3β↑→chemokine receptor CXCR4↓	ASCs	impaired bone repair	Zhang et al. (2016)
	low-level inflammatory microenvironment→disturbed IL6/STAT3 signaling pathway	MSCs	delayed wound healing	van de Vyver et al. (2016)
Secretory Dysfunction	fibroblast markers↑VEGF-A↓	ASCs	various	Kočí et al. (2014)
	VEGF-A↓IGF-1↓	BMMSCs	various	Jin et al. (2010)
	hepatocyte growth factor↓VEGF-A↓IGF-1↓→keratinocyte and fibroblast proliferation and migration↓	ASCs	diabetic ulcer	Cianfarani et al. (2013)
	IGF-1↓	MSCs	delayed wound healing	Gao et al. (2014)
	T1DM→altered peripheral IGF-1/IGFBP3→dysfunction of colonic stem cells	Stem cells	diabetic enteropathy	D'Addio et al. (2015)
Impaired Viability	high glucose	MSCs	various	(Silva et al., 2015), (Ali et al., 2017)
Protein Abnormality	high glucose→ERK↓WNT↓p38↑→alkaline phosphatase activity↑ collagen synthesis↓	MSCs	various	Silva et al. (2015)
	lactate dehydrogenase release↑	MSCs	various	Ali et al. (2017)
	nestin protein expression↓	Cardiac neural stem cells	diabetic cardiomyopathy	El-Helou et al. (2009)

VCAM1, vascular cell adhesion molecule-1; SDF-1, stromal cell derived factor-1; VEGF, vascular endothelial growth factor; DPP-4, dipeptidylpeptidase-4; BM, bone marrow; HSPCs, hematopoietic stem and progenitor cells; G-CSF, granulocyte colony-stimulating factor; SNS, sympathetic nervous system; MSCs, mesenchymal stem cells; CXCL12, chemokine (C-X-C motif) ligand 12; BMMΦ, bone marow macrophages; OSM, oncostatin M; APN, adiponectin; BMMSCs, bone marrow mesenchymal stem cells; MPCs, mesenchymal progenitor cells; ROS, reactive oxygen species; T1DM, type 1 diabetes mellitus; ERK, extracellular regulated protein kinases; T2DM, type 2 diabetes mellitus; BMP, bone morphogenetic protein; ASCs, adipose derived stem cells; SSCs, spermatogonia stem cells; CXCR4, chemokine (C-X-C motif) receptor 4; MAPK, mitogen-activated protein kinase; SCF, stem cells factor; CSCs, cardiac stem cells; GSK3β, glycogen synthase kinase-3β; IL6, interleukin 6; STAT3, signal transducer and activator of transcription 3; VEGF-A, vascular endothelial growth factor-A; IGF-1, insulin-like growth factor-1; IGFBP3, insulin-like growth factor binding protein 3.

TABLE 2 | Summarizes the mechanisms, objects, complications and the corresponding references of stem cells quantity alteration in diabetes.

Quantity alteration		Mechanism	Object	Complication	References
Decrease in Quantity	Decreased Proliferation	Bmi1↓	HSPCs	various	Orlandi et al. (2010)
		Unknown	MSCs	various	Kim et al. (2015), Silva et al. (2015), Jin et al. (2010)
		high glucose	ASCs	various	Cramer et al. (2010)
		Unknown	ASCs	diabetic ulcer	Cianfarani et al. (2013)
		high glucose→GSK3β↑→cyclin D1 and CXCR4↓	BMMSCs	various	Zhang et al. (2016)
		high glucose→AGE↑→disturbed RAGE signaling pathway	MSCs	various	Aikawa et al. (2016)
		high glucose→activation of ROS-p38 mediated pathway→chemokines/cytokines↑	MPCs	various	Yang et al. (2010)
		cellular stress↑→p21↑	BMMSCs	various	Gu et al. (2013), Hernandez et al. (2013)
		inflammatory state→TNF-α levels↑	MSCs	delayed fracture healing	Ko et al. (2015)
	Increased Apoptosis	high glucose→ERK↓WNT↓p38↑	MSCs	various	Silva et al. (2015)
		inflammatory state→activation of caspase 3 and caspase 9→TNF-α levels↑	ASCs	various	Cramer et al. (2010)
		high glucose→AGE↑→disturbed RAGE signaling pathway	MSCs	various	Aikawa et al. (2016)
		cellular stress↑→p21↑	BMMSCs	various	Gu et al. (2013), Hernandez et al. (2013)
		inflammatory state→TNF-α levels↑	MSCs	delayed fracture healing	Ko et al. (2015)
		ROS↑	CPCs	cardiomyopathy	Rota et al. (2006)
		microRNA-155↓→FOXO3a↑and nuclear localization→p21↑p27kip1↑	BMPCs	various	Spinetti et al. (2013)
		endoplasmic reticulum stress→p-S6↓→autophagy↑→apoptosis ↑	BMMSCs	various	Meng et al. (2016)
		complement C5a→Fas-associated protein↑BAX/Bcl-2↑	MSCs	various	Zhu et al. (2017)
		metformin→AMPK-mediated mTOR suppression	MSCs	various	He et al. (2018)
	Accelerated Senescence	Bmi1↓	HSPCs	various	Orlandi et al. (2010)
		high glucose	ASCs	various	Cramer et al. (2010)
		high glucose→AGE↑→disturbed RAGE signaling pathway	MSCs	various	Aikawa et al. (2016)
	Increased Cellular Death	unknown	BMMSCs	various	Rezabakhsh et al. (2017)
	Induction of Autophagy	high level of p62	BMMSCs	various	Rezabakhsh et al. (2017)
	Growth Reduction	high glucose	MPCs	vascular disease	Keats and Khan, (2012)
Increase in Quantity	Enhanced Proliferation	unknown	Cardiac MSCs	cardiomyopathy	de Paula et al. (2017)
		BMP4↑glucose↑	ASCs	lipodystrophy	Jumabay et al. (2015)
Complex Changes	Concentration	low blood glucose levels→promote proliferation; high blood glucose levels→inhibit proliferation	MSCs	osteoporosis	Deng et al. (2018)
	Location	BM↓PB↓spleen↑	EPCs	various	Saito et al. (2012)
	Selectivity	T1DM→inflammation→Sertoli cells↓→differentiating c-kit+/CD90+ SSC↑CD51-/CD24+/CD52+ SSC↑sc-kit-/CD90+ SSC↓	SSCs	male reproductive disorder	Skurikhin et al. (2017)
		selectively depleted a subpopulation with a highly vasculogenic transcriptional profile	ASCs	vascular disease	Rennert et al. (2014)

HSPCs, hematopoietic stem and progenitor cells; MSCs, mesenchymal stem cells; ASCs, adipose derived stem cells; GSK3β, glycogen synthase kinase-3β; CXCR4, chemokine (C-X-C motif) receptor 4; BMMSCs, bone marrow mesenchymal stem cells; AGE, advanced glycation end-product; RAGE, receptor for AGE; ROS, reactive oxygen species; MPCs, mesenchymal progenitor cells; TNF-α, tumor necrosis factor-α; ERK, extracellular regulated protein kinases; CPCs, cardiac progenitor cells; BMPCs, bone marrow progenitor cells; BAX, Bcl-2-associated X protein; Bcl-2, B cell lymphoma 2; BMP4, bone morphogenetic protein 4; BM, bone marrow; PB, peripheral blood; EPCs, endothelial progenitor cells; T1DM, type 1 diabetes mellitus; SSCs, spermatogonia stem cells.

mobilizing effect of hrG-CSF (Fadini et al., 2013a; Fadini et al., 2013b).

In addition, diabetic autonomic neuropathy is involved in the mobilopathy of stem cells. The sympathetic nervous system is prominently involved in BM-derived stem cells trafficking, and the function of sympathetic nervous system in BM is abnormal under the condition of DM. Ferraro et al. found that HSPCs are aberrantly localized in the marrow niche of the diabetic mice, and abnormalities in the number and function of sympathetic nerve termini are associated with this mis-localization. The MSCs innervated by these sympathetic nervous system fibers fail to downregulate chemokine CXCL12 in response to G-CSF or adrenergic stimulation, thus inhibiting the release of HSPCs from BM and making it aberrantly localized in the marrow niche (Ferraro et al., 2011). Furthermore, Diabetic autonomic neuropathy may increase the expression of various adhesion

molecules through regulating the expression of 66-kDa protein and Sirtuin 1, leading to BM-derived stem cells mobilization dysfunctions eventually (Albiero et al., 2014).

Stem cells "mobilopathy" in diabetes is also associated with the increase of BM macrophages. Diabetes skews macrophage phenotypes, increases the number of M1/CD169 macrophages in both diabetic mice and DM patients. These macrophages secrete large quantities of soluble mediator oncostatin M, which induce chemokine CXCL12 expression of MSCs *via* a mitogen-activated protein kinase kinase-p38-signal transducer and activator of a transcription 3-dependent pathway (Albiero et al., 2015). Another abnormal pathway is related with adiponectin. Reduction of adiponectin level found in T2DM impairs the mobilization of BMMSCs for bone regeneration, which might be one of the possible mechanisms of bone disease in diabetes. *In vitro* studies found that this is because the reduced adiponectin could not effectively lead to Smad1/5/8 phosphorylation and nuclear localization, thus decreasing the expression of chemokine SDF-1 mRNA (Yu et al., 2015).

Abnormal Differentiation

Stem cells have significant plasticity and can differentiate into specialized cells. MSCs are especially multipotent and can differentiate into variety of cell types, including the cells of bone, cartilage, fat and other connective tissue. Within a diabetic microenvironment, however, the differentiation ability of stem cells changes so that they cannot successfully differentiate into the cells required at the injury sites, thus leading to diabetic complications.

Hyperglycemia caused by diabetes can directly act on vascular endothelial cells, leading to vascular dysfunctions, tissue ischemia and many other problems which ultimately result in the complications. Normally, MSCs and mesenchymal progenitor cells can aggregate in the injured area and differentiate into new vascular endothelial cells to restore homeostasis. However, in the case of diabetes, their angiogenic differentiation ability is aberrant and are not able to repair damaged blood vessels (Kim et al., 2015). This is also proved by a group of scientists in 2012. They reported that high glucose drastically increased the differentiation of mesenchymal progenitor cells into adipocytes rather that vascular endothelial cells required for repair (Keats and Khan, 2012). Molecular mechanism is further demonstrated that diabetes can induce the expression of Nox4 which further induce ROS that are essential for the terminal differentiation of MSCs into adipocytes (Yan et al., 2012).

In addition to circulatory vessels, DM can directly affect specific tissues, such as the myocardium, which ultimately progress to diabetic cardiomyopathy (DCM). As one of the most common and severe complication of DM, DCM is characterized by abnormal myocardial metabolism, diastolic cardiac dysfunction, heart failure, cardiomyocyte hypertrophy, cardiac fibrosis and even death in severe patients (Ke et al., 2021). It has been reported that adverse alteration of stem cells found in the heart may be related to the pathogenesis of DCM. Cardiac MSCs are observed with a shift in the differentiation potential toward active fibroblasts that secrete collagen and promote myocardial fibrosis. Reduced capacity for osteogenic and adipogenic differentiation are also reported in DM rats. However, bone or fat is irrelevant to cardiac repair, so whether these changes are associated with DCM remain in doubt (de Paula et al., 2017). Besides differentiation dysfunctions, cardiac stem cells also show abnormalities in migration ability, protein expression, quantity and et al. under diabetes, which are discussed in the later paragraphs. It is worth noting that whether stem cells exist in the heart is controversial at present. Many researchers insist that there are no stem cells in the heart, while some believe a small number do exist (Han et al., 2021). We should be cautious about this issue.

Many patients with diabetes, both T1DM and T2DM, also suffer from an increased risk of osteoporosis-associated fractures according to the influence of DM on skeletal metabolism. In T1DM, patients have reduced bone mineral density (BMD) which may ultimately increase risk of fracture (Kurra et al., 2014). This sustained bone alterations seem to result from a decreased osteoblastic activity. Moreover, osteoporosis is often accompanied by a histologically detectable increase in adipose tissue in the BM. As expected, in T1DM rats, MSCs are observed with the diminished osteogenic and increased adipogenic differentiation. The decreased activity of ERK and WNT, and an increased signaling through p38 may act as its molecular mechanism (Silva et al., 2015). In T2DM, the decreased osteogenic differentiation of MSCs is also significant. Diabetes might alter the circulating factors in microenvironment, which leads to the transformation of MSCs into fat rather than bone, leading to diabetic osteoporosis (Moseley et al., 2018). This changed differentiation ability may also be attributed to the decrease of BMP-2 in BMMSCs, inhibiting the activation of BMP signaling pathway (Wang et al., 2013). However, the influence of T2DM on BMD remains controversial. Studies have reported increased, reduced and even normal BMD of T2DM patients. The conflicting results may partly explained by the combined effects of different quality alteration and degree of decreased osteogenic differentiation ability of MSCs, according to the differences in long-term glycemic control among diabetic patients (Deng et al., 2018).

Most diabetics usually weigh in an abnormal range, either overweight or underweight and some of them also have lipodystrophy. Lipodystrophy is an adipose dysfunction in which your body produces, uses, and stores fat. This kind of disease is mainly related to the obstacle of differentiation of adipose derived stem cells (ASCs) (Cramer et al., 2010; Kočí et al., 2014). Scientists reported that under the condition of diabetes, ASCs lost their ability to differentiate into mature and functional adipocytes. Therefore, DM patients might develop obesity through a hypertrophy of existing mature adipocytes due to failure turnover of adipose tissue (Barbagallo et al., 2017). Based on this, the enhanced expression of BMP4, together with high glucose are further discovered to play a role in increasing endothelial and adipogenic lineage differentiation of ASCs. This promotes adipose vascularity and expression of multiple endothelial cell markers in adipose tissue which changes its normal state (Jumabay et al., 2015).

Moreover, male reproductive disorder are serious complications of T1DM. There are three main cells in the

male reproductive system that are related to the disorder, spermatogonia stem cells (SSCs), Sertoli cells and Leydig cells. T1DM results in the inflammation development in the testes and further decreases the number of Leydig cells located in the interstitial tissue of testicles. A great decrease in the number of Leydig cells thus decreases the testosterone level and disturbs the differentiation ability of SSCs. On the contrary, Sertoli cells are hardly affected and form a niche for SSCs, thus minimizing the severity of spermatogenesis disorders in T1DM (Skurikhin et al., 2017).

Above studies *in vivo* indicate that the differentiation abilities of stem cells in diabetic microenvironment are modified. Interestingly, an *in vitro* study found that the properties of stem cells impaired by the diabetic inner environment seems to be irreversible. BMMSCs cultured *in vitro* under normal culture conditions possess decreased myogenic differentiation in induced differentiation experiment, suggesting that the impairment cannot be recovered by *ex-vivo* culture (Jin et al., 2010).

Migration Dysfunctions

Cell migration is a crucial process throughout the life of human beings. This is no exception to stem cells. The migration of stem cells is a significant and highly regulated process that enables them to maintain tissue homoeostasis and mediate repair and regeneration. This property, however, can be subverted during the development of diabetes, weakening stem cells abilities of reaching the required position to repair the damaged sites. Untimely repair thus results in the development of diabetic complications (de Lucas et al., 2018).

It has been reported that in patients with diabetes, wounds of tissue or organ are difficult to heal and the prognosis is poor. Patients often suffer from great pain according to pyogenic and ulcerative skin wounds, irreparable vascular injuries and irrecoverable damaged myocardium, et al. All of these are thought to be associated with stem cells migration disorders (Keats and Khan, 2012; She et al., 2012; Cianfarani et al., 2013). Diabetic ulcer, also called diabetic foot is a serious complication of DM, which mainly occurs in the feet of patients and serve as the leading cause of leg amputation. The experimental results show that this was closely related to the decline of migration function of diabetic ASCs (Cianfarani et al., 2013). Similarly, Keats, E. and Z.A. Khan claimed that neovascularization dysfunctions after tissue ischemia was due to reduced cell migration of mesenchymal progenitor cells in hyperglycemia (Keats and Khan, 2012). In addition, for diabetic patients with myocardial infarction, scientists have reported that the inhibition of migration of cardiac stem cells toward the ischemic area post-myocardial infarction was the main cause of the difficulty to recover damaged myocardium (She et al., 2012).

Furthermore, deeper molecular mechanisms of stem cells migration dysfunctions caused by DM have been revealed. The ability of stem cells to express chemokine receptors is related to their ability to migrate to injury sites and mediate damage repair. Under the condition of diabetes, ASCs reduce expression of chemokine receptor CXCR4, causing the dysfunctions (Kočí et al., 2014). Later, Zhang, B, et al. suggested that the suppression of chemokine receptor CXCR4 was due to the activation of its upstream signal transduction pathway, glycogen synthase kinase-3β by high glucose (Zhang et al., 2016). Another research explained the cause of irrecoverable damaged myocardium after myocardial infarction. Diabetic hyperglycemia decreases stem cells factor expression *via* reduction in ERK1/2 and p38 MAPK activities and further inhibits the migration of cardiac stem cells towards the ischemic area post-myocardial infarction (She et al., 2012). Additionally, for MSCs, it has been reported that diabetes creates a low-level inflammatory microenvironment which leads to dysregulation of inflammation-modulated IL6/STAT3 signaling pathway and finally bring about migration dysfunctions. It's comforting, though, that the dysfunctions can be improved to a certain extent by using recombinant IL-6 (van de Vyver et al., 2016).

Secretory Dysfunctions

The paracrine mechanism suggests that stem cells can secrete a variety of substances, such as cytokines and exosomes, promoting different cellular functions including angiogenesis, wound healing, anti-apoptosis and attenuation of fibrosis (Alrefai et al., 2019). However, it has been reported that DM may cause stem cells secretory dysfunctions and result in diabetic complications.

Cytokines released by stem cells play important roles in stimulating endothelial cell migration, inhibiting endothelial apoptosis, promoting angiogenesis and et al. Many researches have reported that under the condition of diabetes, stem cells have a different composition of secretome, containing different levels of angiogenic factors for instance. Either excessive or deficient angiogenesis can lead to diabetic complications (Kim et al., 2015; Ribot et al., 2017). The cytokine vascular endothelial growth factor-A (VEGF-A), an important factor in vascular growth, displays a significant decrease under DM (Jin et al., 2010; Cianfarani et al., 2013). Moreover, the high expression of fibroblast marker, detected by monoclonal anti-human fibroblast surface protein, is associated with this reduced expression of VEGF-A. This suggests the decrease of angiogenesis and the increase of fibrogenesis, which breaks the homeostasis of fiber and vessel formation during wound healing (Kočí et al., 2014).

In addition, lower expression of insulin-like growth factor-1 (IGF-1) has been found under diabetic environment. The delayed wound healing in diabetes is closely related to it (Jin et al., 2010; Gao et al., 2014). According to Cianfarani, growth factors play important roles in skin repair. The decreased release of growth factors results from a reduced paracrine activity of diabetic stem cells at the wound site. This further reduces proliferation and migration of keratinocytes and fibroblasts, resulting in diabetic ulcer (Cianfarani et al., 2013). Interestingly, IGF-1 can also act on stem cells. The level of IGF-1 and its binding protein 3 (IGFBP3) are disrupted in diabetic enteropathy which is common in individuals with long-standing T1DM. And the altered peripheral IGF-1/IGFBP3 results in the dysfunctions of colonic stem cells in diabetic enteropathy (D'Addio et al., 2015).

MSCs also have the ability to secrete exosomes, extracellular nanoparticles containing functional mRNAs, miRNAs, lncRNAs, proteins and lipids (Zhang et al., 2019; van Niel et al., 2018). The therapeutic effect of MSC-derived exosomes has been demonstrated in

preclinical studies of DM and the resulting complications. In a rat model of T2DM, intravenous infusion of exosomes from human umbilical cord MSCs can alleviate T2DM by enhancing peripheral insulin sensitivity and inhibiting β-cell apoptosis (Sun et al., 2018). MSC-derived exosomes are also reported to improve functional recovery in mice with diabetic neuropathy and rats with DM-induced myocardial injury *via* suppression of proinflammatory genes and inhibition of TGF-β1/Smad2 signaling pathway, respectively (Fan et al., 2020; Lin et al., 2019). However, so far, most studies have focused on the therapeutic effects of exogenous exosomes. Evidence on the ability of endogenous MSCs to secrete exosomes under DM is limited.

Others

In addition to the typical dysfunctions mentioned above, DM also leads to many other stem cells dysfunctions. Many studies have found an impaired viability of MSCs caused by high glucose (Silva et al., 2015; Ali et al., 2017).

Protein abnormality is also one of the factors that are often reported. In diabetic rats, MSCs display increased alkaline phosphatase activity and decreased collagen synthesis through a decreased activity of ERK and WNT, and an increased signaling through p38 resulted from DM. This is associated with abnormal metabolism and regeneration of bone tissue in DM (Silva et al., 2015). It has also been reported that diabetes induce harmful effects on MSCs, increasing the release of lactate dehydrogenase, thus affecting the repair capability (Ali et al., 2017). Besides, El-Helou et al. find that nestin protein expression in cardiac neural stem cells was significantly reduced. The aberrant cardiac neural stem cells phenotype may compromise their biological role and predispose the diabetic heart to maladaptive healing following ischemic injury (El-Helou et al., 2009). **Table 2** summarizes the mechanisms, objects, complications and the corresponding references of stem cells quantity alteration in diabetes.

Stem Cells Quantity Alteration in Diabetes

Decrease in Quantity

Most of the studies have reported that acute exposure to high levels of glucose under diabetic condition decreases the number of various types of stem cells, leading to insufficiency of stem cells used for repair and regeneration, which strongly relates to different diabetic complications (Keats and Khan, 2012; Skurikhin et al., 2017).

Abnormal Proliferation

Inhibition of stem cells proliferation is one of the main reasons for the decrease of stem cells number. Many studies have shown that the proliferation ability of MSCs is obviously impaired within a diabetic microenvironment (Jin et al., 2010; Kim et al., 2015; Silva et al., 2015). It has also been reported that the proliferative potential of ASCs decrease in T1DM (Cianfarani et al., 2013).

This proliferation inhibition may be due to high glucose conditions (Cramer et al., 2010). It is well known that in diabetes, chronic hyperglycemic conditions drive glycation reactions between proteins and glucose or its derivatives, resulting in the formation of AGE. AGE may decrease MSCs proliferation by signaling through receptor for AGE (RAGE) (Aikawa et al., 2016). They may also be responsible for an inhibitory effect on MPCs proliferation by inducing production of chemokines/cytokines *via* activation of ROS-p38 mediated pathway (Yang et al., 2010). Additionally, high glucose may activate glycogen synthase kinase-3beta, which plays an important role in inhibiting the proliferation of BMMSCs by inhibiting cyclin D1 and CXCR4 (Zhang et al., 2016).

Besides high glucose, many other mechanisms have also been proposed. Orlandi et al. show that long-term diabetes decreases the repopulation capacity of HSPCs by reducing the expression of Bmi1 (Orlandi et al., 2010). Another study suggests that the significant decrease of proliferation of BMMSCs is associated with the increase of p21, which is due to increased cellular stress during the pathogenesis of diabetes (Gu et al., 2013; Hernandez et al., 2013). Also, diabetes causes an inflammatory state of the body and increases TNF-α levels, thus reducing stem cells number in new bone area (Ko et al., 2015).

Increased Apoptosis

The activation of apoptosis pathway of stem cells by DM is another important reason for the decrease of number (Jin et al., 2010; Baban et al., 2016). Many of the factors mentioned above that reduce the proliferation of stem cells also affect their apoptosis ability. For example, high glucose, p21, TNF-α, AGE and RAGE (Cramer et al., 2010; Stolzing et al., 2010; Gu et al., 2013; Ko et al., 2015). Deeper connections between these factors have also been found. Apoptosis is reported to be induced by high glucose *via* activation of caspase 3 and caspase 9 which is associated with TNF-α (Cramer et al., 2010). High glucose also plays a role in a decreased activity of ERK and WNT, and an increased signaling through p38 (Silva et al., 2015).

Other different mechanisms have also been put forward. The generation of ROS can lead to the apoptosis of cardiac progenitor cells and damage the growth reserve of the heart (Rota et al., 2006). Additionally, the activation of proapoptotic pathway can cause the shortage of CD34(+) bone marrow progenitor cells (BMPCs). Upregulation and nuclear localization of the proapoptotic factor FOXO3a and induction of FOXO3a targets, p21 and p27kip1 play a significant role. Moreover, microRNA-155, which regulates cell survival through inhibition of FOXO3a, is downregulated in diabetic CD34(+)-BMPCs and inversely correlated with FOXO3a levels (Spinetti et al., 2013).

In 2016, it has been reported for the first time that endoplasmic reticulum stress induces apoptosis of BMMSCs, which is mediated by autophagy associated with the decrease of p-S6 (Meng et al., 2016). Later, Zhu et al. found that DM induces MSCs apoptosis through complement C5a-dependent up regulation of Fas-associated protein with death domain and the Bcl-2-associated X protein (BAX)/B cell lymphoma 2 (Bcl-2) ratios (Zhu et al., 2017). More recently, it is suggested that when metformin is used to enhance glucose control in diabetic patients, it might induce MSCs apoptosis through AMPK-mediated mTOR suppression, while high glucose (standard glucose control) can significantly reverse its adverse reactions in an AMPK-mTOR pathway dependent manner (He et al., 2018; He et al., 2019).

Others

In addition to inhibiting proliferation and promoting apoptosis, a few reports have suggested that diabetes can reduce the number of stem cells by some other mechanisms.

Long-term diabetes may accelerate the senescence of HSPCs by reducing the expression of Bmi1 (Orlandi et al., 2010). The accelerated aging of stem cells also relates to the increase of glucose in T2DM and the change of AGE and RAGE (Cramer et al., 2010; Stolzing et al., 2010).

It has been reported that diabetic serum is found to induce a higher cellular death rate and decrease human BMMSCs angiogenic properties by the induction of autophagy signaling which is marked by high level of p62 (Rezabakhsh et al., 2017). Additionally, Keats and Khan found that MPCs show a transient reduction in growth upon glucose challenge (Keats and Khan, 2012).

Increase in Quantity

Although most of the literatures report the damage of diabetes to the number of stem cells, still, some have reported that diabetes increases their quantity.

A higher number of cardiac MSCs in DM rats has been observed *in vitro*, which is associated with a significantly higher proliferative rate. However, the confirmation of this assertion requires more experiments to evaluate their mitotic rate *in vivo* (de Paula et al., 2017). Additionally, cautiousness is required on the existence of stem cells in the heart. For ASCs, this enhanced proliferative rate results from the change of glucose and BMP4 (Jumabay et al., 2015).

Complex Changes in Quantity

Moreover, some studies have reported complex changes in the number of stem cells under DM condition.

The number of stem cells is related to the level of glucose. A certain degree of hyperglycemia promotes MSCs proliferation, whereas high blood glucose levels (>10%), which reflects poor glycemic control, significantly inhibits MSCs proliferation (Deng et al., 2018).

Additionally, the location of stem cells may also be connected with their quantity. The number of circulating endothelial progenitor cells (EPCs) significantly decreases in BM and peripheral blood, but paradoxically increases in spleen under diabetic conditions. This may be attributed to the damage of EPCs production in BM and the reduction of mobilization of spleen EPCs (Saito et al., 2012). However, Keats and Khan reported that EPCs were resistant to the effects of high levels of glucose, even following chronic exposure (Keats and Khan, 2012).

A study further claimed that this quantity change was not overall or random. For ASCs, diabetes selectively depletes a subpopulation with a highly vasculogenic transcriptional profile, thus impairing new blood vessel formation and wound healing (Rennert et al., 2014). Among the male reproductive disorders caused by T1DM, the proliferation of SSCs plays a critical role. The pronounced inflammatory component of T1DM slightly decreases the number of Sertoli cells which can regulate the SSCs *via* secretion of various factors. Thus, the number of SCCs with c-kit-/CD90+ immunophenotype significantly decreases and the number of differentiating c-kit+/CD90+ SSC and CD51-/CD24+/CD52+ SSCs significantly increases (Skurikhin et al., 2017).

Stem Cell-Based Therapy for Diabetic Complications

We can see that diabetes indeed does damage to the endogenous stem cells of the body in all aspects, which leads to severe diabetic complications. Therefore, it is possible that exogenous stem cells can be used to treat the complications. Some studies have reported the effectiveness of the treatment basic *in vitro* experiments and animal experiments. But to the best of our knowledge, existing clinical studies are of low quality and none has proven clinical safety nor efficacy (Li et al., 2021). Here, we briefly put forward some therapies, hoping to inspire more researchers to improve and perfect the therapeutic methods of diabetic complications.

Diabetes damages stem cells from quality and quantity. In most cases, the number of stem cells decreases under DM. Therefore, supplementing exogenous stem cells can relieve the damage of diabetes on the quality of stem cells. Additionally, stem cell dysfunctions caused by diabetes can also be relieved through the normal function of exogenous stem cells. Three specific mechanisms might play a role, including migration, differentiation and secretion ability. Firstly, stem cells undergo homing and further migrate to the injured site, which may be due to chemoattraction mediated by cell surface receptors (Teo et al., 2012). Secondly, exogenous stem cells can differentiate into multiple cell types to replace damaged tissue and induce functional recovery (Aggarwal and Pittenger, 2005). Thirdly, stem cells can secrete growth/bioactive factors and exosomes, which may have potential positive effects on local and systemic physiological processes (Raffaghello et al., 2008). It is important to note that various mechanisms exist in the therapeutic potential of stem cells, above mentioned might not be generally true for all stem cell therapies.

Microvascular Complications

The microvascular complications of diabetes mainly include retinopathy, neuropathy, and nephropathy. These three major microvascular complications seriously affect the quality of life of diabetic patients and even threaten their lives. Stem cells seem to be an effective long-term treatment option for these complications due to their repair and regeneration potential.

It has been reported that stem cells may delay the progression and alleviate the symptoms of diabetic retinopathy through secretion and differentiation abilities (Scalinci et al., 2011; Davey et al., 2014). Recent studies on MSCs, EPCs and ASCs have shown that cell-based therapy may be a feasible option to prevent neurovascular injury and promote retinal regeneration (Megaw and Dhillon, 2014; Gaddam et al., 2019). However, current authoritative studies mainly focus on basic researches and animal studies. Although these researches have tentatively confirmed the effectiveness of cell regeneration therapy and consolidated the foundation of preclinical research in this field, the stem cell therapy has not yet been widely accepted in clinical practice (Ludwig et al., 2019; Li et al., 2021).

Effectiveness for reversing various manifestations of experimental diabetic neuropathy has also been proved through attempts for treating experimental diabetic

neuropathy with BM-derived stem or progenitor cells. In previous studies, MSCs transplantation has been reported to have therapeutic effects on diabetic neuropathy through paracrine actions of growth factors (Shibata et al., 2008). Additionally, MSCs transplantation are able to improve diabetic neuropathy through direct peripheral nerve angiogenesis, neurotrophic effects, and restoration of myelination (Han et al., 2016). More recently, application of MSCs-derived exosomes to diabetic mice cast light on the feasibility and efficacy of the exosome-based therapy for diabetic neuropathy (Fan et al., 2021).

For the treatment of diabetic nephropathy, some studies have reported that in the presence of certain growth factors, embryonic stem cells can differentiate into renal cells and play a therapeutic effect on diabetic neuropathy (Kim and Dressler, 2005; Narayanan et al., 2013). iPSCs have also been successfully differentiated into renal cells (Song et al., 2012). Moreover, the role of MSCs in the treatment of diabetic neuropathy is prospective. MSCs have been introduced into diabetic rats to repair renal damage and regenerate insulin-secreting cells (Ezquer et al., 2008). MSCs can also protect the kidney by stimulating the regeneration microenvironment through paracrine action (Ezquer et al., 2015). It has been further demonstrated that BMMSCs treatment are able to regulate the serum level of insulin, hemeoxygenase-1, AGE, and glucose with recovery in renal function (Hamza et al., 2017).

Macrovascular Complications

Diabetic patients are prone to atherosclerosis, and eventually develop into macrovascular complications. Vascular stem cells have the ability to differentiate into EPCs, which is a potential target for the treatment of diabetic macrovascular complications (Peng et al., 2018).

DISCUSSION

Diabetes causes various stem cells dysfunctions such as mobilopathy, abnormal differentiation, migration dysfunctions, secretory dysfunctions and et al. through different molecular pathways. DM also results in abnormal changes in the number of stem cells, which may due to abnormal proliferating rate, increased apoptosis and et al. These may further lead to diabetic complications, which are the main cause of high mortality in patients with diabetes.

Fortunately, in the past few years, the role of stem cells in the treatment of diabetic pathology and related complications has been widely studied. The ability of stem cells to regenerate and differentiate makes it possible for researchers to explore their potential in treating diabetic complications. It has been suggested that normal functional exogenous stem cells might improve microvascular complications and macrovascular complications, which are the major complications of DM. This therapeutic approach not only helps to overcome the limitations of modern treatment, but also provides a new way for long-term treatment of diabetic complications. Therefore, the use of exogenous stem cells in the treatment of diabetic complications is very promising, worthy of further exploration. However, it can't be denied that stem cells therapy for diabetic complications is still in the imperfect stage of exploration. Extensive research is needed to establish a standard procedure for stem cells therapy of diabetic complications. We hope that this review can provide an in-depth understanding of the association between stem cells and diabetic complications, pave the way for novel insights into the mechanisms underlying diabetes complications, and inspire more researchers to explore new methods for the treatment of diabetic complications.

AUTHOR CONTRIBUTIONS

JX: design the study, collection of the data, analysis the data and preparation of the manuscript. JX, CZ: review and final approval of the manuscript. All authors contributed to the article and approved the submitted version.

FUNDING

This study was supported by the National Natural Science Foundation of China (81970808).

REFERENCES

2. Classification and Diagnosis of Diabetes: Standards of Medical Care in Diabetes-2020. *Diabetes Care*, 2020. 43(Suppl. 1): p. S14-s31.doi:10.2337/dc20-S002

Aggarwal, S., and Pittenger, M. F. (2005). Human mesenchymal stem cells modulate allogeneic immune cell responses. *Blood* 105 (4), 1815–1822. doi:10.1182/blood-2004-04-1559

Aikawa, E., Fujita, R., Asai, M., Kaneda, Y., and Tamai, K. (2016). Receptor for Advanced Glycation End Products-Mediated Signaling Impairs the Maintenance of Bone Marrow Mesenchymal Stromal Cells in Diabetic Model Mice. *Stem Cell Dev.* 25 (22), 1721–1732. doi:10.1089/scd.2016.0067

Alberti, K. G. M. M., and Zimmet, P. Z. (1998). Definition, diagnosis and classification of diabetes mellitus and its complications. Part 1: diagnosis and classification of diabetes mellitus. Provisional report of a WHO Consultation. *Diabet. Med.* 15 (7), 539–553. doi:10.1002/(sici)1096-9136(199807)15:7<539:aid-dia668>3.0.co;2-s

Albiero, M., Poncina, N., Ciciliot, S., Cappellari, R., Menegazzo, L., Ferraro, F., et al. (2015). Bone Marrow Macrophages Contribute to Diabetic Stem Cell Mobilopathy by Producing Oncostatin M. *Diabetes* 64 (8), 2957–2968. doi:10.2337/db14-1473

Albiero, M., Poncina, N., Tjwa, M., Ciciliot, S., Menegazzo, L., Ceolotto, G., et al. (2014). Diabetes causes bone marrow autonomic neuropathy and impairs stem cell mobilization via dysregulated p66Shc and Sirt1. *Diabetes* 63 (4), 1353–1365. doi:10.2337/db13-0894

Ali, F., Aziz, F., and Wajid, N. (2017). Effect of type 2 diabetic serum on the behavior of Wharton's jelly-derived mesenchymal stem cells *in vitro*. *Chronic Dis. Translational Med.* 3 (2), 105–111. doi:10.1016/j.cdtm.2017.02.006

Alrefai, M. T., Tarola, C. L., Raagas, R., Ridwan, K., Shalal, M., Lomis, N., et al. (2019). Functional Assessment of Pluripotent and Mesenchymal Stem Cell Derived Secretome in Heart Disease. *Ann. Stem Cel Res* 2 (1), 29–36.

Angelini, A., Castellani, C., Vescovo, G., and Thiene, G. (2004). Pathological evidence of stem cell regeneration in the heart. *Int. J. Cardiol.* 96 (3), 499–504. doi:10.1016/j.ijcard.2004.07.001

Baban, B., Liu, J. Y., Payne, S., Abebe, W., Yu, J. C., and Mozaffari, M. S. (2016). Status of stem cells in diabetic nephropathy: predictive and preventive potentials. *EPMA J.* 7 (1), 21. doi:10.1186/s13167-016-0070-6

Barbagallo, I., Li Volti, G., Galvano, F., Tettamanti, G., Pluchinotta, F. R., Bergante, S., et al. (2017). Diabetic human adipose tissue-derived mesenchymal stem cells fail to differentiate in functional adipocytes. *Exp. Biol. Med. (Maywood)* 242 (10), 1079–1085. doi:10.1177/1535370216681552

Berebichez-Fridman, R., and Montero-Olvera, P. R. (2018). Sources and Clinical Applications of Mesenchymal Stem Cells: State-of-the-art review. *Sultan Qaboos Univ. Med. J.* 18 (3), e264–e277. doi:10.18295/squmj.2018.18.03.002

Brownlee, M. (2001). Biochemistry and molecular cell biology of diabetic complications. *Nature* 414 (6865), 813–820. doi:10.1038/414813a

Charbord, P. (2010). Bone marrow mesenchymal stem cells: historical overview and concepts. *Hum. Gene Ther.* 21 (9), 1045–1056. doi:10.1089/hum.2010.115

Chen, C. W., Corselli, M., Péault, B., and Huard, J. (2012). Human blood-vessel-derived stem cells for tissue repair and regeneration. *J. Biomed. Biotechnol.* 2012, 597439. doi:10.1155/2012/597439

Cianfarani, F., Toietta, G., Di Rocco, G., Cesareo, E., Zambruno, G., and Odorisio, T. (2013). Diabetes impairs adipose tissue-derived stem cell function and efficiency in promoting wound healing. *Wound Repair Regen.* 21 (4), 545–553. doi:10.1111/wrr.12051

Cramer, C., Freisinger, E., Jones, R. K., Slakey, D. P., Dupin, C. L., Newsome, E. R., et al. (2010). Persistent high glucose concentrations alter the regenerative potential of mesenchymal stem cells. *Stem Cell Dev.* 19 (12), 1875–1884. doi:10.1089/scd.2010.0009

D'Addio, F., La Rosa, S., Maestroni, A., Jung, P., Orsenigo, E., Ben Nasr, M., et al. (2015). Circulating IGF-I and IGFBP3 Levels Control Human Colonic Stem Cell Function and Are Disrupted in Diabetic Enteropathy. *Cell Stem Cell* 17 (4), 486–498. doi:10.1016/j.stem.2015.07.010

Davey, G. C., Patil, S. B., Oâ€™Loughlin, A., and Oâ€™Brien, T. (2014). Mesenchymal stem cell-based treatment for microvascular and secondary complications of diabetes mellitus. *Front. Endocrinol.* 5, 86. doi:10.3389/fendo.2014.00086

de Lucas, B., Pérez, L. M., and Gálvez, B. G. (2018). Importance and regulation of adult stem cell migration. *J. Cel Mol Med* 22 (2), 746–754. doi:10.1111/jcmm.13422

de Paula, D. R. M., Capuano, V., Filho, D. M., Carneiro, A. C. D. M., de Oliveira Crema, V., de Oliveira, L. F., et al. (2017). Biological properties of cardiac mesenchymal stem cells in rats with diabetic cardiomyopathy. *Life Sci.* 188, 45–52. doi:10.1016/j.lfs.2017.08.034

Deng, X., Xu, M., Shen, M., and Cheng, J. (2018). Effects of Type 2 Diabetic Serum on Proliferation and Osteogenic Differentiation of Mesenchymal Stem Cells. *J. Diabetes Res.* 2018, 5765478. doi:10.1155/2018/5765478

Domingueti, C. P., Dusse, L. M. S. A., Carvalho, M. d. G., de Sousa, L. P., Gomes, K. B., and Fernandes, A. P. (2016). Diabetes mellitus: The linkage between oxidative stress, inflammation, hypercoagulability and vascular complications. *J. Diabetes its Complications* 30 (4), 738–745. doi:10.1016/j.jdiacomp.2015.12.018

Du, X.-L., Edelstein, D., Rossetti, L., Fantus, I. G., Goldberg, H., Ziyadeh, F., et al. (2000). Hyperglycemia-induced mitochondrial superoxide overproduction activates the hexosamine pathway and induces plasminogen activator inhibitor-1 expression by increasing Sp1 glycosylation. *Proc. Natl. Acad. Sci.* 97 (22), 12222–12226. doi:10.1073/pnas.97.22.12222

El-Helou, V., Proulx, C., Béguin, P., Assimakopoulos, J., Gosselin, H., Clement, R., et al. (2009). The cardiac neural stem cell phenotype is compromised in streptozotocin-induced diabetic cardiomyopathy. *J. Cel. Physiol.* 220 (2), 440–449. doi:10.1002/jcp.21785

Ezquer, F., Giraud-Billoud, M., Carpio, D., Cabezas, F., Conget, P., and Ezquer, M. (2015). Proregenerative Microenvironment Triggered by Donor Mesenchymal Stem Cells Preserves Renal Function and Structure in Mice with Severe Diabetes Mellitus. *Biomed. Res. Int.* 2015, 164703. doi:10.1155/2015/164703

Ezquer, F. E., Ezquer, M. E., Parrau, D. B., Carpio, D., Yañez, A. J., and Conget, P. A. (2008). Systemic administration of multipotent mesenchymal stromal cells reverts hyperglycemia and prevents nephropathy in type 1 diabetic mice. *Biol. Blood Marrow Transplant.* 14 (6), 631–640. doi:10.1016/j.bbmt.2008.01.006

Fadini, G. P., Albiero, M., Seeger, F., Poncina, N., Menegazzo, L., Angelini, A., et al. (2013). Stem cell compartmentalization in diabetes and high cardiovascular risk reveals the role of DPP-4 in diabetic stem cell mobilopathy. *Basic Res. Cardiol.* 108 (1), 313. doi:10.1007/s00395-012-0313-1

Fadini, G. P., Albiero, M., Vigili de Kreutzenberg, S., Boscaro, E., Cappellari, R., Marescotti, M., et al. (2013). Diabetes impairs stem cell and proangiogenic cell mobilization in humans. *Diabetes Care* 36 (4), 943–949. doi:10.2337/dc12-1084

Fadini, G. P., Ciciliot, S., and Albiero, M. (2017). Concise Review: Perspectives and Clinical Implications of Bone Marrow and Circulating Stem Cell Defects in Diabetes. *Stem Cells* 35 (1), 106–116. doi:10.1002/stem.2445

Falanga, V. (2012). Stem cells in tissue repair and regeneration. *J. Invest. Dermatol.* 132 (6), 1538–1541. doi:10.1038/jid.2012.77

Fan, B., Chopp, M., Zhang, Z. G., and Liu, X. S. (2021). Treatment of diabetic peripheral neuropathy with engineered mesenchymal stromal cell-derived exosomes enriched with microRNA-146a provide amplified therapeutic efficacy. *Exp. Neurol.* 341, 113694. doi:10.1016/j.expneurol.2021.113694

Fan, B., Li, C., Szalad, A., Wang, L., Pan, W., Zhang, R., et al. (2020). Mesenchymal stromal cell-derived exosomes ameliorate peripheral neuropathy in a mouse model of diabetes. *Diabetologia* 63 (2), 431–443. doi:10.1007/s00125-019-05043-0

Ferraro, F., Lymperi, S., Mendez-Ferrer, S., Saez, B., Spencer, J. A., Yeap, B. Y., et al. (2011). Diabetes impairs hematopoietic stem cell mobilization by altering niche function. *Sci. Translational Med.* 3 (104), 104ra101. doi:10.1126/scitranslmed.3002191

Forbes, J. M., and Cooper, M. E. (2013). Mechanisms of diabetic complications. *Physiol. Rev.* 93 (1), 137–188. doi:10.1152/physrev.00045.2011

Fox, C. S., Coady, S., Sorlie, P. D., Levy, D., Meigs, J. B., D'Agostino SR, R. B., et al. (2004). Trends in cardiovascular complications of diabetes. *Jama* 292 (20), 2495–2499. doi:10.1001/jama.292.20.2495

Gaddam, S., Periasamy, R., and Gangaraju, R. (2019). Adult Stem Cell Therapeutics in Diabetic Retinopathy. *Int. J. Mol. Sci.* 20 (19). doi:10.3390/ijms20194876

Gao, D., Gu, C., Wu, Y., Xie, J., Yao, B., Li, J., et al. (2014). Mesenchymal stromal cells enhance wound healing by ameliorating impaired metabolism in diabetic mice. *Cytotherapy* 16 (11), 1467–1475. doi:10.1016/j.jcyt.2014.05.014

Giacco, F., and Brownlee, M. (2010). Oxidative stress and diabetic complications. *Circ. Res.* 107 (9), 1058–1070. doi:10.1161/circresaha.110.223545

Gu, Z., Jiang, J., Xia, Y., Yue, X., Yan, M., Tao, T., et al. (2013). p21 is associated with the proliferation and apoptosis of bone marrow-derived mesenchymal stem cells from non-obese diabetic mice. *Exp. Clin. Endocrinol. Diabetes* 121 (10), 607–613. doi:10.1055/s-0033-1354380

Hamza, A. H., Al-Bishri, W. M., Damiati, L. A., and Ahmed, H. H. (2017). Mesenchymal stem cells: a future experimental exploration for recession of diabetic nephropathy. *Ren. Fail.* 39 (1), 67–76. doi:10.1080/0886022x.2016.1244080

Han, J. W., Choi, D., Lee, M. Y., Huh, Y. H., and Yoon, Y.-S. (2016). Bone Marrow-Derived Mesenchymal Stem Cells Improve Diabetic Neuropathy by Direct Modulation of Both Angiogenesis and Myelination in Peripheral Nerves. *Cel Transpl.* 25 (2), 313–326. doi:10.3727/096368915x688209

Han, M. A., Jeon, J. H., Shin, J. Y., Kim, H. J., Lee, J. S., Seo, C. W., et al. (2021). Intramyocardial delivery of human cardiac stem cell spheroids with enhanced cell engraftment ability and cardiomyogenic potential for myocardial infarct repair. *J. Controlled Release* 336, 499–509. doi:10.1016/j.jconrel.2021.06.040

He, X., Yang, Y., Yao, M.-W., Ren, T.-t., Guo, W., Li, L., et al. (2019). Full title: High glucose protects mesenchymal stem cells from metformin-induced apoptosis through the AMPK-mediated mTOR pathway. *Sci. Rep.* 9 (1), 17764. doi:10.1038/s41598-019-54291-y

He, X., Yao, M.-W., Zhu, M., Liang, D.-L., Guo, W., Yang, Y., et al. (2018). Metformin induces apoptosis in mesenchymal stromal cells and dampens their therapeutic efficacy in infarcted myocardium. *Stem Cel Res Ther* 9 (1), 306. doi:10.1186/s13287-018-1057-0

Hernandez, A. M., Colvin, E. S., Chen, Y.-C., Geiss, S. L., Eller, L. E., and Fueger, P. T. (2013). Upregulation of p21 activates the intrinsic apoptotic pathway in β-cells. *Am. J. Physiology-Endocrinology Metab.* 304 (12), E1281–E1290. doi:10.1152/ajpendo.00663.2012

Intensive blood-glucose control with sulphonylureas or insulin compared with conventional treatment and risk of complications in patients with type 2

diabetes (UKPDS 33). UK Prospective Diabetes Study (UKPDS) Group. *Lancet*, 1998. 352(9131): p. 837–853.

Jin, P., Zhang, X., Wu, Y., Li, L., Yin, Q., Zheng, L., et al. (2010). Streptozotocin-induced diabetic rat-derived bone marrow mesenchymal stem cells have impaired abilities in proliferation, paracrine, antiapoptosis, and myogenic differentiation. *Transplant. Proc.* 42 (7), 2745–2752. doi:10.1016/j.transproceed.2010.05.145

Jumabay, M., Moon, J. H., Yeerna, H., and Boström, K. I. (2015). Effect of Diabetes Mellitus on Adipocyte-Derived Stem Cells in Rat. *J. Cel. Physiol.* 230 (11), 2821–2828. doi:10.1002/jcp.25012

Ke, X., Lin, Z., Ye, Z., Leng, M., Chen, B., Jiang, C., et al. (2021). Histone Deacetylases in the Pathogenesis of Diabetic Cardiomyopathy. *Front. Endocrinol.* 12, 679655. doi:10.3389/fendo.2021.679655

Keats, E., and Khan, Z. A. (2012). Unique responses of stem cell-derived vascular endothelial and mesenchymal cells to high levels of glucose. *PLoS One* 7 (6), e38752. doi:10.1371/journal.pone.0038752

Kim, D., and Dressler, G. R. (2005). Nephrogenic factors promote differentiation of mouse embryonic stem cells into renal epithelia. *Jasn* 16 (12), 3527–3534. doi:10.1681/asn.2005050544

Kim, H., Han, J. W., Lee, J. Y., Choi, Y. J., Sohn, Y.-D., Song, M., et al. (2015). Diabetic Mesenchymal Stem Cells Are Ineffective for Improving Limb Ischemia Due to Their Impaired Angiogenic Capability. *Cel Transpl.* 24 (8), 1571–1584. doi:10.3727/096368914x682792

Ko, K. I., Coimbra, L. S., Tian, C., Alblowi, J., Kayal, R. A., Einhorn, T. A., et al. (2015). Diabetes reduces mesenchymal stem cells in fracture healing through a TNFα-mediated mechanism. *Diabetologia* 58 (3), 633–642. doi:10.1007/s00125-014-3470-y

Kočí, Z., Turnovcová, K., Dubský, M., Baranovičová, L., Holákň, V., Chudíčková, M., et al. (2014). Characterization of human adipose tissue-derived stromal cells isolated from diabetic patient's distal limbs with critical ischemia. *Cell Biochem Funct* 32 (7), 597–604.

Kurra, S., Fink, D. A., and Siris, E. S. (2014). Osteoporosis-associated fracture and diabetes. *Endocrinol. Metab. Clin. North America* 43 (1), 233–243. doi:10.1016/j.ecl.2013.09.004

Lapidot, T., and Petit, I. (2002). Current understanding of stem cell mobilization. *Exp. Hematol.* 30 (9), 973–981. doi:10.1016/s0301-472x(02)00883-4

Li, X. J., Li, C. Y., Bai, D., and Leng, Y. (2021). Insights into stem cell therapy for diabetic retinopathy: a bibliometric and visual analysis. *Neural Regen. Res.* 16 (1), 172–178. doi:10.4103/1673-5374.286974

Lin, Y., Zhang, F., Lian, X.-f., Peng, W.-q., and Yin, C.-y. (2019). Mesenchymal stem cell-derived exosomes improve diabetes mellitus-induced myocardial injury and fibrosis via inhibition of TGF-β1/Smad2 signaling pathway. *Cel Mol Biol (Noisy-le-grand)* 65 (7), 123–126. doi:10.14715/cmb/2019.65.7.21

Lodi, D., Iannitti, T., and Palmieri, B. (2011). Stem cells in clinical practice: applications and warnings. *J. Exp. Clin. Cancer Res.* 30 (1), 9. doi:10.1186/1756-9966-30-9

Ludwig, P. E., Freeman, S. C., and Janot, A. C. (2019). Novel stem cell and gene therapy in diabetic retinopathy, age related macular degeneration, and retinitis pigmentosa. *Int. J. Retin. Vitr* 5, 7. doi:10.1186/s40942-019-0158-y

Megaw, R., and Dhillon, B. (2014). Stem cell therapies in the management of diabetic retinopathy. *Curr. Diab Rep.* 14 (7), 498. doi:10.1007/s11892-014-0498-9

Meng, Y., Ji, J., Tan, W., Guo, G., Xia, Y., Cheng, C., et al. (2016). Involvement of autophagy in the procedure of endoplasmic reticulum stress introduced apoptosis in bone marrow mesenchymal stem cells from nonobese diabetic mice. *Cel Biochem Funct* 34 (1), 25–33. doi:10.1002/cbf.3161

Moseley, K. F., Doyle, M. E., and Jan De Beur, S. M. (2018). Diabetic serum from older women increases adipogenic differentiation in mesenchymal stem cells. *Endocr. Res.* 43 (3), 155–165. doi:10.1080/07435800.2018.1441868

Naji, A., Eitoku, M., Favier, B., Deschaseaux, F., Rouas-Freiss, N., and Suganuma, N. (2019). Biological functions of mesenchymal stem cells and clinical implications. *Cell. Mol. Life Sci.* 76 (17), 3323–3348. doi:10.1007/s00018-019-03125-1

Narayanan, K., Schumacher, K. M., Tasnim, F., Kandasamy, K., Schumacher, A., Ni, M., et al. (2013). Human embryonic stem cells differentiate into functional renal proximal tubular-like cells. *Kidney Int.* 83 (4), 593–603. doi:10.1038/ki.2012.442

Nathan, D. M., Nathan, D. M., Genuth, S., Lachin, J., Cleary, P., Crofford, O., et al. (1993). The effect of intensive treatment of diabetes on the development and progression of long-term complications in insulin-dependent diabetes mellitus. *N. Engl. J. Med.* 329 (14), 977–986. doi:10.1056/NEJM199309303291401

Nishikawa, T., Edelstein, D., Du, X. L., Yamagishi, S.-i., Matsumura, T., Kaneda, Y., et al. (2000). Normalizing mitochondrial superoxide production blocks three pathways of hyperglycaemic damage. *Nature* 404 (6779), 787–790. doi:10.1038/35008121

Orlandi, A., Chavakis, E., Seeger, F., Tjwa, M., Zeiher, A. M., and Dimmeler, S. (2010). Long-term diabetes impairs repopulation of hematopoietic progenitor cells and dysregulates the cytokine expression in the bone marrow microenvironment in mice. *Basic Res. Cardiol.* 105 (6), 703–712. doi:10.1007/s00395-010-0109-0

Peng, B. Y., Dubey, N. K., Mishra, V. K., Tsai, F. C., Dubey, R., Deng, W. P., et al. (2018). Addressing Stem Cell Therapeutic Approaches in Pathobiology of Diabetes and Its Complications. *J. Diabetes Res.* 2018, 7806435. doi:10.1155/2018/7806435

Raffaghello, L., Bianchi, G., Bertolotto, M., Montecucco, F., Busca, A., Dallegri, F., et al. (2008). Human mesenchymal stem cells inhibit neutrophil apoptosis: a model for neutrophil preservation in the bone marrow niche. *Stem Cells* 26 (1), 151–162. doi:10.1634/stemcells.2007-0416

Rennert, R. C., Sorkin, M., Januszyk, M., Duscher, D., Kosaraju, R., Chung, M. T., et al. (2014). Diabetes impairs the angiogenic potential of adipose-derived stem cells by selectively depleting cellular subpopulations. *Stem Cel Res. Ther.* 5 (3), 79. doi:10.1186/scrt468

Rezabakhsh, A., Cheraghi, O., Nourazarian, A., Hassanpour, M., Kazemi, M., Ghaderi, S., et al. (2017). Type 2 Diabetes Inhibited Human Mesenchymal Stem Cells Angiogenic Response by Over-Activity of the Autophagic Pathway. *J. Cel. Biochem.* 118 (6), 1518–1530. doi:10.1002/jcb.25814

Ribot, J., Caliaperoumal, G., Paquet, J., Boisson-vidal, C., Petite, H., and Anagnostou, F. (2017). Type 2 diabetes alters mesenchymal stem cell secretome composition and angiogenic properties. *J. Cel. Mol. Med.* 21 (2), 349–363. doi:10.1111/jcmm.12969

Rota, M., LeCapitaine, N., Hosoda, T., Boni, A., De Angelis, A., Padin-Iruegas, M. E., et al. (2006). Diabetes Promotes Cardiac Stem Cell Aging and Heart Failure, Which Are Prevented by Deletion of the p66 shc Gene. *Circ. Res.* 99 (1), 42–52. doi:10.1161/01.res.0000231289.63468.08

Saeedi, P., Petersohn, I., Salpea, P., Malanda, B., Karuranga, S., Unwin, N., et al. (2019). Global and regional diabetes prevalence estimates for 2019 and projections for 2030 and 2045: Results from the International Diabetes Federation Diabetes Atlas, 9th edition. *Diabetes Res. Clin. Pract.* 9157, 107843. doi:10.1016/j.diabres.2019.107843*(th) edition.*

Saito, H., Yamamoto, Y., and Yamamoto, H. (2012). Diabetes alters subsets of endothelial progenitor cells that reside in blood, bone marrow, and spleen. *Am. J. Physiology-Cell Physiol.* 302 (6), C892–C901. doi:10.1152/ajpcell.00380.2011

Scalinci, S. Z., Scalinci, S. Z., Scorolli, L., Corradetti, fnm., Domanico, S., Vingolo, E. M., et al. (2011). Potential role of intravitreal human placental stem cell implants in inhibiting progression of diabetic retinopathy in type 2 diabetes: neuroprotective growth factors in the vitreous. *Opth* 5, 691–696. doi:10.2147/opth.s21161

Sena, C. M., Pereira, A. M., and Seiça, R. (2013). Endothelial dysfunction - a major mediator of diabetic vascular disease. *Biochim. Biophys. Acta (Bba) - Mol. Basis Dis.* 1832 (12), 2216–2231. doi:10.1016/j.bbadis.2013.08.006

She, T., Wang, X., Gan, Y., Kuang, D., Yue, J., Ni, J., et al. (2012). Hyperglycemia suppresses cardiac stem cell homing to peri-infarcted myocardium via regulation of ERK1/2 and p38 MAPK activities. *Int. J. Mol. Med.* 30 (6), 1313–1320. doi:10.3892/ijmm.2012.1125

Shibata, T., Naruse, K., Kamiya, H., Kozakae, M., Kondo, M., Yasuda, Y., et al. (2008). Transplantation of bone marrow-derived mesenchymal stem cells improves diabetic polyneuropathy in rats. *Diabetes* 57 (11), 3099–3107. doi:10.2337/db08-0031

Silva, J. C., Sampaio, P., Fernandes, M. H., and Gomes, P. S. (2015). The Osteogenic Priming of Mesenchymal Stem Cells is Impaired in Experimental Diabetes. *J. Cel. Biochem.* 116 (8), 1658–1667. doi:10.1002/jcb.25126

Skurikhin, E. G., Pakhomova, A. V., Pershina, O. V., Krupin, V. A., Ermakova, N. N., Pan, E. S., et al. (2017). Role of Sertoli and Leydig Cells in the Regulation of Spermatogonial Stem Cell and Development of Reproductive Disorders in Male

C57Bl/6 Mice with Type 1 Diabetes Mellitus. *Bull. Exp. Biol. Med.* 164 (2), 127–131. doi:10.1007/s10517-017-3940-6

Song, B., Smink, A. M., Jones, C. V., Callaghan, J. M., Firth, S. D., Bernard, C. A., et al. (2012). The directed differentiation of human iPS cells into kidney podocytes. *PLoS One* 7 (9), e46453. doi:10.1371/journal.pone.0046453

Spinetti, G., Cordella, D., Fortunato, O., Sangalli, E., Losa, S., Gotti, A., et al. (2013). Global Remodeling of the Vascular Stem Cell Niche in Bone Marrow of Diabetic Patients. *Circ. Res.* 112 (3), 510–522. doi:10.1161/circresaha.112.300598

Stolzing, A., Sellers, D., Llewelyn, O., and Scutt, A. (2010). Diabetes induced changes in rat mesenchymal stem cells. *Cells Tissues Organs* 191 (6), 453–465. doi:10.1159/000281826

Sun, Y., Shi, H., Yin, S., Ji, C., Zhang, X., Zhang, B., et al. (2018). Human Mesenchymal Stem Cell Derived Exosomes Alleviate Type 2 Diabetes Mellitus by Reversing Peripheral Insulin Resistance and Relieving β-Cell Destruction. *ACS Nano* 12 (8), 7613–7628. doi:10.1021/acsnano.7b07643

Teo, G. S. L., Ankrum, J. A., Martinelli, R., Boetto, S. E., Simms, K., Sciuto, T. E., et al. (2012). Mesenchymal Stem Cells Transmigrate Between and Directly through Tumor Necrosis Factor-α-Activated Endothelial Cells via Both Leukocyte-Like and Novel Mechanisms. *Stem Cells* 30 (11), 2472–2486. doi:10.1002/stem.1198

Tripathi, B. K., and Srivastava, A. K. (2006). Diabetes mellitus: complications and therapeutics. *Med. Sci. Monit.* 12 (7), Ra130–47.

van de Vyver, M., Niesler, C., Myburgh, K. H., and Ferris, W. F. (2016). Delayed wound healing and dysregulation of IL6/STAT3 signalling in MSCs derived from pre-diabetic obese mice. *Mol. Cell Endocrinol.* 426, 1–10. doi:10.1016/j.mce.2016.02.003

van den Born, J. C., Hammes, H.-P., Greffrath, W., van Goor, H., and Hillebrands, J.-L. (2016). Gasotransmitters in Vascular Complications of Diabetes. *Diabetes* 65 (2), 331–345. doi:10.2337/db15-1003

van Niel, G., D'Angelo, G., and Raposo, G. (2018). Shedding light on the cell biology of extracellular vesicles. *Nat. Rev. Mol. Cel Biol* 19 (4), 213–228. doi:10.1038/nrm.2017.125

Wang, J., Wang, B., Li, Y., Wang, D., Lingling, E., Bai, Y., et al. (2013). High glucose inhibits osteogenic differentiation through the BMP signaling pathway in bone mesenchymal stem cells in mice. *Excli j* 12, 584–597.

Yan, J., Tie, G., Wang, S., Messina, K. E., DiDato, S., Guo, S., et al. (2012). Type 2 diabetes restricts multipotency of mesenchymal stem cells and impairs their capacity to augment postischemic neovascularization in db/db mice. *J. Am. Heart Assoc.* 1 (6), e002238. doi:10.1161/JAHA.112.002238

Yang, K., Wang, X. Q., He, Y. S., Lu, L., Chen, Q. J., Liu, J., et al. (2010). Advanced glycation end products induce chemokine/cytokine production via activation of p38 pathway and inhibit proliferation and migration of bone marrow mesenchymal stem cells. *Cardiovasc. Diabetol.* 9, 66. doi:10.1186/1475-2840-9-66

Yu, L., Tu, Q., Han, Q., Zhang, L., Sui, L., Zheng, L., et al. (2015). Adiponectin regulates bone marrow mesenchymal stem cell niche through a unique signal transduction pathway: an approach for treating bone disease in diabetes. *Stem Cells* 33 (1), 240–252. doi:10.1002/stem.1844

Zhang, B., Liu, N., Shi, H., Wu, H., Gao, Y., He, H., et al. (2016). High glucose microenvironments inhibit the proliferation and migration of bone mesenchymal stem cells by activating GSK3β. *J. Bone Miner Metab.* 34 (2), 140–150. doi:10.1007/s00774-015-0662-6

Zhang, Z. G., Buller, B., and Chopp, M. (2019). Exosomes - beyond stem cells for restorative therapy in stroke and neurological injury. *Nat. Rev. Neurol.* 15 (4), 193–203. doi:10.1038/s41582-018-0126-4

Zhu, M., He, X., Wang, X.-H., Qiu, W., Xing, W., Guo, W., et al. (2017). Complement C5a induces mesenchymal stem cell apoptosis during the progression of chronic diabetic complications. *Diabetologia* 60 (9), 1822–1833. doi:10.1007/s00125-017-4316-1

Conflict of Interest: The authors declare that the research was conducted in the absence of any commercial or financial relationships that could be construed as a potential conflict of interest.

Publisher's Note: All claims expressed in this article are solely those of the authors and do not necessarily represent those of their affiliated organizations, or those of the publisher, the editors and the reviewers. Any product that may be evaluated in this article, or claim that may be made by its manufacturer, is not guaranteed or endorsed by the publisher.

frontiers in Cell and Developmental Biology

ORIGINAL RESEARCH
published: 02 November 2021
doi: 10.3389/fcell.2021.766815

LRP5-Mediated Lipid Uptake Modulates Osteogenic Differentiation of Bone Marrow Mesenchymal Stromal Cells

*Jiachen Lin[1,2], Zhifa Zheng[1], Jieying Liu[1], Guihua Yang[3], Ling Leng[1], Hai Wang[2], Guixing Qiu[2] and Zhihong Wu[1]**

[1] Medical Science Research Center, State Key Laboratory of Complex Severe and Rare Diseases, Peking Union Medical College Hospital, Chinese Academy of Medical Sciences and Peking Union Medical College, Beijing, China, [2] Department of Orthopedic Surgery, Peking Union Medical College Hospital, Chinese Academy of Medical Sciences and Peking Union Medical College, Beijing, China, [3] Harmony Technology Co., Ltd., Beijing, China

Nutritional microenvironment determines the specification of progenitor cells, and lipid availability was found to modulate osteogenesis in skeletal progenitors. Here, we investigated the implications of lipid scarcity in the osteogenic differentiation of bone marrow mesenchymal stromal cells (BMSCs) and the role of low-density lipoprotein receptor-related protein 5 (LRP5), a co-receptor transducing canonical Wnt/beta-catenin signals, in BMSC lipid uptake during osteogenesis. The osteogenic differentiation of murine BMSCs was suppressed by lipid scarcity and partially rescued by additional fatty acid treatment with oleate. The enhancement of osteogenesis by oleate was found to be dosage-dependent, along with the enhanced activation of beta-catenin and Wnt target genes. Conditional knockout (CKO) of *Lrp5* gene in murine mesenchymal lineage using *Lrp5*$^{fl/fl}$*;Prrx1-cre* mice led to decreased bone quality and altered fat distribution *in vivo*. After *Lrp5* ablation using adenoviral Cre-recombinase, the accumulation of lipid droplets in BMSC cytoplasm was significantly reduced, and the osteogenesis of BMSCs was suppressed. Moreover, the impaired osteogenesis due to either lipid scarcity or *Lrp5* ablation could be rescued by recombinant Wnt3a protein, indicating that the osteogenesis induced by Wnt/beta-catenin signaling was independent of LRP5-mediated lipid uptake. In conclusion, lipid scarcity suppresses BMSC osteogenic differentiation. LRP5 plays a role in the uptake of lipids in BMSCs and therefore mediates osteogenic specification.

Keywords: bone marrow mesenchymal stromal cell (BMSC), low-density lipoprotein receptor-related protein 5 (LRP5), osteogenic differentiation, lipid metabolism, conditional knockout mice

OPEN ACCESS

Edited by:
Xiao Chen,
Second Military Medical University, China

Reviewed by:
Qun Cheng,
Fudan University, China
Shufang Wu,
Xi'an Jiaotong University, China

****Correspondence:***
Zhihong Wu
wuzh3000@126.com

Specialty section:
This article was submitted to Cellular Biochemistry, a section of the journal Frontiers in Cell and Developmental Biology

Received: *30 August 2021*
Accepted: *04 October 2021*
Published: *02 November 2021*

Citation:
Lin J, Zheng Z, Liu J, Yang G, Leng L, Wang H, Qiu G and Wu Z (2021) LRP5-Mediated Lipid Uptake Modulates Osteogenic Differentiation of Bone Marrow Mesenchymal Stromal Cells. Front. Cell Dev. Biol. 9:766815. doi: 10.3389/fcell.2021.766815

INTRODUCTION

Nutritional microenvironment determines the specification of skeletal progenitor cells. As one of the essential metabolites in mammals, lipids serve not only as important fuel sources but also as biological mediators for the proper functioning and homeostasis of bone (Rendina-Ruedy and Rosen, 2020). Recently, lipids were revealed as key modulators to the cell fate of multiple skeletal lineages, including periosteal cells, osteoblasts, and chondrocytes, during the vascularization

and regeneration after bone fracture (van Gastel et al., 2020). Bone marrow mesenchymal stromal cells (BMSCs) harbor a subpopulation of skeletal progenitors with potency to undergo osteogenesis (Yue et al., 2016; Chan et al., 2018; Baccin et al., 2020) and are therefore considered favorable seeding cells in many bone regenerative investigations (Lv et al., 2017; Mazzoni et al., 2020; Ying et al., 2020). However, the regulatory role of lipids in the osteogenic differentiation of BMSCs has not yet been elucidated.

Low-density lipoprotein (LDL) receptor-related protein 5 (LRP5) is a member of LDL receptor family and also known as a co-receptor for canonical Wnt/beta-catenin signaling pathway and transduces key molecular signals in bone development and homeostasis (Cui et al., 2011; Baron and Kneissel, 2013; Kobayashi et al., 2016). Several newly uncovered molecular mechanisms about Wnt-independent LRP5 modulation in bone (Clement-Lacroix et al., 2005; Yadav and Ducy, 2010; Chin et al., 2015; Frey et al., 2015; He et al., 2020) suggested a more complicated role of LRP5 in skeletal progenitors. Notably, recognized as a cell surface endocytic receptor (Li et al., 2001; Schneider and Nimpf, 2003; Chung and Wasan, 2004), LRP5 was also found to participate in the uptake and internalization of lipids in macrophages (Badimon et al., 2020), hepatocytes and adrenal cortex tissues (Kim et al., 1998), and osteoblasts (Frey et al., 2015). There are other studies indicating the modulatory role of LRP5 in lipid metabolism (Magoori et al., 2003; Loh et al., 2015).

In order to investigate the specific role of lipid availability and LRP5 in the osteogenic differentiation of BMSCs, we here carried out *in vivo* and *in vitro* assays using BMSCs isolated from wild-type mice and *Lrp5* gene conditional-ready (i.e., *Lrp5*-floxed) mice. We recorded the suppression of osteogenesis and Wnt-target genes in BMSCs by lipid scarcity and a dosage-dependent rescue of the phenotype using oleate, an unsaturated fatty acid, as a supplement. The $Lrp5^{fl/fl}$;*Prrx1-cre* CKO mice presented with impaired bone formation and altered fat distribution. Moreover, we observed a significant decrease in lipid uptake and suppressed osteogenesis of $Lrp5^{fl/fl}$ BMSCs after adenoviral Cre-recombination, and it was rescued by additional recombinant Wnt3a protein. In summary, these findings suggested that lipid scarcity suppressed osteogenic differentiation of BMSCs, and LRP5-mediated lipid uptake could modulate osteogenic differentiation of BMSCs.

MATERIALS AND METHODS

Mouse Lines and Genotyping

This study was approved by the Ethics Committee of Peking Union Medical College Hospital. C57BL/6J mice were obtained from the Vital River Laboratory Animal Technology (Beijing, China). $Lrp5^{fl/fl}$ conditional-ready mice and *Prrx1-cre* transgenic mice were purchased from the Shanghai Model Organisms Center (Shanghai, China). To generate *Lrp5* CKO mice, $Lrp5^{fl/fl}$ mice were crossed with *Prrx1-cre* mice to get $Lrp5^{fl/fl}$; *Prrx1-cre* genotype. Mouse genome DNA was extracted from tail of mice at postnatal day 10 (P10), and the amplification of target genes (*Lrp5* and *Prrx1-cre*) was done following a described protocol (Truett et al., 2000; Cui et al., 2011). A 2.5% Agarose-TAE gel containing Gel-Green (D0143, Beyotime, Beijing, China) was used for electrophoresis of PCR products.

Cell Culture

Murine BMSCs were obtained using a previous described protocol with minor modifications (Grassel et al., 2012). In brief, murine femur and humerus were dissected from $Lrp5^{fl/fl}$ or wild-type C57BL/6J mice at P14 after euthanasia and washed three times in cold phosphate buffered saline (PBS; Cytiva) with 1% penicillin-streptomycin (Sigma-Aldrich). The isolated long bones were then cut with sterile scissors, and the bone marrow was extracted by centrifuging at 500 *g* for 30 s. Pellet was resuspended in PBS and filtered with 70-μm cell strainer (BD Falcon). Cells were then resuspended and seeded in 10-cm dishes (Corning) in Dulbecco's modified Eagle's medium (DMEM) high glucose (Hyclone), 1% penicillin-streptomycin (Sigma-Aldrich), and 10% fetal bovine serum (FBS; Gibco). BMSCs were cultured at 37°C and 5% CO_2, and the cell medium was changed every 48 h. After 80–90% cell confluence was reached, the adherent cells were washed twice in PBS, trypsinized using 0.25% Trypsin-EDTA (Thermo Fisher Scientific), centrifuged at 1,000 *g* for 3 min, and then seeded in 10-cm dish (Corning) at the next passage.

Cell Viability

Cell viability was determined by the methylthiazolyldiphenyl-tetrazolium bromide (MTT) assay as described previously (Riss et al., 2004). In brief, MTT solution was added to each well 7 days after osteogenic induction with mediums of different lipid treatment. Three hours later, dimethyl sulfoxide (DMSO) was added and the absorbance of the solution was measured at 570 nm with an automatic microplate reader (CFX Connect, Bio-Rad). The survival rate of cells in percentage was calculated using DMSO-treated cells as a standard. One-way ANOVA was conducted with GraphPad Prism software.

Induction of Osteogenic Differentiation

The osteogenic differentiation of BMSCs was induced as described previously (Grassel et al., 2012). The third-passage BMSCs were seeded in 0.1% gelatin (Sigma-Aldrich) pretreated 6- or 12-well plates (Corning) at 5,000 cells/100 μl. The osteogenic induction was initiated at 70–80% cell confluence by using an osteogenic medium composed of DMEM high glucose (Hyclone), 100 nM dexamethasone (Sigma-Aldrich), 0.05 mM ascorbate 2-phosphate (Sigma-Aldrich), 10 mM sodium beta-glycerophosphate (Sigma-Aldrich), and 1% penicillin-streptomycin (Sigma-Aldrich). FBS (Gibco), lipid-reduced serum (Biowest), oleate (Sigma-Aldrich), and recombinant Wnt3a protein (5036-WN, R&D Systems) were added into the medium according to the experiment design.

Assessment of Alkaline Phosphatase Activity

After 5/7/11 days of osteogenic induction, the osteogenic differentiation was assessed by alkaline phosphatase (ALP) staining kit (VectorLab) in the 12-well plate. After 30 min staining, the BMSCs were fixed in 4% paraformaldehyde (P1110,

Solarbio, Beijing, China), washed in PBS (Cytiva). Then, the 12-well plate was scanned and photographed under × 4 magnification using EVOS Cell Imaging System (EVOS M7000, Thermo Fisher Scientific). The ALP activity of each well was quantified with ImageJ Software ([1]National Institutes of Health) as previously described (Dupont et al., 2011). In essence, the ALP + area was determined with ImageJ as the number of blue pixels across the picture, and then this value was normalized to the total number of pixels for each picture. For each well, views of four different zones were adopted for calculations. Multiple *t* tests were conducted with GraphPad Prism software using the Holm–Sidak test.

Fluorescent Staining of Lipid Droplets in Cytoplasm

Bone marrow mesenchymal stromal cells were seeded in six-well plate under different conditions. BODIPY^{TM} staining kit (Thermo Fisher Scientific) was applied to trace the endocytosis of lipid substance in BMSCs (DiDonato and Brasaemle, 2003), and 4,6-diamidino-2-phenylindole staining solution (C00065, Solarbio, Beijing, China) was used to locate the nucleus. After BODIPY^{TM} application, the plate was scanned and photographed under × 40 magnification using EVOS Cell Imaging System (EVOS M7000, Thermo Fisher Scientific). Cells with positive signals in cytoplasm were counted, and the fluorescence intensity was calculated by BODIPY^{TM}-positive cell counts over total cell in the region. Statistical comparisons were conducted with GraphPad Prism software using the Holm–Sidak test. For each analysis, four different views were adopted to carry out the quantification.

Adenoviral Vector Preparation and Infection

Adenoviruses expressing CMV-Cre-recombinase and CMV-Null vectors were purchased from Beyotime (Beijing, China). BMSCs were infected with viruses at 100 multiplicity of infection (MOI) in the presence of 0.1% poly-L-lysine (Sigma-Aldrich) for 1 h as previously described (Buo et al., 2016).

RNA Extraction, Reverse Transcription, and Real-Time PCR

Total protein was extracted from BMSC cell lysates, murine bone tissue, and other organs using TRIzol (Thermo Fisher Scientific) following the standard protocols. cDNA was obtained using PrimerScript RT (TaKaRa, Japan). Real-time PCR was performed using TB Green Master Mix kit (TaKaRa, Japan) on Applied Biosystems StepOnePlus Real-Time PCR System (Thermo Fisher Scientific). The primers used for qPCR analysis were listed in the **Supplementary Table**. mRNA expression levels of *Alpl*, *Sp7*, *Col1a1*, *Tcf1*, *Lef1*, and *Axin2* were normalized to *glyceraldehyde 3-phosphate dehydrogenase* (*Gapdh*). Statistical comparisons were conducted with GraphPad Prism software using the Holm–Sidak test. Each experiment was repeated three times.

[1]https://imagej.nih.gov/ij/

Protein Extraction and Western Blotting

Total protein was extracted from BMSC cell lysates, murine bone tissue, and other organs using radioimmunoprecipitation assay (RIPA) buffer (Thermo Fisher Scientific). The protein concentration was determined by bicinchoninic acid (BCA) protein assay kit (Thermo Fisher Scientific). Western blot was performed using a standard protocol. Anti-LRP5 (rabbit monoclonal, ab223203, Abcam, 1:1,000), anti-Type I Collagen (COL1; rabbit monoclonal, ab270993, Abcam, 1:1,000), anti-RUNX Family Transcription Factor 2 (RUNX2; rabbit monoclonal, ab236639, Abcam, 1:1,000), anti-beta catenin (rabbit monoclonal, ab32572, Abcam, 1:5,000), and anti-GAPDH (rabbit monoclonal, #2118, Cell Signaling Technology, 1:1,000) were applied as primary antibodies, and horseradish peroxidase (HRP) goat anti-rabbit immunoglobulin G (IgG) (H + L) (ZB-2301, ZSGB Biotech, Beijing, China, 1:2,000) was applied as secondary antibody to carry out immunoblotting. Protein expression levels were visualized by automatic chemiluminescence imaging system (C300, Azure Biosystems). The quantification of band intensity was performed by ImageJ Software. Overall expression levels of LRP5, COL1, RUNX2, and beta-catenin were normalized to GAPDH levels. Statistical comparisons were conducted with GraphPad Prism software using the Holm–Sidak test. Three repetitions were carried out for each of the above experiments.

Micro-Computed Tomography and Assessment of Bone Quality

Control and CKO mice at P21 were euthanized. Femora and humeri were obtained and fixed in 4% paraformaldehyde (P1110, Solarbio, Beijing, China) for 48 h, washed in cold PBS three times, and then preserved in 75% ethanol at 4°C. Samples were scanned and analyzed using SCANCO micro-computed tomography (micro-CT) μ100 system (SCANCO Medical). The three-dimensional structural parameters including humerus length, mean bone density, trabecular bone volume fraction (Tb.BV/TV), average cortical thickness (Ct.Th), trabecular number (Tb.N), and trabecular separation (Tb.Sp) were analyzed to determine the bone quality as previously described (Bouxsein et al., 2010). Each analysis was performed in samples collected from 12 individual animals (six control mice and six CKO mice). Statistical comparisons were conducted with GraphPad Prism software using unpaired *t*-test.

Dissection of Adipose Tissue

Here, 2-month-old control or CKO mice were euthanized. Intact adipose tissues in gonadal, mesenteric, and subcutaneous regions were carefully dissected using forceps and scissors. The percentage of fat pad mass (g) over body weight (g) was calculated. Each analysis was repeated with 12 individual animals (six control mice and six CKO mice). Statistical comparisons were conducted with GraphPad Prism software using the Holm–Sidak test.

Statistical Analysis

All data analysis in this study was carried out on GraphPad Prism 8 (GraphPad Software). At least three independent experimental

groups were performed to generate a qualified data set. Statistical strategies adopted in each experiment were described above. *P*-values < 0.05 (*), 0.01 (**), and 0.001 (***) were considered significant. Error bars on all graphs are presented as the standard deviation of the mean unless otherwise indicated.

RESULTS

Lipid Scarcity Suppressed Osteogenic Differentiation of Murine Bone Marrow Mesenchymal Stromal Cells and Wnt/Beta-Catenin Signaling

To investigate the effects of lipid availability on BMSC osteogenesis, we began by performing osteogenic assays using murine BMSCs isolated from P14 wild-type C57BL/6J mice. Osteogenic medium was prepared using normal FBS (10%), lipid-reduced serum (LRS; 10%), serum deprivation (SD), and LRS with additional oleate (OL, 75 μM), an unsaturated fatty acid, and treated with isolated murine BMSCs. ALP staining was performed on days 5, 7, and 11 after osteogenic induction, and ALP activity was measured to determine the osteogenesis in different mediums (**Figures 1A,B**). Moreover, an MTT assay was carried out to evaluate the cell viability 7 days after osteogenic induction under different lipid supplements (**Figure 1C**). Here, we observed significantly decreased ALP activities of BMSCs in LRS or SD medium, and the suppression could be partially rescued by additional supplementation with oleate (**Figure 1B**). Notably, the cell survival was significantly reduced in SD medium (**Figure 1C**; $p < 0.001$), indicating that the viability of BMSCs was impaired due to complete deprivation of serum supplement. Further *in vitro* analysis revealed a significant decrease in protein expression of osteogenic markers such as COL1, RUNX2, and beta-catenin, serving as an intracellular Wnt signaling transducer (**Figures 1D,E**) 7 days post-induction. We then asked whether the suppressed osteogenesis was also related to the downregulation of Wnt/beta-catenin signaling. Relative mRNA expression of several Wnt target genes (*Tcf1*, *Lef1*, *Axin2*) and osteogenic genes (*Alpl*, *Sp7*, *Col1a1*) was examined and turned out to be reduced significantly in qRT-PCR assays 7 days after induction (**Figure 1F**). Notably, the suppressed expressions of protein and

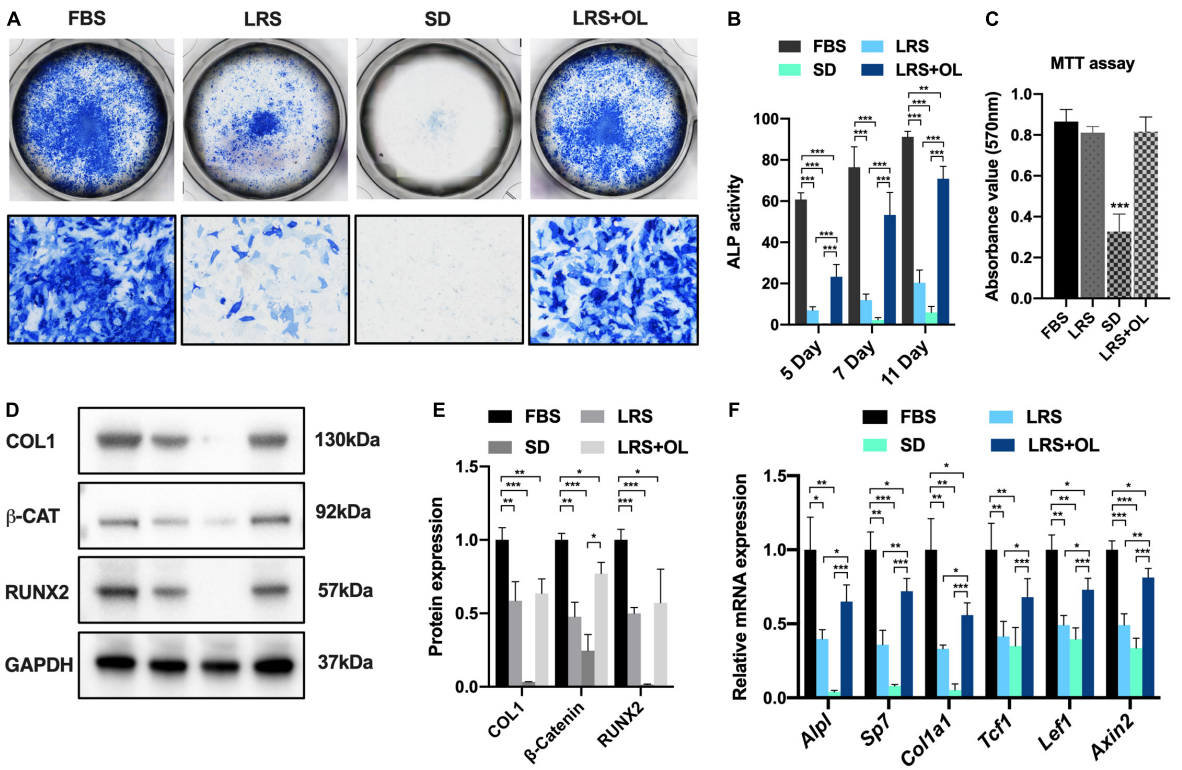

FIGURE 1 | Lipid scarcity suppressed bone marrow mesenchymal stromal cell (BMSC) osteogenesis and Wnt/beta-catenin signaling activation. **(A)** Alkaline phosphatase (ALP) staining of BMSCs 7 days after osteogenic induction in culture medium with normal fetal bovine serum (FBS; 10%), lipid-reduced serum (LRS; 10%), SD, and LRS (10%) with 75 μM oleate treatment. **(B)** ALP activity of BMSCs 5, 7, and 11 days after osteogenic induction in different culture mediums. **(C)** Methylthiazolyldiphenyl-tetrazolium bromide (MTT) assays revealed significantly decreased cell viability in SD treatment BMSCs compared to FBS treatment group, while the cell viability was not significantly changed in LRS and LRS + OL group. **(D,E)** Western blots showed that the protein expression levels of osteogenic markers Type I Collagen (COL1) and RUNX Family Transcription Factor 2 (RUNX2) and beta-catenin were significantly decreased after lipid deprivation and partially restored by additional oleate treatment 7 days after induction. **(F)** qRT-PCR revealed that the mRNA expression levels of osteogenic genes, *Alpl*, *Sp7*, and *Col1a1*, as well as Wnt target genes *Tcf1*, *Lef1*, and *Axin2*, were significantly decreased after lipid deprivation and partially restored by additional oleate treatment 7 days after induction, $*p < 0.05$, $**p < 0.01$, and $***p < 0.001$.

mRNA of both osteogenesis and Wnt/beta-catenin signaling were rescued by oleate supplementation (**Figures 1A–F**).

The Suppressed Osteogenic Differentiation Was Rescued by Oleate Supplementation in a Dosage-Dependent Manner

To further validate the rescue effect of oleate supplementation in lipid-deprived BMSCs, we performed an osteogenic assay of BMSCs using increasing dosage of oleate (0, 25, 50, 75, and 100 μM, respectively) in LRS medium for 5, 7, and 11 days (**Figure 2A**). Quantification of ALP activity revealed that the enhancement of osteogenesis was dosage-dependent on oleate supplementation (**Figure 2B**). Moreover, the protein and mRNA expressions of osteogenic markers and Wnt target genes were also increased dependent on oleate treatment 7 days after induction (**Figures 2C–E**). These results suggested that lipid availability could modulate osteogenic differentiation *via* Wnt/beta-catenin signaling in BMSCs.

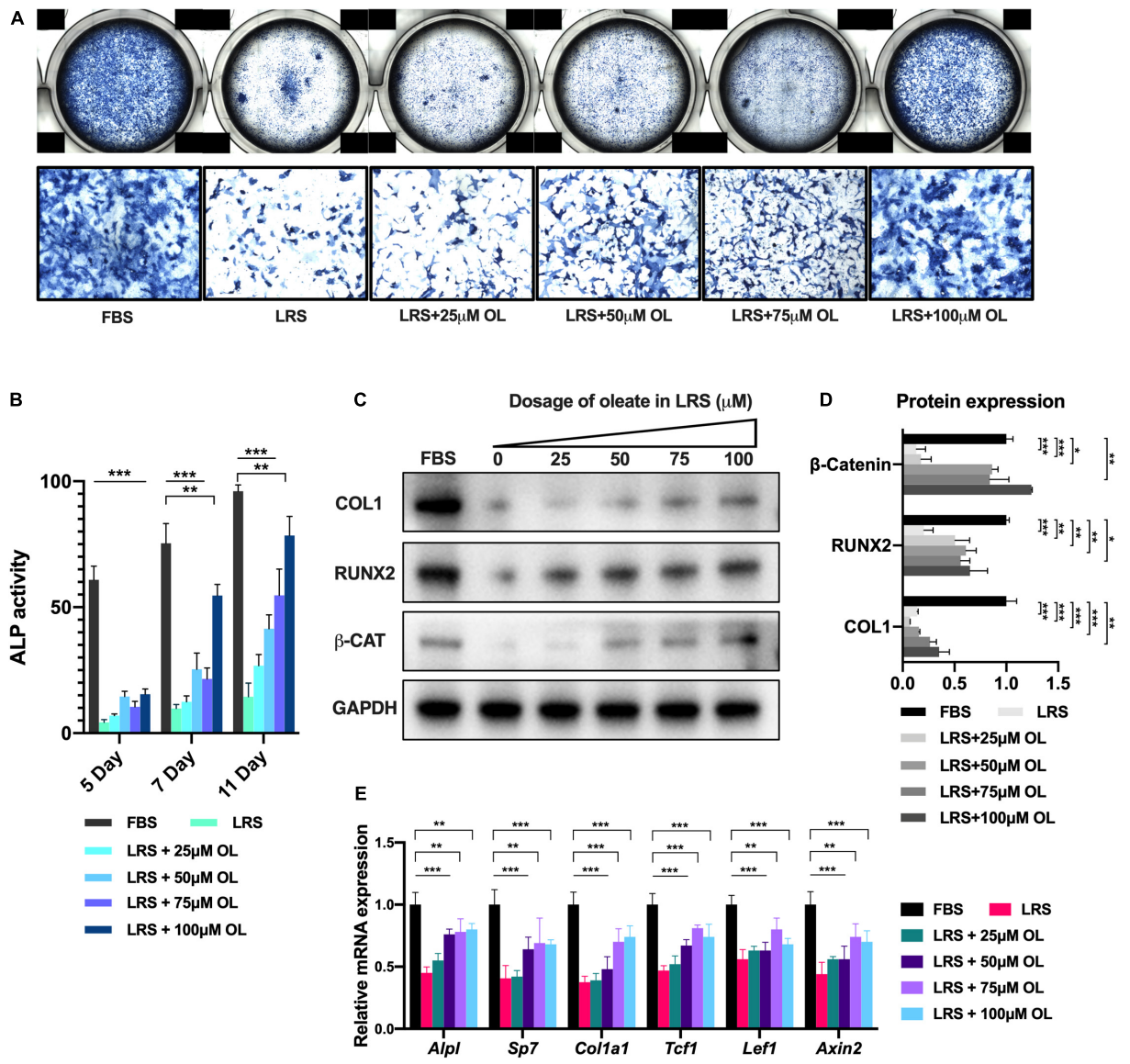

FIGURE 2 | The suppressed osteogenesis was rescued by oleate supplementation in a dosage-dependent manner. **(A)** Alkaline phosphatase (ALP) staining of bone marrow mesenchymal stromal cells (BMSCs) 7 days after osteogenic induction in culture medium with normal fetal bovine serum (FBS; 10%), lipid-reduced serum (LRS; 10%), and LRS (10%) with increasing dosages of oleate (25, 50, 75, 100 μM). **(B)** ALP activity of BMSCs 5, 7, and 11 days after osteogenic induction in different culture mediums. **(C,D)** Western blots showed that the suppressed protein expression levels of osteogenic markers COL1 and RUNX2 and beta-catenin by lipid deprivation were restored by additional oleate treatment in a dosage-dependent manner. **(E)** qRT-PCR revealed that the suppressed mRNA expression levels of osteogenic genes *Alpl*, *Sp7*, and *Col1a1* and Wnt target genes *Tcf1*, *Lef1*, and *Axin2* by lipid deprivation were restored by additional oleate treatment in a dosage-dependent manner, $^{*}p < 0.05$, $^{**}p < 0.01$, and $^{***}p < 0.001$.

Lrp5 Knockout in Limb Mesenchymal Lineage Impaired Bone Formation

As an important co-receptor for Wnt/beta-catenin signaling and potential endocytic mediator of multiple substances (Li et al., 2001; Schneider and Nimpf, 2003; Chung and Wasan, 2004), LRP5 was previously reported essential in bone development (Clement-Lacroix et al., 2005; Yadav and Ducy, 2010; Chin et al., 2015; Frey et al., 2015; He et al., 2020) and lipid metabolism (Magoori et al., 2003; Loh et al., 2015). We generated CKO mice by crossing *Lrp5*-floxed ready mice with *Prrx1-cre* mouse line to inactivate *Lrp5* gene in limb mesenchymal cell lineage, including BMSCs. The loxP sequence was inserted into the murine genome to conditionally remove the exon 2 of *Lrp5* gene in Cre-expressing lineages. We collected the genome DNA from P10 mouse tail, and a PCR program and the following electrophoresis were performed to determine the floxed *Lrp5* allele (**Figure 3A**). To further validate the efficiency of Cre-mediated knockout *in vivo*, we harvested multiple organs from control ($Lrp5^{fl/fl}$) and CKO ($Lrp5^{fl/fl}$; *Prrx1-cre*) mice at P0, including bone and skeletal muscles in forelimbs, skin, brain, heart, kidney, and subcutaneous adipose tissue. The following Western blot and qRT-PCR analysis confirmed that the LRP5 protein expression and *Lrp5* mRNA expression were lost in CKO mice in bone and skeletal muscles of forelimbs compared to control mice (**Figures 3B,G**; all $p < 0.001$). It turned out that the mRNA expression of *Lrp5* was significantly increased in liver tissue ($p < 0.001$), indicating a compensatory enhancement of gene expression in liver. In addition, in P21, the CKO mice presented a reduced body size and shortened limbs in gross appearance (**Figure 3C**). Besides, the body weight was decreased in CKO mice significantly (**Figure 3F**; $p < 0.001$).

To determine the effect of *Lrp5* knockout *in vivo*, we performed micro-CT scan on the humerus and femur samples harvested from P21 mice. The humerus length was remarkably decreased in CKO mice (**Figures 3E,F**; $p < 0.001$). The reconstruction imaging of distal femur recorded decreased density in trabecular architecture and thinner cortical bone in CKO compared to control mice (**Figure 3D**). Further analysis revealed a significant decrease in mean bone density ($p < 0.001$), average Ct.Th. ($p < 0.001$), Tb.BV/TV ($p < 0.001$), and Tb.N ($p < 0.01$) and increased Tb.Sp ($p < 0.001$) in the distal femur of CKO mice. These data indicated that the bone formation in limb was impaired as a result of suppressed osteogenesis differentiation of skeletal progenitors, including BMSCs by *Lrp5* knockout.

Lrp5 Knockout in Bone Marrow Mesenchymal Stromal Cells Altered Fat Distribution in Mice

Previous report showed the lipid metabolism and adipose tissue were changed after *Lrp5* gene was knockout in osteoblast lineage (Frey et al., 2015), indicating the role of LRP5 in modulating lipid availability in skeletal progenitors. In order to test the similar regulatory effect in BMSC-CKO mice, we dissected the adipose tissue from control and CKO mice at 2 months old. Interestingly, there was increased fat pad mass in gonadal ($p < 0.001$) and mesenteric areas ($p < 0.05$; **Figures 3I,J**), but the subcutaneous fat in limb was not changed (data not shown). In addition, the expression of lipid metabolic genes (*Acadl*, *Acat2*, *Acsl1*, *Cpt1b*, and *Hadha*) in limb BMSCs was significantly decreased (**Figure 3K**; all $p < 0.001$). There data suggested that the ability of using lipid substances was impaired in BMSCs after *Lrp5* knockout and the accumulation of adipose tissue was increased in mesenteric and gonadal regions, strongly indicating the role of LRP5 in lipid uptake and metabolism in BMSCs.

Lrp5 Ablation Suppressed Lipid Uptake and Osteogenic Differentiation of Bone Marrow Mesenchymal Stromal Cells

To further understand the role of LRP5 in lipid uptake of BMSCs, we used adenovirus carrying CMV-Cre-recombinase (Ad-Cre) or CMV-null (Ad-CMV) expressing vector to infect BMSCs isolated from P14 $Lrp5^{fl/fl}$ mice. The expression of LRP5 at protein and mRNA levels was examined to validate the efficiency of Cre-recombination (**Figures 4C,D**; $p < 0.001$). To trace the endocytosis of lipids *in vitro*, we applied BODIPY^{TM} staining (DiDonato and Brasaemle, 2003) in FBS and LRS + OL culture condition 48 h after viral infection (**Figure 4A**). The fluorescence intensity of lipid droplet signals in cytoplasm was found significantly decreased after *Lrp5* ablation both in FBS and LRS + OL conditions (**Figure 4B**; both $p < 0.001$), suggesting impaired endocytosis of lipid due to *Lrp5* ablation. We next performed osteogenic assays on adenoviral-treated BMSCs in FBS and LRS mediums (**Figure 4E**). Consistent with *in vivo* results, the osteogenesis of BMSCs was significantly inhibited by *Lrp5* ablation (**Figures 4E,F**; all $p < 0.001$) after 7-day induction in both assays, indicating the modulatory role of LRP5 in BMSC osteogenesis.

The Wnt-Activating Osteogenesis Was Independent of Lipid Scarcity

In light of the fact that Wnt-LRP5 signaling was found to participate in the lipid metabolism and bone formation in skeletal progenitors, we then examined whether this modulation is regulated by lipid availability or not. After 7-day osteogenic induction, *Lrp5* knockout significantly reduced the expression of Wnt target genes (*Tcf1*, *Lef1*, *Axin2*; **Figure 4G**; all $p < 0.001$), as well as osteogenic genes (*Alpl*, *Sp7*, *Col1a1*; **Figure 4G**; all $p < 0.001$) in FBS-treated BMSCs, which was consistent with previous reports (Ayturk et al., 2013; Sebastian et al., 2017). However, the changes in Wnt target gene expression were not significant after *Lrp5* ablation in lipid deprivation medium (**Figure 4G**). These data suggested that the modulation of LRP5 in BMSC osteogenesis was mediated by Wnt/beta-catenin signaling and was dependent on lipid availability. We further used recombinant Wnt3a protein, a classic Wnt ligand, in the lipid-deprived BMSCs with/without *Lrp5* ablation (**Figure 4E**). The osteogenic activity was significantly enhanced even compared with *Lrp5*-intact BMSCs ($Lrp5^{fl/fl}$ treated with Ad-CMV) in FBS medium (**Figures 4E,F**; $p < 0.001$). These

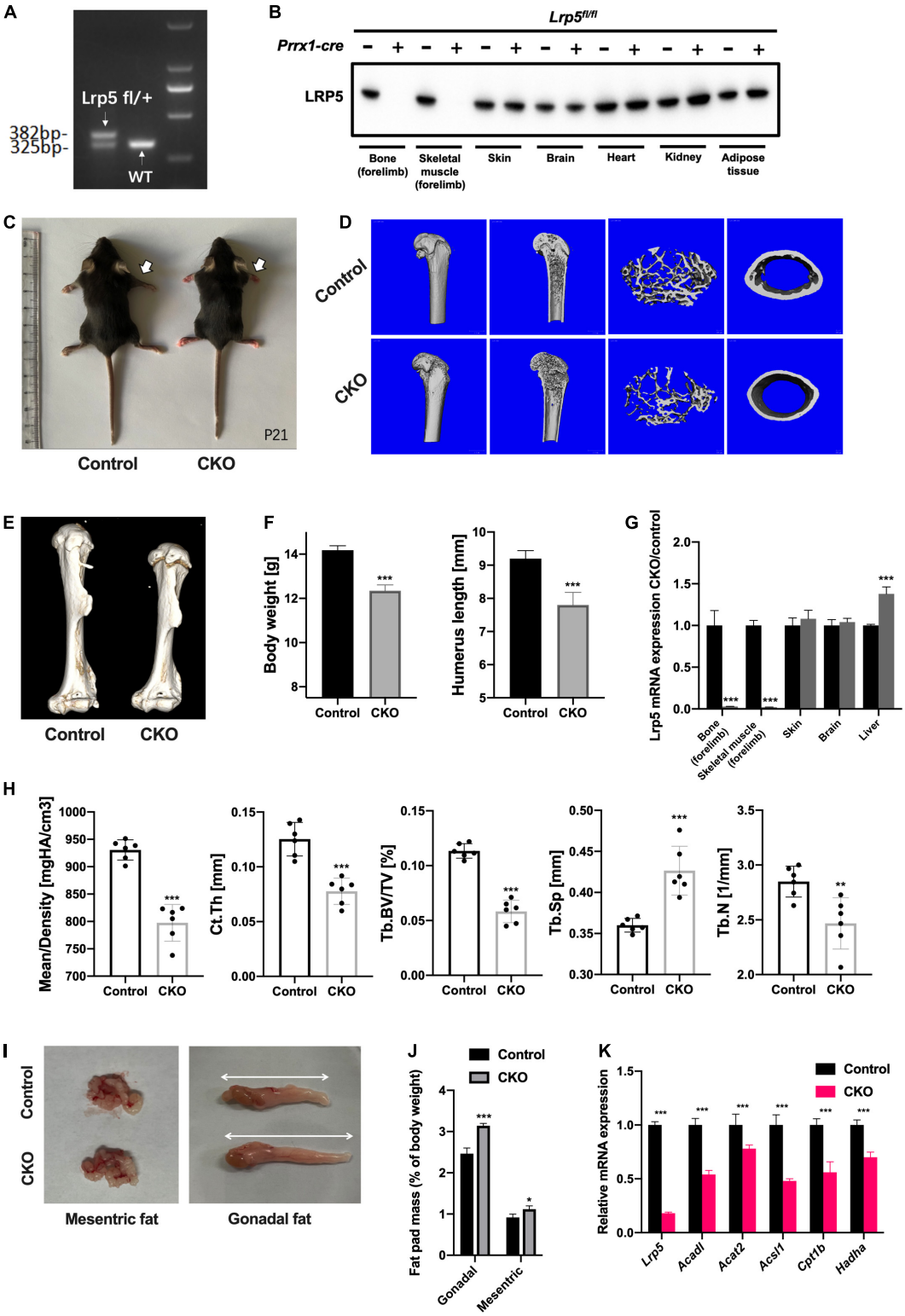

FIGURE 3 | Impaired bone formation and altered adipose tissue distribution in *low-density lipoprotein receptor-related protein 5* (*Lrp5*)$^{fl/fl}$;*Prrx1-cre* conditional knockout (CKO) mice. **(A)** Electrophoresis of PCR products to identify *Lrp5*-flox allele in heterozygous (left band) and wild-type (WT) (right band) samples. The band size for WT allele was ~325 bp and floxed allele was ~382 bp. **(B)** Protein expression of LRP5 in different organs collected from postnatal day 0 (P0) control (*Prrx1-cre* negative) and CKO (*Prrx1-cre* positive) mice. The LRP5 expression was significantly abrupted in bone and skeletal muscles from forelimb. **(C)** Gross

(Continued)

FIGURE 3 | (Continued)
appearance of P21 mice. White arrows indicate shortened forelimbs in CKO (right) mice compared to control (left) mice. **(D)** Representative three-dimensional micro-computed tomography (micro-CT) images of trabecular bony architecture and cortical bone thickness of distal femur harvested from P21 control and CKO mice. **(E)** Representative three-dimensional micro-CT images of humerus harvested from P21 control and CKO mice. **(F)** Body weight and humerus length of CKO mice were quantified (n = 6, mean ± standard deviation). **(G)** qRT-PCR analysis revealed abruptions of *Lrp5* gene expression in bone and skeletal tissues harvested from P0 CKO mice. **(H)** Quantified micro-CT data. Data are shown as mean ± standard deviation (n = 6). **(I)** Gross appearance of dissected mesenteric and gonadal fat from 2-month-old control and CKO mice. White arrows indicate an increase in the volume of gonadal fat in CKO mice. **(J)** Quantification on mesenteric and gonadal fat pad mass as a percentage of body weight in 2-month-old control and CKO mice. The mesenteric and gonadal fat were significantly increased in CKO mice (n = 6, mean ± standard deviation). **(K)** qRT-PCR analysis on bone marrow mesenchymal stromal cells (BMSCs) harvested from mouse forelimbs indicated a significant decrease in mRNA expression levels of lipid metabolism genes, including *Acadl*, *Acat2*, *Acsl1*, *Cpt1b*, and *Hadha*, as well as *Lrp5*, $^{*}p < 0.05$, $^{**}p < 0.01$, and $^{***}p < 0.001$.

results indicated that the Wnt-activating osteogenesis was independent of lipid scarcity.

DISCUSSION

Lipid metabolism dysfunction, including atherosclerosis and hypercholesterolemia, was considered to be related to osteoporosis in many clinical studies (Yamaguchi et al., 2002; Buizert et al., 2009; Lampropoulos et al., 2012), shedding light on the dynamics of mesenchymal stromal cell lineage differentiation and specification (Loh et al., 2015; Yue et al., 2016; van Gastel et al., 2020). Wnt/beta-catenin signaling and its components play essential roles in bone homeostasis and lipid metabolism, while the molecular underpinnings of their regulations remain to be clarified. Here, we showed that lipid scarcity suppressed osteogenic differentiation of BMSCs and Wnt/beta-catenin signaling *in vitro*, and the suppression could be rescued by additional fatty acid supplementation in a dosage-dependent manner. We also demonstrated that the Wnt co-receptor, LRP5, participated in lipid uptake of BMSCs and modulated bone formation and lipid metabolism *in vitro* and *in vivo*.

Lipid depots in bone marrow area can be mobilized into fatty acids and serve as one of the chief fuel sources for bone-residing cells and BMSCs. Recent studies uncovered further essential roles of lipids in bone marrow and other skeletal niche in bone development and functioning (Rendina-Ruedy and Rosen, 2020). Most recently, van Gastel et al. (2020) reported that the lipids in microenvironment were responsible for the specification of multiple skeletal progenitor lineages during bone-healing process. In the study, they recorded that when lipids were scarce, skeletal progenitors preferentially underwent chondrogenesis rather than osteoblastogenesis due to the activated SOX9 signaling and thus adapted to an avascular life. Notably, there are also studies about how lipids modulate mesenchymal stromal cell behaviors (Clemot et al., 2020; Senos Demarco et al., 2020). Another study reported that adipose-derived MSCs could reciprocally modulate lipid metabolism *via* reprogramming macrophages (Souza-Moreira et al., 2019). In the present study, we investigated the impact of lipid scarcity on BMSC osteogenesis *in vitro*. Deprivation of lipid from serum supplement significantly impaired the osteogenic capacity of BMSCs (**Figures 1A,B**) and suppressed Wnt/beta-catenin signaling (**Figures 1D,E**). Moreover, additional supplementation with fatty acid, oleate, was able to restore the osteogenesis deprived by lipid scarcity in a dosage-dependent manner (**Figures 2A,B**). These data suggested that lipids mediated BMSC differentiation by providing fatty acids as sources for oxidation (FAO). The block of FAO would potentially inhibit osteogenesis and activation of Wnt/beta-catenin signaling in BMSC lineages.

As a member of LDL receptor family, LRP5 serves as a transmembrane co-receptor for canonical Wnt/beta-catenin signaling pathway and plays an essential role in bone development and homeostasis (Cui et al., 2011; Baron and Kneissel, 2013; Kobayashi et al., 2016). Mutations in *LRP5* genes are responsible for a spectrum of skeletal phenotypes in human, ranging from low to high bone density (Gong et al., 2001; Van Wesenbeeck et al., 2003; Levasseur et al., 2005; Baron and Kneissel, 2013). The past decade had witnessed frequent breaks in therapeutic development targeting LRP5 signaling, namely, the anti-DKK1 and anti-sclerostin molecules in the treatment of postmenopausal osteoporosis (Li et al., 2005; Niehrs, 2006; Williams, 2017). LRP5 was also observed to be involved in lipid metabolism. In human, gain-of-function *LRP5* mutations led to higher bone mass and lower body fat accumulation, while a low bone mineral density-associated common LRP5 allele correlated with increased abdominal adiposity (Loh et al., 2015). Similarly, LRP5 deficiency led to increased plasma cholesterol levels in mice fed a high-fat diet caused by the decreased hepatic clearance of chylomicron remnant. Meanwhile, LRP5-deficient mice showed a markedly impaired glucose tolerance (Loh et al., 2015). Magoori et al. (2003) used apoE;*Lrp5* double-knockout mice to investigate the role of LRP5 in lipoprotein metabolism and found severe hypercholesterolemia, impaired fat tolerance, and increased atherosclerosis in DKO mice. Previously, Wnt-LRP5 signaling was found to regulate fatty acid oxidation in osteoblasts (Frey et al., 2015). By using *Osx-cre*, researchers also recorded a decrease in bone mass and increase in body fat for CKO mice. In the present study, we generated BMSC CKO mice using *Prrx1-cre* and provided strong evidence for LRP5 participating in the regulation of osteogenesis and lipid uptake of BMSCs. The CKO mice developed less bone formation (**Figures 3D–H**) and increased adipose tissue in mesenteric and gonadal regions (**Figures 3I,K**). Lipid droplets were retained in BMSC cytoplasm after *Lrp5* ablation and the osteogenesis was inhibited (**Figures 4A–F**). Taken together, our data suggested that the loss of LRP5 in BMSC impaired the capacity to uptake and use lipid substances during osteogenesis, which explained the phenotypes of reduced bone quality and accumulated fat mass *in vivo*.

The canonical Wnt/beta-catenin signaling pathway is known as a key regulator of bone development, metabolism,

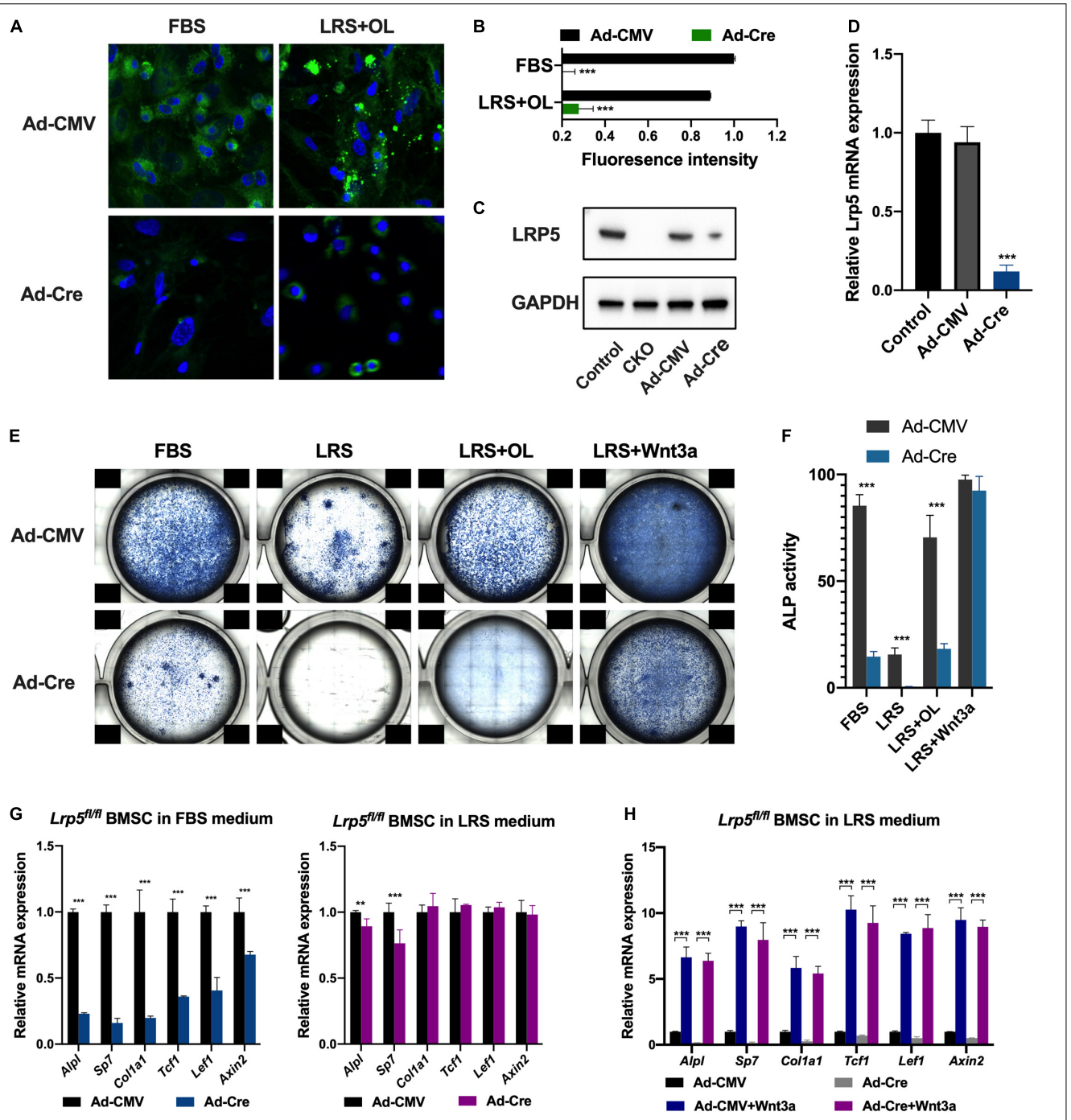

FIGURE 4 | *Low-density lipoprotein receptor-related protein 5 (Lrp5)* ablation in bone marrow mesenchymal stromal cells (BMSCs) impairs lipid uptake and osteogenesis. **(A)** BODIPY^{TM} staining revealed significantly decreased lipid droplets in BMSC cytoplasm after *Lrp5* ablation using adenoviral Cre-recombinase. **(B)** Quantified fluorescence intensity of lipid droplets in BMSC cytoplasm indicating impaired lipid uptake of *Lrp5*-KO BMSCs. **(C)** LRP5 protein expression in BMSCs harvested from postnatal day 0 (P0) control mice, conditional knockout (CKO) mice, *Lrp5*-control BMSC, and *Lrp5*-KO BMSCs. **(D)** qRT-PCR validated the knockout effect of adenoviral-Cre infection on *Lrp5*$^{fl/fl}$ BMSCs. **(E)** Alkaline phosphatase (ALP) staining of control and *Lrp5*-KO BMSCs 7 days after osteogenic induction in culture medium with normal fetal bovine serum (FBS), lipid-reduced serum (LRS), LRS with 100 μM oleate treatment, and LRS with recombinant 100 ng/ml Wnt3a treatment, respectively. **(F)** ALP activity of BMSCs 7 days after osteogenic induction in different culture mediums. **(G)** mRNA expression levels in control and *Lrp5*-KO BMSCs of osteogenic genes *Alpl*, *Sp7*, and *Col1a1* and Wnt target genes *Tcf1*, *Lef1*, and *Axin2* after 7 days of osteogenic induction in FBS or LRS culture medium. **(H)** mRNA expression levels in control and *Lrp5*-KO BMSCs of osteogenic genes *Alpl*, *Sp7*, and *Col1a1* as well as Wnt target genes *Tcf1*, *Lef1*, and *Axin2* after 7 days of induction in LRS culture medium with or without Wnt3a treatment, $^{*}p < 0.05$, $^{**}p < 0.01$, and $^{***}p < 0.001$.

and homeostasis (Niehrs, 2012; Kobayashi et al., 2016). The co-receptors LRP5/6 respond to Wnt ligands including Wnt1, Wnt3a, and Wnt10b to regulate bone formation (Boland et al., 2004; Bennett et al., 2007; Keupp et al., 2013). However, previous study revealed Wnt3a preferentially acted *via* LRP6 in osteoblasts, and LRP5 played a less significant role in mediating Wnt signaling (Sebastian et al., 2017). Another study recorded that lithium chloride activates canonical Wnt/beta-catenin signaling in cultured $Lrp5^{-/-}$ osteoblasts and *in vivo*, also indicating an LRP5-independent way to activate Wnt signaling (Clement-Lacroix et al., 2005). Additionally, duodenum-derived serotonin was found to regulate bone formation in an LRP5-dependent manner (Yadav et al., 2008), suggesting a more complicated role of LRP5 in bone development. In the present study, we found that the regulation of lipids on BMSC osteogenesis was also LRP5-dependent, as *Lrp5* ablation in normal FBS treatment significantly impairs ALP activity of BMSCs (**Figure 4E**, panel 1). Moreover, Wnt3a activated canonical Wnt/beta-catenin signaling and BMSC osteogenesis *via* LRP5-independent manner, as the ALP activity and Wnt downstream targets were significantly enhanced by Wnt3a treatment in *Lrp5*-KO BMSCs (**Figures 4E**, panels 3, 4; **H**). These data provided further evidence in Wnt-LRP5 regulatory network in bone formation and other biological processes.

In summary, we investigated the influence of lipid scarcity on BMSC differentiation and provided more insight to the role of LRP5 in mediating lipid uptake in BMSC osteogenic differentiation and metabolism. These results further unveil the critical role of lipid availability in the biological functions of mesenchymal progenitors. Clinically, LRP5 functions essentially in bone mass and lipid metabolism in osteoporosis or cardiovascular patients. Our data suggested novel therapeutic discoveries targeting LRP5 in the treatment of bone disorders and metabolic diseases.

CONCLUSION

Our study uncovered the regulatory role of LRP5 and lipids in osteogenic differentiation of BMSCs. Lipid scarcity suppressed osteogenic differentiation of BMSCs and Wnt/beta-catenin signaling. LRP5 acted as mediators in lipid uptake of BMSCs and thus modulated osteogenesis and lipid metabolism both *in vitro* and *in vivo*. As a valuable therapeutic target in the treatment of osteoporosis and cardiometabolic disorders, the biological functions and molecular implications of Wnt-LRP5 regulations require further investigation.

DATA AVAILABILITY STATEMENT

The original contributions presented in the study are included in the article/**Supplementary Material**, further inquiries can be directed to the corresponding author.

ETHICS STATEMENT

The animal study was reviewed and approved by the Ethics Committee of Peking Union Medical College Hospital.

AUTHOR CONTRIBUTIONS

JcL and ZW conceptualized and designed the study. ZW and GQ were responsible for the administrative and funding supports. JcL conducted investigations on animals and cell lines and wrote the original draft. ZZ and GY were responsible for the collection and assembly of data. JyL and JcL were responsible for the data analysis and interpretation. ZW, LL, and HW were responsible for the review and editing the final manuscript. All authors made the final approval of the article.

FUNDING

This research was funded in part by the Beijing Natural Science Foundation (7191007 to ZW) and the National Natural Science Foundation of China (81930068 and 81772299 to ZW).

ACKNOWLEDGMENTS

We thank Harmony Technology Co., Ltd. (Beijing, China), for the technical support in cell culture experiment and data analysis.

SUPPLEMENTARY MATERIAL

The Supplementary Material for this article can be found online at: https://www.frontiersin.org/articles/10.3389/fcell.2021.766815/full#supplementary-material

REFERENCES

Ayturk, U. M., Jacobsen, C. M., Christodoulou, D. C., Gorham, J., Seidman, J. G., Seidman, C. E., et al. (2013). An RNA-seq protocol to identify mRNA expression changes in mouse diaphyseal bone: applications in mice with bone property altering Lrp5 mutations. *J. Bone Miner. Res.* 28, 2081–2093. doi: 10.1002/jbmr.1946

Baccin, C., Al-Sabah, J., Velten, L., Helbling, P. M., Grunschlager, F., Hernandez-Malmierca, P., et al. (2020). Combined single-cell and spatial transcriptomics reveal the molecular, cellular and spatial bone marrow niche organization. *Nat. Cell Biol.* 22, 38–48. doi: 10.1038/s41556-019-0439-6

Badimon, L., Luquero, A., Crespo, J., Pena, E., and Borrell-Pages, M. (2020). PCSK9 and LRP5 in macrophage lipid internalization and inflammation. *Cardiovasc. Res.* 117, 2054–2068. doi: 10.1093/cvr/cvaa254

Baron, R., and Kneissel, M. (2013). WNT signaling in bone homeostasis and disease: from human mutations to treatments. *Nat. Med.* 19, 179–192. doi: 10.1038/nm.3074

Bennett, C. N., Ouyang, H., Ma, Y. L., Zeng, Q., Gerin, I., Sousa, K. M., et al. (2007). Wnt10b increases postnatal bone formation by enhancing osteoblast differentiation. *J. Bone Miner. Res.* 22, 1924–1932. doi: 10.1359/jbmr.070810

Boland, G. M., Perkins, G., Hall, D. J., and Tuan, R. S. (2004). Wnt 3a promotes proliferation and suppresses osteogenic differentiation of adult

human mesenchymal stem cells. *J. Cell. Biochem.* 93, 1210–1230. doi: 10.1002/jcb.20284

Bouxsein, M. L., Boyd, S. K., Christiansen, B. A., Guldberg, R. E., Jepsen, K. J., and Muller, R. (2010). Guidelines for assessment of bone microstructure in rodents using micro-computed tomography. *J. Bone Miner. Res.* 25, 1468–1486. doi: 10.1002/jbmr.141

Buizert, P. J., van Schoor, N. M., Lips, P., Deeg, D. J., and Eekhoff, E. M. (2009). Lipid levels: a link between cardiovascular disease and osteoporosis? *J. Bone Miner. Res.* 24, 1103–1109. doi: 10.1359/jbmr.081262

Buo, A. M., Williams, M. S., Kerr, J. P., and Stains, J. P. (2016). A cost-effective method to enhance adenoviral transduction of primary murine osteoblasts and bone marrow stromal cells. *Bone Res.* 4:16021. doi: 10.1038/boneres.2016.21

Chan, C. K. F., Gulati, G. S., Sinha, R., Tompkins, J. V., Lopez, M., Carter, A. C., et al. (2018). Identification of the human skeletal stem cell. *Cell* 175, 43–56.e21. doi: 10.1016/j.cell.2018.07.029

Chin, E. N., Martin, J. A., Kim, S., Fakhraldeen, S. A., and Alexander, C. M. (2015). Lrp5 has a Wnt-independent role in glucose uptake and growth for mammary epithelial cells. *Mol. Cell Biol.* 36, 871–885. doi: 10.1128/MCB.00800-15

Chung, N. S., and Wasan, K. M. (2004). Potential role of the low-density lipoprotein receptor family as mediators of cellular drug uptake. *Adv. Drug Deliv. Rev.* 56, 1315–1334. doi: 10.1016/j.addr.2003.12.003

Clement-Lacroix, P., Ai, M., Morvan, F., Roman-Roman, S., Vayssiere, B., Belleville, C., et al. (2005). Lrp5-independent activation of Wnt signaling by lithium chloride increases bone formation and bone mass in mice. *Proc. Natl. Acad. Sci. U. S. A.* 102, 17406–17411. doi: 10.1073/pnas.0505259102

Clemot, M., Senos Demarco, R., and Jones, D. L. (2020). Lipid mediated regulation of adult stem cell behavior. *Front. Cell. Dev. Biol.* 8:115. doi: 10.3389/fcell.2020.00115

Cui, Y., Niziolek, P. J., MacDonald, B. T., Zylstra, C. R., Alenina, N., Robinson, D. R., et al. (2011). Lrp5 functions in bone to regulate bone mass. *Nat. Med.* 17, 684–691. doi: 10.1038/nm.2388

DiDonato, D., and Brasaemle, D. L. (2003). Fixation methods for the study of lipid droplets by immunofluorescence microscopy. *J. Histochem. Cytochem.* 51, 773–780. doi: 10.1177/002215540305100608

Dupont, S., Morsut, L., Aragona, M., Enzo, E., Giulitti, S., Cordenonsi, M., et al. (2011). Role of YAP/TAZ in mechanotransduction. *Nature* 474, 179–183. doi: 10.1038/nature10137

Frey, J. L., Li, Z., Ellis, J. M., Zhang, Q., Farber, C. R., Aja, S., et al. (2015). Wnt-Lrp5 signaling regulates fatty acid metabolism in the osteoblast. *Mol. Cell. Biol.* 35, 1979–1991. doi: 10.1128/MCB.01343-14

Gong, Y., Slee, R. B., Fukai, N., Rawadi, G., Roman-Roman, S., Reginato, A. M., et al. (2001). LDL receptor-related protein 5 (LRP5) affects bone accrual and eye development. *Cell* 107, 513–523. doi: 10.1016/s0092-8674(01)00571-2

Grassel, S., Stockl, S., and Jenei-Lanzl, Z. (2012). Isolation, culture, and osteogenic/chondrogenic differentiation of bone marrow-derived mesenchymal stem cells. *Methods Mol. Biol.* 879, 203–267. doi: 10.1007/978-1-61779-815-3_14

He, X., Cheng, R., Huang, C., Takahashi, Y., Yang, Y., Benyajati, S., et al. (2020). A novel role of LRP5 in tubulointerstitial fibrosis through activating TGF-beta/Smad signaling. *Signal. Transduct. Target. Ther.* 5:45. doi: 10.1038/s41392-020-0142-x

Keupp, K., Beleggia, F., Kayserili, H., Barnes, A. M., Steiner, M., Semler, O., et al. (2013). Mutations in WNT1 cause different forms of bone fragility. *Am. J. Hum. Genet.* 92, 565–574. doi: 10.1016/j.ajhg.2013.02.010

Kim, D. H., Inagaki, Y., Suzuki, T., Ioka, R. X., Yoshioka, S. Z., Magoori, K., et al. (1998). A new low density lipoprotein receptor related protein, LRP5, is expressed in hepatocytes and adrenal cortex, and recognizes apolipoprotein E. *J. Biochem.* 124, 1072–1076. doi: 10.1093/oxfordjournals.jbchem.a022223

Kobayashi, Y., Uehara, S., Udagawa, N., and Takahashi, N. (2016). Regulation of bone metabolism by Wnt signals. *J. Biochem.* 159, 387–392. doi: 10.1093/jb/mvv124

Lampropoulos, C. E., Papaioannou, I., and D'Cruz, D. P. (2012). Osteoporosis–a risk factor for cardiovascular disease? *Nat. Rev. Rheumatol.* 8, 587–598. doi: 10.1038/nrrheum.2012.120

Levasseur, R., Lacombe, D., and de Vernejoul, M. C. (2005). LRP5 mutations in osteoporosis-pseudoglioma syndrome and high-bone-mass disorders. *Joint Bone Spine* 72, 207–214. doi: 10.1016/j.jbspin.2004.10.008

Li, X., Zhang, Y., Kang, H., Liu, W., Liu, P., Zhang, J., et al. (2005). Sclerostin binds to LRP5/6 and antagonizes canonical Wnt signaling. *J. Biol. Chem.* 280, 19883–19887. doi: 10.1074/jbc.M413274200

Li, Y., Cam, J., and Bu, G. (2001). Low-density lipoprotein receptor family: endocytosis and signal transduction. *Mol. Neurobiol.* 23, 53–67. doi: 10.1385/MN:23:1:53

Loh, N. Y., Neville, M. J., Marinou, K., Hardcastle, S. A., Fielding, B. A., Duncan, E. L., et al. (2015). LRP5 regulates human body fat distribution by modulating adipose progenitor biology in a dose- and depot-specific fashion. *Cell Metab.* 21, 262–273. doi: 10.1016/j.cmet.2015.01.009

Lv, B., Li, F., Han, J., Fang, J., Xu, L., Sun, C., et al. (2017). Hif-1alpha overexpression improves transplanted bone mesenchymal stem cells survival in rat MCAO stroke model. *Front. Mol. Neurosci.* 10:80. doi: 10.3389/fnmol.2017.00080

Magoori, K., Kang, M. J., Ito, M. R., Kakuuchi, H., Ioka, R. X., Kamataki, A., et al. (2003). Severe hypercholesterolemia, impaired fat tolerance, and advanced atherosclerosis in mice lacking both low density lipoprotein receptor-related protein 5 and apolipoprotein E. *J. Biol. Chem.* 278, 11331–11336. doi: 10.1074/jbc.M211987200

Mazzoni, E., Mazziotta, C., Iaquinta, M. R., Lanzillotti, C., Fortini, F., D'Agostino, A., et al. (2020). Enhanced osteogenic differentiation of human bone marrow-derived mesenchymal stem cells by a hybrid hydroxylapatite/collagen scaffold. *Front. Cell. Dev. Biol.* 8:610570. doi: 10.3389/fcell.2020.610570

Niehrs, C. (2006). Function and biological roles of the Dickkopf family of Wnt modulators. *Oncogene* 25, 7469–7481. doi: 10.1038/sj.onc.1210054

Niehrs, C. (2012). The complex world of WNT receptor signalling. *Nat. Rev. Mol. Cell Biol.* 13, 767–779. doi: 10.1038/nrm3470

Rendina-Ruedy, E., and Rosen, C. J. (2020). Lipids in the bone marrow: an evolving perspective. *Cell Metab.* 31, 219–231. doi: 10.1016/j.cmet.2019.09.015

Riss, T. L., Moravec, R. A., Niles, A. L., Duellman, S., Benink, H. A., Worzella, T. J., et al. (2004). "Cell viability assays," in *Assay Guidance Manual*, eds S. Markossian, A. Grossman, K. Brimacombe, M. Arkin, D. Auld, C. P. Austin, et al. (Bethesda (MD)).

Schneider, W. J., and Nimpf, J. (2003). LDL receptor relatives at the crossroad of endocytosis and signaling. *Cell Mol. Life Sci.* 60, 892–903. doi: 10.1007/s00018-003-2183-Z

Sebastian, A., Hum, N. R., Murugesh, D. K., Hatsell, S., Economides, A. N., and Loots, G. G. (2017). Wnt co-receptors Lrp5 and Lrp6 differentially mediate Wnt3a signaling in osteoblasts. *PLoS One* 12:e0188264. doi: 10.1371/journal.pone.0188264

Senos Demarco, R., Clemot, M., and Jones, D. L. (2020). The impact of ageing on lipid-mediated regulation of adult stem cell behavior and tissue homeostasis. *Mech. Ageing Dev.* 189:111278. doi: 10.1016/j.mad.2020.111278

Souza-Moreira, L., Soares, V. C., Dias, S., and Bozza, P. T. (2019). Adipose-derived mesenchymal stromal cells modulate lipid metabolism and lipid droplet biogenesis via AKT/mTOR -PPARgamma signalling in macrophages. *Sci. Rep.* 9:20304. doi: 10.1038/s41598-019-56835-8

Truett, G. E., Heeger, P., Mynatt, R. L., Truett, A. A., Walker, J. A., and Warman, M. L. (2000). Preparation of PCR-quality mouse genomic DNA with hot sodium hydroxide and tris (HotSHOT). *Biotechniques* 29, 52,54. doi: 10.2144/00291bm09

van Gastel, N., Stegen, S., Eelen, G., Schoors, S., Carlier, A., Daniels, V. W., et al. (2020). Lipid availability determines fate of skeletal progenitor cells via SOX9. *Nature* 579, 111–117. doi: 10.1038/s41586-020-2050-1

Van Wesenbeeck, L., Cleiren, E., Gram, J., Beals, R. K., Benichou, O., Scopelliti, D., et al. (2003). Six novel missense mutations in the LDL receptor-related protein 5 (LRP5) gene in different conditions with an increased bone density. *Am. J. Hum. Genet.* 72, 763–771. doi: 10.1086/368277

Williams, B. O. (2017). LRP5: from bedside to bench to bone. *Bone* 102, 26–30. doi: 10.1016/j.bone.2017.03.044

Yadav, V. K., and Ducy, P. (2010). Lrp5 and bone formation : a serotonin-dependent pathway. *Ann. N. Y. Acad. Sci.* 1192, 103–109. doi: 10.1111/j.1749-6632.2009.05312.x

Yadav, V. K., Ryu, J. H., Suda, N., Tanaka, K. F., Gingrich, J. A., Schütz, G., et al. (2008). Lrp5 controls bone formation by inhibiting serotonin synthesis in the duodenum. *Cell* 135, 825–837. doi: 10.1016/j.cell.2008.09.059

Yamaguchi, T., Sugimoto, T., Yano, S., Yamauchi, M., Sowa, H., Chen, Q., et al. (2002). Plasma lipids and osteoporosis in postmenopausal women. *Endocr. J.* 49, 211–217. doi: 10.1507/endocrj.49.211

Ying, C., Wang, R., Wang, Z., Tao, J., Yin, W., Zhang, J., et al. (2020). BMSC-exosomes carry mutant HIF-1alpha for improving angiogenesis and osteogenesis in critical-sized calvarial defects. *Front. Bioeng. Biotechnol.* 8:565561. doi: 10.3389/fbioe.2020.565561

Yue, R., Zhou, B. O., Shimada, I. S., Zhao, Z., and Morrison, S. J. (2016). Leptin receptor promotes adipogenesis and reduces osteogenesis by regulating mesenchymal stromal cells in adult bone marrow. *Cell Stem Cell* 18, 782–796. doi: 10.1016/j.stem.2016.02.015

Conflict of Interest: GY is employed by Harmony Technology Co., Ltd. (Beijing, China).

The remaining authors declare that the research was conducted in the absence of any commercial or financial relationships that could be construed as a potential conflict of interest.

Publisher's Note: All claims expressed in this article are solely those of the authors and do not necessarily represent those of their affiliated organizations, or those of the publisher, the editors and the reviewers. Any product that may be evaluated in this article, or claim that may be made by its manufacturer, is not guaranteed or endorsed by the publisher.

frontiers in Cell and Developmental Biology

REVIEW
published: 29 November 2021
doi: 10.3389/fcell.2021.770705

Bone Marrow Adipocytes: A Critical Player in the Bone Marrow Microenvironment

Lipeng Wang[1†], *Hao Zhang*[2†], *Sicheng Wang*[3*], *Xiao Chen*[2*] *and Jiacan Su*[1,2*]

[1]Institute of Translational Medicine, Shanghai University, Shanghai, China, [2]Department of Orthopedics Trauma, Shanghai Changhai Hospital, Naval Medical University, Shanghai, China, [3]Department of Orthopedics, Shanghai Zhongye Hospital, Shanghai, China

Recognized for nearly 100 years, bone marrow adipocytes (BMAs) form bone marrow niches that contain hematopoietic and bone cells, the roles of which have long been underestimated. Distinct from canonical white, brown, and beige adipocytes, BMAs derived from bone marrow mesenchymal stromal cells possess unique characteristics and functions. Recent single-cell sequencing studies have revealed the differentiation pathway, and seminal works support the tenet that BMAs are critical regulators in hematopoiesis, osteogenesis, and osteoclastogenesis. In this review, we discuss the origin and differentiation of BMAs, as well as the roles of BMAs in hematopoiesis, osteogenesis, osteoclastogenesis, and immune regulation. Overall, BMAs represent a novel target for bone marrow-related diseases, including osteoporosis and leukemia.

Keywords: bone marrow adipocytes, bone marrow mesenchymal stromal cells, hematopoiesis, osteogenesis, osteoclastogenesis, immune regulation

OPEN ACCESS

Edited by:
Giorgio Malpeli,
University of Verona, Italy

Reviewed by:
Ormond MacDougald,
University of Michigan, United States
Stuart Rushworth,
University of East Anglia,
United Kingdom

***Correspondence:**
Sicheng Wang
w.s.c@sina.com
Xiao Chen
sirchenxiao@126.com
Jiacan Su
drsujiacan@163.com

†*These authors have contributed equally to this work*

Specialty section:
This article was submitted to Cellular Biochemistry, a section of the journal Frontiers in Cell and Developmental Biology

Received: *04 September 2021*
Accepted: *29 October 2021*
Published: *29 November 2021*

Citation:
Wang L, Zhang H, Wang S, Chen X and Su J (2021) Bone Marrow Adipocytes: A Critical Player in the Bone Marrow Microenvironment. Front. Cell Dev. Biol. 9:770705. doi: 10.3389/fcell.2021.770705

INTRODUCTION

Bone marrow niches are specialized microenvironments that include hematopoietic cells, mesenchymal lineage cells, endothelial cells, and nerves. Erythroid, myeloid, and lymphoid cells constitute the hematopoietic lineage, and mesenchymal stromal cells (MSCs) mainly differentiate into adipocytes, osteoblasts, and chondrocytes (de Paula and Rosen, 2020).

Bone marrow adipocytes (BMAs) were first described in 1922, but it was not until recently that scientists began to understand the basic tenets of BMAs. BMAs are developmentally and functionally distinct from classical white, brown, and beige adipocytes (Sebo et al., 2019). White adipocytes are large, lipid-laden cells that act as an energy source for other tissues and make up 99% of the volume of the subcutaneous and visceral adipose tissue depot. Brown adipocytes are small, mitochondria-abundant cells that burn fatty acids to generate heat. Beige adipocytes reside in subcutaneous depots together with white adipocytes but share some functional features of brown adipocytes, especially in terms of thermogenic capacity through uncoupling protein 1 and morphology (multilocular small cells). BMAs, derived from a unique origin, are metabolically active cells with abundant lipid stores, mitochondria, and endoplasmic reticulum. The amount of BMAs is dynamic during development and in several conditions including osteoporosis, aging, and caloric restriction (de Paula and Rosen, 2020). These observations have encouraged the scientists to explore the roles of BMAs.

BMA IDENTIFICATION

Origin and classification

Lineage tracing results have indicated that BMAs arise from bone marrow mesenchymal stromal cells (BMSCs), not white adipocytes, brown adipocytes, or hematopoietic progenitors. Efforts are ongoing to identify the adipocyte progenitors *in vivo*. It remains unclear whether BMAs originate from a single population or different sources.

Lepr$^+$ BMSCs are a major source of BMAs in adults. BMSCs are heterogeneous and labeled according to the absence of hematopoietic or endothelial markers accompanied by the expression of several stem cell markers (Zhou et al., 2014). In adults, *Lepr*$^+$ stromal cells are situated around the vascular network and account for 94% of BMSCs. *Lepr*$^+$ cells arise postnatally and form most bone cells and BMAs in adults (Zhou et al., 2014). After irradiation, fracture, or transplantation, *Lepr*$^+$ cells are accountable for the generation of bone and BMAs (Zhou et al., 2014).

Comprising approximately 70% of adult marrow volume and 10% of adipose tissue mass in healthy individuals, bone marrow adipose tissue (BMAT) is mainly formed by BMAs and two distinct compositions exist: constitutive (cBMAT) and regulated (rBMAT) compartments (Scheller et al., 2015). Micro-computed tomography (CT) on osmium tetroxide-stained bone imaging has shown that cBMAT is located in the distal region of the tibia. cBMAT forms immediately after birth and represents a more stable form of BMAT that rarely responds to environmental stimuli. cBMAT development results in an accumulation of cells. rBMAT resides in vertebrae and the proximal region of the tibia and is sensitive to global and local cues, including cold exposure and radiation; it also participates in physiological adaptation. Although the classification of rBMAT and cBMAT is clear within rodents, the extent to which this nomenclature can be applied to humans remains to be determined.

Differentiation

Although the differentiation routes of BMSCs into adipocytes have been elucidated, the identification and characteristics of the precursors are poorly explored. A recent study depicts the adipose precursor hierarchy of BMSCs (Ambrosi et al., 2017). Focusing on cell surface markers, they showed that CD45$^-$CD31$^-$Sca$^+$CD24$^+$ multipotent precursor cells differentiate into both BMAs and osteoblasts. CD45 and CD31 are hematopoietic lineage markers, while Sca and CD24 are adipose precursor markers. This population further differentiates into CD45$^-$CD31$^-$Sca$^+$CD24$^-$ adipogenic precursors, which give rise to CD45$^-$CD31$^-$Sca$^-$Zfp234$^+$ preadipocytes and then mature BMAs (Grandl and Wolfrum, 2017). Another group identifies new subtypes of *Lepr*$^+$ BMSCs that differentiate into BMAs: *Mpg*^{high} and *Lpl*^{high} clusters (Tikhonova et al., 2019).

To delineate the development of BMSCs into terminal BMAs through hierarchical differentiation paths *in vivo*, Qin et al. performed extensive single-cell RNA-sequencing on BMSCs (Zhong et al., 2020). Mesenchymal lineage cells are divided into nine subpopulations. Analysis of lineage-unique gene markers identified collections of BMAs, osteoblasts, osteocytes, and chondrocytes. Trajectory pattern analysis using the slingshot method identified the most primordial subgroup in the sequencing dataset: early mesenchymal progenitors (EMPs). The results show that EMPs express some stem cell markers, including Sca-1, Thy1, and Cd34. Based on the expression level of osteogenic genes, they also identified intermediate mesenchymal progenitors (IMPs), late mesenchymal progenitors (LMPs), and lineage committed progenitors (LCPs) before differentiation into osteoblasts or BMAs. The authors found that α-smooth muscle actin (SMA) labels mesenchymal progenitors before bifurcated differentiation and can act as a marker for LMPs. Notably, they identified an original adipogenic lineage cell subpopulation, which are lipid-poor, labeled by adiponectin (*Adipoq*)-Cre and can be observed after LCPs and before mature BMAs during adipogenic differentiation. This novel population of adipogenic lineage cells is referred to as marrow adipogenic lineage precursors (MALPs). MALPs maintain marrow vasculature and inhibit bone formation by secreted factors such as vascular endothelial growth factor (VEGF) and angiopoietin 4 (ANGPT4) (Zhong et al., 2020). This study showed relatively comprehensive *in vivo* differentiation of BMSCs into BMAs inside the bone marrow (**Figure 1**). Overall, there is heterogeneity in adipocytes in bone marrow, and BMAs at different stages of differentiation may play distinct biological roles.

ROLES OF BMAS

Adipose tissue is a substantial endocrine organ that regulates physiological activities by secreting hormones and cytokines (Cawthorn et al., 2014; Suchacki et al., 2020). It is predicted that 263 distinct proteins are secreted by primary human adipocytes (Lehr et al., 2012). Although the function of BMAs in marrow niches is under investigation, their regulatory role in hematopoiesis, bone metabolism, and immunity are only partially understood.

The role of BMAs in hematopoiesis is controversial

Evidence indicates that BMAs negatively regulate hematopoiesis (Naveiras et al., 2009; Scheller et al., 2016). Adipocyte-abundant caudal vertebrae retain fewer hematopoietic stem cells (HSCs) and short-term progenitors compared with adipocyte-free thoracic vertebrae. Furthermore, the genetic and pharmacologic inhibition of adipogenesis accelerates hematopoietic recovery after irradiation and bone marrow transplant (Naveiras et al., 2009). However, it is still unclear if this reflects the influence of BMAs on HSCs or a secondary impact on the marrow environment.

A recent study reported that adipocytes in long bones support hematopoietic restoration following irradiation by providing stem cell factor (SCF), a critical factor for HSC survival

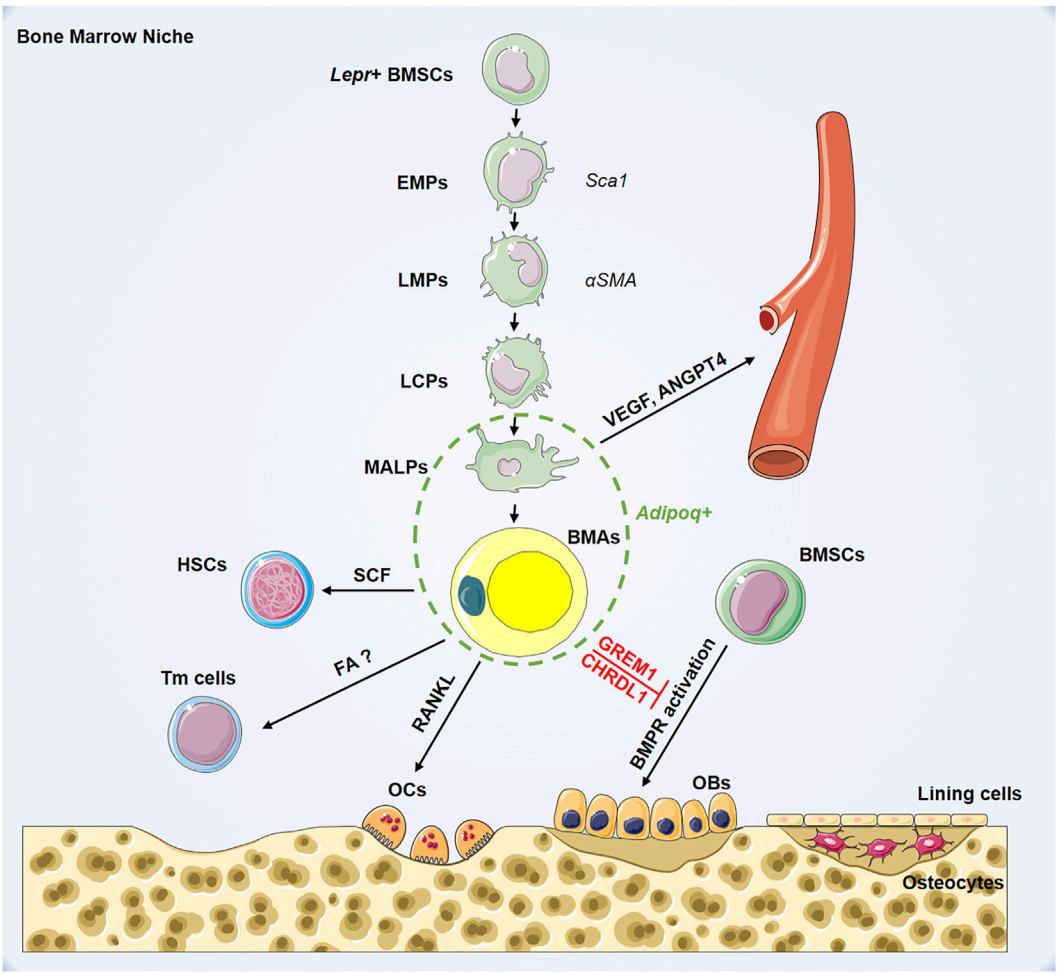

FIGURE 1 | Hierarchy of bone marrow adipocyte lineage cell and its role in bone marrow niche. BMSCs: bone marrow mesenchymal stromal cells; EMPs: early mesenchymal progenitors; LMPs: late mesenchymal progenitors; LCPs: lineage committed progenitors; MALPs: marrow adipogenic lineage precursors; BMAs: bone marrow adipocytes; HSCs: hematopoietic stem cells; Tmcells: T memory cells; OCs: osteoclasts; OBs: osteoblasts; *Lepr*: leptin receptor; *Sca1*: stem cell antigen 1; *αSMA*: smooth muscle actin alpha; *Adipoq*: adiponectin; SCF: stem cell factor; RANKL: receptor activator for nuclear factor-κ B ligand; FAO; VEGF: vascular endothelial growth factor; ANGPT4: angiopoietin 4; GREM1: gremlin1; CHRDL1: chordin-like1; BMPR: bone morphogenetic protein receptor.

(Oguro et al., 2013), whereas in tail vertebrae adipocytes impair hematopoiesis (Zhou et al., 2017). After irradiation, fatless A-ZIP/F1 mice have reduced overall marrow cells and HSCs in long bones, yet exhibit an increased number in caudal vertebrae (Zhou et al., 2017). This difference was attributed to the presence of a high number of blood vessels in the tail vertebrae of A-ZIP/F1 mice, a phenomenon not seen in femurs (Zhou et al., 2017). Suppression of marrow vascularization impairs HSC frequency and hematopoietic regeneration (Hooper et al., 2009). In addition to SCF, BMAs also synthesize adiponectin and leptin, which promote HSC proliferation (DiMascio et al., 2007; Poloni et al., 2013). Although the finding that BMA expansion is accompanied by reduced hematopoiesis has conventionally been interpreted to reflect an inhibitory effect of BMAs on hematopoiesis, these data suggest that adipogenesis is an emergency response that produces HSC niche factors and promotes hematopoiesis in most bones. Compared with constructing new perivascular niches, adipogenesis is a faster way to produce HSC niche factors, which involves the promotion of marrow vascularization (Zhou et al., 2017).

To confirm further the connections between BMAs and hematopoiesis in primates, the rhesus macaque model has been used to determine that hematopoietic stem and progenitor cells (HSPCs) reside abreast of BMAs. Furthermore, BMAT-conditioned medium promotes the expansion and differentiation of HSPCs *ex vivo* (Robino et al., 2020). To explore the underlying mechanism, quantitative proteomic examination of BMAT-conditioned medium was performed. A total of 994 proteins were found to be released from BMAT, including TGFB1, FBLN1, IGFBP2, LGALS1, TIMP1, and C3, which have been identified as positive regulators of HSPC differentiation, motility, and adhesion (Robino et al., 2020). Among them, 430 proteins are of microvesicular/exosomal origin, indicating complex

composition and paracrine activity. Of note, BMAT contains many types of cells in addition to BMAs, including granulocytes and monocytes/macrophages (Robino et al., 2020). Several proteins identified from BMAT are derived from these cellular neighborhoods of BMAs. Thus, BMAs may also regulate HSPC activity through these immune cells.

The function of BMAs in leukemia is debatable and lineage specific. In acute lymphoblastic leukemia (ALL), *in vitro* and *in vivo* studies indicate that BMAs inhibit T-ALL proliferation (Cahu et al., 2017). In acute myeloid leukemia (AML), Shafat et al. report that AML blasts cocultured with BMA show reduced apoptosis and enhanced proliferation (Shafat et al., 2017). AML blasts promote BMA lipolysis, and the fatty acids generated are transmitted from BMAs to AML cells for β-oxidation. However, a recent study showed that AML caused a reduction in adipocytes in human marrow and AML xenografts (Boyd et al., 2017), suggesting that AML mainly influences the adipocyte population, in addition to promoting the lipolysis of preexisting adipocytes (Boyd et al., 2017). Furthermore, global transcriptome analysis of BMSCs from AML patients or healthy bone marrow donors revealed that adipogenic differentiation is compromised by AML (Boyd et al., 2017). To explore further the relationship between BMA decline and deficient myelo-erythropoiesis in AML, the researchers performed Transwell assays, which showed that BMAs promote myeloid and erythroid lineage maturation. The PPARγ agonist GW1929 was used to stimulate adipogenesis and was found to rescue hematopoietic maturation while suppressing leukemic growth (Boyd et al., 2017). Overall, BMAs promote normal myelo-erythroid maturation and may be a useful therapeutic target to improve bone marrow failure in AML. However, the high sensitivity of BMAs to the change of metabolic status hampers a clear definition of its function in distinct clinical situations and further studies are needed to fully unveil the function of BMA in physiology and different pathology conditions (Zinngrebe et al., 2020).

BMAs inhibit osteogenesis

Findings in healthy individuals indicate that regardless of age (age 5–88 years), BMAs are negatively related to bone mass (Shen et al., 2007; Shen et al., 2014). BMAs have also been reported to inhibit bone formation and fracture healing, although the underlying mechanism is still under investigation (Ambrosi et al., 2017).

BMA ablation enhances osteogenesis. In a recent study, researchers mated mice bearing diphtheria toxin receptor (DTR), under control of a STOP-flox, to *Adipoq*-Cre mice (Zou et al., 2020). The DTR^{Adipoq} mice showed eliminated peripheral and marrow adipocytes following administration of the diphtheria toxin. The bone mass of *Adipoq*-deficiency mice increased 10-fold with 10 days of diphtheria toxin treatment. To exclude the effect of peripheral adipocytes, the authors performed parabiosis between wild-type and DTR^{Adipoq} mice and found that diphtheria toxin treatment to control mice induced DTR^{Adipoq} mice osteosclerosis, while administration of diphtheria toxin to DTR^{Adipoq} mice had no impact on the bone volume of wild-type partners (Zou et al., 2020). Thus, enhanced osteogenesis in DTR^{Adipoq} mice is mediated by BMA ablation. To uncover the mechanism of enhanced bone formation following BMA deletion, they further mated DTR^{Adipoq} mice to *2.3Col*-GFP reporter mice to characterize osteoblasts. Four days after diphtheria toxin induction, more GFP^{+} cells were observed in DTR^{Adipoq} mice. They next mated DTR^{Adipoq} *2.3Col*-GFP mice to *TK-3.6Col1a1* mice, a specific strain transduced by mitotic pre-osteoblastic cells (Zou et al., 2020). Diphtheria toxin-induced osteosclerosis is reversed in *TK-3.6Col1a1* mice by ganciclovir, an agent that targets replicating pre-osteoblasts (Zou et al., 2020). These results suggest that BMA ablation promotes pre-osteoblast recruitment and their differentiation into mature osteoblasts. This impact is a result of activation of bone morphogenetic protein receptor (BMPR) and epidermal growth factor receptor pathways. BMAs express chordin-like1 (CHRDL1) and gremlin1 (GREM1), specific BMPR inhibitors, and thus suppress osteogenesis (Zou et al., 2020). Another group reported that BMAs also secrete interleukin (IL)-6 and palmitate to suppress osteoblast activity (Gasparrini et al., 2009; Gunaratnam et al., 2014).

BMAs mediate myeloma-induced osteoblastogenesis suppression. Multiple myeloma is distinguished by overactive bone absorption and impaired bone generation (Palumbo and Anderson, 2011). When BMSCs are cultured with conditioned medium from BMAs obtained from myeloma patients or pre-exposed to myeloma cells, the researchers observed reduced Alizarin red S staining, alkaline phosphatase levels, and osteoblastic gene expression (Liu et al., 2019). Furthermore, using an extramedullary model of osteogenesis and calvarial bone defect, they found that myeloma-associated adipocytes weakened new bone formation (Liu et al., 2019). To explore the mechanism, microarray analysis and qPCR were performed to examine adipokine expression profiles in adipocytes from the bone marrow of patients and healthy controls. Three downregulated genes (adiponectin, adipsin, and visfatin) and one upregulated gene (*Tnfa*) were identified. The changes in expression of these adipokines inhibited osteoblastogenesis (Liu et al., 2019).

BMAs and osteoblasts are derived from the same stem cell, and the direction toward adipocytes occurs at the cost of osteoblast reduction. Thus, regulating the lineage allocation of BMSCs is an effective way to enhance osteoblastogenesis (Suresh et al., 2019; Yu et al., 2019). However, it is notable that the mutual exclusivity between adipocytes and osteoblasts in BM has not yet been proven. During puberty, bone marrow changes from red toward yellow but bone-forming activity has reached its peak (Moore and Dawson, 1990; Devlin and Rosen, 2015). Various animal models show elevated bone mass and excessive BMAT (Ackert-Bicknell et al., 2009).

BMAs enhance osteoclastogenesis

BMAs promote osteoclastogenesis and recent studies by Hu et al. and Yu et al. have begun to address how BMAs regulate osteoclast formation and bone remodeling (Hu et al., 2021b; Yu et al., 2021). Receptor activator of NF-κB (RANK) and its ligand RANKL play pivotal roles in osteoclastogenesis (Theill et al., 2002). RANKL is predominantly found in osteoblasts, osteocytes, and hypertrophic

chondrocytes and binds RANK of osteoclast progenitors to induce osteoclastogenesis (Onji et al., 2021). Notably, BMAs also express RANKL (Fan et al., 2017). Yu et al. crossed *Rankl*-floxed mice with the *Adipoq*-Cre line to uniquely knock out *Rankl* in adipogenic lineage cells ($Adipoq^{cre}$;$Rankl^{fl/fl}$). Under physiological conditions, these mice showed impaired osteoclastogenesis and bone resorption (Yu et al., 2021). In ovariectomy-induced osteoporosis, we found no decrease in cancellous bone density or cortical bone thickness after *Rankl* deletion in adipose cells (Hu et al., 2021b). To explore the role of RANKL in pathological BMA expansion, $Adipoq^{cre}$;$Rankl^{fl/fl}$ mice were administered the PPARγ activator rosiglitazone to increase bone marrow adipogenesis and the possibility of fracture (Aubert et al., 2010). $Adipoq^{cre}$;$Rankl^{fl/fl}$ mice showed similar BMA expansion but a reduced number of osteoclasts compared with control $Rankl^{fl/fl}$ mice (Aubert et al., 2010). These findings suggest that expanded BMA are crucial sources of RANKL for increased osteoclastogenesis and bone resorption. Overall, these two independent studies revealed that BMAs mediate bone remodeling through RANK/RANKL-dependent regulation of osteoclastogenesis in physiological and pathological states. Thus, targeting bone marrow adipogenesis and RANKL signaling in BMAs may be useful to treat osteoporosis.

BMAs regulate immune function

BMAs contribute to inflammation and plasma cell malfunction inside the bone marrow. Memory T cells and long-lasting plasma cells settle primarily in the marrow to provide protection against recurrent infections (Tokoyoda et al., 2009). To investigate the function of BMAs in immune regulation, global gene expression analysis was performed to compare mRNA expression of adipocytes from human BMAs and white adipose tissue (WAT) (Miggitsch et al., 2019). Several cytokines, including CCL2 CCL5, IL6, IL8, IL10, IL15, CCR7, CCRL2, and CXCL1 were elevated in BMAs, indicating its immune regulatory function within the bone marrow (Miggitsch et al., 2019). Furthermore, the production of reactive oxygen species (ROS) is elevated inside BMAs. ROS secretion accounts for the inhibition of IgG producing plasma cells (Miggitsch et al., 2019).

BMAs promote memory T cell gathering in the bone marrow upon dietary restriction (DR). While WAT collapses after caloric restriction, BMAs are paradoxically increased, with unclear significance. Recent findings have revealed that memory T cells redistribute from the periphery toward the bone marrow in response to the nutritional challenge (Collins et al., 2019). To determine if BMA expansion contributes to memory T cell viability and aggregation, the *Adipoq*-Cre^{ERT2}×*Rosa26*-DTA mice were generated to delete BMAs. *Rosa26*-DTA mice carry a loxP-flanked stop cassette linked to the active fragment of diphtheria toxin. When crossed with *Adipoq*-Cre mice, specific ablation of adipocytes is achieved. In mice with reduced BMAs, memory T cells are no longer sustained in the marrow after DR, indicating BMAs are important for memory T cells homing to the bone marrow. Moreover, these T cells show strengthened protection resisting secondary cancers and infections (Collins et al., 2019). Previous studies have revealed that long-chain fatty acids are indispensable for T cell survival, but how BMAs contribute to memory T cell maintenance and homing is still unclear. Collectively, BMAs help maintain and optimize immunological retention upon DR with an unknown mechanism.

REGULATION OF BONE MARROW ADIPOGENESIS

An increase in BMAT is a shared reaction to various clinical circumstances and medication, such as diabetes, obesity, anorexia, senescence, and glucocorticoid treatment. Based on the role of BMAs, regulating bone marrow adipogenesis is a promising method for treating bone marrow-related diseases and controlling the differentiation fate of BMSCs is a feasible way.

Several regulators participate in BMSC differentiation. PPARγ, C/EBPα, platelet-derived growth factor receptor β and zinc finger proteins 423, 467, and 521 are well-known factors required for adipogenesis (de Paula and Rosen, 2020); additional regulators are under investigation. Forkhead box P1 (FOXP1) can interact with the CEBPβ/δ complex and RBPjκ to regulate BMSC fate switches (Li et al., 2017). Expressed on BMSCs, Thy-1 (CD90) is a glycosylphosphatidyl-anchored protein of the immunoglobulin family. Thy-1-deficient mice show increased adipogenesis (Picke et al., 2018), and Thy-1 deficiency results in a reduction in Wnt ligand concomitantly with upregulation of the Wnt inhibitors dickkopt-1 and sclerostin, which inhibit osteogenesis (Picke et al., 2018). microRNAs (miRs) participate in cell metabolism by regulating the mRNA degradation of target mRNA. Antagonism of miR-188 can affect the differentiation fate of BMSCs and promote bone formation (Hu et al., 2021a). BMSC differentiation is also epigenetically regulated: histone demethylases KDM4B and KDM6B inhibit adipogenic differentiation of BMSCs *via* elimination of H3K9me3 and H3K27me3 (Ye et al., 2012).

The bone marrow niche also provides information that regulates BMSC lineage commitment. Sensory nerves can induce osteogenic differentiation of BMSCs by downregulating sympathetic nerve activity. Local elevation of prostaglandin E2 triggers EP4 receptors in sensory nerves and inhibits adipogenesis (Hu et al., 2020). Mechanical forces facilitate osteogenic differentiation of BMSCs and prohibit BMA production (Ozcivici et al., 2010). During mechanical loading, modulation of actin regulates ERK and AKT pathways to induce BMSC differentiation (Li et al., 2015). mTORC2 also plays a role in strain-induced cytoskeletal reorganization. Deletion of mTORC2 in BMSCs abolishes osteogenic differentiation and facilitates adipogenic differentiation (Sen et al., 2014). Endocrine molecules also influence BMSC differentiation. Estrogen acts on estrogen receptor-α and has been shown to suppress adipogenesis (Rooney and van der Meulen, 2017). Both BMSCs and BMAs express the follicle-stimulating hormone (FSH) receptor, and inhibition of its interaction with FSH prevents adipogenesis (Liu et al., 2017). Parathyroid hormone (PTH) regulates bone metabolism and inhibits the differentiation of BMSCs toward BMAs (Fan et al., 2017). Moreover, BMAs express PTH1R, and PTH can induce adipogenic lipolysis, which further diminishes adipogenesis in the bone marrow niche

(Maridas et al., 2019). Leptin also regulates bone metabolism (Cohen et al., 1996); hypothalamic or subcutaneous administration of leptin has been shown to impair obesity-induced marrow adiposity (Hamrick et al., 2005; Ambati et al., 2010). Overall, several factors control BMSCs differentiation fate, and further work are needed to identify novel regulators.

PERSPECTIVE

BMAs are unique adipocytes that reside in the skeletal space. Previous studies have suggested that mature and premature adipocytes exert various influences on hematopoiesis, bone remodeling, and immune regulation in bone marrow niches (**Figure 1**). However, it is worth noting that the specificity of *Adipoq*-Cre is questionable (Onji et al., 2021). Many studies have targeted BMAs with *Adipoq*-Cre; however, in aged mice, some osteocytes and osteoblasts are also Cre-positive (Mukohira et al., 2019; Yu et al., 2021). Moreover, *Adipoq* is a marker of mature adipocytes as well as their progenitors, MALPs (Yu et al., 2021). Further studies using more specific Cre lines are warranted to uncover the function of BMAs and adipocyte precursors in distinct phases of differentiation.

Lineage allocation of BMSCs is regulated by niche inputs that involve mechanical, neural, and endocrine modulators. Efforts are being made to genetically or pharmacologically manipulate bone marrow adipogenesis, and it may constitute a novel therapeutic strategy for bone marrow-related disorders.

AUTHOR CONTRIBUTIONS

LW, SW, XC, and JS conceived the article. LW and HZ wrote the article. SW, XC, and JC reviewed and edited the article. All authors listed have made a substantial, direct, and intellectual contribution to work and approved it for publication.

FUNDING

This project was supported by the National Key Research and Development Plan (2018YFC2001500), National Natural Science Foundation of China (NSFC) Key Research Program in Aging (91749204), National Natural Science Foundation of China (81771491, 81871099, 81972254, and 82172098), and Shanghai Rising-Star Program (21QA1412000).

REFERENCES

Ackert-Bicknell, C. L., Shockley, K. R., Horton, L. G., Lecka-Czernik, B., Churchill, G. A., and Rosen, C. J. (2009). Strain-specific Effects of Rosiglitazone on Bone Mass, Body Composition, and Serum Insulin-like Growth Factor-I. *Endocrinology* 150 (3), 1330–1340. doi:10.1210/en.2008-0936

Ambati, S., Li, Q., Rayalam, S., Hartzell, D. L., Della-Fera, M. A., Hamrick, M. W., et al. (2010). Central Leptin versus Ghrelin: Effects on Bone Marrow Adiposity and Gene Expression. *Endocr* 37 (1), 115–123. doi:10.1007/s12020-009-9274-z

Ambrosi, T. H., Scialdone, A., Graja, A., Gohlke, S., Jank, A.-M., Bocian, C., et al. (2017). Adipocyte Accumulation in the Bone Marrow during Obesity and Aging Impairs Stem Cell-Based Hematopoietic and Bone Regeneration. *Cell Stem Cell* 20 (6), 771–784. e776. doi:10.1016/j.stem.2017.02.009

Aubert, R. E., Herrera, V., Chen, W., Haffner, S. M., and Pendergrass, M. (2010). Rosiglitazone and Pioglitazone Increase Fracture Risk in Women and Men with Type 2 Diabetes. *Diabetes Obes. Metab.* 12 (8), 716–721. doi:10.1111/j.1463-1326.2010.01225.x

Boyd, A. L., Reid, J. C., Salci, K. R., Aslostovar, L., Benoit, Y. D., Shapovalova, Z., et al. (2017). Acute Myeloid Leukaemia Disrupts Endogenous Myelo-Erythropoiesis by Compromising the Adipocyte Bone Marrow Niche. *Nat. Cel Biol* 19 (11), 1336–1347. doi:10.1038/ncb3625

Cahu, X., Calvo, J., Poglio, S., Prade, N., Colsch, B., Arcangeli, M.-L., et al. (2017). Bone Marrow Sites Differently Imprint Dormancy and Chemoresistance to T-Cell Acute Lymphoblastic Leukemia. *Blood Adv.* 1 (20), 1760–1772. doi:10.1182/bloodadvances.2017004960

Cawthorn, W. P., Scheller, E. L., Learman, B. S., Parlee, S. D., Simon, B. R., Mori, H., et al. (2014). Bone Marrow Adipose Tissue Is an Endocrine Organ that Contributes to Increased Circulating Adiponectin during Caloric Restriction. *Cel Metab.* 20 (2), 368–375. doi:10.1016/j.cmet.2014.06.003

Cohen, S. L., Halaas, J. L., Friedman, J. M., Chait, B. T., Bennett, L., Chang, D., et al. (1996). Human Leptin Characterization. *Nature* 382 (6592), 589. doi:10.1038/382589a0

Collins, N., Han, S.-J., Enamorado, M., Link, V. M., Huang, B., Moseman, E. A., et al. (2019). The Bone Marrow Protects and Optimizes Immunological Memory during Dietary Restriction. *Cell* 178 (5), 1088–1101. e1015. doi:10.1016/j.cell.2019.07.049

de Paula, F. J. A., and Rosen, C. J. (2020). Marrow Adipocytes: Origin, Structure, and Function. *Annu. Rev. Physiol.* 82, 461–484. doi:10.1146/annurev-physiol-021119-034513

Devlin, M. J., and Rosen, C. J. (2015). The Bone-Fat Interface: Basic and Clinical Implications of Marrow Adiposity. *Lancet Diabetes Endocrinol.* 3 (2), 141–147. doi:10.1016/s2213-8587(14)70007-5

DiMascio, L., Voermans, C., Uqoezwa, M., Duncan, A., Lu, D., Wu, J., et al. (2007). Identification of Adiponectin as a Novel Hemopoietic Stem Cell Growth Factor. *J. Immunol.* 178 (6), 3511–3520. doi:10.4049/jimmunol.178.6.3511

Fan, Y., Hanai, J.-i., Le, P. T., Bi, R., Maridas, D., DeMambro, V., et al. (2017). Parathyroid Hormone Directs Bone Marrow Mesenchymal Cell Fate. *Cel Metab.* 25 (3), 661–672. doi:10.1016/j.cmet.2017.01.001

Gasparrini, M., Rivas, D., Elbaz, A., and Duque, G. (2009). Differential Expression of Cytokines in Subcutaneous and Marrow Fat of Aging C57BL/6J Mice. *Exp. Gerontol.* 44 (9), 613–618. doi:10.1016/j.exger.2009.05.009

Grandl, G., and Wolfrum, C. (2017). Adipocytes at the Core of Bone Function. *Cell Stem Cell* 20 (6), 739–740. doi:10.1016/j.stem.2017.05.008

Gunaratnam, K., Vidal, C., Gimble, J. M., and Duque, G. (2014). Mechanisms of Palmitate-Induced Lipotoxicity in Human Osteoblasts. *Endocrinology* 155 (1), 108–116. doi:10.1210/en.2013-1712

Hamrick, M. W., Della-Fera, M. A., Choi, Y.-H., Pennington, C., Hartzell, D., and Baile, C. A. (2005). Leptin Treatment Induces Loss of Bone Marrow Adipocytes and Increases Bone Formation in Leptin-Deficient Ob/ob Mice. *J. Bone Miner Res.* 20 (6), 994–1001. doi:10.1359/jbmr.050103

Hooper, A. T., Butler, J. M., Nolan, D. J., Kranz, A., Iida, K., Kobayashi, M., et al. (2009). Engraftment and Reconstitution of Hematopoiesis Is Dependent on VEGFR2-Mediated Regeneration of Sinusoidal Endothelial Cells. *Cell Stem Cell* 4 (3), 263–274. doi:10.1016/j.stem.2009.01.006

Hu, B., Lv, X., Chen, H., Xue, P., Gao, B., Wang, X., et al. (2020). Sensory Nerves Regulate Mesenchymal Stromal Cell Lineage Commitment by Tuning Sympathetic Tones. *J. Clin. Invest.* 130 (7), 3483–3498. doi:10.1172/jci131554

Hu, Y., Li, X., Zhang, Q., Gu, Z., Luo, Y., Guo, J., et al. (2021a). Exosome-guided Bone Targeted Delivery of Antagomir-188 as an Anabolic Therapy for Bone Loss. *Bioactive Mater.* 6 (9), 2905–2913. doi:10.1016/j.bioactmat.2021.02.014

Hu, Y., Li, X., Zhi, X., Cong, W., Huang, B., Chen, H., et al. (2021b). RANKL from Bone Marrow Adipose Lineage Cells Promotes Osteoclast Formation and Bone Loss. *EMBO Rep.* 22, e52481. doi:10.15252/embr.202152481

Lehr, S., Hartwig, S., Lamers, D., Famulla, S., Müller, S., Hanisch, F.-G., et al. (2012). Identification and Validation of Novel Adipokines Released from Primary Human Adipocytes. *Mol. Cell Proteomics* 11 (1), M111. doi:10.1074/mcp.M111.010504

Li, H., Liu, P., Xu, S., Li, Y., Dekker, J. D., Li, B., et al. (2017). FOXP1 Controls Mesenchymal Stem Cell Commitment and Senescence during Skeletal Aging. *J. Clin. Invest.* 127 (4), 1241–1253. doi:10.1172/jci89511

Li, R., Liang, L., Dou, Y., Huang, Z., Mo, H., Wang, Y., et al. (2015). Mechanical Strain Regulates Osteogenic and Adipogenic Differentiation of Bone Marrow Mesenchymal Stem Cells. *Biomed. Res. Int.* 2015, 1–10. doi:10.1155/2015/873251

Liu, H., He, J., Koh, S. P., Zhong, Y., Liu, Z., Wang, Z., et al. (2019). Reprogrammed Marrow Adipocytes Contribute to Myeloma-Induced Bone Disease. *Sci. Transl. Med.* 11 (494), eaau9087. doi:10.1126/scitranslmed.aau9087

Liu, P., Ji, Y., Yuen, T., Rendina-Ruedy, E., DeMambro, V. E., Dhawan, S., et al. (2017). Blocking FSH Induces Thermogenic Adipose Tissue and Reduces Body Fat. *Nature* 546 (7656), 107–112. doi:10.1038/nature22342

Maridas, D. E., Rendina-Ruedy, E., Helderman, R. C., DeMambro, V. E., Brooks, D., Guntur, A. R., et al. (2019). Progenitor Recruitment and Adipogenic Lipolysis Contribute to the Anabolic Actions of Parathyroid Hormone on the Skeleton. *FASEB j.* 33 (2), 2885–2898. doi:10.1096/fj.201800948RR

Miggitsch, C., Meryk, A., Naismith, E., Pangrazzi, L., Ejaz, A., Jenewein, B., et al. (2019). Human Bone Marrow Adipocytes Display Distinct Immune Regulatory Properties. *EBioMedicine* 46, 387–398. doi:10.1016/j.ebiom.2019.07.023

Moore, S. G., and Dawson, K. L. (1990). Red and Yellow Marrow in the Femur: Age-Related Changes in Appearance at MR Imaging. *Radiology* 175 (1), 219–223. doi:10.1148/radiology.175.1.2315484

Mukohira, H., Hara, T., Abe, S., Tani-Ichi, S., Sehara-Fujisawa, A., Nagasawa, T., et al. (2019). Mesenchymal Stromal Cells in Bone Marrow Express Adiponectin and Are Efficiently Targeted by an Adiponectin Promoter-Driven Cre Transgene. *Int. Immunol.* 31 (11), 729–742. doi:10.1093/intimm/dxz042

Naveiras, O., Nardi, V., Wenzel, P. L., Hauschka, P. V., Fahey, F., and Daley, G. Q. (2009). Bone-marrow Adipocytes as Negative Regulators of the Haematopoietic Microenvironment. *Nature* 460 (7252), 259–263. doi:10.1038/nature08099

Oguro, H., Ding, L., and Morrison, S. J. (2013). SLAM Family Markers Resolve Functionally Distinct Subpopulations of Hematopoietic Stem Cells and Multipotent Progenitors. *Cell Stem Cell* 13 (1), 102–116. doi:10.1016/j.stem.2013.05.014

Onji, M., Werschler, N., and Penninger, J. (2021). A Critical Relationship between Bone and Fat: the Role of Bone Marrow Adipose-derived RANKL in Bone Metabolism. *EMBO Rep.* 22, e52986. doi:10.15252/embr.202152986

Ozcivici, E., Luu, Y. K., Adler, B., Qin, Y.-X., Rubin, J., Judex, S., et al. (2010). Mechanical Signals as Anabolic Agents in Bone. *Nat. Rev. Rheumatol.* 6 (1), 50–59. doi:10.1038/nrrheum.2009.239

Palumbo, A., and Anderson, K. (2011). Multiple Myeloma. *N. Engl. J. Med.* 364 (11), 1046–1060. doi:10.1056/NEJMra1011442

Picke, A.-K., Campbell, G. M., Blüher, M., Krügel, U., Schmidt, F. N., Tsourdi, E., et al. (2018). Thy-1 (CD90) Promotes Bone Formation and Protects against Obesity. *Sci. Transl. Med.* 10 (453), eaao6806. doi:10.1126/scitranslmed.aao6806

Poloni, A., Maurizi, G., Serrani, F., Mancini, S., Zingaretti, M. C., Frontini, A., et al. (2013). Molecular and Functional Characterization of Human Bone Marrow Adipocytes. *Exp. Hematol.* 41 (6), 558–566. e552. doi:10.1016/j.exphem.2013.02.005

Robino, J. J., Pamir, N., Rosario, S., Crawford, L. B., Burwitz, B. J., Roberts, C. T., Jr., et al. (2020). Spatial and Biochemical Interactions between Bone Marrow Adipose Tissue and Hematopoietic Stem and Progenitor Cells in Rhesus Macaques. *Bone* 133, 115248. doi:10.1016/j.bone.2020.115248

Rooney, A. M., and van der Meulen, M. C. H. (2017). Mouse Models to Evaluate the Role of Estrogen Receptor α in Skeletal Maintenance and Adaptation. *Ann. N.Y. Acad. Sci.* 1410 (1), 85–92. doi:10.1111/nyas.13523

Scheller, E. L., Cawthorn, W. P., Burr, A. A., Horowitz, M. C., and MacDougald, O. A. (2016). Marrow Adipose Tissue: Trimming the Fat. *Trends Endocrinol. Metab.* 27 (6), 392–403. doi:10.1016/j.tem.2016.03.016

Scheller, E. L., Doucette, C. R., Learman, B. S., Cawthorn, W. P., Khandaker, S., Schell, B., et al. (2015). Region-specific Variation in the Properties of Skeletal Adipocytes Reveals Regulated and Constitutive Marrow Adipose Tissues. *Nat. Commun.* 6, 7808. doi:10.1038/ncomms8808

Sebo, Z. L., Rendina-Ruedy, E., Ables, G. P., Lindskog, D. M., Rodeheffer, M. S., Fazeli, P. K., et al. (2019). Bone Marrow Adiposity: Basic and Clinical Implications. *Endocr. Rev.* 40 (5), 1187–1206. doi:10.1210/er.2018-00138

Sen, B., Xie, Z., Case, N., Thompson, W. R., Uzer, G., Styner, M., et al. (2014). mTORC2 Regulates Mechanically Induced Cytoskeletal Reorganization and Lineage Selection in Marrow-Derived Mesenchymal Stem Cells. *J. Bone Miner Res.* 29 (1), 78–89. doi:10.1002/jbmr.2031

Shafat, M. S., Oellerich, T., Mohr, S., Robinson, S. D., Edwards, D. R., Marlein, C. R., et al. (2017). Leukemic Blasts Program Bone Marrow Adipocytes to Generate a Protumoral Microenvironment. *Blood* 129 (10), 1320–1332. doi:10.1182/blood-2016-08-734798

Shen, W., Chen, J., Punyanitya, M., Shapses, S., Heshka, S., and Heymsfield, S. B. (2007). MRI-measured Bone Marrow Adipose Tissue Is Inversely Related to DXA-Measured Bone mineral in Caucasian Women. *Osteoporos. Int.* 18 (5), 641–647. doi:10.1007/s00198-006-0285-9

Shen, W., Velasquez, G., Chen, J., Jin, Y., Heymsfield, S. B., Gallagher, D., et al. (2014). Comparison of the Relationship between Bone Marrow Adipose Tissue and Volumetric Bone mineral Density in Children and Adults. *J. Clin. Densitom.* 17 (1), 163–169. doi:10.1016/j.jocd.2013.02.009

Suchacki, K. J., Tavares, A. A. S., Mattiucci, D., Scheller, E. L., Papanastasiou, G., Gray, C., et al. (2020). Bone Marrow Adipose Tissue Is a Unique Adipose Subtype with Distinct Roles in Glucose Homeostasis. *Nat. Commun.* 11 (1), 3097. doi:10.1038/s41467-020-16878-2

Suresh, S., de Castro, L. F., Dey, S., Robey, P. G., and Noguchi, C. T. (2019). Erythropoietin Modulates Bone Marrow Stromal Cell Differentiation. *Bone Res.* 7, 21. doi:10.1038/s41413-019-0060-0

Theill, L. E., Boyle, W. J., and Penninger, J. M. (2002). RANK-L and RANK: T Cells, Bone Loss, and Mammalian Evolution. *Annu. Rev. Immunol.* 20, 795–823. doi:10.1146/annurev.immunol.20.100301.064753

Tikhonova, A. N., Dolgalev, I., Hu, H., Sivaraj, K. K., Hoxha, E., Cuesta-Domínguez, Á., et al. (2019). The Bone Marrow Microenvironment at Single-Cell Resolution. *Nature* 569 (7755), 222–228. doi:10.1038/s41586-019-1104-8

Tokoyoda, K., Zehentmeier, S., Hegazy, A. N., Albrecht, I., Grün, J. R., Löhning, M., et al. (2009). Professional Memory CD4+ T Lymphocytes Preferentially Reside and Rest in the Bone Marrow. *Immunity* 30 (5), 721–730. doi:10.1016/j.immuni.2009.03.015

Ye, L., Fan, Z., Yu, B., Chang, J., Al Hezaimi, K., Zhou, X., et al. (2012). Histone Demethylases KDM4B and KDM6B Promotes Osteogenic Differentiation of Human MSCs. *Cell Stem Cell* 11 (1), 50–61. doi:10.1016/j.stem.2012.04.009

Yu, W., Zhong, L., Yao, L., Wei, Y., Gui, T., Li, Z., et al. (2021). Bone Marrow Adipogenic Lineage Precursors Promote Osteoclastogenesis in Bone Remodeling and Pathologic Bone Loss. *J. Clin. Invest.* 131 (2), e140214. doi:10.1172/jci140214

Yu, Y., Newman, H., Shen, L., Sharma, D., Hu, G., Mirando, A. J., et al. (2019). Glutamine Metabolism Regulates Proliferation and Lineage Allocation in Skeletal Stem Cells. *Cel Metab.* 29 (4), 966–978. e964. doi:10.1016/j.cmet.2019.01.016

Zhong, L., Yao, L., Tower, R. J., Wei, Y., Miao, Z., Park, J., et al. (2020). Single Cell Transcriptomics Identifies a Unique Adipose Lineage Cell Population that Regulates Bone Marrow Environment. *Elife* 9, e54695. doi:10.7554/eLife.54695

Zhou, B. O., Yu, H., Yue, R., Zhao, Z., Rios, J. J., Naveiras, O., et al. (2017). Bone Marrow Adipocytes Promote the Regeneration of Stem Cells and Haematopoiesis by Secreting SCF. *Nat. Cel Biol* 19 (8), 891–903. doi:10.1038/ncb3570

Zhou, B. O., Yue, R., Murphy, M. M., Peyer, J. G., and Morrison, S. J. (2014). Leptin-receptor-expressing Mesenchymal Stromal Cells Represent the Main

Source of Bone Formed by Adult Bone Marrow. *Cell Stem Cell* 15 (2), 154–168. doi:10.1016/j.stem.2014.06.008

Zinngrebe, J., Debatin, K.-M., and Fischer-Posovszky, P. (2020). Adipocytes in Hematopoiesis and Acute Leukemia: Friends, Enemies, or Innocent Bystanders? *Leukemia* 34 (9), 2305–2316. doi:10.1038/s41375-020-0886-x

Zou, W., Rohatgi, N., Brestoff, J. R., Li, Y., Barve, R. A., Tycksen, E., et al. (2020). Ablation of Fat Cells in Adult Mice Induces Massive Bone Gain. *Cel Metab.* 32 (5), 801–813. e806. doi:10.1016/j.cmet.2020.09.011

Conflict of Interest: The authors declare that the research was conducted in the absence of any commercial or financial relationships that could be construed as a potential conflict of interest.

Publisher's Note: All claims expressed in this article are solely those of the authors and do not necessarily represent those of their affiliated organizations, or those of the publisher, the editors, and the reviewers. Any product that may be evaluated in this article, or claim that may be made by its manufacturer, is not guaranteed or endorsed by the publisher.

frontiers in Cell and Developmental Biology

ORIGINAL RESEARCH
published: 03 December 2021
doi: 10.3389/fcell.2021.767006

Curculigoside Ameliorates Bone Loss by Influencing Mesenchymal Stem Cell Fate in Aging Mice

Na Wang[1,2†], Ziyi Li[1,2†], Shilun Li[3†], Yukun Li[1,2], Liu Gao[1,2], Xiaoxue Bao[1,2], Ke Wang[1,2], Chang Liu[1,2], Peng Xue[1,2] and Sijing Liu[4*]*

[1]Department of Endocrinology, The Third Hospital of Hebei Medical University, Shijiazhuang, China, [2]Key Orthopaedic Biomechanics Laboratory of Hebei Province, Shijiazhuang, China, [3]Department of Joint Surgery, The Third Hospital of Hebei Medical University, Shijiazhuang, China, [4]Editorial Department of Hebei Medical University, Hebei Medical University, Shijiazhuang, China

Senile osteoporosis is characterized by increased bone loss and fat accumulation in marrow. Curculigoside (CCG) is the major bioactive component of Curculigo orchioides, which has been used as anti-osteoporosis therapy for elder patients since antiquity. We aimed to investigate the underlying mechanisms by which CCG regulated the bone-fat balance in marrow of aging mice. In our study, CCG treatment was identified to interfere with the stem cell lineage commitment both *in vivo* and *in vitro*. *In vivo*, CCG promoted the transcriptional co-activator with PDZ-binding motif (TAZ) expression to reverse age-related bone loss and marrow adiposity. *In vitro*, proper concentration of CCG upregulated TAZ expression to increase osteogenesis and decrease adipogenesis of bone marrow mesenchymal stem cells (BMSCs). This regulating effect was discounted by TAZ knockdown or the use of MEK-ERK pathway inhibitor, UO126. Above all, our study confirmed the rescuing effects of CCG on the differential shift from adipogenesis to osteogenesis of BMSCs in aging mice and provided a scientific basis for the clinical use of CCG in senile osteoporosis.

Keywords: osteoporosis, curculigoside, BMSCs, TAZ, MEK-ERK pathway

OPEN ACCESS

Edited by:
Ce Dou,
Army Medical University, China

Reviewed by:
Jiacan Su,
Second Military Medical University, China
Yinhe Wang,
Nanjing University Medical School, China

***Correspondence:**
Peng Xue
hebmuxuepeng@163.com
Sijing Liu
hbydxbl@126.com

[†]These authors have contributed equally to this work and share first authorship.

Specialty section:
This article was submitted to Cellular Biochemistry, a section of the journal Frontiers in Cell and Developmental Biology

Received: *30 August 2021*
Accepted: *05 November 2021*
Published: *03 December 2021*

Citation:
Wang N, Li Z, Li S, Li Y, Gao L, Bao X, Wang K, Liu C, Xue P and Liu S (2021) Curculigoside Ameliorates Bone Loss by Influencing Mesenchymal Stem Cell Fate in Aging Mice. Front. Cell Dev. Biol. 9:767006. doi: 10.3389/fcell.2021.767006

INTRODUCTION

Osteoporosis is increasingly recognized as a major health concern that affects approximately 50% of women and 20% of men over 50 years old (Sambrook and Cooper, 2006). This age-related systemic impairment of bone loss is characterized by decreased osteogenesis and increased adiposity in bone marrow, resulting in more propensity of fragility fracture (Hu et al., 2018; Sanghani-Kerai et al., 2018; Zanker and Duque, 2019). Bone marrow mesenchymal stem cells (BMSCs) could differentiate to osteoblasts or adipocytes. They held a competition relationship during BMSCs' differentiation (Ambrosi et al., 2017; Muruganandan et al., 2017). The process of stem cell fate determination is constantly changing, and consists of self-renewal and terminal differentiation (Hansen et al., 1999; Dalton, 2015; Urbach and Witte, 2019). Various exogenous and endogenous factors could alter the differentiation switch from adipogenesis to osteogenesis of BMSCs context-dependently (Teitelbaum, 2010; Huang et al., 2018; Wang et al., 2019a). However, the underlying mechanism has not been clearly addressed.

Curculigo orchioides, a small herbal plant belonging to the family Amaryllidacea, has been used as an anti-osteoporosis herb in many Asian countries (Wang et al., 2012; Wu et al., 2012; Tan et al., 2019). The

extracts of this plant contain a wide variety of flavonoids, phytosterols, and phenolic compounds, with curculigoside (CCG) identified as the main active substance (Wang et al., 2017). *In vivo* study, CCG was reported to distribute widely in bone marrow and many other tissues after oral administration (Yuan et al., 2015). Cao et al. (2008) discovered that oral administration of CCG prevented bone loss in the tibia of the ovariectomized rats. As was demonstrated, CCG could up-regulate VEGF expression, reverse iron-overload via GPX4, relieve oxidative stress via Akt-FoxO1 axis, and reduce inflammation via NF-κβ signaling transduction to favor the bone remodeling *in vivo* and *in vitro* (Cao et al., 2008; Ma et al., 2011; Tan et al., 2019; Zhang et al., 2019; Wang et al., 2020). In our research, we tried to elucidate if and how CCG switch the differentiation from adipogenesis to osteogenesis of BMSCs in aging mice.

Senile osteoporotic patients often showed an increased adipogenesis in their bone marrow with a reduction of osteoblastogenesis (Rosen et al., 2009). Transcriptional co-activator with PDZ-binding motif (TAZ) has been demonstrated as a nuclear transcription factor playing crucial roles in stem cell differentiation (Kegelman et al., 2018; Wang et al., 2018; Tan and Dai, 2019). As was proved, TAZ combined to runt-related transcription factor 2 (RUNX2) to promote osteogenesis, and interacted with peroxisome proliferator-activated receptorγ (PPARγ) to suppress adipogenesis (Byun et al., 2013; Matsumoto et al., 2016; Wang et al., 2019b). Besides, TAZ has neuro-protection, angiogenesis, and anti-oxidative stress effects, which were important for bone nutrition and regeneration (Lee et al., 2019; Chen et al., 2021; Jeanette et al., 2021). Yu et al. (2018) revealed that PGC-1 alpha targeted TAZ to alter bone-fat balance during skeletal aging. Previously, our study also pointed a molecular link of MEK-ERK pathway to the TAZ during BMSCs osteogenesis (Wang et al., 2018; Wang et al., 2019a). As the MEK-ERK signaling pathway has been intensively investigated in regulating cells differentiation, it exerts our interest on the role of MEK-ERK/TAZ axis in the CCG-mediated differentiation of BMSCs during aging.

Molecular interactions and protein networks of CCG could predict the functions of its compounds as an anti-osteoporotic drug in clinical. However, the underlying mechanisms whereby CCG promotes osteogenesis in bone marrow have not been well established. In this study, we found that CCG induced the switch from adipogenesis to osteogenesis of BMSCs in aging mice and ameliorated the age-related bone loss by influencing the osteoblasts-adipocytes lineage commitment of BMSCs via MEK/ERK-TAZ interaction axis. Altogether, these findings provided a scientific basis for the clinical use of CCG in the geriatric population.

MATERIALS AND METHODS

Mice and *In Vivo* Treatment

Our experiments were approved by the Local Committee of Animal Use and Protection of the Third Hospital of Hebei Medical University. C57BL/6 mice were bred in a room with the environmental temperature ranging from 20 to 24°C and proper humidity ranging from 30 to 70%. The mice had either free access to food or water. The 3-months mice were regarded as the normal control group. In addition, the three groups of 16-months mice would be received vehicle, 50 mg/kg/d or 100 mg/kg/d CCG (Shanghai Standard Biotech, Shanghai, China) by oral administration, respectively, for 2 months. After the 2 months treatment, we considered the above three groups as 18-mon, 50 mg-CCG, and 100 mg-CCG group.

Micro-Computed Tomography (μCT) Analyses

We fixed the harvested femurs in 4% paraformaldehyde (4°C, 24 h). We used the SkyScan μCT scanner to analyze the bone parameters with 65 kv voltage and 153 μA current. Each image was obtained with high resolution of 9.0 μm per pixel. We used NRecon for image reconstruction (version 1.6), CTAn (version 1.9) for data analysis, and CTVol (version 2.0) for 3D model visualization. With 3D analysis, we collected bone parameters of trabecular bone volume fraction (BV/TV), trabecular bone thickness (Tb.Th), trabecular bone number (Tb.N), and trabecular bone separation (Tb.Sp) to represent the femur character in this part.

OsO4 Staining and μCT Analysis

We decalcified the long bone in 0.5 M EDTA for 21 days. We cut off the proximal of femurs and then discarded it. The rest of the femur was incubated in aqueous osmium tetroxide (OsO4) (2%, 2 h). Then we rinsed the tissues for 48 h and scanned them by using μCT (9-μm pixel; 45kV, 177 μA). The number and the volume of adipocytes (ad. N; ad. V) in bone marrow were quantified for inter-group analyses in this part.

Hematoxylin and Eosin and Tartrated Resistant Acid Phosphatase Staining

After 3-weeks decalcification of the femur samples, we embedded them in paraffin and cut them into 4 μm-thick slices for H&E and TRAP staining. The adipocyte number relative to bone marrow area was then collected for inter-group analysis based on the H&E staining; and the osteoclast (OC) numbers were calculated via TRAP staining.

Immunofluorescence Assay

Harvested femurs were decalcified by 0.5 M EDTA. The tissues were embedded in gelatin (at a concentration of 8%) with sucrose (at a concentration of 20%) in the presence of polyvinylpyrrolidone (at a concentration of 2%). We sliced the tissues into 20 μm-thick sections. Subsequently, we blocked the samples, treated the samples with primary antibodies (the antibodoy for TAZ, 1:200, Abcam; for OCN, 1:200, R&D; for perilipin, 1:400, Sigma), and incubated them with secondary antibodies.

Cell Isolation and Culture

We euthanized the mice and dissected the bilateral femurs as well as tibias to collect the marrow cells. Then we planted the cells in Dulbecco's modified Eagle's medium (DMEM) with fetal bovine serum (FBS, 12%). BMSCs at passage three were incubated with the antibody of CD34, CD45, CD29, and CD90 (Thermo Fisher Scientific, United States) in phycoerythrin and sorted by flow

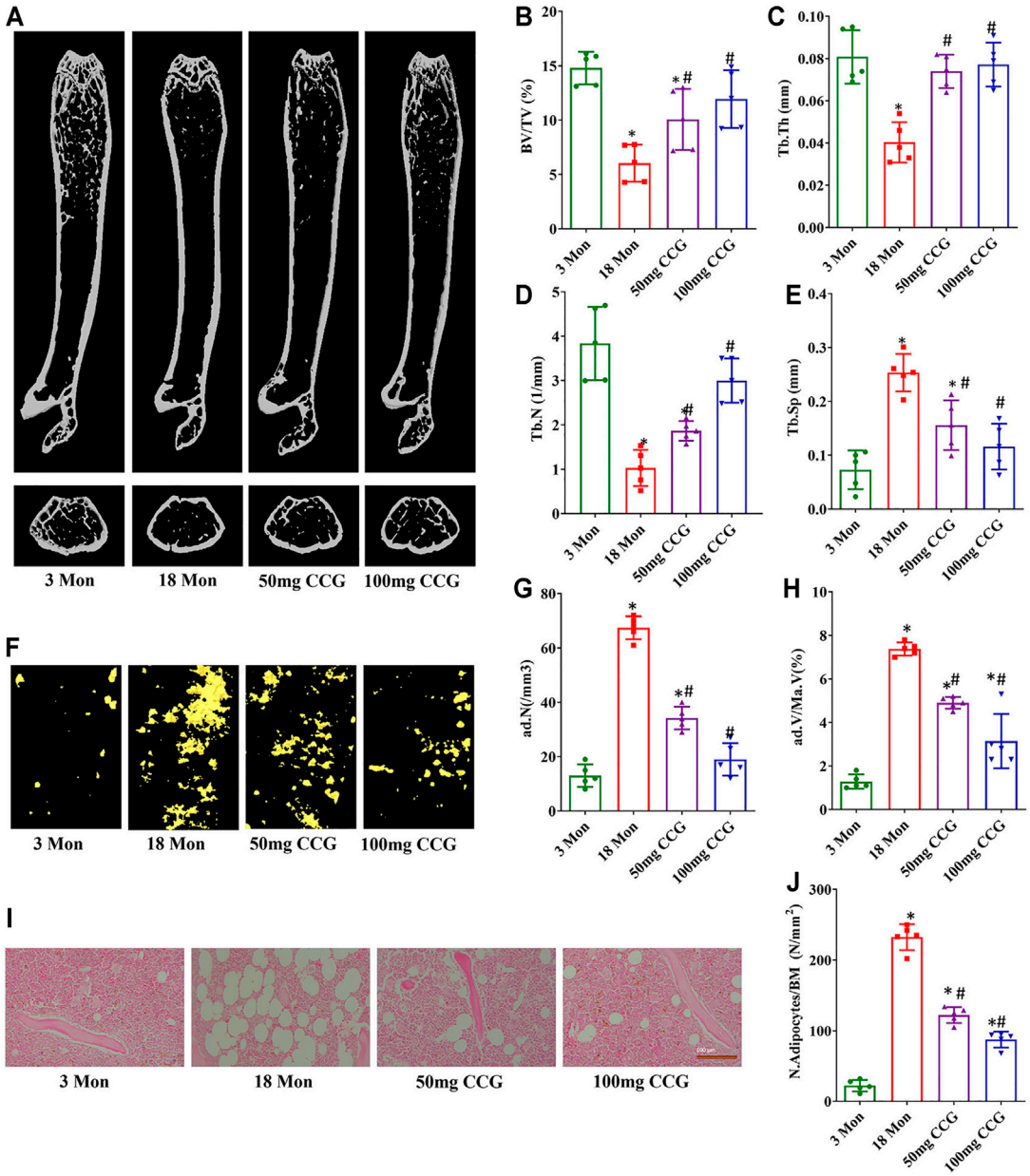

FIGURE 1 | CCG ameliorated bone loss and marrow adiposity of aging mice. **(A–E)** Representative μ-CT images of femurs from the animals in different groups to acquire the quantitative analysis of trabecular bone. **(F–H)** Representative μ-CT images of OsO_4 staining of femurs from the animals in different groups to acquire the quantitative analysis of the volume of adipocytes. **(I, J)** Representative images of H&E staining to show the ratio of adipocyte number to the area of bone marrow. Scale bar: 100 μm (n = 5) *$p < 0.05$ vs. the 3-mon mice group; #$p < 0.05$ vs. the 18-mon mice group.

cytometry by different cell fluorescence for identification. To identify the effect of CCG on cell cycles, 3 days treated cells were harvested and fixed with 70% ethanol. After washing in PBS, cells were stained with propidium iodide (Sigma, United States) (5 mg/ml) for 30 min in the dark at 4°C. Fluorescence was measured with the flow cytometer equipped with a 570-nm argon ion laser (Epics XL, Beckman Coulter Corporation, FL) and the data were analyzed using the Muticycle AV software.

Cell Differentiation

For one thing, we mixed β-glycerophosphoric acid (10 mM, Sigma), dexamethasone (10 nM, Sigma), and ascorbic acid (50 μg/ml, Sigma) with the growth medium to induce osteogenesis. For another thing, we added dexamethasone (1 μM, Sigma), insulin (10 mg/ml, Sigma), and methyl isobutylxanthine (500 mM, Sigma) to the growth medium to induce adipogenesis.

CCG Administration *In Vitro*

We sub-cultured the cells that reached approximately 80% confluence into a new flask and replaced the growth medium with differential medium in the absence or presence of CCG (10, 100, or 1000 μM). Then, we selected an appropriate concentration of CCG for the next research part.

Cell Viability Assay

The cells were incubated with MTT (5 mg/ml, Solarbio) to form crystals. We then added dimethyl sulfoxide (DMSO, Solarbio) to fully dissolve the crystals in 10 min. At a wavelength of 490 nm, we measured the absorbance by using the microplate spectrophotometer (BioTek Instruments, United States) to acquire the cell viability assay.

Plasmid Transfection

We used the plasmid mixed with small interfering RNA sequences for gene knockdown research. The designed and synthesized SiTAZ was used to knock down the TAZ expression (Genechem, China). We used the Lipofectamine 3000 (Thermo Fisher Scientific) for transfection. After 24 h, the transfected cells were ready for the subsequent experiments. Furthermore, we measured the transfection efficiency using flow cytometry (Epics XL, Beckman Coulter Corporation, United States). The sequences of SiTAZ were:

5′-GATCCCCTGGACCAAGTATATGAACCACTCGAG
TGGTTCATATACTTGGTCCAGTTTTTGGAT-3′;
5′-AGCTATCCAAAAACTGGACCAAGTATATGAACC
ACTCGAGTGGTTCATATACTTGGTCCAGGG-3′.

Alizarin Red Staining

We conducted the AR-S after 14-days treatment of osteogenic cocktail. We washed the cells and fixed them with 4% paraformaldehyde. Then we incubated the washed cells with AR (0.1%, Sigma). Then, the cells were de-stained with 10% cetylpyridinium chloride (Sigma) for AR quantification. We detected the OD value at 562 nm wavelength to calculate the calcium concentrations.

Oil Red O Staining

We conducted the oil red O staining after 14-days treatment of the adipogenic medium. The cells were then incubated with oil red O solution (0.5%, Sigma). After fully washed, we acquired the staining images using the microscope. Then we de-stained the treated cells with isopropanol in PBS for quantification study. We detected the OD value at 520 nm wavelength to calculate the lipid droplets using the microscope (Leica).

Real-Time Reverse Transcription-Polymerase Chain Reaction

We extracted the total RNA using TRIzol® reagent (Ambition, United States). A total of 1 μg RNA was reversed-transcribed by using cDNA synthesis Kit (Thermo Fisher Scientific). Real-time RT-PCR was performed on a CFX96 Real-Time PCR Detection System (Bio-Rad, Hercules, CA) using SuperReal PreMix Plus (TIANGEN, Beijing, China). All primers were synthesized by Invitrogen (Carlsbad, CA). The relative expression of mRNAs was calculated according to the ratio of the copy numbers of the target genes (TAZ, RUNX2, OCN, PPARγ, perilipin) to the housekeeping gene GAPDH in each sample. The relative gene expression values were evaluated by the 2-△△Ct method [24]. Forward and reverse primers are listed in **Supplementary Table S1**.

Western Blotting Analysis

We isolated the proteins from the treated cells seeded in 60-mm plastic dishes. We separated the target proteins using 12% sodium dodecyl sulfate polyacrylamide gel electrophoresis (SDS-PAGE; Costar) and transferred them into a polyvinylidene fluoride (PVDF; Costar) membrane. Membranes were blocked with 5% milk and incubated with primary antibodies against TAZ (1:200; Abcam), RUNX2 (1:200; Cell Signaling), OCN (1:200; Takara Bio), PPARγ (1:100; Cell Signaling), perilipin (1:400; Abcam), p-ERK (1:100; Cell Signaling), ERK (1:100; Cell SignalingA), or GAPDH (1:200, Bioworld, United States). Then we induced the conjugated secondary antibody (IRDye800®, 1:2000, Rockland, United States) and scanned the samples using the Odyssey Infrared Imaging System (Li-COR Biosciences, Beijing, China). ImageJ (version 1.46) was used to determine the integrated intensity of the detected band (Tan and Dai, 2019).

Statistics

Quantitative results were expressed as mean ± standard deviation (SD). *In vivo*, there were five mice in each group; *in vitro*, all experiments were replicated at least three times. Independent samples *t*-test for the comparison of two groups, one-way analysis of variance (ANOVA) followed by Student Newman Keuls (S-N-K) post hoc analysis for the parametric data among multiple groups, which were performed by using SPSS (v.21.0). Values were considered statistically significant at $p < 0.05$.

RESULTS

CCG Ameliorated Bone Loss and Reduced Marrow Adiposity of Aging Mice

We used μCT to analyze the trabecular bone structure as well as the marrow adipose tissue volume. The BV/TV, Tb.Th, and Tb.N of the femur bone significantly decreased in the 18-mon mice relative to the 3-mon mice, and the Tb. Sp in marrow significantly increased in the 18-mon mice compared with the 3-mon mice (**Figures 1A–E**). Simultaneously, fat was significantly accumulated with aging, which was demonstrated by more lipid droplets stained with osmium tetroxide (OsO_4) in the marrow (**Figures 1F–H**). After oral administration with 50 mg/kg/d or 100 mg/kg/d CCG for 2 months, the age-related bone loss and fat accumulation by aging were markedly reduced. First, the μCT results showed an increased bone formation compared with the 18-mon group (**Figures 1A–E**). Second, a significantly lower amount of fat droplets appeared in 50 mg/kg/d or 100 mg/kg/d CCG administration group (**Figures 1F–H**). Similarly, H&E staining calculated a lower number of adipocytes after oral administration of CCG (**Figures 1I,J**). These data suggested that oral administration of CCG

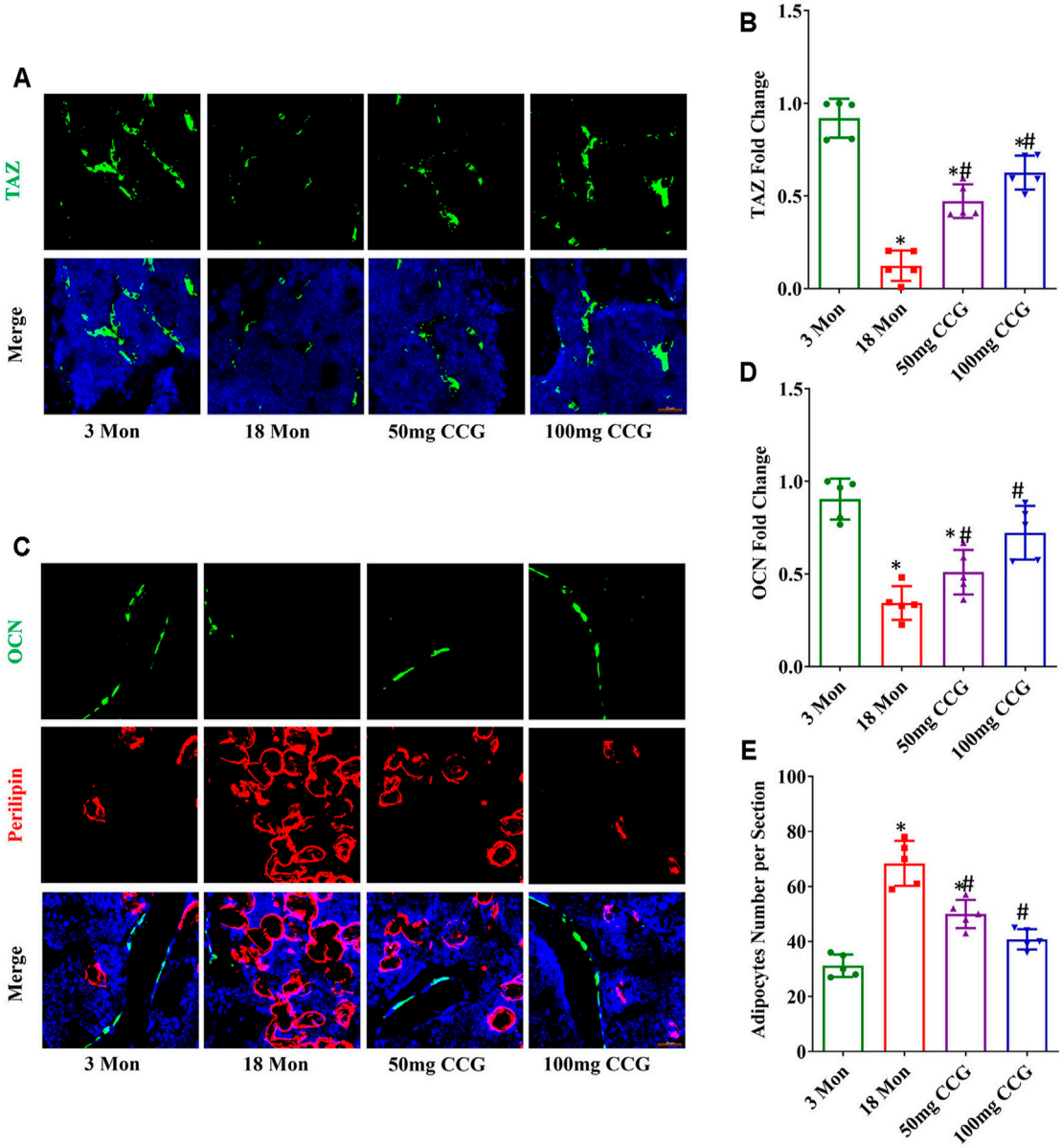

FIGURE 2 | CCG targeted TAZ to regulate the switch from adipogenesis to osteogenesis of BMSCs *in vivo*. **(A, B)** Representative images and quantitative analysis of TAZ (green) expression in the mice femurs from different groups. **(C–E)** Immunofluorescent staining of OCN (green) and perilipin (red) in the mice femurs and the relevant quantitative analysis. Scale bar: 50 μm (n = 5) *$p < 0.05$ vs. the 3-mon mice group; #$p < 0.05$ vs. the 18-mon mice group.

ameliorated bone loss and marrow adiposity of aging mice. Furthermore, CCG was demonstrated to inhibit osteoclasts formation by TRAP staining (**Supplementary Figure S1**).

CCG Increased TAZ Expression to Regulate Switch from Adipogenesis to Osteogenesis in Bone Marrow

TAZ expression was decreased with aging, while 50 mg/kg/d or 100 mg/kg/d dose of CCG offset the age-related down-expression of TAZ (**Figures 2A,B**). Consequently, we found a decreased expression of osteocalcin (OCN) (the marker for osteogenesis) and an increased expression of perilipin (the marker for adipogenesis) in aging mice (**Figures 2C–E**). CCG administration ameliorated the down-expression of OCN and decreased the up-expression of perilipin in aging mice (**Figures 2C–E**). Above all, we speculated that CCG targeted TAZ to regulate the switch from adipocytes to osteoblasts of BMSCs. In order to confirm our hypothesis, we conducted experiments *in vitro* study.

CCG Targeted TAZ to Facilitate Osteogenic Differentiation of BMSCs *In Vitro*

The hematopoietic surface markers CD34, CD45, CD29, and CD90 were detected to identify the BMSCs (**Supplementary Figure S2**). Then, we performed MTT assays and found that the cell viabilities were decreased after 1000 μM CCG treatment but increased after administration with 100 μM of CCG. Of interest, 10 μM CCG did not influence the cell viability (**Figure 3A**). To verify whether the administration of 100 μM CCG influenced the proliferation of BMSCs, we calculated the percentage of the cells in the G1 phase with the flow cytometer after 3 days' treatment. As a result, we found that the percentage of the cells in the G1 phase did not change after the CCG treatment (**Supplementary Figure S3**).

In order to confirm whether CCG had anti-aging effects, we identified the expression of p21 and p16 using real-time RT PCR analyses. We found that the CCG treatment induced the down-expression of p21 and p16 (**Supplementary Figure S4**). Further, CCG was proved to facilitate the most osteogenesis at the concentration of 100 μM. On one hand, 100 μM of CCG accelerated the calcium deposition evidenced by AR-S experiment (**Figures 3B,C**). On the other hand, the highest mRNA levels of RUNX2 and OCN expressed in 100 μM CCG group (**Figures 3D,E**). Thus, 100 μM CCG was administrated on cells in the subsequent experiments. Inevitably, 100 μM of CCG markedly increased the expression of TAZ, RUNX2, and OCN on Day 3, 7, and 14 (**Figures 3F–I**). Meanwhile, the adipogenic markers were down-regulated during osteogenesis by CCG treatment (**Supplementary Figure S5A**). Then, the TAZ expression was knocked down by transfecting with plasmids containing SiTAZ sequences (**Figures 3J–L**). SiTAZ significantly offset the CCG induced up-expression of the markers for osteogenesis, RUNX2, and OCN (**Figures 3M–Q**). Moreover, the AR-S results suggested SiTAZ delayed the recruitment of osteogenic nodules by CCG (**Figures 3R, S**). Above all, CCG might facilitate osteogenesis by targeting TAZ with a peak at the concentration of 100 μM for BMSCs differentiation.

CCG Targeted TAZ to Reduce Adipogenic Differentiation of BMSCs *In Vitro*

As well, we performed MTT assays and found that the cell viabilities were decreased after 1000 μM CCG administration but increased after administration with 100 μM of CCG during adipogenic differentiation of BMSCs, and 10 μM CCG did not influence the cell viability (**Figure 4A**). The Oil Red O staining results demonsrated that 100 μM of CCG decreased the lipid droplets during adipogenesis on Day 14 (**Figures 4B,C**). Consistently, the lowest mRNA levels of PPARγ and perilipin but the highest TAZ expression appeared in 100 μM CCG group during adipogenesis (**Figures 4D,E**). Meanwhile, the osteogenic markers were up-regulated during the administration of CCG treatment (**Supplementary Figure S5B**). Thus, 100 μM CCG was also administrated on cells in the subsequent experiments during adipogenesis. Inevitably, the expression of PPARγ and perilipin was markedly decreased and the TAZ protein levels were significantly increased by 100 μM CCG administration during adipogenesis (**Figures 4F–I**). Then the TAZ expression was knocked down by transfecting with plasmids containing SiTAZ sequences (**Figures 4J–L**). Both at the mRNA and protein levels, TAZ knockdown markedly lessened the CCG induced down-expression of PPARγ and perilipin (**Figures 4M–Q**). Accordingly, the Oil Red O staining also points a link between CCG treatment and TAZ signaling transduction during adipogenesis of BMSCs (**Figures 4R, S**). Taken together, we hypothesized that CCG targeted TAZ to reduce marrow adiposity *in vitro*.

CCG Activated p-ERK Signal to Modulate TAZ Expression and BMSCs Lineage Commitment

To elucidate the signaling transduntion, we conducted inhibitor study using pathway inhibitors. We found that the up-expression of TAZ induced by CCG administration was significantly diminished by UO126, rather than LY294002 (**Figures 5A–C**). Furthermore, the p-ERK/ERK ratio could be augmented by CCG, suggesting CCG could stimulate the MEK-ERK signaling transduction during osteogenesis (**Figures 5D–F**). Additionally, the AR-S results reflected that UO126 attenuated the formation of osteogenic nodules accelerated by CCG (**Figures 5G,H**). Similar results were confirmed during adipogenesis to that during osteogenesis (**Figure 6**). We concluded that the MEK-ERK signaling pathway was involved in the CCG-TAZ axis to facilitate osteogenesis at the expense of adiposity in bone marrow for anti-aging related osteoporosis.

DISCUSSION

Osteoporosis is recognized as a common concern in the aging population worldwide (Curtis et al., 2015). Osteogenesis reduction and fat accumulation triggered an imbalance of bone remodeling (Infante and Rodríguez, 2018). With aging progressing, senile osteoporosis becomes a growing public problem. The importance of developing new anti-osteoporosis therapies targeted at osteoblasts not only to increase bone formation and induce bone growth, but also to prevent age-related fat accumulation (Li et al., 2015). Increasing evidences bestow Chinese herbs vital roles in the therapy of osteoporosis and bone fracture, with Curculigo orchioides identified as widely used in senile osteoporosis (Wang et al., 2012; Wu et al., 2012; Tan et al., 2019). The potential biological functions and molecular mechanisms of the effects of CCG, the major bioactive component of Curculigo orchioides, on the switch from adipocytes into osteoblasts in aging mice has never been reported.

In our present study, the μCT analyses revealed that oral administration of CCG ameliorated the bone loss and marrow adiposity in the bone of aging mice. Previously, researchers

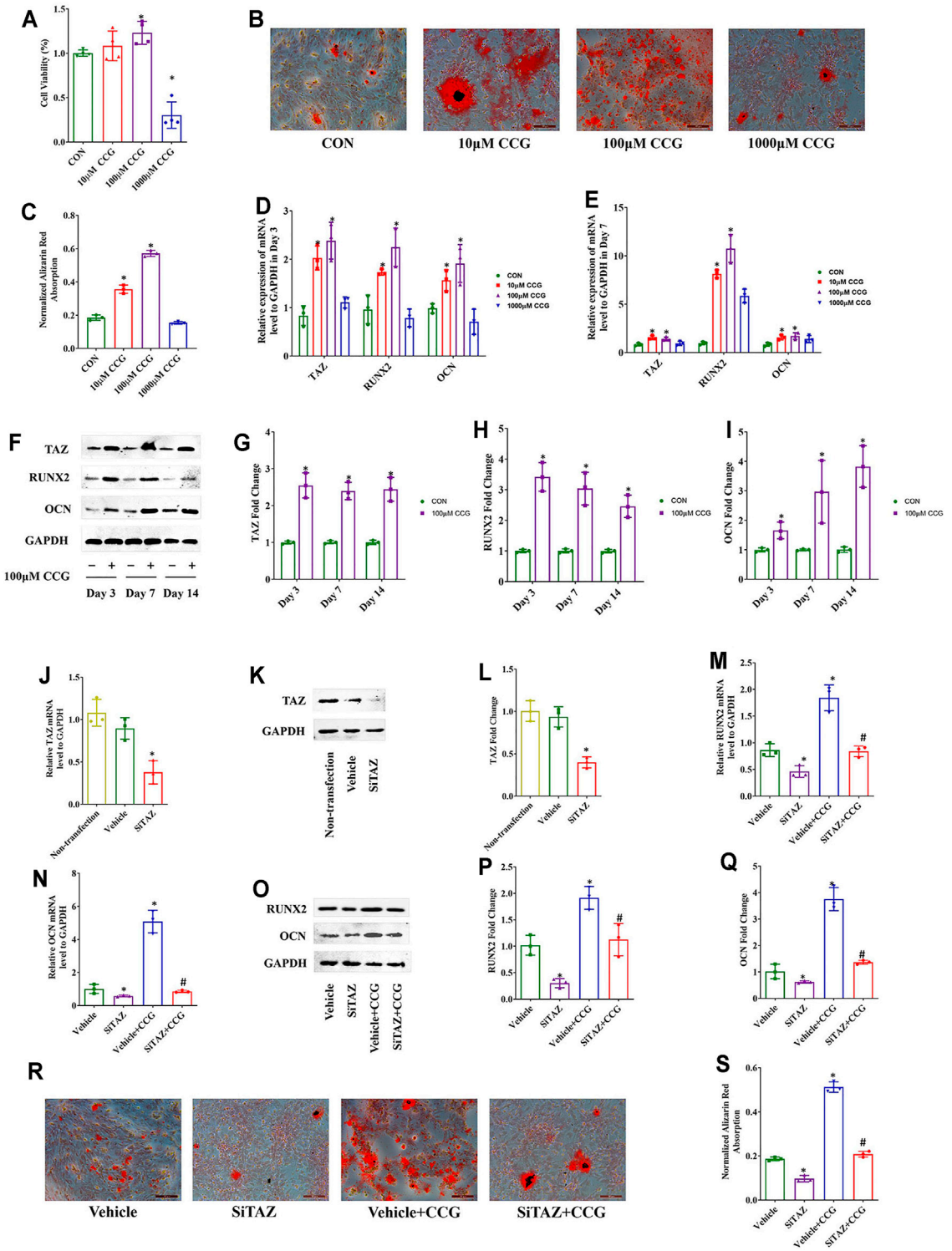

FIGURE 3 | CCG targeted TAZ to facilitate osteogenic differentiation of BMSCs *in vitro*. **(A)** MTT assays presented cell viabilities after CCG administration during osteogenesis of BMSCs. **(B, C)** Representative images of AR-S results in different mice groups. Scale bar: 100 μm. **(D, E)** Relative mRNA levels of TAZ, RUNX2, and OCN with or without CCG treatment. **(F–I)** TAZ, RUNX2, and OCN expression in protein levels with or without CCG treatment. **p* < 0.05 vs. the control group. **(J–L)** SiTAZ plasmid significantly knocked down the mRNA and protein levels of TAZ during the osteogenesis of BMSCs. **(M–Q)** SiTAZ discounted the CCG induced up-regulation of RUNX2 and OCN. **(R, S)** Representative images of AR-S showed the differences of calcium deposits in different groups. Bar graphs showed the means ± SD from three independent experiments. Scale bar: 100 μm (n = 3) **p* < 0.05 vs. the Vehicle group; #*p* < 0.05 vs. the Vehicle + CCG group.

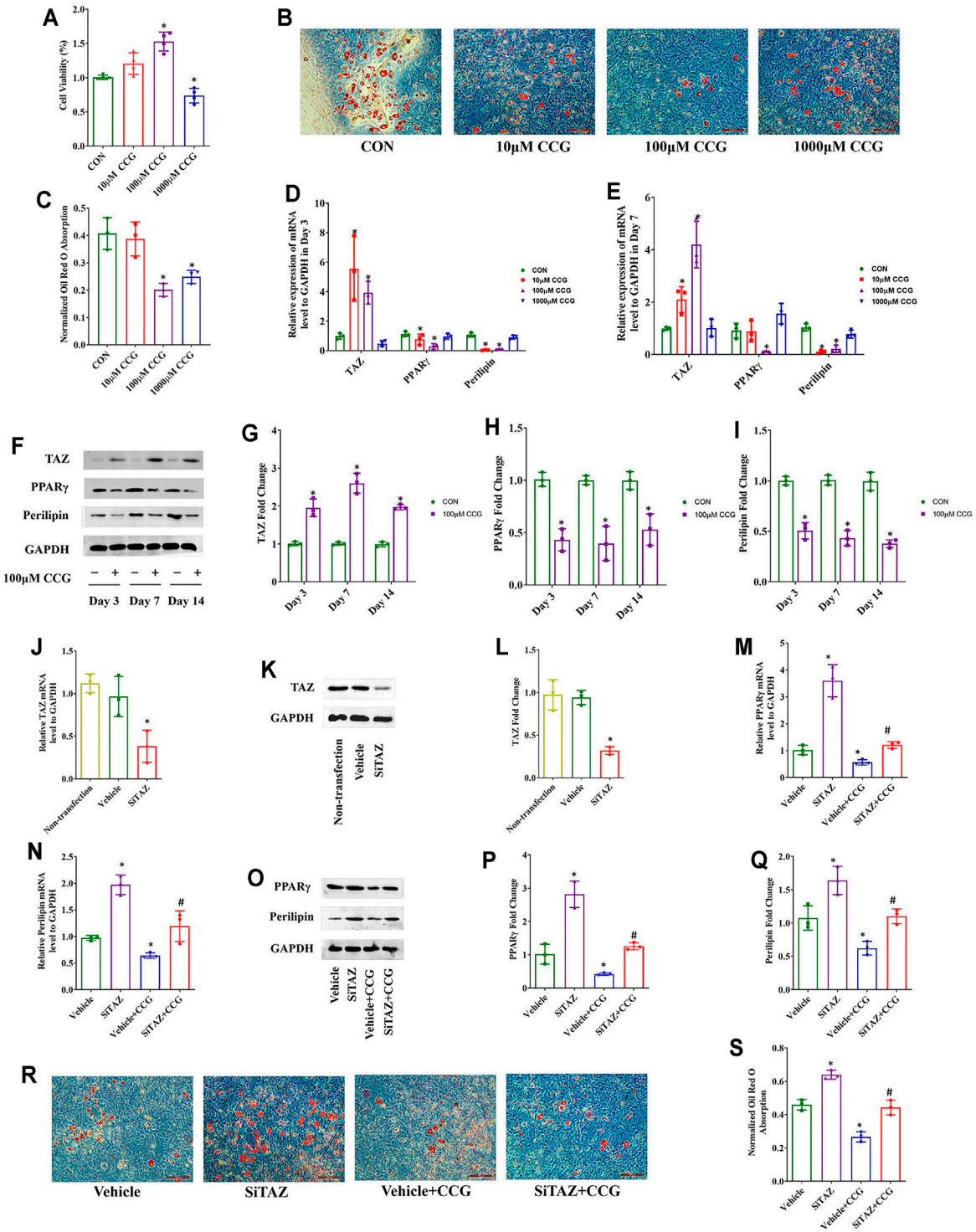

FIGURE 4 | CCG targeted TAZ to reduce adipogenic differentiation of BMSCs *in vitro*. **(A)** MTT assays presented cell viabilities after CCG administration during adipogenesis of BMSCs. **(B, C)** Representative images of Oil Red O staining reflected the lipid droplets. Scale bar: 100 μm. **(D, E)** Relative mRNA levels of TAZ, PPARγ, and perilipin to GAPDH were presented in Day 3 and Day 7 in the absence or presence of CCG during adipogenesis. **(F–I)** Relative protein levels of TAZ, PPARγ, and perilipin to GAPDH were presented in Day 3, in Day 7, and in Day 14 after the treatment. *$p < 0.05$ vs. the control group. **(J–L)** Relative mRNA and protein levels to GAPDH of TAZ were significantly knocked down by the SiTAZ plasmid during adipogenesis. **(M–Q)** SiTAZ discounted the CCG induced up-expression of TAZ and down-expression of PPARγ and perilipin at Day 3 after the treatment. **(R, S)** Representative images of Oil Red O staining showed the lipid droplets in different groups. Bar graphs showed the means ± SD from three independent experiments. Scale bar: 100 μm (n = 3) *$p < 0.05$ vs. the Vehicle group; #$p < 0.05$ vs. the Vehicle + CCG group.

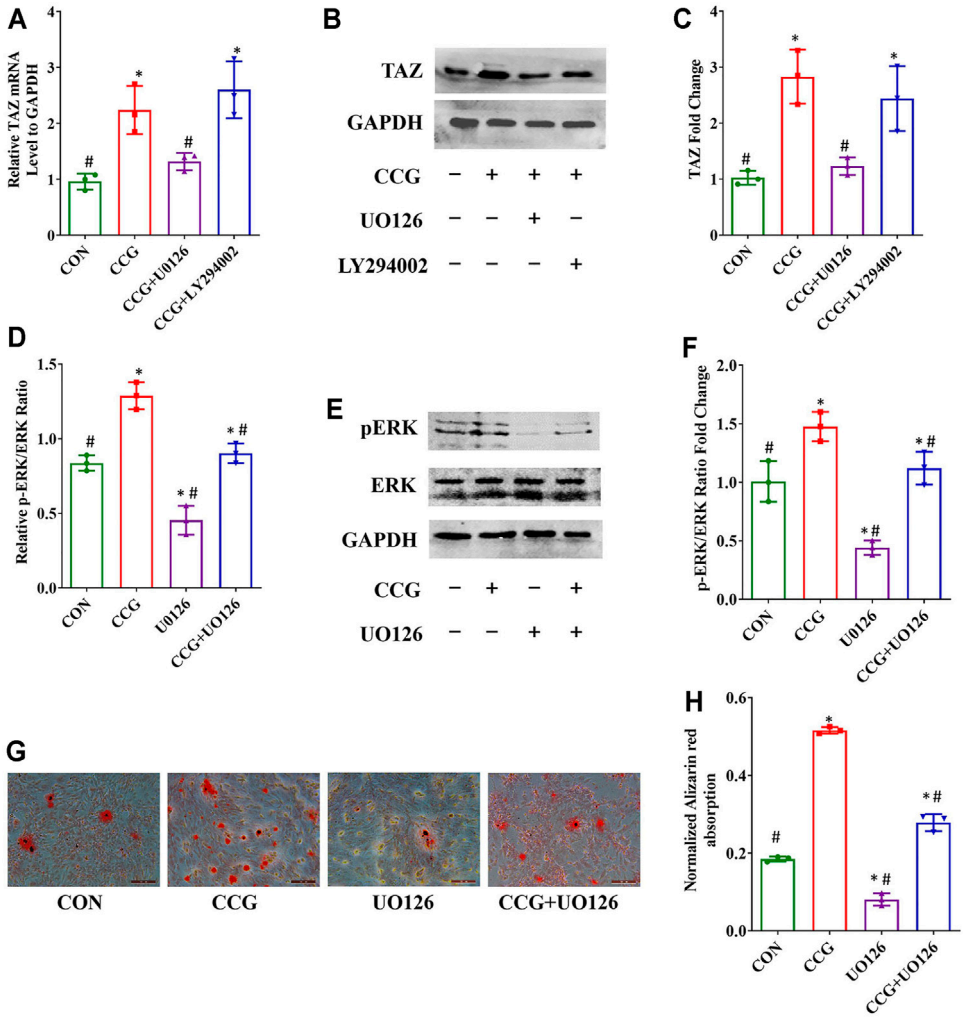

FIGURE 5 | Osteogenic differentiation and TAZ expression were increased by CCG treatment by increasing the p-ERK/ERK ratio. **(A–C)** Relative mRNA and protein levels to GAPDH of TAZ at Day 3 in different groups. **(D–F)** Relative mRNA and protein levels of p-ERK at Day 3 in different groups. **(G, H)** Representative images of AR-S showed the calcium deposits were influenced by CCG treatment. Scale bar: 100 μm *$p < 0.05$ vs. the control group (cells cultured in osteogenic medium during osteogenesis); #$p < 0.05$ vs. the CCG administration group.

reported that CCG prevented bone loss in ovariectomized rats (Shen et al., 2013). Consistently, other researchers have demonstrated that CCG stimulated the secretion of bone morphogenetic protein 2 (BMP-2) to promote osteogenesis (Ma et al., 2011). As was reported, CCG also prevented oxidative damage and inhibited osteoclastogenesis in rat bone marrow cells (Wang et al., 2012). As well, our study provided new insight into the molecular mechanisms how CCG regulates the age-related adipocytes-osteoblasts lineage commitment through MEK/ERK-TAZ axis. Thus, CCG might be a good candidate for further development as an anti-osteoporotic remedy in an aging population.

Latent bone-lining osteoblast-adipocyte precursors, including BMSCs, are activated in response to various stimuli including exogenous and endogenous changes causing pre-osteoblasts to increase surface expression of osteogenic markers at the expense of reduced adipogenic markers (Paspaliaris and Kolios, 2019). In addition, the microenvironment significantly affects bone mass by the regulation of vital factors (Du et al., 2019). For instance, TAZ exerted pivotal effects on stem cell fate determination (Panciera et al., 2017; Salem and Hansen, 2019; Zheng and Pan, 2019). In our previous study, we confirmed TAZ as an important transcriptional modulator during osteoblastogenesis, which was evoked by insulin-like growth factor 1 (IGF-1) (Xue et al., 2013). In the present study, we confirmed that the TAZ signaling was involved in the regulation of the differential shift from adipogenesis to osteogenesis by CCG. *In vivo*, the down-expression of TAZ in aging mice was ameliorated by the oral administration of CCG with up-expression of osteogenic genes and down-expression of adipogenic genes. *In vitro*, TAZ knockdown could offset CCG-regulated expression of osteogenic genes and adipogenic genes. Hereby, our results suggested that CCG influenced the

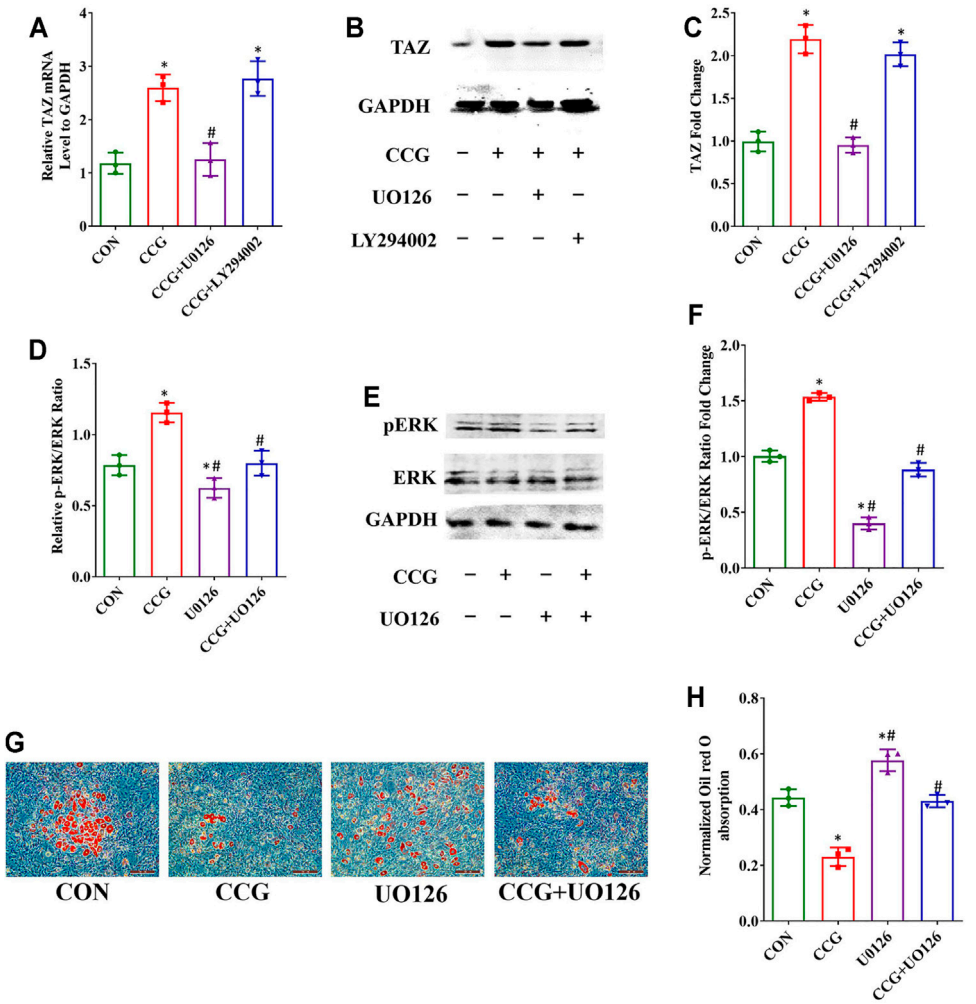

FIGURE 6 | Decreased adipogenic differentiation accompanied by increased TAZ expression was also mediated by p-ERK/ERK signaling after CCG treatment. **(A–C)** Relative mRNA and protein levels of TAZ to GAPDH at Day 3 after the treatment during adipogenesis. **(D–F)** Relative mRNA and protein levels of p-ERK at Day 3 after the treatment during adipogenesis. **(G, H)** Representative images of Oil Red O staining showed the lipid droplets were lessened by CCG. Scale bar: 100 μm (n = 3) *$p < 0.05$ vs. the control group (cells cultured in adipogenic medium during adipogenesis); #$p < 0.05$ vs. the CCG treatment group.

age-related switch of cells lineage commitment of BMSCs via TAZ signal pathway.

As recognized commonly, mitogen activated protein kinases (MAPKs)-mediated signaling pathways pronounced markedly in cell differentiation and proliferation (Elango et al., 2019; Kim et al., 2019). Differential molecular in signaling pathways goes through the plasma membrane from extracellular to intracellular environment, then regulates the osteogenesis and adipogenesis (Husain and Jeffries, 2017; Wu et al., 2017; Bukowska et al., 2018). In the early 1990s, as one of the members of the MAPK family, the MEK-ERK pathway was first recognized (Xu et al., 2016). The activation of p-ERK had been shown to be essential for RUNX2 up-regulation and transcriptional activity previously (Li et al., 2017). As was proved, TAZ directly combined to RUNX2 to promote osteogenesis (Wang et al., 2019b). Previously, our study also pointed a molecular link of MEK-ERK pathway to the TAZ during BMSCs osteogenesis (Xue et al., 2013; Wang et al., 2019a; Tan and Dai, 2019). Here, we found that CCG up-regulated TAZ signaling via the MEK-ERK pathway, which might be identified as the underlying regulation network. The MEK-ERK pathway was activated upon CCG-mediated osteogenic differentiation of BMSCs, while the MEK-ERK inhibitors, UO126 reduced the CCG-mediated calcium deposits during cell differentiation. These findings suggested that MRK-ERK activation was the upstream signal by which CCG-induced TAZ up-expression and then regulated the cell differentiation.

CONCLUSION

Our present study confirmed that CCG ameliorated age-related bone loss by upregulating TAZ expression to induce

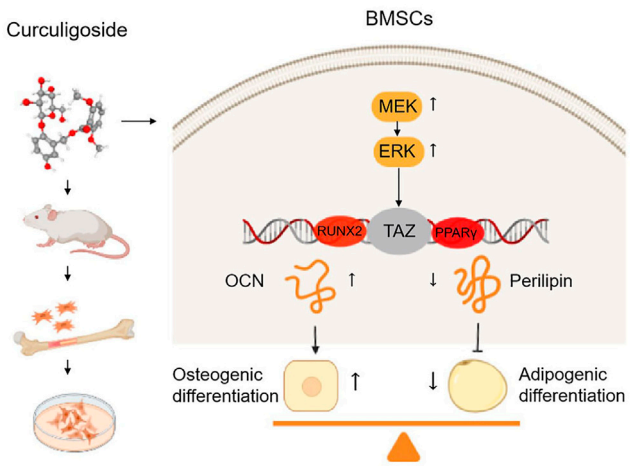

FIGURE 7 | Curculigoside ameliorates bone loss by influencing mesenchymal stem cell fate in aging mice. CCG ameliorated age-related bone loss by upregulating TAZ expression to induce switch from adipogenesis to osteogenesis of BMSCs in aging mice through MEK/ERK-TAZ axis.

the switch from adipogenesis to osteogenesis of BMSCs in aging mice through MEK/ERK-TAZ axis. *In vivo*, oral administration of CCG significantly increased the bone mass and decreased the adipocyte numbers in the bone marrow of aging mice. *In vitro*, a proper concentration of CCG regulated TAZ expression through the MEK-ERK pathway to facilitated osteogenesis at the expense of reduced adipogenesis of BMSCs (**Figure 7**).

All these results revealed that CCG targeted TAZ to ameliorate bone loss in aging mice, which provided the evidence for the clinical use in age-related osteoporosis. In summary, our study pointed the new link of CCG to TAZ signaling and provided a novel therapeutic target for senile osteoporosis.

DATA AVAILABILITY STATEMENT

The raw data supporting the conclusions of this article will be made available by the authors, without undue reservation.

ETHICS STATEMENT

The animal study was reviewed and approved by the ethics committee of the third hospital of hebei medical university.

AUTHOR CONTRIBUTIONS

PX and SL designed the research; NW, ZL and SL carried out most of the experiments, generated data, and drafted the manuscript; LG, XB, KW and CL helped to collect the samples; PX, SL and YL supervised the experiments and proofread the manuscript.

FUNDING

This work was supported by Basic Research Program for Beijing-Tianjin-Hebei Coordination (No: 19JCZDJC65500Z), Medical application technology program of Hebei Province (No: G2019008), Osteoporosis Program for Young Doctors (No: GX20191107) and Government Foundation to Train Clinical Talents and Leading Specialists (No: 361005).

SUPPLEMENTARY MATERIAL

The Supplementary Material for this article can be found online at: https://www.frontiersin.org/articles/10.3389/fcell.2021.767006/full#supplementary-material

REFERENCES

Ambrosi, T. H., Scialdone, A., Graja, A., Gohlke, S., Jank, A.-M., Bocian, C., et al. (2017). Adipocyte Accumulation in the Bone Marrow during Obesity and Aging Impairs Stem Cell-Based Hematopoietic and Bone Regeneration. *Cell Stem Cell* 20, 771–784. doi:10.1016/j.stem.2017.02.009

Bukowska, J., Frazier, T., Smith, S., Brown, T., Bender, R., McCarthy, M., et al. (2018). Bone Marrow Adipocyte Developmental Origin and Biology. *Curr. Osteoporos. Rep.* 16, 312–319. doi:10.1007/s11914-018-0442-z

Byun, M. R., Lee, C. H., Hwang, J.-H., Kim, A. R., Moon, S. A., Sung, M. K., et al. (2013). Phorbaketal A Inhibits Adipogenic Differentiation through the Suppression of PPARγ-Mediated Gene Transcription by TAZ. *Eur. J. Pharmacol.* 718, 181–187. doi:10.1016/j.ejphar.2013.08.035

Cao, D. P., Zheng, Y. N., Qin, L. P., Han, T., Zhang, H., Rahman, K., et al. (2008). Curculigo Orchioides, a Traditional Chinese Medicinal Plant, Prevents Bone Loss in Ovariectomized Rats. *Maturitas* 59, 373–380. doi:10.1016/j.maturitas.2008.03.010

Chen, T., Wang, H., Jiang, C., and Lu, Y. (2021). PKD1 Alleviates Oxidative Stress-Inhibited Osteogenesis of Rat Bone Marrow-Derived Mesenchymal Stem Cells through TAZ Activation. *J. Cel Biochem.* 122 (11), 1715–1725. doi:10.1002/jcb.30124

Curtis, E., Litwic, A., Cooper, C., and Dennison, E. (2015). Determinants of Muscle and Bone Aging. *J. Cel. Physiol.* 230, 2618–2625. doi:10.1002/jcp.25001

Dalton, S. (2015). Linking the Cell Cycle to Cell Fate Decisions. *Trends Cel. Biol.* 25, 592–600. doi:10.1016/j.tcb.2015.07.007

Du, Y., Guo, J. L., Wang, J., Mikos, A. G., and Zhang, S. (2019). Hierarchically Designed Bone Scaffolds: From Internal Cues to External Stimuli. *Biomaterials* 218, 119334. doi:10.1016/j.biomaterials.2019.119334

Elango, J., Robinson, J., Zhang, J., Bao, B., Ma, N., de Val, J. E. M. S., et al. (2019). Collagen Peptide Upregulates Osteoblastogenesis from Bone Marrow Mesenchymal Stem Cells through MAPK- Runx2. *Cells* 8, 446. doi:10.3390/cells8050446

Hansen, J. B., Petersen, R. K., Larsen, B. M., Bartkova, J., Alsner, J., and Kristiansen, K. (1999). Activation of Peroxisome Proliferator-Activated Receptor γ Bypasses the Function of the Retinoblastoma Protein in Adipocyte Differentiation. *J. Biol. Chem.* 274, 2386–2393. doi:10.1074/jbc.274.4.2386

Hu, L., Yin, C., Zhao, F., Ali, A., Ma, J., and Qian, A. (2018). Mesenchymal Stem Cells: Cell Fate Decision to Osteoblast or Adipocyte and Application in Osteoporosis Treatment. *Int. J. Mol. Sci.* 19, 360. doi:10.3390/ijms19020360

Huang, L., Wang, X., Cao, H., Li, L., Chow, D. H.-K., Tian, L., et al. (2018). A Bone-Targeting Delivery System Carrying Osteogenic Phytomolecule Icaritin Prevents Osteoporosis in Mice. *Biomaterials* 182, 58–71. doi:10.1016/j.biomaterials.2018.07.046

Husain, A., and Jeffries, M. A. (2017). Epigenetics and Bone Remodeling. *Curr. Osteoporos. Rep.* 15, 450–458. doi:10.1007/s11914-017-0391-y

Infante, A., and Rodríguez, C. I. (2018). Osteogenesis and Aging: Lessons from Mesenchymal Stem Cells. *Stem Cel. Res. Ther.* 9, 244. doi:10.1186/s13287-018-0995-x

Jeanette, H., Marziali, L. N., Bhatia, U., Hellman, A., Herron, J., Kopec, A. M., et al. (2021). YAP and TAZ Regulate Schwann Cell Proliferation and Differentiation during Peripheral Nerve Regeneration. *Glia* 69 (4), 1061–1074. doi:10.1002/glia.23949

Kegelman, C. D., Mason, D. E., Dawahare, J. H., Horan, D. J., Vigil, G. D., Howard, S. S., et al. (2018). Skeletal Cell YAP and TAZ Combinatorially Promote Bone Development. *FASEB j.* 32, 2706–2721. doi:10.1096/fj.201700872r

Kim, J. M., Yang, Y. S., Park, K. H., Oh, H., Greenblatt, M. B., and Shim, J. H. (2019). The ERK MAPK Pathway Is Essential for Skeletal Development and Homeostasis. *Int. J. Mol. Sci.* 20, 1803. doi:10.3390/ijms20081803

Lee, E., Ko, J.-Y., Kim, J., Park, J.-W., Lee, S., and Im, G.-I. (2019). Osteogenesis and Angiogenesis Are Simultaneously Enhanced in BMP2-/VEGF-Transfected Adipose Stem Cells through Activation of the YAP/TAZ Signaling Pathway. *Biomater. Sci.* 7 (11), 4588–4602. doi:10.1039/c9bm01037h

Li, C.-J., Cheng, P., Liang, M.-K., Chen, Y.-S., Lu, Q., Wang, J.-Y., et al. (2015). MicroRNA-188 Regulates Age-Related Switch between Osteoblast and Adipocyte Differentiation. *J. Clin. Invest.* 125, 1509–1522. doi:10.1172/jci77716

Li, Y., Ge, C., and Franceschi, R. T. (2017). MAP Kinase-dependent RUNX2 Phosphorylation Is Necessary for Epigenetic Modification of Chromatin during Osteoblast Differentiation. *J. Cel. Physiol.* 232, 2427–2435. doi:10.1002/jcp.25517

Ma, C., Zhang, J., Fu, J., Cheng, L., Zhao, G., and Gu, Y. (2011). Up-regulation of VEGF by MC3T3-E1 Cells Treated with Curculigoside. *Phytother. Res.* 25, 922–926. doi:10.1002/ptr.3449

Matsumoto, Y., La Rose, J., Kent, O. A., Wagner, M. J., Narimatsu, M., Levy, A. D., et al. (2016). Reciprocal Stabilization of ABL and TAZ Regulates Osteoblastogenesis through Transcription Factor RUNX2. *J. Clin. Invest.* 126, 4482–4496. doi:10.1172/jci87802

Muruganandan, S., Govindarajan, R., McMullen, N. M., and Sinal, C. J. (2017). Chemokine-Like Receptor 1 Is a Novel Wnt Target Gene that Regulates Mesenchymal Stem Cell Differentiation. *Stem Cells* 35, 711–724. doi:10.1002/stem.2520

Panciera, T., Azzolin, L., Cordenonsi, M., and Piccolo, S. (2017). Mechanobiology of YAP and TAZ in Physiology and Disease. *Nat. Rev. Mol. Cel Biol.* 18, 758–770. doi:10.1038/nrm.2017.87

Paspaliaris, V., and Kolios, G. (2019). Stem Cells in Osteoporosis: From Biology to New Therapeutic Approaches. *Stem Cell Int.* 2019, 1730978. doi:10.1155/2019/1730978

Rosen, C. J., Ackert-Bicknell, C., Rodriguez, J. P., and Pino, A. M. (2009). Marrow Fat and the Bone Microenvironment: Developmental, Functional, and Pathological Implications. *Crit. Rev. Eukar Gene Expr.* 19 (2), 109–124. doi:10.1615/critreveukargeneexpr.v19.i2.20

Salem, O., and Hansen, C. G. (2019). The Hippo Pathway in Prostate Cancer. *Cells* 8, 370. doi:10.3390/cells8040370

Sambrook, P., and Cooper, C. (2006). Osteoporosis. *Lancet* 367, 2010–2018. doi:10.1016/s0140-6736(06)68891-0

Sanghani-Kerai, A., McCreary, D., Lancashire, H., Osagie, L., Coathup, M., and Blunn, G. (2018). Stem Cell Interventions for Bone Healing: Fractures and Osteoporosis. *Cscr* 13, 369–377. doi:10.2174/1574888x13666180410160511

Shen, Q., Zeng, D., Zhou, Y., Xia, L., Zhao, Y., Qiao, G., et al. (2013). Curculigoside Promotes Osteogenic Differentiation of Bone Marrow Stromal Cells from Ovariectomized Rats. *J. Pharm. Pharmacol.* 65, 1005–1013. doi:10.1111/jphp.12054

Tan, F. Z., and Dai, H. L. (2019). TAZ Accelerates Osteogenesis Differentiation of Mesenchymal Stem Cells via Targeting PI3K/Akt. *Eur. Rev. Med. Pharmacol. Sci.* 23, 81–88. doi:10.26355/eurrev_201908_18633

Tan, S., Xu, J., Lai, A., Cui, R., Bai, R., Li, S., et al. (2019). Curculigoside Exerts Significant Anti-arthritic E-ffects I-n vivo and I-n vitro via R-egulation of the JAK/STAT/NF-κB S-ignaling P-athway. *Mol. Med. Rep.* 19, 2057–2064. doi:10.3892/mmr.2019.9854

Teitelbaum, S. L. (2010). Stem Cells and Osteoporosis Therapy. *Cell Stem Cell.* 7, 553–554. doi:10.1016/j.stem.2010.10.004

Urbach, A., and Witte, O. W. (2019). Divide or Commit - Revisiting the Role of Cell Cycle Regulators in Adult Hippocampal Neurogenesis. *Front. Cel Dev. Biol.* 7, 55. doi:10.3389/fcell.2019.00055

Wang, Y., Zhao, L., Wang, Y., Xu, J., Nie, Y., Guo, Y., et al. (2012). Curculigoside Isolated from Curculigo Orchioides Prevents Hydrogen Peroxide-Induced Dysfunction and Oxidative Damage in Calvarial Osteoblasts. *Acta Biochim. Biophys. Sin.* 44, 431–441. doi:10.1093/abbs/gms014

Wang, N., Zhao, G., Zhang, Y., Wang, X., Zhao, L., Xu, P., et al. (2017). A Network Pharmacology Approach to Determine the Active Components and Potential Targets of Curculigo Orchioides in the Treatment of Osteoporosis. *Med. Sci. Monit.* 23, 5113–5122. doi:10.12659/msm.904264

Wang, N., Xue, P., Li, Z., and Li, Y. (2018). IRS-1 Increases TAZ Expression and Promotes Osteogenic Differentiation in Rat Bone Marrow Mesenchymal Stem Cells. *Biol. Open* 7, bio036194. doi:10.1242/bio.036194

Wang, N., Li, Y., Li, Z., Ma, J., Wu, X., Pan, R., et al. (2019). IRS-1 Targets TAZ to Inhibit Adipogenesis of Rat Bone Marrow Mesenchymal Stem Cells through PI3K-Akt and MEK-ERK Pathways. *Eur. J. Pharmacol.* 849, 11–21. doi:10.1016/j.ejphar.2019.01.064

Wang, N., Li, Y., Li, Z., Liu, C., and Xue, P. (2019). Sal B Targets TAZ to Facilitate Osteogenesis and Reduce Adipogenesis through MEK-ERK Pathway. *J. Cel Mol Med.* 23, 3683–3695. doi:10.1111/jcmm.14272

Wang, S., Liu, W., Wang, J., and Bai, X. (2020). Curculigoside Inhibits Ferroptosis in Ulcerative Colitis through the Induction of GPX4. *Life Sci.* 259, 118356. doi:10.1016/j.lfs.2020.118356

Wu, X.-Y., Li, J.-Z., Guo, J.-Z., and Hou, B.-Y. (2012). Ameliorative Effects of Curculigoside from Curculigo Orchioides Gaertn on Learning and Memory in Aged Rats. *Molecules* 17, 10108–10118. doi:10.3390/molecules170910108

Wu, X., Li, S., Xue, P., and Li, Y. (2017). Liraglutide, a Glucagon-Like Peptide-1 Receptor Agonist, Facilitates Osteogenic Proliferation and Differentiation in MC3T3-E1 Cells through Phosphoinositide 3-kinase (PI3K)/protein Kinase B (AKT), Extracellular Signal-Related Kinase (ERK)1/2, and cAMP/protein Kinase A (PKA) Signaling Pathways Involving β-Catenin. *Exp. Cel Res.* 360, 281–291. doi:10.1016/j.yexcr.2017.09.018

Xu, Z., Sun, J., Tong, Q., Lin, Q., Qian, L., Park, Y., et al. (2016). The Role of ERK1/2 in the Development of Diabetic Cardiomyopathy. *Int. J. Mol. Sci.* 17, 2001. doi:10.3390/ijms17122001

Xue, P., Wu, X., Zhou, L., Ma, H., Wang, Y., Liu, Y., et al. (2013). IGF1 Promotes Osteogenic Differentiation of Mesenchymal Stem Cells Derived from Rat Bone Marrow by Increasing TAZ Expression. *Biochem. Biophys. Res. Commun.* 433, 226–231. doi:10.1016/j.bbrc.2013.02.088

Yu, B., Huo, L., Liu, Y., Deng, P., Szymanski, J., Li, J., et al. (2018). PGC-1α Controls Skeletal Stem Cell Fate and Bone-Fat Balance in Osteoporosis and Skeletal Aging by Inducing TAZ. *Cell Stem Cell.* 23 (2), 193–209.e5. doi:10.1016/j.stem.2018.06.009

Yuan, T.-t., Xu, H.-t., Zhao, L., Lv, L., He, Y.-j., Zhang, N.-d., et al. (2015). Pharmacokinetic and Tissue Distribution Profile of Curculigoside after Oral and Intravenously Injection Administration in Rats by Liquid Chromatography-Mass Spectrometry. *Fitoterapia* 101, 64–72. doi:10.1016/j.fitote.2014.12.012

Zanker, J., and Duque, G. (2019). Osteoporosis in Older Persons: Old and New Players. *J. Am. Geriatr. Soc.* 67, 831–840. doi:10.1111/jgs.15716

Zhang, Q., Zhao, L., Shen, Y., He, Y., Cheng, G., Yin, M., et al. (2019). Curculigoside Protects against Excess-Iron-Induced Bone Loss by Attenuating Akt-FoxO1-dependent Oxidative Damage to Mice and Osteoblastic MC3T3-E1 Cells. *Oxid Med. Cel Longev.* 2019, 9281481. doi:10.1155/2019/9281481

Zheng, Y., and Pan, D. (2019). The Hippo Signaling Pathway in Development and Disease. *Dev. Cel.* 50, 264–282. doi:10.1016/j.devcel.2019.06.003

Conflict of Interest: The authors declare that the research was conducted in the absence of any commercial or financial relationships that could be construed as a potential conflict of interest.

Publisher's Note: All claims expressed in this article are solely those of the authors and do not necessarily represent those of their affiliated organizations, or those of the publisher, the editors, and the reviewers. Any product that may be evaluated in this article, or claim that may be made by its manufacturer, is not guaranteed or endorsed by the publisher.

frontiers in Cell and Developmental Biology

ORIGINAL RESEARCH
published: 17 December 2021
doi: 10.3389/fcell.2021.748831

IL-18-Mediated SLC7A5 Overexpression Enhances Osteogenic Differentiation of Human Bone Marrow Mesenchymal Stem Cells *via* the c-MYC Pathway

Feifei Ni[1], *Tao Zhang*[1], *Wanan Xiao*[1], *Hong Dong*[2], *Jian Gao*[2], *YaFeng Liu*[1] *and Jianjun Li*[1]*

[1]Department of Orthopaedics, Shengjing Hospital of China Medical University, Shenyang, China, [2]Liaoning Qifu Stem Cell Biotechnology Co, Ltd, Shenyang, China

OPEN ACCESS

Edited by:
Chao Xie,
University of Rochester, United States

Reviewed by:
Dwijendra K. Gupta,
Jai Prakash Vishwavidyalaya, India
Thanaphum Osathanon,
Chulalongkorn University, Thailand

***Correspondence:**
Jianjun Li
Chinan888999@163.com

Specialty section:
This article was submitted to Cellular Biochemistry, a section of the journal Frontiers in Cell and Developmental Biology

Received: *28 July 2021*
Accepted: *30 November 2021*
Published: *17 December 2021*

Citation:
Ni F, Zhang T, Xiao W, Dong H, Gao J, Liu Y and Li J (2021) IL-18-Mediated SLC7A5 Overexpression Enhances Osteogenic Differentiation of Human Bone Marrow Mesenchymal Stem Cells via the c-MYC Pathway. Front. Cell Dev. Biol. 9:748831. doi: 10.3389/fcell.2021.748831

Objective: To investigate the role of IL-18 in the regulation of osteogenic differentiation in human bone marrow mesenchymal stem cells (hBMSCs).

Methods: To assess whether IL-18 affects the osteogenic differentiation of hBMSCs through the c-MYC/SLC7A5 axis, IL-18 dose-response and time-course experiments were performed to evaluate its impact on osteogenic differentiation. To confirm osteogenic differentiation, alizarin red staining calcium measurement were performed. RT-qPCR and western blotting were used to determine the expression levels of bone-specific markers ALP, RUNX2, and BMP2, as well as those of SLC7A5 and c-MYC. Furthermore, SLC7A5 and c-MYC expression was evaluated *via* immunofluorescence. To elucidate the roles of SLC7A5 and c-MYC in osteoblast differentiation, cells were transfected with SLC7A5 or c-MYC siRNAs, or treated with the SLC7A5-specific inhibitor JPH203 and c-MYC-specific inhibitor 10058-F4, and the expression of SLC7A5, c-MYC, and bone-specific markers ALP, RUNX2, and BMP2 was assessed.

Results: Our results demonstrated that IL-18 increased calcium deposition in hBMSCs, and upregulated the expression of SLC7A5, c-MYC, ALP, RUNX2, and BMP2. Silencing of SLC7A5 or c-MYC using siRNA reduced the expression of ALP, RUNX2, and BMP2, while IL-18 treatment partially reversed the inhibitory effect of siRNA. Similar results were obtained by treating hBMSCs with SLC7A5 and c-MYC specific inhibitors, leading to significant reduction of the osteogenesis effect of IL-18 on hBMSCs.

Conclusion: In conclusion, our results indicate that IL-18 promotes the osteogenic differentiation of hBMSCs *via* the SLC7A5/c-MYC pathway and, therefore, may play an important role in fracture healing. These findings will provide new treatment strategies for delayed fracture healing after splenectomy.

Keywords: IL-18, human bone marrow mesenchymal stem cells, c-Myc, osteogenic differentiation, SLC7A5

INTRODUCTION

In a preliminary clinical study, we previously demonstrated that fracture healing was significantly delayed in patients undergoing splenectomy, while inflammatory factors were significantly reduced during the acute phase (Xiao et al., 2017; Xiao et al., 2018). These results indicated that during certain stages of bone healing, the inflammatory immune response at the fracture site is indispensable (Claes et al., 2012). However, the specific role of pro-inflammatory factors during fracture healing is still not clear.

Early inflammatory response is a key aspect of fracture repair. The administration of anti-inflammatory drugs, such as steroids, at the early stage of fracture healing is not advantageous based on reported outcomes (Chan et al., 2015). In response to a fracture, the inflammatory microenvironment formed around the edges of the fracture recruits bone marrow mesenchymal stem cells (BMSCs) to the site to participate in fracture repair (Reich et al., 2020). In this microenvironment, BMSCs express numerous cytokines and induce the release of a series of cytokines, leading to the activation of autocrine and paracrine pathways, BMSC homing, and osteoblast differentiation, which is beneficial to fracture repair (Zhao et al., 2020). As inflammation subsides, mesenchymal stem cells (MSCs) and other progenitor cells proliferate and form granulation tissue, which is eventually converted to a cartilaginous callus to stabilize the fracture site.

Interleukin 18 (IL-18), a pro-inflammatory cytokine, has been shown to enhance the activity of natural killer (NK) cells, T cells, B cells, and macrophages in the spleen to produce interferon-γ (INF-γ), and plays an important role in inflammation and immune responses (Apalset et al., 2014). Monocytes, macrophages, osteoblasts, BMSCs, and other cells can also express IL-18 (Vecchié et al., 2021). Furthermore, it has been reported that IL-18 can inhibit collagen synthesis and regulate osteoblast differentiation and function. IL-18 expression has been detected in several organs and tissues, such as liver, kidney, spleen, pancreas, lungs, and skeletal muscles. IL-18 plays an important role in fracture repair by coordinating the homing of BMSCs, as well as the differentiation of osteoblasts and osteoclasts; however, the exact mechanism is still unclear (Gibon et al., 2016; Lima Leite et al., 2020).

Amino acids play an important role in the maintenance of cellular homeostasis and various physiological and biochemical processes in cells. Solute carrier family 7, member 5 (SLC7A5) is a Na^+ and pH-independent large neutral amino acid transporter involved in the uptake of essential amino acids, such as leucine, phenylalanine, and valine. The gene is located on human chromosome 16, contains 39,477 nucleotides and 10 exons, and encodes a 507 amino acid 12-pass transmembrane protein with a molecular mass of 55 kDa (Singh and Ecker, 2018). SLC7A5 is highly expressed in the spleen, bone marrow, and placenta, as well as by monocytes and macrophages. SLC7A5 can act as a cellular nutrient signal receptor by regulating the transport of amino acids and providing key components for numerous cellular processes, such as cell proliferation and differentiation (Kandasamy et al., 2018). It has been recently reported that IL-18 can upregulate the expression of SLC7A5 in NK cells, and that amino acid transport mediated by SLC7A5 has an impact on the expression levels of c-MYC. When SLC7A5 is inhibited, c-MYC protein levels drop rapidly, leading to a significant reduction in NK cell metabolism (Liu et al., 2017; Almutairi et al., 2019). Furthermore, research shows that c-MYC expression in T cells is affected by the intracellular amino acid levels (Loftus et al., 2018). Studies have shown that SLC7A5 and c-MYC are highly expressed in stem cells and play roles in most tissues and cells where terminal differentiation occurs (Melnik et al., 2019; Poncet et al., 2020). However, the roles of SLC7A5 and c-MYC in the osteogenic differentiation of human BMSCs (hBMSCs) has not been reported.

Based on these findings, we hypothesized that IL-18 regulates the osteogenic differentiation of hBMSCs *via* the SLC7A5/c-MYC axis. In this study, we investigated the potential roles of IL-18, SLC7A5, and c-MYC during osteogenic differentiation.

MATERIALS AND METHODS

Cell Culture

hBMSCs were provided by the Liaoning Qifu Stem Cell Biotechnology Co, Ltd, China. Cells were cultured in DMEM/F12 (Heyclone, United States) medium supplemented with 15% FBS (Excell Bio, China) and 1% penicillin/streptomycin (Sigma, United States), and passage 3 cells were used for all experiments. To induce osteogenic differentiation, hBMSCs were plated at a density of 10×10^4 cells in 6-well plates and cultured in the classical osteogenic differentiation medium (DMEM/F12 containing 15% FBS and 1% penicillin/streptomycin and supplemented with 100 nM dexamethasone (Sigma, United States), 10 mM β-glycerophosphate (Sigma, United States), and 50 μM ascorbic acid (Sigma, United States)). Cells were cultured in a 37°C, 5% CO_2 incubator, and the medium was changed every 2 days. The cells were seeded in a six-well plate for osteogenic differentiation at 150,000 per well. To evaluate the effect of recombinant human IL-18 (R&D, United States) on osteogenic differentiation, the cells were treated with different concentrations of IL-18 (0 ng/ml as control, 1, 10, 50, 100 ng/ml) for 12 h. In another set of experiments, cells were treated with 100 ng/ml IL-18 and incubated for 0 (control), 3, 6, 12, and 24 h. Based on the results of these dose-response and time-course experiments, we selected 100 ng/ml as the IL-18 concentration for all subsequent experiments. To investigate the involvement of the SLC7A5/c-MYC axis, hBMSCs were pretreated with SLC7A5 specific inhibitor JPH203 (5 μM) (MCE, United States) and c-MYC specific inhibitor 10058-F4 (5 μM) (APExBIO, United States) for 48 or 72 h, and then cultured with IL-18 (100 ng/ml) for 12 h. JPH203, and 10058-F4 were dissolved in DMSO (final concentration of DMSO<0.01%)

Alizarin Red Staining and Calcium Measurement

To confirm the formation of calcium deposits, hBMSCs were cultured in osteogenic medium for 7 days. Next, the cells were fixed with 4% paraformaldehyde for 20 min, washed 3 times with

PBS, stained with Alizarin Red (Sigma, United States) for 20 min at room temperature, washed 3 times with PBS, and then observed under the microscope. Then use the Calcium Colorimetric Assay Kit (Beyotime, China) for calcium measurement. Follow the instructions. In short, wash and dilute the cells and extracellular matrix in a buffer solution, and add the active solution to each well. After 15 min of incubation in the dark at room temperature, the calcium concentration is measured at 575 nm wavelength.

RNA Extraction and Reverse Transcription Quantitative Real-Time Polymerase Chain Reaction

Total RNA was extracted from BMSCs cultured in osteogenic medium using RNAiso Plus reagent (9108, Takara, Japan). Samples with optical density (OD) 260/280 nm between 1.8 and 2.0 were used for cDNA synthesis. Reverse transcription was conducted using a PrimeScript RT Reagent Kit (RR037A, Takara). Quantitative PCR was performed on an ABI 7500fast System (Life Technologies, United States) using TB Green™ Premix Ex Taq ™II (RR820A, Takara) according to the manufacturer's instructions. conditions of real-time PCR were as follows: denaturation at 95°C for 30 s, 40 cycles at 95°C for 3 s and 60°C for 30 s, The dissociation stage was added to the end of the amplification procedure. The following primers (Takara) were used:

SLC7A5 forward: 5′-GCATCGGCTTCACCATCATC-3′,
reverse: 5′-ACCACCTGCATGAGCTTCTGAC-3′;
c-MYC forward: 5′-GGAGGCTATTCTGCCCATTTG-3′,
reverse: 5′-CGAGGTCATAGTTCCTGTTGGTG-3′;
ALP forward: 5′-CAAATGCCTGGATCCTGTTGAC-3′,
reverse: 5′-TGCACTGGCCATCCATCTC-3′;
RUNX2 forward: 5′-CACTGGCGCTGCAACAAGA-3′,
reverse: 5′-CATTCCGGAGCTCAGCAGAATAA-3';
BMP2 forward: 5′-AACACTGTGCGCAGCTTCC-3′
reverse: 5′-CCTAAAGCATCTTGCATCTGTTCTC-3';
β-actin forward: 5′-TGGCACCCAGCACAATGAA-3′
reverse: 5′-CTAAGTCATAGTCCGCCTAGAAGCA-3'.

Gene expression analyses were calculated using the $2^{-\Delta\Delta Ct}$ method.

siRNA and Transfection

Small interfering RNAs (siRNAs) targeting SLC7A5 (5′-GCG UCAUGUCCUGGAUCAUTTAUGAUCCAGGACAUGACG CTT-3′), c-MYC (5′-CACCUAUGAACUUGUUUCATTUGA AACAAGUUCAUAGGUGTT-3′), and the negative control (NC, 5′-UUCUCCGAACGUGUCACGUTT-3′) were purchased from Genepharma (Suzhou, China). Cells were transfected with 75 nmol/L of either SLC7A5 siRNA, c-MYC siRNA, or NC siRNA using Lipofectamine™ 3000 Transfection Reagent (Thermo Scientific, United States) according to the manufacturer's guidelines. The cells were collected for RNA or protein isolation 24–72 h post-transfection to evaluate the effects of the treatment on osteogenic differentiation.

Western Blotting

Cells were cultured as described above, washed with PBS, and scraped off the culture plates, and the total cell protein was extracted with radioimmunoprecipitation assay buffer containing protease and phosphatase inhibitors according to the instructions. The protein concentration was determined using the bicinchoninic acid protein assay (Biyotime, China). Equal amounts of protein/sample (20 μg) were separated using sodium dodecyl-sulfate polyacrylamide gel electrophoresis (SDS-PAGE) and then transferred to a polyvinylidene difluoride membrane (Millipore, United States). The membranes were blocked in 5% skim milk in tris-buffered saline with Tween 20 (TBST) and then incubated with primary antibodies at 4°C overnight. The following primary antibodies were used: GAPDH (60004-1-Ig, Proteintech, United States), SLC7A5 (13752-1-AP, Proteintech), c-MYC (10828-1-AP, Proteintech), ALP (11187-1-AP, Proteintech), BMP2 (18933-1-AP, Proteintech), RUNX2 (AF5186, Affinity, United States). All primary antibodies were diluted according to the manufacturers' instructions. Next, the membranes were washed 3 × 15 min with TBST and then incubated with a secondary antibody goat anti-rabbit IgG (HRP-6004, Proteintech) at room temperature for 2 h. Finally, the target bands were visualized using the enhanced chemiluminescence reagent (Biosharp, China) and a Plus Western Blotting Detection System (GE680, United States).

Immunofluorescence Staining

In a 24-well plate, the slides that have climbed up cells were washed 3 × 3 min in PBS, fixed with 4% paraformaldehyde for 15 min, permeabilized with 0.5% Triton X-100 in PBS preparation at room temperature 20 min, and then blocked with normal goat serum for 30 min at room temperature. The blocking solution was removed using the absorbent paper and a sufficient amount of diluted anti-SLC7A5 or anti-c-MYC primary antibody was added to each slide. Slides were incubated overnight at 4°C in a humidified container. Next, the cells were incubated with CoraLite488-conjugated secondary antibody (1:100, SA00013-2, Proteintech) or CoraLite594-conjugated secondary antibody (1:100, SA00013-4, Proteintech) for 2 h at room temperature. 4′,6-Diamidino-2-phenylindole was added dropwise, and the cells were incubated for 5 min in the dark to stain the nuclei. The slides were mounted using an anti-quenching mounting solution, and the cells were observed under an inverted phase contrast microscope and image acquisition system for observing and acquiring images (Eclipse NI, Nikon).

Statistical Analysis

Statistical analyses were conducted using the SPSS software version 16.0 (SPSS Inc, United States). All quantitative data are expressed as the mean ± standard deviation (SD) of three independent experiments. Differences between groups were analyzed using One-way ANOVA with a subsequent Bonferroni post-hoc test. $p < 0.05$ was considered statistically significant.

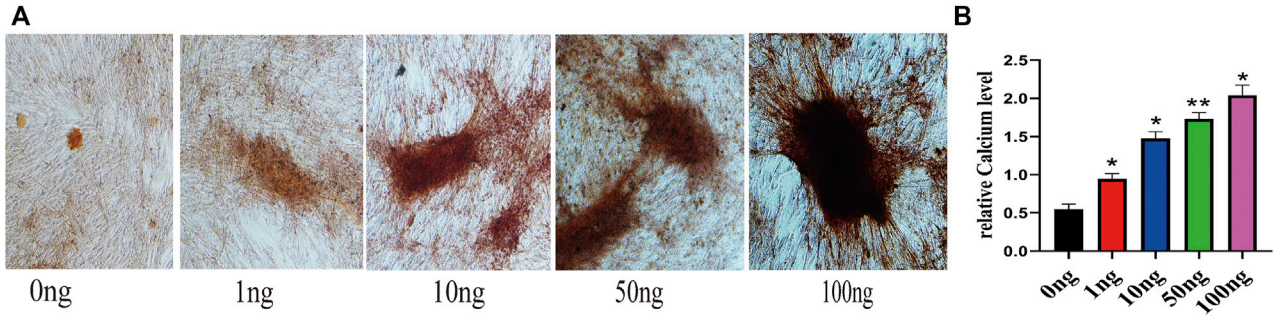

FIGURE 1 | IL-18 promotes the osteogenic differentiation of hBMSCs. hBMSCs were treated with different concentrations of IL-18 for 7 days and calcium deposition was evaluated using Alizarin Red staining **(A)** and quantitative calcium assay is used to measure calcium concentration **(B)**. Data are expressed as the mean ± standard deviation (SD). Concentration groups vs. the control (0 ng) group. Experiments were repeated three times. Scale bars: 200 μm for A, $*p < 0.05$, $**p < 0.01$.

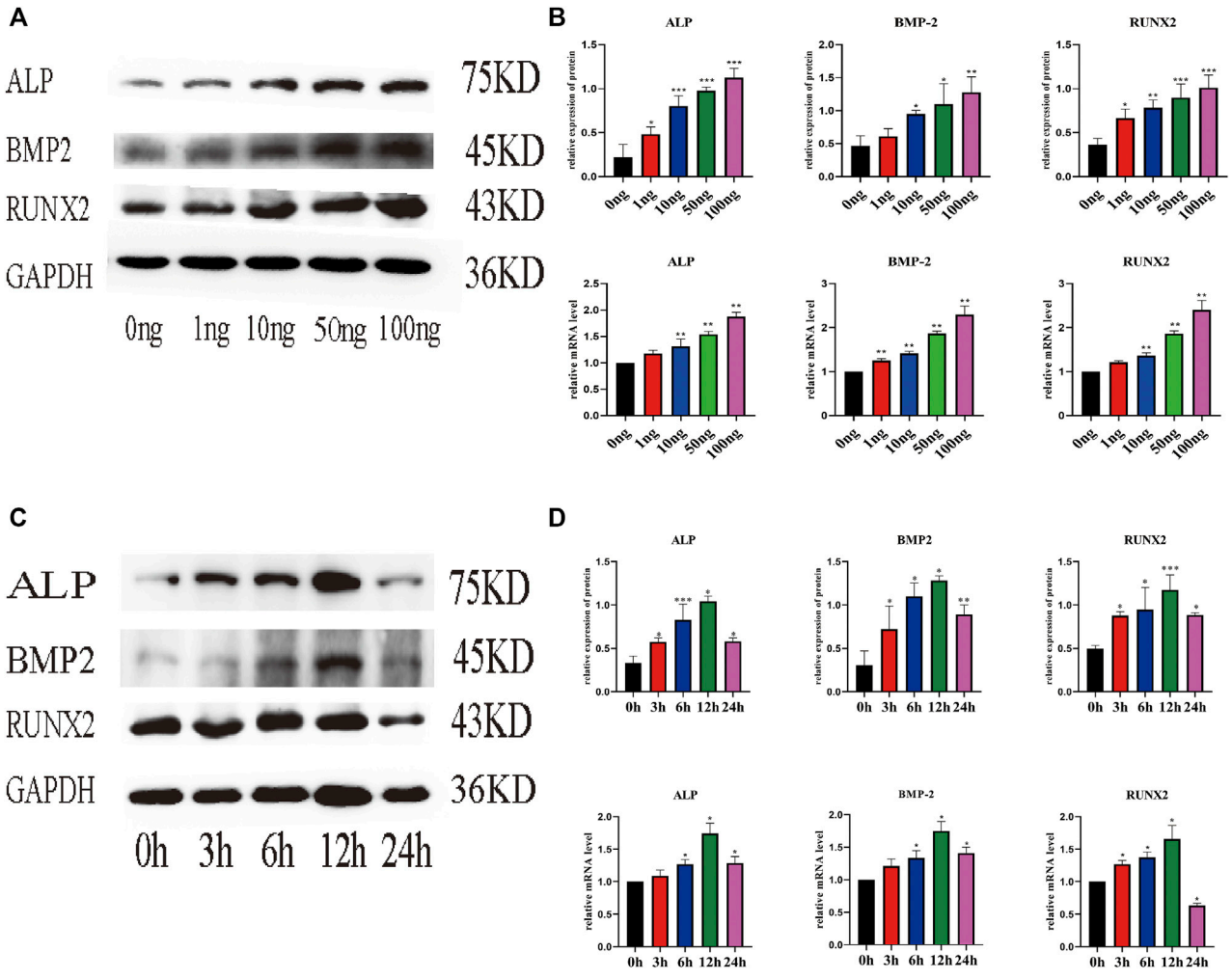

FIGURE 2 | IL-18 induced the expression of osteoblast-specific markers in a dose- and time-dependent manner. hBMSCs were treated with different culture concentrations (0, 1, 10, 50, 100 ng) of IL-18, western blot and qPCR were used to evaluate the protein and mRNA **(A, B)** expression levels of ALP, BMP2, RUNX2, GAPDH. hBMSCs were treated with 100 ng/ml IL-18 for 0, 3, 6, 12 and 24 h, and Western Blotting and qPCR were used to evaluate the protein expression of osteoblast-specific markers ALP, BMP2, RUNX2, GAPDH and their mRNA expression **(C, D)**. GAPDH was used as an internal control. Data are expressed as the mean ± standard deviation (SD). Concentration groups vs. the control (0 ng) group; time-point groups vs. the control (0 h) group, $*p < 0.05$, $**p < 0.01$, $***p < 0.001$.

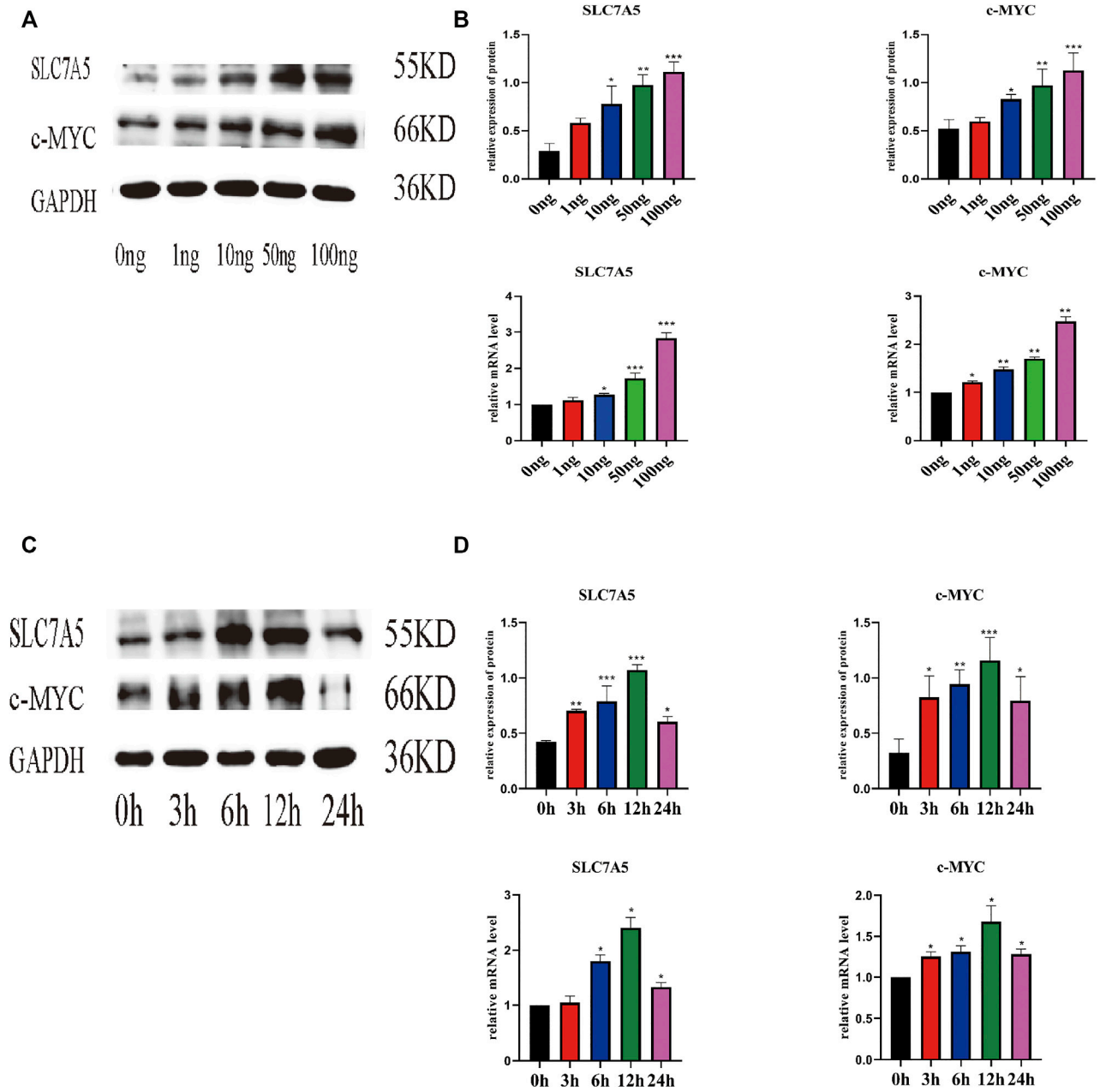

FIGURE 3 | IL-18 induced the expression of SLC7A5 and –MYC in a dose- and time-dependent manner. hBMSCs were treated with different culture concentrations (0, 1, 10, 50, 100 ng) of IL-18, western blot and qPCR were used to evaluate the protein and mRNA **(A, B)** expression levels of SLC7A5, c-MYC, and GAPDH. hBMSCs were treated with 100 ng/ml IL-18 for 0, 3, 6, 12, and 24 h, and Western Blotting and qPCR were used to evaluate the protein expression of SLC7A5,c-MYC and GAPDH (as internal control) and their mRNA expression **(C, D)**. Data are expressed as the mean ± standard deviation (SD). Concentration groups vs. the control (0 ng) group; time-point groups vs. the control (0 h) group, Experiments were repeated three times. $^{*}p < 0.05$, $^{**}p < 0.01$, $^{***}p < 0.001$.

RESULTS

IL-18 Enhances Calcium Deposition

To investigate the effect of IL-18 on osteogenesis in hBMSCs *in vitro*, Alizarin Red staining was performed. Mineralization is commonly used as a late marker of osteogenesis; therefore, the cells were evaluated on day 7 after osteogenic induction by Alizarin red staining. Alizarin red staining showed that the number of mineralized nodules also increased significantly at higher IL-18 concentrations, with the highest staining intensity being observed at 100 ng/ml IL-18 (**Figure 1A**). According to the quantitative analysis of calcium, Compared with 0ng group hBMSCs cultured in osteogenic induction medium showed that the amount of calcium deposition increased with the concentration (**Figure 1B**).

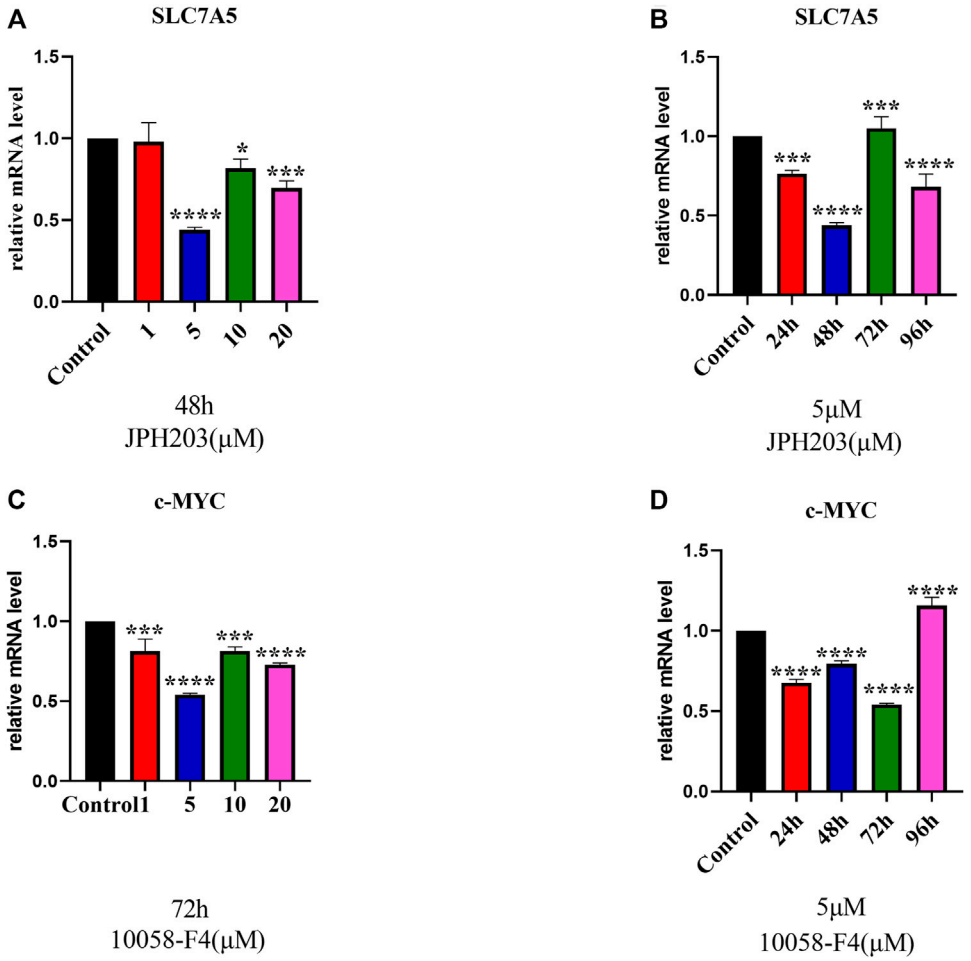

FIGURE 4 | RT-qPCR evaluation of SLC7A5 **(A, B)** and c-MYC **(C, D)** gene expression. hBMSCs were cultured in the osteogenesis induction medium and then treated 10058-F4 and JPH203 with different concentrations (0, 1, 5, 10, 20 μM) and for different time periods (0, 24, 48, 72, 96 h). GAPDH was used as an internal control. Data are presented as the mean ± SEM, Concentration groups vs. the control group; time-point groups vs. the control group. Experiments were repeated three times. $^{*}p < 0.05$, $^{**}p < 0.01$, $^{***}p < 0.001$, $^{****}p < 0.0001$.

IL-18 Promotes the Differentiation of hBMSCs Into Osteoblasts in a Time- and Dose-dependent Manner

Real-time PCR (qPCR) and WB were used to evaluate the effect of IL-18 on the expression of osteoblast-specific markers. IL-18 increased the mRNA expression of ALP, BMP2, and RUNX2 in a dose-dependent manner, with the highest expression levels being observed at the 100 ng/ml IL-18 dose. Similar results were observed in WB experiments (**Figures 2A,B**). Next, we performed time-course experiments (3–24 h) to assess the effect of IL-18 (100 ng/ml dose) on the expression of ALP, BMP2, and RUNX2 in hBMSCs. Our results demonstrated that BMP2 expression started to increase at the 6 h time-point, while ALP and RUNX2 expression started to increase at the 3 h time-point. The expression levels of all markers were the highest at 12 h and decreased by 24 h (**Figures 2C,D**).

IL-18 Promotes the Increase of c-MYC Expression *via* SLC7A5 in a Time- and Dose-dependent Manner

Next, we evaluated the effect of IL-18 on the expression of SLC7A5 and c-MYC using qPCR and western blot. qPCR results showed that IL-18 affected SLC7A5 and c-MYC expression in a dose-dependent manner; SLC7A5 expression started to increase at 10 ng/ml, while c-MYC expression was induced at 1 ng/ml, and the expression of both genes reached maximum levels at 100 ng/ml (**Figures 3A,B**). Time-course experiments demonstrated that SLC7A5 expression was initiated at the 6-h time point, while c-MYC expression was induced at the 3 h time point, and the expression of both genes reached their highest levels by 12 h. Western blot results confirmed these findings; the protein expression levels of SLC7A5 and c-MYC were the highest at 100 ng/ml dose, while

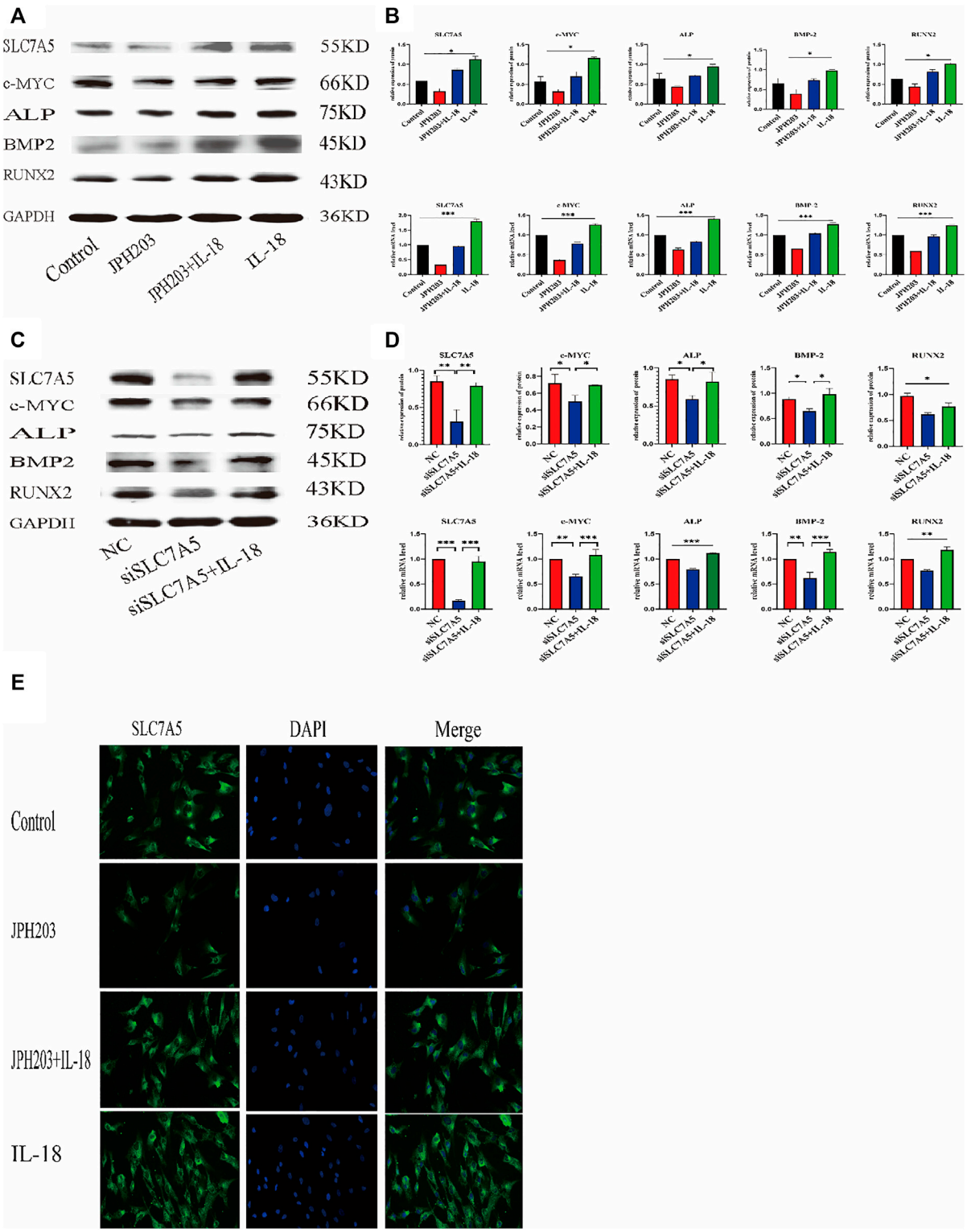

FIGURE 5 | Inhibition of SLC7A5 reduces the bone-forming ability of hBMSCs induced by IL-18. The cells were treated with JPH203 (5 μM) for 48 h, and then with 100 ng/ml IL-18 for 12 h western blotting and q-PCR experiments were conducted to evaluate the expression of osteoblast-specific markers, as well as SLC7A5 and c-MYC mRNA; GAPDH was used as an internal control **(A, B)**. Cells were transfected for 48 h and then treated with 100 ng/ml IL-18 for 12 h, mRNA levels of SLC7A5, c-MYC and osteoblast-specific factors were quantied by qRT-PCR ,Cells were transfected for 72 h and then treated with 100 ng/ml IL-18 for 12 h and then western blotting experiments were conducted to evaluate the expression of osteoblast-specific factors, as well as SLC7A5 and c-MYC; GAPDH was used as an internal control **(C, D)**.Cells were treated with JPH203 (5 μM) and IL-18 (100 ng/ml) for 48 h, and the protein levels of SLC7A5 were assessed by immunofluorescence **(E)**. Data expressed as the mean ± standard deviation (SD). Experiments were repeated three times. Scale bars: 200 μm for F, G. $^{*}p < 0.05$, $^{**}p < 0.01$, $^{***}p < 0.001$ (multiple comparisons use one-way ANOVA with a subsequent Bonferroni post-hoc test).

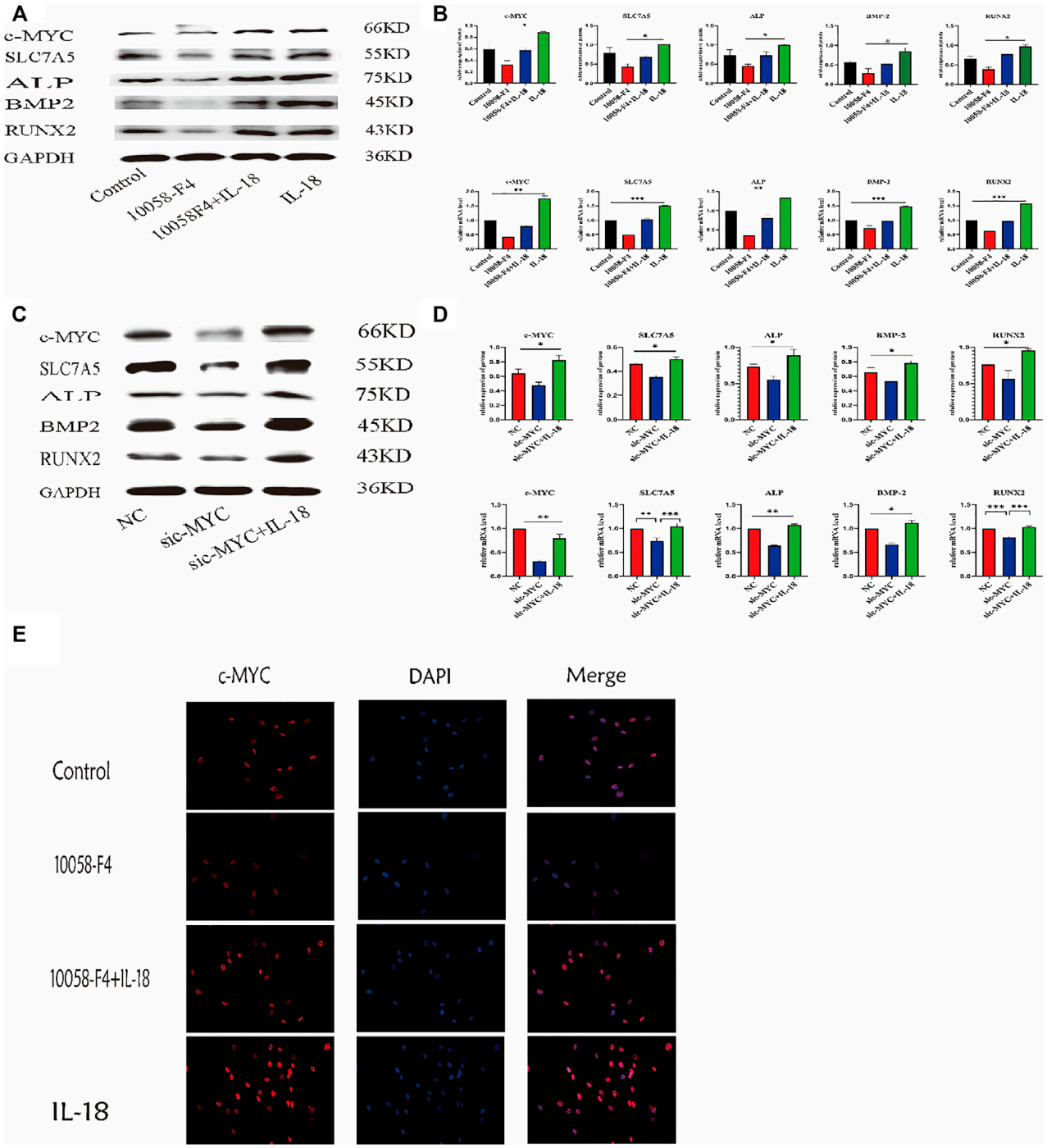

FIGURE 6 | Inhibition of c-MYC can reduce the bone-forming ability of HBMSC induced by IL-18. The cells were treated with 10058-F4 (5 μM) for 72 h, and then with 100 ng/ml IL-18 for 12 h western blotting and q-PCR experiments were conducted to detect osteogenic factors and the protein and mRNA expression of c-MYC and SLC7A5, ALP, BMP2, RUNX2; GAPDH was used as an internal control **(A, B)**. Cells were transfected for 48 h and then treated with 100 ng/ml IL-18 for 12 h, mRNA levels of SLC7A5, c-MYC and osteoblast-specific factors were quantied by qRT-PCR, Cells were transfected for 72 h and then treated with 100 ng/ml IL-18 for 12 h and then western blotting experiments were conducted to evaluate the expression of osteoblast-specific factors, as well as c-MYC and SLC7A5; GAPDH was used as an internal control **(C, D)**. After treatment with 10058-F4 (5 μM) for 72 h and 100 ng/ml IL-18 for 12 h, immunofluorescence staining was used to observe c-MYC protein levels **(E)**. Data expressed as the mean ± standard deviation (SD). Experiments were repeated three times.*$p < 0.05$, **$p < 0.01$, ***$p < 0.001$ (multiple comparisons use one-way ANOVA with a subsequent Bonferroni post-hoc test).

time-course experiments showed that the protein expression levels of SLC7A5 and c-MYC were upregulated at 3 h, reached the maximum levels at 12 h, and decreased by 24 h (**Figures 3C,D**).

Determination of Optimal Concentrations for SLC7A5 and c-MYC Inhibitors

To evaluate the involvement of SLC7A5 and c-MYC in osteoblast differentiation, first, we determined the optimal concentration of JPH203 (a specific SLC7A5 inhibitor) and 10058-F4 (a specific c-MYC inhibitor) using real-time PCR. The cells were treated with different concentrations of JPH203 for 48 h and 10058-F4 (5 μM) for 72 h. SLC7A5 and c-MYC mRNA expression decreased significantly (**Figures 4A,B**).

Osteogenic Differentiation Ability of hBMSCsis Reduced by SLC7A5 Inhibition and Enhanced by IL-18

To investigate whether SLC7A5 is involved in the IL-18-induced osteogenic differentiation of hBMSCs, we transfected cells with siSLC7A5 to specifically downregulate the expression of SLC7A5. In another set of experiments, we used JPH203, a SLC7A5 specific inhibitor, to evaluate the role of SLC7A5 in the osteogenic differentiation of hBMSCs. Our results demonstrated that, compared to the control group, the expression levels of SLC7A5 and c-MYC in the siSLC7A5 and JPH203 treatment groups were significantly reduced, and the expression levels of osteogenic markers ALP, BMP2, and RUNX2 were also decreased (**Figures 5A–D**). Furthermore, our results showed that IL-18-induced SLC7A5 expression could be reversed either by JPH203 treatment or siSLC7A5. As to the immunofluorescent staining results, compared with the IL-18 + JPH203 group, the IL-18 group showed the highest expression levels, and the JPH203 group showed the lowest expression levels (**Figure 5E**).

Osteogenic Differentiation Ability of hBMSCs That Inhibit the Decrease of c-MYC Expression can Be Enhanced by IL-18

To further investigate whether the inhibition of c-MYC can reverse the IL-18-induced osteogenic differentiation of hBMSCs, cells were treated with c-MYC antagonists 10058-F4 and sic-MYC to inhibit c-MYC expression. Compared to the control group, 10058-F4 and sic-MYC significantly reduced the expression of c-MYC at the mRNA and protein levels, with expression of c-MYC reduced, it's also reduced the expression of SLC7A5,ALP,BMP2 and RUNX2; however, IL-18 treatment partially restored the bone formation ability in 10058-F4 and sic-MYC groups (**Figures 6A–D**). Immunofluorescent staining also showed that IL-18 promoted the nuclear expression of c-MYC, while 10058-F4 significantly reduced the nuclear expression of c-MYC that was induced by IL-18 (**Figure 6E**).

DISCUSSION

Currently, an increasing number of studies are involved in the investigation of the role of immune response mechanisms during fracture healing. It has been reported that, within 24 h of an injury, the expression of cytokines is increased in the fracture hematoma; however, the role of cytokines in these hematomas has not been fully understood. Here we showed that IL-18 induced the mineralization and osteogenic differentiation of hBMSCs at a biologically relevant concentration, which is crucial for the investigation of its molecular mechanism *in vitro*. Our results also indicated that 100 ng/ml of IL-18 induced the strongest osteogenic effect. We also tested 120 ng/ml concentration of IL-18 in the cells; however, this concentration was found to be toxic to the cells, and cells died and floated within a few minutes. Therefore, 100 ng/ml was considered to be the optimal concentration. Our results demonstrated that SLC7A5 and c-MYC played an important role in the IL-18-induced expression of osteogenic markers in hBMSCs; IL-18 upregulated the expression of SLC7A5 and c-MYC at the early stage of hBMSC osteogenic differentiation, and SLC7A5 and c-MYC inhibition blocked the osteogenic differentiation that was induced by IL-18. To the best of our knowledge, this is the first report demonstrating that SLC7A5 is involved in the activation of c-MYC in hBMSCs (**Figure 3**, **Figure 5**).

Previous studies have shown that the levels of IL-18 in the blood are significantly increased after a fracture, while the levels of IL-18 return to normal levels after the fracture is repaired (Ko et al., 2018; Li and Wang, 2018). We previously demonstrated that the levels of proinflammatory factors in hematoma and peripheral blood are significantly increased after a fracture. Other studies have shown that IL-18 induces the expression of osteoprotegerin (OPG) in mouse osteoblasts to inhibit the formation of osteoclasts (Makiishi-Shimobayashi et al., 2001). The bone density of elderly patients with osteoporosis increases significantly after anti-osteoporosis treatment. This may be related to the ability of IL-18 to inhibit osteoclast activity, induce the proliferation and differentiation of bone marrow-derived lymphoid progenitor cells, and promote NK cell proliferation and cytotoxicity (Maugeri et al., 2005; Gandhapudi et al., 2015; Choi et al., 2019). These findings suggest that IL-18 has some beneficial impacts; however, it has a negative effect on rheumatoid arthritis (RA) and osteoarthritis (OA). For example, IL-18 induces inflammatory responses in synovial cells and chondrocytes (Fu et al., 2012); however, the upregulation of splenic suppressors of cytokine signaling (SOCS) can reduce the release of pro-inflammatory cytokine IL-18 and relieve the symptoms of RA. It is possible that, in these two chronic diseases, the continued release of IL-18 leads to abnormal bone formation (Nozaki et al., 2019), while during bone fracture, an acute condition with an early phase lasting approximately 3 days, pro-inflammatory factors and immune cells in the fractured hematoma tissue promote hBMSC migration and fracture healing (Pountos et al., 2019). However, the effect of IL-18 on other bone-related factors in hBMSCs is still unclear. Here, in this study, we observed that IL-18 can induce the

expression of osteogenic factors, such as ALP, BMP2, and RUNX2, in a dose-dependent manner. At the same time, IL-18 (100 ng/ml) can promote mineralization, confirming the osteogenic differentiation of hBMSCs (**Figure 1**). Runx2 is a transcription factor that regulates the expression of early osteoblast-specific genes, while BMP-2 is a growth factor known to induce osteoblast differentiation and the expression of osteogenic genes, and therefore plays an important role in bone repair (Salazar et al., 2016). ALP is another osteoblast-specific factor involved in the regulation of bone morphogenesis by generating the phosphoric acid necessary for the deposition of hydroxyapatite during mineralization. The higher the ALP activity, the stronger the osteogenic differentiation ability (Wang et al., 2018). Therefore, our results confirm that the regulation of cell surface molecules by pro-inflammatory cytokines after fracture plays an important role in the activation of BMSCs. Accurately increasing the levels of IL-18 at the fracture site after fracture, in combination with splenectomy, may provide a new treatment strategy for fracture healing in the early stage of fracture.

Amino acids can affect the proliferation, differentiation, and mineralization of BMSCs through intracellular oxidative stress and the tricarboxylic acid cycle (TCA) cycle (Dirckx et al., 2019; Zhou et al., 2019). Furthermore, a low essential amino acid diet in mice can lead to bone loss and osteoporosis. SLC7A5 is an essential amino acid transporter that plays a key role in cell metabolism and growth. The importance of SLC7A5 was demonstrated using an animal global knockout model, with the embryos not surviving past the second trimester. Furthermore, BMSCs grown in a medium with low amino acid levels have significantly reduced proliferation and differentiation ability. At the same time, the abnormal expression of SLC7A5 can cause diseases, such as tumors, Parkinson's, neurodevelopmental abnormalities, and autism, confirming that SLC7A5 plays a crucial role in physiological processes (Tărlungeanu et al., 2016; Ding et al., 2018; Scalise et al., 2018). The expression of SLC7A5 in osteoclasts of a mouse osteoporosis model was reportedly significantly reduced. By regulating nuclear factor of activated T cells, cytoplasmic 1 (NFATc1) in osteoclasts, it plays a key role in bone resorption and bone homeostasis. It was shown that SLC7A5 knockout mice developed osteoporosis. The femur bone density was significantly reduced, while the levels of osteoclast markers in the blood were significantly increased (Ozaki et al., 2019), confirming that SLC7A5 plays an important role in bone homeostasis. However, the specific role of SLC7A5 in BMSCs is not clear. Several studies have shown that stem cells express a variety of amino acid transporters, while high expression levels of SLC7A5 and energy metabolism are essential for the osteogenic differentiation of hBMSCs (Moravcikova et al., 2018). Our results, using hBMSCs, showed that in response to IL-18 treatment, SLC7A5 expression increased in a concentration-dependent manner, while the expression levels of SLC7A5 were significantly decreased by SLC7A5 inhibitors and siRNA.

SLC7A5 is necessary for the growth of T cells. T cells lacking SLC7A5 do not undergo metabolic reprogramming, expansion, and differentiation in response to antigen stimulation. Furthermore, SLC7A5 knockout mouse embryos have serious nerve and limb growth defects (Sinclair et al., 2013; Poncet et al., 2020). Another study demonstrated that in tumor cells SLC7A5 can regulate the expression of c-MYC, forming a mechanism that connects essential amino acid transport and tumorigenesis. The positive feedback loop mechanism is probably due to the fact that tumor cells have higher energy and nutrient demands to maintain cell survival and proliferation (Yue et al., 2017). Here, in our study, we used SLC7A5 inhibitor JPH203 and siSLC7A5 to investigate whether IL-18 promoted the osteogenic differentiation of hBMSCs *via* SLC7A5. We found that JPH203 and siSLC7A5 significantly inhibited the expression of IL-18-induced osteogenic markers, such as Runx2, ALP, and BMP2, and significantly reduced the expression of c-MYC. These results suggested that IL-18 induced the osteogenic differentiation of hBMSCs *via* SLC7A5 (**Figure 5**). These findings are consistent with previous studies demonstrating osteoporosis in SLC7A5 knockout mice. JPH203 is a selective inhibitor of SLC7A5 which can effectively block the amino acid transport mediated by SLC7A5 (Enomoto et al., 2019; Ozaki et al., 2019).

Recent studies have shown that c-MYC is a downstream target gene of multiple signaling pathways and plays key roles in numerous physiological processes, such as embryonic development, self-renewal of stem cells, and tissue regeneration, as well as cellular differentiation (Liu et al., 2017). Under normal physiological conditions, the expression of c-MYC is strictly regulated and increases in response to extracellular growth factors; in response to these growth factors, c-MYC is quickly activated (Meyer and Penn, 2008). The expression of c-MYC in osteoblast culture medium is significantly increased. c-MYC is widely regarded as a marker of pluripotent stem cells such as ESCs and iPSCs and is highly expressed in stem cells, and regulates the pluripotency of mouse ESCs, neural stem cells (NSC), and hematopoietic stem cells (HSC). The key role of sex and self-renewal ability is known (Nair et al., 2014; Foroutan, 2016), but research on the specific mechanism of action is limited. Studies have found that β-catenin signaling can upregulate the expression of OSX in human pre-osteoblasts and bone marrow stromal cells through c-MYC to promote osteogenesis. These findings suggest that c-MYC plays an important role in osteogenesis (Liu et al., 2015). The c-MYC pathway also plays a key role in the maintenance of T cell function and metabolic reprogramming and is independent of the mTOR pathway. The physiological condition, in terms of the transcription levels of c-MYC, reflects tissue and cell growth status; tissues with high proliferation rates have high c-MYC transcription levels (Lu et al., 2020). Several studies have demonstrated that many types of tumors are characterized by high c-MYC expression levels; however, in the absence of other mutations, c-MYC overexpression alone is not sufficient for tumorigenic transformation. These findings suggest that c-MYC plays a pivotal role in physiological and pathological conditions (Wolfer and Ramaswamy, 2011; Cascón and Robledo, 2012; Sinclair et al., 2013).

Whole genome analysis of rat fibroblasts showed that SLC7A5 is the direct action site of c-MYC. The increase of c-MYC activity

upregulates the expression of several glutamine transporters, and in c-MYC knockout mice resulted in embryonic death and significantly reduced SLC7A5 levels (Zhao et al., 2019). Previous studies have shown that c-MYC enhances the expression of SLC7A5 by binding to specific promoters (Gao et al., 2009; Hayashi et al., 2012). Other studies have also found that c-MYC in cells can be activated by directly binding to specific E-box sequences to initiate SLC7A5 transcription, while SLC7A5-mediated uptake of essential amino acids stimulates c-MYC protein synthesis and downstream target gene transcription, leading to reprogramming of the entire metabolic process, including glycolysis, glutamine breakdown, and lipogenesis (Yue et al., 2017). In tumor cells, the expression of c-MYC has been shown to significantly decrease after the JPH203-mediated inhibition of SLC7A5, thereby affecting the metabolic function controlled by c-MYC (Rosilio et al., 2015). It has also been shown that high expression levels of c-MYC appear to be essential for the maintenance of MSC proliferation and differentiation potential. However, low c-MYC expression or loss of function leads to the inhibition of MSC proliferation and differentiation. It was recently demonstrated that c-MYC overexpression increases type X collagen one (COL10A1) expression, suggesting that c-MYC plays an important role in cartilage formation (Wang et al., 2017; Melnik et al., 2019). These findings indicate that c-MYC is an important regulatory factor in stem cells and are consistent with our results. Here we showed that the use of siRNA and c-MYC inhibitor 10058-F4 resulted in the downregulation of SLC7A5 expression, as well as of osteogenic markers, indicating that c-MYC inhibition can decrease the osteogenic differentiation ability of hBMSCs *in vitro*. Moreover, IL-18 reversed the downregulation of c-MYC and osteogenic markers induced by siRNA and the c-MYC specific inhibitor 10058-F4, indicating that IL-18 plays a role *via* c-MYC regulation (**Figure 6**). Our study determined the close relationship between the SLC7A5 and c-MYC signaling pathway and the expression of Runx2, BMP2, and ALP, as well as the close relationship between SLC7A5 and c-MYC. The results indicate that IL-18 promotes the osteogenic differentiation of hBMSCs through the SLC7A5/c-MYC regulatory axis. Therefore, activating the SLC7A5/c-MYC axis can promote fracture healing after splenectomy.

Our results show that IL-18 promotes bone formation *in vitro*. It activates SLC7A5 to enhance the osteogenic differentiation of hBMSCs mainly through the c-MYC pathway. Blocking SLC7A5/c-MYC reduces the osteogenic differentiation of hBMSCs, indicating that the SLC7A5/c-MYC axis plays an important role in the osteogenic differentiation of hBMSCs, suggesting that the spleen plays an important role in the fracture healing process. Therefore, when fractures with splenic injury require surgical treatment, the spleen should be preserved as much as possible during the operation to ensure stability of the patient's immune function after surgery. These findings will provide new treatment strategies for delayed fracture healing after splenectomy.

DATA AVAILABILITY STATEMENT

The original contributions presented in the study are included in the article/Supplementary Materials, further inquiries can be directed to the corresponding author.

ETHICS STATEMENT

The studies involving human participants were reviewed and approved by the China Medical University ethics committee. The patients/participants provided their written informed consent to participate in this study.

AUTHOR CONTRIBUTIONS

FN performed the experiments, wrote the manuscript, and analyzed the data; JL designed the experiments. TZ, WX, HD, JG, and YL assisted with the preparation of the experiments. All authors read and approved the final manuscript.

FUNDING

This work was supported by the National Natural Science Foundation of China (grant number: 81971829), and the 50 Engineering Project of Shengjing Hospital, Affiliated to China Medical University (project number: M0414).

REFERENCES

Almutairi, S. M., Ali, A. K., He, W., Yang, D.-S., Ghorbani, P., Wang, L., et al. (2019). Interleukin-18 Up-Regulates Amino Acid Transporters and Facilitates Amino Acid-Induced mTORC1 Activation in Natural Killer Cells. *J. Biol. Chem.* 294 (12), 4644–4655. doi:10.1074/jbc.RA118.005892

Apalset, E. M., Gjesdal, C. G., Ueland, P. M., Øyen, J., Meyer, K., Midttun, Ø., et al. (2014). Interferon Gamma (IFN-Γ)-Mediated Inflammation and the Kynurenine Pathway in Relation to Risk of Hip Fractures: the Hordaland Health Study. *Osteoporos. Int.* 25 (8), 2067–2075. doi:10.1007/s00198-014-2720-7

Cascón, A., and Robledo, M. (2012). MAX and MYC: A Heritable Breakup: Figure 1. *Cancer Res.* 72 (13), 3119–3124. doi:10.1158/0008-5472.Can-11-3891

Chan, J. K., Glass, G. E., Ersek, A., Freidin, A., Williams, G. A., Gowers, K., et al. (2015). Low-dose TNF Augments Fracture Healing in normal and Osteoporotic Bone by Up-regulating the Innate Immune Response. *EMBO Mol. Med.* 7 (5), 547–561. doi:10.15252/emmm.201404487

Choi, Y. H., Lim, E. J., Kim, S. W., Moon, Y. W., Park, K. S., and An, H.-J. (2019). IL-27 Enhances IL-15/IL-18-mediated Activation of Human Natural Killer Cells. *J. Immunotherapy Cancer* 7 (1), 168. doi:10.1186/s40425-019-0652-7

Claes, L., Recknagel, S., and Ignatius, A. (2012). Fracture Healing under Healthy and Inflammatory Conditions. *Nat. Rev. Rheumatol.* 8 (3), 133–143. doi:10.1038/nrrheum.2012.1

Ding, K.-H., Cain, M., Davis, M., Bergson, C., McGee-Lawrence, M., Perkins, C., et al. (2018). Amino Acids as Signaling Molecules Modulating Bone Turnover. *Bone* 115, 15–24. doi:10.1016/j.bone.2018.02.028

Dirckx, N., Moorer, M. C., Clemens, T. L., and Riddle, R. C. (2019). The Role of Osteoblasts in Energy Homeostasis. *Nat. Rev. Endocrinol.* 15 (11), 651–665. doi:10.1038/s41574-019-0246-y

Enomoto, K., Sato, F., Tamagawa, S., Gunduz, M., Onoda, N., Uchino, S., et al. (2019). A Novel Therapeutic Approach for Anaplastic Thyroid Cancer through Inhibition of LAT1. *Sci. Rep.* 9 (1), 14616. doi:10.1038/s41598-019-51144-6

Foroutan, T. (2016). Comparison of Differentiation of Induced Pluripotent Stem Cells and Bone-Marrow Mesenchymal Stem Cells to Osteoblast: Osteogenesis versus Pluripotency. *Int. J. Organ. Transpl. Med* 7 (2), 91–96.

Fu, Z., Liu, P., Yang, D., Wang, F., Yuan, L., Lin, Z., et al. (2012). Interleukin-18-induced Inflammatory Responses in Synoviocytes and Chondrocytes from Osteoarthritic Patients. *Int. J. Mol. Med.* 30 (4), 805–810. doi:10.3892/ijmm.2012.1073

Gandhapudi, S. K., Tan, C., Marino, J. H., Taylor, A. A., Pack, C. C., Gaikwad, J., et al. (2015). IL-18 Acts in Synergy with IL-7 to Promote *Ex Vivo* Expansion of T Lymphoid Progenitor Cells. *J.I.* 194 (8), 3820–3828. doi:10.4049/jimmunol.1301542

Gao, P., Tchernyshyov, I., Chang, T.-C., Lee, Y.-S., Kita, K., Ochi, T., et al. (2009). c-Myc Suppression of miR-23a/b Enhances Mitochondrial Glutaminase Expression and Glutamine Metabolism. *Nature* 458 (7239), 762–765. doi:10.1038/nature07823

Gibon, E., Lu, L., and Goodman, S. B. (2016). Aging, Inflammation, Stem Cells, and Bone Healing. *Stem Cel Res Ther* 7, 44. doi:10.1186/s13287-016-0300-9

Hayashi, K., Jutabha, P., Endou, H., and Anzai, N. (2012). c-Myc Is Crucial for the Expression of LAT1 in MIA Paca-2 Human Pancreatic Cancer Cells. *Oncol. Rep.* 28 (3), 862–866. doi:10.3892/or.2012.1878

Kandasamy, P., Gyimesi, G., Kanai, Y., and Hediger, M. A. (2018). Amino Acid Transporters Revisited: New Views in Health and Disease. *Trends Biochem. Sci.* 43 (10), 752–789. doi:10.1016/j.tibs.2018.05.003

Ko, F. C., Rubenstein, W. J., Lee, E. J., Siu, A. L., and Sean Morrison, R. (2018). TNF-α and sTNF-RII Are Associated with Pain Following Hip Fracture Surgery in Older Adults. *Pain Med.* 19 (1), 169–177. doi:10.1093/pm/pnx085

Li, Y., and Wang, L. (2018). Changes in Inflammatory Factors in Patients with Osteoporotic Vertebral Compression Fracture and Influences of Rehabilitation Training on Postoperative Functional Recovery and Inflammation. *J. Musculoskelet. Neuronal Interact* 18 (2), 272–279.

Lima Leite, E., Gautron, A., Deplanche, M., Nicolas, A., Ossemond, J., Nguyen, M. T., et al. (2020). Involvement of Caspase-1 in Inflammasomes Activation and Bacterial Clearance in *S. aureus* -infected Osteoblast-like MG -63 Cells. *Cell Microbiol.* 22 (8), e13204. doi:10.1111/cmi.13204

Liu, B., Wu, S., Han, L., and Zhang, C. (2015). β-Catenin Signaling Induces the Osteoblastogenic Differentiation of Human Pre-osteoblastic and Bone Marrow Stromal Cells Mainly through the Upregulation of Osterix Expression. *Int. J. Mol. Med.* 36 (6), 1572–1582. doi:10.3892/ijmm.2015.2382

Liu, P., Ge, M., Hu, J., Li, X., Che, L., Sun, K., et al. (2017). A Functional Mammalian Target of Rapamycin Complex 1 Signaling Is Indispensable for C-Myc-Driven Hepatocarcinogenesis. *Hepatology* 66 (1), 167–181. doi:10.1002/hep.29183

Loftus, R. M., Assmann, N., Kedia-Mehta, N., O'Brien, K. L., Garcia, A., Gillespie, C., et al. (2018). Amino Acid-dependent cMyc Expression Is Essential for NK Cell Metabolic and Functional Responses in Mice. *Nat. Commun.* 9 (1), 2341. doi:10.1038/s41467-018-04719-2

Lu, W., Yang, C., He, H., and Liu, H. (2020). The CARM1-P300-C-Myc-Max (CPCM) Transcriptional Complex Regulates the Expression of CUL4A/4B and Affects the Stability of CRL4 E3 Ligases in Colorectal Cancer. *Int. J. Biol. Sci.* 16 (6), 1071–1085. doi:10.7150/ijbs.41230

Makiishi-Shimobayashi, C., Tsujimura, T., Iwasaki, T., Yamada, N., Sugihara, A., Okamura, H., et al. (2001). Interleukin-18 Up-Regulates Osteoprotegerin Expression in Stromal/osteoblastic Cells. *Biochem. Biophysical Res. Commun.* 281 (2), 361–366. doi:10.1006/bbrc.2001.4380

Maugeri, D., Mamazza, C., Giudice, F. L., Puglisi, N., Muscoso, E. G., Rizzotto, M., et al. (2005). Interleukin-18 (IL-18) and Matrix Metalloproteinase-9 (MMP-9) in post-menopausal Osteoporosis. *Arch. Gerontol. Geriatr.* 40 (3), 299–305. doi:10.1016/j.archger.2004.10.001

Melnik, S., Werth, N., Boeuf, S., Hahn, E.-M., Gotterbarm, T., Anton, M., et al. (2019). Impact of C-MYC Expression on Proliferation, Differentiation, and Risk of Neoplastic Transformation of Human Mesenchymal Stromal Cells. *Stem Cel Res Ther* 10 (1), 73. doi:10.1186/s13287-019-1187-z

Meyer, N., and Penn, L. Z. (2008). Reflecting on 25 Years with MYC. *Nat. Rev. Cancer* 8 (12), 976–990. doi:10.1038/nrc2231

Moravcikova, E., Meyer, E. M., Corselli, M., Donnenberg, V. S., and Donnenberg, A. D. (2018). Proteomic Profiling of Native Unpassaged and Culture-Expanded Mesenchymal Stromal Cells (MSC). *Cytometry* 93 (9), 894–904. doi:10.1002/cyto.a.23574

Nair, R., Roden, D. L., Teo, W. S., McFarland, A., Junankar, S., Ye, S., et al. (2014). c-Myc and Her2 Cooperate to Drive a Stem-like Phenotype with Poor Prognosis in Breast Cancer. *Oncogene* 33 (30), 3992–4002. doi:10.1038/onc.2013.368

Nozaki, Y., Ri, J., Sakai, K., Niki, K., Kinoshita, K., Funauchi, M., et al. (2019). Inhibition of the IL-18 Receptor Signaling Pathway Ameliorates Disease in a Murine Model of Rheumatoid Arthritis. *Cells* 9 (1), 11. doi:10.3390/cells9010011

Ozaki, K., Yamada, T., Horie, T., Ishizaki, A., Hiraiwa, M., Iezaki, T., et al. (2019). The L-type Amino Acid Transporter LAT1 Inhibits Osteoclastogenesis and Maintains Bone Homeostasis through the mTORC1 Pathway. *Sci. Signal.* 12 (589), eaaw3921. doi:10.1126/scisignal.aaw3921

Poncet, N., Halley, P. A., Lipina, C., Gierliński, M., Dady, A., Singer, G. A., et al. (2020). Wnt Regulates Amino Acid Transporter Slc7a5 and So Constrains the Integrated Stress Response in Mouse Embryos. *EMBO Rep.* 21 (1), e48469. doi:10.15252/embr.201948469

Pountos, I., Walters, G., Panteli, M., Einhorn, T. A., and Giannoudis, P. V. (2019). Inflammatory Profile and Osteogenic Potential of Fracture Haematoma in Humans. *Jcm* 9 (1), 47. doi:10.3390/jcm9010047

Reich, K. M., Viitanen, P., Apu, E. H., Tangl, S., and Ashammakhi, N. (2020). The Effect of Diclofenac Sodium-Loaded Poly(Lactide-Co-Glycolide) Rods on Bone Formation and Inflammation: A Histological and Histomorphometric Study in the Femora of Rats. *Micromachines* 11 (12), 1098. doi:10.3390/mi11121098

Rosilio, C., Nebout, M., Imbert, V., Griessinger, E., Neffati, Z., Benadiba, J., et al. (2015). L-type Amino-Acid Transporter 1 (LAT1): a Therapeutic Target Supporting Growth and Survival of T-Cell Lymphoblastic lymphoma/T-Cell Acute Lymphoblastic Leukemia. *Leukemia* 29 (6), 1253–1266. doi:10.1038/leu.2014.338

Salazar, V. S., Gamer, L. W., and Rosen, V. (2016). BMP Signalling in Skeletal Development, Disease and Repair. *Nat. Rev. Endocrinol.* 12 (4), 203–221. doi:10.1038/nrendo.2016.12

Scalise, M., Galluccio, M., Console, L., Pochini, L., and Indiveri, C. (2018). The Human SLC7A5 (LAT1): The Intriguing Histidine/Large Neutral Amino Acid Transporter and its Relevance to Human Health. *Front. Chem.* 6, 243. doi:10.3389/fchem.2018.00243

Sinclair, L. V., Rolf, J., Emslie, E., Shi, Y.-B., Taylor, P. M., and Cantrell, D. A. (2013). Control of Amino-Acid Transport by Antigen Receptors Coordinates the Metabolic Reprogramming Essential for T Cell Differentiation. *Nat. Immunol.* 14 (5), 500–508. doi:10.1038/ni.2556

Singh, N., and Ecker, G. (2018). Insights into the Structure, Function, and Ligand Discovery of the Large Neutral Amino Acid Transporter 1, LAT1. *Ijms* 19 (5), 1278. doi:10.3390/ijms19051278

Tărlungeanu, D. C., Deliu, E., Dotter, C. P., Kara, M., Janiesch, P. C., Scalise, M., et al. (2016). Impaired Amino Acid Transport at the Blood Brain Barrier Is a Cause of Autism Spectrum Disorder. *Cell* 167 (6), 1481–1494. doi:10.1016/j.cell.2016.11.013

Vecchié, A., Bonaventura, A., Toldo, S., Dagna, L., Dinarello, C. A., and Abbate, A. (2021). IL-18 and Infections: Is There a Role for Targeted Therapies? *J. Cel Physiol* 236 (3), 1638–1657. doi:10.1002/jcp.30008

Wang, J.-Y., Wu, P.-K., Chen, P. C.-H., Lee, C.-W., Chen, W.-M., and Hung, S.-C. (2017). Generation of Osteosarcomas from a Combination of Rb Silencing and C-Myc Overexpression in Human Mesenchymal Stem Cells. *STEM CELLS Translational Med.* 6 (2), 512–526. doi:10.5966/sctm.2015-0226

Wang, X., Zhang, Y., Choukroun, J., Ghanaati, S., and Miron, R. J. (2018). Effects of an Injectable Platelet-Rich Fibrin on Osteoblast Behavior and Bone Tissue Formation in Comparison to Platelet-Rich Plasma. *Platelets* 29 (1), 48–55. doi:10.1080/09537104.2017.1293807

Wolfer, A., and Ramaswamy, S. (2011). MYC and Metastasis: Figure 1. *Cancer Res.* 71 (6), 2034–2037. doi:10.1158/0008-5472.Can-10-3776

Xiao, W. a., Hu, Z., Li, T., and Li, J. (2017). Bone Fracture Healing Is Delayed in Splenectomic Rats. *Life Sci.* 173, 55–61. doi:10.1016/j.lfs.2016.12.005

Xiao, W., Yang, X., Wang, Y., and Li, J. (2018). Splenectomy Delays Fracture Healing by Affecting the Level of Tumor Necrosis Factor Alpha, Interleukin 6 and Bone Morphogenetic Protein. *Adv. Clin. Exp. Med.* 27 (2), 165–171. doi:10.17219/acem/67755

Yue, M., Jiang, J., Gao, P., Liu, H., and Qing, G. (2017). Oncogenic MYC Activates a Feedforward Regulatory Loop Promoting Essential Amino Acid Metabolism and Tumorigenesis. *Cel Rep.* 21 (13), 3819–3832. doi:10.1016/j.celrep.2017.12.002

Zhao, S.-J., Kong, F.-Q., Jie, J., Li, Q., Liu, H., Xu, A.-D., et al. (2020). Macrophage MSR1 Promotes BMSC Osteogenic Differentiation and M2-like Polarization by Activating PI3K/AKT/GSK3β/β-catenin Pathway. *Theranostics* 10 (1), 17–35. doi:10.7150/thno.36930

Zhao, X., Petrashen, A. P., Sanders, J. A., Peterson, A. L., and Sedivy, J. M. (2019). SLC1A5 Glutamine Transporter Is a Target of MYC and Mediates Reduced mTORC1 Signaling and Increased Fatty Acid Oxidation in Long-lived Myc Hypomorphic Mice. *Aging Cell* 18 (3), e12947. doi:10.1111/acel.12947

Zhou, T., Yang, Y., Chen, Q., and Xie, L. (2019). Glutamine Metabolism Is Essential for Stemness of Bone Marrow Mesenchymal Stem Cells and Bone Homeostasis. *Stem Cell Int.* 2019, 1–13. doi:10.1155/2019/8928934

Conflict of Interest: Authors HD and JG are employed by Liaoning Qifu Stem Cell Biotechnology Co, Ltd.

The remaining authors declare that the research was conducted in the absence of any commercial or financial relationships that could be construed as a potential conflict of interest.

frontiers in Cell and Developmental Biology

REVIEW
published: 03 January 2022
doi: 10.3389/fcell.2021.787118

Bone Marrow Mesenchymal Stromal Cells: Identification, Classification, and Differentiation

Qianmin Gao [1,2,3,4†], Lipeng Wang [1†], Sicheng Wang [5†], Biaotong Huang [1,4,6], Yingying Jing [1,4*] and Jiacan Su [7*]*

[1]Institute of Translational Medicine, Shanghai University, Shanghai, China, [2]School of Medicine, Shanghai University, Shanghai, China, [3]School of Life Sciences, Shanghai University, Shanghai, China, [4]Shanghai University Institute of Advanced Interdisciplinary Materials Science, Shanghai, China, [5]Department of Orthopedics, Shanghai Zhongye Hospital, Shanghai, China, [6]Wenzhou Institute of Shanghai University, Wenzhou, China, [7]Department of Orthopedics Trauma, Shanghai Changhai Hospital, Naval Medical University, Shanghai, China

OPEN ACCESS

Edited by:
Ce Dou,
Army Medical University, China

Reviewed by:
Peng Xue,
Third Hospital of Hebei Medical University, China
Qian Cong,
Harvard University, United States

***Correspondence:**
Biaotong Huang
hbt021@sina.com
Yingying Jing
jingy4172@shu.edu.cn
Jiacan Su
drsujiacan@163.com

†These authors have contributed equally to this work

Specialty section:
This article was submitted to Cellular Biochemistry, a section of the journal Frontiers in Cell and Developmental Biology

Received: 30 September 2021
Accepted: 25 November 2021
Published: 03 January 2022

Citation:
Gao Q, Wang L, Wang S, Huang B, Jing Y and Su J (2022) Bone Marrow Mesenchymal Stromal Cells: Identification, Classification, and Differentiation. Front. Cell Dev. Biol. 9:787118. doi: 10.3389/fcell.2021.787118

Bone marrow mesenchymal stromal cells (BMSCs), identified as pericytes comprising the hematopoietic niche, are a group of heterogeneous cells composed of multipotent stem cells, including osteochondral and adipocyte progenitors. Nevertheless, the identification and classification are still controversial, which limits their application. In recent years, by lineage tracing and single-cell sequencing, several new subgroups of BMSCs and their roles in normal physiological and pathological conditions have been clarified. Key regulators and mechanisms controlling the fate of BMSCs are being revealed. Cross-talk among subgroups of bone marrow mesenchymal cells has been demonstrated. In this review, we focus on recent advances in the identification and classification of BMSCs, which provides important implications for clinical applications.

Keywords: bone marrow mesenchymal stromal cells, multipotent stem cells, skeletal stem cells, adipocyte lineage cells, BMSC

INTRODUCTION

BMSCs, first identified by Frieden (Friedenstein et al., 1976; Owen and Friedenstein, 1988), are a group of heterogeneous cells composed of multipotent stem cells, including osteochondral and adipocyte progenitors (Ashton et al., 1980; Pittenger et al., 1999; Wolock et al., 2019). BMSCs with niche forming and immunomodulatory ability are of great clinical significance and are widely explored in the treatment of autoimmune disorders and biological engineering (Orkin, 2000; Kong et al., 2009; Amini et al., 2012; Laranjeira et al., 2015).

Although the differentiation and hierarchies of hematopoietic stem cells have long been well clarified, those of BMSCs are less well defined (Azadniv et al., 2020), which limits BMSC application. Traditional RNA sequencing can only obtain the average data of cells, which fails to reflect cellular heterogeneity (Tang et al., 2019). The development of single-cell sequencing offers the opportunity to identify and classify BMSCs at the single-cell level. Through single-cell sequencing, several new BMSC subgroups have been identified, and their roles are clarified under normal physiological and pathological conditions.

In this review, we focus on recent advances in the identification and classification of BMSCs, key regulators, and mechanisms controlling BMSC fate and cross-talk among subgroups of BMSCs, to find important implications for clinical applications.

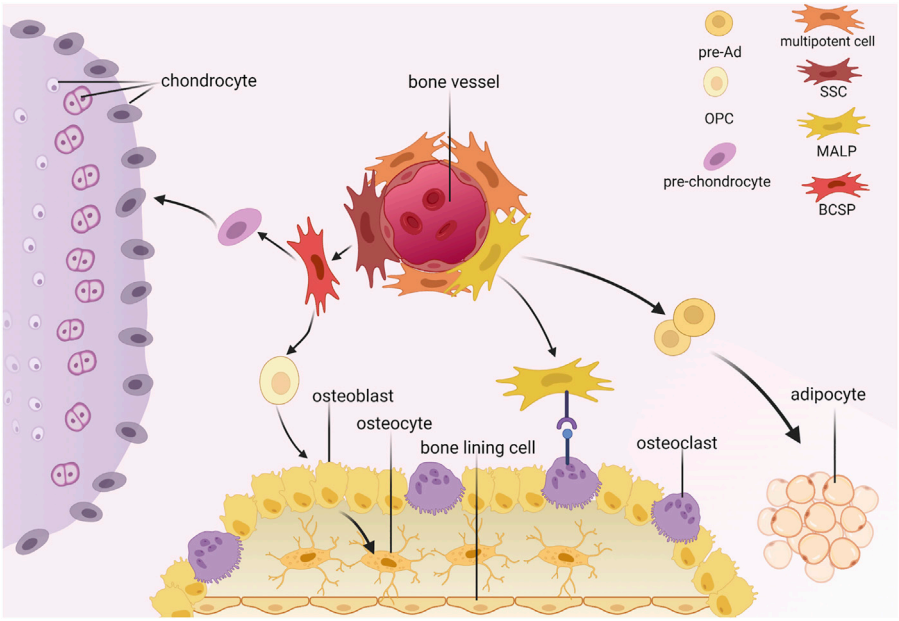

FIGURE 1 | Hierarchy of bone marrow mesenchymal stromal cells. SSC, skeletal stem cell; MALP, marrow adipogenic lineage precursors; BCSP, bone, cartilage and stromal progenitor; pre-Ad, pre-adipocyte; OPC, osteo progenitor cell.

Identification and Classification

According to the International Society for Cellular Therapy, BMSCs are plastic-adherent when maintained in standard culture conditions and express CD105, CD73, and CD90 but not CD45, CD34, CD14, or CD11b, CD79α, or CD19 or HLA-DR surface molecules. In addition, BMSCs can differentiate into osteoblasts, adipocytes, and chondroblasts *in vitro* (Dominici et al., 2006). In this review, we emphasize the multipotent stem cells (MSCs), skeletal stem cells (SSCs), and adipocyte lineage cells (**Figure 1**).

Multipotent Stem Cells

The identification of MSCs is mainly based on morphological observation (Li et al., 2016) and detection of surface markers (Baddoo et al., 2003; Ambrosi et al., 2017).

Novel molecular markers are continually being investigated to identify MSCs. LepR+ cells are a highly heterogeneous population containing multipotent stem cells. They are the main source of osteo-lineage cells and adipo-lineage cells in adult mice and generate the hematopoietic niche around bone vessels. Leptin receptor (LepR)+ cells are the primary source of multipotent stem cells that are stem cell factor (SCF)^{high} Cxcl12 ^{high} Nestin^{low} NG2^{low} (Zhou et al., 2014). Platelet-derived growth factor-α (PDGFRα)+ is another marker used individually or in combination for enriching MSCs (Suire et al., 2012; Grandl and Wolfrum, 2017). Its combinations include CD45-Ter119- (a nonhematopoietic marker) CD31-CD51+Sca1+ (Wolock et al., 2019), and CD45-Ter119-vascular cell adhesion molecule (VCAM) + CD146^{low}CD31–PDGFRα+ (Chou et al., 2012). Glioma-associated oncogene (Gli1) +, a transcription factor and an effector of the Hedgehog pathways, enriches metaphysis mesenchymal progenitor cells (MMPs) located at the junction of cartilage just below the growth plate of postnatal mice. Hox11+ enriches MSCs in adult mice (Swinehart et al., 2013), especially in the periosteum and perivascular areas (Rux et al., 2016). In addition, CXCL12-abundant reticular (CAR) cells enrich bipotent progenitors of osteoblasts and adipocytes (Omatsu et al., 2010).

With the development of single-cell sequencing, we are able to further classify highly heterogeneous MSCs (Tikhonova et al., 2019). In addition, with a single trajectory, we can further characterize the hierarchy and differentiation routes of osteoblasts, chondrocytes, and adipocytes (Wolock et al., 2019). Wolock assigned cell state labels to each cluster of the scRNA-seq dataset and inferred the gene expression trajectories of MSCs isolated by flow cytometry. In this study, mesenchymal stromal cells represented the starting states and the most abundant population in the dataset. Gene sets of extracellular matrices, BMP2 targets, adipose tissue stromal cells, and HSC-supportive stromal cell lines were enriched in mesenchymal stromal cells, including B3galnt1, Cebpa, Cxcl12, Cybb, Il7, Kitl, Lpl, and Snai2. Mesenchymal stromal cells differentiate into adipocyte progenitors and osteoblast-chondrocyte progenitors. The second layer of hierarchy consists of adipocyte progenitors (AdPs) and osteoblast-chondrocyte progenitors (OsPs). The third group consists of preadipocytes (pre-Ad) and preosteoblast chondrocytes (Pre-OCs). Gene set enrichment analysis of TNFA signaling *via* NFKB showed that during adipogenesis, adult tissue stem cells are enriched in AdPs and pre-Ad, including Adipoq, Ccl2, Cebpb, Cxcl12, Fos, Il6, Jun,

and Kitl. OsPs and pre-OCs were enriched in the gene sets of extracellular matrices, epithelial–mesenchymal transition, extracellular space, and tissue development, including Alpl, Mmp13, Poxstn, Sp7, and Wif1. Pro-osteoblasts and prochondrocytes served as end states of this dataset. Pro-osteoblasts were enriched in the gene set of endoplasmic reticula, Golgi apparatus, skeletal system development, and ossification, including Bglap, Col1a1, Col1a2, Creb3l1, Mef2c, Nupr1, Spare, and Sp7. Prochondrocytes were enriched in tissue development, extracellular space, and biomineral tissue development genes, including Ackr3, Ank, Cd44, Dmp1, Mepa, Mmp13 Nupr1, and Spp1 (Wolock et al., 2019).

Tikhonova classified LepR+ cells into four clusters by scRNA-seq: adipogenesis-associated clusters were P1 (Mgp high) and P2 (Lpl high), suggesting a poised pro-adipogenic state; clusters P3 (Wif1 high) and P4 (Spp1 high Ibsp high) represented osteoprimed LEPR+ cells (Tikhonova et al., 2019).

Zhong and others subdivided MSCs. They further classified LepR+ cells and reported the following hierarchy of LepR+ cells: early mesenchymal progenitors (EMPs) as the state status (highly expressing the genes Ly6a, Cd34, Thy1, Mfap5, Gsn, and Cles3b); intermediate mesenchymal progenitors (IMPs) (expressing higher levels of osteogenic genes than EMPs and located after EMPs); late mesenchymal progenitors (LMPs) (highly expressing the genes Aspn, Edil3, Tnn, Pstn, Ostn, and Dkk3); lineage committed progenitors (LCPs); and three final states of osteoblast/osteocyte (highly expressing the genes Sp7, Runx3, Col1a1, Ibsp, Bglap2, and Dmp1), adipocyte (highly expressing the genes Cebpa, Cebpb, Pparg, Lpl, Adipoq, and Apoe), and chondrocyte clusters (highly expressing the genes Sox9, Col2a1, Col10a1, Pth1r, Acan, and Ihh) (Zhong et al., 2020).

In the studies mentioned above, some functional features of MSCs have arisen. LepR+ MSCs are located around sinusoids and arterioles, are a main source of adipocytes in adult bone marrow (Tikhonova et al., 2019), and are regulated by the Pten gene to promote osteogenesis and to restrain adipogenesis (Zhou et al., 2014). CAR LepR+ MSCs can retain HSCs and colony-forming progenitors. During growth, Hox11 + can form perichondrium, tendons, and muscle connective tissue (Swinehart et al., 2013). Under irradiation, LepR+ MSCs can form osteoblasts and adipocytes (Zhou et al., 2014).

When discussing MSCs, we emphasize their potential for differentiation in multiple directions. The starting point of the branch of BMSCs has long been discussed, yet there is still no common resolution. After assembling the current studies that identify and classify MSCs through various markers or their combination, we tried to illustrate some functional relations and provide some implications for clinical applications.

Skeletal Stem Cells

SSCs were once thought to be equal to BMSCs (Li et al., 2016) and to functionally give rise not only to osteoblasts and chondrocytes but also to adipocytes (Robey and Riminucci, 2020). However, recent studies have determined that SSCs, as a lineage-restricted subset of BMSCs, are especially characterized by self-renewal and osteochondral (Méndez-Ferrer et al., 2010; Chan et al., 2013; Marecic et al., 2015a; Worthley et al., 2015) differentiation (Méndez-Ferrer et al., 2010; Chan et al., 2013; Marecic et al., 2015a; Worthley et al., 2015).

Various studies have identified and defined different SSCs by detecting different sites of active bone growth. Therefore, it may be easier to understand SSCs from a clinical and functional perspective.

In the mouse growth plate, the system of SSCs and their downstream progenitors can be described as lineage hierarchy. Determination of the mouse SSC (mSSC) lineage hierarchy included mSSCs and pre-mBCSP cells (CD45-TER119-TIE2-ITGAV+THY1-6C3-CD200-CD105-). Then, mBCSP cells (CD45-TER119-TIE2-ITGAV+THY1-6C3-CD105+) were generated, followed by chondro-lineage/PCP cells (CD45-TER119-TIE2-ITGAV+THY1+6C3-CD200 + CD105+), osteo-lineage cells, and stroma cells. The osteo-lineage can be further classified into two subgroups, namely, THY (CD45-TER119-TIE2-ITGAV+THY1+6C3-CD200-CD105+) and B-cell lymphocyte stroma progenitors (BLSPs) (CD45-TER119-TIE2-ITGAV+THY1+6C3-CD105-). The stroma can also be further classified into two subgroups, that is, 6C3 (CD45-TER119-TIE2-ITGAV+THY1-6C3+CD105+) and hepatic leukemia factor-expressing HECs (CD45-TER119-TIE2-ITGAV+THY1-6C3+CD105-) (Chan et al., 2015). The same group also reported on SSCs in human tissue. Nonhematopoietic SSCs can be prospectively isolated and characterized by PDPN+CD146-CD73+CD164+ (Chan et al., 2018). Another study isolated an intermediate cell type (CD200+ CD105-) between the start cluster mSSCs and BCSPs. These cells are self-renewing, pluripotent, and give rise to all other cells at the single-cell level. Pre-mBCSPs and mSSCs are functionally indistinguishable, so this population may be collectively referred to as phenotypic mSSCs (Gulati et al., 2018). PTHrP+ resting chondrocytes were identified as SSCs in the stationary region of the growth plate partially overlapping with mouse skeletal stem cells and progenitor cells previously identified by Chan and others. These cells are distributed in the perichondrium during the fetal stage (Mizuhashi et al., 2018) (**Figure 2**).

A study reported the existence of an SSC pool within the periosteum. Compared with bone marrow SSCs, periosteum SSCs are more clonal and have stronger growth and bone regeneration ability (Allen et al., 2004). Ctsk was found to label a type of SSC called periosteum stem cells that exist in the periosteum mesenchyme of long bones or the skull (Debnath et al., 2018). Gli1+ cells are osteogenic, chondrogenic, and weakly adipogenic cells in the sutura cranii (Zhao et al., 2015; Farmer et al., 2021). Axin2+ can label osteogenic and cartilaginous cells in the cranii (Maruyama et al., 2016).

In the hematopoietic microenvironment in human bone marrow, Sacchetti found a cluster of CD146+TIE2- cells around sinusoids defined as SSCs (Sacchetti et al., 2007). Another study from the same group illustrated that CD146 is able to functionally regenerate bone and stroma and to form a homotopic niche (Serafini et al., 2014).

As shown above, we can see that the tight relationship between active bone generation and the location of SSCs was vividly shown above.

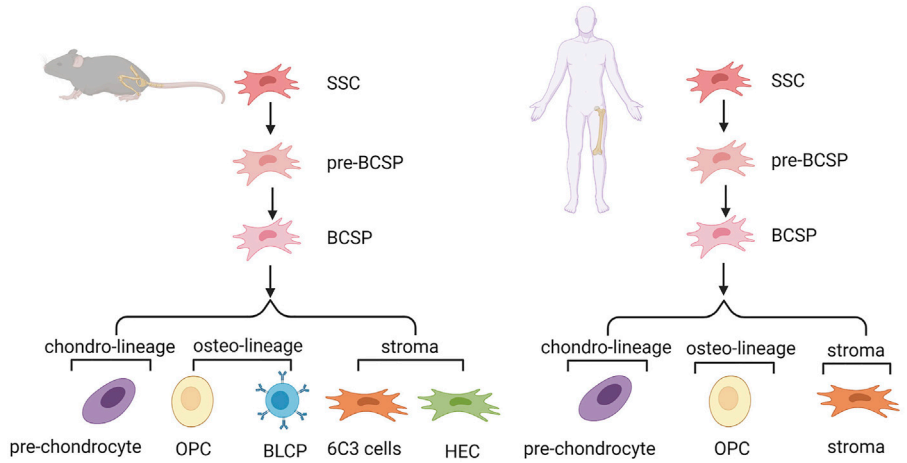

FIGURE 2 | Hierarchy of skeletal stem cells in mouse and human growth plate. SSC, skeletal stem cell; pre-BCSP, pre-bone, cartilage and stromal progenitor; BCSP, bone, cartilage and stromal progenitor; BLSP, B-cell lymphocyte stroma progenitor; OPC, osteo progenitor cell.

Adipocyte Lineage Cells

Adipocyte lineage cells represent a branch of BMSCs after the differentiation point in the pseudotime trajectory according to several studies.

Berry and Rodeheffer described adipocyte lineage cells consisting of CD24+ cells (generating adipocyte progenitors) and CD24$^-$cells (generating preadipocytes) (Berry and Rodeheffer, 2013). Gupta reported the use of the transcription factor zinc-finger protein (Zfp)423 to enrich preadipocytes in bone marrow, which is generally used to label adipogenic cells in white adipose tissue (WAT) (Gupta et al., 2012). In addition, Zfp423 is able to distinguish preadipocytes from adipogenic progenitor cells in bone marrow. According to Ambrosi's study, marker combination adipogenic progenitor cells can be enriched in CD45-CD31-Sca1+Pα+CD24-Zfp423- and pre-Ads by CD45-CD31-Sca1-CD24-Zfp423+ (Ambrosi et al., 2017). Another study mentioned above identified adipocyte lineage cells of LepR+ cells. Tikhonova reported but did not clearly define two adipogenesis-associated clusters P1 (Mgp high) and P2 (Lpl high), which presented a continuous relationship among four subsets of LepR+ cells. They were specifically found covering the sinusoidal capillaries as LepR+Esm1+ cells (Tikhonova et al., 2019). However, the association between these two has not been fully developed (Tencerova and Kassem, 2016).

There were significant differences in cell size and fatty acid content between intramedullary and extramedullary fat cells. Zhong first classified adipocyte lineage cells from a morphological perspective. There was a novel population of adipocyte lineage cells containing no lipid droplets in the cytoplasm. Zhong further identified a novel population that does not express Plin1, a lipid droplet coating protein gene, but does express Pparg, Cebpa, Adipoq, Apoe, Lpl, Lepr, Cxcl12, Il1rn, Serpina3g, Kng1, Kng2, Agt, Esm1, and Gdpd2 *in vivo* and named them marrow adipogenic lineage precursors (MALPs). In conclusion, MALPs express adipocyte markers but do not contain lipid droplets. As nonproliferative precursors of adipocytes, they are abundant in the form of pericytes and stromal cells, forming ubiquitous 3D networks in the bone marrow cavity, maintaining the bone marrow vascular system and inhibiting bone formation (Zhong et al., 2020). However, the pericyte function of these cells is not totally clear. The MALP knockout experiment did not change anything with respect to hematopoiesis. Zhou claimed that bone marrow adipocytes secrete SCF to promote the regeneration of stem cells and hematopoiesis (Zhou et al., 2017).

In brief, the identification and classification of adipocyte lineage cells seems simpler than that of MSCs and SSCs at present. More attention should be given to functional studies in the future.

Linkage Between Fat and Bone

Regulation of Differentiation Fate

As illustrated in many studies, the differentiation fate of BMSCs to osteo-lineage cells and to adipo-lineage bone cells is located on two branches. The differentiation fate is specifically regulated by an increase in intracellular transcription factors (TFs), signaling pathways, and microRNAs. In addition, extracellular elements such as hypoxia and mechanical stimulation are also involved in this vital process (**Figure 3**).

For osteogenesis, TFs regulate the differentiation fate of BMSCs by increasing the expression of genes that are responsible for the corresponding osteo-cell type. Runt-related transcription factor 2 (Runx2) and Osterix are two key TFs that promote osteoblast differentiation (Augello and De Bari, 2010). Runx2 enhanced by core-binding factor beta (Cbfβ) promotes osteoblast differentiation (Yoshida et al., 2002), but inhibits adipocyte differentiation of BMSCs by disturbing PPARγ (Komori, 2006). Runx2 is also called core binding factor α1 (Cbfa1) and is upregulated in BMSCs through single-cell sequencing (Wolock et al., 2019). Many other factors can increase the TF level of Runx2 and then cooperate with it, such as bone morphogenetic protein-2 (BMP2), Dlx5, Sprouty

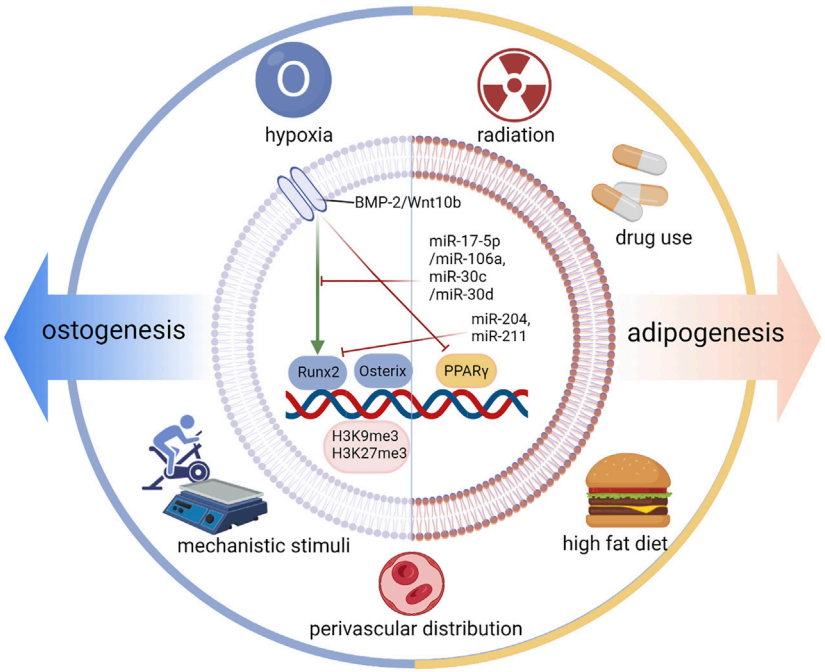

FIGURE 3 | Regulation of differentiation fate. The differentiation fate of BMSCs is specifically regulated by an increase in intracellular transcription factors (TFs), Osterix and PPARγ; signaling pathways; and microRNAs. In addition, extracellular elements such as hypoxia and mechanical stimulation are also involved in this vital process. Runx2, Runt-related transcription factor 2; BMP2, bone morphogenetic protein-2.

2 (Spry2), Twist-1, and Twist-2 (Gori et al., 1999; Bialek et al., 2004; Kronenberg, 2004; Augello and De Bari, 2010; Schneider et al., 2017). Under pathological conditions, unexpected upregulation of Runx2 causes heterotopic ossification (Wang et al., 2019). BMP2 is proven to be a key signaling pathway by targeting Runx2/Cbfa1. High concentrations of BMP2 show dose-dependent effects on osteogenesis (Javed et al., 2008). Furthermore, microRNAs are another important coeffector in this process. MiR-204 and miR-211 are induced during adipogenesis and downregulate Runx2 expression (Huang et al., 2010). MiR-17-5p/miR-106a and miR-30c/miR-30 days inhibit BMP signaling by targeting key components of the pathway, namely, BMP2 and Smad1 (Kang and Hata, 2015). In addition to runx2, a vital factor related to many important signaling pathways and microRNAs, osterix is another primary TF for the osteogenesis of BMSCs. Osterix has been demonstrated to play a role downstream of runx2 and can be activated by runx2 (Nakashima et al., 2002). In osterix-null mice, MSCs cannot differentiate into osteoblasts, and no bone formation occurs (Nakashima et al., 2002). Osterix, also called Sp7, is upregulated in OBs and pre-OBs based on single-cell sequencing (Wolock et al., 2019; Zhong et al., 2020). miR-637 and miR-31 can directly suppress osterix expression (Zhang et al., 2011; Baglìo et al., 2013). In addition to Runx2 and osterix, other transcription factors, such as TAZ and Forkhead box C2 (Foxc2), can also promote osteogenesis and suppress adipogenesis (Hong et al., 2005; Park et al., 2011; Yu et al., 2018). The expression of Wnt10b signaling promotes osteogenesis by inducing the expression of runx2, osterix, distal-less homeobox 5 (Dlx5), and TAZ and suppresses adipogenesis by inhibiting PPARγ and C/EBPα (Bennett et al., 2005; Byun et al., 2014), which demonstrates the pro-osteoblastic and anti-adipocytic differentiation effect of Wnt/β-catenin signaling (Kang and Hata, 2015; Gu et al., 2016). The regulatory function of H3K9me3 and H3K27me3 works in balancing the osteogenic and adipogenic differentiation of mesenchymal stem cells. Ye et al. reported that the histone demethylase KDM4B in BMSCs increases bone marrow fat cells by epigenetic coordination of β-catenin/Smad1-mediated transcription by removing inhibitory H3K9me3, ultimately contributing to bone aging and osteoporosis (Ye et al., 2012). Xue et al. reported that H3K9me3 can activate Wnt-5a and repress PPAR-γ (Xu et al., 2016).

For adipogenesis, PPARγ plays a vital role by regulating the expression of adipogenic genes. PPARγ shows pro-adipocytic and anti-osteoblastic effects (Zhuang et al., 2016). Upstream of FOXO1, it could regulate lipogenesis through PPARγ and the adipocyte cell cycle through p21 and p27 (Chen et al., 2019). PPARγ agonists induce adipocyte differentiation by modulating the expression of Lipin-1 downstream (Kim et al., 2016). PPARγ is a secretory BMP inhibitor (Gustafson et al., 2015). As mentioned above, a high concentration of BMP2 accelerates osteoblast differentiation, while a low concentration of BMP2 promotes adipocyte formation in the C3H10T1/2 mesenchymal cell line (Tang et al., 2004). Additionally, CCAAT/enhancer binding protein α (C/EBPα), platelet-derived growth factor receptor β (PDGFβ) and zinc finger proteins 423 and 521 also take part in adipogenesis (Lin and Lane, 1994; Gupta et al., 2012; Huang et al., 2012; Dang et al., 2021).

In addition to transcription factors, signaling pathways, miRNAs, and other intracellular influencing factors, there are extracellular factors that can also play an important regulatory role, typically including hypoxia, mechanistic stimuli, radiation, a high-fat diet, drug use, and perivascular distribution.

Hypoxia promotes osteogenesis but suppresses adipogenesis of human mesenchymal stromal cells in a hypoxia-inducible factor-1 (HIF-1)-dependent manner (Wagegg et al., 2012). Hypoxia and hypoxia-mimetic microRNA miR-675-5p mediate the angiogenesis response and osteochondroblast commitment of hMSCs (Costa et al., 2017; Wang et al., 2007). Clinically, an FDA-approved iron chelator promotes angiogenesis and osteogenesis, thereby enhancing the rate of fracture repair (Yellowley and Genetos, 2019), while hypoxia promotes osteogenesis but suppresses adipogenesis of human mesenchymal stromal cells in a hypoxia-inducible factor-1 (HIF-1) dependent manner (Wagegg et al., 2012). Hypoxia and hypoxia-mimetic microRNA miR-675-5p in angiogenesis response and osteo-chondroblast commitment of hMSCs (Costa et al., 2017; Wang et al., 2007). Clinically, an FDA-approved iron chelator promotes angiogenesis and osteogenesis, thereby enhancing the rate of fracture repair (Yellowley and Genetos, 2019). Mechanical factors, such as exercise and vibration, have been confirmed by many studies to regulate the differentiation fate of BMSCs. Climbing exercise was reported to significantly increase bone volume and OB number while decreasing bone marrow fat volume and adipocyte number (Mori et al., 2003; Menuki et al., 2008). *In vivo* studies have demonstrated that vibrations with low-magnitude mechanical signals upregulate Runx2 and downregulate PPARγ (Luu et al., 2009). In addition, low-magnitude high-frequency vibration may promote osteoblast differentiation of MSCs *via* the Wnt/β-catenin signaling pathway, the estrogen receptor α signaling pathway, and cytoskeletal remodeling (Haffner-Luntzer et al., 2018; Wang et al., 2020; Yi et al., 2020) (Wang et al., 2020a; Haffner-Luntzer et al., 2018; Yi et al., 2020).

In addition to mechanical stimuli, other chemical factors, such as a high-fat diet and drug use, also play roles in regulating MSC differentiation. Obesity caused by a high-fat diet and aging impair osteogenesis and hematopoietic regeneration by regulating osteoblastic or adipocytic genes, probably through PPAR-γ (Parhami et al., 2001; da Silva et al., 2016; Ambrosi et al., 2017). Yue et al. reported that in diabetes and obesity, LepR signaling in BMSCs has been shown to promote adipogenesis and inhibit osteoblast production in response to diet (Yue et al., 2016). In addition, both obesity and osteoporosis are associated with elevated oxidative stress and increased production of proinflammatory cytokines. The expression levels of DLL1/delta-like one and DLL4/delta-like four ligands decreased under stress conditions. In the absence of vascular Dll4, hematopoietic stem cells prematurely induce bone marrow transcriptional programming (Tikhonova et al., 2019). Deacetylated histone 3 (Hdac3) inhibits lipid storage in osteoblasts and controls fat production (Pierce et al., 2019). Regarding drug use, long-term use of steroid hormones, such as glucocorticoids, can lead to obesity with rapid bone loss (Body, 2010).

In addition, previous studies have suggested that the differentiation directions appear to be correlated with distinguishing the perivascular distribution of cells. Perivascular multipotent stem cells fall into two categories based on the differential expression of the accepted adipose precursor marker stem cell antigen (Sca) 1+ (Ambrosi et al., 2017): around arterioles (PDGFRα+Sca-1-CD45-Ter119- cells) (Morikawa et al., 2009; Ambrosi et al., 2017) and around sinusoids [PDGFRα+Sca-1-CD45-Ter119-, as well as CAR cells (Greenbaum et al., 2013)]. Osteolectin is an osteogenic growth factor that enhances the maintenance of adult skeletal bone cells. It has also been reported that a group of peri-arteriolar LepR+Oln+ cells express osteogenic genes by gene set enrichment analysis. However, LepR+Oln- cells were distributed around the venous sinus and expressed lipogenic genes (Shen et al., 2021).

Taken together, internal factors, such as epigenetic regulation and perivascular distribution, and external factors, such as exercise, drug use, and a high-fat diet, are also critical in regulating osteogenesis and adipogenesis of BMSCs. These factors may take effect through cross-talk with the key transcription factors and signaling pathways mentioned above.

In brief, the differentiation fate regulation of BMSCs presents a complex network.

Cross-Talk Between Bone and Fat

Bone growth is the coupling of bone formation by osteoblasts and bone absorption by osteoclasts. In childhood, bone growth is dominated by osteogenesis. During aging, cross-talk occurs between bone and fat. Osteogenesis weakens, bone absorption increases, and fat cells in the bone marrow increase.

Fat is negatively related to bone mass (Shen et al., 2007; Shen et al., 2014). Fat is reported to inhibit bone formation and fracture healing (Ambrosi et al., 2017). Fat can affect bone growth through two or more mechanisms. It was reported that adipo-lineage progenitors specifically and highly express osteoclast regulatory factors. RANKL is the most widely studied one. MALPs can specifically secrete several osteoclast regulatory factors, especially RANKL, which is involved in the progression of bone remodeling (Robling and Bonewald, 2020; Hu et al., 2021; Yu et al., 2021). Adipokines, such as leptin, adiponectin, and chemerin, are typically secreted by adipocytes and are directly or indirectly involved in bone metabolism and correlated with bone mineral density (Fang and Judd, 2018; Helfer and Wu, 2018; Reid et al., 2018; Maeda et al., 2020; Zhao et al., 2020; Fang and Judd, 2018; Helfer and Wu, 2018; Reid et al., 2018; Maeda et al., 2020; Zhao et al., 2020). In pathological situations, such as postmenopausal osteoporosis, obesity has long been considered a beneficial factor for bone health (Felson et al., 1993) that can reduce the risk of fracture (Compston et al., 2014). However, as soon as fracture occurs, the opposite condition occurs. Adipocytic cells significantly impair bone fracture healing and hematopoietic repopulation by secreted dipeptidyl peptidase-4 (DPP4), an important target of antidiabetes treatments (Ambrosi et al., 2017). This adipocyte ablation-mediated enhancement of bone

mass reflects the activation of BMP receptors after the elimination of its inhibitor, which is associated with simultaneous epidermal growth factor receptor signaling. Diphtheria toxin receptor adiponectin-induced osteosclerosis was not due to ablation of surrounding fat cells but may reflect the elimination of cells expressing adiponectin in the bone marrow (Zou et al., 2020). To our knowledge, acute fat loss through dieting does not affect bone mass (Lagerquist et al., 2021).

Regarding the effect of bone on fat, there are few studies. However, in many pathological conditions, such as osteoporosis, the phenomenon of expanding the volume and number of adipocytes in BM is generally observed (Justesen et al., 2001). Bone loss is often regarded as a consequence but not an impact factor. The clinical influence of bone on fat needs to be further explored. What is more, many other well-known ways are able to restrain the fat accumulation so that there may be no need to regulate fat through bone and fat cross-talk.

As shown above, cross-talk exists between differentiated bone tissue and fat. The balance between these two is tightly related to physiological homeostasis and pathological situations.

CONCLUSION

In conclusion, BMSCs are highly heterogeneous. Different researchers have defined subsets of markers or combinations that are discrete or partially overlapping. Otherwise, those single-cell sequencing studies report their classic and newly discovered roles and connections in the context of physiological or pathological states. The diversity and assortative nature of different cell markers makes it difficult to classify BMSCs, let alone find associations between them. We tried our best to review the identification and classification and to find a link among the overlapping clues of multipotent stem cells, skeletal stem cells, and adipocyte lineage cells for more applicable and clinical explanations.

AUTHOR CONTRIBUTIONS

QG and SW conceived the manuscript. QG and LW wrote the manuscript. BH, YJ, and JS reviewed and edited the manuscript. All authors listed have made a substantial, direct, and intellectual contribution to work, and approved it for publication.

FUNDING

This work was funded by the National Key Research and Development Plan (2018YFC2001500), the National Natural Science Foundation of China (NSFC) Key Research Program in Aging (91749204), the National Natural Science Foundation of China (81771491, 81972254, and 82172098), and Shanghai Municipal Health Commission (202040372).

REFERENCES

Allen, M. R., Hock, J. M., and Burr, D. B. (2004). Periosteum: Biology, Regulation, and Response to Osteoporosis Therapies. *Bone* 35, 1003–1012. doi:10.1016/j.bone.2004.07.014

Ambrosi, T. H., Scialdone, A., Graja, A., Gohlke, S., Jank, A.-M., Bocian, C., et al. (2017). Adipocyte Accumulation in the Bone Marrow during Obesity and Aging Impairs Stem Cell-Based Hematopoietic and Bone Regeneration. *Cell Stem Cell* 20, 771–784. doi:10.1016/j.stem.2017.02.009

Amini, A. R., Laurencin, C. T., and Nukavarapu, S. P. (2012). Bone Tissue Engineering: Recent Advances and Challenges. *Crit. Rev. Biomed. Eng.* 40, 363–408. doi:10.1615/critrevbiomedeng.v40.i5.10

Ashton, B. A., Allen, T. D., Howlett, C. R., Eaglesom, C. C., Hattori, A., and Owen, M. (1980). Formation of Bone and Cartilage by Marrow Stromal Cells in Diffusion chambers *In Vivo*. *Clin. Orthopaedics Relat. Res.* &NA;, 294–307. doi:10.1097/00003086-198009000-00040

Augello, A., and De Bari, C. (2010). The Regulation of Differentiation in Mesenchymal Stem Cells. *Hum. Gene Ther.* 21, 1226–1238. doi:10.1089/hum.2010.173

Azadniv, M., Myers, J. R., McMurray, H. R., Guo, N., Rock, P., Coppage, M. L., et al. (2020). Bone Marrow Mesenchymal Stromal Cells from Acute Myelogenous Leukemia Patients Demonstrate Adipogenic Differentiation Propensity with Implications for Leukemia Cell Support. *Leukemia* 34, 391–403. doi:10.1038/s41375-019-0568-8

Baddoo, M., Hill, K., Wilkinson, R., Gaupp, D., Hughes, C., Kopen, G. C., et al. (2003). Characterization of Mesenchymal Stem Cells Isolated from Murine Bone Marrow by Negative Selection. *J. Cel. Biochem.* 89, 1235–1249. doi:10.1002/jcb.10594

Baglìo, S. R., Devescovi, V., Granchi, D., and Baldini, N. (2013). MicroRNA Expression Profiling of Human Bone Marrow Mesenchymal Stem Cells during Osteogenic Differentiation Reveals Osterix Regulation by miR-31. *Gene* 527, 321–331. doi:10.1016/j.gene.2013.06.021

Bennett, C. N., Longo, K. A., Wright, W. S., Suva, L. J., Lane, T. F., Hankenson, K. D., et al. (2005). Regulation of Osteoblastogenesis and Bone Mass by Wnt10b. *Proc. Natl. Acad. Sci.* 102, 3324–3329. doi:10.1073/pnas.0408742102

Berry, R., and Rodeheffer, M. S. (2013). Characterization of the Adipocyte Cellular Lineage *In Vivo*. *Nat. Cel Biol* 15, 302–308. doi:10.1038/ncb2696

Bialek, P., Kern, B., Yang, X., Schrock, M., Sosic, D., Hong, N., et al. (2004). A Twist Code Determines the Onset of Osteoblast Differentiation. *Dev. Cel* 6, 423–435. doi:10.1016/s1534-5807(04)00058-9

Body, J.-J. (2010). Prevention and Treatment of Side-Effects of Systemic Treatment: Bone Loss. *Ann. Oncol.* 21 (Suppl. 7), vii180–vii185. doi:10.1093/annonc/mdq422

Byun, M. R., Hwang, J.-H., Kim, A. R., Kim, K. M., Hwang, E. S., Yaffe, M. B., et al. (2014). Canonical Wnt Signalling Activates TAZ through PP1A during Osteogenic Differentiation. *Cell Death Differ* 21, 854–863. doi:10.1038/cdd.2014.8

Chan, C. K. F., Gulati, G. S., Sinha, R., Tompkins, J. V., Lopez, M., Carter, A. C., et al. (2018). Identification of the Human Skeletal Stem Cell. *Cell* 175, 43–56. doi:10.1016/j.cell.2018.07.029

Chan, C. K. F., Seo, E. Y., Chen, J. Y., Lo, D., McArdle, A., Sinha, R., et al. (2015). Identification and Specification of the Mouse Skeletal Stem Cell. *Cell* 160, 285–298. doi:10.1016/j.cell.2014.12.002

Chen, J., Lu, Y., Tian, M., and Huang, Q. (2019). Molecular Mechanisms of FOXO1 in Adipocyte Differentiation. *J. Mol. Endocrinol.* 62, R239–R253. doi:10.1530/JME-18-0178

Chou, D. B., Sworder, B., Bouladoux, N., Roy, C. N., Uchida, A. M., Grigg, M., et al. (2012). Stromal-derived IL-6 Alters the Balance of Myeloerythroid Progenitors duringToxoplasma Gondiiinfection. *J. Leukoc. Biol.* 92, 123–131. doi:10.1189/jlb.1011527

Compston, J. E., Flahive, J., Hosmer, D. W., Watts, N. B., Siris, E. S., Silverman, S., et al. (2014). Relationship of Weight, Height, and Body Mass index with Fracture Risk at Different Sites in Postmenopausal Women: the Global Longitudinal Study of Osteoporosis in Women (GLOW). *J. Bone Miner Res.* 29, 487–493. doi:10.1002/jbmr.2051

da Silva, S. V., Renovato-Martins, M., Ribeiro-Pereira, C., Citelli, M., and Barja-Fidalgo, C. (2016). Obesity Modifies Bone Marrow Microenvironment and Directs Bone Marrow Mesenchymal Cells to Adipogenesis. *Obesity* 24, 2522–2532. doi:10.1002/oby.21660

Dang, T. N., Taylor, J. L., Kilroy, G., Yu, Y., Burk, D. H., and Floyd, Z. E. (2021). SIAH2 Is Expressed in Adipocyte Precursor Cells and Interacts with EBF1 and ZFP521 to Promote Adipogenesis. *Obesity* 29, 98–107. doi:10.1002/oby.23013

Debnath, S., Yallowitz, A. R., McCormick, J., Lalani, S., Zhang, T., Xu, R., et al. (2018). Discovery of a Periosteal Stem Cell Mediating Intramembranous Bone Formation. *Nature* 562, 133–139. doi:10.1038/s41586-018-0554-8

Dominici, M., Le Blanc, K., Mueller, I., Slaper-Cortenbach, I., Marini, F. C., Krause, D. S., et al. (2006). Minimal Criteria for Defining Multipotent Mesenchymal Stromal Cells. The International Society for Cellular Therapy Position Statement. *Cytotherapy* 8, 315–317. doi:10.1080/14653240600855905

Fang, H., and Judd, R. L. (2018). Adiponectin Regulation and Function. *Compr. Physiol.* 8, 1031–1063. doi:10.1002/cphy.c170046

Farmer, D. J. T., Mlcochova, H., Zhou, Y., Koelling, N., Wang, G., Ashley, N., et al. (2021). The Developing Mouse Coronal Suture at Single-Cell Resolution. *Nat. Commun.* 12, 4797. doi:10.1038/s41467-021-24917-9

Felson, D. T., Zhang, Y., Hannan, M. T., and Anderson, J. J. (1993). Effects of Weight and Body Mass index on Bone mineral Density in Men and Women: the Framingham Study. *J. Bone Miner Res.* 8, 567–573. doi:10.1002/jbmr.5650080507

Friedenstein, A. J., Gorskaja, J. F., and Kulagina, N. N. (1976). Fibroblast Precursors in normal and Irradiated Mouse Hematopoietic Organs. *Exp. Hematol.* 4, 267–274.

Gori, F., Thomas, T., Hicok, K. C., Spelsberg, T. C., and Riggs, B. L. (1999). Differentiation of Human Marrow Stromal Precursor Cells: Bone Morphogenetic Protein-2 Increases OSF2/CBFA1, Enhances Osteoblast Commitment, and Inhibits Late Adipocyte Maturation. *J. Bone Miner Res.* 14, 1522–1535. doi:10.1359/jbmr.1999.14.9.1522

Grandl, G., and Wolfrum, C. (2017). Adipocytes at the Core of Bone Function. *Cell Stem Cell* 20, 739–740. doi:10.1016/j.stem.2017.05.008

Greenbaum, A., Hsu, Y.-M. S., Day, R. B., Schuettpelz, L. G., Christopher, M. J., Borgerding, J. N., et al. (2013). CXCL12 in Early Mesenchymal Progenitors Is Required for Haematopoietic Stem-Cell Maintenance. *Nature* 495, 227–230. doi:10.1038/nature11926

Gu, C., Xu, Y., Zhang, S., Guan, H., Song, S., Wang, X., et al. (2016). miR-27a Attenuates Adipogenesis and Promotes Osteogenesis in Steroid-Induced Rat BMSCs by Targeting PPARγ and GREM1. *Sci. Rep.* 6, 38491. doi:10.1038/srep38491

Gulati, G. S., Murphy, M. P., Marecic, O., Lopez, M., Brewer, R. E., Koepke, L. S., et al. (2018). Isolation and Functional Assessment of Mouse Skeletal Stem Cell Lineage. *Nat. Protoc.* 13, 1294–1309. doi:10.1038/nprot.2018.041

Gupta, R. K., Mepani, R. J., Kleiner, S., Lo, J. C., Khandekar, M. J., Cohen, P., et al. (2012). Zfp423 Expression Identifies Committed Preadipocytes and Localizes to Adipose Endothelial and Perivascular Cells. *Cel Metab.* 15, 230–239. doi:10.1016/j.cmet.2012.01.010

Gustafson, B., Hammarstedt, A., Hedjazifar, S., Hoffmann, J. M., Svensson, P.-A., Grimsby, J., et al. (2015). BMP4 and BMP Antagonists Regulate Human White and Beige Adipogenesis. *Diabetes* 64, 1670–1681. doi:10.2337/db14-1127

Haffner-Luntzer, M., Kovtun, A., Lackner, I., Mödinger, Y., Hacker, S., Liedert, A., et al. (2018). Estrogen Receptor α- (ERα), but Not ERβ-Signaling, Is Crucially Involved in Mechanostimulation of Bone Fracture Healing by Whole-Body Vibration. *Bone* 110, 11–20. doi:10.1016/j.bone.2018.01.017

Helfer, G., and Wu, Q.-F. (2018). Chemerin: a Multifaceted Adipokine Involved in Metabolic Disorders. *J. Endocrinol.* 238, R79–R94. doi:10.1530/JOE-18-0174

Hong, J.-H., Hwang, E. S., McManus, M. T., Amsterdam, A., Tian, Y., Kalmukova, R., et al. (2005). TAZ, a Transcriptional Modulator of Mesenchymal Stem Cell Differentiation. *Science* 309, 1074–1078. doi:10.1126/science.1110955

Hu, Y., Li, X., Zhi, X., Cong, W., Huang, B., Chen, H., et al. (2021). RANKL from Bone Marrow Adipose Lineage Cells Promotes Osteoclast Formation and Bone Loss. *EMBO Rep.* 22. doi:10.15252/embr.202152481

Huang, J., Zhao, L., Xing, L., and Chen, D. (2009). MicroRNA-204 Regulates Runx2 Protein Expression and Mesenchymal Progenitor Cell Differentiation. *Stem Cells* 28, A–N. doi:10.1002/stem.288

Huang, Y., Das, A. K., Yang, Q.-Y., Zhu, M.-J., and Du, M. (2012). Zfp423 Promotes Adipogenic Differentiation of Bovine Stromal Vascular Cells. *PLoS One* 7, e47496. doi:10.1371/journal.pone.0047496

Javed, A., Bae, J.-S., Afzal, F., Gutierrez, S., Pratap, J., Zaidi, S. K., et al. (2008). Structural Coupling of Smad and Runx2 for Execution of the BMP2 Osteogenic Signal. *J. Biol. Chem.* 283, 8412–8422. doi:10.1074/jbc.M705578200

Justesen, J., Stenderup, K., Ebbesen, E. N., Mosekilde, L., Steiniche, T., and Kassem, M. (2001). Adipocyte Tissue Volume in Bone Marrow Is Increased with Aging and in Patients with Osteoporosis. *Biogerontology* 2, 165–171. doi:10.1023/a:1011513223894

Kang, H., and Hata, A. (2015). The Role of microRNAs in Cell Fate Determination of Mesenchymal Stem Cells : Balancing Adipogenesis and Osteogenesis. *BMB Rep.* 48, 319–323. doi:10.5483/bmbrep.2015.48.6.206

Kim, J., Lee, Y.-J., Kim, J. M., Lee, S. Y., Bae, M.-A., Ahn, J. H., et al. (2016). PPARγ Agonists Induce Adipocyte Differentiation by Modulating the Expression of Lipin-1, Which Acts as a PPARγ Phosphatase. *Int. J. Biochem. Cel Biol.* 81, 57–66. doi:10.1016/j.biocel.2016.10.018

Komori, T. (2006). Regulation of Osteoblast Differentiation by Transcription Factors. *J. Cel. Biochem.* 99, 1233–1239. doi:10.1002/jcb.20958

Kong, Q.-f., Sun, B., Bai, S.-s., Zhai, D.-x., Wang, G.-y., Liu, Y.-m., et al. (2009). Administration of Bone Marrow Stromal Cells Ameliorates Experimental Autoimmune Myasthenia Gravis by Altering the Balance of Th1/Th2/Th17/Treg Cell Subsets through the Secretion of TGF-β. *J. Neuroimmunology* 207, 83–91. doi:10.1016/j.jneuroim.2008.12.005

Kronenberg, H. M. (2004). Twist Genes Regulate Runx2 and Bone Formation. *Dev. Cel* 6, 317–318. doi:10.1016/s1534-5807(04)00069-3

Lagerquist, M. K., Gustafsson, K. L., Henning, P., Farman, H., Wu, J., Sjögren, K., et al. (2021). Acute Fat Loss Does Not Affect Bone Mass. *Sci. Rep.* 11, 14177. doi:10.1038/s41598-021-93450-y

Laranjeira, P., Pedrosa, M., Pedreiro, S., Gomes, J., Martinho, A., Antunes, B., et al. (2015). Effect of Human Bone Marrow Mesenchymal Stromal Cells on Cytokine Production by Peripheral Blood Naive, Memory, and Effector T Cells. *Stem Cel Res Ther* 6, 3. doi:10.1186/scrt537

Li, H., Ghazanfari, R., Zacharaki, D., Lim, H. C., and Scheding, S. (2016). Isolation and Characterization of Primary Bone Marrow Mesenchymal Stromal Cells. *Ann. N.Y. Acad. Sci.* 1370, 109–118. doi:10.1111/nyas.13102

Lin, F. T., and Lane, M. D. (1994). CCAAT/enhancer Binding Protein Alpha Is Sufficient to Initiate the 3T3-L1 Adipocyte Differentiation Program. *Proc. Natl. Acad. Sci.* 91, 8757–8761. doi:10.1073/pnas.91.19.8757

Luu, Y. K., Capilla, E., Rosen, C. J., Gilsanz, V., Pessin, J. E., Judex, S., et al. (2009). Mechanical Stimulation of Mesenchymal Stem Cell Proliferation and Differentiation Promotes Osteogenesis while Preventing Dietary-Induced Obesity. *J. Bone Mineral Res.* 24, 50–61. doi:10.1359/jbmr.080817

Maeda, N., Funahashi, T., Matsuzawa, Y., and Shimomura, I. (2020). Adiponectin, a Unique Adipocyte-Derived Factor beyond Hormones. *Atherosclerosis* 292, 1–9. doi:10.1016/j.atherosclerosis.2019.10.021

Maruyama, T., Jeong, J., Sheu, T.-J., and Hsu, W. (2016). Stem Cells of the Suture Mesenchyme in Craniofacial Bone Development, Repair and Regeneration. *Nat. Commun.* 7, 10526. doi:10.1038/ncomms10526

Menuki, K., Mori, T., Sakai, A., Sakuma, M., Okimoto, N., Shimizu, Y., et al. (2008). Climbing Exercise Enhances Osteoblast Differentiation and Inhibits Adipogenic Differentiation with High Expression of PTH/PTHrP Receptor in Bone Marrow Cells. *Bone* 43, 613–620. doi:10.1016/j.bone.2008.04.022

Mizuhashi, K., Ono, W., Matsushita, Y., Sakagami, N., Takahashi, A., Saunders, T. L., et al. (2018). Resting Zone of the Growth Plate Houses a Unique Class of Skeletal Stem Cells. *Nature* 563, 254–258. doi:10.1038/s41586-018-0662-5

Mori, T., Okimoto, N., Sakai, A., Okazaki, Y., Nakura, N., Notomi, T., et al. (2003). Climbing Exercise Increases Bone Mass and Trabecular Bone Turnover through Transient Regulation of Marrow Osteogenic and Osteoclastogenic Potentials in Mice. *J. Bone Miner Res.* 18, 2002–2009. doi:10.1359/jbmr.2003.18.11.2002

Morikawa, S., Mabuchi, Y., Kubota, Y., Nagai, Y., Niibe, K., Hiratsu, E., et al. (2009). Prospective Identification, Isolation, and Systemic Transplantation of Multipotent Mesenchymal Stem Cells in Murine Bone Marrow. *J. Exp. Med.* 206, 2483–2496. doi:10.1084/jem.20091046

Nakashima, K., Zhou, X., Kunkel, G., Zhang, Z., Deng, J. M., Behringer, R. R., et al. (2002). The Novel Zinc finger-containing Transcription Factor Osterix Is Required for Osteoblast Differentiation and Bone Formation. *Cell* 108, 17–29. doi:10.1016/s0092-8674(01)00622-5

Omatsu, Y., Sugiyama, T., Kohara, H., Kondoh, G., Fujii, N., Kohno, K., et al. (2010). The Essential Functions of Adipo-Osteogenic Progenitors as the Hematopoietic Stem and Progenitor Cell Niche. *Immunity* 33, 387–399. doi:10.1016/j.immuni.2010.08.017

Orkin, S. H. (2000). Stem Cell Alchemy. *Nat. Med.* 6, 1212–1213. doi:10.1038/81303

Owen, M., and Friedenstein, A. J. (1988). Stromal Stem Cells: Marrow-Derived Osteogenic Precursors. *Ciba Found. Symp.* 136, 42–60. doi:10.1002/9780470513637.ch4

Parhami, F., Tintut, Y., Beamer, W. G., Gharavi, N., Goodman, W., and Demer, L. L. (2001). Atherogenic High-Fat Diet Reduces Bone Mineralization in Mice. *J. Bone Miner Res.* 16, 182–188. doi:10.1359/jbmr.2001.16.1.182

Park, S. J., Gadi, J., Cho, K.-W., Kim, K. J., Kim, S. H., Jung, H.-S., et al. (2011). The Forkhead Transcription Factor Foxc2 Promotes Osteoblastogenesis via Up-Regulation of Integrin β1 Expression. *Bone* 49, 428–438. doi:10.1016/j.bone.2011.05.012

Pittenger, M. F., Mackay, A. M., Beck, S. C., Jaiswal, R. K., Douglas, R., Mosca, J. D., et al. (1999). Multilineage Potential of Adult Human Mesenchymal Stem Cells. *Science* 284, 143–147. doi:10.1126/science.284.5411.143

Reid, I. R., Baldock, P. A., and Cornish, J. (2018). Effects of Leptin on the Skeleton. *Endocr. Rev.* 39, 938–959. doi:10.1210/er.2017-00226

Robey, P. G., and Riminucci, M. (2020). "Skeletal Stem Cells," in *Principles of Bone Biology*. Editors J. P. Bilezikian, T. J. Martin, T. L. Clemens, and C. J. Rosen. Fourth Edition (Academic Press), 45–71. doi:10.1016/B978-0-12-814841-9.00002-6

Robling, A. G., and Bonewald, L. F. (2020). The Osteocyte: New Insights. *Annu. Rev. Physiol.* 82, 485–506. doi:10.1146/annurev-physiol-021119-034332

Rux, D. R., Song, J. Y., Swinehart, I. T., Pineault, K. M., Schlientz, A. J., Trulik, K. G., et al. (2016). Regionally Restricted Hox Function in Adult Bone Marrow Multipotent Mesenchymal Stem/Stromal Cells. *Dev. Cel* 39, 653–666. doi:10.1016/j.devcel.2016.11.008

Sacchetti, B., Funari, A., Michienzi, S., Di Cesare, S., Piersanti, S., Saggio, I., et al. (2007). Self-Renewing Osteoprogenitors in Bone Marrow Sinusoids Can Organize a Hematopoietic Microenvironment. *Cell* 131, 324–336. doi:10.1016/j.cell.2007.08.025

Schneider, A. K., Cama, G., Ghuman, M., Hughes, F. J., and Gharibi, B. (2017). Sprouty 2 , an Early Response Gene Regulator of FosB and Mesenchymal Stem Cell Proliferation during Mechanical Loading and Osteogenic Differentiation. *J. Cel. Biochem.* 118, 2606–2614. doi:10.1002/jcb.26035

Serafini, M., Sacchetti, B., Pievani, A., Redaelli, D., Remoli, C., Biondi, A., et al. (2014). Establishment of Bone Marrow and Hematopoietic Niches *in vivo* by Reversion of Chondrocyte Differentiation of Human Bone Marrow Stromal Cells. *Stem Cell Research* 12, 659–672. doi:10.1016/j.scr.2014.01.006

Shen, B., Tasdogan, A., Ubellacker, J. M., Zhang, J., Nosyreva, E. D., Du, L., et al. (2021). A Mechanosensitive Peri-Arteriolar Niche for Osteogenesis and Lymphopoiesis. *Nature* 591, 438–444. doi:10.1038/s41586-021-03298-5

Suire, C., Brouard, N., Hirschi, K., and Simmons, P. J. (2012). Isolation of the Stromal-Vascular Fraction of Mouse Bone Marrow Markedly Enhances the Yield of Clonogenic Stromal Progenitors. *Blood* 119, e86–e95. doi:10.1182/blood-2011-08-372334

Swinehart, I. T., Schlientz, A. J., Quintanilla, C. A., Mortlock, D. P., and Wellik, D. M. (2013). Hox11 Genes Are Required for Regional Patterning and Integration of Muscle, Tendon and Bone. *Development* 140, 4574–4582. doi:10.1242/dev.096693

Tang, Q.-Q., Otto, T. C., and Lane, M. D. (2004). Commitment of C3H10T1/2 Pluripotent Stem Cells to the Adipocyte Lineage. *Proc. Natl. Acad. Sci.* 101, 9607–9611. doi:10.1073/pnas.0403100101

Tang, X., Huang, Y., Lei, J., Luo, H., and Zhu, X. (2019). The Single-Cell Sequencing: New Developments and Medical Applications. *Cell Biosci* 9, 53. doi:10.1186/s13578-019-0314-y

Tencerova, M., and Kassem, M. (2016). The Bone Marrow-Derived Stromal Cells: Commitment and Regulation of Adipogenesis. *Front. Endocrinol.* 7. doi:10.3389/fendo.2016.00127

Tikhonova, A. N., Dolgalev, I., Hu, H., Sivaraj, K. K., Hoxha, E., Cuesta-Domínguez, Á., et al. (2019). The Bone Marrow Microenvironment at Single-Cell Resolution. *Nature* 569, 222–228. doi:10.1038/s41586-019-1104-8

Wang, C., Xu, W., An, J., Liang, M., Li, Y., Zhang, F., et al. (2019). Poly(ADP-ribose) Polymerase 1 Accelerates Vascular Calcification by Upregulating Runx2. *Nat. Commun.* 10, 1203. doi:10.1038/s41467-019-09174-1

Wang, J., Cui, C., Chim, Y. N., Yao, H., Shi, L., Xu, J., et al. (2020). Vibration and β-hydroxy-β-methylbutyrate Treatment Suppresses Intramuscular Fat Infiltration and Adipogenic Differentiation in Sarcopenic Mice. *J. Cachexia, Sarcopenia Muscle* 11, 564–577. doi:10.1002/jcsm.12535

Wolock, S. L., Krishnan, I., Tenen, D. E., Matkins, V., Camacho, V., Patel, S., et al. (2019). Mapping Distinct Bone Marrow Niche Populations and Their Differentiation Paths. *Cel Rep.* 28, 302–311. doi:10.1016/j.celrep.2019.06.031

Xu, C., Wang, J., Zhu, T., Shen, Y., Tang, X., Fang, L., et al. (2016). Cross-Talking between PPAR and WNT Signaling and its Regulation in Mesenchymal Stem Cell Differentiation. *Cscr* 11, 247–254. doi:10.2174/1574888x10666150723145707

Ye, L., Fan, Z., Yu, B., Chang, J., Al Hezaimi, K., Zhou, X., et al. (2012). Histone Demethylases KDM4B and KDM6B Promotes Osteogenic Differentiation of Human MSCs. *Cell Stem Cell* 11, 50–61. doi:10.1016/j.stem.2012.04.009

Yi, X., Wright, L. E., Pagnotti, G. M., Uzer, G., Powell, K. M., Wallace, J. M., et al. (2020). Mechanical Suppression of Breast Cancer Cell Invasion and Paracrine Signaling to Osteoclasts Requires Nucleo-Cytoskeletal Connectivity. *Bone Res.* 8, 40. doi:10.1038/s41413-020-00111-3

Yoshida, C. A., Furuichi, T., Fujita, T., Fukuyama, R., Kanatani, N., Kobayashi, S., et al. (2002). Core-binding Factor β Interacts with Runx2 and Is Required for Skeletal Development. *Nat. Genet.* 32, 633–638. doi:10.1038/ng1015

Yu, B., Huo, L., Liu, Y., Deng, P., Szymanski, J., Li, J., et al. (2018). PGC-1α Controls Skeletal Stem Cell Fate and Bone-Fat Balance in Osteoporosis and Skeletal Aging by Inducing TAZ. *Cell Stem Cell* 23, 193–209. doi:10.1016/j.stem.2018.06.009

Yu, W., Zhong, L., Yao, L., Wei, Y., Gui, T., Li, Z., et al. (2021). Bone Marrow Adipogenic Lineage Precursors Promote Osteoclastogenesis in Bone Remodeling and Pathologic Bone Loss. *J. Clin. Invest.* 131. doi:10.1172/JCI140214

Yue, R., Zhou, B. O., Shimada, I. S., Zhao, Z., and Morrison, S. J. (2016). Leptin Receptor Promotes Adipogenesis and Reduces Osteogenesis by Regulating Mesenchymal Stromal Cells in Adult Bone Marrow. *Cell Stem Cell* 18, 782–796. doi:10.1016/j.stem.2016.02.015

Zhang, J.-f., Fu, W.-m., He, M.-l., Wang, H., Wang, W.-m., Yu, S.-c., et al. (2011). MiR-637 Maintains the Balance between Adipocytes and Osteoblasts by Directly Targeting Osterix. *MBoC* 22, 3955–3961. doi:10.1091/mbc.E11-04-0356

Zhao, H., Feng, J., Ho, T.-V., Grimes, W., Urata, M., and Chai, Y. (2015). The Suture Provides a Niche for Mesenchymal Stem Cells of Craniofacial Bones. *Nat. Cel Biol* 17, 386–396. doi:10.1038/ncb3139

Zhao, S., Kusminski, C. M., Elmquist, J. K., and Scherer, P. E. (2020). Leptin: Less Is More. *Diabetes* 69, 823–829. doi:10.2337/dbi19-0018

Zhong, L., Yao, L., Tower, R. J., Wei, Y., Miao, Z., Park, J., et al. (2020). Single Cell Transcriptomics Identifies a Unique Adipose Lineage Cell Population that

Regulates Bone Marrow Environment. *Elife* 9, e54695. doi:10.7554/eLife.54695

Zhou, B. O., Yu, H., Yue, R., Zhao, Z., Rios, J. J., Naveiras, O., et al. (2017). Bone Marrow Adipocytes Promote the Regeneration of Stem Cells and Haematopoiesis by Secreting SCF. *Nat. Cel Biol* 19, 891–903. doi:10.1038/ncb3570

Zhou, B. O., Yue, R., Murphy, M. M., Peyer, J. G., and Morrison, S. J. (2014). Leptin-receptor-expressing Mesenchymal Stromal Cells Represent the Main Source of Bone Formed by Adult Bone Marrow. *Cell Stem Cell* 15, 154–168. doi:10.1016/j.stem.2014.06.008

Zhuang, H., Zhang, X., Zhu, C., Tang, X., Yu, F., wei Shang, G., et al. (2016). Molecular Mechanisms of PPAR-γ; Governing MSC Osteogenic and Adipogenic Differentiation. *Cscr* 11, 255–264. doi:10.2174/1574888x10666150531173309

Zou, W., Rohatgi, N., Brestoff, J. R., Li, Y., Barve, R. A., Tycksen, E., et al. (2020). Ablation of Fat Cells in Adult Mice Induces Massive Bone Gain. *Cel Metab.* 32, 801–813. doi:10.1016/j.cmet.2020.09.011

Conflict of Interest: The authors declare that the research was conducted in the absence of any commercial or financial relationships that could be construed as a potential conflict of interest.

frontiers in Molecular Biosciences

ORIGINAL RESEARCH
published: 11 February 2022
doi: 10.3389/fmolb.2021.782054

Transcriptome Sequencing Reveals Key Genes in Three Early Phases of Osteogenic, Adipogenic, and Chondrogenic Differentiation of Bone Marrow Mesenchymal Stem Cells in Rats

*Fanxiao Liu, Jun Dong, Peng Zhang, Dongsheng Zhou and Qingyu Zhang**

Department of Orthopaedics, Shandong Provincial Hospital Affiliated to Shandong First Medical University, Jinan, China

Bone mesenchymal stem cells (BMSCs) of multi-directional differentiation and reproductive activity are attractive candidates for bone and cartilage repair. However, the molecular mechanisms underlying the early phase of osteogenesis, adipogenesis, and chondrogenesis of BMSCs are still far from understood. In the current study, BMSCs are isolated from rats, and the gene expressions during the initiation of differentiation (phase I), lineage acquisition (phase II), and early lineage progression (phase III) of three-directional differentiation of BMSCs were detected by using high-throughput sequencing. Then, 356, 540, and 299 differentially expressed genes (DEGs) were identified in phases I, II, and III of osteogenesis, respectively. The numbers are 507, 287, and 428 for adipogenesis, respectively, and 412, 336, and 513 for chondrogenesis, respectively. Time-dependent expression patterns of genes were also validated during three-directional differentiation in BMSCs. Hub genes including *Ccna2*, *Cdc20*, and *Il6* may act as common participants in initiating osteogenesis, adipogenesis, and chondrogenesis. *Mex3b*, *Sertad1*, and *Hopx* showed an enhanced expression throughout three early phases during the osteogenic differentiation but no significant change in other two-directional differentiation. A similar pattern of *Dtx4* and *Ibsp* expression occurred in adipogenesis and chondrogenesis, respectively. Our findings will help understand the underlying mechanism determining the differentiation fate of BMSCs and provide theoretical support for the clinical treatment of osteoporosis, osteoarthritis, and other age-related bone diseases.

Keywords: bone marrow mesenchymal stem cells, high-throughput sequencing, osteogenic differentiation, chondrogenic differentiation, adipogenic differentiation, differentially expressed genes

OPEN ACCESS

Edited by:
Xiao Chen,
Second Military Medical University, China

Reviewed by:
Changliang Peng,
Second Hospital of Shandong University, China
Yan Wang,
Peking Union Medical College Graduate School, China

****Correspondence:***
Qingyu Zhang
zhangqingyu@sdfmu.edu.cn

Specialty section:
This article was submitted to Cellular Biochemistry, a section of the journal Frontiers in Molecular Biosciences

Received: *23 September 2021*
Accepted: *27 December 2021*
Published: *11 February 2022*

Citation:
Liu F, Dong J, Zhang P, Zhou D and Zhang Q (2022) Transcriptome Sequencing Reveals Key Genes in Three Early Phases of Osteogenic, Adipogenic, and Chondrogenic Differentiation of Bone Marrow Mesenchymal Stem Cells in Rats. Front. Mol. Biosci. 8:782054. doi: 10.3389/fmolb.2021.782054

INTRODUCTION

The microenvironment within the bone marrow cavity consists of both stromal lineage and hematopoietic lineage. Mesenchymal stem cells (MSCs) are discovered by Friedenstein et al. from stromal tissues of the bone marrow (BM) more than 50 years ago and have the potential to give rise to multiple mesodermal progenies such as osteocytes, adipocytes, and chondrocytes (Arthur and Gronthos, 2020; Jiang et al., 2021; Johnson et al., 2021; Saeedi et al., 2021). Meanwhile,

bone MSCs (BMSCs) possess immune-modulatory and anti-inflammatory abilities (Li et al., 2012). Therefore, cell therapy with BMSCs has been proposed as an eligible paradigm for treating trauma, bone defects, and bone metabolic disorders (e.g., osteonecrosis and osteonecrosis) (Galderisi et al., 2021; Mabuchi et al., 2021). However, to date, clinical trials of MSC transplantation for osteoporosis predominantly focused on applying autologous cells, and no results have been reported (Jiang et al., 2021). Many unsolved problems and challenges still exist (Galderisi et al., 2021; Mabuchi et al., 2021; Saeedi et al., 2021). The first one is the patient selection and source of stem cells. A small number of MSCs can be readily obtained for autologous cellular transplantation, and therefore, extensive expansion may be required for therapeutic utility (Tamama et al., 2006). Meanwhile, there is a lack of homogenous criteria for isolating and cultivating MSCs and standardized procedures for transplantation. Last but not least, the differentiation fate of transplanted BMSCs is not controllable *in vivo*.

Adipogenesis, osteogenesis, and chondrogenesis of BMSCs are closely related. The specific differentiation direction is highly regulated by biological, physical, and chemical incentives (Hu et al., 2018). As the most studied terminally differentiated cell of BMSCs, the osteocyte is a mechanosensory commander maintaining homeostasis of the bone by osteoclasts and osteoblasts (Kim and Adachi, 2021). An imbalance resulting BMSCs toward a higher rate of adipogenesis is detrimental to bone health and associates with loss of bone mass and development of musculoskeletal diseases. Bone marrow adipocytes (BMAs) account for 50–70% of the marrow volume in adults (Piotrowska and Tarnowski, 2021). Besides acting as an energy reservoir, this kind of adipose tissue has been proved to possess paracrine, endocrine, and immunomodulatory functions (Sulston and Cawthorn, 2016). It, therefore, is critical for the homeostasis of the bone environment. Chondrocytes can be found in the articular surface of adults, which has poor regenerative capacity. Autologous chondrocyte transplantation is appealing for treating osteoarthritis, but the requirement for biopsies of chondrocytes from a healthy area of the cartilage cap is an evident disadvantage (Boeuf and Richter, 2010). Multiple key genes, non-coding RNAs (miRNA, lncRNA, and circRNA), and signaling pathways deciding the fate of BMSCs have been proposed to act at different time points during differentiation. For instance, the early stage of adipogenic differentiation is marked by augmentation of AMP cyclic production and phosphorylation of CREB (Chen et al., 2016). While during early osteogenesis, there is an upregulation of hedgehog proteins, Wnt/β-catenin signaling, BMPs, endocrine hormones, growth factors, and transcription factors (TFs) represented by RUNX2 (Pierce et al., 2019). SOX9 is pivotal for chondrogenesis by securing chondrocyte lineage commitment, promoting cell survival, and transcriptionally activating the genes for many cartilage-specific structural components (Lefebvre and Dvir Ginzberg, 2017).

Lineage commitment refers to the process of differentiation in which BMSCs lose their multipotency. During this phase, changes consistent with their respective lineage occur in the transcriptional profile, cellular metabolism, and morphology of BMSCs (van de Peppel et al., 2017). A primary question about the differentiation process is at what moment during the differentiation course MSCs become committed to a specific phenotype. Robert and his colleagues suggested that key genes related to osteogenesis were not significantly modulated in the first 24 h of osteogenesis of MSCs, and conversely, in MSCs treated with the adipogenic medium for 24 h, TFs related to adipogenesis and genes associated with lipid metabolism were already differentially expressed (Robert et al., 2020). van de Pepple et al. (2017) divided the early stage (4 d) of osteogenic and adipogenic lineage commitment of human BMSCs into three distinct phases: initiation of differentiation (0–3 h), lineage acquisition (6–24 h), and early lineage progression (48–96 h). The first phase is characterized by expression changes of many TFs and during the second phase, more than 50% of regulated genes are direct targets of the crucial TFs identified in the first phase. In the third phase, the number of differentially expressed genes (DEGs) is stable, indicating that differentiating cells have reached a stable phenotype. However, the author only applied BMSCs of human sources and key genes during chondrogenesis which are not investigated.

Many studies suggested that BMSCs from four species (human, pig, rat, and guinea pig) functioned across species barriers and act as promising sources for xenograft (Li et al., 2012). Currently, a change at the transcriptional level of rat BMSCs during the lineage-commitment phase of differentiation, especially chondrogenesis, remains unclear. In this study, using high-throughput sequencing data and multiple bioinformatics methods, we attempted to reveal key genes deciding osteogenic, adipogenic, and chondrogenic differentiation of rat BMSCs in early phases and analyze the enriched functions and their correlations. Meanwhile, potentially related microRNAs (miRNAs) and signaling pathways were predicted to elucidate underlying regulatory networks. These findings may help to characterize regulatory programs controlling the early stages of lineage commitment of rat BMSCs, to develop novel therapies for age- and pathology-related musculoskeletal diseases and to protect transplanted xenogeneic MSCs from immune detection and enable their long-term survival.

MATERIALS AND METHODS

This study was approved by the Animal Ethics Committee of Shandong Provincial Hospital affiliated to Shandong First Medical University. The experimental design is depicted in **Figure 1A**.

BMSC Isolation and Induced Differentiation

BMSCs were extracted from femurs and tibia of three female Sprague–Dawley (SD) rats about 3 weeks old by washing the marrow cavity using the high glucose Dulbecco's Modified Eagle medium (DMEM) (Gibco, Rockville, MD, United States). The cells were cultured in the DMEM supplemented with 10% fetal bovine serum (FBS) and placed in an incubator with a temperature of 37°C, 5% CO_2 concentration, and 95% relative

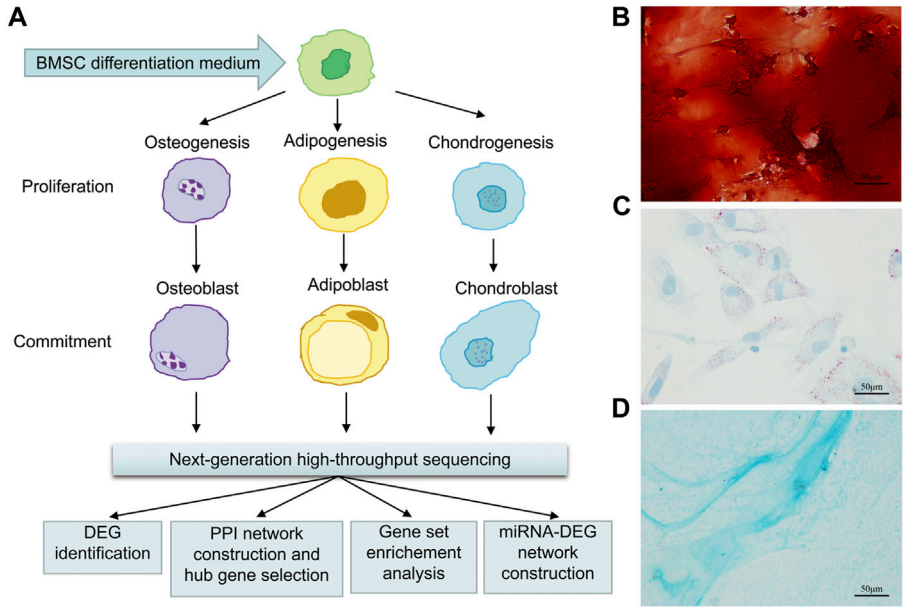

FIGURE 1 | Flow chart of osteogenic, adipogenic, and chondrogenic differentiation of rat BMSCs, data gathering and analysis **(A)**, and histochemical staining of calcium **(B)** with Alizarin red or adipocyte **(C)** with oil red O or cartilage **(D)** with Alcian blue staining after 21 days of osteogenic or adipogenic or chondrogenic differentiation. Scale bars, 50 μm.

humidity. BMSCs at passage 2 were seeded in 12-well cell culture plates. After 2 days of incubation (query), these cells were induced to give rise to osteoblasts by using the osteogenic differentiation medium (Promocell, Germany, C-28013), or to adipocytes using the adipogenic differentiation medium (Promocell, Germany, C-28016), or to chondrocytes using the chondrogenic differentiation medium (Promocell, C-28012). Differentiation media were replaced every 3–4 days.

BMSCs Staining

For confirming the result of induced differentiation, Alizarin red staining, Oil Red O (ORO) staining, and Alcian blue staining assays were conducted, as previously described (Bruedigam et al., 2011; Gari et al., 2016).

RNA Isolation

To obtain enough RNA for the gene expression profiling analyses, we pooled three individual cultures in TRIzol (Life Technologies). A total of three experimental samples per time point (3 time points, namely, 3, 12, and 72 h) per lineage (osteogenic, adipogenic, or chondrogenic) were used for gene expression profiling analyses. In addition to the control samples, there were a total of 30 samples.

Next-Generation High-Throughput Sequencing and Identification of DEGs

The RNA quality assessment, mRNA library construction, and mRNA sequencing were performed using methods described in the previous study (Zhang et al., 2021). Based on the annotation information in the platform, the probe sets were transformed into the corresponding gene symbol. The mean value was calculated if multiple probes corresponded to the same gene symbol. The data were normalized using quantile normalization with Illumina in R software (Version 3.6.2). After data normalization, the DEGs were identified using the limma package (Version 3.42.2) in R software. Individual *p*-values were converted to adjusted *p*-values (adj. *p*. val) by false discovery rate correction of the Benjamini and Hochberg test. The threshold of $|\log_2 \text{fold change (FC)}| \geq 1$ with an adj. *p*. val <0.05 was used as the threshold for selecting DEGs. The volcano plot of the DEGs was drawn using the R ggplot2 package.

Functional and Pathway Enrichment Analyses of DEGs

The DEGs were uploaded to an online biological information database, the Database for Annotation, Visualization, and Integrated Discovery (DAVID) version 6.8 Beta (https://david-d.ncifcrf.gov/) for gene ontology (GO) enrichment (http://www.geneontology.org/) and Kyoto Encyclopedia of Genes and Genomes (KEGG) pathway enrichment (https://www.genome.jp/kegg/pathway) analysis, which was visualized in the R ggplot2 package. The significance criterion was set at *p*. val <0.05.

Protein–Protein Interaction Network Construction and Module Analysis

The protein–protein interaction (PPI) network of identified genes was constructed using the multiple protein online tool in the STRING database (Liu et al., 2021), a Search Tool for the Retrieval of Interacting Genes database (version 11.0b, http://string-db.

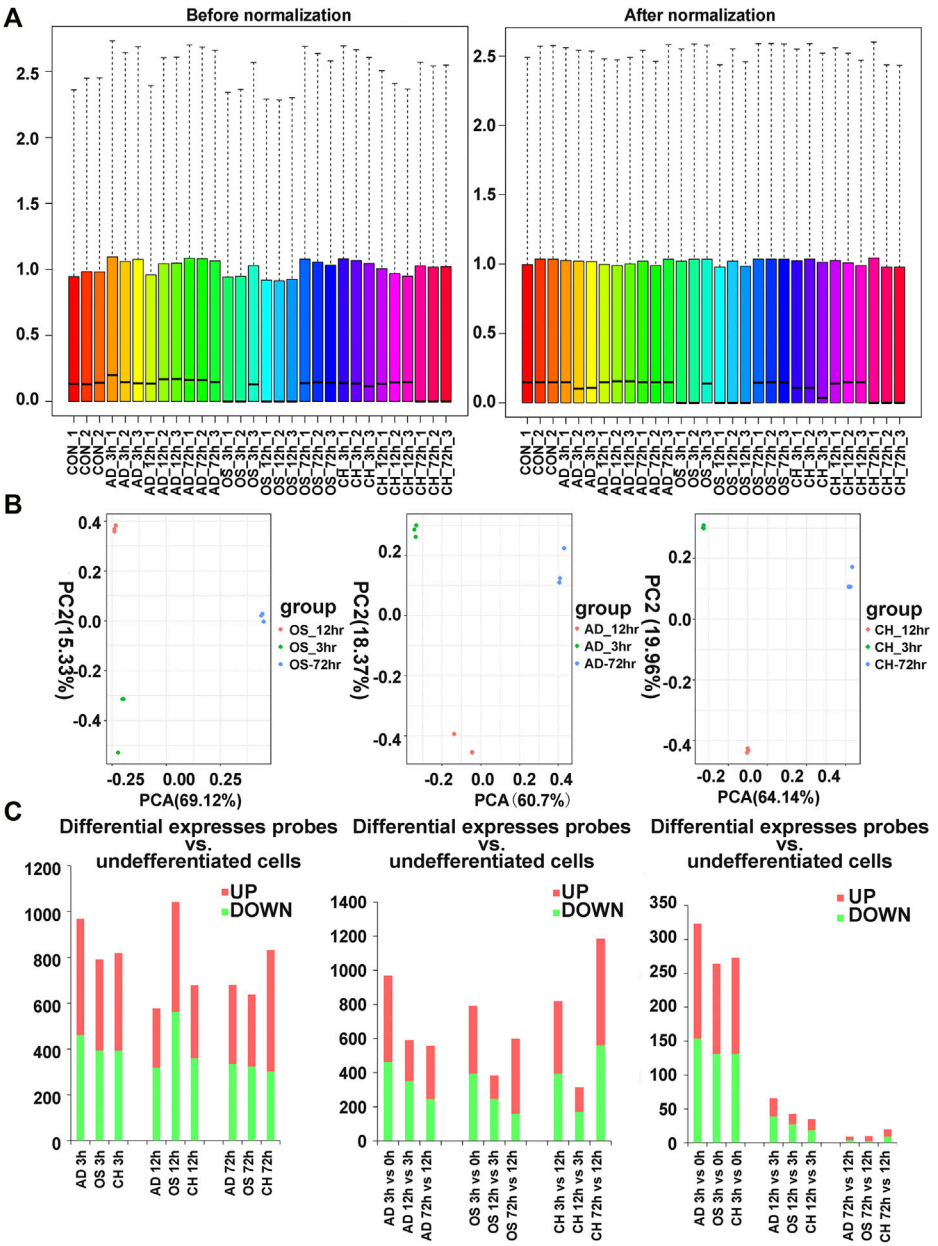

FIGURE 2 | (A) Distribution of expression of 27 samples before and after normalization. **(B)** Distribution of expression of 27 samples involving principal component analysis (PCA) for confirming biological variability between different samples. **(C)** Dynamic transcriptional changes upon osteogenic, adipogenic, and chondrogenic differentiation of rat BMSCs with the number of significant differential genes relative to the previous time point (based on three independent experiments) and the number of differentially expressed genes per hour compared to the previous time point (based on three independent experiments). AD, adipogenesis; OS, osteogenesis; CH, chondrogenesis.

org), and visualized by Cytoscape software (Version 3.6.2). The most significant modules in the PPI network were visualized using the molecular complex detection (MCODE) tool in Cytoscape, and the hub genes were selected by the cytoHubba plugin. The selection criteria were as follows: MCODE scores >5, node score cutoff = 0.2, degree cutoff = 2, max depth = 100, and k-score = 2.

Key Gene Selection

The hub genes (top 10) in the PPI network were identified by using three methods, including maximal clique centrality (MCC), degree, and maximum neighborhood component (MNC) from the cytoHubba plugin in Cytoscape. The biological process analysis of the top 10 genes was performed and visualized

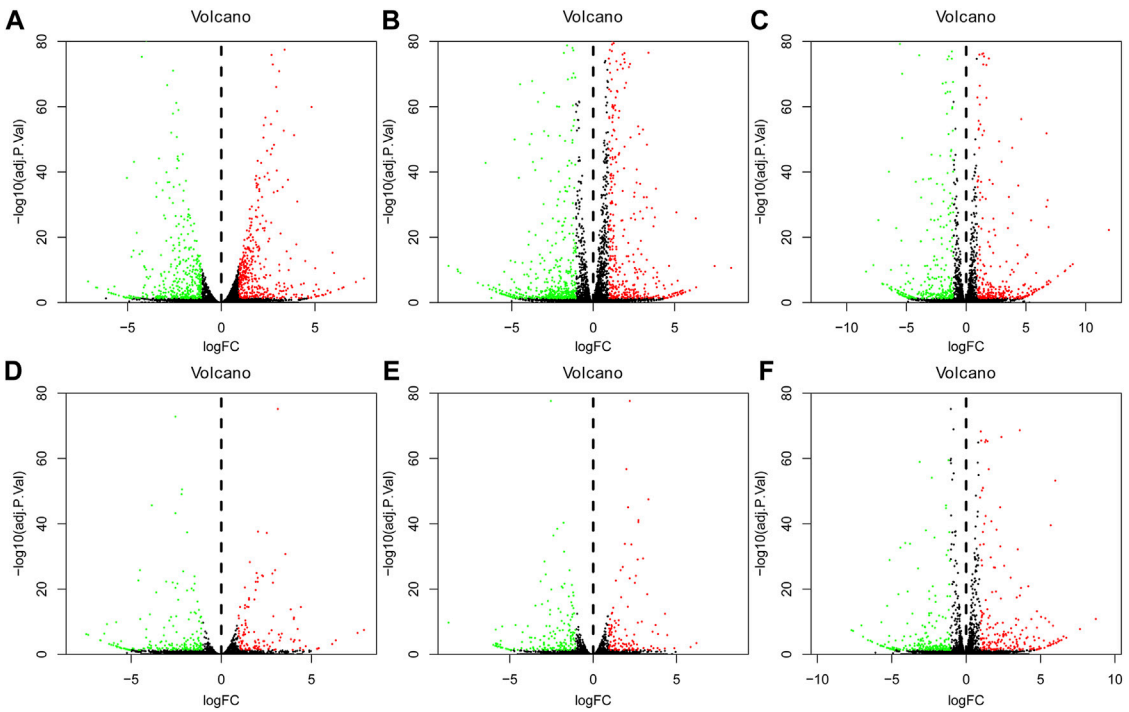

FIGURE 3 | Volcano plot of differentially regulated genes during osteogenesis at 3 h, **(A)** 12 h, and **(B)** 72 h **(C)** Compared with undifferentiated cells (t = 0 h); Volcano plot of differentially regulated genes between every two lineages at 3 h after inductive differentiation (t = 0 h). **(D)** Comparison between osteogenesis and adipogenesis, **(E)** Comparison between osteogenesis and chondrogenesis, and **(F)** Comparison between chondrogenesis and adipogenesis. AD, adipogenesis; OS, osteogenesis; CH, chondrogenesis.

using the Biological Networks Gene Ontology tool (BiNGO) (version 3.0.3) plugin in Cytoscape.

DEG–miRNA Network Construction

After hub genes were selected, the DEG–miRNA pairs were identified using the miRDB database (http://mirdb.org/) and visualized in Cytoscape.

RESULTS

Confirmation of the Three-Directional Differentiation of Rat BMSCs

On day 21 after induced differentiation, Alizarin red staining for calcium in the osteogenic differentiation group showed mineralization of the extracellular matrix (**Figure 1B**); meanwhile, intracellular lipid vesicles accumulated in the adipogenic group (**Figure 1C**), and cartilage formed in the chondrocyte differentiation group (**Figure 1D**). Taken together, these results confirmed that rat BMSCs differentiated in accordance with their expected multi-lineage potential.

Data Normalization

The box plot visualization of the gene expression of all samples (**Figure 2A**) was used to evaluate the data normalization and cross-comparability, which demonstrated that the black lines were almost in the same position after data normalization. Principal component analysis (PCA) confirmed the biological variability between different samples, indicating globally distinct expression profiles (**Figure 2B**).

Identification of DEGs at Three Time Points

Analysis of gene expression dynamics during rat BMSC differentiation revealed that transcript levels changed significantly at 3 h upon induction of differentiation (**Figure 2C**). During induction of osteogenic differentiation, 792 genes (398 upregulated and 394 downregulated ones) were significantly different at 3 h, and this increased further to 1,042 (480 upregulated and 562 downregulated ones) at 12 h. The number of significantly modulated genes decreased to 638 (314 upregulated and 324 downregulated ones) at 72 h. During adipogenic differentiation, the number of DEGs was 969 at 3 h, 577 at 12 h, and 680 at 72 h. During chondrogenic differentiation, the number of DEGs was 819 at 3h, 678 at 12 h, and 832 at 72 h. Remarkably, at 3 h after differentiation, the number of upregulated DEGs was higher than the downregulated ones. Next, we calculated the number of differentially expressed DEGs at each time point compared with the preceding time point, and in three directions of differentiation, the number of DEGs that changed per hour decreased as time extended (**Figure 2C**).

The volcano plot of DEGs at 3, 12, and 72 h of osteogenesis and the comparison results between every two lineages at 3 h after

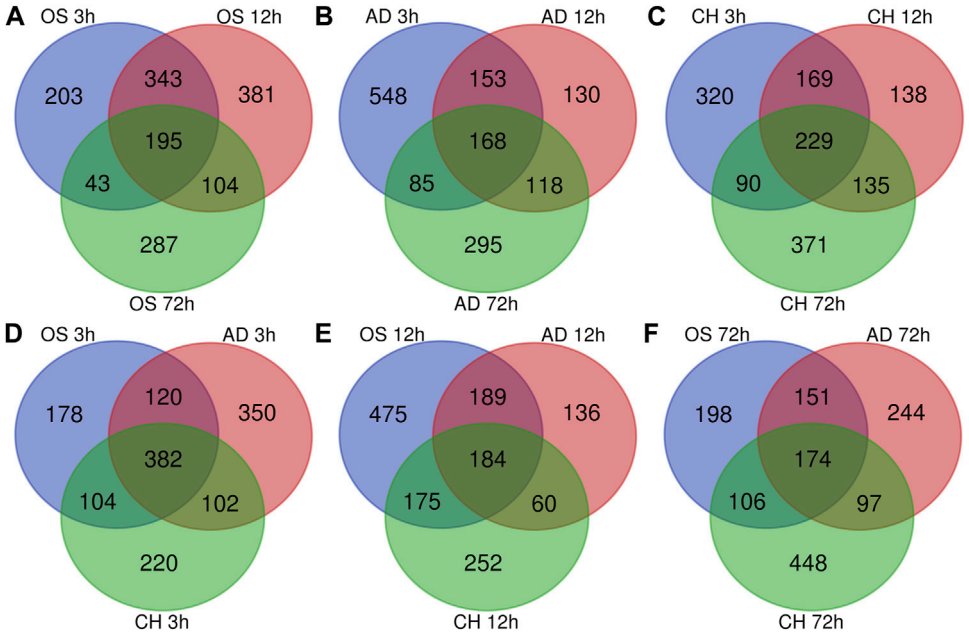

FIGURE 4 | Venn Diagrams of differentially expressed genes during osteogenesis **(A)**, adipogenesis **(B)**, and chondrogenesis **(C)** at three time points compared with undifferentiated cells (t = 0 h). Venn Diagrams of differentially expressed genes at 3 h **(D)**, 12 h **(E)**, and 72 h **(F)** of three directions of differentiation compared with undifferentiated cells (t = 0 h). AD, adipogenesis; OS, osteogenesis; CH, chondrogenesis.

inductive differentiation are presented in **Figure 3**. **Supplementary Figure S1** describes the visualized results of DEGs at three time points of adipogenic and chondrogenic differentiation.

Identification of Specific DEGs at Three Time Points

In osteogenesis of BMSCs, 203, 381, and 287 DEGs were identified to be differentially expressed only at 3, 12, and 72 h after inductive differentiation (**Figure 4A**). In adipogenesis of BMSCs, the numbers were 548, 130, and 295 (**Figure 4B**), and for chondrogenesis of BMSCs, the numbers were 320, 138, and 371 (**Figure 4C**). Notably, 195 (e.g., Mex3b and Sertad1), 168(e.g., Dtx4 and Il6), and 229 (e.g., Glra1 and Fdps) genes showed differentially expressed levels at all three time points in osteogenesis, adipogenesis, and chondrogenesis, respectively.

Comparison of DEGs Between Different Lineages

At 3 h after induction of differentiation, it was noticed that there were 178, 350, and 220 DEGs only differentially expressed in osteogenesis, adipogenesis, and chondrogenesis, respectively (**Figure 4D**). At 12 h after inductive differentiation, the numbers were 475, 136, and 252 (**Figure 4E**), and at 72 h, the numbers were 198, 244, and 448 (**Figure 4F**). Notably, 382 (e.g., *Hmg20a* and *Mmp24*), 184 (e.g., *Galnt2* and *Cxcl6*), and 174 (e.g., *Ccnd2* and *Sgcd*) genes showed differential expression at all three directions of differentiation at 3, 12, and 72 h after inductive differentiation, respectively.

Functional Enrichment Analysis of DEGs

GO and KEGG pathway enrichment analyses of differentially expressed DEGs at different time points of three directions of differentiation were performed to identify the most relevant biological processes (BPs), molecular functions (MFs), cellular components (CCs), and pathways. The top enriched terms of DEGs in BP, CC, MF, and KEGG at 3 h after osteogenesis are presented in **Figure 5A** and **Supplementary Figure S2A**. The DEGs at 3 h of osteogenesis were significantly enriched in the "PI3K-Akt signaling pathway" and BP terms such as "negative regulation of transcription from RNA polymerase II promoter" and "response to drug." The enriched terms at 12 and 72 h after osteogenesis are presented in **Figures 5B,C** and **Supplementary Figures S2B,C**, while results of the other two directions of differentiation are presented in **Supplementary Figures S3, S4**.

The DEGs between osteogenesis and adipogenesis at 3 h after inductive differentiation were also significantly enriched in BP terms such as "positive regulation of cell migration" and "negative regulation of transcription from RNA polymerase II promoter." Results of functional enrichment analysis of the DEGs between every two lineage commitment at 3 h of inductive differentiation are presented in **Figure 6** and **Supplementary Figure S5**.

PPI Network Construction and Module Analysis

The most significant module of DEGs at 3 h of osteogenesis consisted of 65 nodes and 907 edges, with the Rrp15 gene being identified to have a relatively high connectivity degree (**Figure 7A**). The most significant modules at 12 and 72 h

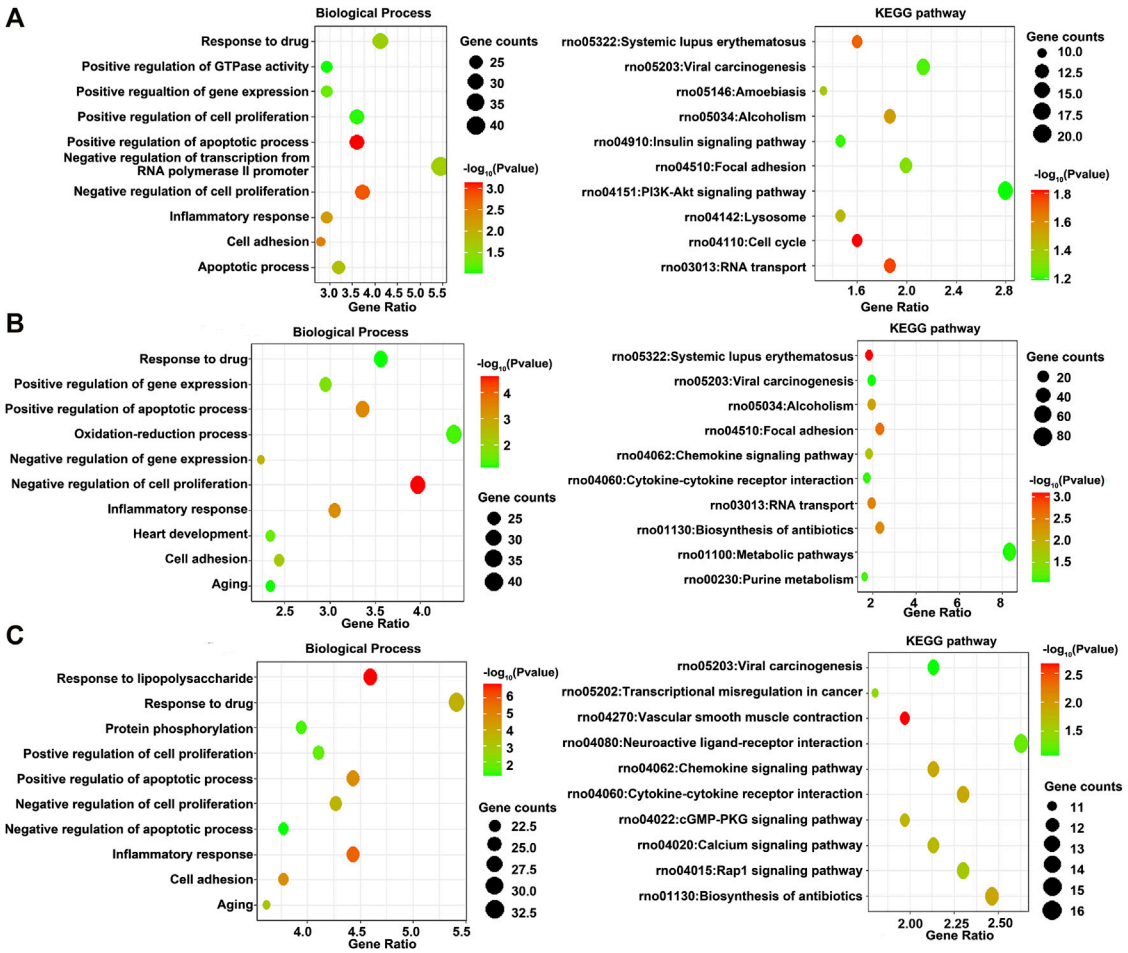

FIGURE 5 | GO including the biological process and KEGG enrichment analysis of differentially expressed genes at 3 h, **(A)** 12 h, and **(B)** 72 h **(C)** of osteogenesis compared with undifferentiated cells (t = 0 h).

after osteogenesis are presented in **Figures 7B,C**, respectively. Meanwhile, the most significant modules of the other two-directional differentiation at three time points are presented in **Supplementary Figure S6**. The most significant module about interactions of DEGs between osteogenesis and adipogenesis at 3 h after inductive differentiation consisted of 7 nodes and 14 edges, with the *Vcl* gene being identified to have a relatively high connectivity degree (**Figure 7D**). The most significant modules regarding interactions of DEGs between osteogenesis and chondrogenesis and between adipogenesis and chondrogenesis at 3 h after inductive differentiation are presented in **Figures 7E,F**. Hub genes were selected by CytoHubba. The top 10 hub genes, which were selected based on the three most commonly used classification methods in cytoHubba, are presented in **Figure 8** and **Supplementary Figure S7**. The top 10 hub genes selected by degree in different comparisons are presented in **Table 1**. The fold change (FC) and adj. p. val of the top 10 hub genes at 3, 12, and 72 h of osteogenesis compared with undifferentiated cells are presented in **Table 2**. The biological process analysis of the top 10 hub genes was performed and visualized using BiNGO in Cytoscape, as shown in **Figure 9** and **Supplementary Figures S8, S9**.

Construction of DEG-miRNA

The miRNA-DEG pairs were identified through network analysis of 10 DEGs using the miRDB databases. At 3 h of osteogenesis, a total of 32 associations between 22 miRNAs and 7 DEGs were identified, and then, the network was visualized in Cytoscape (**Figure 10A**). As is shown, *Rrm1* interacts with four miRNAs (rno-miR-320-3p, rno-miR-145-3p, rno-miR-330-3p, and rno-miR-291a-5p) and four genes (*Top2a*, *Ccna2*, *Mcm4*, and *Kif11*). The DEG-miRNA networks regarding osteogenesis at 12 and 72 h are presented in **Figures 10B,C**. The DEG-miRNA networks about comparisons between every two lineage commitment at 3 h after inductive differentiation are presented in **Figures 10D–F**. The DEG-miRNA networks regarding adipogenesis and chondrogenesis at 3, 12, and 72 h after differentiation are presented in **Supplementary Figure S10**.

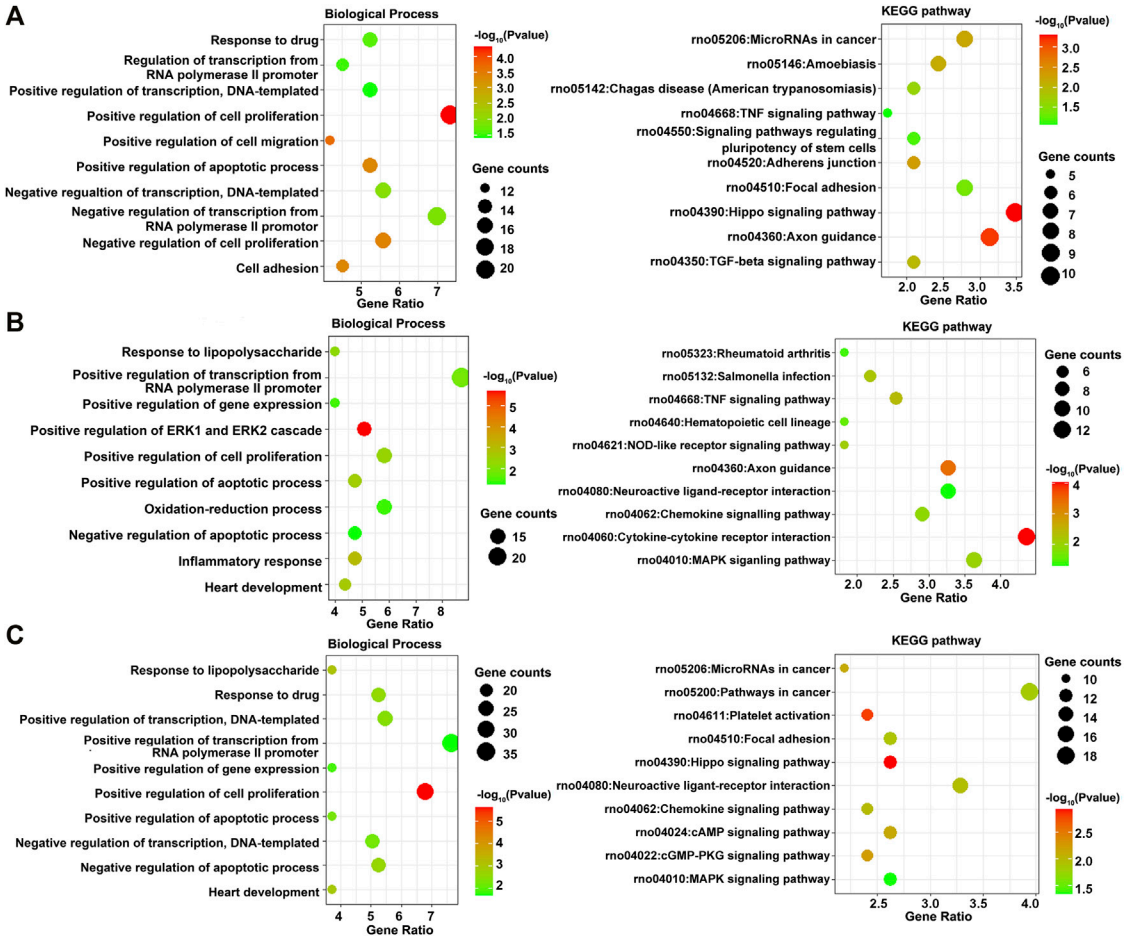

FIGURE 6 | GO including the biological process and KEGG enrichment analysis of differentially expressed genes between every two lineages at 3 h after inductive differentiation (*t* = 0 h). **(A)** Comparison between osteogenesis and adipogenesis, **(B)** Comparison between osteogenesis and chondrogenesis, and **(C)** Comparison between chondrogenesis and adipogenesis.

DISCUSSION

There were no previous studies paying special attention to the lineage commitment of rat BMSCs (Arthur and Gronthos, 2020; Zhu et al., 2020). In the current investigation, three time points (3, 12, and 72 h) after inductive differentiation were chosen to represent the three phases of early lineage commitment of rat BMSCs. Next-generation high-throughput sequencing was adapted to generate potential key genes. At the first time point (3 h), gene expression analyses revealed many DEGs in all three directions of differentiation. The first phase of early lineage commitment represents the initiation stage of the differentiation program. It is characterized by expression changes of many transcription factors that regulate the lineage commitment and set the multipotential stem cells toward a stable phenotype (van de Peppel et al., 2017). As for the second phase, differentiating lineages begin to deviate. In this study, most genes related to osteogenesis were modulated later than those related to adipogenesis, which confirmed the finding of the study conducted by Robert and his colleagues (Robert et al., 2020). In the third stage, the differentiating cells reach a stable phenotype (van de Peppel et al., 2017).

Integrated analysis of differential gene expression at 3 h of osteogenesis indicated that the top 10 DEGs (*Ccna2*, *Cdc20*, *Il6*, *Mad2l1*, *Top2a*, *Kif11*, *Mcm4*, *Asf1b*, *Rrm1*, and *Pa2g4*) in the PPI network were the hub genes; only one gene (*Il6*) showed a decreasing trend compared to the control group. Similarly, at 12 h of osteogenesis, nine (*Mad2l1*, *Top2a*, *Ccna2*, *Cdc20*, *Mcm6*, *Mcm3*, *Kif11*, *Mcm4*, and *Cdc6*) of the identified top 10 hub genes in the PPI network were upregulated except *Il6*. This trend was reversed at 72 h of osteogenesis as it has been shown that at this moment, nine (*Il6*, *Cd44*, *Il1b*, *Ccl2*, *Kif11*, *Asf1b*, *Cdc20*, *Mcm3*, and *Pbk*) of the top 10 DEGs were downregulated except Notch1. For adipogenesis, eight (*Ccna2*, *Cdc20*, *Kif11*, *Top2a*, *Mad2l1*, *Mcm6*, *Asf1b*, and *Mcm3*) hub genes were upregulated and two (*Il6* and *Gsk3b*) were downregulated at 3 h of differentiation, while for chondrogenesis, only two (*Il6* and *Sspo*) hub genes were downregulated at this time point. In fact, there is rather a large overlap regarding hub genes identified at 3 h of osteogenesis,

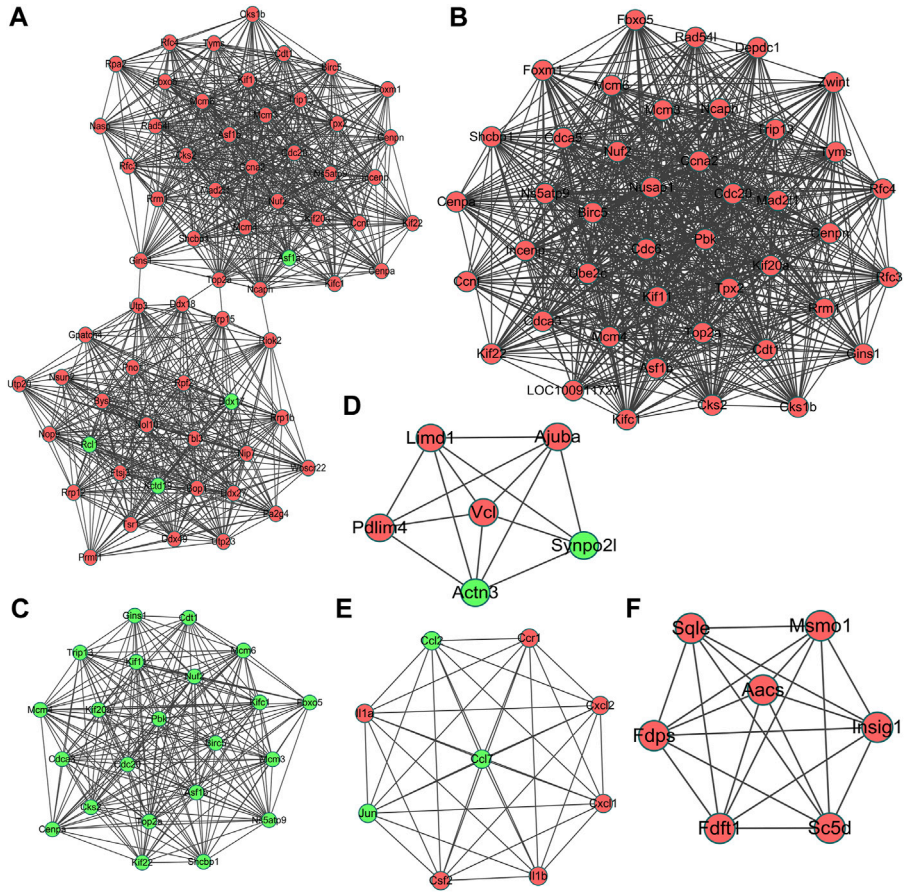

FIGURE 7 | Most significant module in protein–protein interaction (PPI) network analysis of differentially expressed genes at 3 h, **(A)** 12 h, and **(B),** and 72 h **(C)** of osteogenesis compared with undifferentiated cells (t = 0 h); The most significant module of differentially regulated genes between osteogenesis and adipogenesis, **(D)** between osteogenesis and chondrogenesis, and **(E)** between chondrogenesis and adipogenesis **(F)** at 3 h after inductive differentiation (t = 0 h). Red indicates upregulated genes, and green indicates the downregulated genes.

chondrogenesis, and adipogenesis. Three genes (*Ccna2*, *Cdc20*, and *Il6*) were upregulated in all three groups, which suggested that most identified hub genes at this phase may not play independent roles in determining the lineage commitment of BMSCs but act as common participants in initiating differentiation. *Ccna2* is ubiquitously expressed and acts as an essential regulator of the cell division cycle at the G1/S transition and mitotic entry (Bendris et al., 2012; Loukil et al., 2014). *Cdc20* is a key regulator of ubiquitylation of FRET and could colocalize with *Ccna2*, LC3-B, p62 or lysosomes (Loukil et al., 2014). Il6 is a well-known pleiotropic cytokine and shows multiple functions such as the regulation of inflammation and immunity (Hunter and Jones, 2015). Deng et al. (2020) have demonstrated that the expression of *Il6* increased during adipogenesis of MSCs and was positively correlated with the Oil Red O quantification result.

Unique DEGs that occurred in only one lineage may play pivotal roles in determining the fate of BMSCs. Five genes (*LOC689899*, *Mex3b*, *Sertad1*, *LOC100362684*, and *Hopx*) were dysregulated in three time points of osteogenesis but showed non-significant changes during two other lineages (**Supplementary Table S1**). *Mex3B*, which is reportedly to induce apoptosis after cell stimulations such as heat, radiation, and reactive oxygen species, is downregulated in osteogenesis (Umehara et al., 2020). *Hopx* has been demonstrated to be a promoter of BMSC proliferation and an inhibitor of adipogenesis by suppressing adipogenic pathway–related genes such as *PLIN1*, *FABP4*, and *PLIN5* (Hng et al., 2020). *Dtx4* was exclusively upregulated in three time points during adipogenesis and was involved in cell development and cell differentiation (Wang et al., 2017). Wang et al. (2017) indicated that knockdown of this gene could inhibit adipogenesis through restraining C/EBPα and PPARγ and therefore arresting mitotic clonal expansion. Sixteen genes were upregulated through the early lineage of chondrogenesis. Among them, the expression of *Ibsp* is driven by RUNX3 and MEF2C, which appears more critical than RUNX2 for chondrogenesis (Dreher et al., 2020). It could be noticed that a lot of genes are exclusively dysregulated at the first phase of differentiation, and their effect for determining the fate of rat BMSCs needs to be further confirmed (**Supplementary Table S1**). A total of 207 unique DEGs were only identified at 3 h of adipogenesis, which suggested that key genes related to adipogenesis were significantly modulated earlier than osteogenesis.

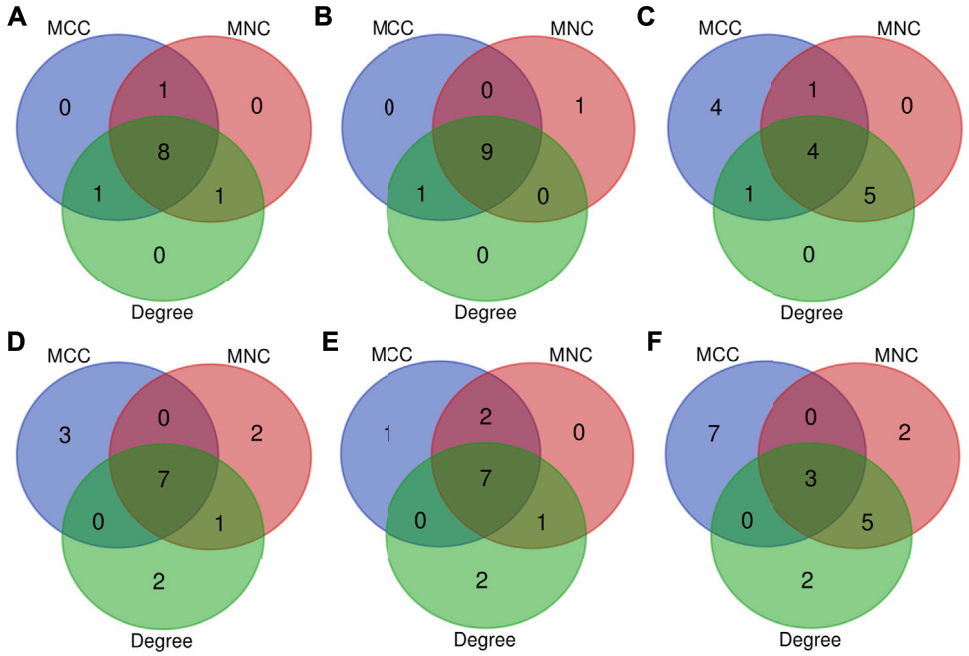

FIGURE 8 | Top 10 key genes at 3 h, **(A)** 12 h, and **(B)** 72 h **(C)** of osteogenesis compared with undifferentiated cells (*t* = 0 h); The top 10 key genes identified from comparisons between osteogenesis and adipogenesis, **(D)** between osteogenesis and chondrogenesis, and **(E)** between chondrogenesis and adipogenesis **(F)** at 3 h after inductive differentiation (*t* = 0 h), which were selected based on the three most commonly used classification methods (MCC, MNC, and Degree) in cytoHubba.

TABLE 1 | List of the top 10 hub genes selected by degree methods in cytoHubba.

Comparisons	Hub genes
OS3h vs BMSCs	Ccna2, Cdc20, Il6, Mad2l1, Top2a, Kif11, Mcm4, Asf1b, Rrm1, Pa2g4
OS12 h vs BMSCs	Il6, Mad2l1, Top2a, Ccna2, Cdc20, Mcm6, Mcm3, Kif11, Mcm4, Cdc6
OS72 h vs BMSCs	Il6, Cd44, Il1b, Ccl2, Kif11, Notch1, Asf1b, Cdc20, Mcm3, Pbk
AD3h vs BMSCs	Il6, Ccna2, Cdc20, Kif11, Top2a, Mad2l1, Gsk3b, Mcm6, Asf1b, Mcm3
AD12 h vs BMSCs	Ccna2, Mad2l1, Mcm3, Top2a, Mcm6, Kif11, Cdc20, Rrm1, Mcm4, Asf1b
AD72 h vs BMSCs	Il6, Notch1, Igf1, Il1b, Kif11, Cdc20, Asf1b, Kif20a, Top2a, Rhoc
CH3h vs BMSCs	Il6, Mad2l1, Top2a, Cdc20, Kif11, Ccna2, Mcm3, Sspo, Mcm6, Mcm4
CH12 h vs BMSCs	Il6, Jun, Notch1, Lep, Mmp2, Acta1, Pik3r1, Csf2, Ldlr, Gja1
CH72 h vs BMSCs	Il6, Rac1, Il1b, Acta1, Ccl2, Vcl, Ctnna1, Sox9, Actn2, Actg2
OS3h vs AD3h	Il6, Jun, Notch1, Pik3r1, Sox9, Vcl, Ctgf, Nck1, Rhoq, Gnai1
OS3h vs CH3h	Il6, Jun, Notch1, Sox9, Vcl, Rnd1, Ccl2, Ctgf, Notch2, Lpl
CH3h vs AD3h	Jun, Csf2, Sox9, Ccl2, Rasa1, Il1b, Epha2, Cxcl1, Il1a, Rnd1

OS, osteogenic differentiation; CH, chondrogenic differentiation; AD, adipogenic differentiation.

Then, various bioinformatics analysis methods were used to reveal the enriched functional terms regarding identified DEGs. As a result, GO terms of 792 DEGs identified at 3 h of osteogenesis for biological process categories included "negative regulation of transcription from RNA polymerase II promoter" and "response to drug." Furthermore, the KEGG pathway enrichment analysis revealed that these DEGs were predominantly associated with the "PI3K-Akt signaling pathway." The DEGs in the "PI3K-Akt signaling pathway" were *Chrm2*, *Pdgfra*, *Ngfr*, *Col24a1*, *Lama1*, *Lama4*, *Flt4*, *Pik3r5*, *Rbl2*, *Il6*, *Ppp2r1b*, *Fgf9*, *Col5a1*, *Col5a2*, *Col4a3*, *Eif4ebp1*, *Tek*, *Ywhah*, *Ifnar1*, *Pck2*, and *Epha2*. As to 12 h of osteogenesis, the most involved BP terms are "oxidation-reduction process" and "negative regulation of cell proliferation," which suggest that BMSCs start from proliferation to differentiation at this phase. While in this phase, the most enriched KEGG pathway is "metabolic pathways." Similar changes occurred early in adipogenesis in comparison with osteogenesis. It can be noticed that at 3 h of adipogenesis, the most enriched BP terms are "oxidation-reduction process," "positive regulation of cell proliferation," "negative regulation of apoptotic process," and "response to drug," while the most involved KEGG pathways are "metabolic pathways."

miRNAs have been demonstrated to be important regulatory factors in the differentiation of BMSCs by binding the 3′-untranslated region of targeted mRNAs (Zhou et al., 2020; Liu et al., 2021). Thus, we constructed a DEG-miRNA regulatory

TABLE 2 | The fold change (FC) and adj. *p*. val of the top 10 hub genes at 3, 12, and 72 h of osteogenesis compared with undifferentiated cells.

3 h			12 h			72 h		
Gene	**log_2FC**	**adj. *p*. val**	**Gene**	**log_2FC**	**adj. *p*. val**	**Gene**	**log_2FC**	**adj. *p*. val**
Asf1b	2.07865	<0.01	Kif11	2.83993	<0.01	Il1b	−6.1996	<0.01
Ccna2	2.52671	<0.01	Mcm4	2.40732	<0.01	Asf1b	−2.4827	<0.01
Cdc20	2.35907	<0.01	Mcm6	3.31951	<0.01	Cd44	−1.1223	<0.01
Il6	−4.6024	<0.01	Mcm3	3.30175	<0.01	Cdc20	−2.2716	<0.01
Kif11	1.67841	<0.01	Cdc20	2.7624	<0.01	Ccl2	−3.2291	<0.01
Mad2l1	1.56818	0.0128	Il6	−6.5453	<0.01	Kif11	−2.833	<0.01
Mcm4	1.13145	<0.01	Top2a	3.34705	<0.01	Notch1	1.86226	<0.01
Pa2g4	1.31558	<0.01	Mad2l1	2.81097	<0.01	Pbk	−5.2452	<0.01
Rrm1	1.53775	<0.01	Ccna2	3.14156	<0.01	Il6	−6.3788	<0.01
Top2a	2.4447	<0.01	Cdc6	3.9125	0.0111	Mcm3	−1.8955	<0.01

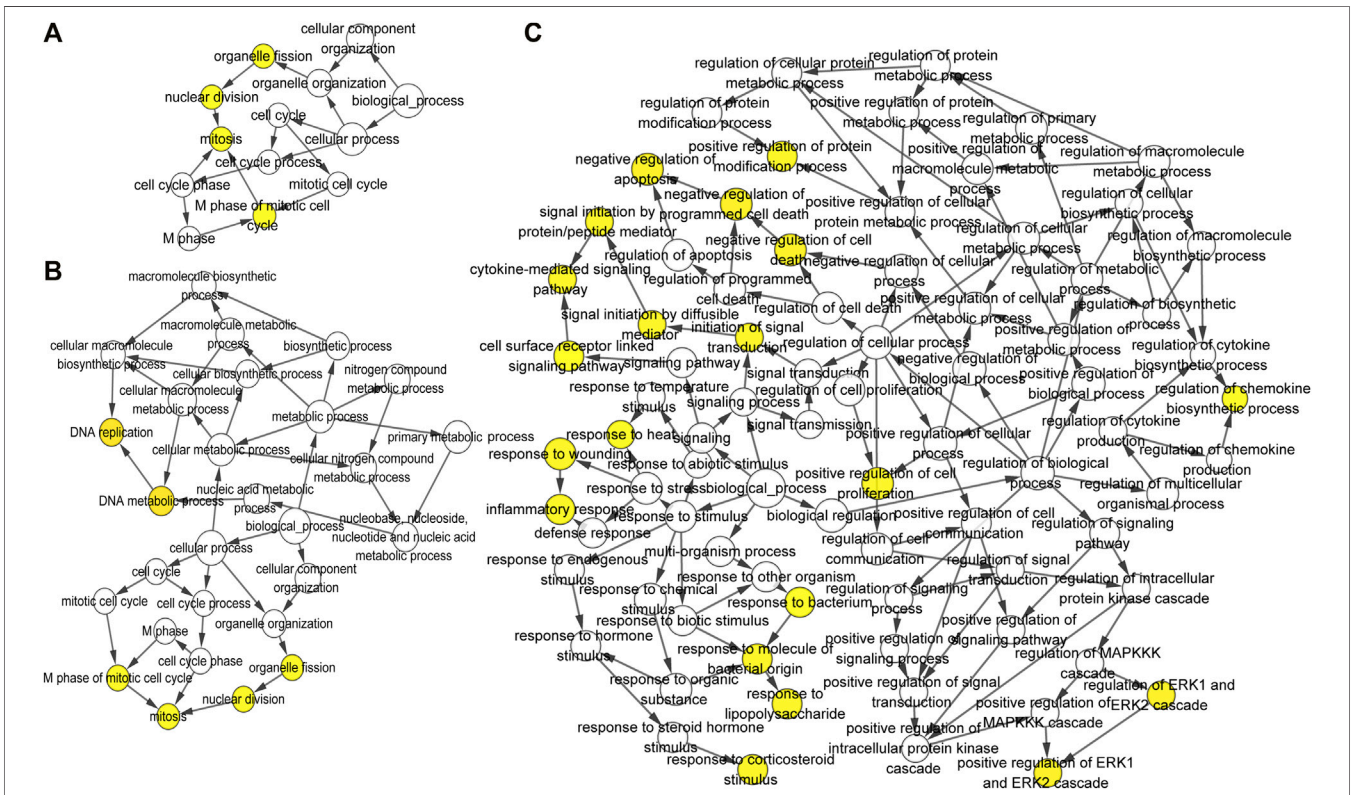

FIGURE 9 | Biological process analysis of the top 10 differentially expressed genes was constructed using BiNGO at 3 h, **(A)** 12 h, and **(B)** 72 h **(C)** of osteogenesis compared with undifferentiated cells ($t = 0$ h). The color depth of nodes refers to the corrected *p*-value of ontologies. The size of nodes refers to the number of genes that are involved in the ontologies. $p < 0.001$ was considered statistically significant.

network to show the potential interactions among identified DEGs and RNAs during osteogenesis, adipogenesis, and chondrogenesis. In the networks of DEGs about comparisons between adipogenesis and osteogenesis at 3h, rno-miR-449-5p may play an important role because it connects with three key genes. This miRNA, along with rno-miR-153-5p, also occurred in the network about comparisons between osteogenesis and chondrogenesis. Rno-miR449a-5p are essential for both mitochondria metabolic dysfunction and phenotype transformation of pulmonary arterial smooth muscle cells (Zhang et al., 2019), but currently, there is no direct evidence to prove the role of this miRNA for the lineage commitment of rat BMSCs.

For the first time, the gene transcription of rat BMSCs during osteogenesis, adipogenesis, and chondrogenesis was systematically detected and analyzed. The current study provided directions and molecular targets for further investigations on the lineage commitment of rat BMSCs by high-throughput sequencing and rigorous bioinformatics analysis. However, it should be admitted that there were shortcomings that merit consideration. First, this is only a very fundamental research study using two-dimensional culture. The differentiation in the internal environment may possess

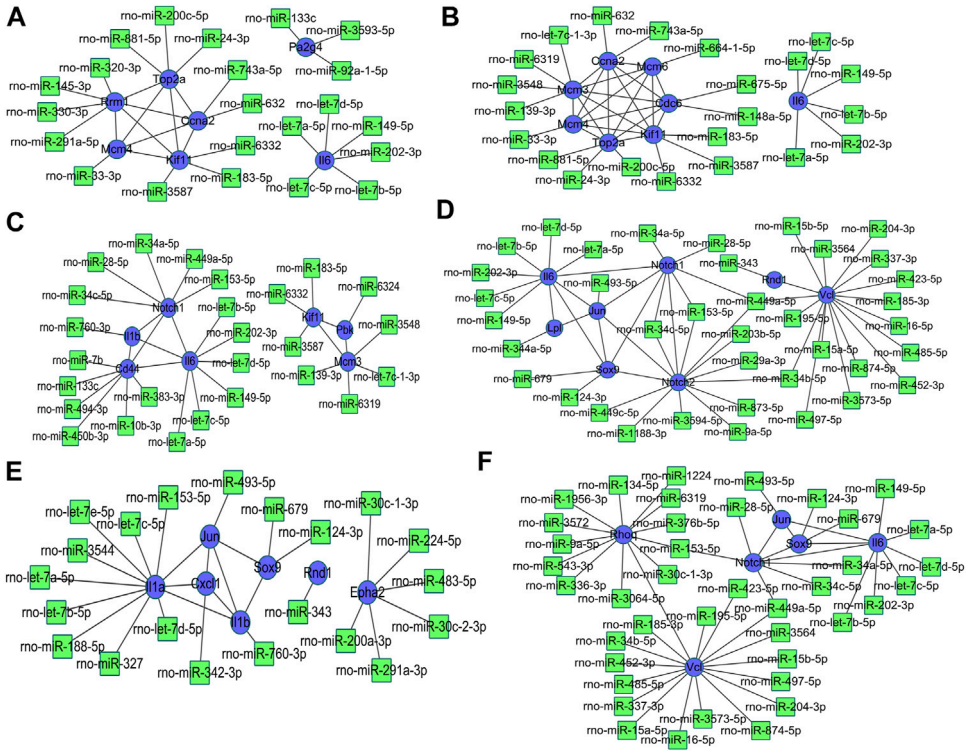

FIGURE 10 | Regulatory network of DEG-miRNA was obtained from the miRDB database using the DEGs at 3 h, **(A)** 12 h, and **(B)** 72 h **(C)** in osteogenesis compared with undifferentiated cells (t = 0 h), and the DEGs identified from comparisons between osteogenesis and adipogenesis, **(D)** between osteogenesis and chondrogenesis, and **(E)** between chondrogenesis and adipogenesis **(F)** at 3 h after inductive differentiation (t = 0 h). Blue indicates genes, and green indicates targeted miRNA. DEG, differentially expressed gene; miRNA, microRNA.

different characteristics in comparison with the *in vitro* experiment. These results cannot completely represent the normal physiological processes. The role of predicted genes and miRNAs in the three-directional differentiation of BMSCs merits further investigation. Second, only three time points distributed so-called "three phases of lineage commitment" were selected in this study as representatives. More detailed results may be acquired if more time points during differentiation were selected. Third, the DEG-miRNA network was constructed by using the miRDB database. In the future, we will detect the expression of non-coding RNA using our samples and then construct a competing endogenous RNA network. Last but not least, because there is a large number of differentially expressed genes identified in the diverse comparisons, validation by Western blot assay or protein array was not available. In the future, specific molecules could be selected for in-depth investigation.

CONCLUSION

These hub genes, functional terms, and predicted targeted genes identified in the current study may provide information for further clarification of the molecular mechanism underlying the lineage commitment of rat bone mesenchymal stem cells. Hub genes including *Ccna2*, *Cdc20*, and *Il6* may act as typical participants in initiating osteogenesis, adipogenesis, and chondrogenesis. *Mex3b*, *Sertad1*, and *Hopx* showed enhanced expression throughout three early phases during the osteogenic differentiation but no significant change in other two-directional differentiation. A similar pattern of *Dtx4* and *Ibsp* expressions occurred in adipogenesis and chondrogenesis, respectively. Additionally, rno-miR-449-5p is a potential regulator for the early lineage commitment of osteogenesis. Our findings will help understand the underlying mechanism determining the differentiation fate of BMSCs and provide theoretical support for the clinical treatment of osteoporosis, osteoarthritis, and other age-related bone diseases.

DATA AVAILABILITY STATEMENT

The datasets presented in this study can be found in online repositories. The names of the repository/repositories and accession number(s) can be found below: https://www.ncbi.nlm.nih.gov/geo/, accession ID: GSE185140.

ETHICS STATEMENT

This study was approved by the Animal Ethics Committee of Shandong Provincial Hospital affiliated to Shandong First Medical University

AUTHOR CONTRIBUTIONS

FL and QZ conceived and designed the study. FL, QZ, JD, and DZ analyzed RNA sequencing data. FL, QZ, and PZ performed the basic experiment. FL, and QZ wrote the manuscript, which was commented on by all authors.

FUNDING

This work was partially supported by the China Scholarship Council (CSC) (Grant number 201808080126), the Incubation Fund of Shandong Provincial Hospital (Grant number 2020FY019), the Young Scholars Program of Shandong Provincial Hospital, the Young Taishan Scholars Program of Shandong Province (Grant number tsqn201909183), the Academic Promotion Program of Shandong First Medical University (Grant number 2020RC008), and the Natural Science Foundation of Shandong Province (Grant numbers ZR2020QH072 and ZR2021QH307).

SUPPLEMENTARY MATERIAL

The Supplementary Material for this article can be found online at: https://www.frontiersin.org/articles/10.3389/fmolb.2021.782054/full#supplementary-material

REFERENCES

Arthur, A., and Gronthos, S. (2020). Clinical Application of Bone Marrow Mesenchymal Stem/Stromal Cells to Repair Skeletal Tissue. *Ijms* 21 (24), 9759. doi:10.3390/ijms21249759

Bendris, N., Loukil, A., Cheung, C., Arsic, N., Rebouissou, C., Hipskind, R., et al. (2012). Cyclin A2: A Genuine Cell Cycle Regulator. *Biomol. Concepts* 3 (6), 535–543. doi:10.1515/bmc-2012-0027

Boeuf, S., and Richter, W. (2010). Chondrogenesis of Mesenchymal Stem Cells: Role of Tissue Source and Inducing Factors. *Stem Cel Res. Ther.* 1 (4), 31. doi:10.1186/scrt31

Bruedigam, C., Driel, M. v., Koedam, M., Peppel, J. v. d., van der Eerden, B. C. J., Eijken, M., et al. (2011). Basic Techniques in Human Mesenchymal Stem Cell Cultures: Differentiation into Osteogenic and Adipogenic Lineages, Genetic Perturbations, and Phenotypic Analyses. *Curr. Protoc. Stem Cel Biol.* 17, t1H–t3H. doi:10.1002/9780470151808.sc01h03s17

Chen, Q., Shou, P., Zheng, C., Jiang, M., Cao, G., Yang, Q., et al. (2016). Fate Decision of Mesenchymal Stem Cells: Adipocytes or Osteoblasts. *Cell Death Differ* 23 (7), 1128–1139. doi:10.1038/cdd.2015.168

Deng, W., Chen, H., Su, H., Wu, X., Xie, Z., Wu, Y., et al. (2020). IL6 Receptor Facilitates Adipogenesis Differentiation of Human Mesenchymal Stem Cells through Activating P38 Pathway. *Ijsc* 13 (1), 142–150. doi:10.15283/ijsc19073

Dreher, S. I., Fischer, J., Walker, T., Diederichs, S., and Richter, W. (2020). Significance of MEF2C and RUNX3 Regulation for Endochondral Differentiation of Human Mesenchymal Progenitor Cells. *Front. Cel Dev. Biol.* 8, 81. doi:10.3389/fcell.2020.00081

Galderisi, U., Peluso, G., and Di Bernardo, G. (2021). Clinical Trials Based on Mesenchymal Stromal Cells Are Exponentially Increasing: Where Are We in Recent Years. *Stem Cel Rev. Rep.* 16. doi:10.1007/s12015-021-10231-w

Gari, M., Alsehli, H., Gari, A., Abbas, M., Alkaff, M., Abuzinadah, M., et al. (2016). Derivation and Differentiation of Bone Marrow Mesenchymal Stem Cells from Osteoarthritis Patients. *Tissue Eng. Regen. Med.* 13 (6), 732–739. doi:10.1007/s13770-016-0013-2

Hng, C. H., Camp, E., Anderson, P., Breen, J., Zannettino, A., and Gronthos, S. (2020). HOPX Regulates Bone Marrow-Derived Mesenchymal Stromal Cell Fate Determination via Suppression of Adipogenic Gene Pathways. *Sci. Rep.* 10 (1), 11345. doi:10.1038/s41598-020-68261-2

Hu, L., Yin, C., Zhao, F., Ali, A., Ma, J., and Qian, A. (2018). Mesenchymal Stem Cells: Cell Fate Decision to Osteoblast or Adipocyte and Application in Osteoporosis Treatment. *Ijms* 19 (2), 360. doi:10.3390/ijms19020360

Hunter, C. A., and Jones, S. A. (2015). IL-6 as a keystone Cytokine in Health and Disease. *Nat. Immunol.* 16 (5), 448–457. doi:10.1038/ni.3153

Jiang, Y., Zhang, P., Zhang, X., Lv, L., and Zhou, Y. (2021). Advances in Mesenchymal Stem Cell Transplantation for the Treatment of Osteoporosis. *Cell Prolif* 54 (1), e12956. doi:10.1111/cpr.12956

Johnson, J., Shojaee, M., Mitchell Crow, J., and Khanabdali, R. (2021). From Mesenchymal Stromal Cells to Engineered Extracellular Vesicles: A New Therapeutic Paradigm. *Front. Cel Dev. Biol.* 9, 705676. doi:10.3389/fcell.2021.705676

Kim, J., and Adachi, T. (2021). Cell-fate Decision of Mesenchymal Stem Cells toward Osteocyte Differentiation Is Committed by Spheroid Culture. *Sci. Rep.* 11 (1), 13204. doi:10.1038/s41598-021-92607-z

Lefebvre, V., and Dvir-Ginzberg, M. (2017). SOX9 and the many Facets of its Regulation in the Chondrocyte Lineage. *Connect. Tissue Res.* 58 (1), 2–14. doi:10.1080/03008207.2016.1183667

Li, J., Ezzelarab, M. B., and Cooper, D. K. C. (2012). Do mesenchymal Stem Cells Function across Species Barriers? Relevance for Xenotransplantation. *Xenotransplantation* 19 (5), 273–285. doi:10.1111/xen.12000

Liu, F., Dong, J., Zhou, D., and Zhang, Q. (2021). Identification of Key Candidate Genes Related to Inflammatory Osteolysis Associated with Vitamin E-Blended UHMWPE Debris of Orthopedic Implants by Integrated Bioinformatics Analysis and Experimental Confirmation. *Jir* Vol. 14, 3537–3554. doi:10.2147/JIR.S320839

Loukil, A., Zonca, M., Rebouissou, C., Baldin, V., Coux, O., Biard-Piechaczyk, M., et al. (2014). High Resolution Live Cell Imaging Reveals Novel Cyclin A2 Degradation Foci Involving Autophagy. *J. Cel Sci.* 127 (Pt 10), 2145–2150. doi:10.1242/jcs.139188

Mabuchi, Y., Okawara, C., Méndez-Ferrer, S., and Akazawa, C. (2021). Cellular Heterogeneity of Mesenchymal Stem/Stromal Cells in the Bone Marrow. *Front. Cel Dev. Biol.* 9, 689366. doi:10.3389/fcell.2021.689366

Pierce, J. L., Begun, D. L., Westendorf, J. J., and McGee-Lawrence, M. E. (2019). Defining Osteoblast and Adipocyte Lineages in the Bone Marrow. *Bone* 118, 2–7. doi:10.1016/j.bone.2018.05.019

Piotrowska, K., and Tarnowski, M. (2021). Bone Marrow Adipocytes-Role in Physiology and Various Nutritional Conditions in Human and Animal Models. *Nutrients* 13 (5), 1412. doi:10.3390/nu13051412

Robert, A. W., Marcon, B. H., Dallagiovanna, B., and Shigunov, P. (2020). Adipogenesis, Osteogenesis, and Chondrogenesis of Human Mesenchymal Stem/Stromal Cells: A Comparative Transcriptome Approach. *Front. Cel Dev. Biol.* 8, 561. doi:10.3389/fcell.2020.00561

Saeedi, M., Nezhad, M. S., Mehranfar, F., Golpour, M., Esakandari, M. A., Rashmeie, Z., et al. (2021). Biological Aspects and Clinical Applications of Mesenchymal Stem Cells: Key Features You Need to Be Aware of. *Cpb* 22 (2), 200–215. doi:10.2174/1389201021666200907121530

Sulston, R. J., and Cawthorn, W. P. (2016). Bone Marrow Adipose Tissue as an Endocrine Organ: Close to the Bone. *Horm. Mol. Biol. Clin. Investig.* 28 (1), 21–38. doi:10.1515/hmbci-2016-0012

Tamama, K., Fan, V. H., Griffith, L. G., Blair, H. C., and Wells, A. (2006). Epidermal Growth Factor as a Candidate for *Ex Vivo* Expansion of Bone Marrow-Derived Mesenchymal Stem Cells. *Stem Cells* 24 (3), 686–695. doi:10.1634/stemcells.2005-0176

Umehara, T., Kagawa, S., Tomida, A., Murase, T., Abe, Y., Shingu, K., et al. (2020). Body Temperature-dependent microRNA Expression Analysis in Rats: Rno-miR-374-5p Regulates Apoptosis in Skeletal Muscle Cells via Mex3B under Hypothermia. *Sci. Rep.* 10 (1), 15432. doi:10.1038/s41598-020-71931-w

van de Peppel, J., Strini, T., Tilburg, J., Westerhoff, H., van Wijnen, A. J., and van Leeuwen, J. P. (2017). Identification of Three Early Phases of Cell-Fate Determination during Osteogenic and Adipogenic Differentiation by Transcription Factor Dynamics. *Stem Cel Rep.* 8 (4), 947–960. doi:10.1016/j.stemcr.2017.02.018

Wang, Z., Dai, Z., Pan, Y., Wu, S., Li, Z., and Zuo, C. (2017). E3 Ubiquitin Ligase DTX4 Is Required for Adipogenic Differentiation in 3T3-L1 Preadipocytes Cell Line. *Biochem. Biophysical Res. Commun.* 492 (3), 419–424. doi:10.1016/j.bbrc.2017.08.083

Zhang, C., Ma, C., Zhang, L., Zhang, L., Zhang, F., Ma, M., et al. (2019). MiR-449a-5p Mediates Mitochondrial Dysfunction and Phenotypic Transition by Targeting Myc in Pulmonary Arterial Smooth Muscle Cells. *J. Mol. Med.* 97 (3), 409–422. doi:10.1007/s00109-019-01751-7

Zhang, Q., Dong, J., Zhang, P., Zhou, D., and Liu, F. (2021). Dynamics of Transcription Factors in Three Early Phases of Osteogenic, Adipogenic, and Chondrogenic Differentiation Determining the Fate of Bone Marrow Mesenchymal Stem Cells in Rats. *Front. Cel Dev. Biol.* 9, 768316. doi:10.3389/fcell.2021.768316

Zhou, L., Qiu, M., Yang, L., Yang, L., Zhang, Y., Mu, S., et al. (2020). MicroRNA-1-3p Enhances Osteoblast Differentiation of MC3T3-E1 Cells by Interacting with Hypoxia-Inducible Factor 1 α Inhibitor (HIF1AN). *Mech. Develop.* 162, 103613. doi:10.1016/j.mod.2020.103613

Zhu, B., Xue, F., Li, G., and Zhang, C. (2020). CRYAB Promotes Osteogenic Differentiation of Human Bone Marrow Stem Cells via Stabilizing β-catenin and Promoting the Wnt Signalling. *Cel Prolif* 53 (1), e12709. doi:10.1111/cpr.12709

Conflict of Interest: The authors declare that the research was conducted in the absence of any commercial or financial relationships that could be construed as a potential conflict of interest.

Publisher's Note: All claims expressed in this article are solely those of the authors and do not necessarily represent those of their affiliated organizations, or those of the publisher, the editors, and the reviewers. Any product that may be evaluated in this article, or claim that may be made by its manufacturer, is not guaranteed or endorsed by the publisher.

frontiers in Molecular Biosciences

ORIGINAL RESEARCH
published: 23 February 2022
doi: 10.3389/fmolb.2022.800288

Bioinformatics-Guided Analysis Uncovers AOX1 as an Osteogenic Differentiation-Relevant Gene of Human Mesenchymal Stem Cells

Lingtong Sun[1†], *Jianfei Ma*[2†], *Juan Chen*[1], *Zhijun Pan*[3,4,5*] and *Lijun Li*[3,4,5*]

[1]Affiliated Hangzhou Xixi Hospital, Zhejiang University School of Medicine, Hangzhou, China, [2]Key Laboratory of Image Information Processing and Intelligent Control, School of Artificial Intelligence and Automation, Huazhong University of Science and Technology, Wuhan, China, [3]Department of Orthopedics Surgery, The Second Affiliated Hospital, Zhejiang University School of Medicine, Hangzhou, China, [4]Orthopedics Research Institute of Zhejiang University, Hangzhou, China, [5]Key Laboratory of Motor System Disease Research and Precision Therapy of Zhejiang Province, Hangzhou, China

Background: The available therapeutic options of bone defects, fracture nonunion, and osteoporosis remain limited, which are closely related to the osteogenic differentiation of bone marrow–derived mesenchymal stem cells (BMSCs). Thus, there remains an urgent demand to develop a prediction method to infer osteogenic differentiation–related genes in BMSCs.

Method: We performed differential expression analysis between hBMSCs and osteogenically induced samples. Association analysis, co-expression analysis, and PPI analysis are then carried out to identify potential osteogenesis-related regulators. GO enrichment analysis and GSEA are performed to identify significantly enriched pathways associated with AOX1. qRT-PCR and Western blotting were employed to investigate the expression of genes on osteogenic differentiation, and plasmid transfection was used to overexpress the gene AOX1 in hBMSCs.

Result: We identified 25 upregulated genes and 17 downregulated genes. Association analysis and PPI network analysis among these differentially expressed genes show that AOX1 is a potential regulator of osteogenic differentiation. GO enrichment analysis and GSEA show that AOX1 is significantly associated with osteoblast-related pathways. The experiments revealed that AOX1 level was higher and increased gradually in differentiated BMSCs compared with undifferentiated BMSCs, and AOX1 overexpression significantly increased the expression of osteo-specific genes, thereby clearly indicating that AOX1 plays an important role in osteogenic differentiation. Moreover, our method has ability in discriminating genes with osteogenic differentiation properties and can facilitate the process of discovery of new osteogenic differentiation–related genes.

Conclusion: These findings collectively demonstrate that AOX1 is an osteogenic differentiation-relevant gene and provide a novel method established with a good performance for osteogenic differentiation-relevant genes prediction.

Keywords: bioinformatics, human bone marrow mesenchymal stem cells, osteogenic differentiation, novel, prediction

OPEN ACCESS

Edited by:
Ce Dou,
Army Medical University, China

Reviewed by:
Xiaoxiao Cai,
Sichuan University, China
庆刚 代,
Shanghai Jiaotong University, China

****Correspondence:***
Zhijun Pan
zrpzj@zju.edu.cn
Lijun Li
lilijun@zju.edu.cn

[†]These authors have contributed equally to this work and share first authorship

Specialty section:
This article was submitted to Cellular Biochemistry, a section of the journal Frontiers in Molecular Biosciences

Received: *22 October 2021*
Accepted: *04 January 2022*
Published: *23 February 2022*

Citation:
Sun L, Ma J, Chen J, Pan Z and Li L (2022) Bioinformatics-Guided Analysis Uncovers AOX1 as an Osteogenic Differentiation-Relevant Gene of Human Mesenchymal Stem Cells. Front. Mol. Biosci. 9:800288. doi: 10.3389/fmolb.2022.800288

INTRODUCTION

The rate of bone defects, fracture nonunion, and osteoporosis incidence continues to rise, and available therapeutic options remain limited. These diseases, closely related to the osteogenic differentiation of bone marrow–derived mesenchymal stem cells (BMSCs), have been confirmed by numerous studies (Marongiu et al., 2020; Xiao et al., 2020; Xiong et al., 2020; Jiang et al., 2021).

BMSCs possess self-renewal capabilities and the potential to differentiate into a variety of cell types, including osteoblasts, chondrocytes, and adipocytes (Bianco et al., 2001; Liao et al., 2017). As a key contributor to the bone formation, BMSCs are regulated by genetic factors (Zhang et al., 2018). However, relying solely on the experimental identification of genes that regulate osteogenic differentiation of BMSCs is generally costly and time-consuming, which leads to an urgent demand to develop a prediction method to infer osteogenic differentiation–related genes in a short time.

High-throughput sequencing including RNA-seq and microarray is a novel technique, which plays an important role in the exploration for genome-level differences and is providing valuable insights into the landscape of the identification of key genes and functional pathways associated with osteogenic differentiation in BMSCs (Fan et al., 2020). In our study, we performed a bioinformatics-guided methodology to identify potential regulators of osteogenic differentiation. We first identified 25 upregulated and 17 downregulated genes between hBMSCs and osteogenically induced samples. Association analysis, co-expression analysis, and PPI analysis are then carried out to infer potential regulators. As a result, AOX1 is identified as a new potential regulator. Association analysis, GO enrichment analysis, and GSEA show that AOX1 is significantly associated with osteogenic differentiation.

Aldehyde oxidase (AOX) is a complex enzyme present in the cytosol of eukaryotes (Garattini et al., 2008; Garattini et al., 2009). In humans, only one *AOX1* functional gene is present (Terao et al., 2006), which is expressed predominantly in the liver but detectable amounts are also found in other organs (Garattini and Terao, 2012). Although its physiological substrates are still unclear, AOX1 is suggested to have an important role in the metabolism of drugs and xenobiotics in the liver (Pryde et al., 2010; Garattini and Terao, 2011). However, its role with respect to the regulation of osteogenic differentiation has not previously been reported.

In this study, we examined the role of AOX1 in the osteogenic differentiation of human BMSCs (hBMSCs) through bioinformatics analysis and experimental verification. The results indicate that AOX1 plays an important role in the osteogenic differentiation *via* multiple pathways, meanwhile providing a novel method for the further study of osteogenic differentiation of human bone marrow–derived mesenchymal stem cells.

RESULT

Identification of Differentially Expressed Genes That Are Associated With Osteogenic Differentiation

To characterize the process of osteogenic differentiation, we performed differential expression analysis between hBMSCs and osteogenically induced samples using the limma R package (Ritchie et al., 2015). As a result, 42 genes are identified to be differentially expressed. Among all of these differentially expressed genes, 25 genes are upregulated and the remaining 17 genes are downregulated in the osteogenically induced samples (**Figure 1A**). Clustering analysis of samples based on these differentially expressed genes shows that samples within the same group tend to be clustered together (**Figure 1B**), suggesting that these differentially expressed genes can differentiate between the control group and osteogenically induced samples. Furthermore, in the osteogenically induced group, samples in the advanced stages of the osteogenic process are found to be clustered with each other, suggesting that the osteogenic stage can indeed affect the expression of these differentially expressed genes.

To analyze the expression variation of these differentially expressed genes during the osteogenic process and identify to which extent the osteogenic stage can affect the expression of these genes, we analyzed the expression of these differentially expressed genes of different osteogenic stages. The median expression of upregulated and downregulated genes is calculated respectively for samples within the same osteogenic stage. Among all upregulated genes, we found that nearly half of these genes tend to display expression variation after day 1, such as OLFML2A, CORIN, MAOA, SUSD2, FRZB, APOD, and ADH1A (**Figure 1C**). Moreover, in the downregulated genes, we observed similar variations. Some genes start downregulating after the osteogenic stage day 1 and then maintain stability in the following stages (**Figure 1D**). Among these differentially expressed genes, CXCL12, FLG, IL6, JCHAIN, and SHISA2 are the top five downregulated genes, and APOD, CORIN, FKBP5, IGFBP2, and RGCC are the top five upregulated genes. The expression profiles of these genes, presented in **Figures 1E,F**, show that the expression is distinct between different stages. These results collectively suggest that the osteogenic stage can indeed affect the expression of these genes, especially in the early stage of the osteogenic process.

Analysis of Osteoblast-Related Pathway in the Differentiation Process

Differentially expressed genes with osteogenic differentiation are analyzed, but the activity of osteoblast-related pathways during the osteogenic process is unknown. To analyze whether these osteoblast-related pathways are activated or inhibited, we collected 15 osteoblast-related pathways from the Molecular Signatures Database (MSigDb) (Subramanian et al., 2005). Single-sample gene set enrichment analysis is used to quantify the activity of osteoblast-related pathways and calculate an enrichment score for each pathway of individual sample. Similar with differentially expressed genes, we found that samples within the same group and stage tend to be clustered together based on the enrichment score of these osteoblast-related pathways (**Figure 2A**), suggesting that osteogenic stages can indeed affect the activity of these pathways.

The median enrichment score of these osteoblast-related pathways for different osteogenic stages is calculated to

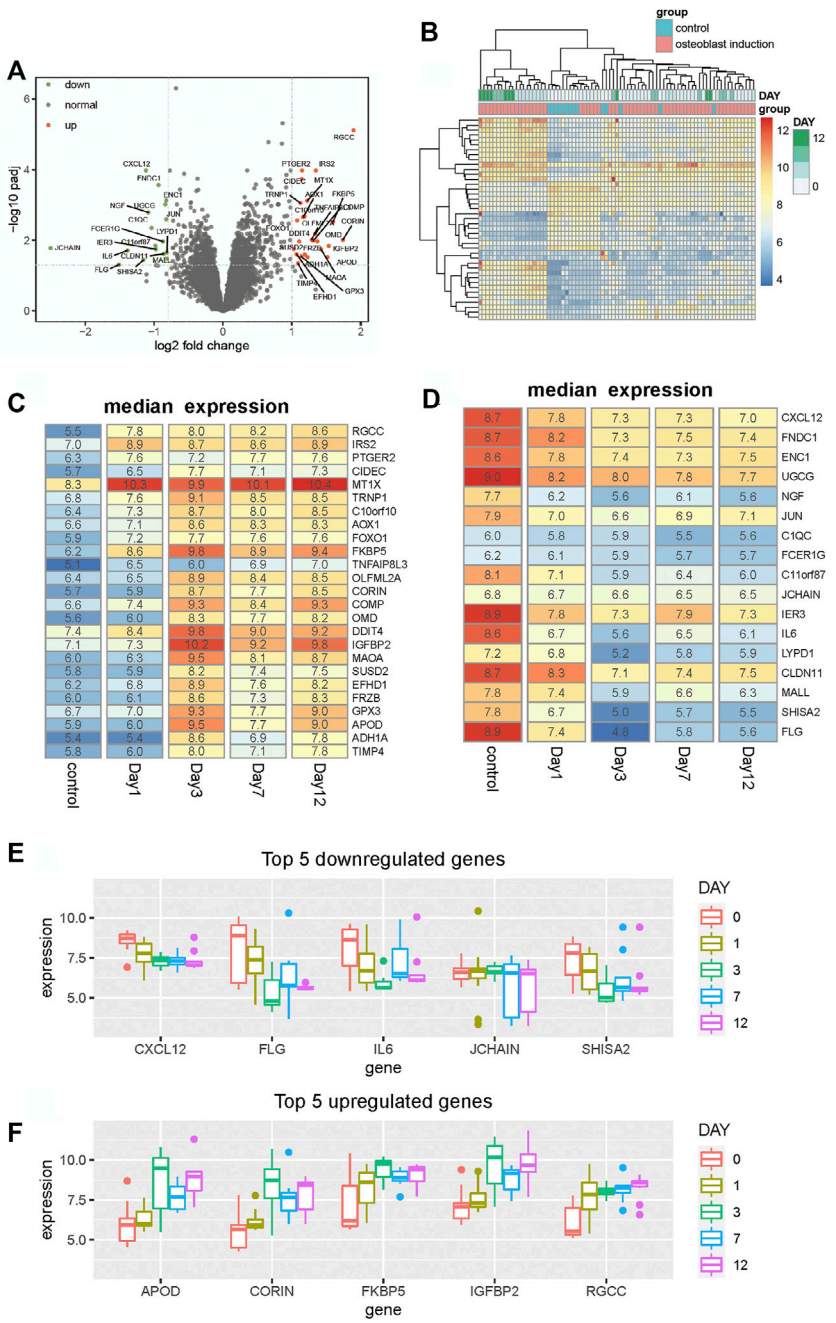

FIGURE 1 | Identification of differentially expressed genes between hBMSCs and osteogenically induced samples. **(A)** Volcano plot shows the differentially expressed genes based on fold change and BH-adjusted *p*-value. Upregulated and downregulated genes are displayed using red and blue nodes, respectively. **(B)** Heat map shows the expression pattern of these differentially expressed genes. Samples are annotated into different groups. Day means the time of osteogenically induced samples in the differentiation process. **(C,D)** Heat map shows the median expression of upregulated and downregulated genes respectively for samples in different differentiation stages. **(E,F)** Boxplot shows the top five downregulated and upregulated genes respectively in the osteogenic process.

identify differentially enriched pathways. We found that most of these osteoblast-related pathways tend to display upregulated trends during the osteogenic process (**Figure 2B**). Four representative pathways are then identified to be upregulated, in which three are associated with osteogenic differentiation and one is associated with osteoblast transcription factors (**Figure 3A**), suggesting that osteoblast differentiation–related pathways are specifically enhanced and activated during the osteogenic process. Interestingly, one pathway associated with osteoblast development is found to be downregulated during the

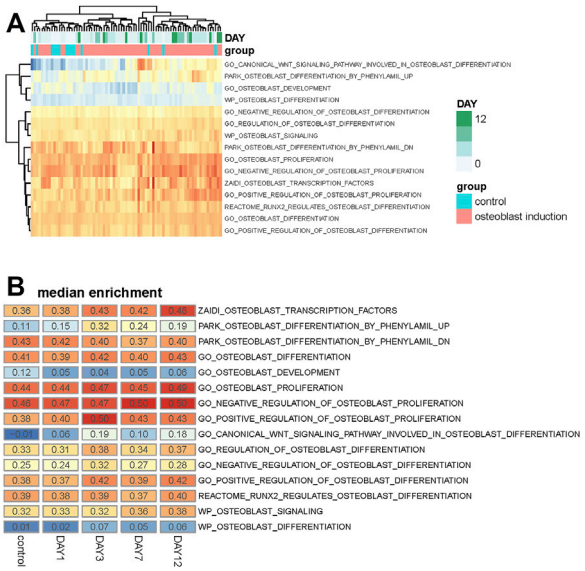

FIGURE 2 | Analysis of osteoblast-related pathways in the osteogenic process. **(A)** Heat map shows the enrichment score of 15 osteoblast-related pathways across all samples. Samples are annotated into different groups and days. **(B)** Heat map shows the median value of the enrichment score of these osteoblast-related pathways across different osteogenic stages.

osteogenic process (**Figure 3B**), suggesting that the differentiation and development of hBMSCs are mutually exclusive during the osteogenic process. The enrichment pattern of these pathways is presented in **Figure 3C**.

Selection of Candidate Genes That Are Associated With Osteogenic Differentiation

To identify candidate genes that are significantly associated with the osteogenic process, we performed association analysis between these differentially expressed genes and osteoblast-related pathways. Most of these genes are found to be positively or negatively associated with osteoblast-related pathways (**Figure 4A**). Furthermore, analysis shows that upregulated genes tend to be positively associated with these pathways, such as C10orf10, AOX1, OLFML2A, CORIN, COMP, OMD, DDIT4, MAOA, and SUSD2, suggesting that these genes are significant determinants in promoting the osteogenic process. Analysis of downregulated genes shows that they are more likely to be negatively correlated with these osteoblast-related pathways, such as UGCG, NGF, C11orf87, LYPD1, CLDN11, and MALL, suggesting significant regulation of these genes in inhibiting the osteogenic process.

Co-expression analysis is then used to identify candidate genes associated with osteogenic differentiation. We evaluated the expression association among these differentially expressed genes based on the Pearson correlation coefficient and constructed the co-expression network for upregulated and downregulated genes respectively (**Figure 4B**). To make sure that the co-expression network is reliable and hub genes identified indeed capture the topological structure of the network, the network is constructed based on a varied association threshold from 0.6 to 0.9. Degree analysis for these upregulated co-expression networks shows that MAOA, FRZB, CIDEC, TRNP1, and APOD are hub genes (**Figure 4C**). Analysis for downregulated co-expression networks shows that NGF, IL6, and IER3 are hub genes (**Figure 4D**).

Additionally, the protein–protein interaction network is also used to identify hub genes that may be associated with the osteogenic process. We constructed a protein–protein interaction network for these differentially expressed genes using the STRING database (Szklarczyk et al., 2019) and then rank these genes by degree. As a result, nine genes are identified as hub genes based on the degree (**Figure 4E**). Among these hub genes, ADH1A, AOX1, MAOA, IRS2, and FOXO1 are upregulated and JUN, NGF, IL6, and CXCL12 are downregulated.

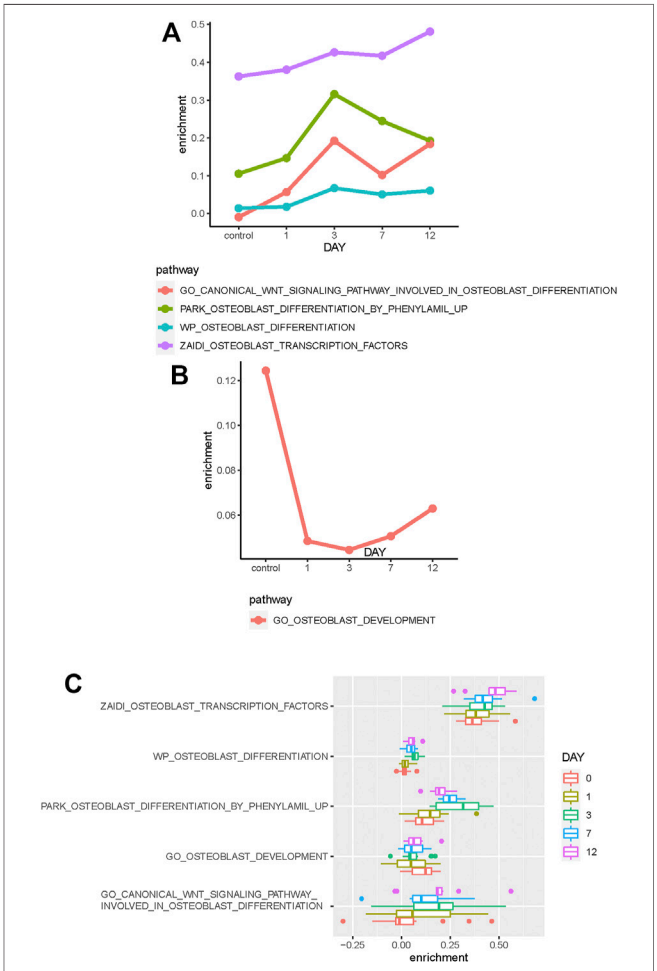

FIGURE 3 | Identification of differentially enriched pathways. **(A)** Four osteoblast-related pathways tend to be upregulated in the osteogenic process. **(B)** One osteoblast-related pathway tends to be downregulated in the osteogenic process. **(C)** Boxplot shows these differentially enriched pathways of samples. Samples are divided into different groups based on osteogenic days.

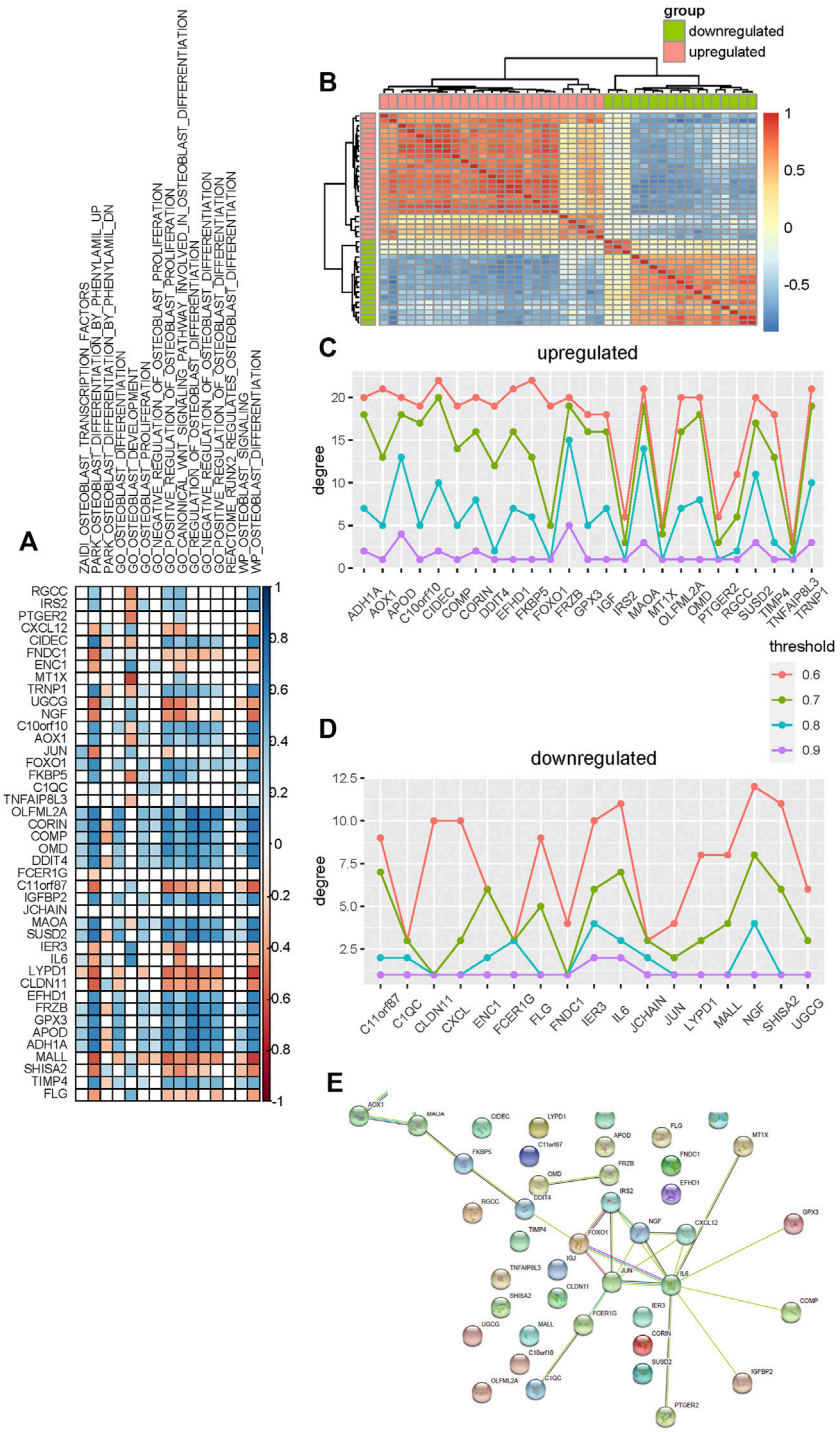

FIGURE 4 | Selection of candidate genes that are significantly associated with the osteogenic process. **(A)** Association analysis between these differentially expressed genes and osteoblast-related pathways. Blue and red colors indicate the positive and negative correlations, respectively. Blank indicates that there is no significance. **(B)** Heat map shows the co-expression pattern of these differentially expressed genes. Association is evaluated using the Pearson correlation coefficient. **(C,D)** Degree of upregulated and downregulated genes in the co-expression network constructed using different thresholds. **(E)** Protein–protein interaction network of these differentially expressed genes is constructed.

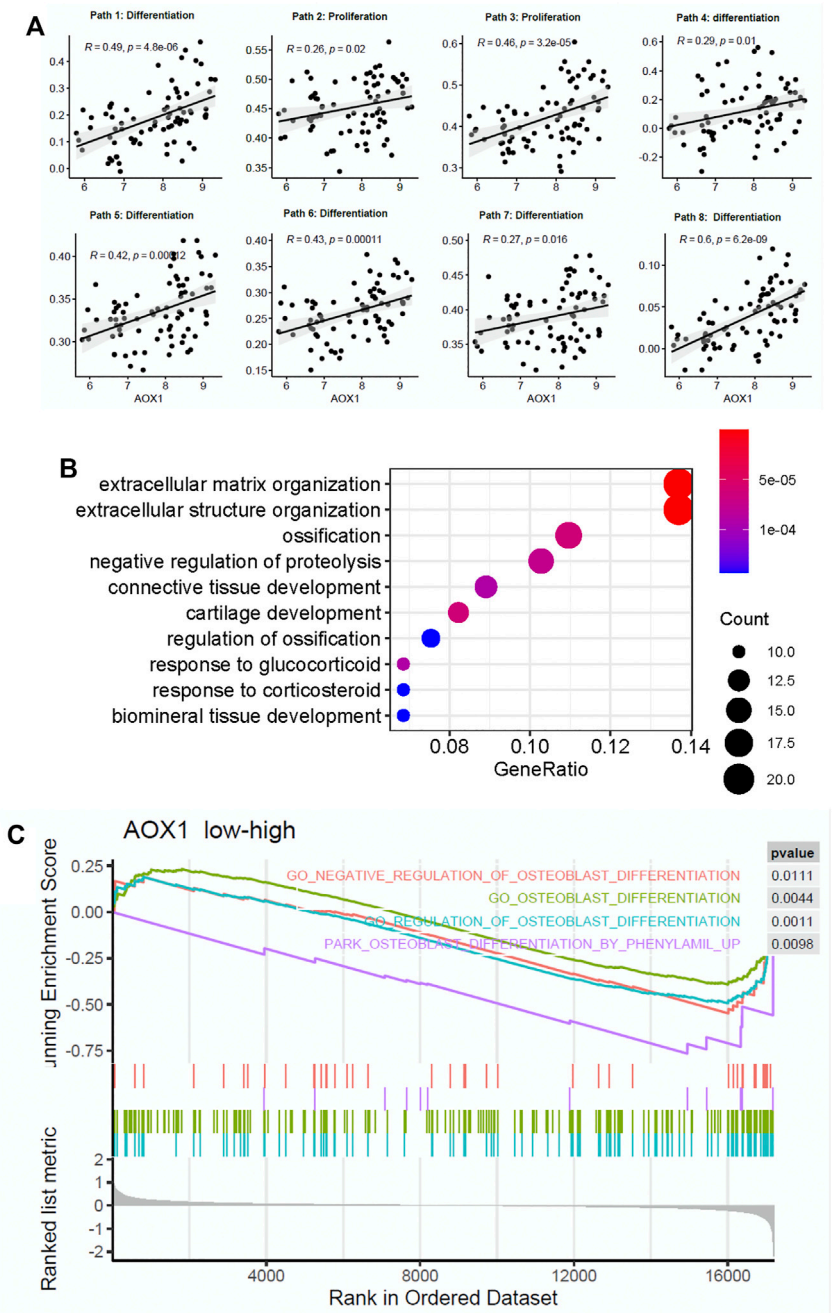

FIGURE 5 | AOX1 is a potential gene positively regulating the osteogenic process. **(A)** Point diagram shows the positive correlation between AOX1 expression and the enrichment score of osteogenic pathways (the detailed information of osteogenic pathways are presented in Supplementary Table). **(B)** Gene ontology enrichment analysis of these differentially expressed genes between the high AOX1 expression group and the low expression group. **(C)** Gene set enrichment analysis between the high AOX1 expression group and the low expression group.

Based on these results, a few genes are identified as potential targets that may promote or inhibit osteogenic differentiation during the osteogenic process. Among these candidate genes, some of them are involved in osteoblast-related pathways, and some genes have been previously studied to be associated with osteogenic differentiation. These genes are then removed from the candidate gene set. In the remaining candidate genes, AOX1 has not yet been studied extensively and no literature reports its relationship with osteogenic differentiation. Due to the strong statistical evidence of AOX1 in the osteogenic process, it is necessary and important to elucidate the interaction between AOX1 and osteogenic differentiation.

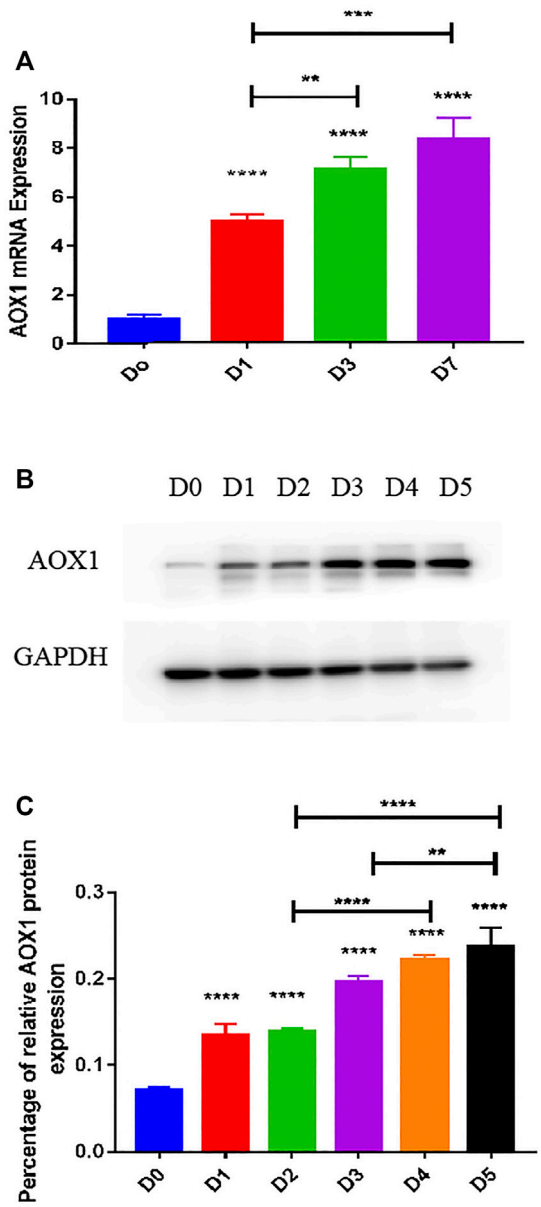

FIGURE 6 | Endogenous AOX1 mRNA expression and the endogenous AOX1 protein expression on osteogenic differentiation of hBMSCs. **(A)** Endogenous expression of AOX1 mRNA was determined by qPCR at days 0, 1, 3, and 7 of osteogenic differentiation. **(B)** Endogenous expression of AOX1 protein was determined by Western blotting analysis at days 0, 1, 2, 3, 4, and 5 of osteogenic differentiation **(C)** Relative quantitative analysis of Western blot analyses for AOX1, data are used by percentage and expressed as the mean ± SD.

AOX1 Plays an Important Role in the Process of Osteogenic Differentiation

To determine the potential role of AOX1 in regulating the osteogenic process, we analyzed the association between AOX1 and osteoblast-related pathways. We found that AOX1 expression is positively associated with the enrichment of eight osteoblast-related pathways, in which two are associated with osteoblast proliferation and six are associated with osteogenic differentiation (**Figure 5A**), suggesting that AOX1 is a potential regulator in the osteogenic process.

Additionally, we divided samples into high AOX1 expression and low expression groups based on the median of AOX1 expression. Differential expression analysis is applied between these two groups to identify differentially expressed genes associated with AOX1. As a result, 152 genes are identified as differentially expressed between these two groups. The GO enrichment analysis is then used to identify whether these differentially expressed genes are enriched in some specific pathways. The GO enrichment analysis shows that these genes are enriched in ossification and regulation of ossification, further demonstrating the regulation of AOX1 in the osteogenic process. The top 10 enriched pathways are presented in **Figure 5B**.

Apart from the GO enrichment analysis, the gene set enrichment analysis is used to determine whether some pathways are enriched in a specific AOX1 group. All genes ranked by fold change between AOX1 groups are inputted into the gene set enrichment analysis, and 15 osteoblast differentiation–related pathways are inputted to analyze whether these genes are enriched in specific pathways. As a result, four osteoblast differentiation–related pathways are found to be enriched in the high-AOX1 expression group (**Figure 5C**). In conclusion, all these results suggest that AOX1 is indeed a potential regulator in the process of osteogenic differentiation.

AOX1 Level Was Higher and Increased Gradually in Differentiated BMSCs Compared With Undifferentiated BMSCs

To determine the expression level of AOX1 associated with osteogenic differentiation of MSCs, we examined endogenous AOX1 expression in hBMSCs at days 0, 1, 3, and 7. Compared with undifferentiated BMSCs, both the mRNA (**Figure 6A**) and protein expression (**Figures 6B,C**) of AOX1 were higher and increased gradually in osteogenic differentiation.

AOX1 Overexpression in hBMSCs

To clarify the role of AOX1 in osteogenic differentiation, plasmid transfection was used to efficiently overexpress AOX1 of third-generation hBMSCs. AOX1 expression was quantified by qRT-PCR after infection. Compared with the Ctrl-OE (control-overexpression) group, the mRNA expression of AOX1 was increased in the AOX1-OE (AOX1-overexpression) group (**Figure 7E**).

AOX1 Overexpression Increased the Levels of Osteo-Specific Genes

To evaluate the effect of AOX1 overexpression in osteogenic differentiation, the levels of osteo-specific genes including the runt-related transcription factor 2 (RUNX2), osteocalcin (OCN), osteopontin (OPN), and osterix (specificity protein 7, SP7) were determined by quantitative real-time PCR (qRT-PCR). qRT-PCR

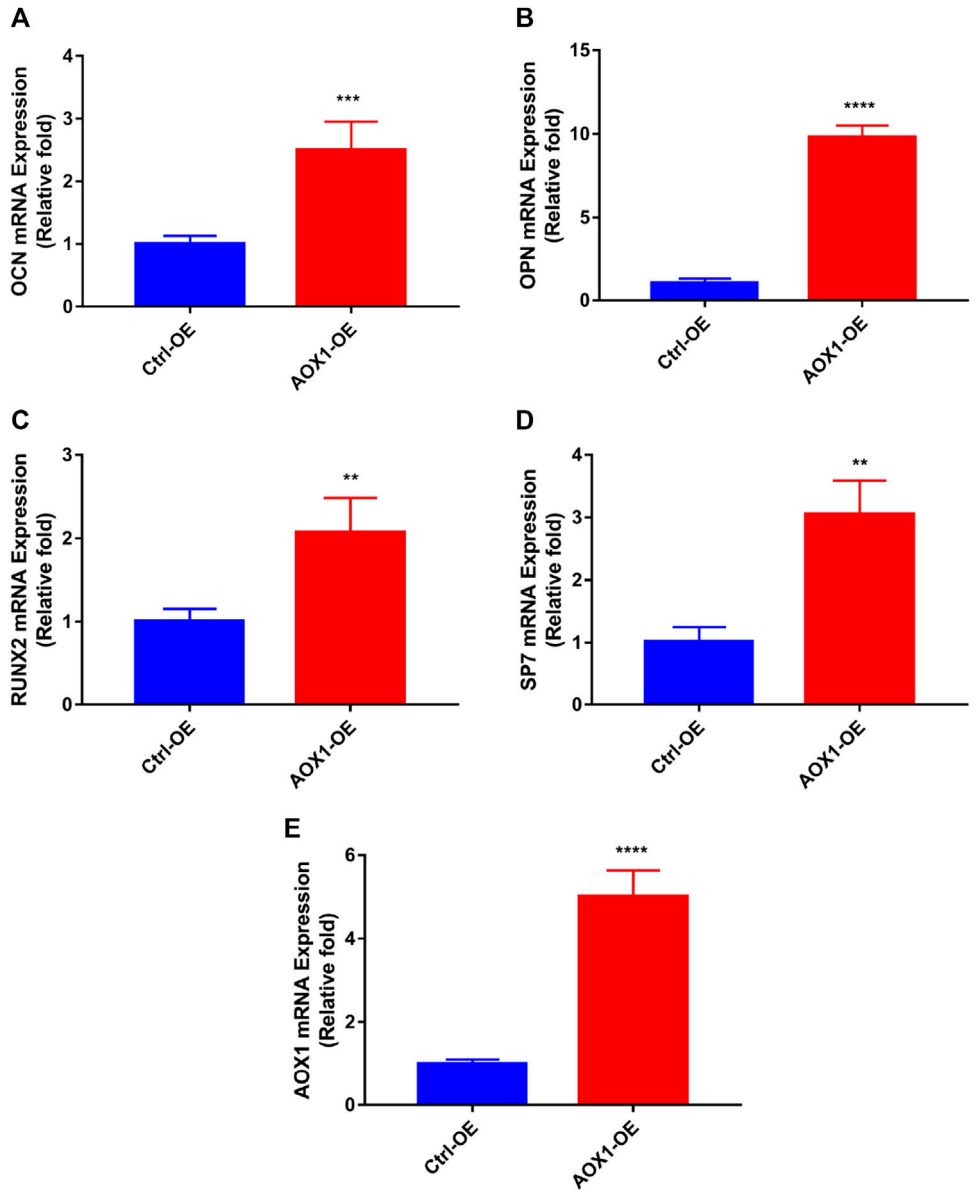

FIGURE 7 | Effects of AOX1 overexpression on osteo-specific genes. **(A–D)** Relative mRNA expression of osteo-specific genes and **(E)** AOX1 on day three of osteogenesis after AOX1 overexpression. The mRNA expression levels were normalized to that of 18S ribosomal RNA.

analysis revealed that RUNX2, OCN, OPN, and SP7 mRNA levels were significantly higher in the AOX1 overexpression group than in the control-overexpression group at day three(p<0.05, **Figures 7A–D**).

DISCUSSION

Mesenchymal stem cells have been proved to be ideal seed cells for bone tissue engineering and are closely associated with bone defects fracture nonunion and osteoporosis. Better understanding of the molecular mechanism in osteogenesis will enable researchers to design suitable targets for more effectively inducing bone tissue regeneration and treat related diseases. Microarray technology enables us to explore the genetic alterations and identify novel biomarkers in mesenchymal stem cells osteogenesis.

In this study, we performed differential expression analysis between hBMSCs and osteogenically induced samples and identified differentially expressed genes. These genes are found to be significantly associated with osteoblast-related pathways, suggesting a significant value of these genes in regulating osteogenic pathways. The co-expression and PPI network analyses show that AOX1 is a newly discovered potential regulator in osteogenic differentiation of hBMSCs. The GO analysis and GSEA among different AOX1 groups show that

osteoblast-related pathways are significantly associated with AOX1 expression.

To verify the gene AOX1 associated with osteogenic differentiation, we performed preliminary verification in hBMSCs. We report here that significant upregulation of AOX1 during the osteogenic differentiation of hBMSCs through the results of PCR and Western blotting. This study revealed that AOX1 overexpression significantly promotes osteogenesis and increases the expression of key genes that regulate the induction of osteogenesis, thereby clearly indicating that AOX1 plays an important role in osteogenic differentiation. As part of a study that was directed toward elucidating the mechanism of action of AOX1, expression of ROS, involved in the osteogenic differentiation (Tao et al., 2020), thereby clearly indicating that AOX1 plays an important role in osteogenic differentiation.

AOX1 is a molybdo-flavoenzyme with complex evolutionary profile, catalyzing the oxidation of a wide variety of substrates (Garattini and Terao, 2012), which is involved in electron transfer (Coelho et al., 2015). The important aspect of AOX1 is that it contributes to the endogenous production of H_2O_2 as reactive oxygen species (ROS), thereby regulating intracellular signaling pathways and determining cell proliferation, apoptosis, migration, and differentiation (Kundu et al., 2007; Gough and Cotter, 2011). It is currently believed that absolute levels of ROS is harmful under pathological conditions, whereas moderately elevated ROS have beneficial effects on osteogenic differentiation (Guzik and Harrison, 2006; Mandal et al., 2011; Li et al., 2017; Rossi et al., 2017; Zhu et al., 2018; Gardin et al., 2020; Khalid et al., 2020; Tao et al., 2020; Li et al., 2021). ROS enables induction of FOXO activation, which promotes bone formation in part by modulating the differentiation of osteoblastic cells (Ambrogini et al., 2010) and is also known to suppress the expression and transcriptional activity of PPARγ (a potent repressor of osteoblastogenesis) (Armoni et al., 2006). FOXO1 acts upstream of RUNX2 induction and plays an important role in promoting osteogenic differentiation and suppressing proliferation in differentiating cells (Siqueira et al., 2011).

AOX1 is one of the key enzymes of tryptophan catabolism and loss of AOX1 may lead to the accumulation of kynurenine and NADP (Vantaku et al., 2020). Meanwhile, kynurenine impacts MSCs and causes age-related bone loss (Anaya et al., 2020). AOX1 also contributes to ATRA biosynthesis (Zhong et al., 2021). ATRA-induced osteogenic differentiation of mesenchymal stem cells and its ability to influence osteogenic differentiation has been observed in numerous cell systems (Zhang et al., 2016; Ahmed et al., 2019; Weng et al., 2019).

However, the underlying molecular mechanisms accounting for the role of AOX1 in regulating osteogenic differentiation in hBMSCs need further research. Moreover, these results also suggest that our method has the ability in discriminating genes with osteogenic differentiation properties and can facilitate the process of discovery of new osteogenic differentiation-related genes.

Although more research is necessary to confirm the detailed mechanism during osteogenic differentiation, the present findings indicate that the gene AOX1 plays an important role in the osteogenic differentiation of stem cells and are thus worthy of further exploration. Furthermore, we developed a novel way for the prediction of osteogenic differentiation-relevant genes, and can thus provide potential biomarkers and targets for osteogenic differentiation of stem cells.

METHOD

Data Collection

Gene expression profiles of hBMSCs and osteogenically induced samples are collected from gene expression omnibus (GEO). Four datasets GSE12266, GSE18043, GSE37558, and GSE80614 are downloaded to identify osteogenic differentiation–related genes. GSE12266 contains four hBMSCs and 12 osteogenically induced samples. GSE18043 contains three hBMSCs and nine osteogenically induced samples (Granchi et al., 2010). GSE37558 contains four hBMSCs and 12 osteogenically induced samples (Alves et al., 2014). GSE80614 contains three hBMSCs and 30 osteogenically induced samples. For probes that did not match any gene, we removed them from the expression profiling matrix. For genes that match multiple probes, we averaged the signal intensity of these probes as the expression of the matched gene. To eliminate the platform-based bias and create an integrated dataset, we combined these four datasets using the combat algorithm, which is implemented using the sva R package. In total, 14 controls and 63 osteogenically induced samples are included in our analysis.

MSigDb is an integrated database of annotated gene sets from different sources. Osteoblast-related pathways are retrieved from this database. To identify gene sets that are associated with osteoblast, we search for related gene sets from all of these annotated names using the keyword osteoblast. As a result, 15 gene sets whose name contains osteoblast are identified as osteoblast-related pathways. Among these pathways, one is associated with the osteoblast transcription factor, nine are associated with osteogenic differentiation, one is associated with osteoblast development, three are associated with osteoblast proliferation, and one is associated with osteoblast signaling.

Single-Sample Gene Set Enrichment Analysis

Single-sample gene set enrichment analysis (ssGSEA) is used to evaluate the activity of a specific pathway in an individual sample. It calculates an enrichment score of a pathway based on the relative expression of these genes involved in the pathway. In this study, we calculated the enrichment score of these 15 osteoblast-related pathways for all samples. The ssGSEA is conducted using gsva R package (Hänzelmann et al., 2013).

Differential Expression Analysis

Combined expression profiling dataset is used to identify differentially expressed genes between hBMSCs and osteogenically induced samples. limma R package is then

TABLE 1 | Sequences of primers for real-time quantitative PCR analysis.

Gene	Primer sequence, 5–3′	
	Forward	Reverse
AOX1	CGTGTTGGTGGAGCGTTTG	ATCGTTCATGAATCCAGCTTTGT
18S	CGCCGCTAGAGGTGAAATTC	TTGGCAAATGCTTTCGCTC
OCN	CACTCCTCGCCCTATTGGC	CCCTCCTGCTTGGACA CAAAG
RUNX2	ACTTCCTGTGCTCGGTGCT	GACGGTTATGGTCAAGGTGAA
OPN	CTCCATTGACTCGAACGACTC	CAGGTCTGCGAAACTTCT TAGAT
SP7	AGCCCATTAGTGCTTGTAAAGG	CCTCTGCGGGACTCAACAAC

applied to identify these genes differentially expressed between the control and osteogenic induction groups based on BH-adjusted *p*-value and fold change. A gene is identified as upregulated if BH-adjusted *p*-value <0.05 and log-transformed fold change >1, and downregulated if BH-adjusted *p*-value <0.05 and log-transformed fold change <−0.8. The reason why we use −0.8 as the threshold for the identification of downregulated genes is that the threshold −1 will lead to a limited number of downregulated genes. As a result, 25 genes are identified as upregulated and 17 genes are identified as downregulated.

Construction of the Co-Expressed Network

The Pearson correlation coefficient is used to evaluate the co-expression pattern for these differentially expressed genes. Upregulated genes and downregulated genes are analyzed separately to identify hub genes in the co-expressed network. The correlation matrix is first calculated for upregulated genes. Due to the uncertainty of the threshold to construct a co-expressed network, we construct multiple networks based on the varied correlation threshold from 0.6 to 0.9. After analyzing the hub genes of each co-expressed network, we can create a final set of hub genes based on the frequency of hub identified in a single network. We note that the hub genes identified based on this method are reliable and can indeed capture the topological structure of multiple networks compared with a single network. This method is then applied in downregulated genes to identify hub genes that are associated with the osteogenic process.

Functional Enrichment Analysis

GO enrichment analysis is used to identify pathways that are associated with AOX1. We first divided samples into high AOX1 expression group and low expression group based on the median expression of AOX1. Differentially expressed genes are then identified between these two groups. The GO enrichment analysis is used to identify pathways that are presented by these differentially expressed genes. BH-adjusted *p*-value <0.05 is considered to be statistically significant. The GO enrichment analysis is conducted using the clusterProfiler R package (Yu et al., 2012).

Gene Set Enrichment Analysis Between Different AOX1 Groups

Gene set enrichment analysis is used to identify pathways that are associated with the AOX1 group. Differential expression analysis between AOX1 groups has been performed earlier. All genes are ranked based on the fold change between AOX1 groups. The ranked gene list and osteoblast-related pathways are then inputted into the gene set enrichment analysis to identify whether osteoblast-related pathways are enriched in the top or the bottom of the ranked gene list. This analysis is conducted using the clusterProfiler R package.

Cell Culture, Reagents, and Antibodies

hBMSCs were provided by Cyagen Biosciences (Guangzhou, China), which can differentiate into osteoblasts, adipocytes, and chondrocytes under specific inductive conditions. Adherent hBMSCs were incubated in culture flasks in the hBMSC special growth medium (Cyagen Biosciences, Inc., Guangzhou, China) in a cell incubator contained at 37 °C with 5% CO_2 and were passaged at nearly 80–90% confluence. Cells from passages 2–6 were used in subsequent experiments. Specific antibodies against glyceraldehyde-3-phosphate dehydrogenase (GAPDH) and AOX1 were purchased from Proteintech Group. Inc. (Chicago, United States).

Osteogenic Differentiation Protocol

hBMSCs were cultured in the special growth medium (Cyagen Biosciences, Guangzhou, China) and 100 IU/ml penicillin/streptomycin) in six- or twelve-well cell culture plates at a density of $3 \times 10^4/cm^2$ and incubated for 48 h at 37 °C under 5% CO_2. Subsequently, the cells were cultured in osteogenic induction medium (L-DMEM with 10% FBS, 100 IU/ml penicillin/streptomycin, 100 nM dexamethasone, 0.2 mM ascorbic acid, and 10 mM β-glycerophosphate). The cells were maintained by the replacement of fresh osteogenic induction medium every 2–3 days.

Plasmid Transfection

AOX1 plasmid transfection and negative control plasmid were used for overexpression experiments (Genomeditech). hBMSCs were prepared at 50–60% confluence in six-well plates. The transfection mixture was prepared by adding 200 μL Opti-MEM containing 4 μL TransMate reagent (GenePharma) to 200 μL Opti-MEM containing 0.66ug AOX1 plasmid and incubating for 10 min at room temperature. The transfection mixture was added in six-well plates containing 800ul α-MEM with FBS. After transfection for 4 h, the medium was changed to the growth medium.

RNA Extraction and Quantitative RT-PCR

Levels of the osteoblast formation gene expression were measured using quantitative RT-PCR (qRT-PCR). hBMSCs (3×104 cells/cm2) were cultured in six-well plates with the medium. Total cellular RNA was isolated and measured using the RNAiso reagent (Takara Bio, Kusatsu, Japan) and NanoDrop 2000. The absorbance of the samples at 260 nm was calculated in accordance with the manufacturer's instructions (Thermo Fisher Scientific, MA, United States). Total RNA was reverse-transcribed into complementary DNA (cDNA) in a 20 μL reaction volume (Takara). A total of 2 μL cDNA was used as the template with Power SYBR® Green PCR Master Mix (Takara), and qRT-PCR was performed in triplicate by the ABI 7500 system (Thermo Fisher Scientific); 18S was used as housekeeping genes and each reaction was repeated three times independently. GenePharma synthesized the primer AOX1 and Sangon Biotech (Shanghai, China) synthesized the other primers used in this experiment. Primer sequences are listed in **Table 1**. The qRT-PCR reaction was at 95°C for 30 s, followed by 45 cycles at 95°C for 5 s, and 60°C for 30 s. The expression levels of all of the genes were evaluated by the $2^{-\triangle\triangle Ct}$ method.

Western Blotting Analysis

Cells were lysed for 30 min on ice in a RIPA buffer containing phosphatase and protease inhibitor cocktails (Beyotime, Shanghai, China). The centrifugation to clear the lysates and collect the supernatants was set at 14,000 rpm for 10 min at 4°C. Equal amounts of proteins were separated by 10% sodium dodecyl sulfate polyacrylamide gel electrophoresis and then transferred to a polyvinylidene fluoride membrane (Millipore, Shanghai, China) which was then probed with the primary antibodies. The membranes were then blocked for 1 h at room temperature in Tris-buffered saline containing 10% non-fat milk and 0.1% Tween. Subsequently, the membranes were incubated with primary antibodies overnight at 4°C. After washing with 0.1% Tween in Tris-buffered saline for three times and incubation with horseradish peroxidase–conjugated secondary antibodies (anti-rabbit; Beyotime) for 1 h at room temperature, proteins were visualized by an enhanced chemiluminescent detection reagent (MilliporeSigma) and an XRS chemiluminescence detection system (Bio-Rad Laboratories, Hercules, CA, United States).

Statistical Analysis

Statistical analysis was performed using GraphPad Prism v.7.0 (GraphPad Software, San Diego, CA, United States). All experiments were performed at least in triplicate. Data are presented as the mean ± SD. Statistical significance was determined using a two-tailed Student's *t* test when comparing two groups, and one-way ANOVA followed by Tukey's *post hoc* test was used when comparing more than two groups. A value of $p- \leq 0.05$ was considered to indicate statistical significance.

DATA AVAILABILITY STATEMENT

The datasets presented in this study can be found in online repositories. The names of the repository/repositories and accession number(s) can be found in the article/ Supplementary Material.

AUTHOR CONTRIBUTIONS

Conception: LS and LL interpretation or analysis of data: JM and JC preparation of the manuscript: LS and LL, JM experiment: LL and LS revision for important intellectual content: ZP, LL and LS supervision: LL and ZP.

FUNDING

The National Natural Science Foundation of China (Grant No. 81672147 and 81874007), Zhejiang Provincial Natural Science Foundation (Y21H070011) and Medical Health Science and Technology Project of Zhejiang Provincial Health Commission (Grant No.2021KY939) funds were received in support of this work. The authors declare no relevant financial activities outside the submitted work.

ACKNOWLEDGMENTS

We thank all clients from the Clinical Research Center of the Second Affiliated Hospital, Zhejiang University. We also appreciate the general help of Lingl Zhang and Sm Feng from the Orthopedic Research Center of the Second Affiliated Hospital, Zhejiang University.

REFERENCES

Ahmed, M. F., El-Sayed, A. K., Chen, H., Zhao, R., Yusuf, M. S., Zuo, Q., et al. (2019). Comparison between Curcumin and All-Trans Retinoic Acid in the Osteogenic Differentiation of Mouse Bone Marrow Mesenchymal Stem Cells. *Exp. Ther. Med.* 17, 4154–4166. doi:10.3892/etm.2019.7414

Alves, R. D., Eijken, M., van de Peppel, J., and van Leeuwen, J. P. (2014). Calcifying Vascular Smooth Muscle Cells and Osteoblasts: Independent Cell Types Exhibiting Extracellular Matrix and Biomineralization-Related Mimicries. *BMC Genomics* 15, 965. doi:10.1186/1471-2164-15-965

Ambrogini, E., Almeida, M., Martin-Millan, M., Paik, J.-H., Depinho, R. A., Han, L., et al. (2010). FoxO-mediated Defense against Oxidative Stress in Osteoblasts Is Indispensable for Skeletal Homeostasis in Mice. *Cel Metab.* 11, 136–146. doi:10.1016/j.cmet.2009.12.009

Anaya, J. M., Bollag, W. B., Hamrick, M. W., and Isales, C. M. (2020). The Role of Tryptophan Metabolites in Musculoskeletal Stem Cell Aging. *Int. J. Mol. Sci.* 21, 6670. doi:10.3390/ijms21186670

Armoni, M., Harel, C., Karni, S., Chen, H., Bar-Yoseph, F., Ver, M. R., et al. (2006). FOXO1 Represses Peroxisome Proliferator-Activated Receptor-Γ1 and -γ2 Gene Promoters in Primary Adipocytes: A Novel Paradigm To Increase Insulin Sensitivity. *J. Biol. Chem.* 281, 19881–19891. doi:10.1074/jbc.m600320200

Bianco, P., Riminucci, M., Gronthos, S., and Robey, P. G. (2001). Bone Marrow Stromal Stem Cells: Nature, Biology, and Potential Applications. *Stem Cells* 19, 180–192. doi:10.1634/stemcells.19-3-180

Coelho, C., Foti, A., Hartmann, T., Santos-Silva, T., Leimkühler, S., and Romão, M. J. (2015). Structural Insights into Xenobiotic and Inhibitor Binding to Human Aldehyde Oxidase. *Nat. Chem. Biol.* 11, 779–783. doi:10.1038/nchembio.1895

Fan, T., Qu, R., Yu, Q., Sun, B., Jiang, X., Yang, Y., et al. (2020). Bioinformatics Analysis of the Biological Changes Involved in the Osteogenic Differentiation of Human Mesenchymal Stem Cells. *J. Cel Mol Med* 24, 7968–7978. doi:10.1111/jcmm.15429

Garattini, E., Fratelli, M., and Terao, M. (2008). Mammalian Aldehyde Oxidases: Genetics, Evolution and Biochemistry. *Cell. Mol. Life Sci.* 65, 1019–1048. doi:10.1007/s00018-007-7398-y

Garattini, E., Fratelli, M., and Terao, M. (2009). The Mammalian Aldehyde Oxidase Gene Family. *Hum. Genomics* 4, 119–130. doi:10.1186/1479-7364-4-2-119

Garattini, E., and Terao, M. (2011). Increasing Recognition of the Importance of Aldehyde Oxidase in Drug Development and Discovery. *Drug Metab. Rev.* 43, 374–386. doi:10.3109/03602532.2011.560606

Garattini, E., and Terao, M. (2012). The Role of Aldehyde Oxidase in Drug Metabolism. *Expert Opin. Drug Metab. Toxicol.* 8, 487–503. doi:10.1517/17425255.2012.663352

Gardin, C., Bosco, G., Ferroni, L., Quartesan, S., Rizzato, A., Tatullo, M., et al. (2020). Hyperbaric Oxygen Therapy Improves the Osteogenic and Vasculogenic Properties of Mesenchymal Stem Cells in the Presence of Inflammation *In Vitro*. *Int. J. Mol. Sci.* 21, 1452. doi:10.3390/ijms21041452

Gough, D. R., and Cotter, T. G. (2011). Hydrogen Peroxide: a Jekyll and Hyde Signalling Molecule. *Cell Death Dis* 2, e213. doi:10.1038/cddis.2011.96

Granchi, D., Ochoa, G., Leonardi, E., Devescovi, V., Baglìo, S. R., Osaba, L., et al. (2010). Gene Expression Patterns Related to Osteogenic Differentiation of Bone Marrow-Derived Mesenchymal Stem Cells DuringEx VivoExpansion. *Tissue Eng. C: Methods* 16, 511–524. doi:10.1089/ten.tec.2009.0405

Guzik, T. J., and Harrison, D. G. (2006). Vascular NADPH Oxidases as Drug Targets for Novel Antioxidant Strategies. *Drug Discov. Today* 11, 524–533. doi:10.1016/j.drudis.2006.04.003

Hänzelmann, S., Castelo, R., and Guinney, J. (2013). GSVA: Gene Set Variation Analysis for Microarray and RNA-Seq Data. *BMC Bioinformatics* 14, 7. doi:10.1186/1471-2105-14-7

Jiang, Y., Zhang, P., Zhang, X., Lv, L., and Zhou, Y. (2021). Advances in Mesenchymal Stem Cell Transplantation for the Treatment of Osteoporosis. *Cell Prolif* 54, e12956. doi:10.1111/cpr.12956

Khalid, S., Yamazaki, H., Socorro, M., Monier, D., Beniash, E., and Napierala, D. (2020). Reactive Oxygen Species (ROS) Generation as an Underlying Mechanism of Inorganic Phosphate (Pi)-Induced Mineralization of Osteogenic Cells. *Free Radic. Biol. Med.* 153, 103–111. doi:10.1016/j.freeradbiomed.2020.04.008

Kundu, T. K., Hille, R., Velayutham, M., and Zweier, J. L. (2007). Characterization of Superoxide Production from Aldehyde Oxidase: an Important Source of Oxidants in Biological Tissues. *Arch. Biochem. Biophys.* 460, 113–121. doi:10.1016/j.abb.2006.12.032

Li, Q., Gao, Z., Chen, Y., and Guan, M.-X. (2017). The Role of Mitochondria in Osteogenic, Adipogenic and Chondrogenic Differentiation of Mesenchymal Stem Cells. *Protein Cell* 8, 439–445. doi:10.1007/s13238-017-0385-7

Li, X., Li, B., Shi, Y., Wang, C., and Ye, L. (2021). Targeting Reactive Oxygen Species in Stem Cells for Bone Therapy. *Drug Discov. Today* 26, 1226–1244. doi:10.1016/j.drudis.2021.03.002

Liao, J., Tian, T., Shi, S., Xie, X., Ma, Q., Li, G., et al. (2017). The Fabrication of Biomimetic Biphasic CAN-PAC Hydrogel with a Seamless Interfacial Layer Applied in Osteochondral Defect Repair. *Bone Res.* 5, 17018. doi:10.1038/boneres.2017.18

Mandal, C. C., Ganapathy, S., Gorin, Y., Mahadev, K., Block, K., Abboud, H. E., et al. (2011). Reactive Oxygen Species Derived from Nox4 Mediate BMP2 Gene Transcription and Osteoblast Differentiation. *Biochem. J.* 433, 393–402. doi:10.1042/bj20100357

Marongiu, G., Dolci, A., Verona, M., and Capone, A. (2020). The Biology and Treatment of Acute Long-Bones Diaphyseal Fractures: Overview of the Current Options for Bone Healing Enhancement. *Bone Rep.* 12, 100249. doi:10.1016/j.bonr.2020.100249

Pryde, D. C., Dalvie, D., Hu, Q., Jones, P., Obach, R. S., and Tran, T.-D. (2010). Aldehyde Oxidase: an Enzyme of Emerging Importance in Drug Discovery. *J. Med. Chem.* 53, 8441–8460. doi:10.1021/jm100888d

Ritchie, M. E., Phipson, B., Wu, D., Hu, Y., Law, C. W., Shi, W., et al. (2015). Limma powers Differential Expression Analyses for RNA-Sequencing and Microarray Studies. *Nucleic Acids Res.* 43, e47. doi:10.1093/nar/gkv007

Rossi, M. C., Bezerra, F. J. B., Silva, R. A., Crulhas, B. P., Fernandes, C. J. C., Nascimento, A. S., et al. (2017). Titanium-released from Dental Implant Enhances Pre-osteoblast Adhesion by ROS Modulating Crucial Intracellular Pathways. *J. Biomed. Mater. Res.* 105, 2968–2976. doi:10.1002/jbm.a.36150

Siqueira, M. F., Flowers, S., Bhattacharya, R., Faibish, D., Behl, Y., Kotton, D. N., et al. (2011). FOXO1 Modulates Osteoblast Differentiation. *Bone* 48, 1043–1051. doi:10.1016/j.bone.2011.01.019

Subramanian, A., Tamayo, P., Mootha, V. K., Mukherjee, S., Ebert, B. L., Gillette, M. A., et al. (2005). Gene Set Enrichment Analysis: a Knowledge-Based Approach for Interpreting Genome-wide Expression Profiles. *Proc. Natl. Acad. Sci.* 102, 15545–15550. doi:10.1073/pnas.0506580102

Szklarczyk, D., Gable, A. L., Lyon, D., Junge, A., Wyder, S., Huerta-Cepas, J., et al. (2019). STRING V11: Protein-Protein Association Networks with Increased Coverage, Supporting Functional Discovery in Genome-wide Experimental Datasets. *Nucleic Acids Res.* 47, D607–D613. doi:10.1093/nar/gky1131

Tao, H., Ge, G., Liang, X., Zhang, W., Sun, H., Li, M., et al. (2020). ROS Signaling Cascades: Dual Regulations for Osteoclast and Osteoblast. *Acta Biochim. Biophys. Sin (Shanghai)* 52, 1055–1062. doi:10.1093/abbs/gmaa098

Terao, M., Kurosaki, M., Barzago, M. M., Varasano, E., Boldetti, A., Bastone, A., et al. (2006). Avian and Canine Aldehyde Oxidases. *J. Biol. Chem.* 281, 19748–19761. doi:10.1074/jbc.m600850200

Vantaku, V., Putluri, V., Bader, D. A., Maity, S., Ma, J., Arnold, J. M., et al. (2020). Epigenetic Loss of AOX1 Expression via EZH2 Leads to Metabolic Deregulations and Promotes Bladder Cancer Progression. *Oncogene* 39, 6265–6285. doi:10.1038/s41388-019-0902-7

Weng, Z., Wang, C., Zhang, C., Xu, J., Chai, Y., Jia, Y., et al. (2019). All-Trans Retinoic Acid Promotes Osteogenic Differentiation and Bone Consolidation in a Rat Distraction Osteogenesis Model. *Calcif Tissue Int.* 104, 320–330. doi:10.1007/s00223-018-0501-6

Xiao, B., Wang, G., and Li, W. (2020). Weighted Gene Correlation Network Analysis Reveals Novel Biomarkers Associated with Mesenchymal Stromal Cell Differentiation in Early Phase. *PeerJ* 8, e8907. doi:10.7717/peerj.8907

Xiong, Y., Cao, F., Chen, L., Yan, C., Zhou, W., Chen, Y., et al. (2020). Identification of Key microRNAs and Target Genes for the Diagnosis of Bone Nonunion. *Mol. Med. Rep.* 21, 1921–1933. doi:10.3892/mmr.2020.10996

Yu, G., Wang, L.-G., Han, Y., and He, Q.-Y. (2012). clusterProfiler: an R Package for Comparing Biological Themes Among Gene Clusters. *OMICS: A J. Integr. Biol.* 16, 284–287. doi:10.1089/omi.2011.0118

Zhang, S., Chen, X., Hu, Y., Wu, J., Cao, Q., Chen, S., et al. (2016). All-trans Retinoic Acid Modulates Wnt3A-Induced Osteogenic Differentiation of Mesenchymal Stem Cells via Activating the PI3K/AKT/GSK3β Signalling Pathway. *Mol. Cell Endocrinol.* 422, 243–253. doi:10.1016/j.mce.2015.12.018

Zhang, W., Chen, E., Chen, M., Ye, C., Qi, Y., Ding, Q., et al. (2018). IGFBP7 Regulates the Osteogenic Differentiation of Bone Marrow-derived Mesenchymal Stem cellsviaWnt/β-catenin Signaling Pathway. *FASEB j.* 32, 2280–2291. doi:10.1096/fj.201700998rr

Zhong, G., Seaman, C. J., Paragas, E. M., Xi, H., Herpoldt, K.-L., King, N. P., et al. (2021). Aldehyde Oxidase Contributes to All-Trans-Retinoic Acid Biosynthesis in Human Liver. *Drug Metab. Dispos* 49, 202–211. doi:10.1124/dmd.120.000296

Zhu, X.-W., Ding, K., Dai, X.-Y., and Ling, W.-Q. (2018). β-Aminoisobutyric Acid Accelerates the Proliferation and Differentiation of MC3T3-E1 Cells via Moderate Activation of ROS Signaling. *J. Chin. Med. Assoc.* 81, 611–618. doi:10.1016/j.jcma.2017.12.005

Conflict of Interest: The authors declare that the research was conducted in the absence of any commercial or financial relationships that could be construed as a potential conflict of interest.

Publisher's Note: All claims expressed in this article are solely those of the authors and do not necessarily represent those of their affiliated organizations, or those of the publisher, the editors, and the reviewers. Any product that may be evaluated in this article, or claim that may be made by its manufacturer, is not guaranteed or endorsed by the publisher.

frontiers | Frontiers in Molecular Biosciences

ORIGINAL RESEARCH
published: 28 April 2022
doi: 10.3389/fmolb.2022.767536

Lateral Mesoderm-Derived Mesenchymal Stem Cells With Robust Osteochondrogenic Potential and Hematopoiesis-Supporting Ability

Yili Wei[1†], Bin Wang[1†], Lei Jia[2†], Weijun Huang[1], Andy Peng Xiang[1,3], Cong Fang[2], Xiaoyan Liang[2] and Weiqiang Li[1,3]**

[1]Center for Stem Cell Biology and Tissue Engineering, Key Laboratory for Stem Cells and Tissue Engineering, Ministry of Education, Zhongshan School of Medicine, Sun Yat-Sen University, Guangzhou, China, [2]Reproductive Medicine Research Center, Sixth Affiliated Hospital of Sun Yat-Sen University, Guangzhou, China, [3]Department of Biochemistry, Zhongshan Medical School, Sun Yat-Sen University, Guangzhou, China

Mesenchymal stem cells (MSCs) are among the most promising cell sources for the treatment of various diseases. Nonetheless, the therapeutic efficacy in clinical trials has been inconsistent due to the heterogeneity of MSCs, which may be partially attributed to their undefined developmental origins. The lateral mesoderm is also a developmental source of MSCs that constitute appendicular skeletal elements in the developing vertebrate embryo. However, it is difficult to isolate homogeneous lateral mesoderm (LM)-derived MSCs from bone tissues or bone marrow due to the lack of understanding of their characteristics. Herein, we successfully established an efficient differentiation protocol for the derivation of MSCs with a LM origin from human pluripotent stem cells (hPSCs) under specific conditions. LM-MSCs resembled bone marrow-derived MSCs (BMSCs) with regard to cell surface markers, global gene profiles, and immunoregulatory activity and showed a homeodomain transcription factor (HOX) gene expression pattern typical of skeletal MSCs in long bones. Moreover, we demonstrated that LM-MSCs had an increased osteogenic/chondrogenic differentiation capacity and hematopoietic support potential compared to BMSCs. These homogeneous LM-MSCs may serve as a powerful tool for elucidating their precise role in bone formation and hematopoiesis and could be a potentially ideal cell source for therapeutic applications.

Keywords: lateral mesoderm, mesenchymal stem cells, human pluripotent stem cells, differentiation, Hox genes

OPEN ACCESS

Edited by:
Ce Dou,
Army Medical University, China

Reviewed by:
Ritu Chakravarti,
University of Toledo, United States
Hongyuan Zhang,
Amgen, United States
Lijun Li,
Zhejiang University, China
Peng Xue,
Third Hospital of Hebei Medical University, China
Jian Jun Li,
China Medical University, China

****Correspondence:***
Xiaoyan Liang
liangxy2@mail.sysu.edu.cn
Weiqiang Li
liweiq6@mail.sysu.edu.cn

[†]These authors have contributed equally to this work and share first authorship

Specialty section:
This article was submitted to Cellular Biochemistry, a section of the journal Frontiers in Molecular Biosciences

Received: *31 August 2021*
Accepted: *14 March 2022*
Published: *28 April 2022*

Citation:
Wei Y, Wang B, Jia L, Huang W, Xiang AP, Fang C, Liang X and Li W (2022) Lateral Mesoderm-Derived Mesenchymal Stem Cells With Robust Osteochondrogenic Potential and Hematopoiesis-Supporting Ability. Front. Mol. Biosci. 9:767536. doi: 10.3389/fmolb.2022.767536

Abbreviations: MSCs: mesenchymal stem cells; hPSCs: human pluripotent stem cells; hESCs: human embryonic stem cells; hiPSCs: human induced pluripotent stem cells; BMSCs: bone marrow mesenchymal stem cells; HOX: homeodomain transcription factor; LM: lateral mesoderm; NEAA: nonessential amino acids; ITS: insulin-transferrin-selenium; L-GLU: l-glutamic acid; BMP-7: bone morphogenetic protein-7; qRT-PCR: quantitative reverse transcription-polymerase chain reaction; LM-MSCs: LM-derived MSCs; FCM: flow cytometry; CCK8: Cell Counting Kit-8; HA/TCP: hydroxyl-apatite/tricalcium phosphate ceramic powder; EDTA: ethylenediaminetetraacetic acid; H&E: hematoxylin and eosin; PBMCs: peripheral blood mononuclear cells; CFSE: carboxyfluorescein succinimidyl ester; DAPI: 4′,6-diamino-2-phenylindole; RNA-Seq: RNA sequencing; PCA: principal component analysis; TBXT: brachyury; CHIR: CHIR99021; TGF-β1: transforming growth factor-β1; PM: paraxial mesoderm; IM: intermediate mesoderm; TIMP: tissue inhibitors of metalloproteinases; TNF-α: tumor necrosis factor α; IFN-γ: interferon γ.

INTRODUCTION

Mesenchymal stem cells (MSCs) are present in various organs and tissues, including bone marrow, adipose tissue, and the umbilical cord (Jiang et al., 2019). Due to their multilineage differentiation, immunomodulatory profiles, and hematopoietic support capabilities, MSCs have become one of the most promising sources in cell replacement therapy for the treatment of different diseases (Kassem et al., 2004; Augello and De Bari, 2010). According to ClinicalTrials.gov, the number of MSC-related clinical trials has expanded consistently since 2006, and more than 1300 MSC clinical trials have been registered to date for evaluating the treatment of neurological, joint, and graft-versus-host diseases. However, the translation of MSCs to the clinic is still progressing slowly (Herman et al., 1988; Kabat et al., 2020). The major clinical challenges with MSC therapies include the inconsistent therapeutic efficacy caused by the functional heterogeneity of MSCs (Costa et al., 2021; Mabuchi et al., 2021), which may be due to variations in donors, tissue types, and even the isolation protocols and the number of passages of MSCs (Kern et al., 2006; Chen et al., 2015; Yin et al., 2019; Costa et al., 2021).

MSCs also have multiple developmental origins, including the neural crest (neural ectoderm), mesoderm, and trophoblast. For example, craniofacial bones are generated by neural crest-derived MSCs, but the axial and appendicular bones are derived from paraxial and lateral mesoderm (LM)-derived MSCs, respectively (Olsen et al., 2000; Isern et al., 2014). Furthermore, maxilla-derived MSCs are negative for homeodomain transcription factor (HOX) gene expression, while ilium-derived MSCs highly express HOX genes and exhibit superior differentiation to chondrocytes compared with maxilla- and mandible-derived MSCs (Matsubara et al., 2005; Onizuka et al., 2020), further suggesting that MSCs of different origins possess variable functions. The above evidence indicates that the functional heterogeneity of MSCs may be partially due to their undefined developmental origins.

The LM forms the progenitor cells that constitute the heart and cardiovascular system, blood, and appendicular skeletal elements (bone and cartilage) in the developing vertebrate embryo (Prummel et al., 2020). Previous studies have shown that LM-derived MSCs (LM-MSCs) exist in the bone marrow of long bones (Isern et al., 2014). However, the lack of understanding of their characteristics (e.g., specific surface markers) makes it critically challenging to discriminate and isolate MSCs of LM origin directly from human tissues. In recent years, human pluripotent stem cells (hPSCs), including human embryonic stem cells (hESCs) and human induced pluripotent stem cells (hiPSCs), have shown promise for regenerative medicine. hPSCs can indefinitely proliferate and differentiate into almost all cell types of the three germ layers *in vitro*, including nerve cells, skeletal muscle, kidney cells, cardiomyocytes, and hepatocytes (Loh et al., 2016). More recently, studies have demonstrated that MSCs can be obtained from hPSCs through different intermediate stages, including the neural crest, neuromesoderm, mesoderm, and trophoblast (Wang et al., 2016; Chijimatsu et al., 2017; Slukvin and Kumar, 2018; Wang et al., 2019). Accordingly, we assumed that it would be possible to generate homogeneous MSCs through the intermediate stage of LM from hPSCs, which would be valuable in elucidating their distinct biological characteristics and may help to minimize the heterogeneity and variability of treatment effects in the clinical translation of MSCs.

Herein, we successfully established an efficient differentiation protocol for the derivation of MSCs with LM origin from hPSCs. LM-MSCs derived from hPSCs expressed traditional MSC surface markers and HOX genes typical of skeletal MSCs in long bones. LM-MSCs also shared similar immunoregulatory activity as bone marrow-derived MSCs (BMSCs). Moreover, we found that LM-MSCs showed an increased capacity for osteogenic and chondrogenic differentiation and hematopoietic support potential compared to BMSCs.

MATERIALS AND METHODS

Cell Culture

We used the hESC lines H1 and H9 (Thomson et al., 1998) and the hiPSC lines HEF-hiPSCs and HDF-hiPSCs, which were established in our laboratory (Li et al., 2018), for MSC differentiation. Undifferentiated hPSCs were cultured on Matrigel (BD Biosciences, San Diego, CA, United States)-coated plates in mTeSR1 medium (StemCell Technologies, Vancouver, Canada). The medium was changed daily, and the cells were passaged every 3–4 days using ReLeSR™ (StemCell Technologies). Human BMSCs were used as a control (Chen et al., 2019). BMSCs were maintained in StemFit medium, a chemically defined medium (Ajinomoto, Tokyo, Japan), and passaged using StemPro Accutase Cell Dissociation Reagent (Life Technologies, Carlsbad, CA, United States) when the cell confluence reached 80–90%.

Differentiation of Human Pluripotent Stem Cells Into Lateral Mesoderm-Mesenchymal Stem Cells

For induction of differentiation, confluent hPSCs were digested into single cells by incubation in Accutase at 37°C for 2–3 min. These cells were seeded onto Matrigel-coated plates at a density of $1–2\times10^4$ cells/cm^2 and cultured in mTeSR medium containing 10 μM Y27632 (ROCK inhibitor; Sigma-Aldrich, St. Louis, MO, United States) for 24 h. Next, the cells were incubated in Stage 1 medium, which consisted of DMEM/F12, 1% (v/v) penicillin/streptomycin, 1% (v/v) nonessential amino acids (NEAAs), 1% (v/v) insulin-transferrin-selenium (ITS), 1% (v/v) L-glutamic acid (L-GLU) (all from Gibco, Grand Island, NY, United States), and 3 μM CHIR99021 (Sigma-Aldrich), for an additional 48 h to differentiate into primitive streak (PS) cells. PS cells were differentiated into LM by Stage 2 medium with DMEM/F12, 1% (v/v) penicillin/streptomycin, 1% (v/v) NEAA, 1% (v/v) ITS, 1% (v/v) L-GLU, 3 μM CHIR99021, and 100 ng/ml bone morphogenetic protein-7 (BMP-7) (Peprotech, Rocky Hill, New Jersey, United States) for another 6 days. For Stage 3 MSC differentiation, LM cells were cultured in StemFit MSC medium (Ajinomoto, Tokyo, Japan) for 3–4 weeks. Accutase was

used for cell passaging when differentiated cells reached subconfluence. Gene expression levels of markers typical of pluripotency, primitive streak, ectoderm, mesoderm, or endoderm were analyzed by quantitative real-time PCR (qRT-PCR) and immunostaining during each stage of differentiation. The phenotype and multipotency of LM-derived MSCs (LM-MSCs) were assessed by flow cytometry (FCM) analysis and multilineage (osteogenic, adipogenic, and chondrogenic) differentiation assays, respectively.

Flow Cytometry Analysis

FCM was used to detect the protein expression of the intranuclear transcription factors HAND1 and FOXF1 in LM cells, surface antigens (including CD29, CD44, CD73, CD90, CD105, CD166, CD45, CD34, CD11b, CD19, and HLADR) in LM-MSCs, and CD34 in *vitro* expanded hematopoietic stem cells (all from BD Biosciences, Palo Alto, CA, United States) (**Supplementary Table S1**). An irrelevant isotype-identical antibody (BD Biosciences) was used as a negative control. The cells were digested by Accutase, filtered, and incubated with a special human monoclonal antibody. FCM was performed using a Beckman Coulter flow cytometer, and the data were analyzed with FlowJo software (BD Biosciences) or CytExpert (Beckman Coulter GmbH, Krefeld, Germany).

Multilineage Differentiation of Lateral Mesoderm-Mesenchymal Stem Cells

For osteogenic differentiation, LM-MSCs were seeded at 100,000 cells/well in 6-well plates and cultured with osteogenic medium containing 0.1 mM dexamethasone, 50 mM ascorbate-2-phosphate, 10 mM b-glycerophosphate (all from Sigma-Aldrich), and 1% (v/v) penicillin/streptomycin (Gibco) for 21 days. The medium was replaced every 3 days. After 21 days, the osteogenic differentiation ability of LM-MSCs was evaluated by qRT-PCR for osteoblast-specific genes and Alizarin Red S staining to detect calcium deposits. Fifteen minutes after Alizarin Red S staining, the excess Alizarin Red solution was removed. Cells were washed 4 times with PBS and photographed with a phase-contrast microscope. Then, 10% cetylpyridinium solution was added to dissolve the color for 15 min, and the staining intensity was quantified by measuring the absorbance at 562 nm by a microplate reader (Tecan Trading AG, Switzerland).

For chondrogenic differentiation, a pellet culture system was applied. In brief, LM-MSCs were seeded at 500,000 cells/pellet in a 15 ml centrifuge tube and cultured with ACF chondrogenic medium (Stem Cell Technologies) for 21 days. Subsequently, the chondrogenic differentiation ability of LM-MSCs was evaluated by qRT-PCR analysis for chondrocyte-specific genes and Alcian blue staining to detect acid mucins. ImageJ software (National Institutes of Health) was used to analyze the diameter of cartilage micromass.

For the adipogenic differentiation assay, LM-MSCs were seeded at 100,000 cells/well in 6-well plates and cultured with adipogenic medium, which contained 0.5 mM isobutyl-methylxanthine (Sigma-Aldrich), 1 mM dexamethasone, 10 mM insulin (Sigma-Aldrich), 200 mM indomethacin (Sigma-Aldrich), and 1% (v/v) penicillin/streptomycin (Gibco), for 3 weeks. The medium was replaced every other day. The adipogenic differentiation ability of LM-MSCs was evaluated by qRT-PCR analysis for adipocyte-specific genes and oil red O staining to detect lipid droplets. After removal of the dye solution, the cells were washed three times with PBS and photographed with a phase-contrast microscope. Then, the cells were incubated with 100% isopropanol for 15 min to extract the oil red O dye from the stained lipid droplets. The OD values were measured at 510 nm by a microplate reader.

Cell Counting Kit-8 Assay

The cell proliferation of LM-MSCs was analyzed using the fluorescence-based Cell Counting Kit-8 (CCK8) Cell Proliferation Assay (Dojindo, Kumamoto, Japan). The cells were dissociated using Accutase and seeded onto a 96-well plate at 1,500 cells/well. After 24 h, 100 µl of fresh culture medium containing 10% CCK8 solution was added to each well, and the plate was incubated for 2 h. Cell proliferation was assessed by measuring absorbance at 450 nm using a microplate reader (Tecan Trading AG, Switzerland) daily until the cells reached confluence.

In vitro Immunoregulatory Activity of Lateral Mesoderm-Mesenchymal Stem Cells

For the lymphocyte proliferation assay, blood samples were collected from healthy donors after receiving informed consent. Peripheral blood mononuclear cells (PBMCs) were enriched using standardized density gradient techniques. The $CD3^+$ T lymphocytes were isolated from PBMCs by FCM and then stained with 5 µm carboxylated fluorescein succinimide (CFSE; Life Technologies) according to the manufacturer's instructions. The proliferation of labeled $CD3^+$ T cells that were cocultured with or without LM-MSCs was stimulated with anti-CD3 and anti-CD28 (both from BD Biosciences) for 96 h and evaluated by FCM analysis.

For analysis of $CD3^+$ T-cell intracellular cytokine production, $CD3^+$ T cells were cultured with or without MSCs for 72 h. Then, 10 ng/ml brefeldin A (BFA), 50 ng/ml phorbol-12-myristate-13-acetate (PMA), and 1 µg/ml ionomycin (all from Sigma-Aldrich) were added to the culture medium for the last 6 h. Next, $CD3^+$ cells were fixed, permeabilized, and incubated with antibodies against CD3, and intracellular cytokines were detected with anti-human IFN-γ-PECY7 and anti-TNF-α-PE antibodies by FCM.

For analysis of intracellular cytokine production in human THP-1-derived macrophages, THP-1 cells were seeded at 2,000,000 cells/well in 6-well plates for macrophage induction using 100 ng/ml PMA on the first day. BMSCs and LM-MSCs were preseeded onto a 24-well plate at a density of nearly 100%. On Day 2, macrophages were digested and cocultured with BMSCs or LM-MSCs at a density of 200,000 cells/well for 24 h. On Day 3, 1 ng/ml LPS and 20 ng/ml IFN-γ were added to the coculture system for another 24 h. On Day 4, the macrophages were stimulated with 10 µg/ml BFA for 6 h before FCM. Then, the cells were collected, and the expression of TNF-α in $CD45^+$ macrophages was detected by FCM.

For the pro-inflammatory cytokine stimulation assay, 20 ng/ml IFN-γ was added to the culture medium when LM-MSCs reached 60% confluence, and the cells were cultured for 24 or 48 h. Next, the cells were collected, and the mRNA transcripts of pro-inflammatory mediators (IL6, IL8, and CCL2) and anti-inflammatory mediators (IDO, PDL1, and TSG6) were analyzed by qRT-PCR.

In vitro Culture of Hematopoietic Stem Cells With Lateral Mesoderm-Mesenchymal Stem Cells

Human umbilical cord blood $CD34^+$ hematopoietic stem cells were collected from healthy donors following the Declaration of Helsinki protocols with fully ethical informed consent and enriched with FCM. BMSCs and LM-MSCs were preseeded onto a 24-well plate at a density of 90%. On the second day, BMSCs and LM-MSCs were treated with mitomycin c (0.5 mg/ml) for 3 h and washed with PBS 3 times. Then, $CD34^+$ HSCs (5,000 cells) were inoculated into each well of 24-well plates and cocultured with BMSCs or LM-MSCs in StemSpan^{Tm} $CD34^+$ Expansion medium (Stem Cell Technologies) for 9 days. The $CD34^+$ HSCs cultured alone in the same media acted as controls. After 9 days of culture, FCM was used to detect the maintenance of $CD34^+$ HSCs in different coculture conditions.

Long-Term Culture Initiating Cell Assays

BMSCs and LM-MSCs were treated with mitomycin c as described above. Then, $CD34^+$ HSCs (1,000 cells) were inoculated onto each well of 24-well plates and cocultured with BMSCs or LM-MSCs in StemSpan^{Tm} $CD34^+$ Expansion medium (Stem Cell Technologies). After culture for 35 days, 10,000 cells isolated from the supernatant of the coculture system were seeded in methylcellulose (Stem Cell Technologies) plates and incubated at 37°C in 5% CO_2. Fourteen days later, the colonies that were formed were counted and analyzed.

Tumor Formation Assay

For evaluation of the potential tumor formation risk of hPSC-derived LM-MSCs, 5×10^6 cells were premixed with 100 μl of PBS containing 30% Matrigel and injected subcutaneously into 6-week-old male NCG mice (n = 5 for each cell line; obtained from Vital River, Beijing, China). BMSCs and undifferentiated hPSCs were used as controls. Tumor occurrence was evaluated 8 weeks after cell injection. All experimental procedures involving animals were approved by the Animal Ethics Committee of Sun Yat-Sen University.

In vivo Bone Formation Assay

For evaluation of the *in vivo* bone formation capacity of LM-MSCs, we used hydroxyl-apatite/tricalcium phosphate ceramic powder (HA/TCP; Zimmer Scandinavia, Denmark) assembled with LM-MSCs and transplanted the cell-scaffold complexes subcutaneously onto the dorsal surfaces of 8-week-old male NCG mice (n = 5 for each group), as previously described (Wang et al., 2019). The subcutaneous grafts were collected 8 weeks after transplantation, decalcified in 10% ethylenediaminetetraacetic acid (EDTA) for 3 weeks and embedded in paraffin. For microstructure observation, 4-μm-thick sections of the grafts were analyzed by Masson's trichrome staining, hematoxylin and eosin (H&E) staining, and immunostaining for the detection of osteogenic-related markers and hematopoietic-related markers. All experimental procedures involving animals were approved by the Animal Ethics Committee of Sun Yat-Sen University.

Quantitative Reverse Transcription-Polymerase Chain Reaction

Total RNA was extracted using RNAzol (Molecular Research Center, Cincinnati, OH, United States) according to the manufacturer's protocol and then reverse transcribed into cDNA using a Quantitect Reverse Transcription kit (Qiagen, Valencia, CA, United States) in a 10 μl reaction system. qRT-PCR was performed using a DyNAmo ColorFlash SYBR Green qPCR kit (Thermo Fisher Scientific, Rutherford, NJ, United States) on a LightCycler 480 Detection System (Roche Diagnostics, Mannheim, Germany). The thermocycling conditions consisted of 40 cycles of denaturation at 95°C for 10 s, annealing at 60°C for 20 s, and extension at 72°C for 30 s. GAPDH was used as an internal control, and gene expression levels were calculated using the 2-ΔΔCT method. The primer sequences are presented in **Supplementary Table S2**.

Western Blot

Cells or tissues were digested, washed with cold PBS, and lysed in 1x RIPA buffer containing phenylmethanesulfonyl fluoride (PMSF) on ice to extract protein. After sonication, the proteins were separated by SDS-PAGE and electrically transferred to a polyvinylidene difluoride membrane with a pore size of 0.45 μm (Millipore, Bedford, MA, United States). Each membrane was blocked with 5% BSA solution and incubated with appropriate primary antibodies diluted with TBS/T containing 1% BSA overnight at 4°C, followed by reaction with horseradish peroxidase (HRP)-linked secondary antibodies (Cell Signaling Technology, Beverly, MA, United States) at room temperature for 1 h before chemiluminescence detection. The antibodies used in western blotting are listed in **Supplementary Table S3**.

Immunocytochemistry

For immunocytochemistry, differentiated cells were fixed with 4% paraformaldehyde for 20 min, blocked with blocking buffer (0.2% Triton X-100 with 5% human BSA) for 1 h, and incubated with primary antibody (appropriate antibody concentration with 5% human BSA) at 4°C overnight. The cells were washed three times with PBS for 5 min and then incubated at room temperature for 1 h with the secondary antibody in the dark. The nucleus was stained with 4′,6-diamino-2-phenylindole (DAPI; Sigma-Aldrich), and the results were photographed and analyzed by fluorescence microscopy. The utilized antibodies for immunocytochemistry are listed in **Supplementary Table S3**.

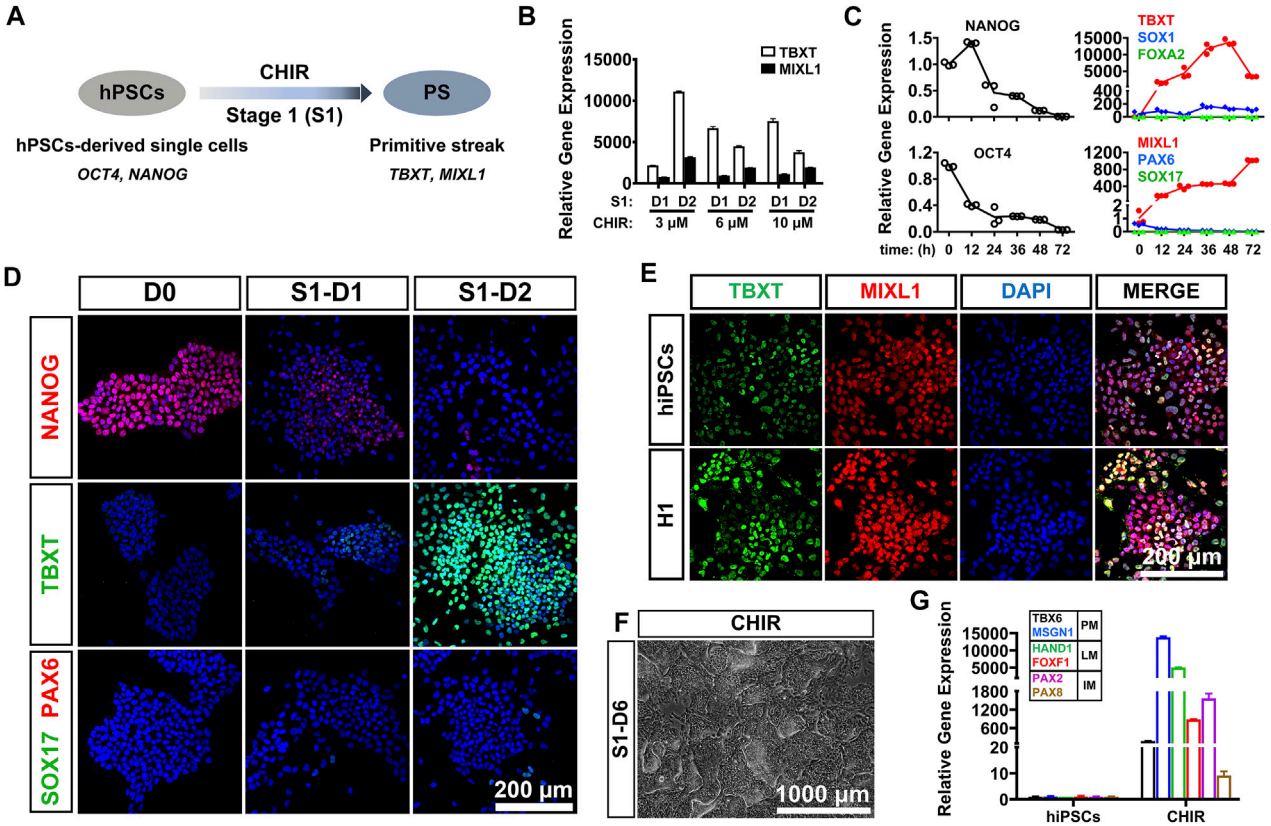

FIGURE 1 | CHIR99021 efficiently induced primitive streak differentiation from hPSCs. **(A)**. Diagram of primitive streak (TBXT; MIXL1) differentiation from hPSCs (OCT4; NANOG) using CHIR99021 (CHIR) at stage 1 (S1). **(B)**. qRT-PCR detection of the expression of primitive streak (PS) markers (TBXT and MIXL1) when hiPSCs were treated with different concentrations (3, 6, and 10 μM) of CHIR for 1 day (D1) and 2 days (D2) at stage 1. **(C)**. Time course of gene expression in the hiPSCs treated with 3 μM CHIR for 72 h at stage 1. qRT-PCR detection of the gene expression levels of markers for pluripotency (OCT4; NANOG), ectoderm (SOX1; PAX6), primitive streak (TBXT; MIXL1), and definitive endoderm (SOX17; FOXA2). **(D)**. Immunostaining assay for the markers of pluripotency (NANOG), primitive streak (TBXT), definitive endoderm (SOX17), and ectoderm (PAX6) in the hiPSCs treated with 3 μM CHIR at Day 0 (D0), Day 1 (S1-D1), and Day 2 (S1-D2). Scale bar: 200 μm. **(E)**. Immunofluorescence staining for the expression of the PS markers TBXT and MIXL1 in the hiPSCs and H1 hESCs treated with CHIR for 2 days. Scale bar: 200 μm. **(F)**. Phase-contrast image of the hiPSCs treated with CHIR for 6 days (S1-D6). Scale bar: 1,000 μm. **(G)**. qRT-PCR detection of the gene expression of markers for paraxial mesoderm (TBX6; MSGN1), lateral mesoderm (HAND1; FOXF1), and intermediate mesoderm (PAX2; PAX8) when hiPSCs were treated with basal medium (basal) or 3 μM CHIR for 6 days. Undifferentiated hiPSCs were used as a negative control.

RNA Sequencing

Samples for RNA sequencing included hiPSC-derived LM cells (LM 1, LM 2), hiPSC-derived LM-MSCs (LM-MSCs 1, LM-MSCs 2), and BMSCs (BMSCs 1, BMSCs 2). Total mRNA was extracted and isolated by RNAzol (Molecular Research Center), and RNA sequencing libraries were constructed using an Illumina mRNA-seq Prep Kit (Illumina, San Diego, CA, United States) as recommended by the manufacturer. The fragmented and randomly primed 150 bp paired-end libraries were sequenced using the Illumina HiSeq X Ten platform. Sequencing data were processed using Consensus Assessment of Sequence and Variation (CASAVA, version 1.8.2; Illumina) under the default settings. The reads per kilobase of transcript per million mapped reads (RPKM) values were used to evaluate the expression levels of genes, and Pearson's correlations were calculated (R^2) to measure the similarities between different cell lines. The RNA-Seq data were also analyzed using Ingenuity Pathways Analysis (IPA) software (Ingenuity Systems, Inc., Redwood City, CA, United States) to categorize the differentially regulated genes. RNA-seq data were deposited in the Gene Expression Omnibus (GEO) under the accession number GSE182161.

Statistical Analysis

All experiments shown were biologically replicated at least three times. All results are shown as the mean ± standard deviation (SD) from at least three independent experiments. Differences between groups were tested by independent sample *t* test and one-way analysis of variance (ANOVA) with a post hoc test using the Student–Newman–Keuls test. Correlation analysis was used to measure the similarities between the different lines. All data were analyzed by GraphPad Prism 7 software and are presented as the mean plus standard deviation. $*p < 0.05$, $**p < 0.01$, and $***p < 0.001$ were considered statistically significant.

RESULTS

Differentiation of Human Pluripotent Stem Cells Into Primitive Streak Cells Using CHIR99021

PS cells serve as a conduit for the generation of mesoderm and definitive endoderm during early embryogenesis (Rivera-Perez and Magnuson, 2005). For development of an induction protocol for LM, it is critical to develop an efficient method to differentiate hPSCs into PS cells, which coexpress BRACHYURY (TBXT) and MIXL1 (**Figure 1A**). Previous studies have shown that treatment with a certain concentration of CHIR99021 (CHIR; a glycogen synthase kinase-3 inhibitor and WNT activator) for 24 or 48 h could effectively induce hPSCs to differentiate into PS cells (Lam et al., 2014; Liu et al., 2020). In this study, we first investigated the differentiation kinetics of the CHIR-treated hPSCs (at 3–10 μM) during PS induction (stage 1 differentiation). Phase-contrast images showed similar morphological changes when hiPSCs were treated with different concentrations of CHIR during PS differentiation (**Supplementary Figure S1A**). qRT-PCR analysis revealed that the mRNA level of TBXT, a PS-specific marker, was rapidly upregulated (5,000–10,000-fold) in all the CHIR-treated cells compared to the undifferentiated hiPSCs 24 h after treatment. However, the TBXT expression in the 6 and 10 μM CHIR-treated cells started to decrease 48 h later, while continuously increased mRNA expression of TBXT (up to 15,000-fold) was observed after treatment with 3 μM CHIR for 2 days. The mRNA expression of MIXL1, the other PS marker, was also upregulated significantly upon CHIR treatment, with the highest level observed with 3 μM CHIR (**Figure 1B**). These results indicated that a CHIR concentration of 3 μM could yield higher expression of TBXT/MIXL1 in differentiated hiPSCs than the other concentrations tested and was then utilized for the subsequent differentiation study.

We then tried to determine the optimal treatment time of CHIR and detected the gene expression patterns of the 3 μM CHIR-treated cells during the 72-h differentiation process. We found that the expression of pluripotency genes (OCT4, NANOG) was downregulated sharply, while the mRNA levels of genes related to ectoderm (PAX6, SOX1) and endoderm (SOX17, FOXA2) were mildly elevated or remained unaffected after treatment with 3 μM CHIR for 2 or 3 days (**Figure 1C**). These data suggested that hiPSCs quickly lost their undifferentiated state, and minimal ectodermal or endodermal progenies were generated in our differentiation system. More importantly, we found that prolonged treatment with CHIR over 48 h resulted in a significant reduction in TBXT expression in hiPSCs, although a continuously increased expression level of MIXL1 was noted (**Figure 1C**). Therefore, we decided to employ a 2-days differentiation protocol for primitive streak commitment from hiPSCs. We performed immunostaining analysis and found that the protein expression of TBXT increased in a time-dependent manner, and almost all of the differentiated cells were TBXT positive after the addition of 3 μM CHIR for 2 days. These results also showed that conditioning with CHIR led to the gradually diminished expression of the pluripotency marker NANOG, while the expression of SOX17 (endoderm progenitor marker) and PAX6 (ectoderm progenitor marker) was rarely activated in these cells during hiPSC differentiation (**Figure 1D**). Furthermore, we discovered that 48 h after 3 μM CHIR treatment, the gene and protein expression patterns in the hESC line (H1) were similar to those in hiPSCs, as illustrated by an immunofluorescence assay with anti-TBXT and anti-MIXL1 antibodies, and nearly 100% TBXT+/MIXL1+ cells were generated in both cell lines (**Figure 1E**). Together, these data indicated that treatment with 3 μm CHIR for 48 h could efficiently induce hPSCs to differentiate into primitive streak cells.

Generation of Lateral Mesoderm From the Primitive Streak by Coactivation of the WNT and Bone Morphogenetic Proteins Signaling Pathways

It was reported that exposure to CHIR resulted in hPSC differentiation toward an LM fate (Lam et al., 2014). To test whether treatment with CHIR alone could efficiently induce LM differentiation, we cultured hiPSCs in medium containing 3 μM CHIR for 6 days. We found that heterogeneous cell populations with diverse cellular morphologies were generated by prolonged treatment with CHIR (**Figure 1F**). qRT-PCR revealed that the mRNA levels of markers for paraxial mesoderm (PM; TBX6/MSGN1), intermediate mesoderm (IM; PAX2/PAX8) and LM (HAND1/FOXF1) were all markedly upregulated in differentiated cells when compared to undifferentiated hiPSCs (**Figure 1G**). Immunofluorescence assays also showed that only 40–50% of cells were HAND1-positive (**Supplementary Figure S1B**). These data suggested that CHIR alone was not sufficient to induce the formation of LM.

Previous studies have demonstrated that TGF-β family-mediated SMAD signaling is involved in mesoderm specification (Schier and Shen, 2000; Casari et al., 2014), and bone morphogenetic proteins (BMPs), such as BMP4 and BMP7, play essential roles in mesoderm formation during embryogenesis (Kim et al., 2019). In particular, high levels of BMP signaling are necessary and sufficient to promote the formation of LM both *in vivo* and *in vitro* (James and Schultheiss, 2005). We attempted to verify the specificity of BMP or TGF-β signaling in LM induction from PS cells (stage 2 differentiation) (**Figure 2A**). hiPSC-derived PS cells were cultured in induction medium with different signaling molecules, such as BMP agonist (BMP4 or BMP7), SMAD1/5/8 inhibitor (LDN193189), or a TGF-β agonist (TGF-β1), in the presence of CHIR for 4 days. We found that supplementation with BMP or TGF-β1 could result in rapid cell expansion and relatively morphologically homogeneous cell cultures compared to CHIR treatment alone (**Supplementary Figure S2A**). qRT-PCR analysis showed that higher expression of LM markers (HAND1; FOXF1) and relatively lower mRNA levels of the PM markers (TBX6; MSGN1) and IM markers (PAX2; PAX8) could be detected in the BMP groups compared to the TGF-β1-, LDN193189-, or

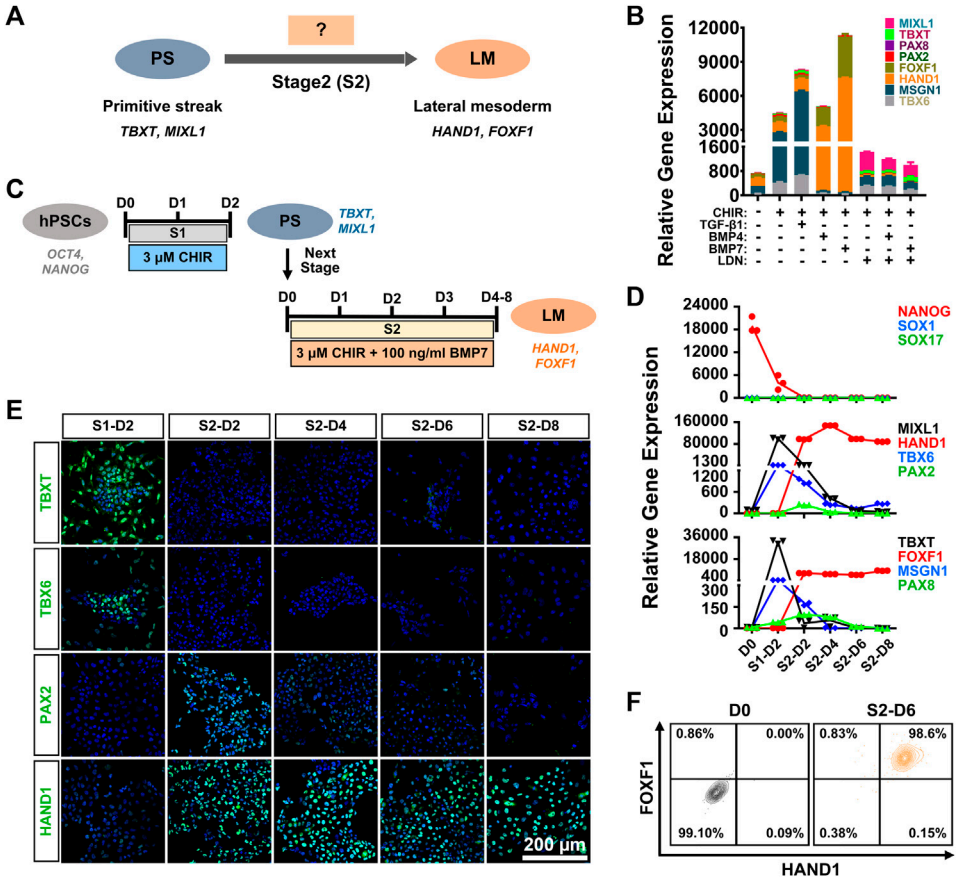

FIGURE 2 | Generation of lateral mesoderm from the primitive streak by activation of the WNT and BMP signaling pathways. **(A)**. Diagram of lateral mesoderm (HAND1; FOXF1) differentiation from the hPSC-derived primitive streak (TBXT; MIXL1) by activating TGFβ1 or BMP signaling at stage 2 (S2). **(B)**. qRT-PCR detection of the gene expression of markers for paraxial mesoderm (TBX6; MSGN1), lateral mesoderm (HAND1; FOXF1), and intermediate mesoderm (PAX2; PAX8) when primitive streak cells were treated with different factors (CHIR, TGFβ1, BMP4, BMP7, or LDN192189) at stage 2 for 4 days (S2-D4). **(C)**. Diagram of the strategy for derivation of lateral mesoderm from hPSCs through the primitive streak with 3 μM CHIR99021 and 100 ng/ml BMP7 for 4–8 days at stage 2 (S2-D4–S2-D8). **(D)**. qRT-PCR detection of the time course of gene expression in markers for pluripotency (NANOG), ectoderm (SOX1), definitive endoderm (SOX17), the primitive streak (TBXT; MIXL1), paraxial mesoderm (TBX6; MSGN1), lateral mesoderm (HAND1; FOXF1), and intermediate mesoderm (PAX2; PAX8) when hiPSCs were treated with 3 μM CHIR99021 at stage 1 (S1) for 2 days, followed by 3 μM CHIR99021 and 100 ng/ml BMP7 at stage 2 (S2) for 8 days. **(E)**. Immunostaining for the markers of the primitive streak (TBXT), paraxial mesoderm (TBX6), lateral mesoderm (HAND1) and intermediate mesoderm (PAX2) during lateral mesoderm differentiation from the hiPSC-derived primitive streak. Scale bar: 200 μm. **(F)**. Quantification of hiPSC-derived lateral mesoderm (HADN1+/FOXF1+) cells at stage 2 for 6 days (S2-D6) by FCM.

CHIR-treated or nontreated groups (**Figure 2B**). Moreover, we found that BMP7 displayed better efficacy in promoting LM commitment than BMP4 (**Figure 2B**). When the BMP pathway was inhibited by LDN193189, these cells proliferated slowly and showed obvious morphological heterogeneity (**Supplementary Figure S2B**), and the expression levels of the detected mesoderm-related genes (MSGN1, HAND1) were downregulated significantly compared to those in the TGF-β1 or BMP group (**Figure 2B**). These results suggested that the BMP signaling pathway, in particular BMP7, was critically involved in the determination of LM fate from the PS *in vitro*. Indeed, western blotting analysis showed that treated with both CHIR and BMP7 (CHIR + BMP7) significantly activated the BMP signaling pathway by inducing SMAD1/5/8 phosphorylation, while "CHIR + TGFβ1" group exhibited stronger level of phosphorylated SMAD2/3 (**Supplementary Figure S2B**). These results further indicated that the activation of BMP-SMAD1/5/8 signaling plays an important role in PS cell-specific induction of LM.

To further determine the optimal induction time for LM differentiation from the PS, we first induced hiPSCs to differentiate into the PS with 3 μM CHIR for 2 days (stage 1; S1) and then cultured them in the presence of both CHIR (3 μM) and BMP7 (100 ng/ml) (stage 2; S2) for 4–8 days (stage 2; **Figure 2C**). A relatively homogeneous cell population could be obtained after LM induction (**Supplementary Figure S2C**). qRT-PCR revealed that the expression of NANOG decreased rapidly on day two at stage 1 differentiation (S1-D2) and showed extremely low levels during the subsequent differentiation process, while genes indicative of ectoderm (SOX1) and

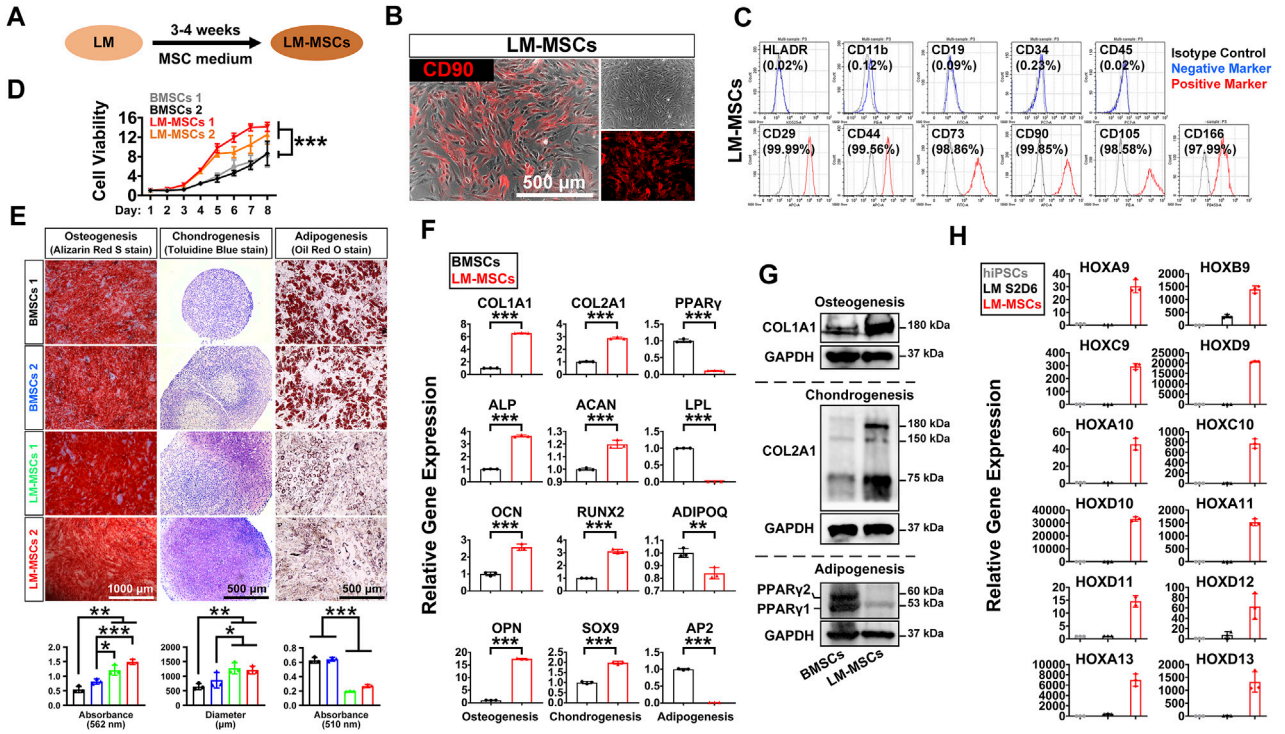

FIGURE 3 | Derivation and characterization of LM-MSCs from hiPSCs. **(A)**. Diagram of the strategy for derivation of MSCs from the hPSC-derived lateral mesoderm by treatment with MSC medium for 3–4 weeks. **(B)**. Phase-contrast image of the hiPSC-derived LM-MSCs and immunostaining of MSC marker (CD90). Scale bar: 500 μm. **(C)**. Flow cytometry for detection of typical MSC surface markers in the hiPSC-derived LM-MSCs. **(D)**. The proliferation of LM-MSCs and BMSCs was detected by CCK8 assays. $^{*}p < 0.05$; $^{**}p < 0.01$; $^{***}p < 0.001$; ns. is nonsignificant. **(E)**. The osteogenic, chondrogenic, and adipogenic differentiation potentials of LM-MSCs and BMSCs were verified by Alizarin Red S staining (scale bar: 1,000 μm), toluidine blue staining (scale bar: 500 μm), and oil red O staining (scale bar: 500 μm) respectively. The OD values of Alizarin Red S staining (562 nm) and oil red O staining (510 nm) were measured by spectrophotometry. ImageJ software was used to analyze the toluidine blue-stained cartilage micromass diameter (n = 3). $^{*}p < 0.05$; $^{**}p < 0.01$; $^{***}p < 0.001$; ns. is nonsignificant. **(F)**. qRT-PCR detection of the gene expression of osteogenic (COL1A1; ALP; OCN; OPN), chondrogenic (COL2A1; ACAN; RUNX2; SOX9), and adipogenic (PPARγ; LPL; ADIPOQ; AP2) markers in LM-MSCs and BMSCs. $^{*}p < 0.05$; $^{**}p < 0.01$; $^{***}p < 0.001$; ns. is nonsignificant. **(G)**. Western blotting for the protein expression of osteogenic (COL1A1), chondrogenic (COL2A1), and adipogenic (PPARγ) markers in differentiated LM-MSCs. **(H)**. qRT-PCR detection of the gene expression of HOX genes in hiPSCs, hiPSC-LM, and LM-MSCs.

endoderm (SOX17) were minimally expressed throughout the differentiation period. The expression of the PS cells (TBXT/MIXL1) reached a peak on S1-D2 and decreased quickly when the medium was switched to stage 2 induction medium. The qRT-PCR results also indicated that PS cells started to differentiate into mesodermal cells, as evidenced by elevated expression of the markers of PM (TBX6/MSGN1), LM (HAND1/FOXF1), and IM (PAX2/PAX8) since S1-D2 or S2-D2. Nonetheless, transcript levels of PM- or IM-specific genes were significantly downregulated from S2-D4, while mRNA levels for LM markers (HAND1/FOXF1) increased constantly during the induction period and maintained a high level up to S2-D6 or S2-D8 (**Figure 2D**). The immunofluorescence assays showed that differentiated cells transiently expressed TBXT (S1-D2), TBX6 (S1-D2), and PAX2 (from S2-D2 to S2-D4) and then expressed only the LM marker HAND1 from S2-D6 (**Figure 2E**). To confirm these findings, we used flow cytometry to quantify the LM differentiation efficiency on S2-D6, showing that 99.6 ± 0.51% of the differentiated cells were HAND1 positive, and 98.6 ± 0.4% of the cells were double positive for HAND1 and FOXF1 (**Figure 2F**). More importantly, a similar high efficiency of LM differentiation could be achieved in the H1 cell line using the same differentiation protocol, as displayed by immunostaining, qRT-PCR, and FCM (**Supplementary Figure S2D–F**). These data demonstrated that PS could be effectively induced into LM when treated with 3 μM CHIR and 100 ng/ml BMP7 for 6 days.

Derivation and Characterization of Mesenchymal Stem Cells Derived From Human Pluripotent Stem Cell-Lateral Mesoderm *in vitro*

LM-derived mesenchymal cells are present throughout the anteroposterior axis of the embryo (Gros and Tabin, 2014) and are closely associated with the formation of adult appendicular skeletal elements (bone and cartilage) (Cohn and Tickle, 1996; Olsen et al., 2000) and visceral white fat (Chau et al., 2014). Such evidence suggests that an MSC-like population exists during both LM differentiation and homeostatic maintenance of

LM-derived tissues (Sheng, 2015). Thus, we hypothesize that MSCs could be obtained *in vitro* from hPSCs via an intermediate stage of LM.

To induce MSC differentiation from LM, we cultured hiPSC-derived LM cells (S2-D6) for 3–4 weeks in chemically defined MSC medium, StemFit for MSC (**Figure 3A**). We observed significant changes in cell morphology during differentiation (**Supplementary Figure S3A**), and cells gradually became spindle-shaped and showed active proliferation, presenting a typical whirlpool-like alignment at a high density (**Figure 3B**). We first tested whether LM-derived cells satisfied the 2006 ISCT's guidelines for MSC characterization (Dominici et al., 2006). FCM analysis showed that over 95% of the differentiated cells expressed the typical surface markers of human MSCs, including CD29, CD44, CD73, CD90, CD105, and CD166, but were negative for HLADR, CD11b, CD19, CD34, and CD45 (**Figure 3C**, **Supplementary Figure S3B**). The CCK8 assay revealed that these cells exhibited stronger proliferation than the BMSCs in StemFit medium (**Figure 3D**). Moreover, when induced to differentiate into osteoblasts, chondrocytes, and adipocytes *in vitro*, LM-derived cells displayed stronger osteogenic and chondrogenic differentiation but less potent adipogenic differentiation than BMSCs, as shown by Alizarin Red S staining, toluidine blue staining, and oil red O staining, respectively (**Figure 3E**, **Supplementary Figure S3C**). Indeed, qRT-PCR revealed a higher expression of osteogenic (COL1A1, ALP, OCN, OPN, SP7) and chondrogenic (COL2A1, ACAN, RUNX2, SOX9) genes, while markers of adipogenesis (PPARγ, LPL, ADIPOQ, AP2) were weakly expressed in the LM-derived cells compared to the BMSCs (**Figure 3F**, **Supplementary Figure S3D**). The western blotting results further showed more abundant COL1A1/COL2A1 during osteogenic/chondrogenic commitment and a lower protein level of PPARγ during adipogenic differentiation of LM-MSCs compared to BMSCs (**Figure 3G**). These results suggested that LM-derived cells resemble primary BMSCs in surface marker expression and differentiation potential, and thus these cells are referred to as LM-MSCs. Moreover, LM-MSCs could be readily generated from H1 and H9-hESC lines and HDF-hiPSCs (**Supplementary Figure S4A,B**).

The HOX gene family plays an essential role during vertebrate limb development, and loss-of-function mutations of some HOX genes, alone or in combination, could lead to severe developmental defects in the limb (Zakany and Duboule, 2007). Thus, we investigated whether LM-MSCs could express typical HOX family members. The qRT-PCR results revealed much more abundant expression of HOX genes 9–13 in LM-MSCs (**Figure 3H**) than in hiPSCs or LM, suggesting that LM-MSCs had HOX expression patterns similar to those of skeletal progenitor cells in the vertebrate limb or limb skeleton-derived BMSCs (Zakany and Duboule, 1999; Rux et al., 2016).

MSCs were reported to have effective immunomodulatory properties and anti-inflammatory abilities and represent a promising therapy in clinical use for a wide range of immune-related diseases (Muller et al., 2021). To explore the immunoregulatory activity of LM-MSCs, we evaluated the suppressive effects of LM-MSCs on the proliferation and pro-inflammatory cytokine production of $CD3^+$ T cells. We found that when cocultured with $CD3^+$ T cells, LM-MSCs exhibited an immunomodulatory function similar to that of BMSCs and could efficiently prevent the proliferation of $CD3^+$ T cells and reduce the percentages of $CD3^+$ T cells that produced TNF-α and IFN-γ (**Figure 4A**). Since macrophages play important roles in the osteogenic environment (Munoz et al., 2020), we asked whether LM-MSCs, in turn, could exert immunoregulatory effects on macrophages. The results showed that LM-MSCs inhibited the production of TNFα from human THP-1-derived macrophages more efficiently than BMSCs (**Figure 4B**). Previous study has revealed that the immunoregulatory function of MSCs is highly plastic. MSCs can not only inhibit the immune response but also promote it (Li et al., 2012; Wang et al., 2014). We therefore investigated the immune response of LM-MSCs when exposed to pro-inflammatory factors by qRT-PCR detection of pro-inflammatory cytokines (IL-6, IL8, and CCL2) and anti-inflammatory mediators (IDO, PDL1, and TSG6). The results indicated that IFN-γ stimulation induced the upregulation of IL-6 expression in both LM-MSCs and BMSCs (approximately 4–6-fold higher than that in the untreated cells). Interestingly, the mRNA level of IL8 was enhanced in the treated LM-MSCs but not the BMSCs, while significantly increased CCL2 transcripts (approximately 15–20-fold higher than untreated cells) were observed only in the stimulated BMSCs. We also found that the expression of anti-inflammatory cytokines was substantially augmented in both cell lines after IFN-γ treatment. Moreover, higher levels of IDO and PDL1 were detected in BMSCs, while increased TSG6 mRNA transcription was observed in LM-MSCs upon IFN-γ stimulation. These preliminary data suggested that LM-MSCs and BMSCs have similar but not identical immunomodulatory properties (**Figure 4C**).

In vivo Transplantation of Lateral Mesoderm-Mesenchymal Stem Cells

We performed subcutaneous transplantation of LM-MSCs into NCG mice to assess their *in vivo* bone formation activity. Eight weeks after transplantation of the combined LM-MSCs and hydroxyapatite scaffolds, samples were collected and analyzed (**Supplementary Figure S5A**). We detected enhanced bone formation (collagen deposition) in the LM-MSC group compared with the BMSC group, as revealed by Masson's trichrome staining and the total area percentage of collagen fiber quantified by ImageJ software (**Figure 5A**). Immunofluorescence assays also showed that more osteoprotegerin (OPG)- and osteocalcin (OCN)-positive cells could be detected in the LM-MSC group than in the BMSC group (**Figure 5B**). These results were consistent with those of the *in vitro* osteogenic differentiation assay described above. More importantly, H&E staining, anti-human mitochondria and anti-mouse CD45 immunostaining revealed that more hematopoietic cell clusters/cells of mouse origin appeared in the samples derived from LM-MSCs than in those from BMSCs, indicating a better hematopoiesis-supporting capacity of LM-MSCs over BMSCs (**Figures 5C,D**; **Supplementary Figure S5B**). qRT-PCR analysis further revealed that the mRNA levels of hematopoietic stem cell maintenance genes, including CXCL12, VCAM-1, MCP1, KITLG, FLT3L, and ANGPT1, were remarkably upregulated in LM-MSCs

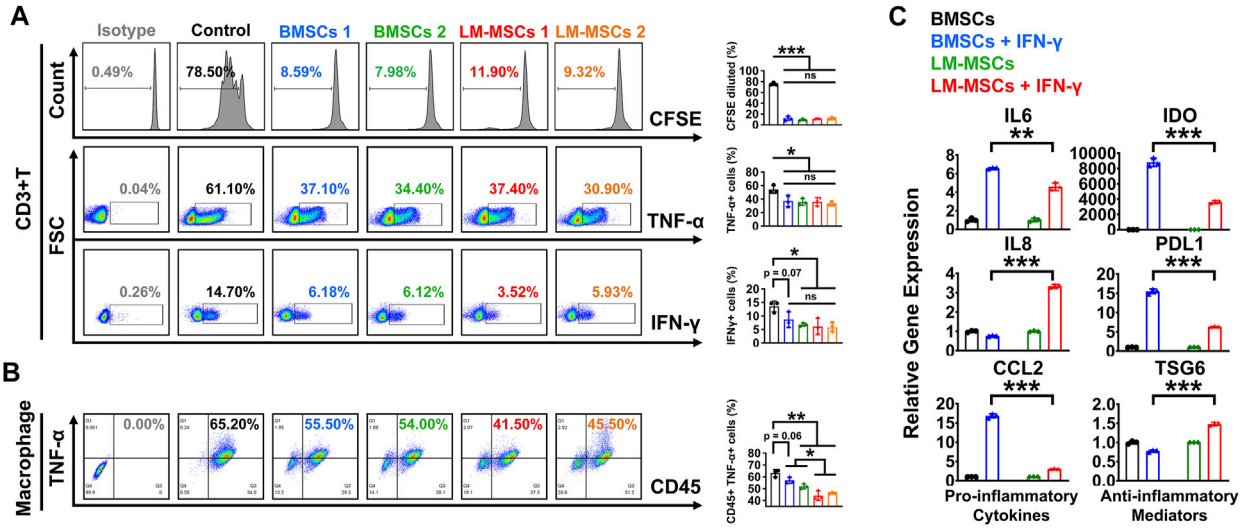

FIGURE 4 | Immunomodulatory properties of LM-MSCs. **(A)**. The proliferation (CFSE assay) and production of TNF-α and IFN-γ were examined by flow cytometry when $CD3^+$ T cells were cultured with or without LM-MSCs or BMSCs for 3 days. *$p < 0.05$; **$p < 0.01$; ***$p < 0.001$, ns. is nonsignificant. **(B)**. The production of TNF-α of human THP-1-derived macrophages was examined by flow cytometry when cells cultured with or without LM-MSCs or BMSCs for 3 days. *$p < 0.05$; **$p < 0.01$; ***$p <$ 0.001, ns. is nonsignificant. **(C)**. qRT-PCR detection of the gene expression of pro-inflammatory cytokines (IL-6, IL-8, and CCL2) and anti-inflammatory mediators (IDO, PDL1, and TSG6) in LM-MSCs and BMSCs exposed to an inflammatory environment. *$p < 0.05$; **$p < 0.01$; ***$p < 0.001$; ns. is nonsignificant.

compared to primary BMSCs (**Figure 5E**). Western blot results confirmed the higher protein level of VCAM-1 in LM-MSCs than in BMSCs (**Figure 5F**). To verify the supportive function for hematopoiesis of LM-MSCs, we performed *in vitro* coculture experiments using MSCs and HSCs. FCM analysis showed that coculture with LM-MSCs generated a significantly greater proportion of $CD34^+$ HSCs than that of the BMSC and control groups. LM-MSCs also produced the highest number of colony-forming unit for granulocytes and macrophages (CFU-GM) and burst-forming unit–erythroid (BFU-E) colonies in the CFU assay (**Figures 5G,H**). The above evidence suggested that the superior hematopoiesis-supporting potential may be attributed to higher expression of hematopoietic supporting genes in LM-MSCs.

Since MSCs show good therapeutic potential for the treatment of various diseases, it is important to evaluate the safety of MSC transplantation. Consequently, 5×10^6 LM-MSCs were subcutaneously injected into NCG mice, and the tumorigenicity of these cells was assessed. After 2 months, we found that the control cells (undifferentiated hiPSCs) could efficiently form tumors (100%), while no evidence of tumor formation was detected in the BMSC and LM-MSC groups (**Supplementary Figure S6**), indicating the safety of *in vivo* transplantation of LM-MSCs.

Global Gene Expression Profiling of Lateral Mesoderm-Mesenchymal Stem Cells

To evaluate changes in the transcriptome profiles during LM-MSC differentiation, we performed RNA sequencing (RNA-Seq) in different datasets to detect genome-wide transcriptional patterns of hiPSC-derived LM (LM1, LM2), hiPSC-derived LM-MSCs (LM-MSCs 1, LM-MSCs 2), and BMSCs (BMSCs 1, BMSCs 2) (GSE182161). We first calculated the coefficients of determination (R2) for all expressed genes and revealed a high level of similarity in the gene expression profile between 2 samples at the same differentiation stage (LM 1 vs LM 2; LM-MSCs 1 vs LM-MSCs 2; R2>0.95; **Figure 6A**), indicating a high reproducibility of our differentiation protocol. However, the R2 value decreased when comparing the data from samples at different stages (LM vs LM-MSCs, R2 = 0.8–0.9), which suggested that significant changes in gene expression patterns occurred in cells during *in vitro* differentiation. Moreover, we determined that the LM-MSCs shared highly similar gene expression patterns with BMSCs (R2>0.90) (**Figure 6A**). The RNA-Seq data also showed that LM-specific transcription factors, such as HAND1 and FOXF1, were enriched in LM cells. More importantly, all the LM-MSC and BMSC samples were highly enriched in transcripts associated with MSC-specific molecules as described, including CD epitope-encoding genes such as CD29/ITGB1, CD44, CD73/NT5E, and CD166/ALCAM (**Figure 6B**). Increased protease (MMP/TIMP) and PTX3 expression was found in LM-MSCs and BMSCs compared to LM cells in RNA-Seq, which was further confirmed by RT-PCR assays (**Supplementary Figure S7**). Upregulation of these genes may be involved in the migration, invasion, ECM remodeling, and angiogenesis properties of LM-MSCs (Lu et al., 2010; Cappuzzello et al., 2016; Doni et al., 2021). In addition, RNA-Seq data indicated that LM-MSCs highly expressed HOX9-13 genes, which was consistent with the qRT-PCR results described above (**Figure 6C**). IPA also showed enrichment for genes involved in the quantity of blood cells, limb development, size of body and others, further suggesting that LM-MSCs possessed higher osteogenic, chondrogenic, and hematopoiesis supporting potential than BMSCs (**Figure 6D**). These findings were in accordance with the above experimental results.

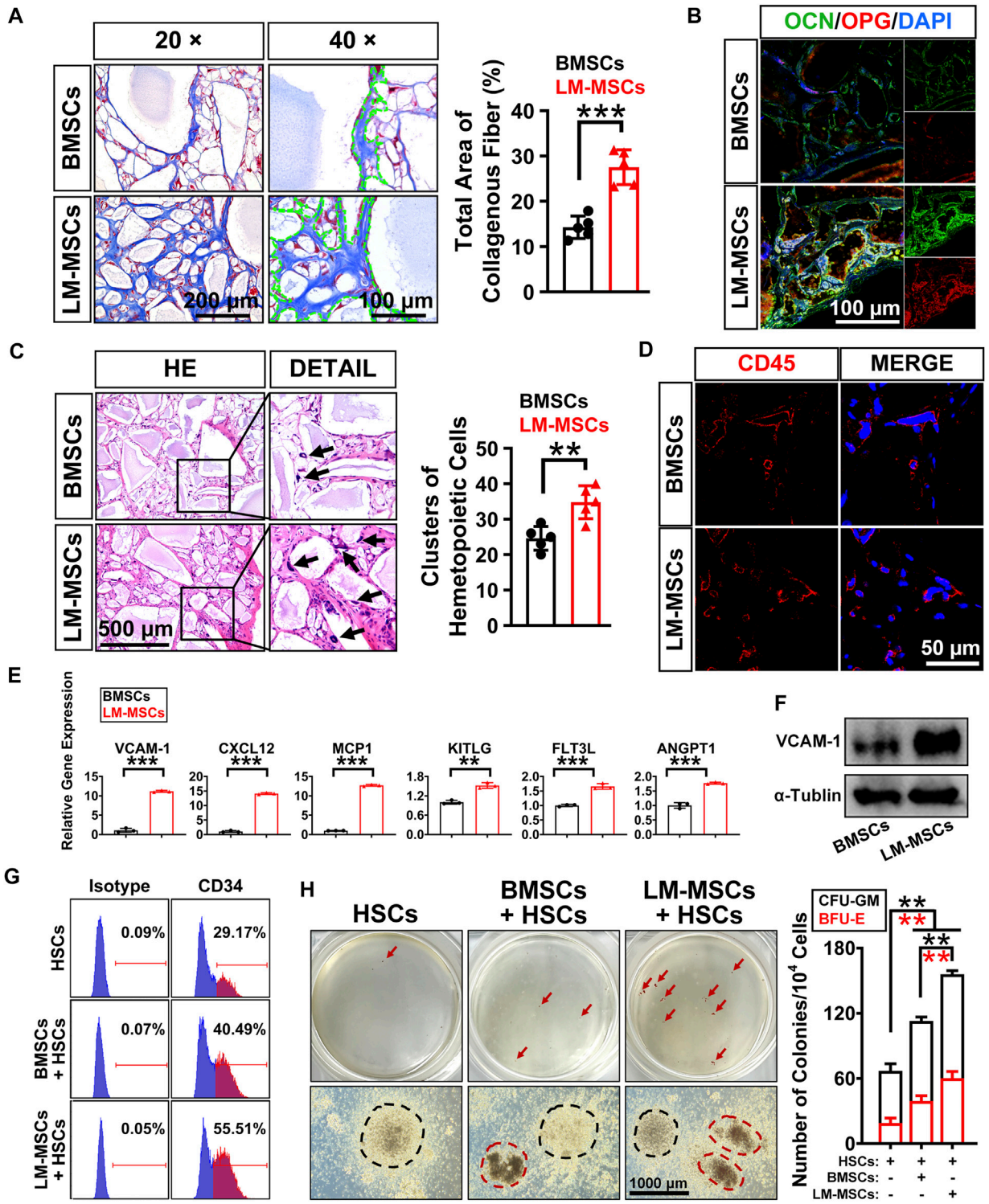

FIGURE 5 | *In vivo* bone formation assay and detection of the hematopoiesis-supporting capacity of LM-MSCs. **(A)**. The samples of *in vivo* bone formation were analyzed by Masson's trichrome staining. 20× (scale bar: 200 μm); 40× (scale bar: 100 μm). The total area percentage of collagen fibers (n = 5) was quantified by ImageJ software. **(B)**. Immunostaining of *in vivo* bone formation samples with anti-osteoprotegerin (OPG) and anti-osteocalcin (OCN) antibodies (scale bar: 100 μm). **(C)**. HE staining (scale bar: 500 μm) was performed, and the hematopoietic clusters were quantified (n = 5). $^{*}p < 0.05$; $^{**}p < 0.01$; $^{***}p < 0.001$; ns. is nonsignificant. **(D)**. Immunostaining with anti-mouse CD45 antibody was applied for the detection of the nucleated cells of mouse origin (scale bar: 50 μm). **(E)**. The expression of hematopoietic supporting genes in cultured LM-MSCs and BMSCs was detected by qRT-PCR. $^{*}p < 0.05$; $^{**}p < 0.01$; $^{***}p < 0.001$; ns. is nonsignificant. **(F)**. Western blotting for the expression of VCAM-1 in BMSCs and LM-MSCs. **(G)**. FCM analysis of the proportion of $CD34^{+}$ HSCs when cocultured with LM-MSCs or BMSCs. **(H)**. The hematopoiesis-supporting function of LM-MSCs and BMSCs was compared by CFU assays. black dotted line indicates CFU-GM, while the red dotted line indicates BFU-E.

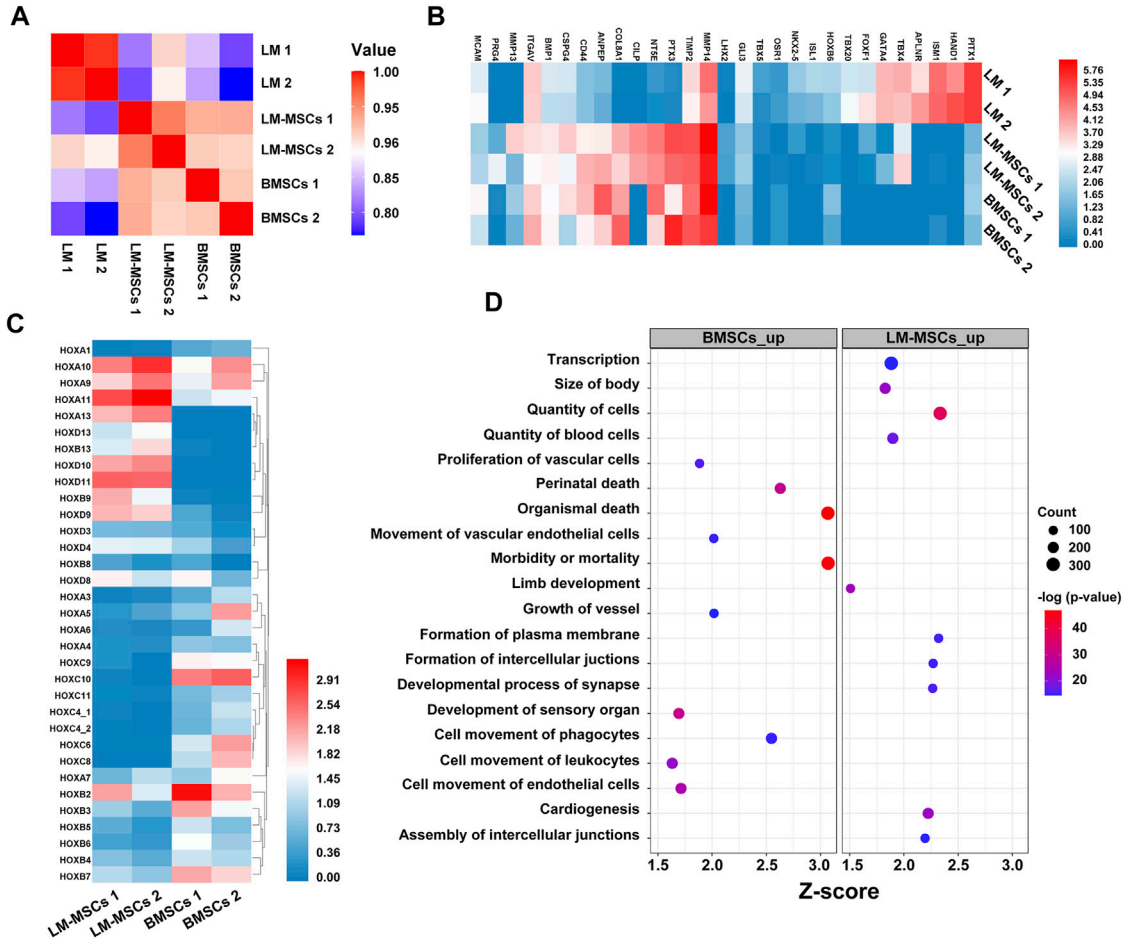

FIGURE 6 | Transcriptome profiles from LM, LM-MSCs, and BMSCs. **(A)**. Pearson's correlation coefficients of pairwise comparisons were calculated for all expressed genes in LM, LM-MSCs, and BMSCs. **(B)**. The heatmap of typical markers labeling LM, LM-MSCs and BMSCs in the RNA-Seq results was analyzed. **(C)**. The HOX gene expression pattern in LM-MSCs and BMSCs in RNA-Seq data was analyzed. **(D)**. IPA functional annotation of differentially expressed mRNAs. The dot plot of partially enriched functions. The color intensity of the nodes indicates the degree of IPA function enrichment. The horizontal axis indicates the gene ratio as the proportion of differentially expressed genes in the whole gene set. The size represents the number counts in a certain function.

DISCUSSION

In this study, we successfully established an efficient and highly reproducible differentiation protocol for the derivation of MSCs with LM origin from hPSCs. hPSC-derived LM-MSCs exhibited characteristic HOX gene profiles and shared similar properties with BMSCs in surface marker expression and immune regulation activity. Moreover, compared to BMSCs, LM-MSCs presented stronger osteogenesis and cartilage differentiation potential *in vitro* and displayed a superior ability to support bone formation and hematopoiesis *in vivo*.

The PM, IM, and LM are generated from PS cells during gastrulation (Loh et al., 2016). Thus, efficient induction of the PS from hPSCs is considered a necessary step toward acquiring mesoderm properties *in vitro*. Preliminary studies have shown that TGF-β superfamily members (including Activin/Nodal and BMP), fibroblast growth factors (FGFs), and WNT signaling are key regulators determining PS cell fate during embryogenesis (Wang and Chen, 2016). Most studies have used high doses of Activin A alone or in synergism with BMP, FGF or WNT activators to induce PS differentiation from hPSCs. However, only a few studies have shown that the activation of the WNT signaling pathway alone was sufficient to direct hPSCs to differentiate into the PS *in vitro* (Wang and Chen, 2016). Sasha et al. reported that significant induction of TBXT transcripts and protein expression could be achieved in hPSCs when treated with only one molecule, CHIR, for 36 h. These researchers also found that 8 μM CHIR yielded higher TBXT expression than 3 μM CHIR, as shown by the immunostaining assay. However, this group did not quantify the PS differentiation efficiency (the proportion of TBXT + cells) induced by CHIR alone. Bone et al. showed that when cultured in mTeSR medium supplemented with 2 μM CHIR, hPSCs started to differentiate into PS cells, and TBXT protein expression was detected on Day 3 and remained elevated until Day 7. Nonetheless, TGF-β and FGF signaling was also activated in their study since the basal medium,

mTeSR, contained TGF-β1 and FGF2 (Arnold and Robertson, 2009; Bone et al., 2011). Lam et al. also demonstrated that treatment with 5 μM CHIR for 24 h resulted in 98.7 ± 1.3% of the cells expressing TBXT during hPSC differentiation (Lam et al., 2014). Herein, we analyzed the time-dependent and dosage-dependent effects of CHIR on hPSC differentiation under serum-free conditions. We found that the mRNA levels of TBXT and MIXL1 increased markedly when cells were treated with 3 μM CHIR for 24 h; however, the pluripotency marker NANOG was still expressed in some of the differentiated hPSCs, as detected by qRT-PCR and immunocytochemistry. Our results also showed that hPSCs could successfully exit pluripotency and differentiate toward TBXT+/MIXL1+ PS cells with high efficiency when treated with 3 μM CHIR for 2 days. Moreover, the expression of TBXT began to decline when hPSCs were treated with CHIR for more than 2 days. Accordingly, we demonstrated that activation of WNT signaling with 3 μM CHIR for 2 days could efficiently induce hPSCs to differentiate into the PS.

Previous studies have shown that WNT signaling is vital for mesoderm specification and separation *in vivo*, and blocking WNT signals in ES cells abrogated the differentiation of FLK1-positive mesoderm *in vitro* (Lindsley et al., 2006; Tanaka et al., 2011). Several protocols have been described for obtaining cells with the characteristics of LM. Kyle et al. found that BMP and WNT signals help drive the bifurcation of lateral versus paraxial mesoderm subtypes from the PS. The authors showed that BMP induces, whereas WNT inhibits, LM from the PS. A 2-days treatment with A8301, BMP4, and C59 (a WNT inhibitor) could direct PS differentiation into HAND1+/FOXF1+ LM cells with an efficiency of 98.1–100% (Loh et al., 2016). Liu et al. established an efficient protocol for the differentiation of LM from hPSCs by the combination of FGF2, BMP4, the ROCK inhibitor Y27632, and follistatin (Liu et al., 2020).

In this study, we first showed that prolonged exposure to CHIR alone (4–8 days) resulted in a heterogeneous population of differentiated cells containing less than 50% LM progenitors. These results suggested that CHIR was not sufficient to induce homogeneous LM cells in the absence of additional exogenous factors. James et al. reported that high levels of BMP repressed both paraxial and intermediate mesoderm gene expression but activated lateral plate genes during chick embryo development (James and Schultheiss, 2005). Indeed, our results confirmed that the addition of BMP to CHIR-containing induction medium could promote the LM fate (nearly 100%) and inhibit the development of intermediate or paraxial mesoderm from the PS *in vitro*. Interestingly, our results indicated that BMP7 had a stronger promoting effect on the expression of LM-related genes than BMP4. The underlying molecular mechanisms need to be further elucidated. Taken together, our results demonstrated that LM progenitors could be readily generated from the PS following treatment with BMP7 and CHIR.

The heterogeneous properties of MSCs have been considered the cause of their inconsistent therapeutic efficacy in many clinical trials. MSCs have multiple developmental origins, including the neural crest (neural ectoderm), mesoderm, and trophoblast (Jiang et al., 2019). Therefore, minimization of the heterogeneity of MSCs by better defining developmental origins may help to stabilize the treatment effects in the clinical translation of MSCs. Previous studies have suggested that an MSC-like population exists during both LM differentiation and homeostatic maintenance of LM-derived tissues (Sheng, 2015). However, to our knowledge, few studies have reported protocols for the derivation of MSCs from LM. Two studies have successfully derived MSCs through the intermediate stages of LM and via subsequent mesenchymoangioblasts of hPSCs (Vodyanik et al., 2010; Ozay et al., 2019). However, these MSCs may represent a mixed population including limb MSCs and pericytes, since the mesenchymoangioblast is the earliest precursor of endothelial cells, mesenchymal cells, and pericytes originating from KDR + hematopoietic mesoderm. Liu et al. established an efficient protocol for the differentiation of skeletal mesenchymal stromal cells through LM from hPSCs. Their results revealed that hPSC-MSCs showed robust mesenchymal trilineage differentiation potential, similar to primary BMSCs. Nevertheless, they did not detect the expression of members of the HOX gene family, immune modulatory function, or hematopoiesis-supporting activity of these skeletal MSCs (Liu et al., 2020). In our study, we successfully acquired LM-MSCs in chemically defined and animal component-free MSC medium, which meets the 2006 ISCT guidelines for MSC characterization (Dominici et al., 2006). We showed that LM-MSCs possessed a stronger osteogenic differentiation capacity than BMSCs *in vitro* and *in vivo*. We hypothesized that the *in vivo* chondrogenic differentiation ability of LM-MSCs may also be stronger than that of BMSCs, since the *in vitro* differentiation assay showed a similar trend and the RNA-Seq data showed that genes of "limb development" were highly enriched in LM-MSCs compared with BMSCs, which needs further experimental verification. LM-MSCs also displayed HOX expression patterns similar to those of skeletal progenitor cells in the vertebrate limb (Cohn et al., 1997). We further confirmed that LM-MSCs resembled primary BM-BMSCs with immunomodulatory properties, as LM-MSCs could efficiently inhibit the proliferation of $CD3^+$ T cells and suppress the percentages of $CD3^+$ T cells and macrophages that produced TNF-α and/or IFN-γ. Intriguingly, we showed that LM-MSCs have a superior ability to support hematopoiesis. Moreover, analysis of RNA-Seq data demonstrated that the R2 between different batches of LM-MSCs from the same hPSC line (LM-MSCs 1 vs LM-MSCs 2) was higher than 0.95, indicating that a relatively homogeneous cell population could be obtained by our differentiation protocol. These results suggested that functional LM-MSCs were successfully generated by a chemically defined MSC medium.

In conclusion, we developed a simple, efficient, and chemically defined protocol for the derivation of MSCs with LM origin from hPSCs. Our findings also supported the critical role of the BMP and WNT signaling pathways in LM commitment from PS cells. These LM-MSCs derived from hPSCs may be valuable in elucidating the

biological characteristics of their *in vivo* counterparts. LM-MSCs may also represent a new source in cell replacement therapy for bone/cartilage defects and hematopoietic diseases.

DATA AVAILABILITY STATEMENT

The datasets presented in this study can be found in online repositories. The names of the repository/repositories and accession number(s) can be found below: https://www.ncbi.nlm.nih.gov/geo/ GSE182161.

ETHICS STATEMENT

The animal study was reviewed and approved by Animal Ethics Committee of Sun Yat-Sen University.

AUTHOR CONTRIBUTIONS

XL and WL conceptualized and designed the study. YW, BW, and LJ were responsible for the collection and assembly of data. WH was responsible for the data analysis and interpretation. AX and CF were responsible for the provision of study materials. All authors contributed to the manuscript writing and approved the final version of the manuscript.

FUNDING

This work was supported by the National Key Research and Development Program of China (2018YFA0107200, 2019YFA0110303); the Strategic Priority Research Program of the Chinese Academy of Sciences (XDA16020701); the National Natural Science Foundation of China (81970474, 81970222, 81730005); the Key Research and Development Program of Guangdong Province (2019B020234001, 2019B020236002); and the Pioneering Talents Project of Guangzhou Development Zone (2017-L163).

SUPPLEMENTARY MATERIAL

The Supplementary Material for this article can be found online at: https://www.frontiersin.org/articles/10.3389/fmolb.2022.767536/full#supplementary-material

REFERENCES

Arnold, S. J., and Robertson, E. J. (2009). Making a Commitment: Cell Lineage Allocation and Axis Patterning in the Early Mouse Embryo. *Nat. Rev. Mol. Cel Biol* 10 (2), 91–103. doi:10.1038/nrm2618

Augello, A., and De Bari, C. (2010). The Regulation of Differentiation in Mesenchymal Stem Cells. *Hum. Gene Ther.* 21 (10), 1226–1238. doi:10.1089/hum.2010.173

Bone, H. K., Nelson, A. S., Goldring, C. E., Tosh, D., and Welham, M. J. (2011). A Novel Chemically Directed Route for the Generation of Definitive Endoderm from Human Embryonic Stem Cells Based on Inhibition of GSK-3. *J. Cel Sci* 124 (Pt 12), 1992–2000. doi:10.1242/jcs.081679

Cappuzzello, C., Doni, A., Dander, E., Pasqualini, F., Nebuloni, M., Bottazzi, B., et al. (2016). Mesenchymal Stromal Cell-Derived PTX3 Promotes Wound Healing via Fibrin Remodeling. *J. Invest. Dermatol.* 136 (1), 293–300. doi:10.1038/JID.2015.346

Casari, A., Schiavone, M., Facchinello, N., Vettori, A., Meyer, D., Tiso, N., et al. (2014). A Smad3 Transgenic Reporter Reveals TGF-Beta Control of Zebrafish Spinal Cord Development. *Develop. Biol.* 396 (1), 81–93. doi:10.1016/j.ydbio.2014.09.025

Chau, Y.-Y., Bandiera, R., Serrels, A., Martínez-Estrada, O. M., Qing, W., Lee, M., et al. (2014). Visceral and Subcutaneous Fat Have Different Origins and Evidence Supports a Mesothelial Source. *Nat. Cel Biol* 16 (4), 367–375. doi:10.1038/ncb2922

Chen, J.-Y., Mou, X.-Z., Du, X.-C., and Xiang, C. (2015). Comparative Analysis of Biological Characteristics of Adult Mesenchymal Stem Cells with Different Tissue Origins. *Asian Pac. J. Trop. Med.* 8 (9), 739–746. doi:10.1016/j.apjtm.2015.07.022

Chen, X., Cai, C., Xu, D., Liu, Q., Zheng, S., Liu, L., et al. (2019). Human Mesenchymal Stem Cell-Treated Regulatory CD23(+)CD43(+) B Cells Alleviate Intestinal Inflammation. *Theranostics* 9 (16), 4633–4647. doi:10.7150/thno.32260

Chijimatsu, R., Ikeya, M., Yasui, Y., Ikeda, Y., Ebina, K., Moriguchi, Y., et al. (2017). Characterization of Mesenchymal Stem Cell-Like Cells Derived From Human iPSCs via Neural Crest Development and Their Application for Osteochondral Repair. *Stem Cell Int.* 2017, 1960965. doi:10.1155/2017/1960965

Cohn, M. J., Patel, K., Krumlauf, R., Wilkinsont, D. G., Clarke, J. D. W., and Tickle, C. (1997). Hox9 Genes and Vertebrate Limb Specification. *Nature* 387 (6628), 97–101. doi:10.1038/387097a0

Cohn, M. J., and Tickle, C. (1996). Limbs: a Model for Pattern Formation within the Vertebrate Body Plan. *Trends Genet.* 12 (7), 253–257. doi:10.1016/0168-9525(96)10030-5

Costa, L. A., Eiro, N., Fraile, M., Gonzalez, L. O., Saá, J., Garcia-Portabella, P., et al. (2021). Functional Heterogeneity of Mesenchymal Stem Cells from Natural Niches to Culture Conditions: Implications for Further Clinical Uses. *Cell. Mol. Life Sci.* 78 (2), 447–467. doi:10.1007/s00018-020-03600-0

Dominici, M., Le Blanc, K., Mueller, I., Slaper-Cortenbach, I., Marini, F. C., Krause, D. S., et al. (2006). Minimal Criteria for Defining Multipotent Mesenchymal Stromal Cells. The International Society for Cellular Therapy Position Statement. *Cytotherapy* 8 (4), 315–317. doi:10.1080/14653240600855905

Doni, A., Mantovani, A., Bottazzi, B., and Russo, R. C. (2021). PTX3 Regulation of Inflammation, Hemostatic Response, Tissue Repair, and Resolution of Fibrosis Favors a Role in Limiting Idiopathic Pulmonary Fibrosis. *Front. Immunol.* 12, 676702. doi:10.3389/fimmu.2021.676702

Gros, J., and Tabin, C. J. (2014). Vertebrate Limb Bud Formation Is Initiated by Localized Epithelial-To-Mesenchymal Transition. *Science* 343 (6176), 1253–1256. doi:10.1126/science.1248228

Herman, T. S., Teicher, B. A., Jochelson, M., Clark, J., Svensson, G., and Coleman, C. N. (1988). Rationale for Use of Local Hyperthermia with Radiation Therapy and Selected Anticancer Drugs in Locally Advanced Human Malignancies. *Int. J. Hyperthermia* 4 (2), 143–158. doi:10.3109/02656738809029305

Isern, J., García-García, A., Martín, A. M., Arranz, L., Martín-Pérez, D., Torroja, C., et al. (2014). The Neural Crest Is a Source of Mesenchymal Stem Cells with Specialized Hematopoietic Stem Cell Niche Function. *Elife* 3, e03696. doi:10.7554/eLife.03696

James, R. G., and Schultheiss, T. M. (2005). Bmp Signaling Promotes Intermediate Mesoderm Gene Expression in a Dose-Dependent, Cell-Autonomous and Translation-Dependent Manner. *Develop. Biol.* 288 (1), 113–125. doi:10.1016/j.ydbio.2005.09.025

Jiang, B., Yan, L., Wang, X., Li, E., Murphy, K., Vaccaro, K., et al. (2019). Concise Review: Mesenchymal Stem Cells Derived from Human Pluripotent Cells, an Unlimited and Quality-Controllable Source for Therapeutic Applications. *Stem Cells* 37 (5), 572–581. doi:10.1002/stem.2964

Kabat, M., Bobkov, I., Kumar, S., and Grumet, M. (2020). Trends in Mesenchymal Stem Cell Clinical Trials 2004-2018: Is Efficacy Optimal in a Narrow Dose Range? *Stem Cell Transl Med* 9 (1), 17–27. doi:10.1002/sctm.19-0202

Kassem, M., Kristiansen, M., and Abdallah, B. M. (2004). Mesenchymal Stem Cells: Cell Biology and Potential Use in Therapy. *Basic Clin. Pharmacol. Toxicol.* 95 (5), 209–214. doi:10.1111/j.1742-7843.2004.pto950502.x

Kern, S., Eichler, H., Stoeve, J., Klüter, H., and Bieback, K. (2006). Comparative Analysis of Mesenchymal Stem Cells from Bone Marrow, Umbilical Cord Blood, or Adipose Tissue. *Stem Cells* 24 (5), 1294–1301. doi:10.1634/stemcells.2005-0342

Kim, H.-S., Neugebauer, J., McKnite, A., Tilak, A., and Christian, J. L. (2019). BMP7 Functions Predominantly as a Heterodimer with BMP2 or BMP4 during Mammalian Embryogenesis. *Elife* 8, e48872. doi:10.7554/eLife.48872

Lam, A. Q., Freedman, B. S., Morizane, R., Lerou, P. H., Valerius, M. T., and Bonventre, J. V. (2014). Rapid and Efficient Differentiation of Human Pluripotent Stem Cells into Intermediate Mesoderm that Forms Tubules Expressing Kidney Proximal Tubular Markers. *J. Am. Soc. Nephrol.* 25 (6), 1211–1225. doi:10.1681/ASN.2013080831

Li, W., Huang, L., Zeng, J., Lin, W., Li, K., Sun, J., et al. (2018). Characterization and Transplantation of Enteric Neural Crest Cells from Human Induced Pluripotent Stem Cells. *Mol. Psychiatry* 23 (3), 499–508. doi:10.1038/mp.2016.191

Li, W., Ren, G., Huang, Y., Su, J., Han, Y., Li, J., et al. (2012). Mesenchymal Stem Cells: A Double-Edged Sword in Regulating Immune Responses. *Cell Death Differ* 19 (9), 1505–1513. doi:10.1038/cdd.2012.26

Lindsley, R. C., Gill, J. G., Kyba, M., Murphy, T. L., and Murphy, K. M. (2006). Canonical Wnt Signaling Is Required for Development of Embryonic Stem Cell-Derived Mesoderm. *Development* 133 (19), 3787–3796. doi:10.1242/dev.02551

Liu, T. M., Yildirim, E. D., Li, P., Fang, H. T., Denslin, V., Kumar, V., et al. (2020). Ascorbate and Iron Are Required for the Specification and Long-Term Self-Renewal of Human Skeletal Mesenchymal Stromal Cells. *Stem Cel Rep.* 14 (2), 210–225. doi:10.1016/j.stemcr.2020.01.002

Loh, K. M., Chen, A., Koh, P. W., Deng, T. Z., Sinha, R., Tsai, J. M., et al. (2016). Mapping the Pairwise Choices Leading from Pluripotency to Human Bone, Heart, and Other Mesoderm Cell Types. *Cell* 166 (2), 451–467. doi:10.1016/j.cell.2016.06.011

Lu, C., Li, X.-Y., Hu, Y., Rowe, R. G., and Weiss, S. J. (2010). MT1-MMP Controls Human Mesenchymal Stem Cell Trafficking and Differentiation. *Blood* 115 (2), 221–229. doi:10.1182/blood-2009-06-228494

Mabuchi, Y., Okawara, C., Méndez-Ferrer, S., and Akazawa, C. (2021). Cellular Heterogeneity of Mesenchymal Stem/Stromal Cells in the Bone Marrow. *Front. Cel Dev. Biol.* 9, 689366. doi:10.3389/fcell.2021.689366

Matsubara, T., Suardita, K., Ishii, M., Sugiyama, M., Igarashi, A., Oda, R., et al. (2005). Alveolar Bone Marrow as a Cell Source for Regenerative Medicine: Differences between Alveolar and Iliac Bone Marrow Stromal Cells. *J. Bone Miner Res.* 20 (3), 399–409. doi:10.1359/JBMR.041117

Müller, L., Tunger, A., Wobus, M., von Bonin, M., Towers, R., Bornhäuser, M., et al. (2021). Immunomodulatory Properties of Mesenchymal Stromal Cells: An Update. *Front. Cel Dev. Biol.* 9, 637725. doi:10.3389/fcell.2021.637725

Muñoz, J., Akhavan, N. S., Mullins, A. P., and Arjmandi, B. H. (2020). Macrophage Polarization and Osteoporosis: A Review. *Nutrients* 12 (10), 2999. doi:10.3390/nu12102999

Olsen, B. R., Reginato, A. M., and Wang, W. (2000). Bone Development. *Annu. Rev. Cel Dev. Biol.* 16, 191–220. doi:10.1146/annurev.cellbio.16.1.191

Onizuka, S., Yamazaki, Y., Park, S.-J., Sugimoto, T., Sone, Y., Sjöqvist, S., et al. (2020). RNA-Sequencing Reveals Positional Memory of Multipotent Mesenchymal Stromal Cells from Oral and Maxillofacial Tissue Transcriptomes. *BMC Genomics* 21 (1), 417. doi:10.1186/s12864-020-06825-2

Ozay, E. I., Vijayaraghavan, J., Gonzalez-Perez, G., Shanthalingam, S., Sherman, H. L., Garrigan, D. T., Jr., et al. (2019). Cymerus iPSC-MSCs Significantly Prolong Survival in a Pre-Clinical, Humanized Mouse Model of Graft-Vs-Host Disease. *Stem Cel Res.* 35, 101401. doi:10.1016/j.scr.2019.101401

Prummel, K. D., Nieuwenhuize, S., and Mosimann, C. (2020). The Lateral Plate Mesoderm. *Development* 147 (12), dev175059. doi:10.1242/dev.175059

Rivera-Pérez, J. A., and Magnuson, T. (2005). Primitive Streak Formation in Mice Is Preceded by Localized Activation of Brachyury and Wnt3. *Develop. Biol.* 288 (2), 363–371. doi:10.1016/j.ydbio.2005.09.012

Rux, D. R., Song, J. Y., Swinehart, I. T., Pineault, K. M., Schlientz, A. J., Trulik, K. G., et al. (2016). Regionally Restricted Hox Function in Adult Bone Marrow Multipotent Mesenchymal Stem/Stromal Cells. *Develop. Cel* 39 (6), 653–666. doi:10.1016/j.devcel.2016.11.008

Schier, A. F., and Shen, M. M. (2000). Nodal Signalling in Vertebrate Development. *Nature* 403 (6768), 385–389. doi:10.1038/35000126

Sheng, G. (2015). The Developmental Basis of Mesenchymal Stem/Stromal Cells (MSCs). *BMC Dev. Biol.* 15, 44. doi:10.1186/s12861-015-0094-5

SlukvinII, and Kumar, A. (2018). The Mesenchymoangioblast, Mesodermal Precursor for Mesenchymal and Endothelial Cells. *Cel. Mol. Life Sci.* 75 (19), 3507–3520. doi:10.1007/s00018-018-2871-3

Tanaka, S. S., Kojima, Y., Yamaguchi, Y. L., Nishinakamura, R., and Tam, P. P. L. (2011). Impact of WNT Signaling on Tissue Lineage Differentiation in the Early Mouse Embryo. *Dev. Growth Differ.* 53 (7), 843–856. doi:10.1111/j.1440-169X.2011.01292.x

Thomson, J. A., Itskovitz-Eldor, J., Shapiro, S. S., Waknitz, M. A., Swiergiel, J. J., Marshall, V. S., et al. (1998). Embryonic Stem Cell Lines Derived from Human Blastocysts. *Science* 282 (5391), 1145–1147. doi:10.1126/science.282.5391.1145

Vodyanik, M. A., Yu, J., Zhang, X., Tian, S., Stewart, R., Thomson, J. A., et al. (2010). A Mesoderm-Derived Precursor for Mesenchymal Stem and Endothelial Cells. *Cell Stem Cell* 7 (6), 718–729. doi:10.1016/j.stem.2010.11.011

Wang, H., Li, D., Zhai, Z., Zhang, X., Huang, W., Chen, X., et al. (2019). Characterization and Therapeutic Application of Mesenchymal Stem Cells with Neuromesodermal Origin from Human Pluripotent Stem Cells. *Theranostics* 9 (6), 1683–1697. doi:10.7150/thno.30487

Wang, L., and Chen, Y.-G. (2016). Signaling Control of Differentiation of Embryonic Stem Cells toward Mesendoderm. *J. Mol. Biol.* 428 (7), 1409–1422. doi:10.1016/j.jmb.2015.06.013

Wang, X., Lazorchak, A. S., Song, L., Li, E., Zhang, Z., Jiang, B., et al. (2016). Immune Modulatory Mesenchymal Stem Cells Derived from Human Embryonic Stem Cells through a Trophoblast-Like Stage. *Stem Cells* 34 (2), 380–391. doi:10.1002/stem.2242

Wang, Y., Chen, X., Cao, W., and Shi, Y. (2014). Plasticity of Mesenchymal Stem Cells in Immunomodulation: Pathological and Therapeutic Implications. *Nat. Immunol.* 15 (11), 1009–1016. doi:10.1038/ni.3002

Yin, J. Q., Zhu, J., and Ankrum, J. A. (2019). Manufacturing of Primed Mesenchymal Stromal Cells for Therapy. *Nat. Biomed. Eng.* 3 (2), 90–104. doi:10.1038/s41551-018-0325-8

Zákány, J., and Duboule, D. (1999). Hox Genes in Digit Development and Evolution. *Cel Tissue Res.* 296 (1), 19–25. doi:10.1007/s004410051262

Zakany, J., and Duboule, D. (2007). The Role of Hox Genes during Vertebrate Limb Development. *Curr. Opin. Genet. Dev.* 17 (4), 359–366. doi:10.1016/j.gde.2007.05.011

Conflict of Interest: The authors declare that the research was conducted in the absence of any commercial or financial relationships that could be construed as a potential conflict of interest.

frontiers | Frontiers in Molecular Biosciences

BRIEF RESEARCH REPORT
published: 09 June 2022
doi: 10.3389/fmolb.2022.806528

Aged Callus Skeletal Stem/Progenitor Cells Contain an Inflammatory Osteogenic Population With Increased IRF and NF-κB Pathways and Reduced Osteogenic Potential

*X. Lin[1], H. Zhang[1], J. Liu[1], C L. Wu[2], A. McDavid[3], B. F. Boyce[1,2] and L. Xing[1,2]**

[1]Department of Pathology and Laboratory Medicine, Rochester, NY, United States, [2]Center for Musculoskeletal Research, Rochester, NY, United States, [3]Biostatistics and Computational Biology, University of Rochester Medical Center, Rochester, NY, United States

Skeletal stem/progenitor cells (SSPCs) are critical for fracture repair by providing osteochondro precursors in the callus, which is impaired in aging. However, the molecular signatures of callus SSPCs during aging are not known. Herein, we performed single-cell RNA sequencing on 11,957 $CD45^-CD31^-Ter119^-$ SSPCs isolated from young and aged mouse calluses. Combining unsupervised clustering, putative makers, and DEGs/pathway analyses, major SSPC clusters were annotated as osteogenic, proliferating, and adipogenic populations. The proliferating cluster had a differentiating potential into osteogenic and adipogenic lineages by trajectory analysis. The osteoblastic/adipogenic/proliferating potential of individual clusters was further evidenced by elevated expression of genes related to osteoblasts, adipocytes, or proliferation. The osteogenic cluster was sub-clustered into house-keeping and inflammatory osteogenic populations that were decreased and increased in aged callus, respectively. The majority of master regulators for the inflammatory osteogenic population belong to IRF and NF-κB families, which was confirmed by immunostaining, RT-qPCR, and Western blot analysis. Furthermore, cells in the inflammatory osteogenic sub-cluster had reduced osteoblast differentiation capacity. In conclusion, we identified 3 major clusters in callus SSPCs, confirming their heterogeneity and, importantly, increased IRF/NF-κB-mediated inflammatory osteogenic population with decreased osteogenic potential in aged cells.

Keywords: skeletal stem/progenitor cell, fracture, aging, IRF, mesenchymal stroma cells, interferon regulatory factor, NF kappa b

OPEN ACCESS

Edited by:
Zhenhong Ni,
Army Medical University, China

Reviewed by:
Sona Kang,
University of California, Berkeley, United States
Jie Zhou,
Tianjin Medical University, China

****Correspondence:***
L. Xing
lianping_xing@urmc.rochester.edu

Specialty section:
This article was submitted to Cellular Biochemistry, a section of the journal Frontiers in Molecular Biosciences

Received: *31 October 2021*
Accepted: *29 April 2022*
Published: *09 June 2022*

Citation:
Lin X, Zhang H, Liu J, Wu CL, McDavid A, Boyce BF and Xing L (2022) Aged Callus Skeletal Stem/Progenitor Cells Contain an Inflammatory Osteogenic Population With Increased IRF and NF-κB Pathways and Reduced Osteogenic Potential. Front. Mol. Biosci. 9:806528. doi: 10.3389/fmolb.2022.806528

INTRODUCTION

Skeletal stem/progenitor cells (SSPCs) are multipotent cells with lineage-committed progeny and self-renewal capacity (Chan et al., 2015). SSPCs are critical for fracture repair by providing osteochondro-precursors in the callus. SSPCs are increased in fracture callus (Chan et al., 2015) while depletion of SSPCs with irradiation results in reduced fracture healing (Mitchell and Logan, 1998). Recent studies report that SSPCs exert inflammatory and senescent phenotypes, contributing to impaired fracture healing in aged mice (Josephson et al., 2019; Ambrosi et al., 2021). However, most

of these studies use SSPCs from the long bone or bone marrow but not from fracture callus where the combination of acute injury and natural aging creates a unique microenvironment. Exploring the molecular signature of callus SSPCs and their potential influence on fracture healing during aging is important because unlike bone/bone marrow SSPCs that are derived from the growth plate, endosteum, and perivascular sites (Ambrosi et al., 2019), callus SSPCs are mainly derived from periosteum (Debnath et al., 2018) and are directly exposed to fracture injury-caused local environmental changes that are often rapid and drastic while bone/bone marrow SSPCs reside in a relatively homeostatic environment. In this study, we performed single-cell RNA sequencing (scRNAseq) on SSPCs that are directly isolated from young and aged mouse callus to discover callus SSPC subsets, gene profiles, and master regulators that may affect fracture healing in aging. We also validated our scRNA-seq findings with immunostaining, RT-qPCR, and Western blot analysis and explored the functional implication of increased inflammatory osteogenic cells in aged callus.

MATERIALS AND METHODS

Animals and Tibial Fracture Procedure

Young (4-month-old, equivalent to 26-year-old in humans) and aged (21-month-old, equivalent to 62-year-old in humans) C57BL/6J mice from the National Institute on Aging were used. Mice were housed in micro-isolator technique rodent rooms. All animal procedures were approved by the University Committee on Animal Research at the University of Rochester. Open tibial fractures were performed according to the standard Operating procedure established in the Center for Musculoskeletal Research (Brown et al., 2014). In brief, an incision of 6 mm in length was made in the skin on the anterior side of the tibia after anesthesia. A sterile 27 G × 1.25-inch needle was inserted into the marrow cavity of the tibia from the proximal end, temporarily withdrawn to facilitate transection of the tibia using a scalpel at midshaft, and then reinserted to stabilize the fracture. The incision was closed with 5–0 nylon sutures. Fractures were confirmed by radiograph. Callus tissues were harvested on day 10, the time when soft callus is formed, following the fracture procedure for cell preparation.

Preparation of Callus Skeletal Stem/Progenitor Cells and Isolation of Cells in the Individual Cluster

For the preparation of callus SSPCs for scRNAseq, two soft calluses were dissected from the fractured tibiae on day 10 of young or aged mice and pooled as a sample, cut into small pieces (<1 mm^3), and digested in 10 ml of Accumax solution (STEMCELL, 1 h, room temperature). Cells were passed through a 35 mm-filter, and red blood cells were lysed with ammonium chloride (5 min, room temperature). Cells were resuspended in a staining medium (PBS with 2% fetal bovine serum) and stained with APC-anti-CD45 (Biolegend, clone 30-F11), FITC-anti-CD31 (eBioscience, clone 390), PerCP/Cy5.5-anti-Ter119 (Biolegend, clone TER-119) antibodies, and Dapi. Callus SSPC cells ($CD45^-CD31^-Ter119^-Dapi^-$) were sorted (85-micron nozzle) by FACS with a BD Aria II instrument. For isolation of cells in individual clusters for qPCR validation, callus cells from young mice on day 10 post fracture were prepared as described earlier. Cells were stained with PE/Cy7-anti-CD45 (Biolegend, clone 30-F11), FITC-anti-CD31 (eBioscience, clone 390), PerCP/Cy5.5-anti-Ter119 (Biolegend, clone TER-119), APC-anti-CXCR2 (Biolegend, clone SA044G4), PE-anti-CCR2 (Biolegend, clone SA203G11) antibodies, and Dapi.

scRNAseq

Cells were loaded onto a chromium chip (10X Genomics) followed by encapsulation in a lipid droplet (Single Cell 3′ kit, 10X Genomics) to generate cDNA and library according to the manufacturer's protocol. cDNA libraries were sequenced to an average of 100,000 reads per cell using Illumina Nextseq 500. scRNA-seq reads were processed with Cell Ranger v2.1, which demultiplexed cells from different samples and quantified transcript counts per putative cell; 5,648 young cells and 7,197 aged cells were sequenced.

Quality Control and Processing of scRNA-Seq Data.

The quality control and cell cluster identification were performed using the Seurat4 R package. After filtering out low-quality cells (<1,000 unique genes, >8% mitochondrial reads) and potential doublets [>12,000 unique molecular identifiers (UMIs)], 5,123 young and 6,834 aged cells were further analyzed. Data were then preprocessed with the Seurat4.0 R package. Data were normalized based on regularized negative binomial models with the SC Transform function. The top 2,000 variable genes were identified and ranked by coefficient of variation. Dimensionality reduction of datasets was performed by the "RunPCA" function with 25 principal components (npcs = 25) at a resolution of 0.1. Find Neighbors function was used to compute the shared nearest-neighbor (SNN) for a given dataset with parameter k = 20. Clusters of the cells were identified based on SNN modularity optimization with the Find Clusters function. The "RunUMAP" function was further used to perform Uniform Manifold Approximation and Projection (UMAP) dimensional reduction. Cell clusters were visualized on reduced UMAP dimensions using the "DimPlot" function. Differentially expressed genes (DEGs) of each cluster were identified with the "FindAllMarkers" function. The top 10 DEGs with the highest average log2-fold-change were presented in a heatmap using the "DoHeatmap" function for cluster functional annotation.

Pathway Analysis

DEGs identified with the "FindAllMarkers" function in Seurat/R and with an average log2-fold-change > 2 and p value < 0.05 were

uploaded to Ingenuity Pathway Analysis software (Qiagen). The top 5 pathways with the highest log10-fold-change were presented and used for cluster functional annotation.

Pseudotime Ordering and Lineage Trajectory Analysis

Monocle2/R package (Qiu et al., 2017) was used to compute and order the sequence of gene expression changes of the cells from each cluster. First, cluster 4 cells that express B cell-related genes were removed from the dataset, which was subsequently converted to a Monocle2 object using the Seurat Wrappers R package. Monocle2 objects were processed with "estimateSizeFactors," "estimateDispersions," "detectGenes," and "reduceDimension" (with "DDRTree" method) functions sequentially to order the cells along a pseudotime trajectory.

Transcription Factor Binding Motif Analysis

To obtain the upstream master regulators and transcription factor (TF) binding motifs that regulate the callus SSPCs, we used DEGs from each cluster, respectively, as input genes to the RcisTarget R package (Aibar et al., 2017) with default parameters and mm9-tss-centered-10kb-7species.mc9nr.feather as the database. For each cluster, the top TF with the corresponding binding motif was selected and visualized. The interaction map between TFs was constructed using STRING v11.0 (Szklarczyk et al., 2019).

Ligand Receptor Analysis

To identify the ligand–receptor pairs among the SSPC sub-clusters (i.e., clusters 1.1, 1.2, 2, and 3), we converted the Seurat object to CellChat/R object, a publicly available database of 2,021 validated molecular interactions for Mus Musculus, for ligand–receptor identification (Jin et al., 2021). The ligand–receptor regulatory potential and downstream target genes in the receptor cells were predicted using the Nichenetr/R package (Browaeys et al., 2020). Cluster 3 was set as the sender cell while the potential target receptors and genes were predicted for clusters 1.1 and 1.2, respectively.

Immunostaining

Tibiae were fixed in 10% formalin for 48 h at 4°C, decalcified in 10% EDTA for two weeks, processed, and embedded in optimal cutting temperature compound (Tissue-Tek). Seven-micron sagittal sections were cut and probed with antibody for CXCR2 (Invitrogen, cat# PA5-100951), followed by goat-anti-rabbit 488 (Abcam, cat# ab150081), and counterstained with Dapi. Sections were imaged with a Zeiss AxioImager motorized fluorescent microscope system with an AxioCam camera. The percentage of CXCR2+/Dapi+ total cells within the callus is quantified with ImageProPlus software.

Osteoblast Differentiation Assay and Alkaline Phosphatase Staining

Callus pieces were prepared with Accumax digestion as described earlier and cultured in α-MEM medium containing 15% fetal bovine serum. Cells that were migrated from callus were continuously cultured to 3rd–5th passages as callus mesenchymal progenitor cells. $CXCR2^{low}$ and $CXCR2^{high}$ callus mesenchymal progenitor cells were purified using CXCR2 antibody (Biolegend cat#149304, clone SA044G4) by fluorescence-activated cell sorting (FACS) or magnetic beads sorting (Miltenyl cat#130-048-801). $CXCR2^{low}$ and $CXCR2^{high}$ cells were seeded in a 96-well plate (1×10^4/well), cultured to 60% confluence, and then cultured in the osteoblast-inducing medium (α-MEM medium containing 15% fetal bovine serum, 50 μg/ml ascorbic acid, and 10 mM β-glycerophosphate) for seven days. The cells were harvested with 100% ethanol for 10 min, washed 3 times with PBS, and stained with 1-step NBT/BCIP reagent for alkaline phosphatase (ALP).

RT-qPCR

Cells that were isolated directly from fracture callus as individual clusters or CXCR2+ or CXCR2- callus mesenchymal progenitor cells were subjected to RNA extraction. RNA was extracted in TRIzol, and cDNA was synthesized using the iSCRIPT cDNA synthesis kit (BioRad). qPCR was performed using primers in **Supplementary Table S1** with iQ SYBR Green Supermix using an iCycler PCR machine (BioRad). The fold change of gene expression was first normalized to actin and then normalized to the values in cluster 1 Dapi-Ter119-CD45-CD31-CXCR2+CCR2- cell or $CXCR2^{low}$ cells, respectively.

Western Blot Analysis

Callus tissues were homogenized after being frozen in liquid nitrogen with a mortar and pestle. Homogenized tissues or cells were lysed in protein lysis buffer containing 1x RIPA buffer (EMD Millipore 20-188), 1 mM DTT (Sigma-Aldrich), 1 mM PMSF (Sigma-Aldrich), and 5 mM N-ethylmaleimide (Millipore Sigma 10197777001) and protease inhibitor cocktail (Millipore Sigma 04693116001). Proteins were loaded onto 15% SDS-PAGE gel and blotted with anti-IFITM1 Ab (Cell Signaling 13126, 1:500) and anti-S100A6 Ab (Cell Signaling 13162, 1:500).

Statistical Analysis

Statistical analysis was performed using GraphPad Prism 5 software (GraphPad Software Inc., San Diego, CA, United States). Data are presented as mean ± SD. Comparisons between two groups were analyzed using a two-tailed unpaired Student's t-test. Comparisons among 3 groups were analyzed using one-way ANOVA followed by the Tukey post-hoc test.

RESULTS

Unsupervised Clustering Reveals 3 Major Clusters in Callus Skeletal Stem/Progenitor Cells

To examine the SSPC populations in callus tissues during the early phase of bone fracture healing, a time when SSPCs were rapidly expanding to form the soft callus, we performed scRNA-

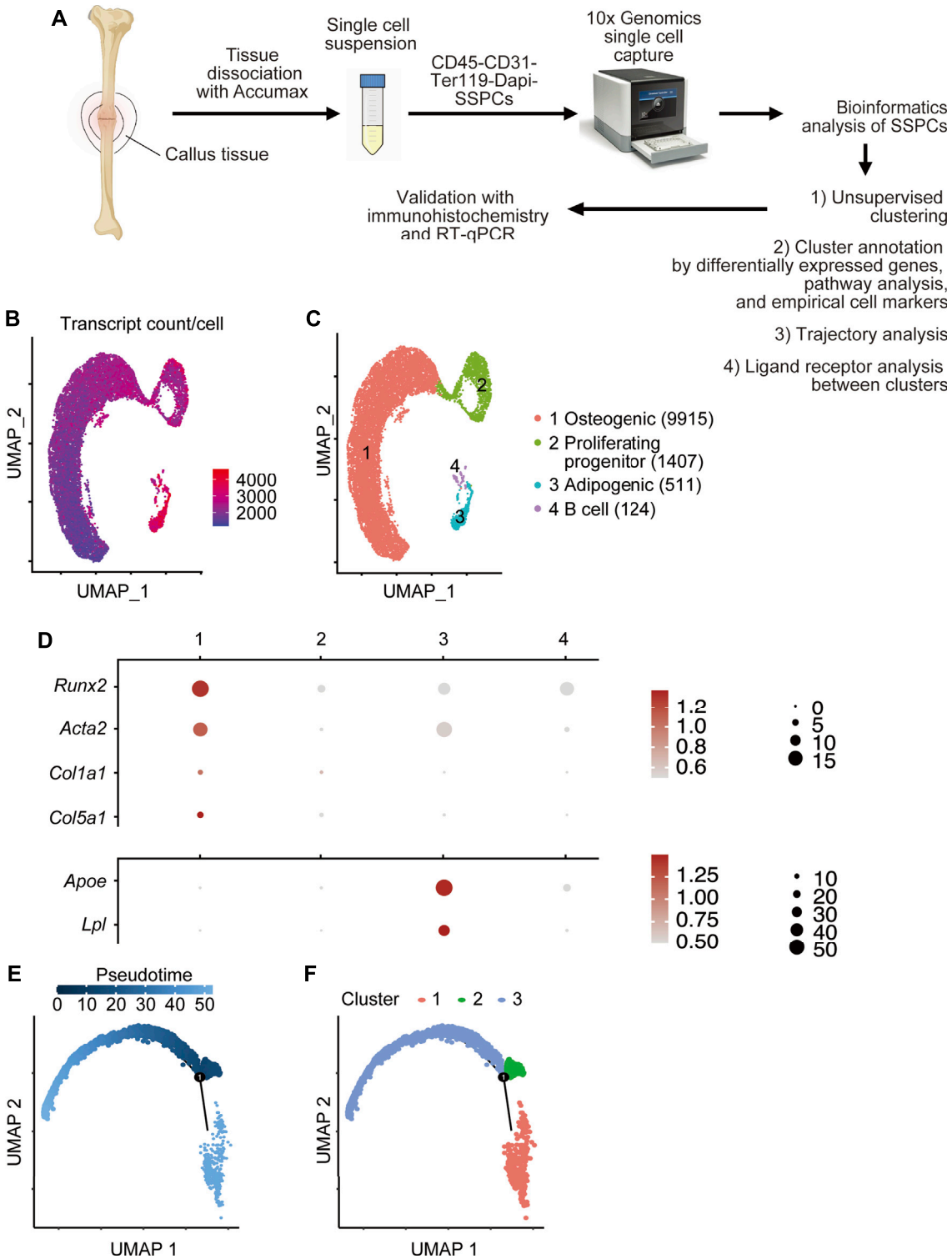

FIGURE 1 | Single-cell RNA sequencing of fracture callus CD45$^-$CD31$^-$Ter119$^-$ SSPC cells. **(A)** Isolation of callus SSPCs for scRNAseq. The tibial fracture was performed on 4-month- (young) and 21-month-old (aged) C57BL/6J male mice, and fracture callus was harvested 10 days after the procedure. A single-cell suspension was prepared by pooling two fracture calluses. CD45$^-$CD31$^-$Ter119$^-$Dapi$^-$ SSPC cells were sorted with FACS and subjected to scRNAseq. Data were analyzed using bioinformatics methods and validated by immunohistochemistry and RT-qPCR. **(B)** The number of transcripts per cell is demonstrated on UMAP. **(C)** A total of 11,957 cells were subjected to unsupervised SNN clustering using Seurat/R and resolved four major clusters. The number of cells within each cluster is indicated in the figure legend: 9,915 cells in the osteogenic cluster, 1,407 cells in the proliferating progenitor cluster, 511 cells in the adipogenic cluster, and 124 cells in the B cell cluster. **(D)** Expression of putative osteogenic and adipogenic markers of SSPCs in clusters 1–3: *Acta2* (SSPC), *Runx2* (osteogenic), *Col1a1* and *Col5a1* (osteoblast), and *Apoe* and *Lpl* (adipocyte). **(E,F)** Pseudotime analysis of cluster 1–3 with Monocle2 demonstrating that cluster2 proliferating progenitor was the earliest along the developmental tree according to pseudotime alignment and could differentiate into cluster 1 osteogenic cells and cluster 3 adipogenic cells.

seq analysis on purified SSPCs defined as CD45$^-$CD31$^-$Ter119$^-$ cells (**Supplementary Figure S1**). This gating strategy would exclude hematopoietic lineage cells *via* CD45 negative selection, endothelial cells *via* CD31 negative selection, and erythroid lineage cells *via* Ter119 negative selection. In order to acquire a comprehensive profile of SSPCs that contributed to fracture repair, we used the triple-negative selection of CD45, CD31, and Ter119 for classically defined stromal cells (Morikawa et al., 2009; Omatsu et al., 2010; Worthley et al., 2015), compared to the more stringent CD45-Ter119-PDPN+CD146-CD73+CD164+ mouse skeletal stem cells defined by Chan et al. (2015) to acquire a comprehensive profile of stromal cells that contributed to fracture repair. A scalable droplet-based scRNA-seq platform (10X Genomics Chromium) was used to profile FACS-purified live (DAPI-negative) SSPCs from the callus of young (4-month-old) and aged (21-month-old) mice following tibial fracture (**Figure 1A**, **Supplementary Figure S1**). A total of 12,845 cells were sequenced at an average depth of 100,000 reads per cell, with 5,648 cells from young and 7,197 cells from aged mice, respectively. The two libraries were aggregated and aligned using the Cell Ranger pipeline (10X Genomics) to compensate for minor differences in library complexity. After quality control filtering to remove cells with low gene detection (<500 genes) and high mitochondrial gene content (>8%), 5,123 young cells and 6,834 aged cells were used for clustering and cell-type identification analysis of combined young and aged datasets using Seurat4.0.3/R (Satija et al., 2015). **Figure 1B** demonstrated that all cells in the analysis had sufficient transcript counts per cell.

Initial unsupervised clustering revealed four clusters (**Figure 1C**). To define these cell clusters, we first assessed the expression of putative markers for SSPCs, specifically osteoblastic markers and adipoblastic markers. *Acta2*, a gene commonly used in lineage tracing and in scRNA-seq study for SSPCs (Josephson et al., 2019; Matthews et al., 2021), and *Runx2* (Komori, 2010), the master transcription factor for osteogenesis, were expressed in cluster 1, which also expressed osteoblast markers (*Col1a1* and *Col5a1*) (Dacic et al., 2001; Lin et al., 2020) (**Figure 1D**) and fibroblast markers *[Pdpn* (Astarita et al., 2012)] (**Supplementary Figure S2**). Adipocyte markers *Apoe* and *Lpl* (Moseti et al., 2016) were expressed in cluster 3 (**Figure 1D**). No chondrocyte-related genes (*Sox9* and *Col2a1*) (Sive et al., 2002) (**Figure 1D**) were detected. Cluster 2 expressed proliferative markers including *Mki67*, *Top2a,* and histones. Cluster 4 expressed genes related to B cells (*Cd79* and *Cd19*) with upregulated B cell pathways (**Supplementary Figure S3**) (Adams et al., 2009). Since B cells are CD45$^+$ hematopoietic cells despite our CD45$^-$CD31$^-$Ter119$^-$ gating strategy for FACS sorting, 124 cells in cluster 4 were likely due to contamination and thereby were removed from subsequent bioinformatics analysis.

To better understand the differentiation hierarchy of SSPC clusters, we performed trajectory analysis to re-order cells along a pseudotime with Monocle2 and found consistent results that cluster 2 was the earliest along the pseudotime trajectory (**Figure 1E**) and could be labeled as the root cells that could differentiate into cluster 1 and cluster 3 populations (**Figure 1F**).

To further characterize purified CD45$^-$CD31$^-$Ter119$^-$ cells, we assessed the expression of putative markers for hematopoietic populations (CD45$^+$) and endothelial cells (CD31$^+$). The expression of *Cd3g*, *Trac* (T cell), *Ighg1* (plasma cell), *Tpsab1* (mast cell), *Krt6a* (epithelial cell), and *Emcn* and *Vwf* (endothelial cells) was low or undetectable while expression of *Cd14* (monocyte), *Adgre* (macrophage), and *Fut4* (neutrophil) was low to moderate (**Supplementary Figure S2**).

Differentially Expressed Genes and Pathway Analysis Further Define the Osteogenic, Proliferating-Progenitor, and Adipogenic Clusters

Heatmap of top 10 DEGs in each cluster (**Figure 2A**) showed that cluster 1 expressed inflammatory [*Retnlg* (Nagaev et al., 2006) and *Cxcr2* (Kawagoe et al., 2020)], and matrix genes [*Mmp8* (Henle et al., 2005) and *Mmp9* (Colnot et al., 2003)]; cluster 2 expressed genes associated with cell proliferation [*Mki67* (Sun and Kaufman, 2018) and *Tuba1b* (Lu et al., 2013)], chromosome regulation [*Top2a* (Nielsen et al., 2020)], and histone modification (*Hist1h2ap* and *Hist1h1b*) (Marzluff et al., 2002); and cluster 3 expressed a miscellany of genes, including oncogene *Crip1* (Ludyga et al., 2013), matrix-related *Fn1* (Klavert and van der Eerden, 2021), inflammatory *S100a4* (Ambartsumian et al., 2019), and stem-cell marker *Sca1* homolog *Ly6e* (Upadhyay, 2019). Pathway analysis revealed that cluster 1 had multiple upregulated pathways that mediate cell adhesion, an important cellular process of inflammation (**Supplementary Figure S4**). Cluster 2 mainly had upregulated pathways related to cell division and cell cycle regulation (**Supplementary Figure S5**). The oxidative phosphorylation pathway and eIF4/p70S6K pathway that are important for adipocyte differentiation (Le Bacquer et al., 2007) were elevated in cluster 3 (**Supplementary Figure S6**). Combining unsupervised clustering, conventional makers, and DEGs/pathway analyses, we annotated clusters 1–3 as the osteogenic population, proliferating-progenitors, and adipogenic population, respectively (**Figure 1C**).

To validate the three major subpopulations of SSPC and their osteogenic/adipogenic/chondrogenic stemness experimentally, we first searched for surface proteins among the DEGs identified in **Figure 2A** and selected CXCR2 from cluster 1 and CCR2 from cluster 3 for our sorting strategy (**Figure 2B**). We sorted CD45$^-$CD31$^-$Ter119$^-$CXCR2$^+$CCR2$^-$ cluster 1, CD45$^-$CD31$^-$Ter119$^-$CXCR2$^-$CCR2$^-$ cluster 2, and CD45$^-$CD31$^-$Ter119$^-$CXCR2$^-$CCR2$^+$ cluster 3 cells from callus cells directly isolated from the callus of wild type mice at 10 days post-fracture (**Figures 2B, C**). We performed RT-qPCR on them to examine the expression of genes related to osteogenic/adipogenic/chondrogenic stemness and cell proliferation. We found that cluster 1 cells expressed the highest level of osteoblastic genes (*Alp*, *Runx2, Col1a1*, and *Acta2*); Cluster 2 cells expressed the highest level of proliferative genes (*Mki67* and *Hist1h1b*); and cluster 3 cells expressed the highest level of adipogenic genes (*Lpl* and *Apoe*). Similar to low levels of genes associated with chondrogenesis, cells in all 3 clusters expressed low levels of chondrogenic genes (*Sox9*) (**Figure 2D**).

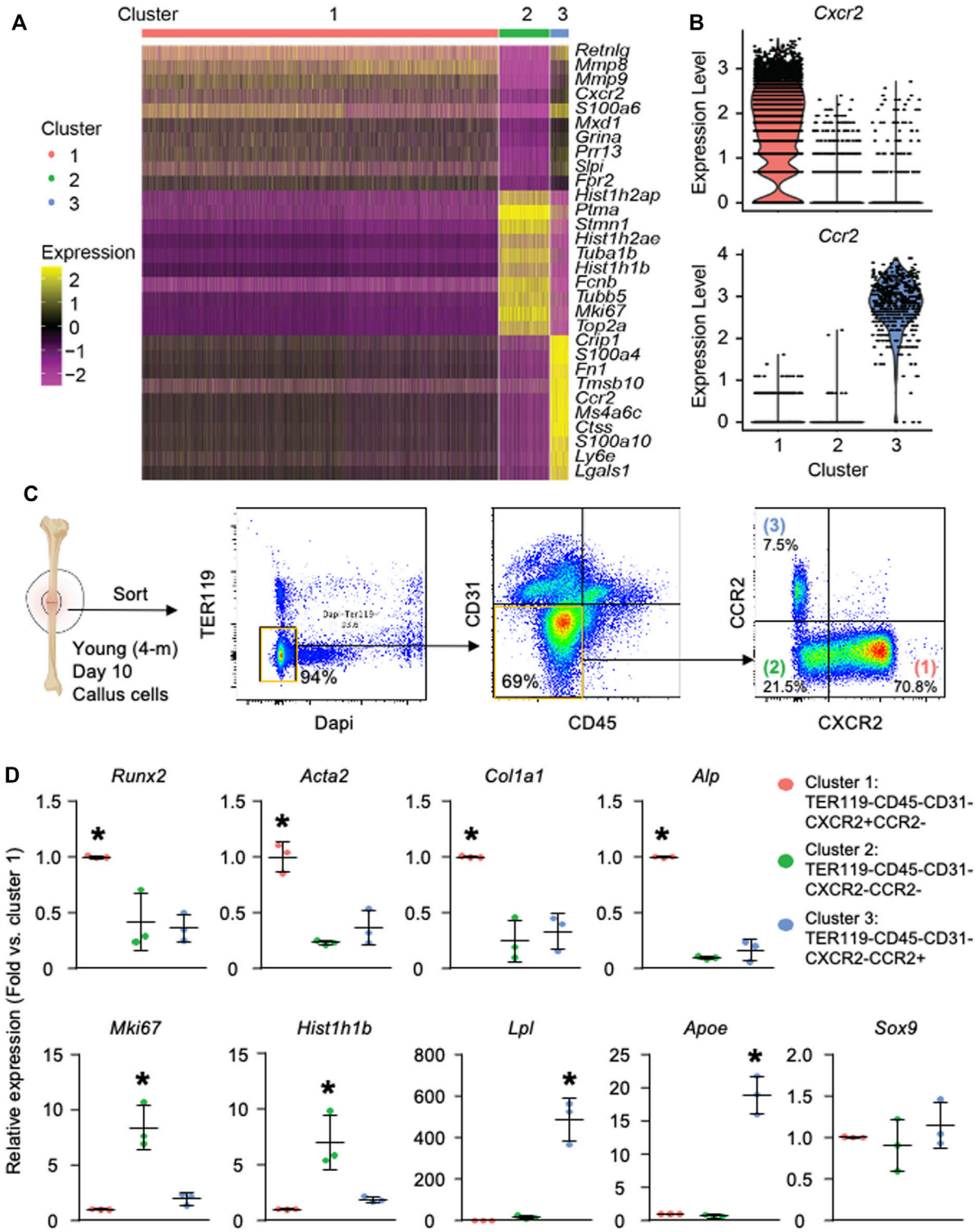

FIGURE 2 | Callus SSPCs are composed of osteogenic, proliferating, and adipogenic clusters. Analysis was performed on clusters 1–3. Cluster 4 was excluded from further analysis due to possible contamination of B cells during cell harvest, which is described in **Supplementary Figure S2**. **(A)** Heatmap of the top 10 DEGs in clusters 1–3 showing cluster 1 expressed inflammatory and matrix related genes, cluster 2 expressed proliferating genes, and cluster 3 expressed a miscellany of inflammatory, stem cell-related, and oncogenes. **(B)** Violin plot of the expression level of surface markers, Cxcr2 and Ccr2, within clusters 1–3. **(C)** Isolation of clusters 1–3 using FACS sorting: Cluster 1: Dapi-TER119-CD45-CD31-CXCR2+CCR2-; Cluster 2: Dapi-TER119-CD45-CD31-CXCR2-CCR2-; Cluster 3: Dapi-TER119-CD45-CD31-CXCR2-CCR2+. **(D)** RT-qPCR of cluster 1–3 cells to assess their osteogenic, proliferative, and adipogenic capacity. Data represent mean ± SD. One-way ANOVA followed by Tukey post-hoc. *$p < 0.05$ for significant difference from any other clusters.

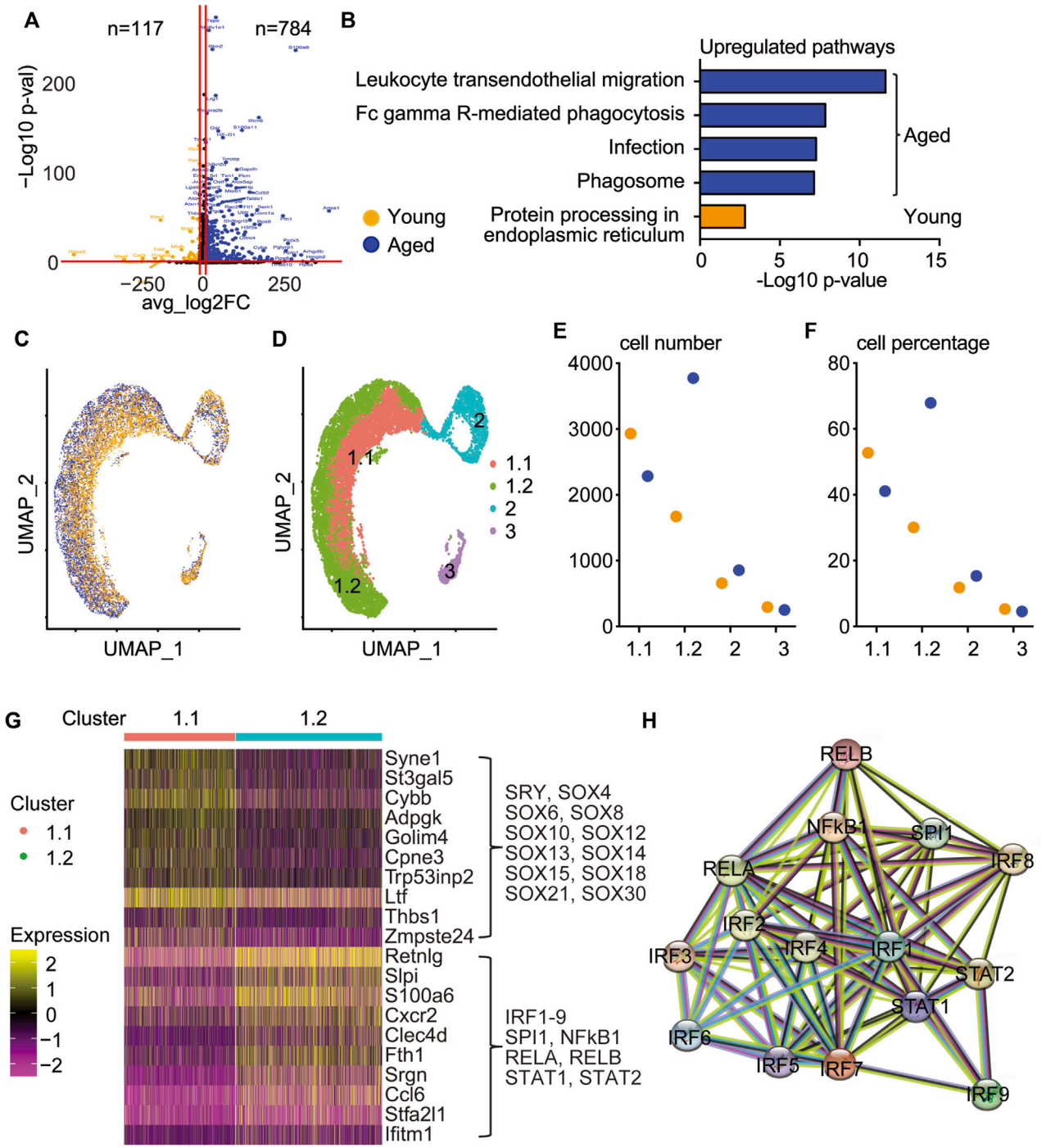

FIGURE 3 | Aged callus SSPCs contain an inflammatory osteogenic sub-cluster with upregulated IRF pathway. Bioinformatics analysis of clusters 1–3 comparing young and aged SSPCs. **(A)** Upregulated genes in young and aged SSPCs were demonstrated on the volcano plot, with each dot representing an individual gene. 117 and 784 genes with a log2FC greater than 2 and a *p*-value less than 0.05 in young and aged samples were colored in orange and blue, respectively. **(B)** Upregulated pathways in young and aged SSPCs were identified using the 117 and 784 upregulated genes in young and aged callus. Only one upregulated pathway was identified in young callus SSPCs, while the top pathways upregulated in aged callus SSPCs were related to inflammation. **(C)** UMAP demonstrated that the distribution of young and aged SSPCs was separated in cluster 1 osteogenic cluster. **(D)** Cluster 1 osteogenic cells were sub-clustered into 1.1 and 1.2 according to the separation of young and aged. **(E,F)** The cell number and percentage of cluster 1.1 were higher in young and vice versa for cluster 1.2 and were comparable in clusters 2 and 3. **(G)** Heatmap showing top 10 DEGs of clusters 1.1 and 1.2 revealing increased genes related to house-keeping and inflammation, respectively, which were driven by SOX family and IRF family transcription factors, respectively, identified by RcisTarget/R analysis. **(H)** The interaction map between master regulators of cluster 1.2.

Aged Callus Skeletal Stem/Progenitor Cells Contain an Inflammatory-Osteogenic Subset With Increased Genes in Interferon Response Factor Pathways

To explore the difference in molecular signature between young and aged callus SSPCs, we identified 117 and 784 upregulated DEGs in young and aged SSPCs, respectively (**Figure 3A**). Pathway analysis revealed that aged cells had increased inflammatory pathways while young cells had increased protein processing pathways (**Figure 3B**). The distribution of young and aged cells on UMAP revealed a clear separation of young and aged cells within cluster 1 osteogenic population (**Figure 3C**), which was further sub-clustered into 1.1 and 1.2 subsets (**Figure 3D**). Interestingly, the cell number and percentage in cluster 1.1 decreased while cells in cluster 1.2 increased in aged SSPCs. Cell numbers in cluster 2 and cluster 3 did not exhibit a clear difference between young and aged cells (**Figures 3E, F**). Heatmap showed that the DEGs of cluster 1.1 were genes related to house-keeping function, including metabolic-related [*Adpgk* (Imle et al., 2019) *and Cybb* (Frazão et al., 2015)], cytoskeletal-related [*Syne1* (Rajgor and Shanahan, 2013) and *Golim4* (Lu et al., 2017), *Ltf* (Cornish et al., 2004; Naot et al., 2005)], and matrix-related [*Zmpste24* (Bergo et al., 2002) *and Thbs1* (Yamashiro et al., 2020)] genes. In contrast, the DEGs of cluster 1.2 were enriched in inflammatory genes [*S100a6* (Xia et al., 2017), *Cxcr2* (Xia et al., 2016), and *Ifitm1* (Liao et al., 2019)] (**Figure 3G**). To further characterize the DEGs in these two sub-clusters, we performed transcription factor analysis to infer their upstream regulators by the RcisTarget R package (Aibar et al., 2017). The master regulators for cluster 1.1 were the Sox family transcription factors (**Figures 3F, G**) and for cluster 1.2 belonged to the IRF-STAT and NF-κB pathways (**Figures 3F, G**). Since Sox family transcription factors regulate multiple cellular functions while IRF-STAT and NF-κB pathways are mainly involved in inflammation, we further sub-clustered the osteogenic cluster in **Figure 1C** and named them as cluster 1.1 house-keeping osteogenic progenitors and cluster 1.2 inflammatory osteogenic progenitors.

To explore the interactions among the SSPC clusters, we performed a ligand–receptor analysis using the CellChat/R package (Jin et al., 2021). CellChat analysis revealed that cluster 3 adipogenic progenitors expressed the most outgoing signals (ligands), whereas cluster 1.1 house-keeping osteogenic and cluster 1.2 inflammatory osteogenic progenitors were the major receivers of incoming signals (**Supplementary Figure S7**). To identify the potential downstream signals activated by the cluster 3 outgoing ligands to cluster 1.1 and cluster 1.2, we utilized the Nichenetr/R package, a computational method to infer the intracellular communications by linking ligands to target genes (Browaeys et al., 2020). Among the inferred target genes of cluster 1.1 that did not overlap with cluster 1.2, *Irf2bp2* has been identified as a repressor for IRF2 signaling (Ramalho-Oliveira et al., 2019). In contrast, among the five target genes of cluster 1.2 that were not inferred in cluster 1.1, *Cebpb* (Pal et al., 2009), *Acvrl1* (Verma et al., 2016), *Anxa1* (Yap et al., 2020), and *Upp1* (Yan et al., 2016) have been reported to be related to IRF signaling and inflammation in various disease models, supporting the argument that cluster 1.2 has the inflammatory osteogenic progenitors mediated by IRF signaling (**Supplementary Figure S8**).

Increased Inflammatory CXCR2^{high} Cells in the Callus of Aged Mice With Elevated Expression of Interferon Response Factor and NF-κB Response Genes and Reduced Osteogenic Potential

To validate our finding that inflammatory osteogenic progenitors are increased in aging (**Figures 3C, D**), we performed immunostaining for CXCR2, one of the top DEGs in this sub-cluster (**Figure 3G**), on young and aged fracture callus tissue sections. Immunohistochemistry detected numerous CXCR2+ cells in the callus and they were mainly localized on the surface of woven bones in both young and aged mice. The percentage of CXCR2+ cells was significantly increased in aged callus (**Figure 4A**). We then assessed the protein levels of IRF-response gene, interferon-induced transmembrane protein 1, *Ifitm1* (Ogony et al., 2016), and NFκB-response gene, *S100a6* (Joo et al., 2003) in young and aged callus, which were among the top DEGs of cluster 1.2 that was predominant in aged callus (**Figure 3G**). Elevated levels of IFITM1 and S100A6 were detected in aged samples (**Figure 4B**). To experimentally validate the inflammatory and functional phenotypes of cluster 1.1 and 1.2 cells, we cultured callus pieces to generate callus-derived mesenchymal progenitor cells as we recently described (Liu et al., 2022) and used surface marker CXCR2 to separate the two sub-clusters in cluster 1. Because the expression of *Cxcr2* was higher in cluster 1.2 compared to cluster 1.1 (**Figure 3G**, **Figure 4C**), we isolated CXCR2^{low} cells as cluster 1.1 cells and CXCR2^{high} cells as cluster 1.2 cells (**Figure 4C**). The expression of *Cxcr2* was about 10-fold higher in CXCR2^{high} cells as a positive control of CXCR2^{high} cell purification. Consistent with the increased corresponding protein levels in aged callus tissues, fitm1 and S100a6 mRNA levels were ~9-fold and ~2-fold higher in CXCR2^{high} cells than in CXCR2^{low} cells, respectively (**Figure 4D**). However, the expression of *Slpi*, an IRF-response gene, was comparable between CXCR2^{low} and CXCR2^{high} cells (**Figure 4E**). These data demonstrated that aged mice had increased callus CXCR2^{high} cells that expressed high levels of IRF and NF-κB response genes. Finally, we assessed the osteogenic capacity of CXCR2^{high} cells to explore their functional implication and found that CXCR2^{high} cells had less ALP+ staining area and decreased *Alp* and *Runx2* mRNA expression levels (**Figure 4F**). This indicates that the reduced osteogenic capacity in inflammatory-osteogenic SSPCs may play a role in decreased fracture healing during aging.

DISCUSSION

Our scRNA-seq study identified three major clusters in callus SSPCs, e.g., osteogenic, proliferating precursors, and adipogenic clusters, confirming the heterogeneity of SSPCs. More importantly, we found that the osteogenic cluster can be further divided into house-keeping and inflammatory sub-clusters, based on significantly differential gene expression profile between young and aged cells, which may indicate the

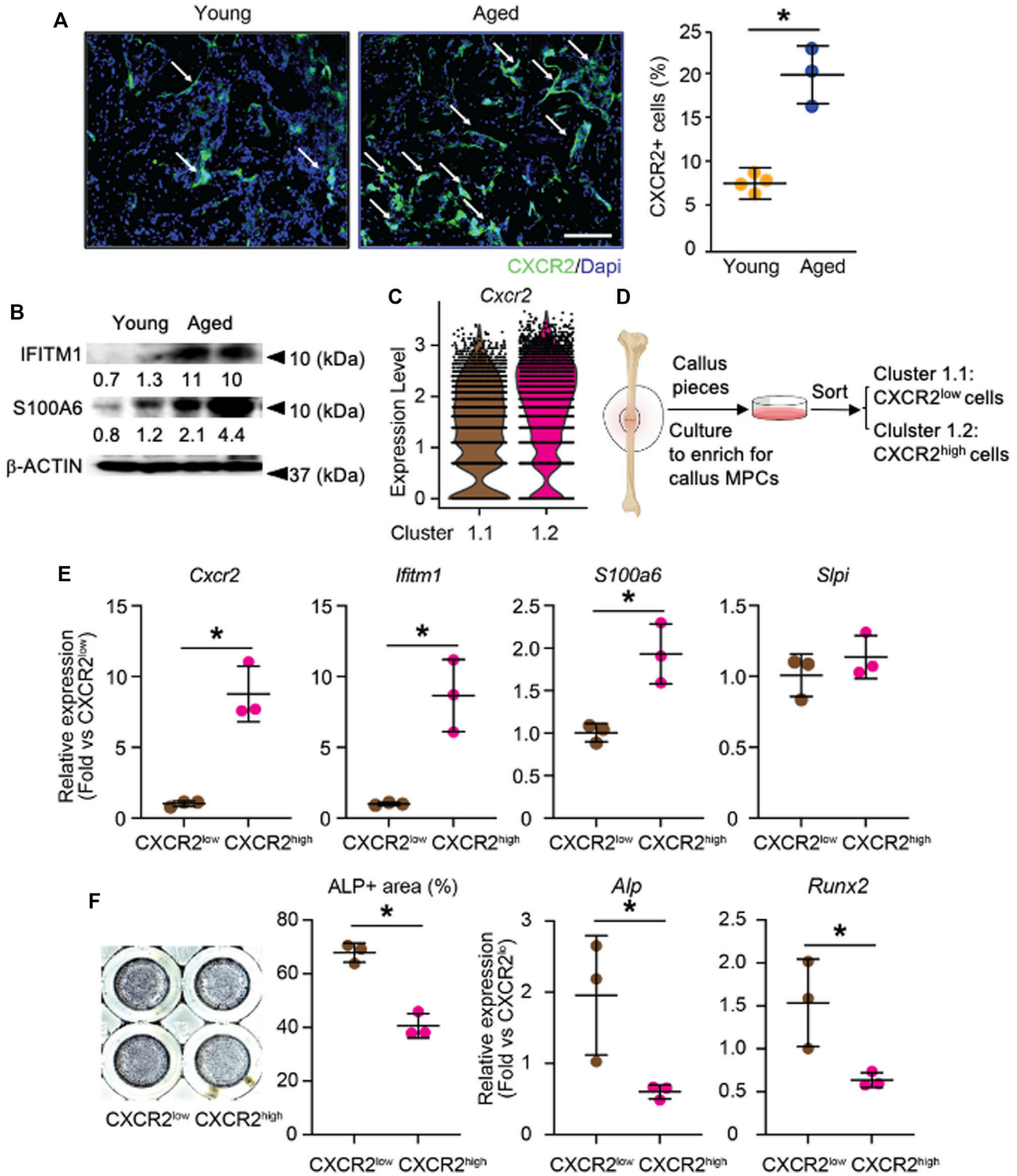

FIGURE 4 | Validation of increased CXCR2^{high} cells in the callus of aged mice with increased IRF and NF-κB pathways and reduced osteogenic potential. The tibial fracture was performed on 4-month- (young) and 21-month-old (aged) C57BL/6J male mice and fracture callus was harvested 10 days after the procedure. **(A)** Immunostaining with anti-CXCR2 antibody in callus sections for CXCR2+ cells. Images show numerous CXCR2+ cells (arrows) localize on the surface of woven bone. The percentage of CXCR2+ cells in the callus of young and aged mice was quantified by Image J software. $n = 4$ mice/young and 3 mice/aged. Data represent mean ± SD. Unpaired two-tailed t-test. *$p < 0.05$. WB: Woven bone. Scale bar = 1 mm. **(B)** Western blot to assess IRF-response protein IFITM1 and NF-κB-response protein S100A6 in young and aged callus tissues. **(C)** Violin plot of the expression level of Cxcr2 in cluster 1.1 and cluster 1.2. **(D)** CXCR2^{low} and CXCR2^{high} cells were isolated from callus-derived mesenchymal progenitor culture. **(E)** The expression levels of target genes for IRF and NF-κB were measured by RT-qPCR. $n = 3$ mice/group. Data represent mean ± SD. Unpaired two-tailed t-test. *$p < 0.05$. **(F)** CXCR2^{low} and CXCR2^{high} cells isolated from callus-derived mesenchymal progenitor culture were cultured in osteoblast inducing medium for 7 days and stained for ALP. The percentage area of ALP+ was measured in Image J software. Expression level of *Alp* and *Runx2* was measured with RT-qPCR. Data represent mean ± SD. Unpaired two-tailed *t*-test. *$p < 0.05$.

different osteogenesis between young and aged mice during bone fracture healing. Compared to the young osteogenic cluster, the aged osteogenic cluster is composed of fewer house-keeping and more inflammatory cells. Increased *Cxcr2* and several other inflammatory genes were detected in the aged inflammatory osteogenic population (cluster 1.2 in **Figure 3**), which was confirmed by immunostaining of CXCR2 on callus sections and by qPCR of IRF and NF-κB target genes in $CXCR2^{high}$ cells, which had decreased osteogenic capacity. Based on these findings, we propose a model to illustrate callus SSPC subsets and their potential roles in fracture healing in aging. In fracture callus, SSPCs can be divided into three clusters: osteogenic, proliferating, and adipogenic populations. The major difference between young and aged mice is the osteogenic population because it can be sub-clustered into the house-keeping osteogenic and inflammatory osteogenic populations. In young mice, the house-keeping osteogenic precursors promote fracture repair by providing metabolic and matrix synthetic functions as well as limiting the development of inflammatory osteogenic population *via* the production of IRF-inhibiting signals. In aged mice, the house-keeping osteogenic population decreased while the inflammatory osteogenic population increased. These inflammatory osteogenic cells express high levels of chemokine receptor *Cxcr2* and other target genes of IRF and NF-κB pathways, which is confirmed in $CXCR2^{high}$ callus cells. Specific targeting of the inflammatory osteogenic population may present a new therapeutic approach for fracture healing in the elderly.

Although a plethora of transcriptomic analyses have been performed on the fracture repair model, our study still provides further insights into the heterogeneity of non-hematopoietic SSPCs directly isolated from young and aged fracture callus tissue. Most importantly, we identified a unique CXCR2 expressing inflammatory osteogenic population and demonstrated that aging increased this inflammatory osteogenic population post-fracture. Our result is consistent with a recent report, in which microarray on callus tissue in 5-month-old and 25-month-old mice revealed increased inflammatory response including increased expression of *Ccl* and *Cxcl* family chemokines in aged mice (Hebb et al., 2018). scRNAseq on callus Ter119- cells of 24-month-old mice revealed that mice treated with vehicle had a prominent enrichment of cells expressing myeloid genes while mice treated with a combination of BMP2 and low dose anti-CSF1 had increased cells expressing SSPC genes and enhanced fracture healing that is comparable to the young mouse level and increasing cells expressing SSPC genes. In their study, the authors proposed that myeloid cells may inhibit SSPCs on fracture healing by creating an inflammatory-degenerative niche in the callus (Ambrosi et al., 2021). Our study indicates that in addition to myeloid cells, osteogenic cells may also function as inflammatory cells.

We found that Cxcr2 is a top DEG for the inflammatory osteogenic population that is increased in aged callus and $CXCR2^{high}$ cells have elevated expression of target genes for IFN and NF-κB signaling pathways. CXCR2 is a chemokine receptor expressed in different types of cells including leukocytes (Cheng et al., 2019), tumor cells (Acosta and Gil, 2009), endothelial cells (Li et al., 2018), chondrocytes (Sherwood et al., 2015), and mesenchymal cells (Kwon et al., 2021). Ligands of CXCR2 include CXCL family chemokines and could activate typical G-protein-mediated signaling cascades that regulate a wide range of cellular functions (Cheng et al., 2019). The level of CXCL8, the most well-known ligand for CXCR2, is increased in human fracture callus (Hoff et al., 2016; Edderkaoui, 2017), while CCL and CXCL family chemokines are among the most upregulated genes in aged fracture callus (Hebb et al., 2018). However, we did not detect the expression of putative CXCR2 ligands in our dataset. This observation is not surprising as chemokines are typically secreted by endothelial and immune cells (Turner et al., 2014), which were excluded from our study. Nevertheless, we identified *Annexin A1* (**Supplementary Figure S7D**) and *Cathelicidin* (**Supplementary Figure S8B**) as specific incoming signals (ligands) for cluster 1.2. Both ligands have been shown to be antagonists for CXCR2 (Zhang et al., 2009; Drechsler et al., 2015). Thus, it is likely that CXCR2 signaling is activated by chemokines produced by immune cells in the fracture callus micro-environment, leading to an increased inflammatory osteogenic population, while callus SSPCs produce negative regulative ligands to inhibit inflammation.

CXCR2 promotes inflammation (Bartek et al., 2008) and promotes cellular senescence *via* $Rb/p16^{INK4a}$ and $p53/p21^{WAF1/CIP1}$ signaling pathways (Acosta et al., 2008; Acosta and Gil, 2009). We did not detect a significant difference in the expression levels of senescent genes ($p16^{INK4a}$, $p21^{WAF1/CIP1}$, and $p18^{INK4c}$) between house-keeping and inflammatory osteogenic populations nor the expression of SASP factors such as *Tgfb1* (**Supplementary Figure S9**). Thus, it is unlikely that the $CXCR2^{high}$ cells in the inflammatory osteogenic population are senescent cells.

We discovered the inflammatory osteogenic cluster is under the control of IRF and NF-κB family transcription factors. IRF and NF-κB family transcription factors initiate the transcription of interferon (IFN) and other inflammatory cytokines (Yanai et al., 2012; Zhao et al., 2015), substantiating the inflammatory phenotype of this subset. Being an important cytokine, the role of IFN in osteoimmunology has been thoroughly investigated (Tang et al., 2018), while less is known about its role in SSPCs in fracture repair. Low levels of IFN have been reported in osteoblasts (Ruiz et al., 2007) and mesenchymal stem cells (Duque et al., 2009) and have been shown to promote osteoblastic and inhibit adipogenic differentiation (Duque et al., 2009). In addition, IFN-primed mesenchymal cells are immunosuppressive by impacting immune cells in the callus (Kim et al., 2018) and have shown promising results in clinical trials in non-union fractures (Medhat et al., 2019).

It is worth noting that the expression of *Irf* or *Nfkb* family genes in our dataset was low and not differentially expressed between clusters 1.1 and 1.2. Although this does not necessarily contradict our findings that IRFs are the master regulators for cluster 1.2, the expression level of a transcription factor does not always positively correlate with its response genes (Joshi et al., 2012). For example, the copy number of altered transcription factors may also affect the expression level of downstream target genes. These altered transcription factors may still lead to the

increased expression of target genes but could not be recognized in RNA sequencing (Joshi et al., 2012). Another factor that may affect the expression level of a transcription factor is whether it is a target gene of itself as in a positive regulation.

Currently, we do not know the exact role of the inflammatory osteogenic sub-cluster in fracture healing apart from that they have decreased osteogenic capacity. Since fracture healing is impaired in aged mice, which is accompanied by increased inflammatory osteogenic cells, we suspect they have a detrimental effect on healing. Thus, the interaction between the osteogenic-inflammatory cluster with other SSPC clusters as well as non-SSPC callus cells should be further investigated. Our initial ligand–receptor analysis with Cellchat (Jin et al., 2021) and NicheNet (Browaeys et al., 2020) did not detect strong outgoing signals between inflammatory osteogenic cells and other SSPC clusters (**Supplementary Figure S7**), which implies this cell population may mainly affect $CD45^+$ myeloid lineage cells that are not included in our samples. The impact and mechanisms of the inflammatory osteogenic population on aging fracture repair warrant further investigation.

In summary, the osteogenic SSPC population can be further sub-clustered into house-keeping and inflammatory populations, in which the former is decreased and the latter, with decreased osteogenic capacity, is markedly increased in aged callus. The combination of housekeeping function stimulation and IRF and NF-κB inhibition may represent a new therapy for fracture in aging.

DATA AVAILABILITY STATEMENT

The datasets presented in this study can be found in online repositories. The names of the repository/repositories and accession number(s) can be found below: GEO, GSE199755.

ETHICS STATEMENT

The animal study was reviewed and approved by the University Committee on Animal Research at the University of Rochester.

AUTHOR CONTRIBUTIONS

XL, JL, HZ, and LX designed the work. XL, JL, and HZ performed experiments. XL, JL, and AM performed bioinformatic analyses. XL and LX wrote the original manuscript. All the authors discussed the result and approved the manuscript.

FUNDING

This work was supported by NIH R01 grant AG059775 (to LX), AG049994 (to BB), NIH R00 grant AR075899, and OREF grant (to CW).

ACKNOWLEDGMENTS

We thank the Genome Research Center of University of Rochester for processing the single cell capture and RNA sequencing. We thank Andrea Baran from the Department of Biostatistics and Computational Biology of University of Rochester for helping with bioinformatics data analysis.

SUPPLEMENTARY MATERIAL

The Supplementary Material for this article can be found online at: https://www.frontiersin.org/articles/10.3389/fmolb.2022.806528/full#supplementary-material

REFERENCES

Acosta, J. C., and Gil, J. (2009). A Role for CXCR2 in Senescence, but what about in Cancer?: Figure 1. *Cancer Res.* 69 (6), 2167–2170. doi:10.1158/0008-5472.can-08-3772

Acosta, J. C., Loghlen, A., Banito, A., Raguz, S., and Gil, J. (2008). Control of Senescence by CXCR2 and its Ligands. *Cell Cycle* 7 (19), 2956–2959. doi:10.4161/cc.7.19.6780

Adams, H., Liebisch, P., Schmid, P., Dirnhofer, S., and Tzankov, A. (2009). Diagnostic Utility of the B-Cell Lineage Markers CD20, CD79a, PAX5, and CD19 in Paraffin-Embedded Tissues from Lymphoid Neoplasms. *Appl. Immunohistochem. Mol. Morphol.* 17 (2), 96–101. doi:10.1097/pai.0b013e3181845ef4

Aibar, S., González-Blas, C. B., Moerman, T., Huynh-Thu, V. A., Imrichova, H., Hulselmans, G., et al. (2017). SCENIC: Single-Cell Regulatory Network Inference and Clustering. *Nat. Methods* 14 (11), 1083–1086. doi:10.1038/nmeth.4463

Ambartsumian, N., Klingelhöfer, J., and Grigorian, M. (2019). The Multifaceted S100A4 Protein in Cancer and Inflammation. *Methods Mol. Biol.* 1929, 339–365. doi:10.1007/978-1-4939-9030-6_22

Ambrosi, T. H., Longaker, M. T., and Chan, C. K. F. (2019). A Revised Perspective of Skeletal Stem Cell Biology. *Front. Cell Dev. Biol.* 7, 189. doi:10.3389/fcell.2019.00189

Ambrosi, T. H., Marecic, O., McArdle, A., Sinha, R., Gulati, G. S., Tong, X., et al. (2021). Aged Skeletal Stem Cells Generate an Inflammatory Degenerative Niche. *Nature* 597 (7875), 256–262. doi:10.1038/s41586-021-03795-7

Astarita, J. L., Acton, S. E., and Turley, S. J. (2012). Podoplanin: Emerging Functions in Development, the Immune System, and Cancer. *Front. Immun.* 3, 283. doi:10.3389/fimmu.2012.00283

Bartek, J., Hodny, Z., and Lukas, J. (2008). Cytokine Loops Driving Senescence. *Nat. Cell Biol.* 10 (8), 887–889. doi:10.1038/ncb0808-887

Bergo, M. O., Gavino, B., Ross, J., Schmidt, W. K., Hong, C., Kendall, L. V., et al. (2002). Zmpste24 Deficiency in Mice Causes Spontaneous Bone Fractures, Muscle Weakness, and a Prelamin A Processing Defect. *Proc. Natl. Acad. Sci. U.S.A.* 99 (20), 13049–13054. doi:10.1073/pnas.192460799

Browaeys, R., Saelens, W., and Saeys, Y. (2020). NicheNet: Modeling Intercellular Communication by Linking Ligands to Target Genes. *Nat. Methods* 17 (2), 159–162. doi:10.1038/s41592-019-0667-5

Brown, M. L., Yukata, K., Farnsworth, C. W., Chen, D.-G., Awad, H., Hilton, M. J., et al. (2014). Delayed Fracture Healing and Increased Callus Adiposity in a C57BL/6J Murine Model of Obesity-Associated Type 2 Diabetes Mellitus. *PLoS One* 9 (6), e99656. doi:10.1371/journal.pone.0099656

Chan, C. K., Seo, E. Y., Chen, J. Y., Lo, D., McArdle, A., Sinha, R., et al. (2015). Identification and Specification of the Mouse Skeletal Stem Cell. *Cell* 160 (1-2), 285–298. doi:10.1016/j.cell.2014.12.002

Cheng, Y., Ma, X.-l., Wei, Y.-q., and Wei, X.-W. (2019). Potential Roles and Targeted Therapy of the CXCLs/CXCR2 axis in Cancer and Inflammatory

Diseases. *Biochimica Biophysica Acta (BBA) - Rev. Cancer* 1871 (2), 289–312. doi:10.1016/j.bbcan.2019.01.005

Colnot, C., Thompson, Z., Miclau, T., Werb, Z., and Helms, J. A. (2003). Altered Fracture Repair in the Absence of MMP9. *Development* 130 (17), 4123–4133. doi:10.1242/dev.00559

Cornish, J., Callon, K. E., Naot, D., Palmano, K. P., Banovic, T., Bava, U., et al. (2004). Lactoferrin Is a Potent Regulator of Bone Cell Activity and Increases Bone Formation *In Vivo*. *Endocrinology* 145 (9), 4366–4374. doi:10.1210/en.2003-1307

Dacic, S., Kalajzic, I., Visnjic, D., Lichtler, A. C., and Rowe, D. W. (2001). Col1a1-driven Transgenic Markers of Osteoblast Lineage Progression. *J. Bone Min. Res.* 16 (7), 1228–1236. doi:10.1359/jbmr.2001.16.7.1228

Debnath, S., Yallowitz, A. R., McCormick, J., Lalani, S., Zhang, T., Xu, R., et al. (2018). Discovery of a Periosteal Stem Cell Mediating Intramembranous Bone Formation. *Nature* 562 (7725), 133–139. doi:10.1038/s41586-018-0554-8

Drechsler, M., de Jong, R., Rossaint, J., Viola, J. R., Leoni, G., Wang, J. M., et al. (2015). Annexin A1 Counteracts Chemokine-Induced Arterial Myeloid Cell Recruitment. *Circ. Res.* 116 (5), 827–835. doi:10.1161/circresaha.116.305825

Duque, G., Huang, D. C., Macoritto, M., Rivas, D., Yang, X. F., Ste-Marie, L. G., et al. (2009). Autocrine Regulation of Interferon γ in Mesenchymal Stem Cells Plays a Role in Early Osteoblastogenesis. *Stem Cells* 27 (3), 550–558. doi:10.1634/stemcells.2008-0886

Edderkaoui, B. (2017). Potential Role of Chemokines in Fracture Repair. *Front. Endocrinol.* 8, 39. doi:10.3389/fendo.2017.00039

Frazão, J. B., Thain, A., Zhu, Z., Luengo, M., Condino-Neto, A., and Newburger, P. E. (2015). Regulation ofCYBBGene Expression in Human Phagocytes by a Distant Upstream NF-Kb Binding Site. *J. Cell. Biochem.* 116 (9), 2008–2017. doi:10.1002/jcb.25155

Hebb, J. H., Ashley, J. W., McDaniel, L., Lopas, L. A., Tobias, J., Hankenson, K. D., et al. (2018). Bone Healing in an Aged Murine Fracture Model Is Characterized by Sustained Callus Inflammation and Decreased Cell Proliferation. *J. Orthop. Res.* 36 (1), 149–158. doi:10.1002/jor.23652

Henle, P., Zimmermann, G., and Weiss, S. (2005). Matrix Metalloproteinases and Failed Fracture Healing. *Bone* 37 (6), 791–798. doi:10.1016/j.bone.2005.06.015

Hoff, P., Gaber, T., Strehl, C., Schmidt-Bleek, K., Lang, A., Huscher, D., et al. (2016). Immunological Characterization of the Early Human Fracture Hematoma. *Immunol. Res.* 64 (5-6), 1195–1206. doi:10.1007/s12026-016-8868-9

Imle, R., Wang, B.-T., Stützenberger, N., Birkenhagen, J., Tandon, A., Carl, M., et al. (2019). ADP-dependent Glucokinase Regulates Energy Metabolism via ER-Localized Glucose Sensing. *Sci. Rep.* 9 (1), 14248. doi:10.1038/s41598-019-50566-6

Jin, S., Guerrero-Juarez, C. F., Zhang, L., Chang, I., Ramos, R., Kuan, C.-H., et al. (2021). Inference and Analysis of Cell-Cell Communication Using CellChat. *Nat. Commun.* 12 (1), 1088. doi:10.1038/s41467-021-21246-9

Joo, J. H., Kim, J. W., Lee, Y., Yoon, S. Y., Kim, J. H., Paik, S.-G., et al. (2003). Involvement of NF-Kb in the Regulation of S100A6 Gene Expression in Human Hepatoblastoma Cell Line HepG2. *Biochem. Biophysical Res. Commun.* 307 (2), 274–280. doi:10.1016/s0006-291x(03)01199-9

Josephson, A. M., Bradaschia-Correa, V., Lee, S., Leclerc, K., Patel, K. S., Muinos Lopez, E., et al. (2019). Age-related Inflammation Triggers Skeletal Stem/progenitor Cell Dysfunction. *Proc. Natl. Acad. Sci. U.S.A.* 116 (14), 6995–7004. doi:10.1073/pnas.1810692116

Joshi, H., Nord, S. H., Frigessi, A., Børresen-Dale, A.-L., and Kristensen, V. N. (2012). Overrepresentation of Transcription Factor Families in the Genesets Underlying Breast Cancer Subtypes. *BMC Genomics* 13, 199. doi:10.1186/1471-2164-13-199

Kawagoe, Y., Kawashima, I., Sato, Y., Okamoto, N., Matsubara, K., and Kawamura, K. (2020). CXCL5-CXCR2 Signaling Is a Senescence-Associated Secretory Phenotype in Preimplantation Embryos. *Aging Cell* 19 (10), e13240. doi:10.1111/acel.13240

Kim, D. S., Jang, I. K., Lee, M. W., Ko, Y. J., Lee, D.-H., Lee, J. W., et al. (2018). Enhanced Immunosuppressive Properties of Human Mesenchymal Stem Cells Primed by Interferon-γ. *EBioMedicine* 28, 261–273. doi:10.1016/j.ebiom.2018.01.002

Klavert, J., and van der Eerden, B. C. J. (2021). Fibronectin in Fracture Healing: Biological Mechanisms and Regenerative Avenues. *Front. Bioeng. Biotechnol.* 9, 663357. doi:10.3389/fbioe.2021.663357

Komori, T. (2010). Regulation of Osteoblast Differentiation by Runx2. *Adv. Exp. Med. Biol.* 658, 43–49. doi:10.1007/978-1-4419-1050-9_5

Kwon, J. H., Kim, M., Um, S., Lee, H. J., Bae, Y. K., Choi, S. J., et al. (2021). Senescence-Associated Secretory Phenotype Suppression Mediated by Small-Sized Mesenchymal Stem Cells Delays Cellular Senescence through TLR2 and TLR5 Signaling. *Cells* 10 (1), 63. doi:10.3390/cells10010063

Le Bacquer, O., Petroulakis, E., Paglialunga, S., Poulin, F., Richard, D., Cianflone, K., et al. (2007). Elevated Sensitivity to Diet-Induced Obesity and Insulin Resistance in Mice Lacking 4E-BP1 and 4E-BP2. *J. Clin. Invest.* 117 (2), 387–396. doi:10.1172/jci29528

Li, Z., Yang, A., Yin, X., Dong, S., Luo, F., Dou, C., et al. (2018). Mesenchymal Stem Cells Promote Endothelial Progenitor Cell Migration, Vascularization, and Bone Repair in Tissue-engineered Constructs via Activating CXCR2-Src-PKL/Vav2-Rac1. *FASEB J.* 32 (4), 2197–2211. doi:10.1096/fj.201700895r

Liao, Y., Goraya, M. U., Yuan, X., Zhang, B., Chiu, S.-H., and Chen, J.-L. (2019). Functional Involvement of Interferon-Inducible Transmembrane Proteins in Antiviral Immunity. *Front. Microbiol.* 10, 1097. doi:10.3389/fmicb.2019.01097

Lin, X., Patil, S., Gao, Y.-G., and Qian, A. (2020). The Bone Extracellular Matrix in Bone Formation and Regeneration. *Front. Pharmacol.* 11, 757. doi:10.3389/fphar.2020.00757

Liu, J., Ali, K., Lou, H., Wang, L, and Wu, L. (2022). Age-associated Callus Senescent Cells Produce TGF Beta1 that Inhibits Fracture Healing in Aged Mice. *J. Clin. Invest.* 132, e148073. doi:10.1172/JCI148073

Lu, C., Zhang, J., He, S., Wan, C., Shan, A., Wang, Y., et al. (2013). Increased α-Tubulin1b Expression Indicates Poor Prognosis and Resistance to Chemotherapy in Hepatocellular Carcinoma. *Dig. Dis. Sci.* 58 (9), 2713–2720. doi:10.1007/s10620-013-2692-z

Lu, Y., Ye, Y., Bao, W., Yang, Q., Wang, J., Liu, Z., et al. (2017). Genome-wide Identification of Genes Essential for Podocyte Cytoskeletons Based on Single-Cell RNA Sequencing. *Kidney Int.* 92 (5), 1119–1129. doi:10.1016/j.kint.2017.04.022

Ludyga, N., Englert, S., Pflieger, K., Rauser, S., Braselmann, H., Walch, A., et al. (2013). The Impact of Cysteine-Rich Intestinal Protein 1 (CRIP1) in Human Breast Cancer. *Mol. Cancer* 12, 28. doi:10.1186/1476-4598-12-28

Marzluff, W. F., Gongidi, P., Woods, K. R., Jin, J., and Maltais, L. J. (2002). The Human and Mouse Replication-dependent Histone Genes. *Genomics* 80 (5), 487–498. doi:10.1006/geno.2002.6850

Matthews, B. G., Novak, S., Sbrana, F. V., Funnell, J. L., Cao, Y., Buckels, E. J., et al. (2021). Heterogeneity of Murine Periosteum Progenitors Involved in Fracture Healing. *Elife* 10, e58534. doi:10.7554/eLife.58534

Medhat, D., Rodríguez, C. I., and Infante, A. (2019). Immunomodulatory Effects of MSCs in Bone Healing. *Int. J. Mol. Sci.* 20 (21), 5467. doi:10.3390/ijms20215467

Mitchell, M. J., and Logan, P. M. (1998). Radiation-induced Changes in Bone. *Radiographics* 18 (5), 1125–1136. doi:10.1148/radiographics.18.5.9747611

Morikawa, S., Mabuchi, Y., Kubota, Y., Nagai, Y., Niibe, K., Hiratsu, E., et al. (2009). Prospective Identification, Isolation, and Systemic Transplantation of Multipotent Mesenchymal Stem Cells in Murine Bone Marrow. *J. Exp. Med.* 206 (11), 2483–2496. doi:10.1084/jem.20091046

Moseti, D., Regassa, A., and Kim, W. K. (2016). Molecular Regulation of Adipogenesis and Potential Anti-adipogenic Bioactive Molecules. *Int. J. Mol. Sci.* 17 (1), 124. doi:10.3390/ijms17010124

Nagaev, I., Bokarewa, M., Tarkowski, A., and Smith, U. (2006). Human Resistin Is a Systemic Immune-Derived Proinflammatory Cytokine Targeting Both Leukocytes and Adipocytes. *PLoS One* 1, e31. doi:10.1371/journal.pone.0000031

Naot, D., Grey, A., Reid, I. R., and Cornish, J. (2005). Lactoferrin - A Novel Bone Growth Factor. *Clin. Med. Res.* 3 (2), 93–101. doi:10.3121/cmr.3.2.93

Nielsen, C. F., Zhang, T., Barisic, M., Kalitsis, P., and Hudson, D. F. (2020). Topoisomerase IIα Is Essential for Maintenance of Mitotic Chromosome Structure. *Proc. Natl. Acad. Sci. U.S.A.* 117 (22), 12131–12142. doi:10.1073/pnas.2001760117

Ogony, J., Choi, H. J., Lui, A., Cristofanilli, M., and Lewis-Wambi, J. (2016). Interferon-induced Transmembrane Protein 1 (IFITM1) Overexpression Enhances the Aggressive Phenotype of SUM149 Inflammatory Breast Cancer Cells in a Signal Transducer and Activator of Transcription 2 (STAT2)-dependent Manner. *Breast Cancer Res.* 18 (1), 25. doi:10.1186/s13058-016-0683-7

Omatsu, Y., Sugiyama, T., Kohara, H., Kondoh, G., Fujii, N., Kohno, K., et al. (2010). The Essential Functions of Adipo-Osteogenic Progenitors as the Hematopoietic Stem and Progenitor Cell Niche. *Immunity* 33 (3), 387–399. doi:10.1016/j.immuni.2010.08.017

Pal, R., Janz, M., Galson, D. L., Gries, M., Li, S., Jöhrens, K., et al. (2009). C/EBPβ Regulates Transcription Factors Critical for Proliferation and Survival of Multiple Myeloma Cells. *Blood* 114 (18), 3890–3898. doi:10.1182/blood-2009-01-201111

Qiu, X., Mao, Q., Tang, Y., Wang, L., Chawla, R., Pliner, H. A., et al. (2017). Reversed Graph Embedding Resolves Complex Single-Cell Trajectories. *Nat. Methods* 14 (10), 979–982. doi:10.1038/nmeth.4402

Rajgor, D., and Shanahan, C. M. (2013). Nesprins: from the Nuclear Envelope and beyond. *Expert Rev. Mol. Med.* 15, e5. doi:10.1017/erm.2013.6

Ramalho-Oliveira, R., Oliveira-Vieira, B., and Viola, J. P. B. (2019). IRF2BP2: A New Player in the Regulation of Cell Homeostasis. *J. Leukoc. Biol.* 106 (3), 717–723. doi:10.1002/JLB.MR1218-507R

Ruiz, C., Pérez, E., García-Martínez, O., Díaz-Rodríguez, L., Arroyo-Morales, M., and Reyes-Botella, C. (2007). Expression of Cytokines IL-4, IL-12, IL-15, IL-18, and IFNγ and Modulation by Different Growth Factors in Cultured Human Osteoblast-like Cells. *J. Bone Min. Metab.* 25 (5), 286–292. doi:10.1007/s00774-007-0767-7

Satija, R., Farrell, J. A., Gennert, D., Schier, A. F., and Regev, A. (2015). Spatial Reconstruction of Single-Cell Gene Expression Data. *Nat. Biotechnol.* 33 (5), 495–502. doi:10.1038/nbt.3192

Sherwood, J., Bertrand, J., Nalesso, G., Poulet, B., Pitsillides, A., Brandolini, L., et al. (2015). A Homeostatic Function of CXCR2 Signalling in Articular Cartilage. *Ann. Rheum. Dis.* 74 (12), 2207–2215. doi:10.1136/annrheumdis-2014-205546

Sive, J. I., Baird, P., Jeziorsk, M., Watkins, A., Hoyland, J. A., Freemont, A. J., et al. (2002). Expression of Chondrocyte Markers by Cells of Normal and Degenerate Intervertebral Discs. *Mol. Pathol.* 55 (2), 91–97. doi:10.1136/mp.55.2.91

Sun, X., and Kaufman, P. D. (2018). Ki-67: More Than a Proliferation Marker. *Chromosoma* 127 (2), 175–186. doi:10.1007/s00412-018-0659-8

Szklarczyk, D., Gable, A. L., Lyon, D., Junge, A., Wyder, S., Huerta-Cepas, J., et al. (2019). STRING V11: Protein-Protein Association Networks with Increased Coverage, Supporting Functional Discovery in Genome-wide Experimental Datasets. *Nucleic Acids Res.* 47 (D1), D607–D613. doi:10.1093/nar/gky1131

Tang, M., Tian, L., Luo, G., and Yu, X. (2018). Interferon-Gamma-Mediated Osteoimmunology. *Front. Immunol.* 9, 1508. doi:10.3389/fimmu.2018.01508

Turner, M. D., Nedjai, B., Hurst, T., and Pennington, D. J. (2014). Cytokines and Chemokines: At the Crossroads of Cell Signalling and Inflammatory Disease. *Biochimica Biophysica Acta (BBA) - Mol. Cell Res.* 1843 (11), 2563–2582. doi:10.1016/j.bbamcr.2014.05.014

Upadhyay, G. (2019). Emerging Role of Lymphocyte Antigen-6 Family of Genes in Cancer and Immune Cells. *Front. Immunol.* 10, 819. doi:10.3389/fimmu.2019.00819

Verma, R., Jaiswal, H., Chauhan, K. S., Kaushik, M., and Tailor, P. (2016). Cutting Edge: ACVRL1 Signaling Augments CD8α+ Dendritic Cell Development. *J. I.* 197 (4), 1029–1034. doi:10.4049/jimmunol.1501849

Worthley, D. L., Churchill, M., Compton, J. T., Tailor, Y., Rao, M., Si, Y., et al. (2015). Gremlin 1 Identifies a Skeletal Stem Cell with Bone, Cartilage, and Reticular Stromal Potential. *Cell* 160 (1-2), 269–284. doi:10.1016/j.cell.2014.11.042

Xia, C., Braunstein, Z., Toomey, A. C., Zhong, J., and Rao, X. (2017). S100 Proteins as an Important Regulator of Macrophage Inflammation. *Front. Immunol.* 8, 1908. doi:10.3389/fimmu.2017.01908

Xia, S., Zhang, X., Zheng, S., Khanabdali, R., Kalionis, B., Wu, J., et al. (2016). An Update on Inflamm-Aging: Mechanisms, Prevention, and Treatment. *J. Immunol. Res.* 2016, 8426874. doi:10.1155/2016/8426874

Yamashiro, Y., Thang, B. Q., Ramirez, K., Shin, S. J., Kohata, T., Ohata, S., et al. (2020). Matrix Mechanotransduction Mediated by Thrombospondin-1/integrin/YAP in the Vascular Remodeling. *Proc. Natl. Acad. Sci. U.S.A.* 117 (18), 9896–9905. doi:10.1073/pnas.1919702117

Yan, M., Wang, H., Sun, J., Liao, W., Li, P., Zhu, Y., et al. (2016). Cutting Edge: Expression of IRF8 in Gastric Epithelial Cells Confers Protective Innate Immunity against Helicobacter pylori Infection. *J. I.* 196 (5), 1999–2003. doi:10.4049/jimmunol.1500766

Yanai, H., Negishi, H., and Taniguchi, T. (2012). The IRF Family of Transcription Factors: Inception, Impact And Implications In Oncogenesis. *Oncoimmunology* 1 (8), 1376–1386. doi:10.4161/onci.22475

Yap, G. L. R., Sachaphibulkij, K., Foo, S. L., Cui, J., Fairhurst, A.-M., and Lim, L. H. K. (2020). Annexin-A1 Promotes RIG-I-dependent Signaling and Apoptosis via Regulation of the IRF3-IFNAR-STAT1-IFIT1 Pathway in A549 Lung Epithelial Cells. *Cell Death Dis.* 11 (6), 463. doi:10.1038/s41419-020-2625-7

Zhang, Z., Cherryholmes, G., Chang, F., Rose, D. M., Schraufstatter, I., and Shively, J. E. (2009). Evidence that Cathelicidin Peptide LL-37 May Act as a Functional Ligand for CXCR2 on Human Neutrophils. *Eur. J. Immunol.* 39 (11), 3181–3194. doi:10.1002/eji.200939496

Zhao, G.-N., Jiang, D.-S., and Li, H. (2015). Interferon Regulatory Factors: at the Crossroads of Immunity, Metabolism, and Disease. *Biochimica Biophysica Acta (BBA) - Mol. Basis Dis.* 1852 (2), 365–378. doi:10.1016/j.bbadis.2014.04.030

Conflict of Interest: The authors declare that the research was conducted in the absence of any commercial or financial relationships that could be construed as a potential conflict of interest.

Publisher's Note: All claims expressed in this article are solely those of the authors and do not necessarily represent those of their affiliated organizations, or those of the publisher, the editors, and the reviewers. Any product that may be evaluated in this article, or claim that may be made by its manufacturer, is not guaranteed or endorsed by the publisher.

Advantages of publishing in Frontiers

OPEN ACCESS
Articles are free to read for greatest visibility and readership

FAST PUBLICATION
Around 90 days from submission to decision

HIGH QUALITY PEER-REVIEW
Rigorous, collaborative, and constructive peer-review

TRANSPARENT PEER-REVIEW
Editors and reviewers acknowledged by name on published articles

Frontiers
Avenue du Tribunal-Fédéral 34
1005 Lausanne | Switzerland

Visit us: www.frontiersin.org
Contact us: frontiersin.org/about/contact

REPRODUCIBILITY OF RESEARCH
Support open data and methods to enhance research reproducibility

DIGITAL PUBLISHING
Articles designed for optimal readership across devices

FOLLOW US
@frontiersin

IMPACT METRICS
Advanced article metrics track visibility across digital media

EXTENSIVE PROMOTION
Marketing and promotion of impactful research

LOOP RESEARCH NETWORK
Our network increases your article's readership